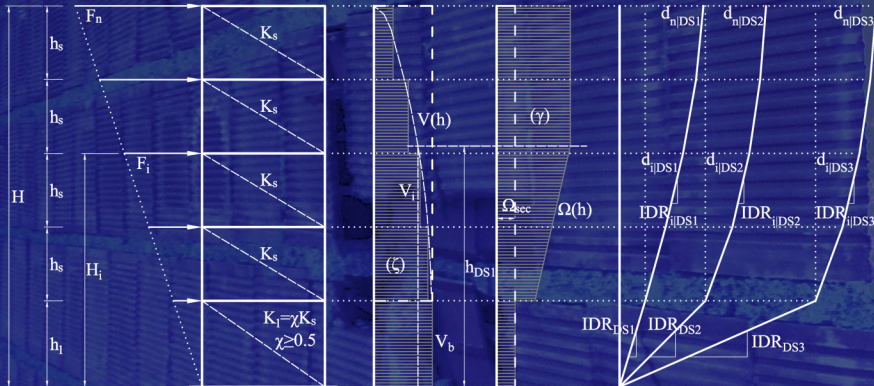




FERNANDO GÓMEZ MARTÍNEZ

**FAST SIMPLIFIED VULNERABILITY APPROACH
FOR SEISMIC ASSESSMENT OF INFILLED
RC-MRF BUILDINGS AND ITS APPLICATION
TO THE 2011 LORCA (SPAIN) EARTHQUAKE**

PH.D. THESIS



UNIVERSITAT POLITÈCNICA DE VALÈNCIA

Escuela Técnica Superior de Arquitectura

Ph.D. Program in Architecture, Building Construction, Urbanism and Landscape



**FAST SIMPLIFIED VULNERABILITY APPROACH
FOR SEISMIC ASSESSMENT OF INFILLED
RC-MRF BUILDINGS AND ITS APPLICATION
TO THE 2011 LORCA (SPAIN) EARTHQUAKE**

PH.D. THESIS

FERNANDO GÓMEZ MARTÍNEZ

Tutor:

Dr. Arch. **Agustín Pérez García**

Co-tutor:

Dr. Arch. **Adolfo Alonso Durá**

Universitat Politècnica
de València



Foreign co-tutors:

Dr. Ing.

Gerardo M.

Verderame

Università degli Studi
di Napoli Federico II



Dr. Ing.

Flavia

De Luca

University
of Bristol



JULY/2015

A mis padres, siempre
A te, per la luce

Acknowledgements

This work represents the end of an important phase of my life, the attainment of the top of the hill that I dreamed. Perhaps it is not so high, but hopefully bigger mountains will appear and the door of knowledge will not close. My research is divided in two different “worlds”, plenty of people who deserve my appreciation: Valencia, Spain (2009-2011) and Napoli, Italy (2012-2015).

Quisiera expresar mi inmensa gratitud a Agustín Pérez, el primero en estimular mi curiosidad por las estructuras y quien me abrió las puertas del Departamento. Siempre me ha hecho sentir como un compañero, dando importancia a mis opiniones, apoyando mis decisiones y ofreciéndome ayuda y consejos desde el interés por mi persona, siendo siempre todo un ejemplo de honradez e integridad. Asimismo debo dar las gracias sinceramente a Adolfo Alonso por su extrema generosidad intelectual y personal. Lo más importante de entre todo lo que he aprendido de él es a amar el trabajo y a encontrar en el conocimiento el mejor de los tesoros. Igualmente, me gustaría agradecer al resto de compañeros de Estructuras 1 su magnífica acogida: Arturo, Verónica, Iván, Ernesto, Begoña, Jéssica y Luis. También a mis alumnos, que hicieron estimulante la docencia, devolviéndome toneladas de gratitud; y a mis compañeros (y sin embargo amigos) del estudio El Fabricante de Esferas por robarme tanto tiempo de Tesis para volcarnos ilusionados en la creación.

Dal mio “mondo” italiano, innanzitutto devo ringraziare sia G. Manfredi che R. Landolfo per possibilitare una permanenza così lunga. Ma soprattutto devo esprimere la mia immensa gratitudine a Gerardo Verderame, chi prese un “architetto gravitazionale” e lo fece diventare un “ingegnere sismico”, chi mi ha fatto crescere e capire cosa sia l’onestà intellettuale e la vera passione per la ricerca, ma soprattutto chi mi ha rispettato, sostenuto e capito fino in fondo. Con moltissimo affetto ringrazio la mia cara “capa” Flavia De Luca, nel ricordo delle nostre liberatorie chiacchiere automobilistiche. Sempre una guida, sempre facendomi distinguere la ricerca della “fantascienza”, fornendomi di tutti gli strumenti, avendo cura di me e incoraggiandomi tanto. Ringrazio pure il resto della squadra per la sua gratissima accoglienza e compagnia: Carlo, Maria Teresa e specialmente Paolo, chi, oltre ad avere estrema pazienza intellettuale, è stato un fratello per me, un vero amico, con chi ho condiviso luce e ombre, gioia, lacrime, dubbi, interessantissime digressioni e tanto divertimento. Tutti loro, insieme agli “Scagnozzi”, la “Contrabbanda”, gli “Scissionisti”, la “Padrona” e il resto di affettuosi napoletani, hanno fatto di questa esperienza la migliore possibile.

Sin embargo, las estructuras colapsan si no tienen buenas condiciones de contorno. Nada habría sido posible sin el equilibrio de los que no pertenecen a esos dos mundos. Doy las gracias a mis amigos calasparreños por aceptarme tal y como soy, respetar mis largas ausencias y sostenerme en mis presencias. Agradezco también a Carmen su inestimable apoyo y afecto, antes y después. Igualmente merece reconocimiento el cariño incondicional de mi familia, especialmente de mi tío y colega Paco, y por supuesto de mi hermano Pedro, quien siempre me ha abierto camino en la vida. Pero sobre todo debo dar las gracias de corazón a mis padres, que están siempre en todo momento. Ellos me han transmitido la cultura del esfuerzo, y su honestidad, abnegación y generosidad es la mejor de las lecciones para la vida, que seguramente es más complicada que cualquier Tesis.

Napoli, July 2015

Abstract

A simplified analytical method (“FAST”) for the estimation of large-scale vulnerability of Reinforced Concrete (RC) Moment Resisting Frames with masonry infills is proposed and subsequently tested by using real damage scenario caused by the 2011 Lorca earthquake as a benchmark.

FAST is a spectral-based approach that allows predicting the average non-structural Damage State expected for each class of building (defined by number of storeys, age of construction, infills ratio in plan and location) for a given demand level. It accounts for non-uniformity of infills in elevation, i.e. a reduction of infills ratio at ground floor.

FAST is based on: (i) the definition of approximate capacity curves of the infilled building, assuming that the RC frame is designed according to the corresponding seismic code; and on (ii) the assumption of “a priori” deformed shapes in accordance with the attainment of each non-structural damage state at 1st storey, estimated through experimental and numerical correlations.

Two versions of FAST are proposed: a “simplified” approach aimed at the evaluation of uniformly infilled frames; and a “generalised” version which can account for any intermediate situation between uniformly infilled frames and pilotis frames (i.e. without infills at 1st storey). Also, some extensions of the method are highlighted.

Aimed at testing FAST, the real damage scenario after the earthquake of Lorca (2011) is used as a benchmark, despite its impulsivity and directivity. In order to define the specific input parameters for the case study, information regarding ground motion, post-earthquake damage scenario and also building design practice must be collected.

Hence, a detailed review of historical Spanish seismic codes and a critical analysis of current Spanish seismic code NCSE-02 in comparison with current reference performance-based codes such as Eurocode 8 are provided. Special emphasis is placed on provisions which can prevent a proper capacity design and that, in turn, can cause brittle failures or favour the interaction with infills. Also, the prescription of lower behaviour factor for wide-beam frames with respect to deep-beam frames—which is not present in most codes—is discussed; outcomes of several case studies suggest that such prescription is obsolete.

Finally, FAST is applied to Lorca earthquake and predicted damage scenarios are obtained, considering different assumptions for input values. Results show proper agreement between predicted and real damages. Structural collapses were rarely observed, even though the PGA was three times higher than the typical acceleration of design, so FAST proves that masonry infills provided additional strength to RC frames.

Keywords: *vulnerability, FAST, infilled frames, pilotis, Damage States, EMS-98, Lorca earthquake, period, Eurocode 8, NCSE-02, wide beams, behaviour factor, capacity design, brittle failures*

Resumen

Se propone un método analítico simplificado (“FAST”) para la estimación de la vulnerabilidad a gran escala de edificios porticados de hormigón armado (HA) con tabiquería de fábrica, posteriormente testado mediante la adopción del escenario de daño real correspondiente al terremoto de Lorca de 2011 como patrón de comparación.

FAST es un procedimiento espectral que permite predecir el nivel medio de daño no estructural para cada clase de edificio (definidas por su número de plantas, año de construcción, densidad de tabiquería en planta y localización geográfica), y para un nivel de demanda dado. El método tiene en cuenta la posible reducción relativa de tabiquería en planta baja.

FAST se basa en: (i) la definición de curvas de capacidad aproximadas para edificios tabicados, asumiendo que la estructura de HA está proyectada según la norma sísmica correspondiente; y en (ii) la asunción de deformadas coherentes con cada grado de daño que se alcanza siempre en planta baja, estimadas a través de correlaciones experimentales y numéricas.

Se proponen dos versiones de FAST: una “simplificada” para la evaluación de edificios uniformemente tabicados en altura, y otra “generalizada”, que es capaz de tener en cuenta cualquier situación intermedia entre el prototipo uniformemente tabicado y el de planta baja diáfana. Además, se proponen ciertas extensiones al método.

A fin de validar FAST, se elige el escenario de daño real correspondiente al terremoto de Lorca (2011) como patrón de comparación, a pesar de su impulsividad y directividad. Para definir los parámetros de input correspondientes al caso de estudio, es necesario recopilar previamente la información concerniente a la señal sísmica, el escenario de daño y las características del parque construido de HA.

Por tanto, se lleva a cabo una revisión de las normas sísmicas históricas en España y un análisis crítico de la actual NCSE-02 en comparación con otras normas actuales de referencia, como el Eurocódigo 8, haciendo énfasis en las provisiones que no garantizan el proyecto por capacidad y que pueden provocar mecanismos frágiles o favorecer la excesiva influencia de la tabiquería. Además, se discute sobre la restricción del coeficiente de ductilidad en estructuras de vigas planas, ausente en la mayoría de normas. Los resultados obtenidos mediante análisis de casos de estudio muestran que dicha prescripción resulta obsoleta para normas actuales.

Finalmente, FAST se aplica al caso del terremoto de Lorca, obteniéndose predicciones de daño medio para diferentes hipótesis. Los resultados muestran una coincidencia aceptable entre la predicción y los daños reales. FAST confirma que la causa principal de la práctica ausencia de colapsos (ante un terremoto con PGA triple que la típica de proyecto) hay que buscarla en la contribución estructural de la tabiquería de fábrica.

Palabras clave: *vulnerabilidad, FAST, edificios tabicados, pilotis, nivel de daño, EMS-98, terremoto de Lorca, periodo, Eurocódigo 8, NCSE-02, vigas planas, coeficiente de ductilidad, diseño por capacidad, roturas frágiles*

Resum

Es proposa un mètode analític simplificat ("FAST") per a l'estimació de la vulnerabilitat a gran escala d'edificis porticats de formigó armat (HA) amb envans de fàbrica. Posteriorment, el mètode ha estat testejat mitjançant l'adopció de l'escenari de dany real corresponent al terratrèmol de Lorca de 2011 com a patró de comparació.

FAST és un procediment espectral que permet predir el nivell de dany mitjà no estructural esperat per a cada classe d'edifici (definit pel seu nombre de plantes, any de construcció, densitat d'envans en planta i localització geogràfica), per a un determinat nivell de demanda. El mètode té en compte la reducció de d'envans a la planta baixa.

FAST es fonamenta en: (i) la definició de corbes de capacitat aproximades per estructures con envans i assumint que l'estructura de HA està projectada segons la norma sísmica corresponent; i en (ii) l'assumpció de deformades coherents amb cada grau de dany a la planta baixa, que han estat estimades a través de correlacions experimentals i numèriques.

Es proposen dues versions de FAST: una "simplificada" per a l'avaluació d'edificis amb envans uniformement repartits per totes les plantes, i una altra "generalitzada", que és capaç de tenir en compte qualsevol situació intermèdia entre el prototip uniformement paredat i el de planta baixa diàfana. A més, es proposen certes extensions al mètode.

Per tal de validar FAST, es tria l'escenari de dany real corresponent al terratrèmol de Lorca (2011) com a patró de comparació, malgrat la seva impulsivitat i directivitat. Per definir els paràmetres de entrada corresponents al cas d'estudi, cal recopilar prèviament la informació concernent al senyal sísmica, l'escenari de dany i les característiques del parc construït.

Per tant, es porta a terme una revisió de les normes sísmiques històriques a Espanya i una anàlisi crítica de la actual NCSE-02 comparant-la amb altres normes actuals de referència, com l'Eurocodi 8, fent èmfasi a les provisions que no garanteixen el projecte per capacitat i que, per tant, poden provocar mecanismes de col·lapse fràgils o afavorir la interacció de la estructura amb els envans. A més, es discuteix sobre la restricció del coeficient de ductilitat de les estructures de bigues planes, absent en la majoria de les normes. Els resultats obtinguts mitjançant l'anàlisi de casos d'estudi mostren que aquesta restricció resulta obsoleta a les normes actuals.

Finalment, FAST s'aplica al cas del terratrèmol de Lorca, obtenint prediccions de dany mitjà per a diferents combinacions del paràmetres de entrada. Els resultats mostren una coincidència acceptable entre la predicció i els danys reals. FAST confirma que la causa principal de la pràctica absència de col·lapses (davant un terratrèmol amb PGA triple que la típica de projecte) cal buscar-la en la contribució estructural dels envans.

Paraules clau: *vulnerabilitat, FAST, edificis amb envans, pilotis, nivell de dany, EMS-98, terratrèmol de Lorca, període, Eurocodi 8, NCSE-02, bigues planes, coeficient de ductilitat, disseny per capacitat, trencaments fràgils*

Contents

<i>Acknowledgements</i>	v
<i>Abstract</i>	vii
<i>Resumen</i>	viii
<i>Resum</i>	ix
<i>Contents</i>	xi
<i>Figures</i>	xix
<i>Tables</i>	xxxi
<i>Symbols</i>	xxxiv
<i>Acronims</i>	xli

<i>Introduction</i>	1
ORGANISATION AND OUTLINE	4
PUBLICATIONS	6

Chapter 1

State of the art	9
1.1 OVERVIEW OF VULNERABILITY ASSESSMENT METHODS FOR RC-MRF BUILDINGS	9
1.1.1 Empirical methods	13
1.1.1.1 <i>Damage Probability Matrices</i>	14
1.1.1.2 <i>Fragility curves</i>	15
1.1.1.3 <i>Vulnerability index</i>	17
1.1.1.4 <i>Screening methods</i>	18

1.1.2	Analytical methods	19
1.1.3	Hybrid methods.....	31
1.2	PBEE FRAMEWORK: SPECTRAL-BASED METHODOLOGIES.....	32
1.2.1	Capacity curves (CC).....	33
1.2.1.1	<i>Static PushOver (SPO) analysis</i>	33
1.2.1.2	<i>Bilinearisation methods</i>	36
1.2.1.3	<i>Behaviour factor and overstrength</i>	37
1.2.1.4	<i>Equivalent SDOF</i>	42
1.2.1.5	<i>Capacity curve of infilled frames</i>	50
1.2.2	Period of the building.....	52
1.2.2.1	<i>Period of bare frames</i>	57
1.2.2.2	<i>Period of uniformly infilled frames</i>	63
1.2.2.3	<i>Period of pilotis frames</i>	65
1.2.2.4	<i>Effective vs. elastic period</i>	65
1.2.3	Demand curves.....	67
1.2.3.1	<i>Smoothed spectra</i>	68
1.2.3.2	<i>Characteristic period</i>	69
1.2.3.3	<i>Equivalent-damped elastic spectra</i>	70
1.2.3.4	<i>Inelastic spectra: R-μ-T relations</i>	71
1.2.3.5	<i>Simplified IDA analysis: IN2 curves</i>	78
1.2.4	Different methods	81
1.2.4.1	<i>Capacity Spectrum Method</i>	81
1.2.4.2	<i>N2 method</i>	82
1.2.4.3	<i>Displacement coefficient method</i>	84
1.3	INFLUENCE OF INFILLS ON RC-MRF BUILDINGS PERFORMANCE	85
1.3.1	In-plane behaviour	86
1.3.1.1	<i>Local performance</i>	86
1.3.1.2	<i>Global performance</i>	89

1.3.2	Mechanic properties of infill panels.....	90
1.3.2.1	<i>Strength and stiffness</i>	90
1.3.2.2	<i>Correlation between non-structural damage states and IDR of infills</i>	90
1.3.3	Distribution and geometry of infills in Mediterranean construction.....	92

Chapter 2

Spanish vs. European seismic codes 95

2.1	CRITICAL REVIEW OF SPANISH SEISMIC CODES	95
2.1.1	Proto-code: MV-101 chapter 7 (1962).....	97
2.1.2	Old-generation codes	98
2.1.3	Medium-generation codes.....	100
2.1.4	New-generation codes.....	102
2.1.5	Comparison of codes.....	104
2.2	DIFFERENCES BETWEEN SPANISH AND EUROPEAN CURRENT CODES	119
2.2.1	Hierarchy of resistances.....	119
2.2.1.1	<i>Capacity design of columns: formulations</i>	123
2.2.1.2	<i>Capacity design of columns: equilibrium</i>	134
2.2.1.3	<i>Axial load in columns</i>	140
2.2.1.4	<i>Hierarchy of resistances in NCSE-02</i>	149
2.2.2	Local detailing of members	159
2.2.3	Restrictions of lateral deformability	160
2.2.4	Interaction with masonry infills	162
2.2.5	Squat columns.....	163
2.2.6	Moment inversion.....	163
2.2.7	Reliability and cost-effectiveness of NCSE-02	164
2.2.8	Regulation of assessment and retrofitting.....	167

2.2.9	Other relevant prescriptions included in RC codes.....	169
2.2.9.1	<i>Partial factors for actions in the accidental seismic situation</i>	169
2.2.9.2	<i>Minimum required amount of stirrups at column ends</i>	172
2.2.9.3	<i>Severity of deflection limitation in beams</i>	173

Chapter 3

Seismic performance of wide-beam frames	177	
3.1	INTRODUCTION.....	177
3.2	REVIEW OF CODE PROVISIONS.....	181
3.2.1	Code provisions on flat-slab structures.....	182
3.2.1.1	<i>Deformability restrictions</i>	184
3.2.1.2	<i>Ductility restrictions</i>	184
3.2.2	Impossibility of using wide-beam frames as the only lateral resisting system.....	185
3.2.3	Impossibility of considering wide-beam frames as high-ductility systems.....	186
3.2.4	Geometrical restrictions for connections of wide-beam frames	187
3.2.4.1	<i>Beam effective width for flexural equilibrium</i>	187
3.2.4.2	<i>Reinforcement placed inside the column core</i>	189
3.2.4.3	<i>Edge beam effective width from eccentricity limitations</i>	189
3.2.4.4	<i>Beam effective width for shear equilibrium</i>	190
3.2.4.5	<i>Upper slab effective width</i>	192
3.2.4.6	<i>Joint effective width</i>	193
3.2.4.7	<i>Member depths for bond development</i>	193
3.2.5	One-way slab as the only lateral resisting system in its direction..	194
3.3	EXPERIMENTAL BEHAVIOUR AND ANALYTICAL MODELS OF WBF	197
3.3.1	Equilibrium of forces in wide beam-column connections	197
3.3.1.1	<i>Effective width and torsional behaviour of transverse beam</i> .	199

3.3.1.2	<i>Joint effective width</i>	203
3.3.1.3	<i>Bond development</i>	204
3.3.1.4	<i>Upper slab contribution</i>	206
3.3.1.5	<i>Joists contribution</i>	209
3.3.1.6	<i>Shear equilibrium</i>	210
3.3.2	Ductility of wide beams	211
3.3.3	Lateral stiffness	219
3.4	SIMPLIFIED SPECTRAL ESTIMATION OF RELATIVE PERFORMANCES BETWEEN DEEP- AND WIDE-BEAM FRAMES	221
3.4.1	Safety Factor ratio.....	222
3.4.2	Estimation of relative performances between WBF and DBF	226
3.5	CASE STUDY: DESIGN.....	232
3.5.1	Case study	233
3.5.2	Three design alternatives: EC8 ₅₀₋₅₀ , EC8 ₁₀₀₋₅₀ and NCSE-02	235
3.5.3	Mechanic properties and design strategies.....	236
3.5.4	Results of design	239
3.6	CASE STUDY: N2 ASSESSMENT	247
3.6.1	Nonlinear local behaviour.....	247
3.6.2	SPO analyses.....	251
3.6.3	Assessment of capacities.....	256
3.7	COMPLEMENTARY ASSESSMENT OF PARAMETRIC SET OF FRAMES	264
3.8	ULTIMATE CHORD ROTATION OF WIDE BEAMS.....	272
3.9	CONCLUSIONS.....	282

Chapter 4

	The 2011 Lorca (Spain) earthquake	285
4.1	CHARACTERISTICS OF THE EVENT	286
4.1.1	General considerations.....	286

4.1.2	Directivity effects.....	291
4.2	CHARACTERISTICS OF RC BUILDING STOCK IN LORCA	295
4.3	DAMAGE SCENARIO	298
4.3.1	Soil influence on damages	299
4.3.2	Disaggregation for RC building stock	300
4.3.3	Observed typology of damages.....	305
4.3.3.1	<i>Structural damage and collapses</i>	305
4.3.3.2	<i>Non-structural damage</i>	308

Chapter 5

FAST approach for seismic assessment of infilled RC-MRF buildings311

5.1	“FAST”: SIMPLIFIED APPROACH FOR UNIFORMLY INFILLED RC-MRF BUILDINGS	311
5.1.1	Code-based assessment of bare frames.....	318
5.1.1.1	<i>Strength capacity</i>	319
5.1.1.2	<i>Fundamental period</i>	326
5.1.1.3	<i>Displacement capacity</i>	327
5.1.1.4	<i>Demand curve and IN2 curve</i>	328
5.1.1.5	<i>Assessment of the performance</i>	329
5.1.2	Capacity curve of uniformly infilled frames.....	329
5.1.2.1	<i>Maximum and residual strength capacities</i>	330
5.1.2.2	<i>Effective period and ductility</i>	333
5.1.3	Damage States displacement thresholds for uniformly infilled frames.....	334
5.1.3.1	<i>Correlation between interstorey drifts and Damage States</i> ...	335
5.1.3.2	<i>Deformed shape</i>	338
5.1.3.3	<i>Elastic stiffness contribution factor (χ)</i>	342
5.1.3.4	<i>Shear contribution factor (ζ)</i>	342

5.1.3.5	<i>Stiffness degradation contribution factor (γ)</i>	344
5.1.3.6	<i>Top displacement for each DS</i>	345
5.1.3.7	<i>Switching into ADRS and into PGA</i>	345
5.1.4	Assessment of the performance	347
5.2	GENERALISED FAST APPROACH FOR NON-UNIFORMLY INFILLED RC-MRF BUILDINGS	348
5.2.1	Non-uniformity of infills: from uniform to pilotis	349
5.2.1.1	<i>Generalised elastic stiffness contribution factor (χ)</i>	350
5.2.1.2	<i>Estimation of dimensions of cross sections of RC columns at 1st storey</i>	352
5.2.2	Generalised Damage States displacement thresholds for non-uniformly infilled frames	356
5.2.2.1	<i>Generalised shear contribution factor (ζ)</i>	357
5.2.2.2	<i>Generalised stiffness degradation contribution factor (γ)</i>	359
5.2.3	Generalised capacity curves for non-uniformly infilled frames	361
5.2.3.1	<i>Global elastic stiffness</i>	361
5.2.3.2	<i>Relative first mode participating mass of the SDOF</i>	362
5.2.3.3	<i>First mode participation factor</i>	363
5.2.3.4	<i>Elastic period of non-uniformly infilled frames</i>	365
5.3	SUITABLE EXTENSIONS OF FAST APPROACH	366
5.3.1	Assessment of “gravitational” buildings	367
5.3.2	DS related to the RC frame	369
5.3.3	Irregularity of infills in plan	371
5.3.3.1	<i>Torsion in multi-storey buildings</i>	372
5.3.3.2	<i>Simplified estimation of the displacement increase due to the torsion</i>	377
5.3.3.3	<i>Influence of torsional behaviour on the vulnerability</i>	394
5.3.4	Cumulative damage	398
5.3.5	Adaptive dynamic properties	403

Chapter 6

Application of FAST to the Lorca earthquake.....	407
6.1 SIMULATED DESIGN	407
6.2 ASSESSMENT OF BARE FRAMES.....	410
6.3 ASSESSMENT OF UNIFORMLY INFILLED FRAMES: SIMPLIFIED FAST	414
6.4 ASSESSMENT OF NON-UNIFORMLY INFILLED FRAMES: GENERALISED FAST.....	425
6.5 DISCUSSION OF RESULTS.....	430
<i>Conclusions</i>	433
<i>References</i>	435

Figures

Figure 1: Flowchart of FAST procedure.....	3
Figure 2: Organisation of contents in the different chapters.....	4
Figure 3: Diagram of the component of the seismic risk assessment and the different vulnerability assessment methodologies (blue rectangles), from (Calvi et al., 2006); the bold path shows a traditional procedure, while red path corresponds to FAST approach.....	10
Figure 4: DS correlation for generic RC frames (from Rossetto and Elnashai, 2003).....	11
Figure 5: DS correlation for infilled RC frames (from Rossetto and Elnashai, 2003).....	11
Figure 6: Characterisation of and vulnerability building classes (a) and Damage States (DS) (b) according to the EMS-98 scale (Grünthal, 1998).....	13
Figure 7: Damage Probability Matrix for a structural typology (Whitman et al., 1973) (from Calvi et al., 2006).....	14
Figure 8: Example of vulnerability (a) and fragility (b) curves according to Lagomarsino and Giovinazzi (2006).....	15
Figure 9: Implicit DPM for vulnerability class A of the EMS-98 scale (a), and interpretations of qualitative quantities as overlapping frequency intervals (b) (from Lagomarsino and Giovinazzi, 2006).....	17
Figure 10: Derived vulnerability curves from EMS-98 implicit DPM: for all the classes (a) and for classes B and C (b) (from Lagomarsino and Giovinazzi, 2006).....	17
Figure 11: Vulnerability functions for different values of vulnerability index (adapted from (Guagenti and Petrini, 1989); image from (Calvi et al., 2006)).....	17
Figure 12: Probability distribution of the damage index of Park and Ang's at a given spectral acceleration (a) and fragility curves for Mid-Rise frames (b) (Singhal and Kiremidjian, 1996)	20
Figure 13: Correlation between MMI intensity and spectral acceleration for a range of periods between 0.5-0.9s (a) and DPM for Mid-Rise buildings (b) (Singhal and Kiremidjian, 1996) ...	21
Figure 14: Predefined collapse mechanisms (Cosenza et al., 2005).....	22
Figure 15: Example of capacity curve of a building with control points (a) and capacity curves and damage states thresholds for five seismic design levels for C1M building class (b) (FEMA, 2001).....	23
Figure 16: Peak response displacement [D] and acceleration [A] obtained from the intersection of demand spectrum and capacity curve (a) and example of fragility curves for each damage state threshold (b) (FEMA, 2001).....	24
Figure 17: example of intersection of capacity areas and demand spectrum (Calvi, 1999).....	26

Figure 18: Deformation-based seismic vulnerability assessment procedure (a, from Glaister and Pinho, 2003) and Joint Probability Density Function (JPDF) of displacement capacity and period (b, from Crowley et al., 2004).....	27
Figure 19: Calculation of pushover curve in the POST approach (Ricci, 2010).....	31
Figure 20: Graphic evaluation of the performance point (a, from Fajfar, 1999) and different post-elastic behaviour of RC bare frames: hardening [i], perfectly plastic [p] and softening [d] (b, from Albanesi and Nuti, 2007)	33
Figure 21: Different capacity curves depending on the selected load pattern (triangular, modal, constant) (from Albanesi and Nuti, 2007).....	35
Figure 22: Different bilinearization strategies; (a) to (f) from (Kadaş, 2006); (g) and (h) from (De Luca et al., 2013)	37
Figure 23: Different combinations of q and μ for equal-performance structures given the equivalent elastic force and the period (a) and relationship between behaviour factor, overstrength, ductility reduction factor and ductility (b, from Mwafy and Elnashai, 2002)	38
Figure 24: Proposed definitions for different sources of contribution of behaviour factor	40
Figure 25: Typical shape of the first mode of vibration of a planar MDOF system with concentrated masses at the storey levels (a) and typical normalisation of amplitudes (b); dynamic and mechanic characteristics of SDOF in comparison with the MDOF (c).....	43
Figure 26: Transformation of the CC from MDOF to SDOF (a), and graphic interpretation of m^*/M for a discrete model (b) and analogous for m^*/M and L^*/M for a continuous model (c).....	45
Figure 27: Three variants of CC obtained from the same pushover curve by assuming different dynamic properties.....	49
Figure 28: Multilinearisation of capacity curve of infilled frames (a) and its conceptual breakdown into their two components ((b), from Dolšek and Fajfar, 2004a).....	51
Figure 29: Definition of different types of stiffnesses (a) and relationship between capacity and demand associated to changes in the global stiffness (b)	53
Figure 30: Examples of the performances of the structures corresponding to the four possible combinations of choices of design: period from code + model with and without stairs (a) and (b); period from physical model + model with and without stairs (c) and (d).....	55
Figure 31: Proposed empirical-based formulations for the fundamental period of bare RC MRF, assuming constant interstorey height $h=3\text{m}$	58
Figure 32: Fourier spectra (dashed line) for the whole time history of one case-study building during the San Fernando (1971) earthquake (a); evolution of the period of a case-study building during the San Fernando (1971) earthquake (b); and evolution of the period of a case-study building during the San Fernando (1971) earthquake, using the “zero-crossings” method (c) (from Bertero et al., 1988)	60
Figure 33: Different expressions for the elastic (grey line) and damaged (black line) period of Mula and Lorca (Spain) infilled frames from ambient noise analysis before and after different earthquakes (from Vidal et al., 2013).....	61

Figures

Figure 34: “Elongation” of “fundamental” (red dotted line) and “equivalent” (blue dotted line) periods of bare (a) and infilled (b) frames during such PGA incremental analysis (from Dolce et al., 2005).....	61
Figure 35: Different contributions to the absolute displacement and “apparent” period history of a building: base translation and rocking, and building deformation (a, from Trifunac et al., 2001a); and analytical periods of gross stiffness European bare MRF in comparison with different experimental formulations (b, from Crowley and Pinho, 2010).....	62
Figure 36: Comparison of analytical-based expressions for elastic period of representative sub-standard European buildings with EC8 formulation, for a transversal direction without beams (a) and for the longitudinal direction with beams (b) (from Verderame et al., 2010b).....	63
Figure 37: Proposed empirical-based (a) and numerical-based (b) formulations for the elastic fundamental period of infilled frames, assuming constant $h=3\text{m}$	64
Figure 38: Comparison of analytical results for elastic period of modern infilled frames with the EC8 formula for “other structures” (a, from Crowley and Pinho, 2010) and approximate ranges of the proposed experimental or numerical expressions for fundamental period of bare, pilotis and infilled frames.....	65
Figure 39: Typical CC and κ for soft-storey and global mechanisms of bare frames.....	66
Figure 40: Normalised pseudo-acceleration response spectrum for El Centro ground motion for damping coefficients of 0, 2, 5, 10 and 20% (a, from Chopra, 1995), and example of smoothing of the media of many spectra (b).....	67
Figure 41: Example of 5%-damped elastic acceleration and displacement spectra (a) and combined in the ADRS format (b) (from Dolšek and Fajfar, 2000).....	68
Figure 42: Construction of smooth response spectrum (from Malhotra, 2006).....	69
Figure 43: Acceleration (a) and velocity (b) response spectra, with the conceptual definition of T_C and T_D (T_1 and T_2 in the figure, respectively) (from Lam et al., 2000).....	70
Figure 44: Analytical values of T_C and T_D obtained from the real (black) and smooth (red) acceleration (a) and velocity (b) response spectra.....	70
Figure 45: Elastic [E_{So}] and hysteretic [E_D] energy for obtaining equivalent hysteretic damping (a), and damping ratios for different cases (b, from Priestley et al., 2007).....	71
Figure 46: Constant-ductility spectra corresponding to the 2011 Lorca mainshock (N-S), and locus of equal performance –blue dotted line— for a given T_{eff} (a); and elastic and constant-ductility spectra (b, from Miranda and Bertero, 1994).....	72
Figure 47: Different R - μ - T relations (from Miranda and Bertero, 1994).....	73
Figure 48: Comparison of R - μ - T relations for $\mu=3$ (from Miranda and Bertero, 1994).....	75
Figure 49: R - μ - T relation (a) and constant-ductility spectra (b) as proposed in Fajfar (1999), and some constant- μ and constant- R inelastic spectra obtained with such expressions (c).....	76
Figure 50: R - μ - T relation for infilled RC frames (a) and some examples of constant-ductility spectra (b) (from Dolšek and Fajfar, 2004a), and comparison of R - μ - T relations for bare (dotted line) and infilled frames (solid line) (c, from Dolšek and Fajfar, 2008a).....	78

Figure 51: Example of inelastic spectrum and displacement demand for an infilled frame (a, from Dolšek and Fajfar, 2005), and IN2 curves for two infilled frames and a bare frame (b, from Dolšek and Fajfar, 2008b).....	78
Figure 52: Characteristics of IDA curves (a, from Vamvatsikos and Cornell, 2002) and comparison of IN2 and IDA curves (b, from Dolšek and Fajfar, 2005)	80
Figure 53: Differences in the IN2 curves of the same structure depending on the characteristics of the ground motion (from Dolšek and Fajfar, 2005)	80
Figure 54: Performance point evaluated through the Capacity Spectrum Method (a, from Freeman, 1998) and through N2 method (b, from Fajfar, 1999).....	82
Figure 55: Graphic comparison between capacity and demand through the IN2 curves in the N2 method: in terms of spectral acceleration (a) (adapted from Fajfar, 1999) and in terms of PGA (b)	83
Figure 56: Monotonic lateral load-displacement response of bare, “weak” infilled or “strong” infilled RC frames (a, from Mehrabi et al., 1996), and force-displacement response of integral and non-integral infilled frames (b, from Crisafulli, 1997).....	86
Figure 57: Normal and shear stresses acting on a loaded corner (a); increase in the stress state along the diagonal of the panel (b) (from Crisafulli, 1997)	87
Figure 58: Bending moment, shear and axial force diagrams for a typical infilled RC frame (from Crisafulli, 1997).....	87
Figure 59: Failure mechanisms of infilled frames (from Shing and Mehrabi, 2002).....	88
Figure 60: Correlation between damage levels in HRC-scale and IDR for different structural types (from Rossetto and Elnashai, 2003).....	91
Figure 61: Fuzzy-probabilistic correlation between damage levels in HAZUS-scale and IDR of infills (from Colangelo, 2012).....	91
Figure 62: Correlation between damage levels IDR for infilled frames (a) and probability density functions of different correlation between damage levels and IDR proposed by different authors (b) (from Colangelo, 2013).....	92
Figure 63: Different positions of infills within the RC frame in a representative Mediterranean layout	93
Figure 64: Soil factor S for the different types depending on the seismicity, in NCSE-02 (a), and transformation of a_b into a_{gR} for the different importance classes of medium-generation Spanish codes, assuming variable $S_{NCSE-02,rock}$ (b).....	105
Figure 65: Hazard maps for each Spanish seismic code (adapted from Cabañas et al., 2011).....	110
Figure 66: Design response spectra for all the codes for different assumptions (I)	116
Figure 67: Design response spectra for all the codes for different assumptions (II).....	117
Figure 68: Soft-storey (a) and beam-sway (b) plastic mechanism of frames (from Fardis, 2009)....	120
Figure 69: Legend for diagrams shown in Figure 70	125

Figures

Figure 70: Diagrams representing different scenarios of evolution of moment demand in members framing into a joint depending on their relative overstrength values	126
Figure 71: Example of capacity design of columns of interior connection, regardless of γ_R , following the procedure of EC8 (a), NTC –alternative— (b) and NCSE-02 (c)	131
Figure 72: Diagrams of moment evolution in members framing into a joint for different assumptions of initial moments due to gravitational load in seismic situation	132
Figure 73: Diagrams of moment evolution in members framing into a joint when inferior column presents negative moment due to only horizontal loading	134
Figure 74: Typical N - M_x - M_y interaction resistance envelope of a generic column with square cross-section.....	143
Figure 75: Alternative consideration of column axial loads for moment resistances calculation for columns-to-beams capacity-design purposes: definition of initial seismic state	144
Figure 76: Alternative consideration of column axial loads for moment resistances calculation for columns-to-beams capacity-design purposes: obtaining of moment resistance	145
Figure 77: Alternative consideration of column axial loads for moment resistances calculation for shear-to-moment capacity-design purposes	147
Figure 78: Alternative consideration of column axial loads for moment resistances calculation for shear-to-moment capacity-design purposes	148
Figure 79: Example of capacity design of joints of interior connection, following the procedure of EC8 (a) and NCSE-02 (b).....	153
Figure 80: Shear capacity design of columns as in NCSE-02.....	154
Figure 81: Conservativeness of shear capacity design of columns depending on shear span proportion, without (a) and with (b) consideration of the increment of 25% to shear of design suggested by NCSE-02.....	158
Figure 82: Maximum allowed ratio between reinforcement in both sides of beam sections correspond to DCH and DCM, for EC8 and NCSE-02	160
Figure 83: NCSE-02 buildings: with likely high contribution of infills to the global strength and stiffness (a), with no compensation of infills reduction at 1 st storey by any increase of resistance of columns (b).....	161
Figure 84: Construction of typical wide-beam frame in Spain	178
Figure 85: Graphic description of variables used in Table 1, corresponding to: plan of interior connection (a), and elevation of connection belonging to central (b) and edge (c) frame.....	182
Figure 86: Typical distribution of elements in a one-way joist slab (a) and detail of joist-wide beam connection (b, from De Andrés and CSCAE, 2009; in grey, gross section concrete outside the beam web).....	188
Figure 87: Perpendicular reinforcement in eccentric edge beams (from De Andrés and CSCAE, 2009)	190
Figure 88: Effective stirrup legs (in black) (a) and arrangement of stirrups within the connection (b) according to NCSE-02 (b from De Andrés and CSCAE, 2009).....	190

Figure 89: Arrangement of stirrups within the connection according to ACI 318-08 (a, b) and ACI 352R-02 (c, d).....	191
Figure 90: Upper slab flexural contribution in a T-beam (a) and typical limitations for effective width of the upper slab tensioned flange for some codes (b).....	192
Figure 91: Joint effective width for NZS 3101.....	193
Figure 92: Typical wide-beam one-way joist slab system solution for common residential building (from De Andrés and CSCAE, 2009).....	195
Figure 93: Possible arrangement of reinforcement within suitable effective width in the joists-column connections.....	196
Figure 94: WB-C subassemblage tested in Quintero-Febres and Wight, 1997.....	198
Figure 95: 3D subassemblage of typical WB-C connection: solid view (a) and strut-and-tie scheme (b and c).....	199
Figure 96: Effective width from failure surface interpretation (a), strut-and-tie interpretation (b) (from Gentry and Wight, 1992) and non-linear finite element analysis of connection (c) (from Benavent-Climent et al., 2010).....	201
Figure 97: Alternative solutions for compressed diagonal strut within the beam effective width: trapezoidal (a) (from Gentry and Wight, 1992) and bi-trapezoidal (b).....	202
Figure 98: Two flexural transfer paths (strut-and-tie and torsional) (a, from Benavent-Climent et al., 2010), and strut-and-tie model of the torsional mechanism outside effective width (b).....	202
Figure 99: Slab contribution to the torsional behaviour of transverse beam (from Cheung et al., 1991).....	203
Figure 100: ACI 318-08 (a) and NZS 3101 (b) models for joint compressed strut.....	204
Figure 101: Effective area according to Gentry and Wight, 1992 (a); and joint mechanism for shallow beam-very deep column (b, from Paulay and Priestley, 1992).....	204
Figure 102: Bond behaviour of beam longitudinal bars placed inside and outside column core; (a) from (Benavent-Climent et al., 2010); (b) from (Gentry and Wight, 1994).....	205
Figure 103: Anchorage within the joint (a, from De Andrés and CSCAE, 2009); debonding strategy (b, from Siah et al., 2003) and (c).....	206
Figure 104: Strut-and-tie model representing upper slab contribution.....	207
Figure 105: Increase of upper slab effective width for larger drifts (a, from Kurose et al., 1991; and b, from LaFave and Wight, 1999).....	208
Figure 106: Upper slab effective width in WB (a) and DB (b) specimens (from LaFave and Wight, 2001).....	208
Figure 107: Strength effective width of flat slab according to (Luo et al., 1994) (a) and (Dovich and Wight, 2005) (b).....	209
Figure 108: Flexural contribution of joist (from Nudo et al., 2004).....	210
Figure 109: Proposed strut-and-tie model for shear equilibrium within the connection.....	211

Figures

Figure 110: DB vs.WB local ductility parametric analysis: ϕ_y (a) and ϕ_u without (b) and with (c) confinement contribution; θ_y (d); θ_{pl} without (e) and with (f) confinement contribution; θ_u without (g) and with (h) confinement contribution; μ_θ without (i) and with (j) confinement contribution; and μ_θ without (g) and with (h) confinement contribution.....	215
Figure 111: Cyclic behaviour of wide-beam (a) and deep-beam (b) subassemblages (from LaFave and Wight, 2001).....	217
Figure 112: Two examples of nonlinear time-history performance of deep- (a) and wide-beam (b) frames; and pushover curve and collapse mechanisms of deep- (c) and wide-beam (d) frames (from Gentry and Wight, 1992)	218
Figure 113: Simplified estimation of the top displacement capacity of a frame	224
Figure 114: ADRS N2 simplified comparison between WBF and DBF showing similar performances, considering similar Γ for both types	226
Figure 115: θ_u in columns for different sections and axial loads, assuming constant $L_V=2m$ and typical distribution of reinforcement bars.....	229
Figure 116: Graphic evaluation of $SF_{W/D}$ corresponding to four different situations, making conservative assumptions ($f_{K,sec}=H_{mec,W/D}=L_{Vc,W/D}=1.0$)	230
Figure 117: Schematic estimation of the probability of occurrence of each situation representing different relative performances between WBF and DBF, with expression of: boundary of $T_{el,W/D}$ for equal-performances (a) and estimated $SF_{W/D}$ (b); dark shadowed areas represent higher probabilities	232
Figure 118: Case study: distribution (a) and structural arrangement in plan (b), and in elevation (c).	234
Figure 119: Elastic horizontal demand acceleration spectrum; parameters follow EC8 terminology.....	235
Figure 120: Lateral deformed shape in both directions for all the models (adapted for comparison).....	242
Figure 121: Distribution (a) and structural arrangement (b) of case-study version EC8 ₅₀₋₅₀ with DB and WB	242
Figure 122: Mean and maximum storey values of ρ_{max}/ρ_{min} in relation with the EC8 limitation for design to DCH, for all the cases.....	243
Figure 123: Mean storey flexural capacity of beams, normalised to spectral design demand acceleration, for all the cases	244
Figure 124: Different fundamental periods for each model: code-based (T_{code}), elastic (T_{el}), design to 100%EI ($T_{100%EI}$), design to 50%EI ($T_{50%EI}$) and effective (T_{eff})	246
Figure 125: θ_y and θ_u ranges in columns in each storey.....	249
Figure 126: θ_y and θ_u ranges in beams in each storey	250
Figure 127: Mean storey μ_θ for columns and beams in all the models	251
Figure 128: Mean ratios between WB and DB regarding ultimate θ_u (a) and μ_θ (b) capacities, depending on the design code	251
Figure 129: Mechanisms of collapse for “MODE” lateral load distribution.....	253

Figure 130: Mean ductility exploitation and capacity of beams in each storey of EC8 models at collapse, for DBF	254
Figure 131: Mean ductility exploitation and capacity of beams in each storey of EC8 models at collapse, for WBF	255
Figure 132: Pushover curves of each model	257
Figure 133: ULS spectral performance and maximum capacity of each model, obtained with N2 method, for DBF	258
Figure 134: ULS spectral performance and maximum capacity of each model, obtained with N2 method, for WBF	259
Figure 135: Bilinear capacity curves (a) and global SF (b) of all the models	260
Figure 136: Interstorey drifts demands corresponding to design to ULS and performance corresponding to the design demand, for each model	262
Figure 137: DLS spectral performance of EC8 models	263
Figure 138: Scheme of pre-emptive yielding occurrence when performing to DLS demand	264
Figure 139: Elastic horizontal demand acceleration spectrum corresponding to both levels of a_{gR} ..	265
Figure 140: Geometry of the different frames of the set	266
Figure 141: Deformed shape for seismic situation of DBF (a) and WBF (b) with $n=9$ and $L=5.5m$ designed to EC8 for $a_{gR}=0.25g$	269
Figure 142: Estimated relative performance between WBF and DBF ($SF_{W/D}$) for each code considering $H_{mec,W/D}=f_{k,sec}=1.0$	271
Figure 143: Predicted vs. experimental values of ϕ_y and θ_y for WB	275
Figure 144: Predicted vs. experimental values of θ_u and μ_0 for WB	276
Figure 145: Predicted vs. experimental values of ϕ_y and θ_y for DB	277
Figure 146: Predicted vs. experimental values of θ_u and μ_0 for DB	278
Figure 147: Corrected-predicted vs. experimental values of θ_u and μ_0 for WB and DB	279
Figure 148: Correction of Figure 142 based on the new expressions proposed for θ_u of beams	281
Figure 149: Lorca: river Guadalentín (discontinuous blue line), limit of the constructed area (green-black line), limits of different soil types (EC8 classification, black dotted line), LOR seismic station (green triangle), mainshock and foreshock epicenter (big and small beach balls, respectively), high (red) and medium (yellow) damaged buildings as classified in the on-site damage survey	287
Figure 150: PGA in cm/s^2 (a) and PGV in cm/s (b) measured at the different stations	288
Figure 151: Elastic response spectra from the signals registered in LOR, ZAR and AM2 stations, closer than 30 km to the epicenter, for foreshock (a) and mainshock (b)	288
Figure 152: Soil classification of Lorca according to Cabañas et al. (2011) and damage level on buildings	289

Figures

Figure 153: Soil classification of Lorca according to Navarro et al. (2012).....	290
Figure 154: Comparison between elastic response spectra registered in LOR station and elastic response spectra proposed by NCSE-02 for Lorca on soil type II (adapted from Goula et al., 2011).....	291
Figure 155: Acceleration, velocity, and relative and absolute energy in terms of equivalent velocity spectra for fault normal FN (a), (b), (c), and fault parallel FP, (d), (e), (f) mainshock signals registered in Lorca (LOR) station with the evaluation of T_C and T_D	293
Figure 156: Baker (2007) quantitative classification of fault normal (FN) (a), and fault parallel (FP) (b) mainshock signals registered at Lorca (LOR) station, characterized by pulse indicators equal to 0.99 and 0.03, respectively	294
Figure 157: Frequency and cumulative distributions in Lorca building stock for: number of storeys (a), age of construction and applied code provision for the design of the building stock (b) (from Feriche et al., 2012)	296
Figure 158: 1 st (left) and upper (right) floors of two representative infilled RC buildings of Lorca; building I (a) and II (b)	297
Figure 159: Damage level in Lorca buildings and soil type for each district (from Cabañas et al., 2011).....	300
Figure 160: Normalised damages depending on soil type for different cases.....	301
Figure 161: Colour code used for each DS of EMS-98	301
Figure 162: Damage survey data according to EMS-98 disaggregated by number of storeys (a) and age of construction (b) for all the buildings (adapted from Feriche et al., 2012)	302
Figure 163: Frequency distribution of EMS-98 damage levels in Lorca	303
Figure 164: Frequency distribution of damage levels for RC structures depending on the number of storeys (a) and seismic code (b).....	304
Figure 165: Damages in RC columns due to lack of shear-to-column (a) and column-to-beam (b) hierarchy of resistances.....	306
Figure 166: Brittle shear failures in RC squat (a) and captive (b) columns, and local interaction with diagonal strut of infills (c).....	307
Figure 167: Brittle shear failures of RC beam-column joint.....	307
Figure 168: The only building collapsed due to the Lorca earthquake, before (Google Street View) (a) and after the event (b and c).....	308
Figure 169: In-plane failures in masonry infill panels: shear diagonal cracking (a), horizontal sliding (b) and corner crushing (c).....	309
Figure 170: Approximate capacity curve of a RC bare frame	322
Figure 171: Conceptual generation of the pushover curve of infilled frame in FAST method (a) and variables defining the corresponding CC and IN2 (b).....	331
Figure 172: Correlation between IDR and DS based on the typical backbone of diagonal-strut masonry infill.....	338

Figure 173: Framework of simplified FAST regarding deformed shape for the different DS: geometry, storey stiffnesses, lateral load pattern, shear diagram, contribution factors, IDR_{DSj} and displacements.....	343
Figure 174: Expression of DS thresholds in PGA units through the IN2 curve of an infilled frame	347
Figure 175: Characterisation of frames depending on the different 1 st storey infills ratio vs. upper storeys.....	350
Figure 176: Two approximate types of infilled frames adopted in generalised FAST framework ...	357
Figure 177: Framework of generalised FAST regarding deformed shape for the different DS: geometry, storey stiffnesses, lateral load pattern, shear diagram, contribution factors, IDR_{DSj} and displacements for uniformly infilled (a) and non-uniformly infilled (b) frames	358
Figure 178: Elastic fundamental period of different non-uniformly infilled frames depending on χ (a) and $\rho_{w,s}$ (b).....	366
Figure 179: Comparison of IDR characterising the attainment of different DS proposed in Table 48	371
Figure 180: Decomposition of torsional behaviour due to lateral loading	373
Figure 181: Two different approaches for the calculation of storey torsional moments: bare frames (adapted from Tso, 1990).....	374
Figure 182: Two different approaches for the calculation of storey torsional moments: non-uniformly infilled frames	375
Figure 183: Distribution of tangential stresses and location of shear centre for two thin-wall sections	376
Figure 184: The two “torsionable” prototypes, without RC structure: “L” (a) and “C” (b).....	378
Figure 185: Torsional behaviour of prototypes “L” (a) and “C” (b).....	379
Figure 186: Torsional out-of-plane behaviour of infill walls (a) and its corresponding translational behaviour (b); and torsional in-plane behaviour of infill walls (c).....	382
Figure 187: Transformation of a rectangle into a square (a) and this into a circle (b); and circular sector chosen as element representing a part of the ensemble of RC columns (c)	383
Figure 188: Torsional behaviour of a part of the ensemble of columns (a) and its corresponding translational behaviour (b).....	384
Figure 189: Hypothetical rectangular plan corresponding to the real centre of twist placed in his barycentre for the “L” prototype	385
Figure 190: Hypothetical rectangular plan corresponding to the real centre of twist placed in his barycentre for the “C” prototype.....	387
Figure 191: Zenithal prospectives of “L” (a) and “C” (b) test case studies	393
Figure 192: Deformed shape of “L” (a) and “C” (b) test case studies without RC columns; the scale of the deformation is not the same in both cases	393
Figure 193: Deformed shape of “L” (a) and “C” (b) test case studies with RC columns; the scale of the deformation is not the same in both cases	393

Figures

Figure 194: Hypothetical comparison between regular and “torsionable” equivalent building class: CC and IN2 (a) and DS thresholds (b).....	396
Figure 195: Four increasing demand spectra (0, 1, 2a-2b and 3) (a) causing the successive DS when acting consecutively on an infilled frame (b).....	399
Figure 196: General backbone of the CC, load paths and IN2 of all the cases	399
Figure 197: General CC backbone, load path, IN2 and DS thresholds of: a non-damaged infilled frame subjected to a demand causing DS1 beyond the beginning of the “plateau” (a) and an infilled frame previously “DS1-beyond-plateau damaged” subjected to a demand causing DS2 scarcely before the drop (b)	400
Figure 198: General CC backbone, load path, IN2 and DS thresholds of: an infilled frame previously “DS1-beyond-plateau damaged” subjected to a demand causing DS2 scarcely after the drop (a) and infilled frame previously “DS2-before-drop damaged” subjected to a demand causing DS3 (b)	401
Figure 199: General CC backbone, load path, IN2 and DS thresholds of: infilled frame previously “DS2-after-drop damaged” subjected to a demand causing DS3 (a) infilled frame previously “DS3 damaged” (b).....	402
Figure 200: CC and IN2 obtained from the same pushover curve of a bare frame assuming three diverse hypotheses (a), and CC and IN2 curve of an infilled frame with modifications for higher DS.....	404
Figure 201: Design acceleration response spectra (a) and normalised base shear demand (b) for the city of Lorca for the different seismic codes.....	409
Figure 202: ADRS of Lorca mainshock for Fault Normal (FN, red) and Fault Parallel (FP, blue) directions (a); and legends for all the graphics of the chapter (b)	410
Figure 203: Preliminary code-base assessment of 3- and 4-storey bare RC frames subjected to mainshock in LOR station in FN and FP directions.....	412
Figure 204: Preliminary code-base assessment of 5- and 6-storey bare RC frames subjected to mainshock in LOR station in FN and FP directions.....	413
Figure 205: Approximate CC and IN2 curves for uniformly infilled frames subjected to mainshock in LOR station in FN and FP directions.....	415
Figure 206: Damage assessment in terms of PGA for 3- and 4-storey uniformly infilled frames subjected to mainshock in LOR station in FN direction	416
Figure 207: Damage assessment in terms of PGA for 5- and 6-storey uniformly infilled frames subjected to mainshock in LOR station in FN direction	417
Figure 208: Damage assessment in terms of PGA for 3- and 4-storey uniformly infilled frames subjected to mainshock in LOR station in FP direction.....	418
Figure 209: Damage assessment in terms of PGA for 5- and 6-storey uniformly infilled frames subjected to mainshock in LOR station in FP direction	419
Figure 210: Damage assessment in terms of PGA for uniformly infilled frames subjected to mainshock in LOR station	420

Figure 211: Fragility curves in terms of PGA for uniformly infilled frames subjected to mainshock in LOR station in FN direction	421
Figure 212: Fragility curves in terms of PGA for uniformly infilled frames subjected to mainshock in LOR station in FP direction	422
Figure 213: Damage assessment in terms of PGA for uniformly infilled frames subjected to mainshock in LOR station, without considering any contribution of the RC frame before infills degradation	423
Figure 214: Damage assessment in terms of PGA for uniformly infilled frames subjected to mainshock in LOR station, for lower-bound [ex] (a) and upper-bound [ex+al+in] (b) infills ratios	424
Figure 215: Damage assessment in terms of PGA for uniformly infilled frames subjected to mainshock in LOR station, for lower-bound (a) and upper-bound (b) for IDR_{DSy}	424
Figure 216: Damage assessment in terms of PGA for uniformly infilled frames subjected to foreshock in LOR station	425
Figure 217: Approximate CC and IN2 curves for non-uniformly infilled frames subjected to mainshock in LOR station in FN and FP directions, assuming hypothesis [ex].....	427
Figure 218: Damage assessment in terms of PGA for non-uniformly infilled frames subjected to mainshock in LOR station, assuming hypothesis [ex]	427
Figure 219: Approximate CC and IN2 curves for non-uniformly infilled frames subjected to mainshock in LOR station in FN and FP directions, assuming hypothesis [ex+al].....	428
Figure 220: Damage assessment in terms of PGA for non-uniformly infilled frames subjected to mainshock in LOR station, assuming hypothesis [ex+al]	428
Figure 221: Approximate CC and IN2 curves for non-uniformly infilled frames subjected to mainshock in LOR station in FN and FP directions, assuming hypothesis [ex+al+in]	429
Figure 222: Damage assessment in terms of PGA for non-uniformly infilled frames subjected to mainshock in LOR station, assuming hypothesis [ex+al+in].....	429

Tables

Table 1: R_S for RC buildings suggested by different authors (from Aguiar Falconi, 2007)	40
Table 2: Dynamic parameters of three typical idealised deformed shapes: linear, sinusoidal and constant.....	48
Table 3: Relation between the choices of design and the overstrength factors and effective period of the resulting structures	56
Table 4: Proposed empirical-based formulations for the fundamental period of bare RC MRF in the form $T_{el}=\alpha H_T^\beta$; * adapted from the original formula $T=\gamma n$ assuming $h=3m$	58
Table 5: Proposed empirical-based formulations for the fundamental period of infilled RC MRF in the form $T_{el,inf}=\gamma n$	64
Table 6: Proposed numerical-based formulations for the fundamental period of infilled RC MRF in the form $T_{el,inf}=\gamma n$	64
Table 7: Relationship between T_{el} and T_{eff} for some case studies of uniformly infilled frames (a) (from Verderame et al., 2013) and pilotis frames (b) (from Ricci et al., 2013), being GD and SD gravitational and seismic design, respectively	66
Table 8: Progressive inclusion of prescriptions in the different seismic codes: included (pale grey), partially included (grey), not included (dark grey) and not susceptible to be regulated (white); in <i>italics</i> : not mandatory in Spain	97
Table 9: Relationship between different hazard scales for representative values used in Spanish codes, corresponding to normal-importance buildings	107
Table 10: Typical ranges of V_P and V_S for some soil types, and their corresponding ratios (from Bourbié et al., 1987)	107
Table 11: Proposed correlation between thresholds of velocity for the different soil types for old- and medium-generation codes	108
Table 12: Thresholds of V_S , homogenised values of S and reference soil for the different Spanish seismic codes	108
Table 13: Comparison of regulations of Spanish seismic codes (I) (<i>italics</i> : implicit)	111
Table 14: Comparison of regulations of Spanish seismic codes (II) (<i>italics</i> : implicit)	112
Table 15: Comparison of regulations of Spanish seismic codes (III) (<i>italics</i> : implicit)	113
Table 16: Comparison of regulations of Spanish seismic codes (IV) (<i>italics</i> : implicit)	114
Table 17: Comparison of regulations of Spanish seismic codes (V) (<i>italics</i> : implicit)	115
Table 18: Amplification of flexural capacity-design factor when expressed in the centre of the joint panel (I)	136

Table 19: Amplification of flexural capacity-design factor when expressed in the centre of the joint panel (II)	137
Table 20: Amplification of flexural capacity-design factor when expressed in the centre of the joint panel (III).....	138
Table 21: Amplification of flexural capacity-design factor when expressed in the centre of the joint panel (IV).....	139
Table 22: Interpretation of the different criteria for the election of the value of axial load in columns adopted for the calculation of bending moment of resistance for capacity-design purposes....	141
Table 23: Defficiencies (grey) detected in capacity-design provisions of NCSE-02	150
Table 24: Generic consequences of the lack of prescriptions in NCSE-02 on the characteristics of the average RC residential building stock.....	165
Table 25: NCSE-02 vs. EC8 regarding infills, and typical damages induced.....	166
Table 26: Chronological comparison of partial factors for actions and combination coefficients between the different seismic and RC Spanish codes (“-“: not proposed; “=”: similar to the corresponding contemporaneous code).....	171
Table 27: Values of c_L for each RC code.....	175
Table 28: Minimum beam effective depth aimed at avoiding any deflection calculation for each RC Spanish code, considering different assumptions.....	175
Table 29: Maximum deflection in beams for each RC Spanish code	175
Table 30: Prescriptions regarding flat-slab and wide-beam frames systems according to different codes.....	183
Table 31: Characteristics of the analysed set of beams.....	213
Table 32: Mean wide-to-deep ratios (W/D) corresponding to different variables.....	214
Table 33: Geometric design properties of each model (^(*) mean)	240
Table 34: Mechanic design properties of each model (^(*) mean)	241
Table 35: Dynamic properties for each model (bold: design to ULS; italics: design to ELS)	245
Table 36: Performance properties for each model	260
Table 37: Estimated and real ratios between capacities of WBF and DBF for EC8 frames belonging to the specific case study, considering similar H_{mec} for both typologies	267
Table 38: Results of design and assessment of the set of frames, considering $H_{mec,W/D}=f_{K,sec}=1.0$ (G: gravitational, S: seismic, D: deformability; I: $T_{el,W/D}\approx 1$, II: $T_{el,W/D}>1$; C: first θ_u attainment in column, B: first θ_u attainment in beam)	268
Table 39: Mean values of ratios of significant parameters between WBF and DBF extracted from Table 38	268
Table 40: Values of θ_{pl} in ASCE/SEI 41-06	274
Table 41: Foreshock and mainshock peak and integral strong motion parameters at Lorca station (LOR).	289

Tables

Table 42: Infills ratios for building I and II	298
Table 43: Normalised damages depending on soil type for different cases	299
Table 44: Input variables of FAST	317
Table 45: Proposal for correlation between <i>IDR</i> and DS of EMS-98	336
Table 46: Values for $\Gamma (C_0)$ suggested by ASCE-SEI 41-06 (ASCE, 2007).....	346
Table 47: Modal properties for some examples of 4- and 8-storey UIF and NIF	365
Table 48: IDR associated to the different DS in the EMS-98 scale, including those corresponding to RC columns	370
Table 49: Error committed when out-of-plane infill torsional contribution to the translational stiffness is neglected	391
Table 50: Suggested values for some input parameters of FAST regardless of the specific case study	408
Table 51: Variables required for code-based simulated design of the different classes of buildings of Lorca, considering soil type II	408
Table 52: Input parameters for the specific case study of Lorca.....	410
Table 53: Demand estimation for 3- and 5-storey bare RC frames for FN and FP mainshock signals in LOR station.....	411
Table 54: Simplified code-based capacity estimation for 3- and 5-storey bare RC frames	411

Symbols

Δd_i	Interstorey displacement
A_b	Area of building in plan
a_b	Reference PGA in hard soil in Spanish framework
a_g	Reference PGA in the corresponding soil
a_{gR}	Reference PGA in rock soil
A_s	Longitudinal reinforcement area in each side of columns
$A_{s,tot}$	Total longitudinal reinforcement area in columns
A_{trib}	Tributary area for columns
a_w	Hardening factor for infill panels with diagonal strut collapse mechanism
A_w	Area of infills in plan
b_b	Cross-sectional width of beam
b_c	Cross-sectional width of column
$b_{c,g1}$	Estimated b_c corresponding to the first gravitational scenario
$b_{c,g2}$	Estimated b_c corresponding to the second gravitational scenario
$b_{c,min}$	Estimated b_c corresponding to the minimum dimension scenario
$b_{c,s}$	Estimated b_c corresponding to the seismic scenario
b_{eff}	Beam effective width
b_{trib}	Tributary transverse distance for beams
b_w	Width of the web of a beam
$C_{P-\Delta}$	Correction factor for second order effects
c_s	Correction factor for switching from a_b to a_{gR} regarding S
C_s	Maximum spectral acceleration capacity
$C_{s,max}$	Maximum spectral acceleration capacity of the infilled frame
$C_{s,min}$	Minimum residual spectral acceleration capacity of the infilled frame
$C_{s,RC}$	Maximum spectral acceleration capacity of the bare RC frame
$C_{s,w}$	Maximum spectral acceleration capacity of the infills
c_{TR}	Correction factor for switching from a_b to a_{gR} regarding T_R
c_χ	Relative contribution of RC with respect to infills to the storey stiffness
d	Effective depth of section
d^*	Displacements of the SDOF
d'	Concrete covering measured from the centreline of the reinforcement bars
d_{bL}	Diameter of longitudinal reinforcement bar
d_n	Top displacement of frame
$d_{n DSj}$	Top displacement thresholds for each DS_j
D_u	Top displacement capacity of the building
$D_{u,pred}$	Predicted top displacement of buildings
e	Beam-column eccentricity

Symbols

e_i^*	Storey eccentricity
e_0	Minimum eccentricity of design in RC columns
E_c	Modulus of elasticity of concrete
e_i	Floor eccentricity
e_j	Eccentricity of each element to the centre of twist
E_w	Masonry elastic modulus
f_{cd}	Concrete design compressive strength
f_{ck}	Concrete characteristic compressive strength
f_{cm}	Concrete mean compressive strength
f_{conf}	Amplification of θ_u due to confinement
F_i	Storey lateral equivalent static force
$f_{K,sec}$	Ratio between secant-to-elastic ratios of WBF and DBF
f_{Lv}	Shear span factor between two members
f_y	Yield strength of steel
$f_{y,nom}$	Nominal yield strength of steel
f_{yd}	Design yield strength of steel
f_{yk}	Characteristic yield strength of steel
f_{ym}	Mean yield strength of steel
G	Permanent loads
G_w	Shear modulus of elasticity
H	Height
h_1	Ground floor interstorey height
h_b	Cross-sectional depth of beam
h_c	Cross-sectional depth of column
H_{cl}	Clear interstorey height
H_{DS1}	Height at which shear force attains the value corresponding to DS1
H_{eff}	Modal effective height
h_f	Thickness of upper slab tension flange
h_i	Interstorey height
H_{mec}	Height of the building involved in the mechanism of collapse
H_n	Total height of the frame
h_s	Upper floors interstorey height
H_T	Total height of the building
I	Cross section moment of inertia
I_A	Arias intensity
I_D	Cosenza and Manfredi index
IDR_{DSj}	Interstorey drift of infill panels causing DS _j
I_{MSK}	MSK intensity
K	Stiffness
K	Azores-Gibraltar fault correction factor to Spanish seismic hazard
K_1'	1 st storey translational stiffness of torsionable buildings
K_{dam}	Damaged stiffness
K_{eff}	Effective stiffness
K_{el}	Elastic stiffness

K_g	Global elastic stiffness of the frame
K_i	Storey stiffness
K_{RC}	Elastic stiffness of RC frame
$K_{RC,T}$	Torsional stiffness of the ensemble of columns
K_{sec}	Secant stiffness
$K_{sec,i}$	Storey secant shear stiffness
K_T	Global torsional stiffness
K_{tan}	Tangent stiffness
K_{VT}	Translational stiffness in torsional regime
K_w	Elastic stiffness of infills
$K_{wm,T}$	In-plane torsional stiffness corresponding to each infill panel
$K_{wp,T}$	Out-of-plane torsional stiffness corresponding to each infill panel
L	Member length
L_{cl}	Clear span
l_j	Length of each element in plan
L_V	Shear span length
M	Total mass in seismic situation
m^*	1 st mode participating mass of the SDOF
M_d	Design total mass in seismic situation
m_d	Superficial storey mass of design
$M_{d,s}$	Design moment in the case of high eccentricity
M_{db}	Design moment in beams
M_{dc}	Design moment in columns
M_{gb}	Moment caused by gravitational load in the seismic situation in beams
M_{gc}	Moment caused by gravitational load in the seismic situation in columns
M_{hb}	Moment caused by horizontal action in beams
M_{hc}	Moment caused by horizontal action in columns
m_i	Storey mass
m_r	Assumed real superficial storey mass
M_r	Assumed real total mass in the seismic situation
M_{Rb}	Moment resistance in beams
M_{Rc}	Moment resistance in columns
M_{Ti}	Storey torsional moment
M_W	Moment magnitude scale
M_y	Bending moment perpendicular to the local y-axis
M_z	Bending moment perpendicular to the local z-axis
n	Number of storeys
N	Axial load
n_c	Number of columns in a storey
$N_{d,g}$	Design axial load in the case of low eccentricity
n_s	Number of reinforcement bars in a side of a section
n_t	Total number of reinforcement bars in section
PGA_c	Capacity PGA
PGA_d	Demand PGA

Symbols

P_R	Reference probability of the reference seismic action
q	Behaviour factor, strength reduction factor
Q	Live loads
R_D	Strength reduction factor due to demand decrease
r_i	Director cosines of the acceleration in the direction of the degree of freedom
R_S	Strength reduction factor due to overstrength
r_u	Ratio between residual and maximum infill strength
R_a	Structural overstrength from first structural yielding until maximum base shear
R_μ	Strength reduction factor due to ductility
R_ω	Structural overstrength until first structural yielding
S	Soil amplification factor
S_a	Spectral acceleration
S_{ae}	Elastic spectral acceleration
$S_{ae}(T)$	Equivalent spectral acceleration of design
$S_{ae,d}$	Elastic spectral acceleration demand
S_D	Earthquake significant duration
$S_{d DSj}$	Spectral displacement thresholds for each DS_j
S_{d1}	Spectral displacement of the infilled frame corresponding to the end of the equivalent elastic branch of the simplified CC
S_{d2}	Spectral displacement of the infilled frame corresponding to the drop of the simplified CC
S_{dc}	Spectral displacement capacity
S_{dd}	Spectral displacement demand
S_{de}	Elastic spectral displacement
S_{du}	Maximum spectral displacement capacity
S_{dy}	Yielding spectral displacement capacity
S_v	Spectral velocity
T	Period of vibration
T_0	Characteristic period of R - μ - T relations
T_1	Assumed real fundamental period of design
$T_{100\%EI}$	Design elastic period considering gross uncracked sections
$T_{50\%EI}$	Design elastic period considering member stiffness reduced in a 50% from gross uncracked sections
T_C	Corner period at the upper limit of the constant acceleration region of the elastic spectrum
T_{code}	Simplified fundamental period suggested by codes
T_D	Corner period at the beginning of the constant displacement region of the elastic spectrum
T_{dam}	Damaged period
T_{eff}	Effective period
$T_{eff,inf}$	Effective period of the infilled frame
T_{el}	Elastic period
$T_{el,inf}$	Elastic period of infilled frame
T_i	Floor torque

T_L	Reference life span of the building
T_R	Reference return period of the seismic action
T_{sec}	Secant period
t_w	Thickness of infill panel
V_1	Base shear corresponding to the attainment of the first structural yielding
V_d	Design base shear
V_{db}	Design shear in beams
V_{dc}	Design shear in columns
V_E	Equivalent velocity
V_{el}	Equivalent elastic base shear
V_i	Storey shear
V_{max}	Maximum base shear of the infilled frame
V_{min}	Minimum residual base shear of the infilled frame
V_P	Velocity of the seismic compression waves through the soil
V_{pc}	Shear force compatible with opposite moments of resistance at column ends
V_{Rb}	Shear resistance in beams
V_{Rc}	Shear resistance in columns
V_S	Velocity of the seismic shear waves through the soil
$V_{w,max}$	Maximum lateral strength of infills at 1 st storey
V_y	Supplied base shear
W	Wind loads
w	Outer cantilevered beam width respect to narrower column core
y	Concrete stress block depth
z	Distance between opposite reinforcement centerlines
α	Confinement effectiveness factor
α	Relative RC contribution to the maximum strength of the infilled frame
$\alpha(T)$	Spectral shape function
α_b	Global moment overstrength in beams
α_c	Global moment overstrength in columns
α_{max}	Maximum spectral amplification
β	Relative infills contribution to the residual strength of the infilled frame
γ	Partial factor for actions
γ	Stiffness degradation contribution factor
γ_d	Design seismic combination factor
γ_I	Importance factor
γ_R	Uncertainty value on resistances for capacity design
δ	Translation of storey due to torsion
ΔK	Relative interstorey difference of stiffness
Δm	Relative interstorey difference of mass
Δ_{max}	Maximum global displacement capacity
Δ_y	Yielding global displacement capacity
ε_y	Yield strain of steel
ζ	Shear contribution factor
η	Damping correction factor

Symbols

θ	Rotation of storey due to torsion
θ_{pl}	Plastic part of ultimate chord rotation
θ_u	Ultimate chord rotation
$\theta_{u,min}$	Minimum ultimate chord rotation within member ends involved in the collapse mechanism
θ_{ub}	Ultimate chord rotation in beams
θ_{uc}	Ultimate chord rotation in columns
θ_{ULS}	Chord rotation at ULS
θ_y	Yielding chord rotation
κ	Factor switching from elastic to effective period
λ	Normalised first mode participating mass of the MDOF
λ_d	Relative MDOF 1 st mode participating mass of design
λ_g	Average geometric slenderness of buildings
λ_r	Assumed real relative MDOF 1 st mode participating mass
μ	Ductility
μ_s	Ductility of infilled frame up to the beginning of strength degradation
μ_θ	Ductility of chord rotation
μ_ϕ	Ductility of curvature
ν	Damping expressed as fraction of the critical one
ν	Normalised axial load in a section
ξ	Viscous damping ratio
ξ_{seq}	Nonlinear equivalent viscous damping
ρ	Tension longitudinal reinforcement ratio
ρ'	Compression longitudinal reinforcement ratio
ρ_d	Diagonal reinforcement ratio
ρ_{max}/ρ_{min}	Relation between longitudinal reinforcement ratios belonging to opposite faces within a section
ρ_{RC}	Equivalent RC area ratio
ρ_s	Average reinforcement ratio of 1 st storey RC columns
ρ_{tot}	Total longitudinal reinforcement ratio
ρ_w	Area of infill panels in plan, normalised to the total area of the building
ρ_w	Transverse reinforcement ratio
$\rho_{w,1}$	Ground floor infills ratio in plan
$\rho_{w,s}$	Upper floors infills ratio in plan
τ_{cr}	Cracking resistance of infills
τ_{max}	Maximum resistance of infills
φ_i	Modal amplitudes normalised to the bigger one
ϕ_i	Modal amplitudes
ϕ_u	Ultimate curvature
ϕ_y	Yielding curvature
χ	Elastic stiffness contribution factor
χ_c	Equivalent RC contribution factor to χ
χ_h	Interstorey height contribution factor to χ
χ_T	Torsional contribution to χ

FAST simplified vulnerability approach for seismic assessment of infilled RC MRF buildings
and its application to the 2011 Lorca (Spain) earthquake

χ_ρ	Infills ratios contribution factor to χ
ψ	Combination coefficient for actions
ω	Angular velocity
ω	Longitudinal tensioned mechanical reinforcement ratio
ω'	Longitudinal compressed mechanical reinforcement ratio
Ω_i	Storey stiffness degradation factor
Ω_{sec}	Relative infills secant stiffness degradation at the attainment of DS2
ω_{tot}	Total longitudinal mechanical reinforcement ratio
ω_w	Transverse mechanical reinforcement ratio
Γ	1 st mode participation factor

Acronims

ADRS	Acceleration-Displacement Response Spectrum
CC	Capacity Curve
CQC	Complete Quadratic Combination
DBELA	Displacement-Based Earthquake Loss Assessment
DPM	Damage Probability Matrix
DS	Damage State
EC8	Eurocode 8
FE	Finite Element
HAZUS	HAZard in United States
IDA	Incremental Dynamic Analysis
IDR	Interstorey Drift
JPDF	Joint Probability Density Function
MCSE	Mercalli-Cancani-Sieberg intensity
MDOF	Multiple Degrees Of Freedom
MMI	Modified Mercalli Intensity
MRF	Moment Resisting Frames
MSK	Medvedev-Sponheuer-Karnik intensity
PBEE	Performance-Based Earthquake Engineering
PDF	Probability Density Functions
PGA	Peak Ground Acceleration
PGD	Peak Ground Displacement
PGV	Peak Ground Velocity
POST	PushOver on Shear Type models
PSHA	Probabilistic Seismic Hazard Analysis
PSI	Parameterless Scale of Intensity
RC	Reinforced Concrete
SDOF	Single Degree Of Freedom
SP-BELA	Simplified Pushover-Based Earthquake Loss Assessment
SPO	Static PushOver
SRSS	Square Root of the Sum of Squares
VC	Reinforced Concrete Vulnerability
DCH	High Ductility Class
DCM	Medium Ductility Class
DCL	Low Ductility Class
ULS	Ultimate Limit State
SLS	Serviceability Limit State
DLS	Damage Limitation Limit State
WB	Wide beams
DB	Deep beams
WBF	Wide-beam frames

FAST simplified vulnerability approach for seismic assessment of infilled RC MRF buildings
and its application to the 2011 Lorca (Spain) earthquake

DBF	Deep-beam frames
WB-C	Wide beam-column
DB-C	Deep beam-column
SF	Safety Factor
LOR	Seismic station of Lorca
ZAR	Seismic station of Zarcilla de Ramos
AM2	Seismic station of Alhama de Murcia
NS	North-South direction
EW	East-West direction
FN	Fault-Normal direction
FP	Fault-Parallel direction

Introduction

A simplified analytical method (“FAST”) for the estimation of large-scale vulnerability of Reinforced Concrete (RC) Moment Resisting Frames with masonry infills is proposed and subsequently tested by using real damage scenario caused by the 2011 Lorca earthquake as a benchmark.

Most of the experience regarding the early earthquake engineering was collected after disastrous earthquakes in seismically prone areas in the world, such as Japan (Edo, 1885), California (San Francisco, 1906) and Italy (Messina, 1908). In the last decades, earthquake engineering, aimed at providing higher control of seismic risk and, more in general, towards the reduction of losses induced by earthquakes (i.e. Cornell and Krawinkler, 2000), has progressed towards "Performance-Based Earthquake Engineering". It is based on the evaluation of the capacity of the buildings together with the demand of the seismic event by using a quantitative and probabilistic framework, in order to predict the vulnerability or provide target performances. The assessment of seismic vulnerability of the existing RC building stock is fundamental for the evaluation and mitigation of seismic risk, since this typology represents a large fraction of the existing stock. In such framework, the family of "spectral-based methodologies" earned interest for large-scale purposes, consisting in the spectral superposition of a capacity curve and a demand spectrum, elastic or inelastic.

This strategy has been widely applied to the assessment of RC buildings. However, in damage surveys of the Mediterranean area (Rossetto and Peiris, 2009; Ricci et al., 2011a) it has been observed that masonry infills, which are "non-structural" elements with no proper design, can substantially increase or conversely decrease the capacity of RC bare frames. Masonry infills are able to provide, on one hand, an increase of the initial stiffness and strength; and on the other hand, they increase the spectral demand, lead to a drop of resistance because of their brittle failure and reduce available displacement capacity.

Besides, different classifications of the level of damage attained by infilled RC buildings are available. One of them is the European Macroseismic Scale (EMS-98, Grünthal, 1998), that distributes damage in 5 Damage States (DS) depending on the condition of both structural and non-structural elements, from DS1 (slight non-structural damage) to DS5 (collapse).

This Thesis proposes a simplified large-scale spectral-based vulnerability approach for the assessment of RC frames with masonry infills: "FAST". It is a spectral-based approach that allows predicting the average non-structural Damage State expected for each class of building (defined by number of storeys, age of construction, infills ratio in plan and location) for a given demand level. It accounts for non-uniformity of infills in elevation, i.e. a reduction of infills ratio at ground floor.

FAST is based on: (i) the definition of approximate capacity curves of the infilled building, assuming that the RC frame has been designed according to the corresponding seismic code; and on (ii) the assumption of "a priori" deformed shapes in accordance with the attainment of each non-structural damage state at 1st storey, according to experimental and numerical correlations.

In Figure 1, a flowchart of FAST basic steps is shown, consisting in two procedures running in parallel. On one hand, capacity curves and IN2 curves in terms of Peak Ground Acceleration (PGA) for the equivalent Single Degree of Freedom (SDOF) of the building are defined. On the other hand, thanks to a mechanical interpretation of non-structural DS (DS 1, 2 and 3) in terms of interstorey drift of the infills, the thresholds of the attainment of such DS in terms of top displacement of the SDOF are carried out. Then, through IN2 curve,

capacity thresholds can be translated from displacement to PGA for each DS. Thus, the approach allows determining the PGA thresholds of the exceedance of each DS.

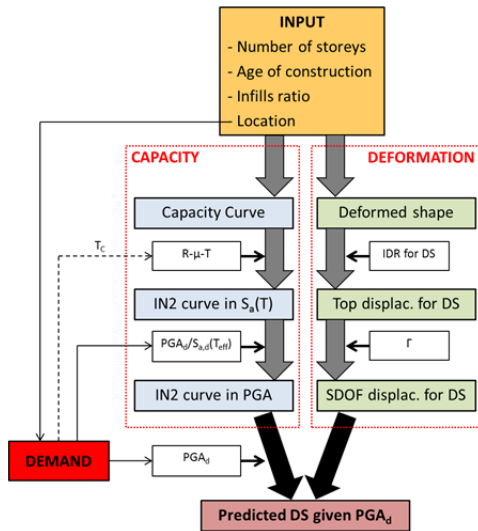


Figure 1: Flowchart of FAST procedure

Two versions of FAST are proposed: a “simplified” approach aimed at the evaluation of uniformly infilled frames; and a “generalised” version which can account for any intermediate situation between uniformly infilled frames and pilotis frames (i.e. without infills at 1st storey). Also, some extensions of the method are highlighted.

Aimed at testing FAST, the real damage scenario after the earthquake of Lorca (Spain, 2011) is used as a benchmark, despite its impulsivity and directivity. In order to define the specific input parameters for the case study, information regarding ground motion, post-earthquake damage scenario and also building design practice must be collected.

Hence, a detailed review of historical Spanish seismic codes and a critical analysis of current Spanish seismic code NCSE-02 in comparison with current

reference performance-based codes as Eurocode 8 are carried out. Special emphasis is placed to provisions which can prevent from capacity design, can cause brittle failures or promote the interaction with infills. Also, the prescription of lower behaviour factor for wide-beam frames with respect to deep-beam frames –which is not present in most codes— is discussed; outcomes of several case studies suggest that such prescription is obsolete.

Finally, FAST is applied to Lorca earthquake and predicted damage scenarios are obtained, considering different assumptions for input values. Results show proper agreement between predicted and real damages. Actually, almost no structural collapse took place although the PGA was three times higher than the typical acceleration of design, so FAST proves that masonry infills provided additional strength.

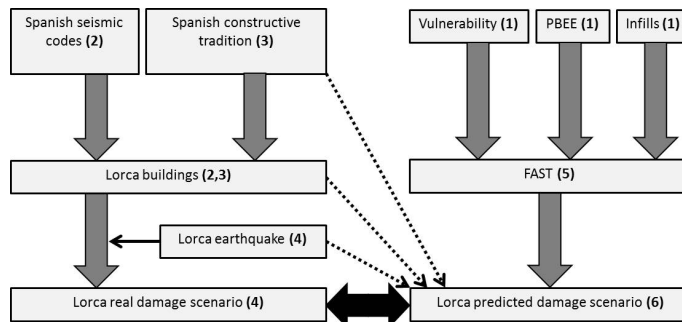


Figure 2: Organisation of contents within the different chapters

ORGANISATION AND OUTLINE

As shown in Figure 2, the organisation of contents within this work reflects the order in which the different information should be collected aimed to the application of FAST approach to any specific case, regardless of the state of the art, which is necessary to define the basis of FAST.

In **Chapter 1**, an overview of the existing vulnerability assessment methods for RC MRF buildings is presented, and some issues concerning the spectral-based

procedures are revisited, focusing in the aspects that are relevant in order to develop FAST vulnerability approach later on. Also, the influence of masonry infills on the performance of Reinforced Concrete (RC) Moment Resisting Frames (MRF) buildings is analysed.

In **Chapter 2**, Spanish seismic codes and typical characteristics of the RC residential building stock in Lorca are studied. Firstly, a compared review of the past and present Spanish seismic codes is presented, in order to establish the demands requested to buildings corresponding to each period, and, afterwards, main drawbacks of NCSE-02 in comparison with the common framework of modern seismic international codes are analysed in detail.

In **Chapter 3**, the prescription of lower behaviour factors for wide-beam frames with respect to deep-beam frames proposed only by Spanish and Italian seismic codes is discussed, and relative performances between wide- and deep-beam frames designed to high ductility are assessed through different approaches.

Chapter 4 is dedicated to the 2011 Lorca earthquake. The special characteristics of the seismic event are analysed, particularities of the RC building stock are studied and the damage scenario is interpreted in the light of the deficiencies of Spanish code provisions.

In **Chapter 5**, FAST method is presented, its theoretical framework is developed and its assumptions –based in literature or experimental works— are detailed. A preliminary approach for code-based assessment of bare frames is followed by two different versions of FAST. The first one, “simplified FAST”, only considers uniformly infilled frames, while the second version, “generalised FAST”, allows accounting for any reduction of infills ratio at 1st storey, i.e. all the intermediate states between the uniformly infilled and the “pilotis” frame. Also, some suitable complementary tools conforming “extended FAST” are highlighted.

Finally, in **Chapter 6** FAST is applied to the case study of Lorca earthquake: firstly to the bare frames, later to the uniformly infilled buildings and finally to the non-uniformly infilled frames. The input variables respond to the local characteristics analysed in the previous chapters. Hence, simulated damage scenarios are obtained and subsequently compared with the real observed damage statistics presented in Chapter 2.

PUBLICATIONS

This Thesis is the result of the research done in the Polytechnic University of Valencia (project BFPI/2009/133, 2009-2011) and the University of Naples Federico II (foreign stage within the same project BFPI/2009/133, 2012; project PROVACI-FORMAZIONE, 2012-2013; and project PON 01_2366/1 STRIT, 2014-2015). The contents of the Thesis consist in a reorganization, improvement and enlargement of the material included in four papers and three contributions to conferences. They are presented and described herein, cronologically:

Gómez-Martínez, F., Pérez-García, A., De Luca, F., Verderame, G.M., Manfredi, G. (2012). Preliminary study of the structural role played by masonry infills on RC buildings performances after the 2011 Lorca, Spain, earthquake. Proceedings of the 15th WCEE – 15 World Conference on Earthquake Engineering, 24-28 September, Lisbon (Portugal).

In this contribution, some characteristics of the Lorca earthquake are briefly described: ground motion and damages; and a first estimation of the capacity of bare frames and infilled frames, still without referencing to the EMS-98 scale, is proposed and applied to the earthquake.

De Luca, F., Verderame, G.M., Gómez-Martínez, F. (2013). FAST vulnerability approach: a simple solution for seismic reliability or RC infilled buildings. Proceedings of ANIDIS 2013 – XV Convegno. Padova (Italy), June 30 – July 04, paper B7.

This work includes the consideration of global variability by furnishing preliminary fragility curves based on lognormal distribution.

Gómez Martínez, F., Pérez García, A., De Luca, F., Verderame, G.M. (2013). Generalized FAST approach for seismic assessment of infilled RC MRF buildings: application to the 2011 Lorca earthquake. 9th World Conference on Earthquake Resistant Engineering Structures, ERES 2013, July 8-10, La Coruña, Spain. In: Proceedings of 13th International Conference on Structures Under Shock and Impact, SUSI 2014.

This contribution is focused in the development of a generalization of FAST for being able to consider a reduction of the infills ratio in the ground floor

(non-uniformly infilled frames). It includes all the theoretical body about the generalized method and a reformulation of the original FAST for uniformly infilled frames. The generalized method is applied again to the Lorca earthquake, using infills ratios from an in-field database.

De Luca, F., Verderame, G.M., Gómez-Martínez, F., Pérez-García, A. (2014). The structural role played by masonry infills on RC building performances after the 2011 Lorca, Spain, earthquake. Bulletin of Earthquake Engineering 12(5):1999-2026.

In this paper, the Lorca earthquake is deeply examined regarding its ground motion, directivity, statistics of building stock, damage scenario and characteristics of the failures. The theoretical construction of FAST for bare and uniformly infilled frames is presented, with a complete justification of the origin of the assumed values for parameters. Finally, the method is applied to the earthquake and results are compared with the real damage scenario.

Gómez Martínez, F., Pérez García, A., De Luca, F., Verderame, G.M. (2015). Comportamiento de los edificios de HA con tabiquería durante el sismo de Lorca de 2011: aplicación del método FAST. Informes de la Construcción 67(537):e065 (in Spanish).

This work adds to the previous one: evaluation of the Spanish codes in relation with the type of damages observed; particularization of the values for the Spanish case; application of FAST considering a reduction of the infills ratio in the ground floor; estimation of the performance for buildings with no seismic design; and application of FAST for the foreshock; and consideration of variability in the input parameters.

Gómez-Martínez, F., Alonso Durá, A., De Luca, F., Verderame, G.M. (2015). Ductility of wide-beam RC frames as lateral resisting system. Bulletin of Earthquake Engineering (under revision).

This work discusses the appropriateness of the prescription of lower behaviour factor for wide-beam frames with respect to deep-beam frames present in Spanish and Italian seismic codes, conversely to Eurocode 8, through: a deep

revision of codes and experimental background, a parametric analysis on local ductility of beams and spectral considerations about performances.

Gómez-Martínez, F., Alonso Durá, A., De Luca, F., Verderame, G.M. (2015). Seismic performance and behaviour factor of wide-beam and deep-beam RC frames. Engineering structures (under revision).

This paper analyses the relative performances of wide- vs. deep-beam frames by means of several case studies, considering different codes of design and diverse modelling strategies

Gómez-Martínez, F., Pérez García, A., Alonso Durá, A., Martínez Boquera, A., Verderame, G.M. (2015). Eficacia de la norma NCSE-02 a la luz de los daños e intervenciones tras el sismo de Lorca de 2011. Proceedings of Congreso Internacional sobre Intervención en Obras Arquitectónicas tras Sismo: L'Aquila (2009), Lorca (2011) y Emilia romagna (2012). 13-14 May, Murcia, Spain (in Spanish).

This contribution summarises the whole work on this Thesis, focusing in the possible cause-effect relationships between the prescriptions of NCSE-02 which are different from Eurocode 8 and the damage scenario after the Lorca earthquake, characterised by high relative contribution of infills, mechanisms of low ductility and brittle failures.

Chapter 1

State of the art

In this chapter, an overview of the existing vulnerability assessment methods for RC MRF buildings is presented, and some issues concerning the spectral-based procedures are revisited, focusing in the aspects that are relevant in order to develop FAST vulnerability approach later on. Finally, the influence of masonry infills on the performance of Reinforced Concrete (RC) Moment Resisting Frames (MRF) buildings is analysed.

1.1 OVERVIEW OF VULNERABILITY ASSESSMENT METHODS FOR RC-MRF BUILDINGS

Vulnerability is one of the three variables that define seismic risk. It is obtained as a symbolical product of three variables:

- Hazard: Probability of suffering in a site an earthquake of a given intensity in a certain exposure time.
- Vulnerability: Probability of a given level of damage to a given building type due to a scenario earthquake.
- Exposition: Territorial factor accounting for the influence of the population density, presence of infrastructures or building uses.

The assessment of seismic risk is necessary for mitigating human and economic losses due to the earthquakes, whose impact can be heavy if it is considered that only a reduced amount of the total building stock of cities placed in areas of high seismic hazard is designed following modern prescriptions.

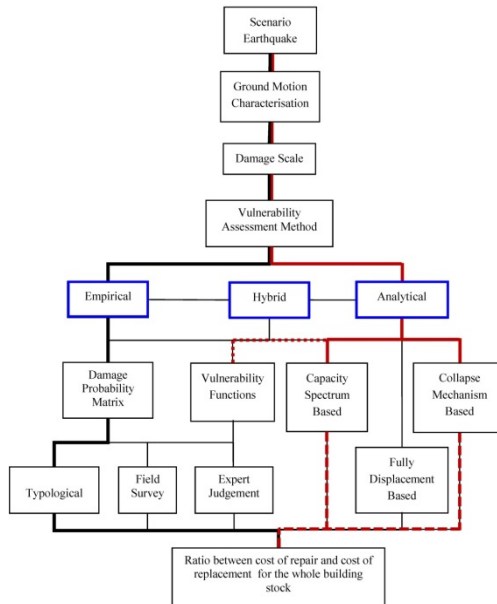


Figure 3: Diagram of the component of the seismic risk assessment and the different vulnerability assessment methodologies (blue rectangles), from (Calvi et al., 2006); the bold path shows a traditional procedure, while red path corresponds to FAST approach

Within this framework, vulnerability assessment approaches are fundamental for the definition of loss models. In the following, main vulnerability assessment procedures are illustrated, referring to RC buildings; it is based in a detailed review available in Calvi et al., (2006). Such methodologies can be classified in: empirical, analytical and hybrid methods, as summarize in Figure 3. The first ones are based on the observation of damaged suffered during past seismic events, while in the second ones a physical model is used for assessing the expected damages. Moreover, other methods are directly based on expert judgement, being each

estimation weighted according to the experience and confidence level of the experts for the considered building class; these ones are not described in this section.

DI _{HRC}	HRC	HAZUS 1999 [17]	VISION 2000 [18]	FEMA 273 [19]	EMS98 [20]	MSK [2]	AIJ [5]	ATC-13 [7]	ATC-21 [21]	EPP0 [22]						
0	None	No damage limit state														
10	Slight	Slight damage	Fully operational	Immediate occupancy	Grade 1	D1	Light	Slight	Green Tag	Green Tag						
20	Light		Operational					Damage control			Grade 2	D2	Light			
30				Moderate												
40	Moderate	Moderate damage	Life safe	Life safe	Grade 3	D3	Moderate	Moderate	Yellow Tag	Yellow Tag						
50								Extensive			Extensive damage	Near collapse	Limited safety	Grade 4	D4	Major
60																
70	Extensive	Extensive damage	Near collapse	Limited safety	Grade 4	D4	Major	Heavy	Yellow Tag	Yellow Tag						
80								Partial collapse			Collapse	Collapse prevention	Collapse prevention	Major	Major	Major
90	Collapse	Collapse	Collapse prevention	Collapse prevention	Major	Major	Partial collapse		Red Tag	Red Tag						
100							Collapse limit state									

Figure 4: DS correlation for generic RC frames (from Rossetto and Elnashai, 2003)

DI _{HRC}	HRC	HAZUS 1999 [17]	VISION 2000 [18]	FEMA 273 [19]	EMS98 [20]	MSK [2]	AIJ [5]	ATC-13 [7]						
0	None	No Damage												
10	Slight	Slight damage	Fully operational	Immediate occupancy	Grade 1	D1	Light	Slight						
20	Light		Operational					Damage control	Grade 2	D2	Minor			
30				Moderate										
40	Moderate	Moderate damage	Life Safe	Life safe	Grade 3	D3	Moderate	Moderate						
50								Extensive	Extensive damage	Near collapse	Limited safety	Grade 4	D4	Major
60														
70	Extensive	Extensive damage	Near collapse	Limited safety	Grade 4	D4	Major	Heavy						
80								Partial collapse	Collapse	Collapse prevention	Collapse prevention	Major	Major	Major
90	Collapse	Collapse	Collapse prevention	Collapse prevention	Major	Major	Major							
100								Collapse						

Figure 5: DS correlation for infilled RC frames (from Rossetto and Elnashai, 2003)

Empirical methods could be quite realistic as they use databases of buildings with similar characteristics to the building stock assessed. However, they present some disadvantages: they do not account for the vibration characteristics of the building and the sources of uncertainty are impossible to be considered. What is more, macroseismic measure is used to define the intensity; considering that it is defined also from the observed damages, it results in a relation of dependence between the prediction (damages) and the input (intensity). Also, the variability in the classifications of damages within different events can be high.

On the other hand, the use of an algorithm allows to take into account the different characteristics of the buildings, even considering new construction or retrofitting practices, and also to account for the different sources of uncertainty. However, they usually need a larger amount of detailed data and a higher computational effort. The critical issue in analytical methods is the confidence in the correlation between the assumed analytical damage index (such as the interstorey drift) and the actual structural damage. Other inconvenient is that it is impossible to consider constructive errors, which are often the main cause of the damages (Verderame et al., 2010a). Anyway, comparison with observed damage data is always required.

Before starting the review of vulnerability methods, it is necessary to present the different classifications of damages existing in literature. Vulnerability methods associate hazard levels to levels of damage in buildings. Those levels are defined generally by the severity of the damages observed in the structure or in non-structural elements, and they are generally characterised by their appearance, as they are meant to be assessed in post-earthquake inspections. There have been proposed several scales. A likely suitable correlation of damage scales have been proposed in Rossetto and Elnashai (2003), which is shown in Figure 4 and Figure 5 for diverse RC structural types.

In this Thesis, European Macroseismic Scale, EMS-98 (Grünthal, 1998) is used. It defines six vulnerability building classes (from A to F, see Figure 6a), based on qualitative characteristics (mainly the material of construction). Then, it define the seismic intensity level, ranging from V to XII, as a function of the proportion of each class of building suffering a given level of damage (from 1 to

6); see Figure 6b for the definition of the corresponding Damage States (DS). These proportions are based on a vague qualitative description of quantities (“few”, “many” and “most”). Thus, Damage Probability Matrices (DPMs) are implicitly defined. However, they are incomplete: some cells are empty, as not all the combinations of damage levels and seismic intensities are provided. Some works (Giovinazzi and Lagomarsino, 2004; and Lagomarsino and Giovinazzi, 2006) have tried to overcome the limits of incompleteness and vagueness of the EMS-98, translating the original DPMs into numerical and complete ones by means of fuzzy set theory, thus permitting to evaluate the expected (mean) damage grade for each building class under growing values of macroseismic intensity.

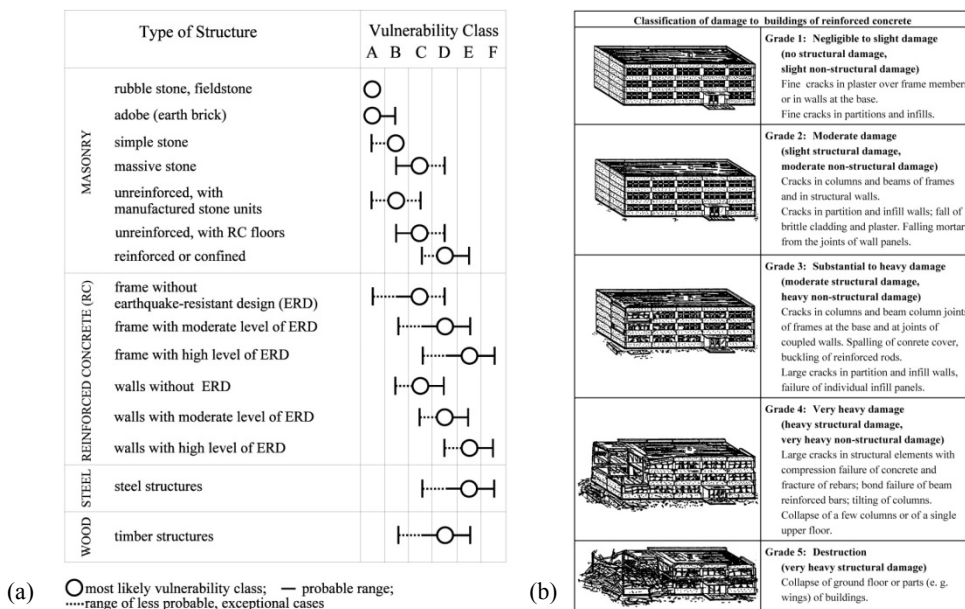


Figure 6: Characterisation of vulnerability building classes (a) and Damage States (DS) (b) according to the EMS-98 scale (Grünthal, 1998)

1.1.1 Empirical methods

Empirical methods can be divided in four types:

- methods furnishing DPM, which express in a discrete form the probability, for each typology of building, of the attainment of a certain damage level when submitted to a ground motion of a certain intensity;
- methods furnishing fragility continuous functions, that are curves that express the probability of equal or exceed such damage level;
- methods based on a so-called “Vulnerability Index”, consisting on the obtaining for each building the vulnerability as a weighted sum of parameters affected by their corresponding indexes;
- screening methods, aimed at prioritising the intervention based on the typologies and observed damages.

1.1.1.1 Damage Probability Matrices

First DPMs were developed thanks to observed damage scenarios of different earthquakes (Figure 7). The probability of being in a given structural and non-structural damage, and the damage ratio –ratio between the cost of repair and the cost of replacement— are provided.

Damage State	Structural Damage	Non-structural Damage	Damage Ratio (%)	Intensity of Earthquake				
				V	VI	VII	VIII	IX
0	None	None	0-0.05	10.4	-	-	-	-
1	None	Minor	0.05-0.3	16.4	0.5	-	-	-
2	None	Localised	0.3-1.25	40.0	22.5	-	-	-
3	Not noticeable	Widespread	1.25-3.5	20.0	30.0	2.7	-	-
4	Minor	Substantial	3.5-4.5	13.2	47.1	92.3	58.8	14.7
5	Substantial	Extensive	7.5-20	-	0.2	5.0	41.2	83.0
6	Major	Nearly total	20-65	-	-	-	-	2.3
7	Building condemned		100	-	-	-	-	-
8	Collapse		100	-	-	-	-	-

Figure 7: Damage Probability Matrix for a structural typology (Whitman et al., 1973) (from Calvi et al., 2006)

The first European version of DPMs is proposed in Braga et al. (1982), based on the damage observed after the 1980 Irpinia (Italy) earthquake. These DPMs are later on improved in Di Pasquale et al. (2005), changing the seismic intensity measure from the MSK to the Mercalli-Cancani-Sieberg (MCS). Also, number of buildings is replaced by the number of dwellings.

In Dolce et al. (2003), the DPMs from Braga et al. (1982) are adapted for the town of Potenza, adding the vulnerability class D for the modern buildings, constructed since 1980. Furthermore, seismic intensity is expressed according to the EMS-98 (Grünthal, 1998).

1.1.1.2 Fragility curves

Fragility curves can be briefly defined as the expression of DPMs in continuous form. They provide the probability of reaching or exceed each discrete damage grade under growing values of macroseismic intensity for a given structural typology. In the literature, often they are also called “vulnerability curves”, which at the same time is used for another kind of function. In this work, the criterion used in Lagomarsino and Giovinazzi (2006) is followed (Figure 8):

- “Vulnerability” functions relate damage level (observed or expected) with macroseismic intensity, for different case-studies of a given typology or for different typologies belonging to a general one;
- “Fragility” functions relate the probability of equal or exceed each discrete damage grade depending on the macroseismic intensity for each typology. They can be understood as cumulative distribution function obtained from the vulnerability curves by assuming probability density functions for the damage grade at each level of intensity for the case studies.

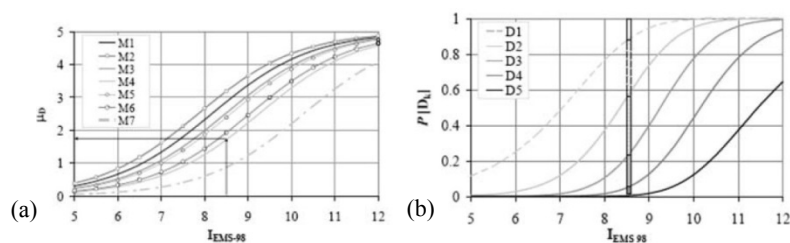


Figure 8: Example of vulnerability (a) and fragility (b) curves according to Lagomarsino and Giovinazzi (2006)

Only methods furnishing fragility curves derived from empirical data are presented in this section. Data of the damage survey carried out after the 1980

Irpinia earthquake are elaborated in Orsini (1999) in order to evaluate, for each municipality, a value of seismic intensity according to the Parameterless Scale of Intensity (PSI) proposed by Spence et al. (1991).

In Sabetta et al. (1998), fragility curves depending on PGA, Arias Intensity and effective peak acceleration based on the elaboration of about 50000 building damage surveys from past Italian earthquakes are derived.

In Rota et al. (2008), more than 91000 damage survey forms from past Italian earthquakes are selected. Both PGA and Housner intensity are considered as ground motion parameters; their values are estimated for each municipality using the attenuation law of Sabetta and Pugliese (1987 and 1996). A similar damage scale to the EMS-98 is used, divided in five levels plus the case of no damage. DPMs are extracted from the data for all of the 23 considered vulnerability classes, according to the defined damage and seismic intensity scales. Thus, continuous fragility curves are obtained by fitting the data from the DPMs.

In Rossetto and Elnashai (2003), parameters related to the spectral acceleration or displacement corresponding to the fundamental period are used instead of macroseismic intensity or PGA. Fragility curves show a better prediction capacity as they take into account the dynamic characteristics of the building stock.

In Lagomarsino and Giovinazzi (2006) two approaches are proposed, a “macroseismic” and a “mechanical” method (for the second one, see section 1.1.2). In both cases, the adopted building typological classification essentially corresponds to the EMS-98 proposal. Vulnerability and fragility curves are derived from EMS-98 macroseismic scale. To this end, the qualitative and incomplete Damage Probability Matrices (DPMs) implicitly defined by EMS-98 are translated into numerical and complete DPMs by means of fuzzy set theory (see Figure 9), thus allowing to evaluate the expected (mean) damage grade for each building class under growing values of macroseismic intensity. Hence, continuous vulnerability curves are obtained (see Figure 10) as interpolating curves, expressed as a function of macroseismic intensity and depending on a “vulnerability index” (see section 1.1.1.3). Then, fragility curves are evaluated starting from the mean damage grade provided by vulnerability curves and assuming a binomial distribution for this probability.

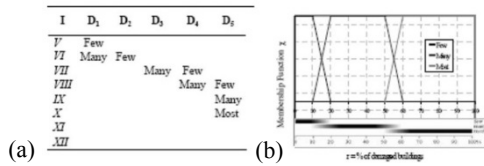


Figure 9: Implicit DPM for vulnerability class A of the EMS-98 scale (a), and interpretations of qualitative quantities as overlapping frequency intervals (b) (from Lagomarsino and Giovinazzi, 2006)

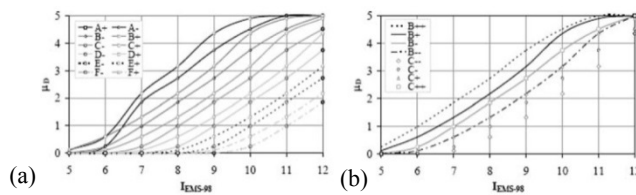


Figure 10: Derived vulnerability curves from EMS-98 implicit DPM: for all the classes (a) and for classes B and C (b) (from Lagomarsino and Giovinazzi, 2006)

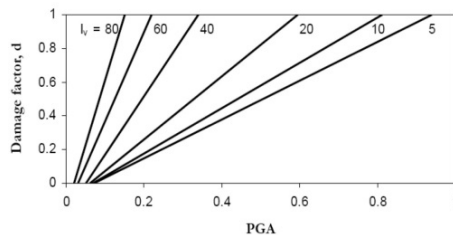


Figure 11: Vulnerability functions for different values of vulnerability index (adapted from Guagenti and Petrini (1989); image from Calvi et al. (2006))

1.1.1.3 Vulnerability index

This index defines the vulnerability of each building as a weighted sum of variables, represented by their corresponding indexes, accounting for all the possible sources of influence. It is first proposed in Benedetti and Petrini (1984) and GNDT (1993). It is evaluated by means of a field survey, considering 11 parameters to be weighted as: plan and elevation configuration, type of foundation, structural and non-structural elements, etc.). Different weight is given to each

variable according to the importance assigned to each one. Then, based on observed damage data from past earthquakes, a relationship is calibrated between seismic intensity and damage ratio for different values of the vulnerability index (see Figure 11). Other works using Vulnerability Index Method are Mouroux and Le Brun (2006), Faccioli et al. (1999) and Faccioli and Pessina (2000).

1.1.1.4 Screening methods

Sometimes the vulnerability of a building is not evaluated taking it as a whole but through an assessment of the different parts. The Japanese Seismic Index Method (JBDPA, 1990) makes a comparison, at each storey, of two different indexes that represent the seismic capacity and demand, being the first one calculated with a screening procedure. The capacity is obtained as the product of three factors:

- one representing the structural performance, calculated as a product of a factor of strength and another one of ductility, depending on the failure mode, the number of storeys and the position of the current storey;
- another one that have into account some design properties as the irregularity of stiffness and/or masses;
- the third one corresponding to the time-dependent deterioration of the building.

Then, the capacity factor is compared with the seismic judgement index, which represents a storey shear force given by the product of four factors:

- a factor that considers the accurateness of the screening procedure;
- a zone index modifying the ground motion intensity;
- a factor accounting for local effects such as ground-building interaction or stratigraphic and topographic amplification;
- an importance factor depending on the function of the building.

Some screening methods based in that of Japan have been proposed also in Turkey, as the “Priority Index” method (Hassan and Sozen, 1997), which asks for the dimensions of the lateral load resisting elements. It is a function of a “wall index” and a “column index”. The “Capacity Index” proposed in Yakut (2004) depends on orientation, size and material properties of the lateral load-resisting

structural system, and also on the quality of workmanship or materials, and other characteristics like short columns or plan irregularities. Seismic Safety Screening Method, SSSM (Ozdemir et al., 2005) also derives from JBDPA.

1.1.2 Analytical methods

In the last 20 years, algorithms and/or physical models have been also used for assessing the vulnerability of buildings. As the other vulnerability methods do, analytical methodologies ask for the choice of a classification of typologies of buildings, a damage scale classification and an intensity measure –typically PGA instead of macroseismic intensity, unlike empirical methods—. However, specific strategies are used in these methodologies, briefly presented herein:

- the general framework in which they are set can be displacement-based or a capacity spectrum one;
- code-based ones require information about some parameters needed for the simulated design, as the type of design (seismic or gravitational) or any overstrength factor;
- the outcome of the simulated design can be a model with specific member definition or conversely only the global dynamic and mechanical properties;
- they need a characteristic parameter defining the damage state thresholds, being often interstorey drift that parameter;
- generally, assumed possible mechanisms of collapse are necessary to define the displacement capacity of the typologies of buildings;
- depending on the framework, different types of periods are evaluated (secant for the displacement-based and effective for the capacity spectrum one) and also different strategy of reduction for the demand spectrum is carried out (equivalent damping and ductility, respectively);
- some of them provide approximate capacity curves, bilinear or curvilinear;
- the probabilistic framework adopted for taking into account the variability and uncertainties of the parameters can be considered globally (adopting general parameters for the distribution function) or individually (considering each variable as a random parameter);

- most of them do not take infill panels into account, at least explicitly (sometimes the damage scale thresholds account indirectly for them);
- almost none of them are able to consider brittle failures in the RC members in their mechanical approaches;
- aimed at testing the approaches, sometimes they are compared with experimental database belonging to past earthquakes or with simulations (time-history analyses).

In Singhal and Kiremidjian (1996), fragility curves and DPMs for different RC frames (from Low-Rise, Mid-rise and High-Rise classes) are estimated by means of nonlinear dynamic analyses and the Monte Carlo simulation technique. The statistics of the Park and Ang damage index (Park and Ang, 1985) are used to obtain the parameters of a lognormal probability distribution function at each level of ground motion (see Figure 12a). Results from this distribution are then used to obtain the vulnerability in each case, adopting given threshold values of the Park and Ang index for the different damage states: “minor” (0.1-0.2), “moderate” (0.2-0.5), “severe” (0.5-1.0) and “collapse” (>1.0).

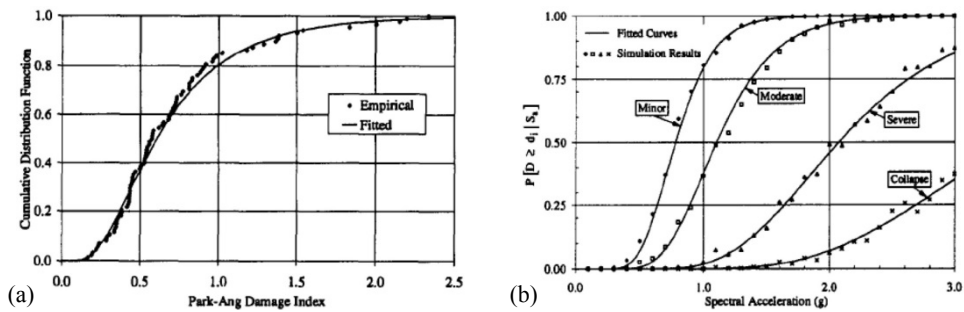


Figure 12: Probability distribution of the damage index of Park and Ang’s at a given spectral acceleration (a) and fragility curves for Mid-Rise frames (b) (Singhal and Kiremidjian, 1996)

Hence, smooth fragility curves (see Figure 12b) are obtained by fitting lognormal distribution functions to discrete points evaluated from the probability distributions of the damage measure. The relationship between the Modified

Mercalli Intensity and the average spectral acceleration in each period band, also assumed to be lognormal, is developed based on average spectral acceleration values of the ground motions recorded on firm sites and the MMI values from these earthquake at the respective recording stations (see Figure 13a). Finally, DPMs are evaluated (see Figure 13b) from the fragility curves.

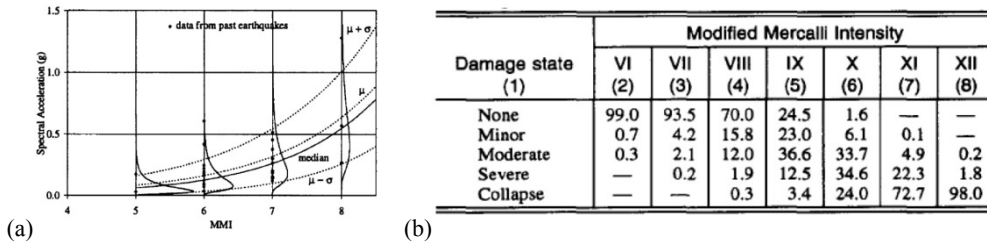


Figure 13: Correlation between MMI intensity and spectral acceleration for a range of periods between 0.5-0.9s (a) and DPM for Mid-Rise buildings (b) (Singhal and Kiremidjian, 1996)

In Masi (2003), a similar methodology is carried out. Three main structural typologies are studied: bare frames, regularly infilled frames and pilotis frames, all of them designed only for gravity loads. Structural models are generated through a simulated design procedure considering current practice and codes at the age of construction. Then, nonlinear dynamic analyses with ground motions of various levels of intensity are carried out. Once results are obtained, each typology of building is classified into a vulnerability class following the EMS-98 scale.

In Rossetto and Elnashai (2003) observational-based fragility curves for European RC structures are derived from a large database of post-earthquake damage distributions for 340000 buildings collected after 19 different earthquakes. “Homogeneous” fragility curves are obtained, which are applicable to different RC structural systems. To this end, a new damage scale is defined, providing a Damage Index for increasing damage levels affecting the above mentioned structural systems. Then, relationships are evaluated between such damage levels and interstorey drift demand, based on experimental tests. Hence, relationships between the defined Damage Index and Inter-Storey Drift demand can be obtained.

The Damage Index corresponding to the damage level reported in each dataset can be evaluated, and the interstorey drift value corresponding to such Damage Index is evaluated depending on the type of structural system. Then, the exceedance probability of each “homogenized” Damage State is obtained. Such probability corresponds to the ground motion intensity of the considered dataset. Fragility curves are finally obtained by fitting the reported intensity-probability points.

In Cosenza et al. (2005), cumulative frequency distributions of capacity parameters within a building class are provided. Each building class is defined by its age of construction and number of storeys. A simulated design procedure based on the probabilistic distribution of the structural parameters is carried out. Seismic capacity is defined in terms of base shear coefficient and global drift through a mechanics-based approach (Figure 14). Base shear is calculated for each mechanism assuming a linear distribution of horizontal seismic forces, and the ultimate roof displacement is determined as a function of the ultimate rotation of the elements in each case. Thus, the collapse mechanism corresponds to the lowest value of the base shear. The response surface method is adopted and the influence of each parameter is investigated from the capacity of the analyzed buildings. Capacity curves expressing the probability of having a capacity lower than the assigned value are obtained through a Monte Carlo simulation technique, including the influence of the knowledge level in the probability.

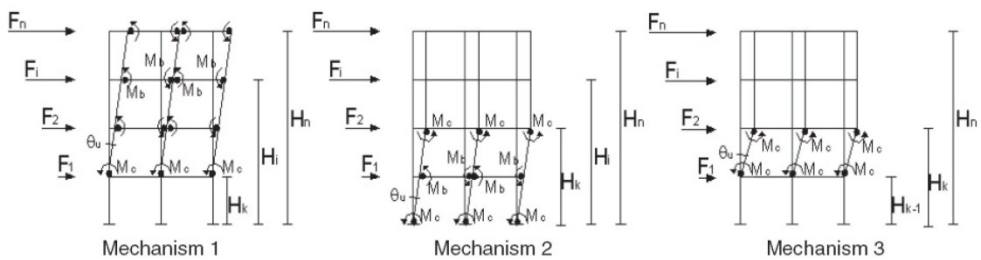


Figure 14: Predefined collapse mechanisms (Cosenza et al., 2005)

This work has been completed in Iervolino et al. (2007), becoming a complete seismic risk assessment framework where the mechanisms-based approach is

overcome. Geometrical and mechanical characteristics are identified as random variables. A simulated design procedure, a nonlinear FE modeling of the structure and a Static PushOver (SPO) analysis are carried out for all the resulting combinations of values. Hence, response surfaces are obtained for the capacity parameters: period, strength and displacement capacity of the equivalent SDOF, expressed as function of the assumed random variables.

One of the most relevant methods for vulnerability assessment is HAZUS (HAZard in United States) (FEMA, 2001; Kircher et al., 1997a; Kircher et al., 1997b; and Whitman et al., 1997). It is actually a complete loss estimation method, able to predict the whole post-earthquake scenario, derived from building damages: casualties, economic impact, emergency planning, damage in lifelines...

HAZUS works with two basic elements: capacity and fragility curves. Two points are needed to define capacity curves: yield and ultimate capacities. The first one is obtained having into account: the base shear of design, redundancies, a certain level of conservatism in the observation of code requirements and the expected resistance of the materials instead of the nominal one. A gradual reduction of the slope characterizes the curve until the ultimate point (Figure 15a). The buildings are classified into a 36 different typologies, being provided the capacity curves for each one (see Figure 15b).

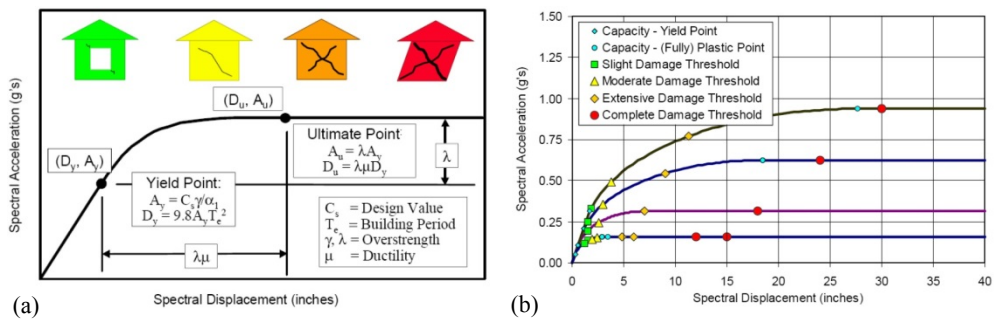


Figure 15: Example of capacity curve of a building with control points (a) and capacity curves and damage states thresholds for five seismic design levels for C1M building class (b) (FEMA, 2001)

Then, the inelastic demand spectrum is obtained through a reduction of the elastic response spectrum by means of an effective damping. The last one depends on the ground motion duration. Thus, it is possible to intersect the capacity and demand curves and so obtaining the peak response acceleration and displacement for each building (Figure 16a).

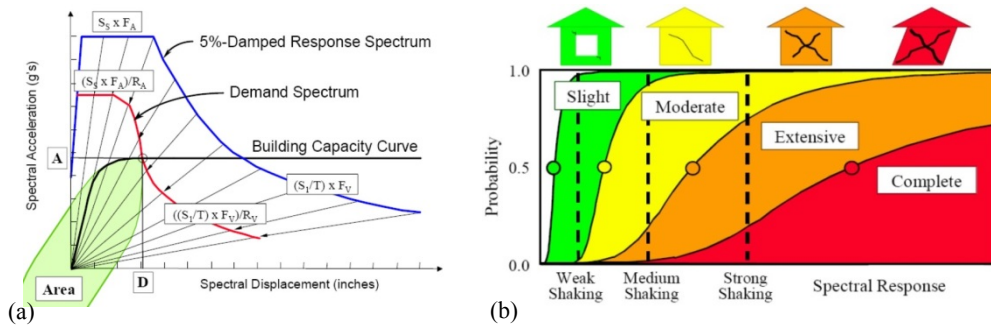


Figure 16: Peak response displacement [D] and acceleration [A] obtained from the intersection of demand spectrum and capacity curve (a) and example of fragility curves for each damage state threshold (b) (FEMA, 2001)

Aimed at defining fragility curves, four damage states (DS) in terms of spectral displacements are considered. Each DS is associated with a median value of spectral displacement obtained from the average interstorey drift corresponding to the step of the SPO at which a certain fraction of structural elements reaches a certain deformation limit. The value of this fraction, for each DS, is defined as the repair or replacement cost of components divided by the total replacement value.

Then, fragility curves are provided (Figure 16b). They account for the variability by a lognormal random variable with a standard deviation that represents the uncertainty associated with capacity curve properties, damage states and ground motion. It is calculated as a combination of those three parameters. The estimation of the variabilities of the capacity and damage states need some judgmental basis, taking in to account the available survey information.

Other methodologies are “code-based”: the evaluation of the capacity of the different typologies of buildings is done assuming that those buildings are design

following all the regulations furnished by the seismic codes in force at the age of construction. Actually, the real capacity of the buildings is much higher than that furnished by the codes, which consists in a lower bound, a minimum value. The issue is that a vulnerability assessment for a large scale earthquake loss model should not be conservative but provide a seismic capacity estimation as reliable as possible. Thus, aimed at obtaining a better fit of the predicted capacity, some factors should be included in order to have in account the sources of overstrength: design conservatism, homogenization of elements, overstrength and real ductility – normally higher than the behaviour factor of design)–.

In Giovinazzi (2005), a code-based vulnerability assessment methodology is proposed. It is based in the consideration of simplified bilinear capacity curves, defined by three parameters: the yield acceleration, the effective period and the ductility. The first variable depends on the base shear provided by the code, multiplied by a factor which accounts for the difference between median and nominal values of the material strength. Simplified code-based expressions are used for the period, and also the ductility capacity is code-based since it is obtained from the behaviour factor. In this case, capacity curve can be assuming a certain collapse mechanism. Displacement demand assessment for a given seismic intensity is carried out according to the Capacity Spectrum Method. An overall uncertainty, representing the same dispersion than that of the observed damage data, is considered through binomial distributions. Then, when this procedure is repeated for different building typologies, a lognormal standard deviation is found. This mechanical approach is compared in Lagomarsino and Giovinazzi, (2006) with the macroseismic approach also presented in this work (see section 1.1.1.2); they are reciprocally calibrated and cross-validated.

Nevertheless, the code-based approach proposed in Grant et al. (2006) does not have into account any overstrength factor, as their scope is to furnish a method able to carry out a first, quick and very simplified multi-level screening procedure aimed at defining priorities and timescales for seismic intervention in school buildings. Then, a “back-analysis” is carried out, having into account concepts included in modern codes as ductility and importance factor. Buildings without specific seismic design are considered to have null capacity. Thus, every building is characterized by a vulnerability factor in terms of “PGA deficit”.

Another family of vulnerability methodologies are those based on the Displacement-based method (e.g. Priestley (1997)); the first work belonging to this family is that of Calvi, (1999). It consists in the evaluation of the displacement capacity of the buildings for each limit state, through an assumption of a displacement shape and a maximum local deformation limit: the material strain capacity leads to a section curvature capacity and so to a drift capacity of the element; finally, assuming a mechanism, displacement capacity is obtained. Secant period is used; also a possible range of variation in its value is defined. This procedure is followed for each limit state. Thus, rectangles representing the possible “positions” of the points corresponding to the building capacity in a period-displacement plane are obtained (see Figure 17). On the other hand, seismic demand is represented by displacement response spectra, reduced in order to account for the nonlinear response, depending on the target displacement and the structural response. Hence, capacity and demand are compared in a period-displacement ambient. The rectangle area represents the expected proportion of buildings reaching or exceeding the corresponding limit state capacity.

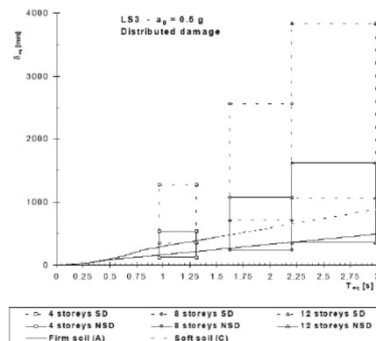


Figure 17: Example of intersection of capacity areas and demand spectrum (Calvi, 1999)

This methodology is developed afterwards (Pinho et al., 2002; Glaister and Pinho, 2003; Crowley et al., 2004; and Crowley et al., 2006) leading to the Displacement-Based Earthquake Loss Assessment (DBELA) procedure. The main improvements to the original procedure can be summarized in: (i) theoretical improvement of displacement capacity equations; (ii) equation between yield

period and height (Crowley and Pinho, 2004; and Crowley and Pinho, 2006); and (iii) fully probabilistic framework able to account for the uncertainties in geometrical and mechanical properties, in capacity models and in demand spectrum. Thus, the displacement capacity can be expressed as a function of the height, which leads also to the definition of the period for each limit state. Hence, at any period, a comparison between the displacement capacity of a building class and the displacement demand predicted from a response spectrum can be carried out (Figure 18a). Thanks to the probabilistic treatment of the uncertainties, it is possible to define a Joint Probability Density Function (JPDF) of displacement capacity and period (Figure 18b).

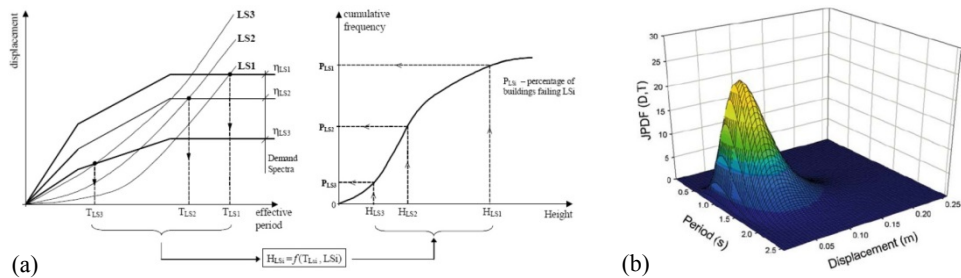


Figure 18: Deformation-based seismic vulnerability assessment procedure (a, from Glaister and Pinho, 2003) and Joint Probability Density Function (JPDF) of displacement capacity and period (b, from Crowley et al., 2004)

DBELA is subsequently developed into a Simplified Pushover-Based Earthquake Loss Assessment (SP-BELA) (Borzi et al., 2008a) by adding the definition of a pushover curve to the general displacement-based framework. The pushover curves are obtained by means of a simplified mechanics-based procedure, similar to Cosenza et al. (2005).

Afterwards, this method has been developed (Borzi et al., 2008b) aimed at accounting approximately for the infill panels (uniform or “pilotis”). Panels are supposed to have an influence on the lateral strength only up to the yield limit state. However, their influence are not considered for the definition of the displacement capacity at the yielding of the structures, as they are often not

perfectly in contact with the frame and so they are assumed to start to influence it after its yielding. Also, their contribution to the stiffness is indirectly considered through a reduction of the secant period to the yielding limit state thanks only to an increase of the lateral strength at that point. Infills are modelled as linear single strut. Authors do not clarify how to account for global influence of the brittle failure of the infills into an elastic-plastic behaviour framework.

Another simplified methodology for the vulnerability assessment of RC buildings, is “Reinforced Concrete Vulnerability” (VC) (Dolce and Moroni, 2005). Only two limit states are considered: slight damage and collapse. The capacity of the building is assessed by evaluating the strength at each storey and applying a ductility coefficient. The method assumes soft-storey collapse as the only possible mechanism, as it is the most probable due to the lack of capacity design and irregularity in the distribution of infills. These elements are also taken into account in terms of stiffness and strength. Elastic behaviour is assumed up to the slight damage limit state. The storey shear stiffness is calculated as the sum of column cracked ones (considering the restrain condition given by the beams) and the stiffness of the infill panels according to the Italian code. Then, the interstorey shear at this limit state is calculated through the stiffness and the corresponding drift. For the collapse limit state, storey shear capacity is evaluated as the sum of the ultimate shear strength of each column derived from their flexural capacity and considering the restrain condition given by the beams on the moment distribution; possible shear failures are considered, too. Infill panels are taken into account for the ultimate shear strength through the consideration of different possible collapse mechanisms. Unlike for slight damage limit state, for the collapse one the displacement capacity is not obtained from an interstorey drift limit but through an assumption of ductility capacity.

Finally, “PushOver on Shear Type models” (POST) method, presented in (Ricci, 2010), from which the approach developed in this PhD thesis, FAST, derives as a simplification. POST evaluate the buildings structural characteristics based on few data such: number of storeys, global dimensions and type of design. Assuming shear type behaviour, it evaluates the nonlinear static response in closed form and applies the N2 method (Fajfar, 1999), so the seismic capacity is evaluated, based on the displacement capacity at each damage state.

The method needs to be given, as input data:

- global geometrical parameters: number of storeys, plan dimensions and number of bays in both directions and interstorey heights of the first and the rest of the storeys;
- distribution of infill panels: uniformly or pilotis distribution in elevation, with definition of opening percentages, or complete absence of them;
- type of design: gravitational or seismic, with specification of the material resistances of design and also of the base shear of design in the last case;
- material characteristics: concrete compressive strength, steel yield strength and infill characteristics (shear cracking strength and shear and longitudinal elastic modulus –assumed to be those proposed in (CMLP, 2009), and ratios relating post-capping degrading stiffness with elastic one and residual and maximum strength), so the envelope of the lateral force-displacement relationship for infills can be defined;
- data for the definition of seismic hazard, from the probabilistic seismic hazard assessment carried out for Italy (INGV-DPC S1, 2007) so location, stratigraphic and topographic condition and type of building are needed.

A code-based simulated design procedure (from Verderame et al. (2010a)) is carried out. Design loads are defined: dead loads are evaluated from a load analysis while live loads and lateral loads are evaluated from past code prescriptions. Then, element dimensions are evaluated. Column area depends on the axial load (estimated from tributary areas), assuming a reduction factor accounting for the combination of axial and bending action (Pecce et al., 2004); dimensions must range between 30 and 70cm and cannot vary more than 10 cm between adjacent storeys. Beams are assumed to be 30cm wide and the height is obtained from gravitational loads.

Reinforcement in columns is distributed uniformly along the faces. In the case of gravitational design, it is based on minimums prescribed by codes. In the case of seismic design, it is calculated from the actions. The storey shear is distributed proportionally to the column's inertias, and shear span equal to half of the interstorey height is assumed. Transverse reinforcement is calculated in a similar way for both cases.

Aimed at defining of the pushover curve, the interstorey shear-displacement relationship of each storey has to be known, so displacement capacities of columns are evaluated. Tri-linear envelopes for moment-chord rotation relationships are assumed, being chord rotation capacities dependant on the section curvature at yielding, calculated in closed-form according to Fardis (2009). Also shear maximum and residual capacities are evaluated according to CEN (2005). For infill panels, force-displacement relationship model proposed in Panagiotakos and Fardis (1996) and Fardis (1997) are assumed, also considering the openings as in Kakaletsis and Karayannis (2009).

Thus, at each storey, a multi-linear shear-displacement relationship is obtained, considering all the RC columns and the infills as acting in parallel, so the building's base shear-top displacement relationship can be evaluated through a closed-form procedure (see Figure 19). The fundamental period and the displacement shape are evaluated through an eigenvalue analysis, once known the mass and stiffness of each storey. Then, the corresponding lateral load shape is obtained and so the interstorey shear demands, which are compared with the interstorey strengths aimed at determining which will be the first (and only) one to reach its maximum resistance. If there are infills at that storey, it will be also the first (and only) one to degrade, thus controlling the global softening. This peak of resistance leads to the calculation of the peak of the pushover curve, given the homothetic shape of the lateral force in all the process. Therefore, the pushover curve is evaluated by means of a force-controlled procedure up to the peak and by means of a displacement-controlled procedure after that. In the latter phase, if there is a softening post-peak behaviour, the interstorey shear of the rest of the storeys will decrease while the one of the damaged storey increases. An unloading stiffness equal to the elastic one is assumed.

Subsequently, the pushover curve is multi- or bilinearized and represented according to the equivalent SDOF. Then, the different limit states thresholds are evaluated depending on the performance of the structure: damage limitation at the beginning of the degradation of the last infill or at the first yielding in a RC column; severe damage, at the attainment of the 75% of the maximum chord rotation of any column; and near collapse, corresponding to the 100%. Afterwards, capacity and demand curves are combined and N2 method (Fajfar, 1999) is applied

in order to obtain the inelastic displacement demand for each limit state through different $R-\mu-T$ relationships (see section 1.2.3.4).

Finally, fragility curves are obtained as cumulative frequency distribution of the PGA capacity for all the limit states, by considering all the variables as random ones, based in the variabilities observed in the results of the nonlinear dynamic analyses carried out for the definition of the $R-\mu-T$ relationships.

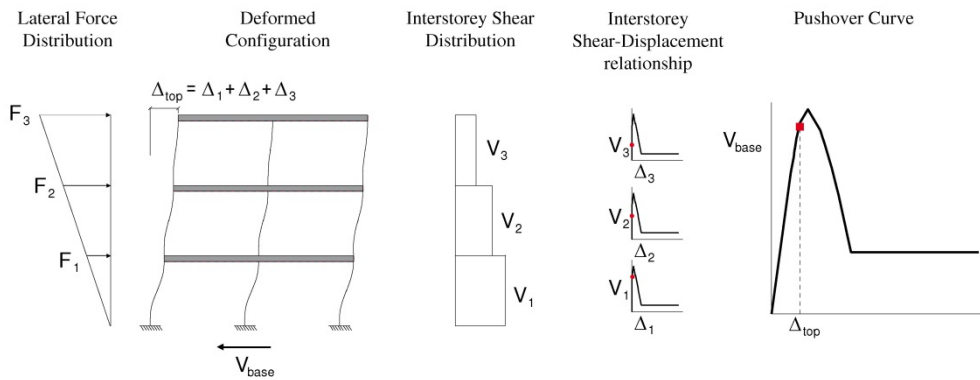


Figure 19: Calculation of pushover curve in POST approach (Ricci, 2010)

1.1.3 Hybrid methods

Some methodologies combine analytical and empirical procedures, providing DPMs and vulnerability curves from mechanical models and empirical data. Sometimes they consist in corrections done to an analytical method by using database from real earthquake. It is worth to note that uncertainties coming from such two different sources can include different variables and levels of uncertainty, not being directly comparable. Hence, it probably would be better to calibrate both sources in order to have equal median values.

In Kappos et al. (1995 and 1998) DPMs are obtained partially from observed damage after the 1978 Thessaloniki earthquake, through the vulnerability index method, and partially from nonlinear dynamic analyses. Aimed at including such analytical results into the DPMs, an empirical correlation between intensity and

PGA values is used, and also another correlation between analytical global damage index and the damage express as the cost of repair.

Another hybrid procedure is presented in Singhal and Kiremidjian (1998). In this case, observational data from the 1994 Northridge earthquake are used for the validation and update of the analytical vulnerability curves for low-rise RC frames proposed in a precedent work Singhal and Kiremidjian (1996). Bayesian updating technique accounting for the reliability of different data sources is used.

1.2 PBEE FRAMEWORK: SPECTRAL-BASED METHODOLOGIES

Most of the vulnerability assessment methodologies presented in the previous section follow the principles of “Performance-Based Earthquake Engineering” (PBEE). It is a framework for both design and assessment of structures against earthquakes aimed at providing higher control of seismic risk and, more in general, towards the reduction of losses induced by earthquakes.

In the last decades, the “performance” philosophy has progressively substituted the “strength” one. However, codes use in most of the cases the force-based framework, implicitly assuming that the strength provided to a structure to avoid collapse would warrant a suitable behaviour when submitted to minor events (Bonett, 2003), and in some cases compelling to a final check of displacements. In fact, increasing strength may not enhance safety, nor necessarily reduce damage. The development of capacity design principles in New Zealand (Park and Paulay, 1975) showed that the distribution of strength through a building was more important than the global strength (Priestley, 2000). Hence, for the last decades seismic codes have been incorporating concepts based in the performance rather than only in the strength, through the definition of different levels of performance: Limit States or Damage States.

Methodologies following the PBEE precepts are based on the evaluation of the capacity of the buildings together with the demand of the seismic event by using a quantitative and probabilistic framework. Most of the approaches allow visual evaluations of the performance of the structures by a graphic superposition, in the

Acceleration-Displacement Response Spectrum (ADRS) format, of the capacity and demand curves, being the “performance point” the intersection of both of them (see Figure 20a). In this section, common issues concerning the definition of capacity and demand curves are presented and some methods are described.

1.2.1 Capacity curves (CC)

In general, the capacity of a structure when subjected to a lateral action can be represented by a force-displacement relationship, i.e. the evolution of the displacement of the top of the frame (abscissa) when subjected to an increasing pattern of lateral forces expressed in terms of total base shear (ordinate). In the following, some issues related to the obtaining and managing of CC are studied: the analysis from which it comes from (SPO), the range of maximum capacities in comparison with the codes’ requirements (overstrength), simplification made to its shape aimed at making it useful (multilinearization), transformation into the ADRS format and the specific shape of CC of infilled frames.

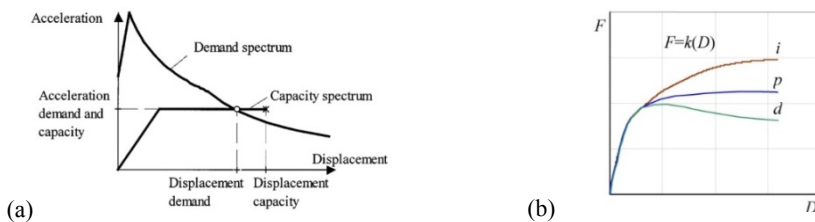


Figure 20: Graphic evaluation of the performance point (a, from Fajfar, 1999) and different post-elastic behaviour of RC bare frames: hardening [i], perfectly plastic [p] and softening [d] (b, from Albanesi and Nuti, 2007)

1.2.1.1 *Static PushOver (SPO) analysis*

Capacity curves are obtained from experimental or simulated pseudo-static inelastic analysis in which the structure is subjected to a lateral pattern of forces that increment monotonically until the collapse of the frame. By means of this procedure, important performance parameters are assessed: cracking, yielding, deterioration and collapse; global and interstorey drifts; redistribution of forces between elements; P - Δ effects; etc. (Krawinkler and Seneviratna, 1998).

The typical shape of the CC of a RC bare MRF is (see Figure 20b):

- a first elastic part with constant slope, which would be shorter if cracking in the $M-\theta$ envelopes of extremities of the elements is considered;
- a second part with decreasing slope until the yielding of the structure;
- a third part with positive (hardening), zero (perfectly plastic) or negative (softening) slope depending on the corresponding definition of the $M-\theta$ envelopes of member ends and on the consideration of $P-\Delta$ effects

Perhaps the most important and critical issue is the assumption of the pattern of forces. The election of a load pattern is based on a “prediction” of the most representative deformed shape of the structure within the process, given that the modal displacements at any degree of freedom are proportional to the corresponding forces and masses. In the case of a non-adaptive approach, that “prediction” is usually carried out considering the initial elastic first-mode behaviour of the frame. In fact, SPO lays on the assumption that the response of the structure is similar to that of the equivalent SDOF, so that the response is controlled by the fundamental mode and that its shape remains constant throughout the process. Different pattern can be selected:

- Equivalent static forces corresponding to the 1st mode of vibration (proportional to the displacement and the masses).
- Linear shape, as an estimation of the previous pattern in order to avoid a modal analysis needed to determine it. It is in good agreement when the storey stiffnesses decrease with the height, as in frame systems.
- Sinusoidal shape, also an estimation of the 1st mode equivalent forces. It is in good agreement when the storey stiffnesses are constant with the height, as in wall systems.
- Equivalent static forces obtained from a SRSS or CQC modal combination, as proposed in the Spanish seismic codes (see section 2.1). This is important for structures severely affected by secondary modes.
- Forces proportional to the masses, emphasizing demand in lower storeys.
- Constant pattern, as an estimation of the previous shape.

Depending on the choice, different curves may be obtained (e.g. Figure 21). A reasonable strategy, suggested by authors and codes, is to use more than one shape

and envelope them (Fajfar, 2000). Other solutions are the adaptive load patterns: storey loads proportional to the displacements in each step, patterns based on the modal response derived from secant stiffness at each step, or loads proportional to storey resistance. It is worth noting that the choice of the load pattern not only influence the maximum strength and displacement capacity of the MDOF but also the subsequent transformation into a capacity curve corresponding to the equivalent SDOF, because the factors switching from one to another depend on the elastic deformed shape (see section 1.2.1.4).

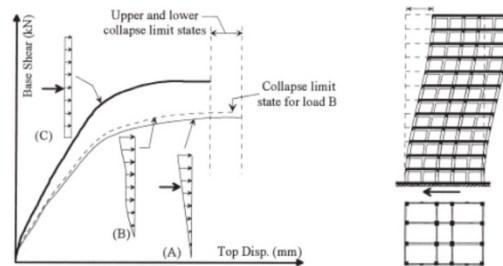


Figure 21: Different capacity curves depending on the selected load pattern (triangular, modal, constant) (from Albanesi and Nuti, 2007)

The main weaknesses of the simple SPO are (López Menjívar, 2004):

- the equivalence to an SDOF is only accurate when there are not significant strength or stiffness irregularities and there is no important influence of the higher modes;
- as it is force-based and not adaptive, it may underestimate storey drift demands due to weaknesses generated when the structure's dynamic characteristics change after formation of the first local mechanism;
- it is difficult to model 3D and torsional effects;
- it only accounts for the dissipation of strain energy, neglecting other sources as kinetic and viscous damping energy;
- the vertical component of the earthquake is ignored.

However, the first two disadvantages can be overcome with the application of a multi-modal fully adaptive pushover procedure (Elnashai, 2001), in which all the

relevant parameters are updated at the end of each incremental step: distribution of stiffness, period of relevant modes, spectral demands, participation factors and load pattern of the increment.

Notwithstanding those drawbacks, non-adaptive SPO is a proper tool for assessing the capacity of structures. Some vulnerability approaches, as FAST, propose direct simplified capacity curves consistent with all the existing background about SPO analyses of RC frames (see section 5.1.2).

1.2.1.2 Bilinearisation methods

In PBEE framework, capacity and demand are not independent. In fact, inelastic demand depends on the estimated ductility and effective period corresponding to the capacity curve (see section 1.2.3.4). Aimed at defining of such two parameters, the CC must be “bilinearised”, i.e., converted into a piecewise function composed of two linear branches: the first one connecting the origin with the estimated yielding point of the structure, and the second one connecting that one with the estimated collapse (or performance) point. The slope of the first branch defines the effective stiffness, inversely proportional to the effective period, and the ratio between the displacement at the collapse and the yielding point defines the ductility.

Lots of strategies aimed at carrying out CC bilinearisation are proposed by authors and codes (see Figure 22). The critical decisions are:

- Slope of the post-yielding branch: it can be zero, i.e. perfect plastic behaviour (see Figure 22 a, b, c, g, h); or positive, i.e. with plastic hardening (see Figure 22 d, e, f).
- The choice between the collapse or the estimated performance point for being the last point of the second branch (requiring iterations).
- Definition of the ultimate displacement: corresponding to the peak resistance (see Figure 22 a to g); corresponding to a decreasing of a 15% of the peak resistance (see Figure 22 h); corresponding to the attainment of the 75% of the ultimate chord rotation in the first plastic hinge; etc.
- Definition of the secant stiffness: the initial tangent elastic one (see Figure 22 a, e); corresponding to a branch passing through the first yielding;

corresponding to a branch passing through a point equivalent to a certain percentage of the collapse load (see Figure 22 b, f, g); or that satisfying the area-balancing rule (equal misfit areas above and below the curve).

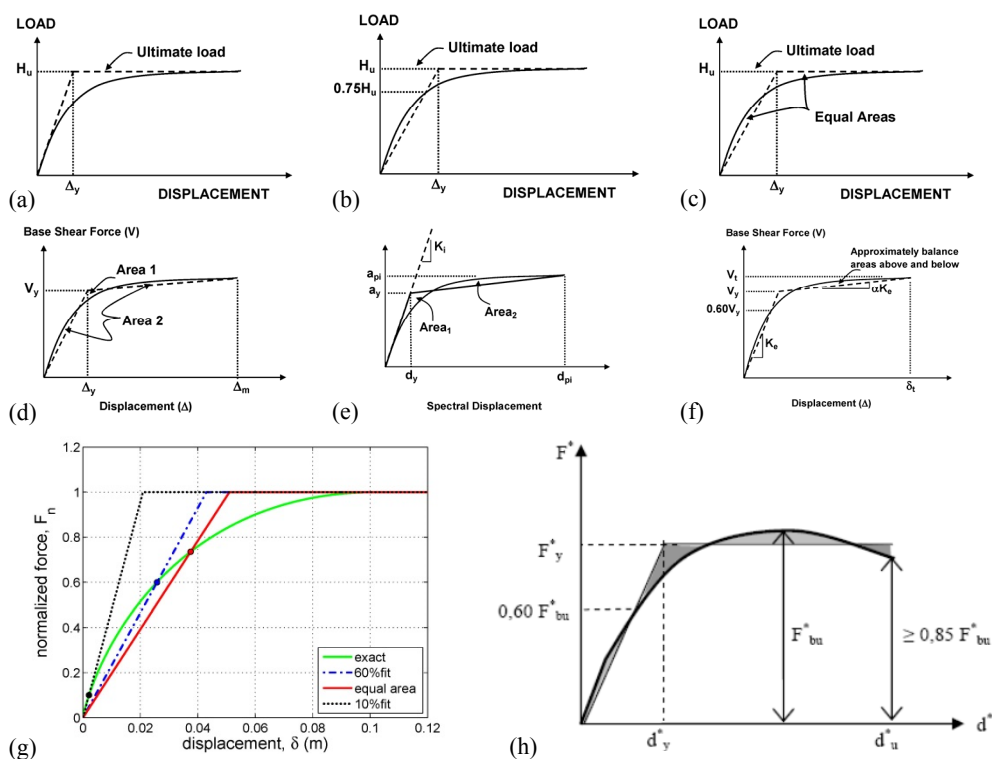


Figure 22: Different bilinearization strategies; (a) to (f) from Kadas (2006); (g) and (h) from De Luca et al. (2013)

1.2.1.3 Behaviour factor and overstrength

Seismic codes conventionally deal with the inelastic behaviour of structures by proposing an equivalent elastic design through the use of behaviour factors (q), which are factors equal or higher than 1.0 aimed at reducing the design force level: $q = V_{el} / V_d$, being V_{el} and V_d the equivalent elastic and design base shear, respectively. This strategy is based in the principle that a system can dissipate energy both by increasing its force (elastic phase) or by increasing its deformation

at a constant force level (inelastic behaviour). Thus, an inelastic structure with a maximum force capacity lower than the equivalent elastic one can perform in a similar way if its displacement capacity reaches a certain level, related with q . This displacement capacity is related with the ductility capacity $\mu = \Delta_{max} / \Delta_y$, being Δ_{max} and Δ_y the maximum and yielding displacement capacities, respectively. Hence, given a period of the structure and target elastic design strength, multiple combinations of q and μ (see section 1.2.3.4) would provide similar performances, as seen in Figure 23a.

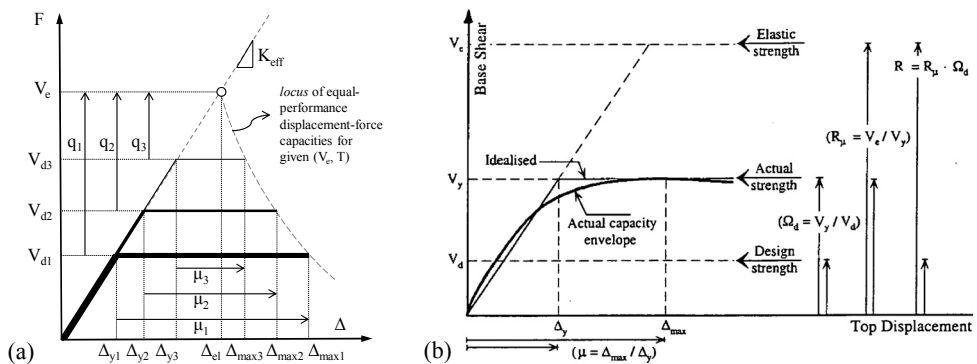


Figure 23: Different combinations of q and μ^\dagger for equal-performance structures given the equivalent elastic force and the period (a) and relationship between behaviour factor, overstrength, ductility reduction factor and ductility (b, from Mwafy and Elnashai, 2002)

The usual design approach of codes is to assign target ductility to the structure depending on the typology and characteristics, and then a behaviour factor is provide or calculated, based not only on this required ductility but also on other expected phenomena as overstrength or other force reducing effects (Borzi and Elnashai, 2000).

[†] In this figure, q and μ , both corresponding to ratios between variables –or as factors switching from one variable to another– are represented graphically as arrows orientated from the value corresponding to the denominator to that of the numerator. All the figures presented in this work follow the same approach. Conversely, magnitudes corresponding to the actual distance marked in the graphic (not to the factor switching) are represented by an arrow in both extremes of the segment (as in Figure 22).

Thus, the supplied or required behaviour factor accounts, implicit or explicitly, for the following contributions (see Figure 24):

- A) Ductility contribution (R_{μ}). It is the reduction of force equivalent to ductility, i.e. due to the hysteretic energy dissipation. It corresponds to the ratio between the elastic demand of the equivalent SDOF with a period similar to the effective period of the structure (T_{eff}), and the supplied strength of the frame (V_y). For more details, see section 1.2.3.4.
- B) Overstrength (R_S). It is the ratio between the “supplied” strength of the structure, i.e. the real base shear, and the design strength provided by the code (see Figure 23b). Different phenomena lead to this increase in the final strength (Vielma et al., 2006; Mwafy and Elnashai, 2002):
- B1. Difference between the mean resistances of the materials in comparison with the reduced nominal design values.
 - B2. Possible benefits of hardening of materials and confining of sections, not taken into account in the design.
 - B3. General conservatism in the design, strategies of homogenisation of elements and discrete quantities in the usual dimensions of RC sections and steel reinforcement bars.
 - B4. Limitations of horizontal displacements and/or interstorey drifts, leading to bigger section areas.
 - B5. Minimum reinforcement areas for ductility or constructive requirements.
 - B6. Contribution of RC structural elements sometimes not considered in the design, as stairs, walls associated to vertical connections (stairs or elevators), solid upper slab or also the joists (when there are not beams in that direction).
 - B7. Consideration of multiple combinations of actions, in all directions.
 - B8. Influence of gravitational and wind design with amplified actions and limited deflections, mainly for low-rise buildings or low-hazard sites (Jain and Navin, 1995).
 - B9. Structural redundancy and capacity of redistribution of the forces between the elements when yielding of the sections occurs sequentially.

Different measures of the global overstrength, obtained from different case studies, are presented in Table 1. Results show values ranging typically from 2 to 3; however, a huge scatter is observed, given that all the contributions are highly dependent on the particularities of the case study and on the strategies and decisions of design. Also, it seems that in some cases also the influence of non-structural elements has been taken into account, leading to extremely high values.

Table 1: R_S for RC buildings suggested by different authors (from Aguiar Falconi, 2007)

Author	Case study	R_S
Osteraas and Krawinkler (1990)	RC MRF, zone 4 of UBC, soil S2	2.1 – 6.5
	RC MRF, only perimeter resistant	1.8 – 3.5
	RC frames with crosses	2.2 – 2.8
Freeman (1990)	4-storey building	2.8
	7-storey building	4.8
Miranda and Bertero (1989)	Low-rise buildings in Mexico	2 – 5
Cassis and Bonelli (1992)	RC SW in Chile	3 – 5
Zhu et al. (1992)	4-storey building in Canada	1.23 – 1.71
Uang and Maarouf (1993)	6-storey building in Loma Prieta (California)	1.9
Hwang and Shinozuka (1994)	4-storey building, zone 2 of UBC	2.2
Fischinger et al. (1994)	Mid- and low-rise buildings	1.6 – 4.6
Jain and Navin (1995)	3-, 6- and 9-storey buildings in zone 5 of India	2.0 – 3.0
Panagiotakos and Fardis (1998)	Any type of RC frame	2.0 – 2.5
Mwafy and Elnashai (2002)	Mid-rise buildings	2.0 – 3.0

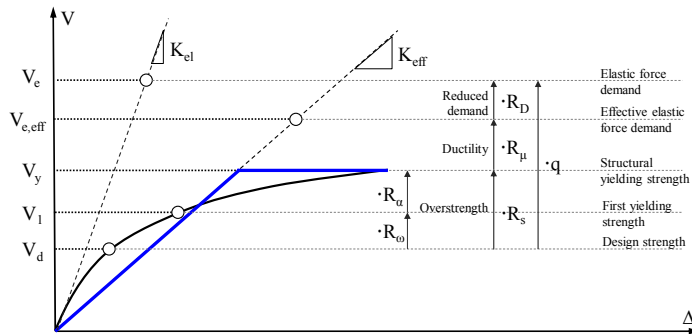


Figure 24: Proposed definitions for different sources of contribution of behaviour factor

Only the first contribution (material real resistance) is independent on the design and can be appropriately individuated. In Galasso et al. (2011a), test data of reinforcing steel bars showed mean values of $f_y/f_{y,nom}$ of 1.27, being f_y and $f_{y,nom}$ the mean and nominal yielding stress of the steel. Similar test carried out for concrete (Cosenza et al., 2009) showed ratios of 1.24.

R_S can be expressed as the product of two factors:

- R_ω , the ratio between the shear force corresponding to the occurrence of the first yielding in any section of the structure (V_1) and that of design (V_d);
- R_α , the ratio between the supplied yielding strength of the structure (V_y) and V_1 .

Unfortunately, it is again hard to classify the 9 sources of overstrength as belonging to one single factor. Only those related to material (B1 and B2), being constant for all the structure, can be assigned respectively to R_ω and R_α , i.e. acting before and after the first yielding of the steel in any section. The rest of the sources' influence is fuzzily distributed, because they result in different overstrength ratios for each element.

Also the source B9 (redundancy) is not clearly included in R_α , as the real redistribution starts before the first yielding in any section occurs, due to the flexural cracking of the concrete. Some codes, as EC8 (CEN, 2004), propose different values for R_α : ranging from 1.1 to 1.3, increasing with the number of bays and storeys. Actually, in general, the higher is the number of elements involved in the collapse mechanism, the higher is R_α , because single overstrength of more elements after first global yielding are employed. However, if a soft ground storey mechanism takes place, the maximum strength provided by the structure is higher than in the case of a global mechanism involving more storeys, because all the columns at ground floor attain their maximum bending moment capacities at both endings, thus providing the maximum base shear of the building (see Figure 39). Still, it is difficult to state a clear relation between this effect and the level of R_α , as the strength corresponding to the first yielding (V_1) may not be comparable in both mechanisms.

- C) Reduced demand contribution (called in this work R_D). It is the ratio between the elastic strength demand considered in the design and the real expected demand, consistent with the seismic hazard. Some authors (Borzi and Elnashai, 2000) consider this as a component of the behaviour factor. In fact, although it is not related to the capacity but with the demand, it is actually a force reducing contribution. However, some other authors do not include it (Fajfar, 1999). Some different origins of this factor are:
- C1. Differences between the conservatively assumed dynamic properties and real ones: overestimation of the total mass acting in the seismic situation, overestimation of the participating mass ratio or underestimation of the viscous damping.
 - C2. Some corrections that may become conservative, as those accounting for accidental torsion or P - Δ effects, or the accidental safety factor provided by some codes.
 - C3. The higher effective period of the structure in comparison with that used in the design (see Figure 24), intended to be the estimated elastic one; see section 1.2.2 for more details.

Finally, it is important to indicate that some authors (De Luca et al., 2014) consider that the behaviour factor comprehends only R_α and R_μ (see Equation (1)), excluding R_ω and R_D from the contributions (as in Equation (1)).

$$q = R_S \cdot R_\mu \cdot R_D = R_\omega \cdot R_\alpha \cdot R_\mu \cdot R_D \quad ; \quad q = R_\alpha \cdot R_\mu \quad (1a,b)$$

1.2.1.4 Equivalent SDOF

The fundamentals of PBEE require expressing the capacity curve in the same format as the demand spectrum, aimed at comparing them. Thus, as demand spectrum corresponds to a SDOF system in ADRS format, both transformations must be also applied to the CC of a MDOF building.

The association of a MDOF system with an equivalent SDOF involve that the dynamic behaviour of the MDOF can be sufficiently represented by its fundamental mode of vibration. Thus, displacements are assumed to be proportional (homothetic) to those corresponding to the first mode (ϕ_i , see Figure 25a) during the structural response to ground motion shape, i.e. the displacement

shape remains constant. This is the basic and the most critical assumption within the procedure (Fajfar, 2000). In all the following, definition of variables and expressions in the equations are referred to planar equivalent systems, as capacity curves derive from pushover analysis carried out separately in each direction.

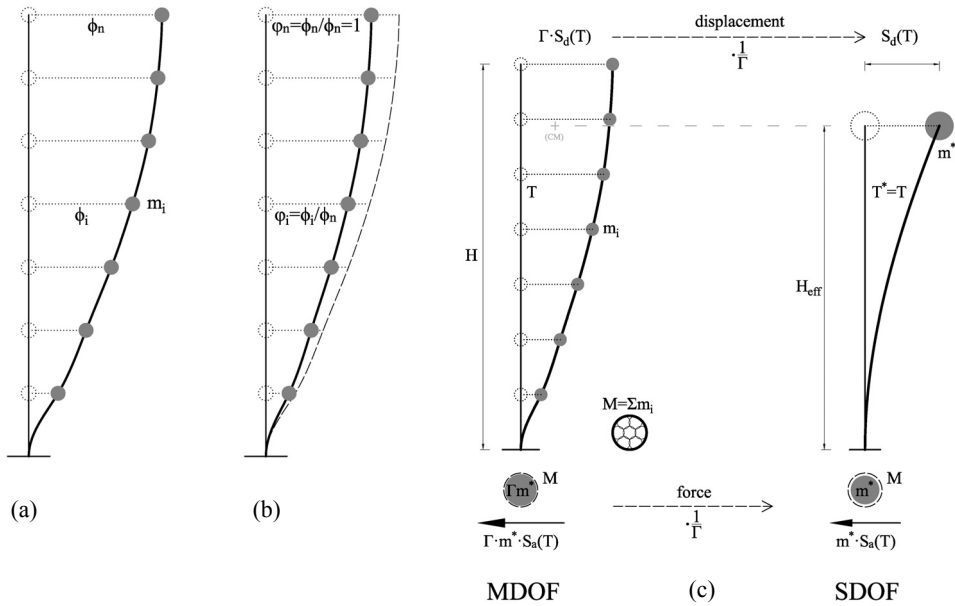


Figure 25: Typical shape of the first mode of vibration of a planar MDOF system with concentrated masses at the storey levels (a) and typical normalisation of amplitudes (b); dynamic and mechanical characteristics of SDOF in comparison with the MDOF (c)

In Figure 25b, dynamic and mechanical characteristics of the SDOF are showed. The equivalent SDOF is a system whose equivalent mass (m^*) is equal to the amount of mass “moved” by the fundamental mode of the MDOF. This mass is called participating mass, see Equation (2a), being $\{\phi\} = \phi_i$ the amplitudes normalised to the bigger one ϕ_n corresponding to the top storey (see Figure 25a), $[M]$ the mass matrix with the concentrated masses m_i in the diagonal, and $\{r\} = r_i$ the director cosines of the acceleration in the direction of the corresponding degree

of freedom, all equal to 1 for planar models. Variables with an asterisk (*) correspond to the SDOF system.

The stiffness of the SDOF –and therefore its fundamental period— is the same as that of the MDOF. Its mass (m^*) is placed at an effective height (H_{eff}) corresponding to the position of the barycentre of the participating mass. At every instant of the motion, both the displacements and the inertial forces of the SDOF system are Γ times lower than in the MDOF, being Γ the first modal participation factor of the structure, expressed in Equation (3a); the denominator of the last expression sometimes is named L^* (Fajfar, 2002). Finally, the first mode participating mass of the MDOF can be expressed as a fraction of the total mass through a factor λ , as shown in Equation (3b).

$$m^* = \{\varphi\}^t [M] \{r\} = \sum m_i \varphi_i \quad ; \quad L^* = \{\varphi\}^t [M] \{\varphi\} = \sum m_i \varphi_i^2 \quad (2a,b)$$

$$\Gamma = \frac{m^*}{L^*} = \frac{\{\varphi\}^t [M] \{r\}}{\{\varphi\}^t [M] \{\varphi\}} = \frac{\sum m_i \varphi_i}{\sum m_i \varphi_i^2} \quad ; \quad \Gamma \cdot m^* = \lambda \cdot M \Rightarrow \lambda = \Gamma \frac{m^*}{M} \quad (3a,b)$$

The fact that Γ is the factor for switching from SDOF to MDOF can be argued as follows. Equations (4) and (5) represents the base-forced movement of a SDOF and MDOF, with scalar and vectorial variables, respectively: d^* and $\{d\}$ are the displacements depending on the time, m^* and $[M]$ the masses, $[C]$ the viscous damping, ν the damping expressed as a fraction of the critical one, ω the angular velocity and $[K]$ the stiffness.

$$\ddot{d}^* + (2 \cdot \omega \cdot \nu) \dot{d}^* + \omega^2 \cdot d^* = -a \quad (4)$$

$$[M] \{\ddot{d}\} + [C] \{\dot{d}\} + [K] \{d\} = -[M] \{r\} a \quad (5)$$

Equation (5) can be transformed into the expression of the 1st mode MDOF top (d_n), see Equation (6a), by pre-multiplying by $\{\varphi\}^t / (\{\varphi\}^t [M] \{\varphi\})$, substituting all the matrix $[A]$ for their first-column vectors $\{a\}_1$ –corresponding to the first mode $j=1$ — and considering that $\{1/m\}_1^t \cdot \{c\}_1 = 2\omega_1 \nu$ and $\{1/m\}_1^t \cdot \{k\}_1 = \omega_1^2$. A comparison between Equations (4) and (6a) demonstrates that the history of displacements of the MDOF is equal to Γ times that of the SDOF, so the spectral

displacement (S_d , maximum displacement of the SDOF in the time-history) can be expressed also as the maximum displacement of the MDOF reduced Γ times (see Equation (6b)). Also the spectral acceleration (S_a) and velocity (S_v) can be defined in similar terms, as well as the base shear and the participating mass.

$$\ddot{d}_n + (2 \cdot \omega_1 \cdot \nu_1) \dot{d}_n + \omega_1^2 \cdot d_n = -\Gamma \cdot a \quad ; \quad \frac{d_{n,\max}}{d_{\max}^*} = \Gamma \quad (6a,b)$$

Thus, the capacity curves –bilinearised or curvilinear— should be reduced by Γ in both axes for obtaining that corresponding to SDOF (see Figure 26a). Besides, aimed at representing it in the ADRS format, as the ordinate axe must be expressed in terms of spectral acceleration, it must be divided by the mass of the SDOF (m^*).

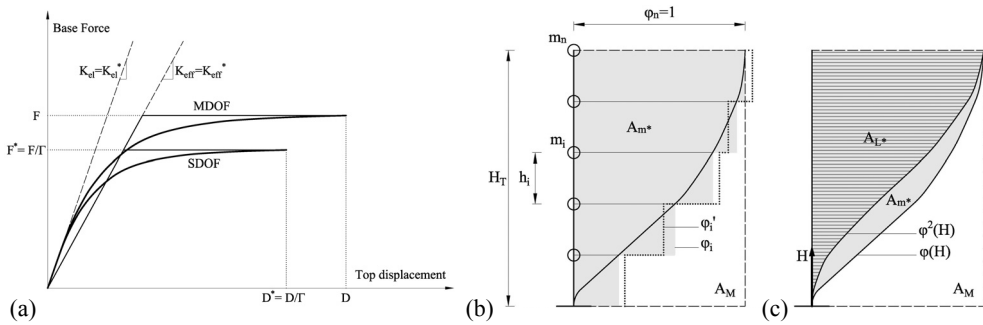


Figure 26: Transformation of the CC from MDOF to SDOF (a); graphic interpretation of (m^*/M) for a discrete model (b) and analogous for (m^*/M) and (L^*/M) for a continuous model (c)

The dynamic properties m^* , L^* and Γ can be interpreted from a graphic point of view as relations between areas generated by the deformed shape. This approach is useful aimed at the definition of some parameters required by generalised FAST (see section 5.2). In Figure 26b, normalised amplitudes ϕ_i corresponding to the first mode are shown, being the degrees of freedom $1 \leq i \leq n$, and m_i and h_i the corresponding storey mass and interstorey height, respectively. The solid line connecting all of them represents a suitable continuous deformed shape of the MDOF, while the stepped outline of the grey surface represents a sort of “discrete” deformed shape, where each “step” corresponds to the amplitude of the degree of

freedom placed just above. In the case of similar interstorey height (see Equation (7)), it makes sense to define the following areas:

- A_M , corresponding to the rectangle circumscribing the deformed shape, whose base is the top amplitude $\varphi_n=1$ and whose height is the total one of the frame H_T (see Equation (8)). It is plotted in Figure 26a with dashed line. Represents graphically the total mass M (Equation (9a)), as if the whole mass of the structure was “moved” by the fundamental mode.
- A_{m^*} represents graphically the SDOF participating mass m^* only if the storey masses are similar. It is the area between the structure and its “discrete” deformed shape, filled in grey in Figure 26a. It can be analytically obtained as the addition of “steps”, the rectangles corresponding to each degree of freedom, identified as A_i (see the upper lines of Equations (10a) and (10b)). The barycentre of A_{m^*} is placed at a height equal to H_{eff} (see Figure 25b).
- $A_{m^{*'}}$ represents m^* for different storey masses. Its graphical construction is analogous to the previous case, as an addition of the rectangles A_i' (see the lower lines of Equations (10a) and (10b)). The difference is that in that case different equivalent amplitudes must be taken (φ_i' , see Equation (9c)), weighted by the ratio between the corresponding storey mass and the average total one \bar{m} , obtained as in Equation (9b).
- A_{L^*} and $A_{L^{*'}}$ are calculated analogously to A_{m^*} and $A_{m^{*'}}$ but using φ_i^2 and $\varphi_i'^2$ instead of φ_i and φ_i' (see Equations (10c)). They represent graphically L^* in the case of similar and different storey masses, respectively.

Then, the ratio between the areas representing m^* and M ($A_{m^{*'}}$ and A_M , respectively) is equal to the fraction of participating mass to the total one in the SDOF, m^*/M (see the lower row of Equation (11)). For the case of equal storey masses, in Equation (12) the expressions for the different dynamic parameters are shown. Thanks to these simplifications, it is possible to demonstrate the expression in the upper row of Equation (11). Similarly, the graphic expressions for the rest of the dynamic parameters are shown in Equation (13).

$$\left. \begin{array}{l} H_T = \sum h_i \\ h_i = h_j = h, \quad \forall i, j \leq n \end{array} \right\} \Rightarrow H_T = n \cdot h \quad (7)$$

$$A_M = H_T \cdot \varphi_n = H_T ; \quad (8)$$

$$M = \sum m_i \quad ; \quad \bar{m} = M/n \quad ; \quad \varphi_i' = \varphi_i \frac{m_i}{m} = \frac{n \cdot m_i \cdot \varphi_i}{M} \quad (9a,b,c)$$

$$\left\{ \begin{array}{l} A_i = \varphi_i \cdot h \\ A_i' = \varphi_i' \cdot h \end{array} \right. ; \quad \left\{ \begin{array}{l} A_m^* = \sum A_i = \sum h \varphi_i = h \sum \varphi_i \\ A_m^{*'} = \sum A_i' = \sum h \varphi_i' = h \sum \varphi_i' \end{array} \right. ; \quad \left\{ \begin{array}{l} A_L^* = h \sum \varphi_i^2 \\ A_L^{*'} = h \sum \varphi_i'^2 \end{array} \right. \quad (10a,b,c)$$

$$\left\{ \begin{array}{l} \frac{A_m^*}{A_M} = \frac{h \sum \varphi_i}{H_T} = \frac{\sum \varphi_i}{n} = \frac{m \sum \varphi_i}{M} = \frac{m^*}{M} \\ \frac{A_m^{*'}}{A_M} = \frac{h \sum \varphi_i'}{H_T} = \frac{\sum \varphi_i'}{n} = \frac{n \sum m_i \varphi_i}{n \cdot M} = \frac{m^*}{M} \end{array} \right. \quad (11)$$

$$\left. \begin{array}{l} M = n \cdot m \\ m^* = \sum m_i \varphi_i = m \sum \varphi_i \\ L^* = \sum m_i \varphi_i^2 = m \sum \varphi_i^2 \end{array} \right\} \Rightarrow \Gamma = \frac{\sum \varphi_i}{\sum \varphi_i^2}, \text{ if } m_i = m_j = m, \forall i, j \leq n \quad (12)$$

$$\left\{ \begin{array}{l} \frac{A_L^*}{A_M} = \frac{L^*}{M} \\ \frac{A_L^{*'}}{A_M} = \frac{L^*}{M} \end{array} \right. ; \quad \left\{ \begin{array}{l} \frac{A_m^*}{A_L^*} = \Gamma \\ \frac{A_m^{*'}}{A_L^{*'}} = \Gamma \end{array} \right. \quad (13a,b)$$

$$m^* = \int_0^{H_T} m(H) \cdot \varphi(H) dH \quad ; \quad L^* = \int_0^{H_T} m(H) \cdot \varphi^2(H) dH \quad (14a,b)$$

If an idealised continuous model –whose number of degrees of freedom tends to be infinite– instead of a discrete one is assumed, as shown in Figure 26c, the expressions for m^* and L^* are integral operations (see Equation (14a) and (14b)). In the case of a constant distribution of the masses –constant density in the

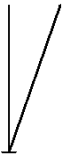
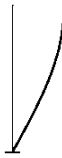
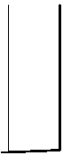
continuous model—, the new expressions (see Equation (15)) can be related to areas, as shown in Figure 26c.

$$\begin{cases} m^* = \frac{M}{H_T} \int_0^{H_T} \varphi(H) dH \\ L^* = \frac{M}{H_T} \int_0^{H_T} \varphi^2(H) dH \end{cases}, \quad \text{if } m(H) \equiv \text{cons} = \frac{M}{H_T} \quad (15)$$

These formulations can be applied to three typical, idealised, deformed shapes, represented by simple functions:

- Linear, typical of a frame with decreasing stiffness with the height:
 $\varphi(H) = H/H_T$
- Sinoidal, typical of a frame with constant stiffness in height:
 $\varphi(H) = \sin(\pi/2 \cdot H/H_T)$
- Constant, typical of a soft-storey frame: $\varphi(H) = 1$

Table 2: Dynamic parameters of three typical idealised deformed shapes: linear, sinusoidal and constant

			
m^*/M	0.50	0.64	$\rightarrow 1.0^-$
L^*/M	0.33	0.50	$\rightarrow 1.0^-$
Γ	1.50	1.27	$\rightarrow 1.0^+$
λ	0.75	0.81	$\rightarrow 1.0^-$

The obtained dynamic parameters corresponding to the three cases are presented in Table 2. L^* , m^* and λ increase with the concavity of the deformed shape, while Γ decreases, being 1.0 the limit for all of them. It is worth noting that this variability of the dynamic parameters is very important when switching from MDOF to SDOF, as briefly pointed in 1.2.1.1. In fact, m^* and Γ —the factors to be applied in the transformation— must be consistent with the origin of each pushover curve, given that usually more than one load pattern is used, being in

each case the deformed shape different. Thus, it is not possible to transform into SDOF all the pushover curves of a structure by using the same dynamic factors.

Moreover, if the pushover curve is obtained by applying a full-adaptive methodology, these changing values may be used also for the transformation of the curve into ADRS (Mohtashami and Shooshtari, 2013). Thus, for each point of the pushover curve, different values of Γ and λ for the abscissa and ordinate, respectively, may be taken. In Figure 27, three different capacity curves obtained from the same pushover curve are shown:

- the first one (red), using the dynamic properties corresponding to a sinusoidal deformed shape (see Table 2), aimed at representing the elastic initial properties, as usual;
- the second one (blue), using the dynamic properties corresponding to a constant deformed shape (see Table 2), aimed at representing the properties at the last step of a performance characterised by a collapse mechanism of soft ground storey, intended to be a lower bound for the spectral acceleration capacity;
- the third one (black), using the “adaptive” dynamic properties at each step, intended to represent kind of “real” behaviour.

The “adaptive” CC fits in its beginning with the first curve and converges to the second one in its end. It is worth noting that the effective periods for the three curves are different, so the comparison of the capacities depends also on the corresponding spectral demands.

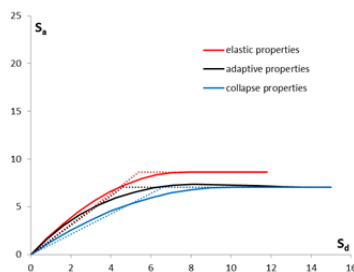


Figure 27: Three variants of CC obtained from the same pushover curve by assuming different dynamic properties

1.2.1.5 Capacity curve of infilled frames

In this case a multilinearisation is required. Conceptually, the pushover curve can be seen as an addition of the curves corresponding to the bare frame and to the infills. The last would be again a combination of backbones corresponding to each single panel; those backbones can be assumed as trilinear. Theoretically, could be possible to contemplate the possibility of obtaining the global multilinear curve as a superposition of the multilinear curves corresponding to the bare frame and infills. But it is impossible to obtain the infills curve as an equivalent trilinear one, unless the global mechanism of the infilled frame is a simple n-storey mechanism and all the infills belonging to them are similar.

The usual procedure is to assume a quadrilinear curve (Dolšek and Fajfar, 2004a):

- the first branch represents both the initial elastic behaviour of infills and bare frame and the post-cracking behaviour of the infills and maybe also of the bare frame;
- the second horizontal branch represents yielding of the infills at the maximum strength of the ensemble;
- the third part represents the strength degradation of the infills;
- the fourth part represents the after-degradation behaviour, in which the infills only contribute with its residual strength.

The multilinearisation procedure would be (see Figure 28a):

- Define the horizontal branch as passing through the maximum strength of the curve (F_{max}).
- Obtain the slope of the first branch (effective stiffness, $K_{w,eff}$) by equalise the misfit areas above and below until the maximum strength point.
- Define the last horizontal branch as passing through the maximum strength of the bare frame accounting with the residual contribution of the infills. If the bilinear curve of the RC frame is available, it is possible to obtain F_{min} by adding the residual contribution to the yielding capacity of the bare frame.
- Define the infills' collapse displacement, and so the end of the third branch by crossing that displacement with the fourth branch.

- Obtain the slope of the third branch (degrading stiffness) by equalising the misfit areas above and below from the maximum strength point until the infill's collapse point. It is possible to simplify the curve by assuming an instantaneous drop (infinite slope), see section 1.2.3.4.

Afterwards, it is possible to breakdown the quadrilinear curve into its components: the bilinear curve of the bare RC frame and an equivalent theoretical trilinear curve of the infills (see Figure 28b). Once obtained the quadrilinear curve, some parameters representing characteristic relations can be defined:

- The degradation of strength (F_3/F_1), ranging typically from 0.5 to 0.75 and suitable to reach 0.25 or 1.00 for sub-standard or capacity-designed buildings (Dolšek and Fajfar, 2004a).
- Available ductility up to the beginning of the degradation of the infills (D_2/D_1), estimated to range between 1.5 and 2.5 (Dolšek and Fajfar, 2004a). For Mediterranean buildings designed only to gravity loads, some assessment studies available in literature (Ricci et al., 2011b; Verderame et al., 2013) suggest values around 2.5.
- Available ductility up to the end of the infills degradation (D_3/D_1), whose uncertainty is much higher than for the precedent parameters. In Dolšek and Fajfar (2004a), it is considered to range between 2.0 and 7.0; however, its influence is not relevant (see section 1.2.3.4).

Finally, in order to transform it to the ADRS format, it is worth noting that both Γ and m^* should be referred to the infilled frame, not to the bare RC frame.

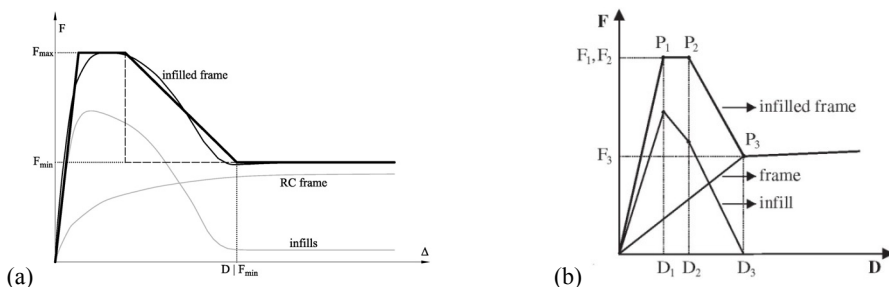


Figure 28: Multilinearisation of capacity curve of infilled frames (a) and its conceptual breakdown into their two components (b, from Dolšek and Fajfar, 2004a)

1.2.2 Period of the building

In general, slopes in the F- Δ format, represent stiffness, which is the same for the MDOF and SDOF system. Each stiffness can be associated with a value of the fundamental period of the equivalent SDOF through the expression $T=2\pi(m^*/K^*)^{0.5}$. Different stiffnesses and corresponding periods can be defined (see Figure 29a):

- Elastic stiffness (K_{el}): Corresponding to the non-damaged structure; is the slope of the tangent line at the initial point of the curve.
- Effective stiffness (K_{eff}): Corresponding to the slope of the first equivalent elastic branch of the bilinear capacity curve.
- Tangent stiffness (K_{tan}): Corresponding to the slope of the tangent line in any point of the capacity curve.
- Damaged stiffness (K_{dam}): Corresponding to the damaged structure; is the slope of the tangent line at the initial point of a reload branch.
- Secant stiffness (K_{sec}): Corresponding to the slope of a line matching the origin with any point of the curve.

Some vulnerability approaches, as FAST, are based in the proposal of a capacity curve attending to the general building properties. Hence, it is necessary to know the common values for the effective period T_{eff} of the structure, which sometimes is obtained as function of the real elastic one T_{el} , or the secant period T_{sec} if the approach uses a direct-displacement framework. Also, aimed at defining the code-based maximum capacity of the building through a simulated design procedure, it is necessary to know the period considered in the design phase.

One of the main differences between seismic design in comparison with the non-seismic one, i.e. design only to gravitational or wind loads, is that seismic global demand (forces or displacements) highly depends on the structural solution of the building. The spectral acceleration of design depends on the period of the structure, which is inversely proportional to the global stiffness; it usually turns the design sequence into an iterative procedure of trial-error. For non-seismic design, the global action is independent on the structural solution (except for self-weight); the only influence is that the local distribution of stiffness can modify the distribution of the action by “attracting” forces to the stiffest members, which seldom makes design requiring iterations.

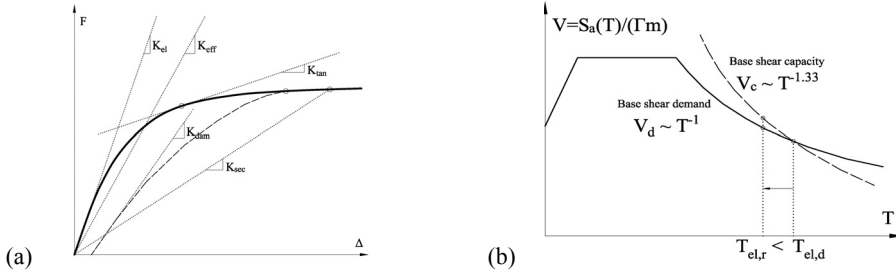


Figure 29: Definition of different types of stiffnesses (a) and relationship between capacity and demand associated to changes in the global stiffness (b)

The acceleration response spectra of most codes show four different parts, proportional to T^1 , T^0 , T^{-1} and T^{-2} , being the second and third parts those corresponding to the usual range of periods. Thus, the demand is usually independent or inversely proportional to the period, which means that, in a middle of the design procedure, assuming that the masses and the modal shape remains constant, an increasing of the section of the members leads to an increase of the demand. It is possible to assume, in a very general, simplified and approximate way[†], that such an increasing of the general stiffness leads to an increasing of the strength capacity which is higher than that of the demand (see Figure 29b).

The last can be also applied to the relationship between the real capacity of the buildings in comparison with the design assumptions. As briefly introduced in section 1.2.1.3, the equivalent demand experimented by a building during an

[†] This approach is based in direct proportionality (\sim) assumptions. Considering pure shear-type frame with constant participant mass ($m^* \Gamma$) and ductility, similar storey masses, stiffnesses and heights, homogeneous distribution of stiffness in plan, linear modal shape, negligible influence of the axial load in vertical elements (conservatively) and constant reinforcement ratio of members, it is possible to express both base shear demand (V_d) and capacity (V_c) as a function of the period T . On one hand, $V_d \sim S_d(T)$ and $S_d(T) \sim T^{-1}$ or I , assuming that $T \leq T_D$; then $V_d \sim (T^{-1}$ or I). On the other hand, $V_c \sim M_c \sim \Sigma h^2$, and $h^3 \sim I \sim k$, being $\Sigma k \sim K \sim T^{-2}$, so $V_c \sim T^{4/3}$. Thus, $V_c/V_d \sim (T^{4/3}$ or $T^{1/3})$, which means that the global safety factor is inversely proportional to the period T . $S_d(T)$, T_D , M_c , h , I , k , K are: spectral acceleration, corner period of the end of the constant-velocity branch of the response spectrum, base moment capacity, hypothetical height of the section of the vertical structural elements, inertia of the elements, stiffness of the elements and global stiffness of the frame, respectively.

earthquake is defined by that corresponding to its effective period. During a seismic event, the building stiffness decrease progressively in the same proportion as the damage increase; thus, the progressive values of the fundamental period of the damage structure (T_{dam}) are higher; this phenomenon is known as “period elongation”. Hence, this period elongation leads to lower seismic demands at each instant of time. The only way to consider a single global seismic demand is to assume that the whole process can be represented by a unique value of effective period (T_{eff}). Being rigorous, this value also depends on the level of performance, but it is possible to consider it independent.

The problem is that it is not easy to predict T_{eff} from T_{el} . That is why codes suggest using T_{el} in the design phase, assuming that the difference between the demand corresponding to both periods is theoretically included in the definition of the behaviour factor q through the contribution R_D . This issue is directly related also to the overstrength factor R_S , as explained in the point B6 of section 1.2.1.3, which refers to the strength provided by the structural elements not considered in the design (e.g. stairs, small shear walls or slabs). If the elastic period is obtained from a physical model –instead of using pre-established approximate formulations— which does not include the stiffness of some of those elements, or even it is obtained by considering the cracked stiffness of the elements (50% of the elastic one, as suggested by EC8) without adding the stiffness of the nodes, the real T_{el} will be lower than that of the model. Hence, the T_{eff} will be closer to the T_{el} considered in the design, resulting in a decrease of R_D . But this decrease, may be less relevant than the increase of the overstrength R_S provided by those elements, always neglecting local effects (see Figure 29b). Anyway, this “compensation” of effects does not make sense if a pre-established approximate formula for elastic period is used and also some elements are not considered as structural; in this case, the final safety factor may be higher. Relations between the assumed period and the physical model used in the phase of design with respect to the resulting overstrength sources are shown in Table 3, without considering any variation of the stiffness of the elements.

In Figure 30, some examples of the performances of the structures corresponding to the four possible combinations of choices are plotted. Different parameters are shown: elastic stiffness (K_e) and elastic base shear (V_e)

corresponding to the period of design; base shear of design (V_d); effective stiffness (K_{eff}); and yielding strength (V_y) obtained at the end of the hypothetical design, assumed approximately that the stiffness of the resulting structure is proportional to the base shear capacity.

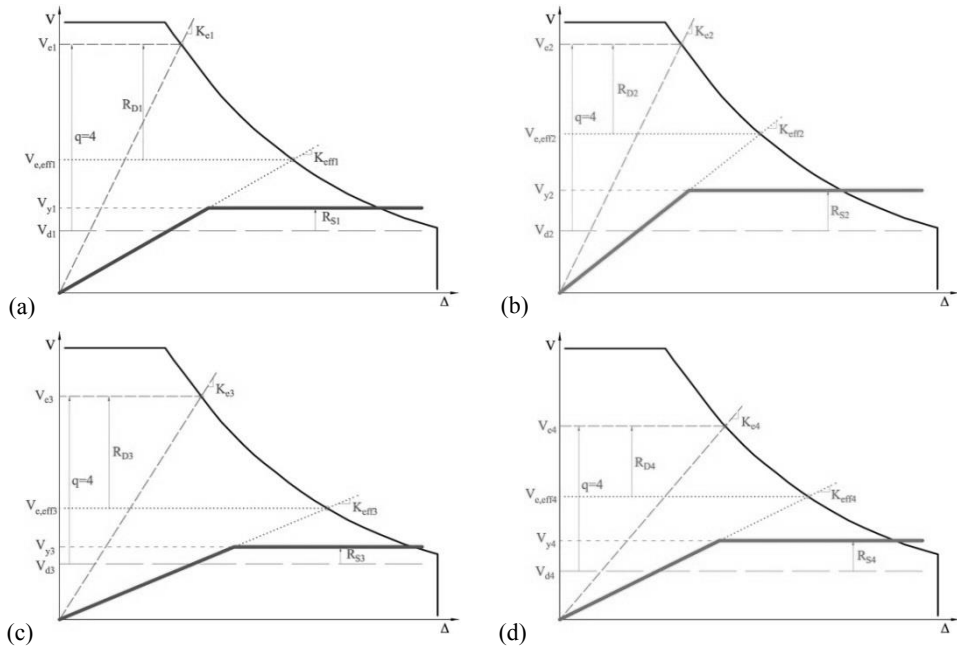


Figure 30: Examples of performances of structures corresponding to the four possible combinations of choices of design: period from code + model with (a) and without (b) stairs; period from physical model + model with (c) and without (d) stairs

Nevertheless, the strategy of neglecting elements in the design model undermines the efforts of the designer and the intention of design codes to control the structural performance (Fardis, 2009). It is very significant for infilled buildings, as most of the codes suggest considering masonry panels as non-structural. This assumption involve consistently, other than the renounce to the initial strength and stiffness provided by the infills, that the elastic period considered in the design is that corresponding to the bare frame.

Table 3: Relation between the choices of design and the overstrength factors and effective period of the resulting structures

Choices of design		R_S	R_D	T_{eff}
Period of design	from code		↑	↓
	from model		↓	↓
Physical model	with stairs and others	↓		↑
	without stairs and others	↑		↑

Thus, it may be globally conservative to design with a model that does not include certain elements that do not affect seriously to the modal behaviour and to the global distribution of the seismic action between the elements. However, many codes apply an upper bound to the period of vibration, in order to provide a base shear not lower than the 85% of that resulting from using a simplified formulation for the period; the difference between base shears is usually higher than 15% (Crowley and Pinho, 2010).

The way in which the elastic period of the bare frame is obtained in the design phase depends on the type of analysis. Former seismic codes only provided the equivalent static method; over time, the linear dynamic analysis (also called modal spectral response analysis) has been included in the codes, and most of modern current codes also allow the use of the nonlinear dynamic one. All of them belong to the force-based framework; in fact, for linear dynamic one, although it is based in the modal superposition of displacement demands, the design is carried out with the forces inferred from these displacements. The considerations of the period in the different methodologies of analysis are presented herein:

- Equivalent static linear analysis: In this method it is necessary to use an approximate elastic period obtained through simplified formulations provided by the codes (see section 1.2.2.1) based in global geometric properties, like the height or number of storeys. Then, the global demand is obtained and assigned to each structural element by pre-defining the first mode displacement shape or the force pattern. Aimed at providing a conservative approach, this pre-established elastic period must be underestimate. Some codes also allow using the Rayleigh method for seeking out the period (see Equation (16), being m , k , ϕ , i , n and h the storey masses, stiffness and amplitudes, the storey level, the number of storeys

and the interstorey height, respectively). This method, based in the principle of conservation of energy, provides the periods of vibration of a MDOF system by assuming, other than the distribution of masses: (i) a modal shape of forces or displacements, and, which is more relevant, (ii) a distribution of stiffnesses across the structure. The last makes this procedure hard to apply without much iteration, unless the dimensions (stiffness) of the structural members are fixed previously due to other reasons, e.g. shear walls in staircases or elevators.

$$T_i = 2\pi \sqrt{\frac{\sum m_i \phi_i^2}{\sum K_i (\phi_i - \phi_{i-1})^2}} \Rightarrow T = \sqrt{\frac{m}{K}} (4n + 2) \text{ if } \begin{cases} m_1 = \dots = m_n = m \\ K_1 = \dots = K_n = K \\ h_1 = \dots = h_n \\ F_i = \frac{i}{n} F_n \end{cases} \quad (16)$$

- Linear dynamic analysis: In this method, the elastic period is obtained through an eigenvalue analysis, which changes every time the analysis is carried out in an iterative process. The pre-eminence of this approach is related to the use of specific computer software which allows repeating the process within a reasonable time consuming.
- Nonlinear dynamic analysis: It may not be considered strictly a design process because, unless the previous two methods, in this case not only the dimensions of the structural members but also the reinforcement must be known. The period of the structure is actualised in each step of the analysis depending of the changes in the stiffness matrix, but it has no influence in the design, because it must have been done previously.

In the following, proposed expressions and common values for fundamental period of RC bare and infilled frames. Most of them are based on numerical regressions of experimental data, and depend on basic geometric parameters such as building height (H) or number of storeys (n).

1.2.2.1 Period of bare frames

In order to provide approximate simplified formulations for the elastic period of bare RC MRF, experimental measurement on buildings have been carried out

for the last four decades. Relevant proposed expressions (Table 4 and Figure 31) are almost all of them in the form $T=\alpha H_T^\beta$, i.e. depending only on the total height of the building (H_T). This expression is based on Rayleigh’s method assuming: (i) linear pattern of forces; (ii) base shear proportional to $T^{-2/3}$; and (iii) linear lateral displacements shape (Goel and Chopra, 1997). Other typical expressions are linear functions depending on the number of storeys n . Some authors offer both upper and lower bound expressions, intended to be applied conservatively within a displacement- or force-based methodology, respectively.

Table 4: Proposed empirical-based formulations for the fundamental period of bare RC MRF in the form $T_{el}=\alpha H_T^\beta$ (* adapted from the original formula $T=\gamma n$ assuming $h=3\text{m}$)

Author or code	α	β
Gates and Foth (1978), ATC3-06 (ATC, 1978)	0.062	0.75
SEAOC-88 (1988)	0.075	0.75
Bertero et al. (1988)	0.085-0.097	0.75
NEHRP (FEMA, 1994)*	0.033	1.00
NCSR-94 (CDNS, 1994)*	0.030	1.00
Goel and Chopra (1997)	0.047-(0.053)-0.068	0.90

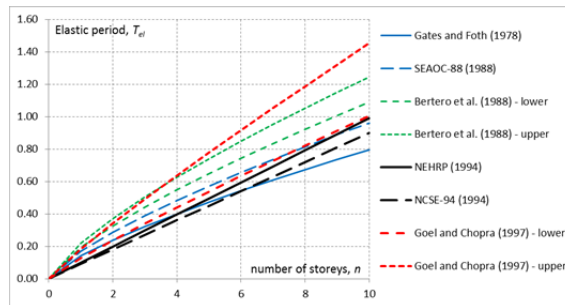


Figure 31: Proposed empirical-based formulations for the fundamental period of bare RC MRF, assuming constant interstorey height $h=3\text{m}$

Most of these expressions have been inferred from measurements carried out during significant earthquakes. Either if the ground motion is real or artificial, and no matter if the intensity of the motion is very low (“ambient noise”) or higher (earthquake), there are two main methodologies for monitoring the instantaneous period or its evolution during an excitation (Trifunac et al., 2001b):

- Fourier analysis: In this case the building is used as a “filter” of frequencies. It is obtained a Fourier spectra corresponding to measurements between top and base of the building, showing which frequencies belonging to the input signal are more predominant in the response of the structure. It is possible to apply this method to the whole event or to apply it to several “windows” of time. In the first case, the “peaks” frequencies correspond to: first modes of vibration, if the building remains in the elastic phase; or to the different periods assumed by the building in its “elongation” process, if it goes into the inelastic behaviour (see Figure 32a). In the case of subdividing in “windows” of time, the evolution of the period can be properly monitored.
- “Zero crossings”: This technique consist on interpreting the history of relative acceleration or displacement between top and ground floor in such a way that the instantaneous period can be associated to the double of the time between two consecutive “zero crossings”, i.e. the points where the function crosses the abscissa (see Figure 32c).

In Bertero et al. (1988), both methods are used to find α and β that best fits with the experimental results. In Figure 32c, period elongation is shown: a previous elastic period of the building with non-structural elements obtained by an ambient noise evaluation; then, a period which the authors consider that corresponds to the elastic one of the bare frame, given that at this point the RC frame does not have yielded yet and all the non-structural elements have collapsed totally; and bigger periods corresponding to diverse steps of structure damage.

It is important to remark that almost all of the expressions of the fundamental period of bare frames were inferred from the behaviour of buildings in America, whose non-structural elements consist on plaster board internal walls and glass curtain walls in the facades; the participation of these components was minimal compared to the RC frame (Bendimerad et al., 1991). In Mediterranean infilled RC MRF, the influence of masonry infills panels is much higher, being it difficult to individuate the period of the bare frame from a monitoring of a building, given that the structural and non-structural damage are often overlapped. Studies done in Mediterranean cities show the effect of period elongation depending on the damage level (structural and non-structural) attained by the building (see Figure 33).

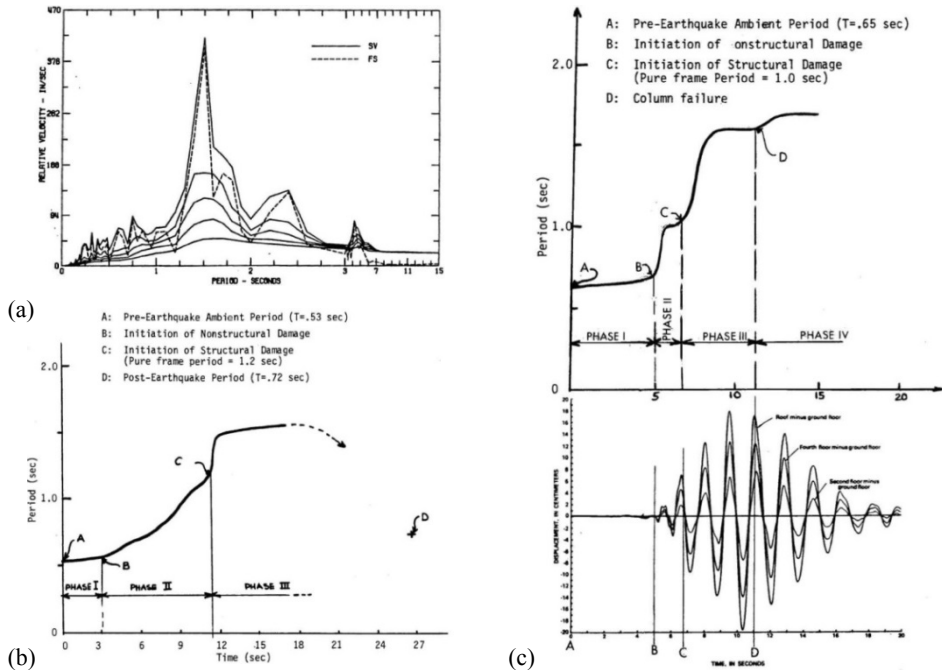


Figure 32: From a case-study building during the San Fernando (1971) earthquake: Fourier spectra (dashed line) for the whole time history (a), evolution of the period (b); and “zero-crossings” method (c) (from Bertero et al., 1988)

The evaluation of the period by assessing the performance in the middle of an earthquake has been a controversial issue. These studies are intended to find out the evolution of the fundamental period at each stage of the building, i.e. the “damaged period” T_{dam} . However, great differences are observed between the last value of T_{dam} and a post-earthquake ambient measurement of the building, whose damage level is the same; the difference can reach the 50%. Trifunac (1999) opines that this is a consequence of the soil-structure interaction. He argues that in all these studies, what is really measured in the middle of the earthquakes is the “apparent” period of the whole system, which includes the influence of the soil lateral compression and the rocking rotation of the building as a rigid-body, which leads to values of period much higher than the “fix-based” period (see Figure 35a).

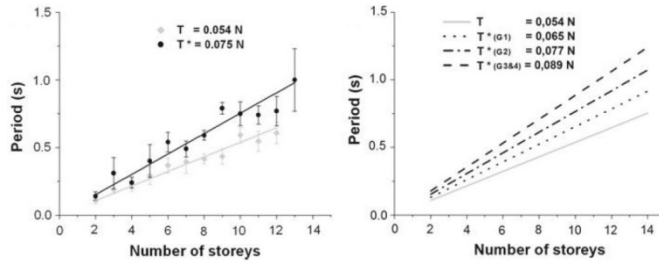


Figure 33: Different expressions for the elastic (grey line) and damaged (black line) period of Mula and Lorca (Spain) infilled frames from ambient noise analysis before and after different earthquakes (from Vidal et al., 2013)

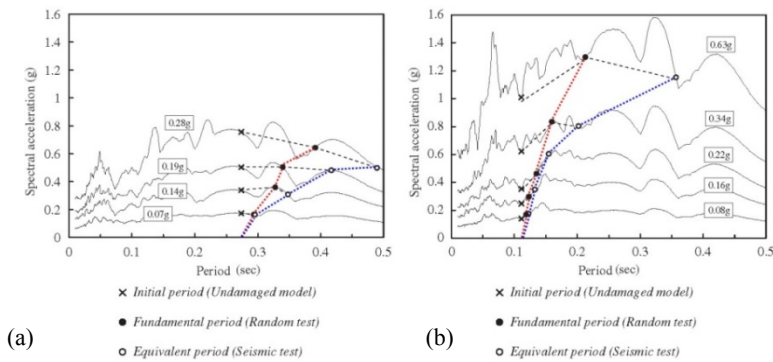


Figure 34: “Elongation” of “fundamental” (red dotted line) and “equivalent” (blue dotted line) periods of bare (a) and infilled (b) frames during such PGA incremental analysis (from Dolce et al., 2005)

However, those differences between “apparent” and post-excitation periods can be observed also in experimental shaking table tests with no influence of soil-structure interaction, as in Dolce et al. (2005). In this work, several tests with incremental PGA are carried out on bare and infilled RC frames. Period is monitored during each seismic test and also after that, with an “ambient” excitation (very low motion). Results show (Figure 34) that the difference between the so-called “equivalent” period (during shaking) and the “fundamental” period (T_{dam}) are important. In author’s opinion, this is due to the closing of cracks in RC and to the friction resistance in masonry panels. Moreover, the affirmation of the authors

about the utility of the “equivalent” period for the application of displacement-based design methods, may suggest that these periods might be “pseudo-secant” ones, perhaps more related to the slope of the hysteretic branches than to the damage period, corresponding to a hypothetical reload branch.

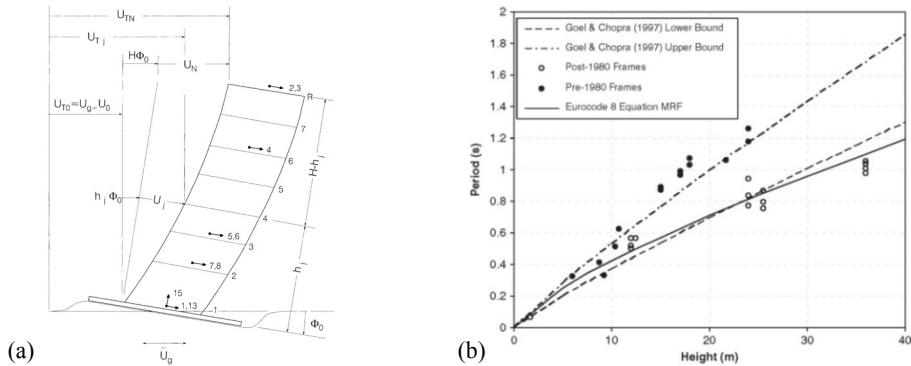


Figure 35: Different contributions to the absolute displacement and “apparent” period history of a building: base translation and rocking, and building deformation (a, from Trifunac et al., 2001a); and analytical periods of gross stiffness European bare MRF in comparison with different experimental formulations (b, from Crowley and Pinho, 2010)

On the other hand, some European studies (as Crowley and Pinho (2004)) show the difference in the fundamental period between structures designed before and after modern codes appeared (referred in this work as sub-standard and capacity-designed structures, respectively). Sub-standard structures were designed with the equivalent static method using a code-based period lower than the period obtained from an eigenvalue of the resulting structure. However, this increasing of the stiffness in old buildings is clearly overcome by the prescriptions of new codes, mainly the capacity design principles and the interstorey drift restrictions, resulting in a much higher stiffness for new buildings. As seen in Figure 35b, the equation proposed by EC8 fits quite well with new buildings.

Other analytical works (Verderame et al., 2010b) also focus into the differences between the periods obtained from eigenvalue analysis of different mechanical models of sub-standard buildings. As explained at the beginning of this

section, often there are significant differences between the stiffness of the model and the real stiffness of the bare frame. In Figure 36, the period of these different models are compared with the EC8 formula; it can be seen that this formula would correspond to higher levels of PGA of design. Also, it is shown the high influence of not having into account the stiffness of the stair or the joists in the transverse direction, when there are not beams in the two directions.

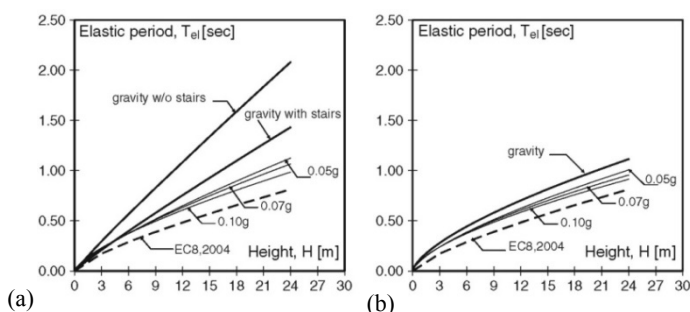


Figure 36: Comparison of analytical-based expressions for elastic period of representative sub-standard European buildings with EC8 formulation, for a transversal direction without beams (a) and for the longitudinal direction with beams (b) (from Verderame et al., 2010b)

1.2.2.2 Period of uniformly infilled frames

The high influence of the masonry infills on the initial stiffness of the RC frames is widely addressed in section 1.3. Several in-situ measurements of the elastic period of uniformly infilled RC MRF buildings of European cities have been carried out; the resulting formulations, directly proportional to the number of storeys n , are resumed in Table 5 and Figure 37a.

On the other hand, some analytical parametric studies have been carried out (see Table 6 and Figure 37b). Only the results in (Ricci et al., 2011c) show fine agreement with the experimental ones; the other considered works provide values of period 2 or 3 times higher. That work offer diverse expressions depending on the type of infills, the consideration of openings or the cracking of the panels. For the most reliable situation (i.e. the elastic initial situation, without cracking of the panels, and presence of openings) the authors propose a formulation whose form is similar to the one proposed in (Goel and Chopra, 1998) for RC SW buildings (see

Equation (17)). It depends not only on the height of the building (H_T) but also on the ratio of the effective infills area in plan to the building area (ρ_w , see Equation (28)). Other works (Crowley and Pinho, 2010) suggest that the formula for “other structures” in Eurocode 8, using $C_T=0.05$, show a good agreement with the analytical results for uniformly infilled frames (see Figure 38a).

$$T_{el,inf} = 0.0023 \frac{H_T}{\sqrt{\rho_w}} \quad (17)$$

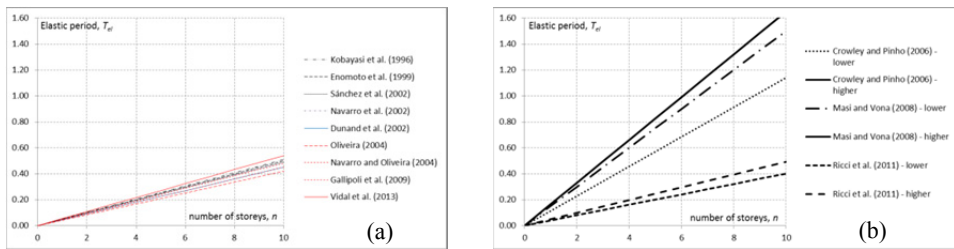


Figure 37: Proposed empirical-based (a) and numerical-based (b) formulations for the elastic fundamental period of infilled frames, assuming constant $h=3m$

Table 5: Proposed empirical-based formulations for the fundamental period of infilled RC MRF in the form $T_{el,inf}=\gamma n$

Author	γ
Kobayashi et al (1996)	0.051
Enomoto et al. (1999)	0.050
Sánchez et al. (2002)	0.049
Navarro et al. (2002)	0.049
Dunand et al. (2002)	0.045
Oliveira (2004)	0.042
Navarro and Oliveira (2004)	0.045
Gallipoli et al. (2009)	0.048
Vidal et al. (2013)	0.054

Table 6: Proposed numerical-based formulations for the fundamental period of infilled RC MRF in the form $T_{el,inf}=\gamma n$

Author	γ
Crowley and Pinho (2006)	0.114-0.165
Masi and Vona (2008)	0.150-0.165
Ricci et al. (2011c)	0.040-0.049

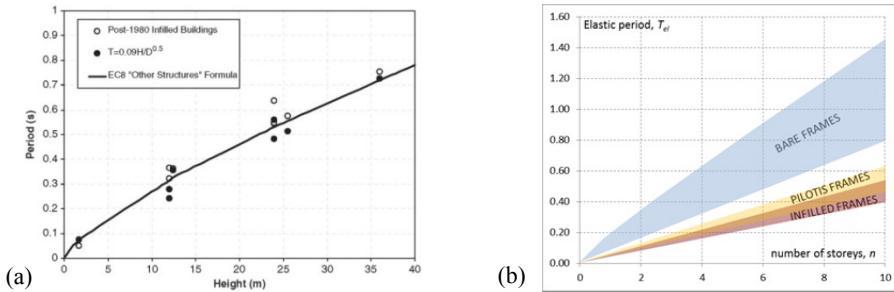


Figure 38: Comparison of analytical results for elastic period of modern infilled frames with the EC8 formula for “other structures” (a, from Crowley and Pinho, 2010); and approximate ranges of the proposed experimental or numerical expressions for fundamental period of bare, pilotis and infilled frames (b)

1.2.2.3 *Period of pilotis frames*

Unfortunately, in literature there are not similar experimental or analytical parametric studies than for bare or uniformly infilled frames, only single analytical case studies can be found. In Kappos et al. (2000), periods of a planar bare 10-storey RC MRF designed to EC8 –without regarding to the specific rules of masonry infills— are evaluated for three situations: bare, fully infilled and pilotis, considering weak or strong masonry and thin or thick panels. Results show that the period of the pilotis frame with respect to the uniformly infilled frame ranges between 1.5% and 11.9% higher. Similar result (8.3% higher) is obtained by the same authors in Dymiotis et al. (2001). Lower increments are obtained in Masi and Vona (2008): only 2.0% higher for pilotis than for fully infilled frames.

1.2.2.4 *Effective vs. elastic period*

In Figure 38b, approximate ranges of the real elastic period of bare, pilotis and fully infilled frames are represented. Knowledge about the elastic period of bare frames allow to an estimation of their maximum code-based capacities. However, aimed at defining of approximate capacity curves, the slope of the first branch is the effective period, T_{eff} . Unfortunately, in literature there are not extensive works furnishing any relationship between T_{el} and T_{eff} for those frames.

An amplification factor κ can be define in the form $T_{el}=\kappa \cdot T_{eff}$. Regarding bare frames, results of the case studies analysed in section 3.6.3 (see Table 36) show

average values of $\kappa=2.2$. It is certainly very difficult to establish a narrow range for κ in the case of bare frames. However, it may be possible to point out that the more local is the mechanism of collapse of the frame (i.e. storey mechanism), the lower values of κ are obtained, as shown in Figure 39.

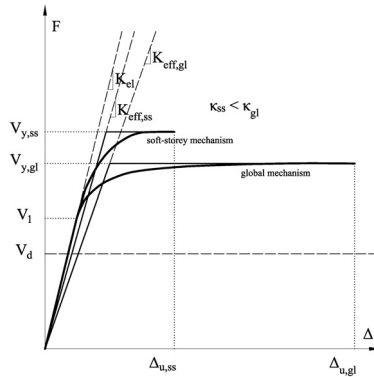


Figure 39: Typical CC and κ for soft-storey and global mechanisms of bare frames.

Table 7: Relationship between T_{el} and T_{eff} for some case studies of uniformly infilled frames (a) (from Verderame et al., 2013) and pilotis frames (b) (from Ricci et al., 2013), being GD and SD gravitational and seismic design, respectively

FULLY INFILLED		T_{el} [s]	T_{eff} [s]	κ	PILOTIS	T_{el} [s]	T_{eff} [s]	κ	
2-storey GD	x	0.082	0.109	1.33	4-storey GD	x	0.387	0.492	1.27
	y	0.106	0.144	1.36		y	0.542	0.680	1.25
4-storey GD	x	0.147	0.188	1.28	4-storey SD	x	0.324	0.485	1.49
	y	0.201	0.253	1.26		y	0.342	0.555	1.62
4-storey GD	x	0.220	0.268	1.22	8-storey GD	x	0.374	0.482	1.29
	y	0.307	0.344	1.12		y	0.551	0.666	1.21
					8-storey SD	x	0.481	0.688	1.43
						y	0.545	0.872	1.60
κ mean				1.26	κ mean				1.40

For uniformly infilled frames, κ has been calibrated on detailed analytical data (Verderame et al., 2013; Manfredi et al., 2013) showing values around 1.3; some of the values of the first reference are shown in Table 7. Regarding pilotis frames, single case studies analysed in Ricci et al. (2013) show values around 1.4.

1.2.3 Demand curves

For a given event, the demand curve changes depending on the inherent characteristics of the building in relation to the performance: damping and ductility. Design demand spectra resemble the collection of maximum values reached by the measured parameter during an event corresponding to a range of effective periods, and assuming constant damping and ductility. They represent the real demand experimented by the equivalent SDOF associated to the buildings.

Design demand spectrum is usually obtained from the elastic one by means of a reduction of their values, following diverse strategies explained in sections 1.2.3.3 and 1.2.3.4. The elastic demand spectrum is defined assuming a certain level of viscous damping for the structures, typically 5% of the critical one. However, other experimental studies (Oliveira and Navarro, 2010) show different values of viscous damping related to the fundamental period of the building. In Figure 40a, spectra corresponding to different damping coefficients are plotted.

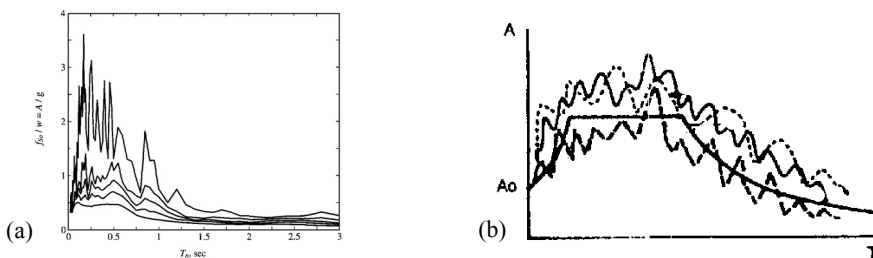


Figure 40: Normalised pseudo-acceleration response spectrum for El Centro ground motion for damping coefficients of 0, 2, 5, 10 and 20% (a, from Chopra, 1995), and example of smoothing of the media of many spectra (b)

For ADRS representation of demand, acceleration and displacement elastic spectra should be obtained, whether they proceed from accelerograms or from codes. Assuming that for low-damped elastic systems in the normal range of periods corresponding to buildings there is not energy dissipation –i.e., all the kinetic energy is transformed into deformation energy—, the acceleration spectrum (S_{ae}) can be approximated by the pseudo-acceleration one, which can be obtained from the displacement spectrum (S_{de}) as $S_{ae} = \omega^2 \cdot S_{de}$ (see Figure 41).

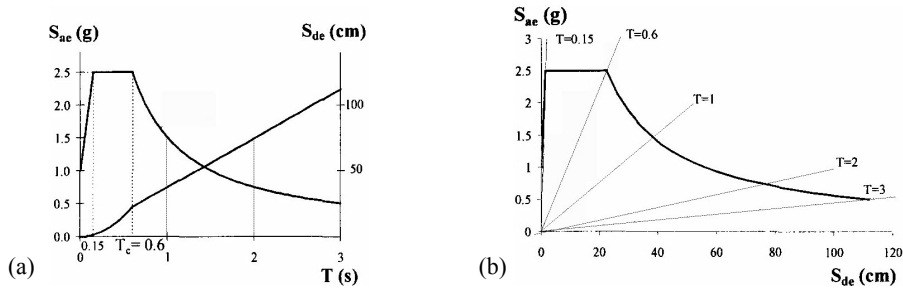


Figure 41: Example of 5%-damped elastic acceleration and displacement spectra (a) and combined in the ADRS format (b) (from Dolšek and Fajfar, 2000)

1.2.3.1 *Smoothed spectra*

Spectra can proceed from real or artificial earthquakes, presenting an irregular shape, or conversely can be design spectra as those proposed by seismic codes, presenting a simplified (smooth) shape. Sometimes it is necessary to convert an irregular spectrum into a smooth one. The irregular spectrum can correspond to a mean (or other fractile) spectrum from different sources (Figure 40b). The disadvantage of real irregular spectra is the higher variability of the demand with respect to little changes of the period, which is not advisable for such approximate approaches given the uncertainty in the period evaluation.

In Malhotra (2006), a simple procedure aimed at obtaining smoothed spectra from irregular ones is presented (Figure 42). It needs to be given the peak values of ground acceleration, velocity and displacement (PGA, PGV and PGD, respectively), and depending on the damping, different amplification factors for such three peak values are provided. Resulting spectra are divided in 7 branches:

- the first three branches, until T_2 , represent the constant-acceleration region;
- the fourth branch, between T_2 and T_3 , represent constant-velocity region;
- the last three branches represent the constant-displacement region.

Maximum values of spectral acceleration, velocity and displacement ($S_{a,max}$, $S_{V,max}$ and $S_{D,max}$, respectively) are obtained from the peak values of the signal (PGA, PGV and PGD, respectively) through such experimental-based amplification factors (α_A , α_V and α_D , respectively).

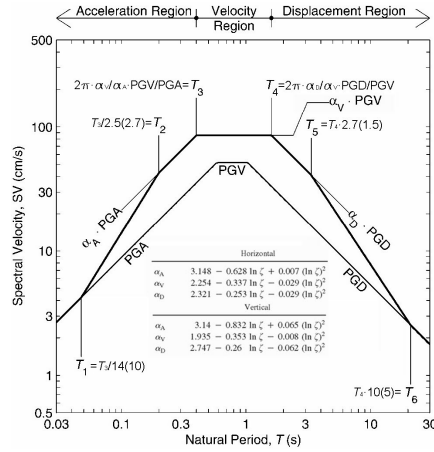


Figure 42: Construction of smooth response spectrum (from Malhotra, 2006)

1.2.3.2 Characteristic period

Most of analytical vulnerability methods ask for characteristic period (T_C) of the demand ground motion, defined as that dividing the constant-acceleration and constant-velocity branches of the corresponding spectrum (see Figure 43). This period is usually close to be that with maximum contribution to the signal, obtained by means of Fourier decomposition, because T_C is close to be the period corresponding to the attainment of the maximum spectral velocity ($S_{V,max}$). In fact, in Jennings (1974) it is stated that, given a ground motion, its 0%-damped velocity spectrum motion represents an upper limit for the Fourier spectrum of acceleration—which has the units of velocity—. Thus, approximately, the “peaks” (relative maximums) of both spectra may coincide for the same values of period, and the same can be guess for the 5%-damped velocity spectrum (see Figure 32).

In Equations (18a) and (18b), the expression proposed in Lam et al. (2000) for the definition of T_C and T_D are shown; they are consistent with the expressions shown in Figure 42. It is important to consider that, if response spectra from real accelerograms are used, different values for each direction would be obtained.

$$T_C = 2\pi \frac{S_{V,max}}{S_{a,max}} \quad ; \quad T_D = 2\pi \frac{S_{V,max}}{S_{D,max}} \quad (18a,b)$$

Depending on whether these expressions are applied to a real or smooth spectrum, T_C and T_D may be different, due to the lower value of $S_{a,max}$, $S_{V,max}$ and $S_{D,max}$ for the smooth spectra in comparison with the real one. Hence, depending on which reduction is larger, the periods for the smooth case will be higher or lower. In Figure 44, an example is shown in which the reduction of $S_{V,max}$ is larger than that of $S_{a,max}$, so T_C obtained from the smooth spectra is higher than that corresponding to the real spectra. In this work, response spectra from real accelerograms are used directly; the other possibility would be also feasible.

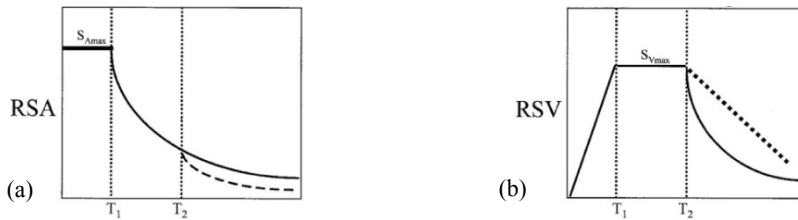


Figure 43: Acceleration (a) and velocity (b) response spectra, with the conceptual definition of T_C and T_D (T_1 and T_2 in the figure, respectively) (from Lam et al., 2000)

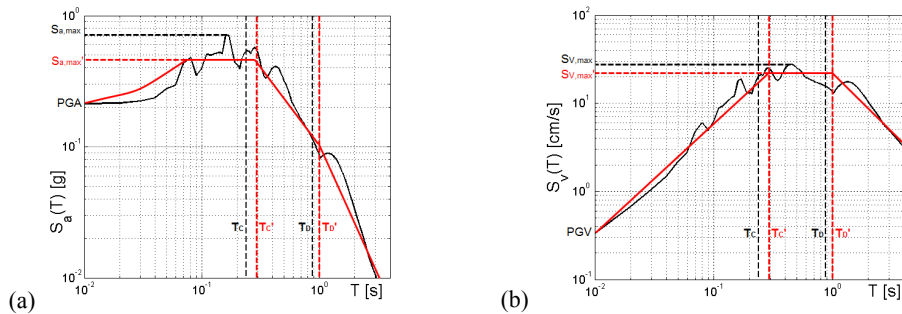


Figure 44: Analytical values of T_C and T_D obtained from the real (black) and smooth (red) acceleration (a) and velocity (b) response spectra

1.2.3.3 *Equivalent-damped elastic spectra*

Several methodologies about how to obtain real demand spectra by reducing values of the elastic one have been proposed. The main two methodologies are:

- The application of an equivalent, artificial, viscous damping (higher than the 5%) to the elastic spectra, in order to simulate the hysteretic energy dissipation ($\xi_{eq}-\mu$ relation).
- The use of inelastic spectra, obtained as a collection of points whose associated ductility is function of the corresponding effective period and strength of the structure ($R-\mu-T$ relation, see 1.2.3.4)

The first solution was proposed in Freeman et al. (1975). Different relationships $\xi_{eq}-\mu$ are suggested depending on the structural typology and material (see Figure 45b). It might represent the addition of the viscous damping plus an equivalent hysteretic damping that depends on the energy dissipated in the elastic phase (E_{So}) and in the hysteretic cycles (E_D) see Figure 45a. In Chopra (1995), the proposed expression for the equivalent hysteretic damping is $(E_D/E_{So})/4\pi$.

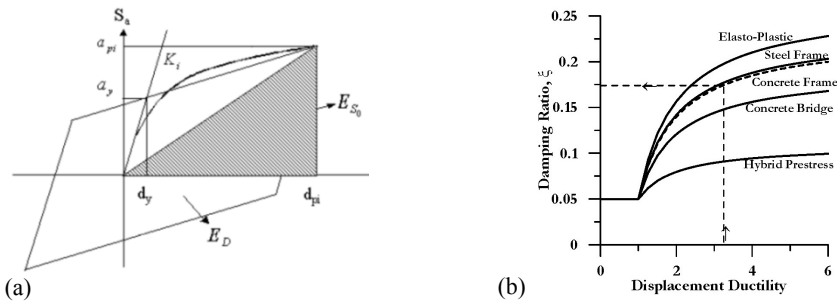


Figure 45: Elastic [E_{So}] and hysteretic [E_D] energy for obtaining equivalent hysteretic damping (a), and damping ratios for different cases (b, from Priestley et al., 2007)

The use of highly damped elastic spectra for the representation of the demand of an inelastic system, is controversial. In Krawinkler (1994), the author asserts that “there is no physical principle that justifies the existence of a stable relationship between the hysteretic energy dissipation of the maximum excursion and equivalent viscous damping, particularly for highly inelastic systems”.

1.2.3.4 *Inelastic spectra: $R-\mu-T$ relations*

Real seismic demand may be represented by inelastic demand spectra. They correspond to the demand experimented by equivalent elastic-plastic SDOF when

subjected to a given ground motion. Inelastic spectra can be of two types: constant-strength or constant-ductility, depending on the fixed parameter: R_μ or μ , respectively. In this section, R_μ is called R .

If not only the elastic spectra but the ground motion (real or not) is known, inelastic spectra can be obtained directly. Constant-strength spectrum can be easily obtained by assigning to each inelastic SDOF a maximum strength equal to the elastic demand strength divided by the selected R . Conversely, constant-ductility spectrum requires iteration (Chopra, 1995): for each inelastic SDOF, it is necessary to try with different values of R aimed at catching the selected μ . In Figure 46a, some constant-ductility spectra corresponding to a real earthquake are shown.

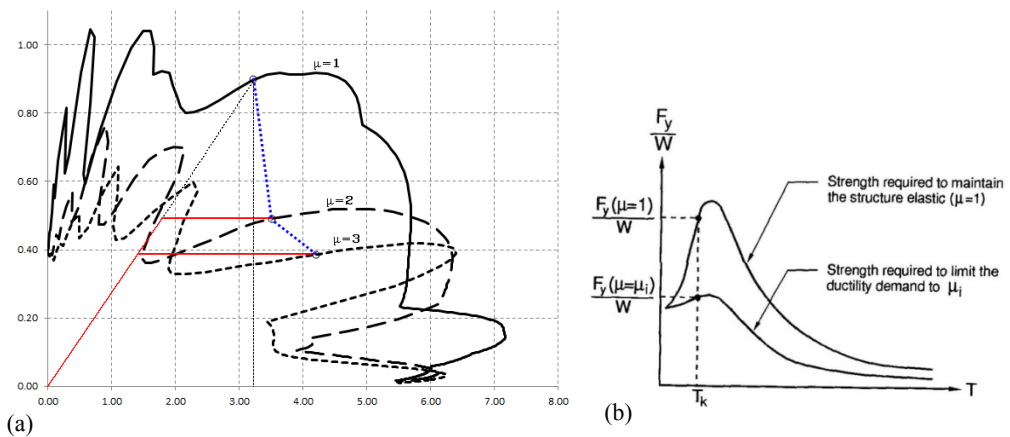


Figure 46: Constant-ductility spectra corresponding to the 2011 Lorca mainshock (N-S), and locus of equal performance—blue dotted line—for a given T_{eff} (a); and elastic and constant-ductility spectra (b, from Miranda and Bertero, 1994)

However, direct calculation is not always possible. If ground motion is not available, as for design purposes, it is impossible to obtain; also in assessment phase the direct method can be hard to use, as many inelastic spectra would be needed to cover the range of possible performances with enough accurateness.

Aimed at obtaining inelastic spectra from elastic ones, analytical expressions relating R_μ and μ for each period (R - μ - T relations) are needed. As explained in 1.2.1.3, the component R_μ of the behaviour factor provided by the codes come

from an estimation of the lateral strength of the structure that is required in order to limit the global ductility demand to a certain pre-determined value which results in the adequate control of local ductility demands (see Figure 46b).

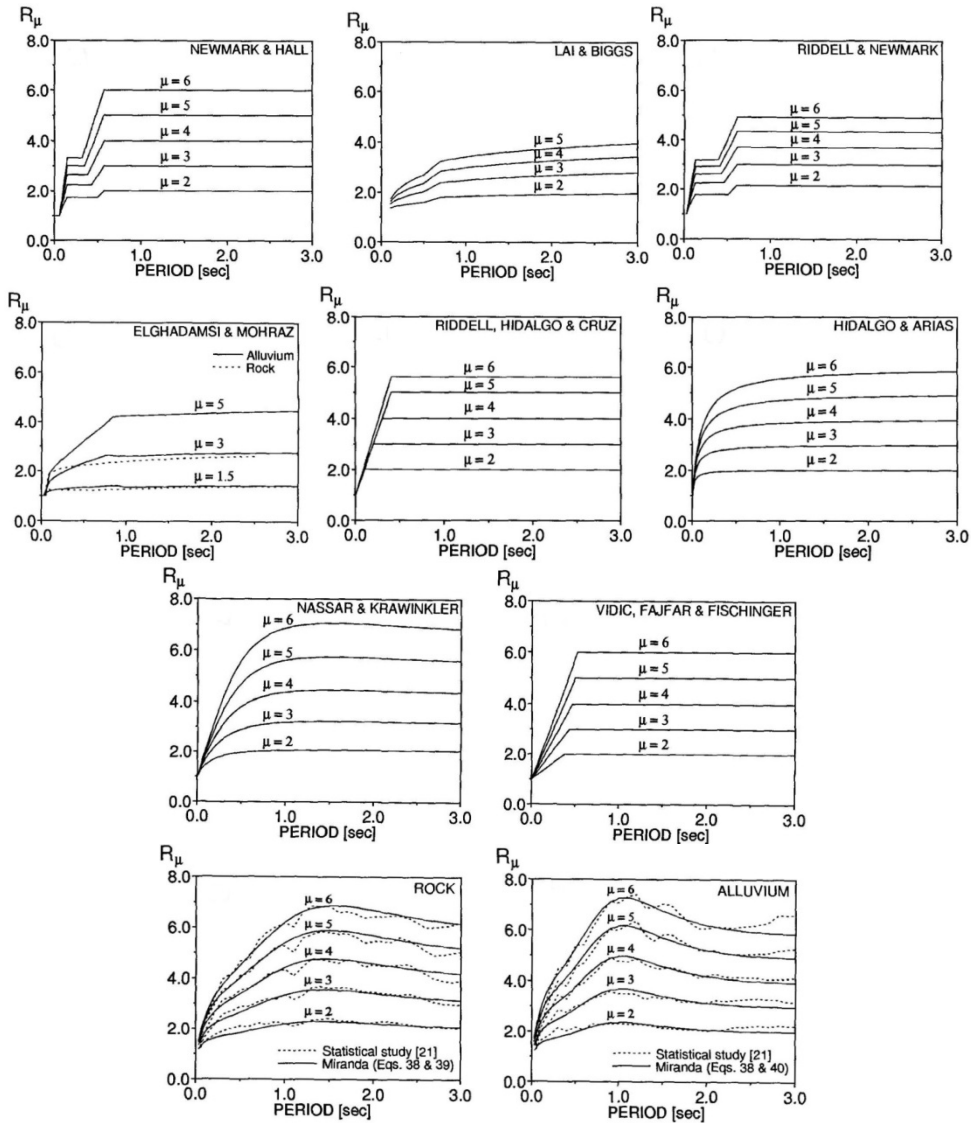


Figure 47: Different R - μ - T relations (from Miranda and Bertero, 1994)

In Miranda and Bertero (1994), an in-depth revision of the different expressions suggested in literature is presented; they are plotted in Figure 47 and compared in Figure 48. Most of them are obtained as regression analysis from case studies of real earthquakes. Usually, these expressions:

- are piecewise functions in the form $R=f(\mu)$ for each interval of T ;
- are divided in two branches: an increasing function up to the characteristic period of the ground motion (see section 1.2.3.2) and an approximately constant branch from this point forward;
- assume values of $R=1.0$ for very low periods and $R=\mu$ for medium and large periods (“equal displacement” principle).

The first formulation is proposed in Newmark and Hall (1973), being the expression for the low periods based in the conservation of energies. This work is slightly modified in Riddell and Newmark (1979) by including the damping influence. Lai and Biggs (1980) suggested a three-branched function with very low values. Similar values are obtained in Elghadamsi and Mohraz (1987), which is the first study considering the effect of soil conditions. Riddell et al. (1989) propose a simple bilinear function, while in Hidalgo and Arias (1990), a single expression for the whole period range is presented. In Nassar and Krawinkler (1991), sensitivity to epicentral distance, yield level, strain-hardening ratio and stiffness degradation is taken into account. Then, in Vidic et al. (1994), a very simple bilinear function is presented; and finally, more complex expressions having into account the local site conditions, magnitude and epicentral distance are developed in Miranda (1993), which is the only one showing $R>\mu$ for medium-long period range.

Among all those proposals, the relations provided in (Fajfar, 1999) – constituting a simplification of those presented in Vidic et al. (1994)— have achieved great divulgation, being included in the Annex B of EC8. Both works belong to a very relevant continuous research activity developed in the University of Ljubljana since the middle 80’s. In Equation (19a), the bilinear $R-\mu-T$ relation is expressed. The characteristic period T_0 is function of the ductility (see Equation (19b)), thus compelling to the use of iterations for the case of low periods. Despite that, the author suggests to assume, conservatively, an approximate value of corner period independent of the ductility (see Equation (19c)).

The expressions come from a statistical study of a stiffness-degrading system with 10% strain hardening and 5% mass-proportional damping, assuming a bilinear hysteretic model and damping proportional to the instantaneous stiffness. Minor influence of the magnitude of the strain hardening ratio and moderate influence of hysteretic behaviour and damping were observed; hence, simplified expressions are independent of those variables.

In Figure 49a and Figure 49b, differences between using the exact (bold line) or the simplified (fine line) expression of the corner period are shown. In Figure 49c, some constant-ductility and constant-strength inelastic spectra obtained with the simplified expression are shown. Dashed lines represent locus of equal-performance, being in this specific case rectilinear ones[†]. Nevertheless, this method loses feasibility when applied to some particular cases:

$$\mu = \begin{cases} (R-1)\frac{T_0}{T} + 1 & , \quad T \leq T_0 \\ R & , \quad T > T_0 \end{cases} ; \quad T_0 = 0.65 \cdot \mu^{0.3} \cdot T_c \leq T_c ; \quad T_0 \approx T_c \quad (19a,b,c)$$

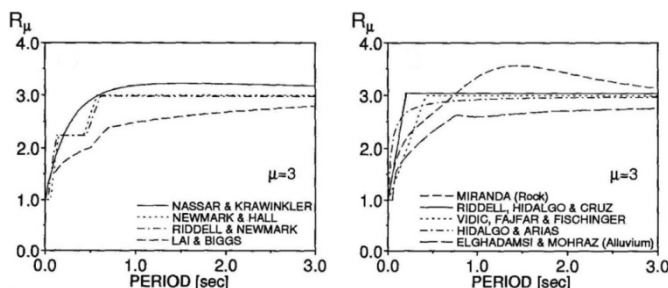


Figure 48: Comparison of R - μ - T relations for $\mu=3$ (from Miranda and Bertero, 1994)

[†] It is possible to express that curve as a relationship between $S_{ae}-S_a$ and S_d-S_{de} . Firstly, Equation (19a) is substituted into $S_d=S_{de} \cdot \mu/R$ so $(S_d-S_{de}) = S_{de} \cdot [(1-T_0/T)/R - (1-T_0/T)]$. Then, $(S_{ae}-S_a) = S_{ae}(1-R)$ so $S_{ae} = (S_{ae}-S_a) \cdot R/(R-1)$, which is substituted into $\omega^2 = g \cdot S_{ae}/S_{de}$ resulting in $S_{de} = g[T/(2\pi)]^2 \cdot R/(R-1) \cdot (S_{ae}-S_a)$. Finally, S_{de} is substituted into the expression of (S_d-S_{de}) resulting in $(S_d-S_{de}) = g[T/(2\pi)]^2 \cdot (T_0/T-1) \cdot (S_{ae}-S_a)$, which is a linear function whose negative slope $m(T) = (2\pi/T)^2/[g \cdot (1-T_0/T)]$ —expressed in the ADRS format—reaches a relative minimum for $T=T_0/2$, the value for which $m'(T)=0$.

- For near-fault, impulsive type of ground motions, it has been not statistically tested
- For long- and very long-period range it may be not conservative.
- For system with low strength (less than the 20% of the elastic demand), it also may be not conservative.
- The case of extremely narrow-band ground motions, like those recorded on very soft soil deposits, needs special consideration.
- The method is feasible when applied to smooth spectra that follow the typical shape. Elastic spectra for specific accelerograms or spectra which deviate from the typical shape should not be combined with smooth R_μ spectra because they are not compatible.

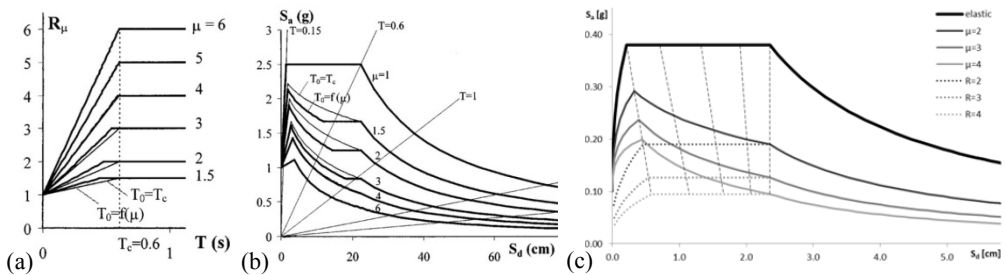


Figure 49: R - μ - T relation (a) and constant-ductility spectra (b) as proposed in Fajfar (1999), and some constant- μ and constant- R inelastic spectra obtained with such expressions (c)

All the previous is referred to bare frames. In Fajfar and Drobnič (1998), these methods have been also applied to infilled frames. In this case, given that the strength of the bare frame is not too much lower than the maximum strength of the infilled frame, results could be suitable. However, for poor seismic designed structures this is not possible, being necessary to find out new formulations.

In Dolšek and Fajfar (2004) a R - μ - T relation for infilled RC frames is proposed, which depends on more parameters than that for bare frames. It has into account:

- the ratio between the strength when the infills have collapsed and the previous maximum strength (r_u);

- the ductility at the beginning of the degradation of the infills (μ_s);
- the slope of the drop of resistance due to infills degradation, which finally is not considered in the expressions given its low relevance.

$$\mu = \frac{1}{c}(R - R_0) + \mu_0 \quad (20)$$

$$c = \begin{cases} \left. \begin{array}{l} 0.7 \frac{T}{T_C} \\ 0.7 + 0.3 \cdot \Delta T \end{array} \right\} , & \begin{array}{l} T \leq T_C \\ T_C < T \leq T_D^* \end{array} \\ \left. \begin{array}{l} 0.7 \cdot \sqrt{r_u} \left(\frac{T}{T_C} \right)^{\frac{1}{\sqrt{r_u}}} \\ 0.7 \cdot \sqrt{r_u} (1 - \Delta T) + \Delta T \end{array} \right\} , & \begin{array}{l} T \leq T_C \\ T_C < T \leq T_D^* \end{array} \\ 1 & , \quad T > T_D^* \end{cases} , \quad \begin{array}{l} R \leq R(\mu_s) \\ R > R(\mu_s) \end{array} \quad (21)$$

$$T_D^* = T_D \sqrt{2 - r_u} \quad ; \quad \Delta T = \frac{T - T_C}{T_D \sqrt{2 - r_u} - T_C} \quad (22a,b)$$

$$\mu_0 = \begin{cases} 1 & , \quad R \leq R(\mu_s) \\ \mu_s & , \quad R > R(\mu_s) \end{cases} \quad ; \quad R_0 = \begin{cases} 1 & , \quad R \leq R(\mu_s) \\ R(\mu_s) & , \quad R > R(\mu_s) \end{cases} \quad (23a,b)$$

$$R(\mu_s) = \begin{cases} 0.7 \frac{T}{T_C} (\mu_s - 1) + 1 & , \quad T \leq T_C \\ (0.7 + 0.3 \Delta T) (\mu_s - 1) + 1 & , \quad T_C < T \leq T_D^* \\ \mu_s & , \quad T > T_D^* \end{cases} \quad (24)$$

The main relation (Equation (20)) is formally similar to that of bare frames (Equation (19a)). The different variables are shown in Equations (21) to (24). The shape of the R - μ - T relation can be seen in Figure 50a, together with the some constant-ductility spectra. In this case the relation it is a trilinear function, reaching

the “equal-displacement” principle at a value of period even bigger than T_D , when for bare frames it happens approximately for T_C (see Figure 50c). This implies that the ratio between inelastic and equivalent elastic displacement demand is much bigger than for bare frames in the usual range of periods, as seen in Figure 51a.

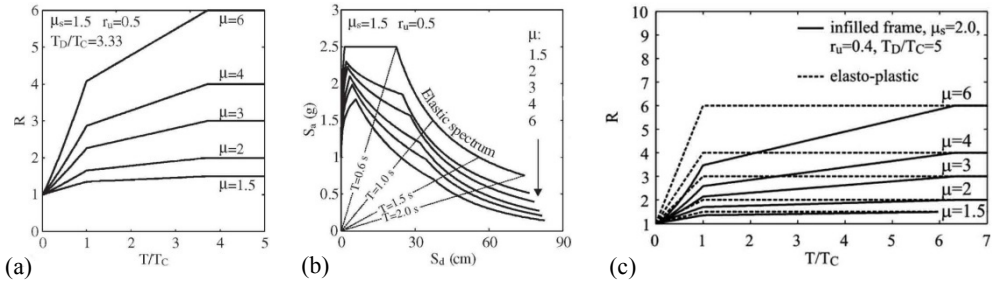


Figure 50: R - μ - T relation for infilled RC frames (a) and some examples of constant-ductility spectra (b) (from Dolšek and Fajfar, 2004a), and comparison of R - μ - T relations for bare (dotted line) and infilled frames (solid line) (c, from Dolšek and Fajfar, 2008a)

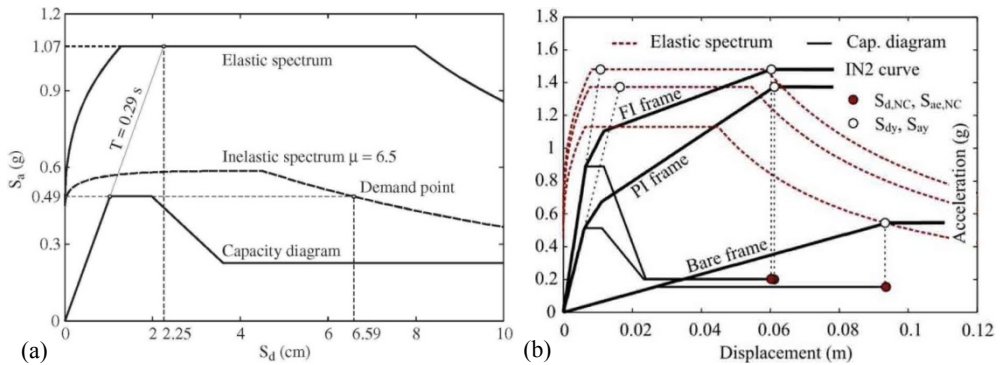


Figure 51: Example of inelastic spectrum and displacement demand for an infilled frame (a, from Dolšek and Fajfar, 2005), and IN2 curves for two infilled frames and a bare frame (b, from Dolšek and Fajfar, 2008b)

1.2.3.5 Simplified IDA analysis: IN2 curves

For a given capacity curve, the evaluation of the displacement demands corresponding to the different elastic strength demands –corresponding to demand

spectrums with the same “corner” period— from the maximum strength capacity on, results in a set of couples (S_d , S_a). If plotted, it results in an increasing curve whose shape is closely related to that of the capacity curve. It is called IN2 curve (Dolšek and Fajfar, 2004b).

The IN2 curves are essentially simplified representations of the IDA curves, which are the output of Incremental Dynamic Analysis, “IDA” (Vamvatsikos and Cornell, 2002). This is a parametric seismic analysis method, in which a structural model is subjected to multiple levels of seismic intensity using one or more ground motion records and non-linear dynamic analysis, in order to understand the structural behaviour under increasing demand (from scaled accelerograms).

IDA curves relate any “intensity measure” in ordinates –PGA, PGV, first mode 5% damped spectral acceleration $S_d(T)$, etc.— that represents the input, with a “structural state variable” in abscissa –maximum roof displacement, peak roof or interstorey drift, maximum base shear, node rotations, peak storey ductilities, damage indices, etc.— that represents the output. The shape of the IDA curve depends on that of the capacity curve (CC) (see Figure 52a):

- the elastic region is approximately common to both curves;
- a subsequent perfectly plastic part in the CC corresponds to an approximate equal-displacement rule for the IDA, thus a slope approximately similar to the elastic, except for short periods, showing lower slopes;
- in this region, positive or negative slope in the CC corresponds to higher or lower slopes than the elastic one in the IDA, respectively;
- a non-negative region in the CC after a softening cause a new equal-displacement region in the IDA.

IN2 curves, although constitute a very simplified approach to the IDA curves, have been widely tested and represent a reasonable agreement with the real behaviour (see Figure 52b). In Figure 51b, typical shapes of IN2 curves for infilled and bare frames are shown. For bare frames, IN2 curve is a linear function with the same slope as the elastic part for medium and high periods, or a slightly lower slope for short periods. In the case of infilled frames, IN2 curve is a bilinear

function, whose first branch (before softening) has a slope lower than the elastic one, and the second branch even more. It is worth to note that the shape of the IN2 not only depend on the structure but also on the characteristics of the ground motion, i.e. on the characteristic (“corner”) period. In Figure 53 can be observed how the slope of both branches of the IN2 of the same structure is much lower when subjected to a set of ground motions whose corner period is higher.

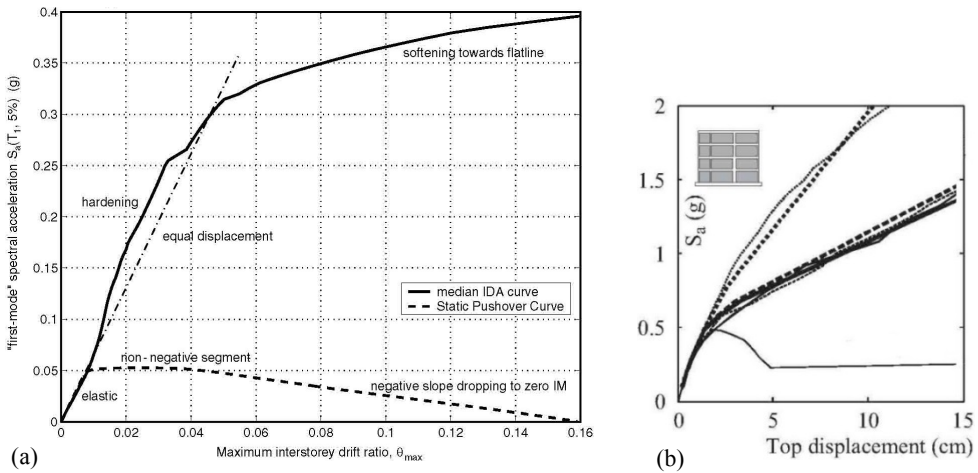


Figure 52: Characteristics of IDA curves (a, from Vamvatsikos and Cornell, 2002) and comparison of IN2 and IDA curves (b, from Dolšek and Fajfar, 2005)

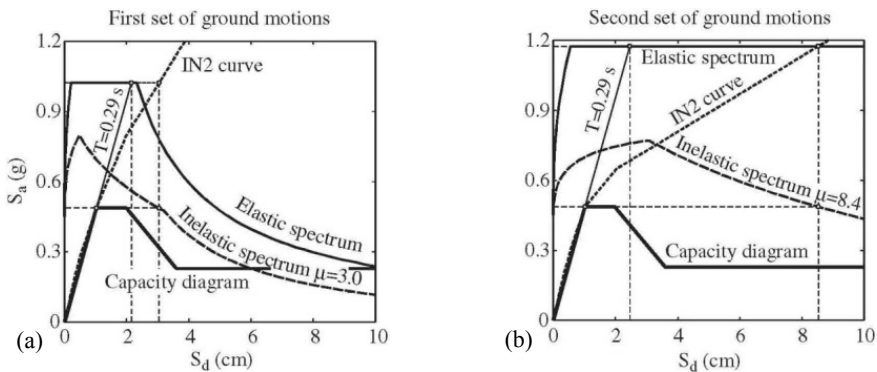


Figure 53: Differences in the IN2 curves of the same structure depending on the characteristics of the ground motion (from Dolšek and Fajfar, 2005)

1.2.4 Different methods

Finally, in this section three different spectral performance-based methods for the assessment of structures are presented. Some of them share similar graphic frameworks or tools exposed previously.

1.2.4.1 *Capacity Spectrum Method*

Firstly proposed by Freeman et al. (1975) as a quick graphical procedure for the estimation of the performance point of structures. It was assumed in the ATC-10 for the assessment of existing structures (ATC, 1982). Afterwards, it has been properly settled in Freeman (1998). It is the first method that uses the graphic superposition of capacity and demand curves in the ADRS format, establishing that a structure is safe if the capacity curve can extend through the envelope of the corresponding demand curve, being the performance point the intersection of both.

It uses highly-damped elastic spectrum for representing the demand curve (see section 1.2.3.3). The capacity curve is bilinearised, but the slope of the plastic part can be different from zero.

In Figure 54a, the graphic approximate procedure is shown. Firstly, several secant periods are marked in the ADRS format. Then, demand spectra corresponding to different equivalent damping values are plotted. Subsequently, the bilinear capacity curve is plotted, marking the points corresponding to different values of ductility (i.e. 1, 2...). Later, these values of ductility must be related with levels of damping; different methods are explained in section 1.2.3.3). Finally, the performance point is placed in the interval of the capacity curve where the value of damping associated with the ductility coincides with the damping of the demand curve passing through the interval. For an accurate solution, interpolation is needed. A secant period is associated to performance period, evaluated graphically.

Another possible strategy is to proceed with iterations. Firstly, an arbitrarily first performance point is chosen; it can be the one corresponding to the equal-displacement rule applied using the elastic period, i.e., the point on the capacity curve corresponding to a displacement demand obtained by intersecting the elastic period with the elastic demand spectrum. Then, the highly-damped spectrum associated to the ductility represented by the first performance point is plotted. So,

the intersection of this spectrum with the capacity curve represents the performance point in the second iteration; and so on. The method can be used for designing of structures instead of for assessing in an inverse way.

The graphic framework of this method is the main advantage but the use of highly-damped spectra as demand ones is controversial (see section 1.2.3.3).

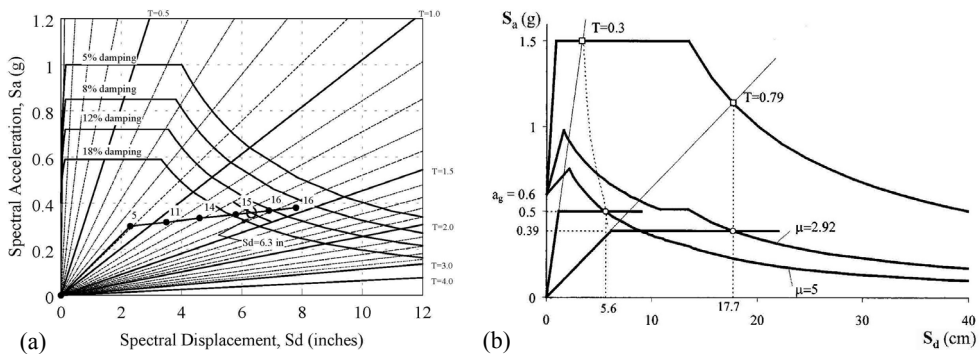


Figure 54: Performance point evaluated through the original Capacity Spectrum Method (a, from Freeman, 1998) and through N2 method (b, from Fajfar, 1999)

1.2.4.2 *N2 method*

This method (Fajfar and Fischinger, 1988; Fajfar and Gašperšič, 1996; Fajfar, 1999; and Fajfar, 2000) combines the graphic approach of the Capacity Spectrum Method with the use of inelastic spectra as demand curves (see section 1.2.3.4). This method is used in the Eurocode 8 (CEN, 2004). The graphic process can be observed in Figure 54b: the equivalent elastic period defines an elastic strength demand, from with it is possible to obtain the value of R by comparing it with the maximum strength of the capacity curve, defined as elastic-perfectly plastic. Then, the ductility corresponding to the performance point is obtained from R through any R - μ - T relationship, so the displacement demand can be calculated. It is worth noting that the obtaining of the inelastic demand curve is not necessary.

Aimed at evaluating performance of the structure, the spectral displacement demand should be compared with the maximum spectral displacement capacity. The construction of the IN2 curve of the structure (see section 1.2.3.5) allows

carrying out this comparison in terms of spectral acceleration instead. In Figure 55a, the IN2 curves corresponding to the two capacity curves are obtained. The end of the IN2 curves correspond to the maximum spectral acceleration capacity ($S_{a,e}$), which is compared in both cases with the spectral acceleration demand ($S_{a,d}$); the red arrow show the difference between capacity and demand.

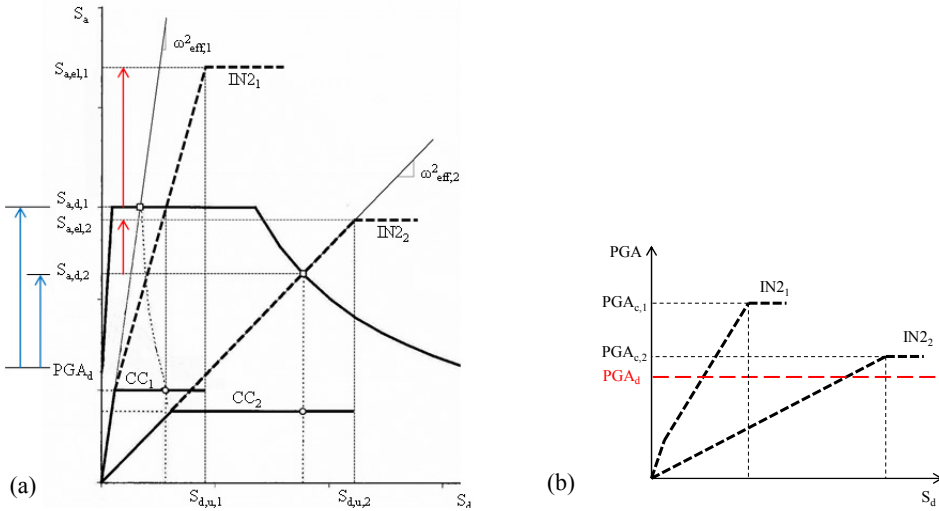


Figure 55: Graphic comparison between capacity and demand through the IN2 curves in the N2 method: in terms of spectral acceleration (a) (adapted from Fajfar, 1999) and in terms of PGA (b)

However, maximum capacities of several structures and their relative performances (capacities vs. demand) when subjected to the same event cannot be compared directly in a graphical way if the IN2 curves are expressed in terms of spectral acceleration. In fact, given the same event with defined by its demand PGA_d , the spectral demand acceleration $S_{a,d}$ for each structure depends on its effective period; the relations between PGA_d and the spectral demands are marked with blue arrows in Figure 55a. Thus, aimed at allowing a direct comparison, the IN2 curves can be expressed in PGA units by applying the transformation shown in Equation (25). As a result, the PGA capacities (PGA_c) can be directly compared with the demand (see Figure 55b).

$$PGA_c = S_{a,c} \frac{PGA_d}{S_{a,d}(T_{eff})} \quad (25)$$

Likewise to the Capacity Spectrum Method, the N2 method can be used inversely with design purposes, both force- and displacement-based. There are four parameters defining structural behaviour: strength, stiffness, ductility and displacement, from which only two are known in any case. Those two known variables are, depending on the case:

- Force-based design: stiffness and ductility
- Displacement-based design: displacement and ductility
- Assessment: stiffness and strength

1.2.4.3 *Displacement coefficient method*

This is the method proposed in FEMA 273 (ATC, 1997). There is no substantial difference with the N2 method, except for the consideration of any post-yielding slope and two conservative modification factors accounting for the eventual pinching in the hysteresis loops or the second order effects (C_2 and C_3 , respectively).

The displacement demand is calculated as the displacement corresponding to the elastic strength demand, multiplied by four factors:

- C_0 , equivalent to the first mode participation factor Γ ;
- C_1 , equivalent to μ/R calculated with the simplified $R-\mu-T$ presented in (Fajfar, 1999), with a maximum amplification of 1.5 for $T < 0.1s$;
- C_2 , which assumes values ranging from 1.1 to 1.3 for Life Safety Level or from 1.2 to 1.5 for Collapse Prevention Level, corresponding in both cases the lower and upper bounds to the values for the corner period and 0.1s, respectively;
- C_3 , equal to 1.0 for positive post-yielding stiffness or the value given by the Equation (26) for negative slope.

$$C_3 = 1 + \frac{|\alpha|(R-1)^{3/2}}{T} \quad (26)$$

1.3 INFLUENCE OF INFILLS ON RC-MRF BUILDINGS PERFORMANCE

Infill walls are usually employed in reinforced concrete buildings for partition use and for thermal/acoustic insulation. Hence, they are considered as non-structural elements; nevertheless, post-earthquake damage observation, experimental and numerical research have shown that their influence on seismic behaviour of RC buildings can be not negligible at all. Modern seismic codes prescribe to account for the possible influence of infills on seismic behaviour of RC frames, both at local and global level. Even though the awareness about this issue in earthquake engineering is not very recent, it is likely to state that practically no existing RC building was designed accounting for the presence of these elements.

Generally speaking, infill walls can provide a considerable contribution to a RC structure in terms of strength and stiffness. However, their post-peak response is usually quite brittle. Moreover, many uncertainties affect the evaluation of their behaviour; the first (and obvious) reason is that those elements are not designed to have a specific behaviour under seismic action. Different collapse modes are possible, both in-plane and out-of-plane. Also, many differences in materials and constructive methods are observed.

The interaction between infill panels and RC structural elements under seismic action develops at global level, leading to an increase in lateral stiffness and base shear capacity, but also at local level, potentially leading to brittle failure mechanisms in surrounding elements such as columns or beam-column joints.

It is not easy to determine whether infill influence on seismic behaviour of RC buildings is beneficial or not, on the whole. Probably, the best synthetic description of this issue can be drawn from the conclusions reported in Dolšek and Fajfar (2001): the infill walls can have a beneficial effect on the structural response, provided that they are placed regularly throughout the structure, and that they do not cause shear failures of columns.

1.3.1 In-plane behaviour

1.3.1.1 *Local performance*

First, the response of the infilled RC frame is influenced, obviously, by the material characteristics of the infill panel (see Figure 56a). These characteristics are influenced both by mortar and masonry unit properties; nevertheless, when evaluating the behaviour of an infilled RC frame the material mechanical characteristics are usually referred to the equivalent homogeneous material, and are expressed through different parameters such as the Young's elastic modulus, the shear elastic modulus, the compressive strength or the shear cracking stress. These parameters are usually determined from vertical or diagonal (i.e., with different angles between the bed joint direction and the applied load) tests on masonry specimens. However, material types and constructive methods can vary greatly in infill panels. Hence, high uncertainties and dispersion affect the determination of these characteristics when they have to be evaluated in order to model the influence of infill panels on structural behaviour.

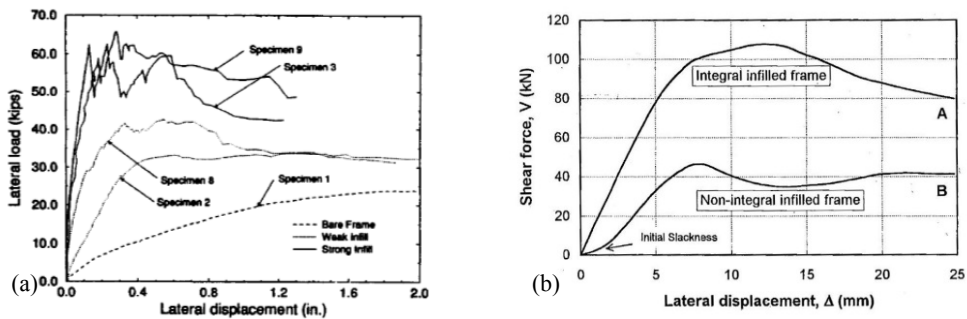


Figure 56: Monotonic lateral load-displacement response of bare, “weak” infilled or “strong” infilled RC frames (a, from Mehrabi et al., 1996), and force-displacement response of integral and non-integral infilled frames (b, from Crisafulli, 1997)

Behaviour of an infilled RC frame is also strongly influenced by the interaction between the masonry panel and the surrounding RC structure, both in terms of stiffness and strength. Generally, some distinct phases in the response of

an infilled frame can be distinguished, focusing the attention on the monotonic envelope of a typical lateral force-displacement curve.

In a first phase, for very low values of lateral displacement, the response of the infilled frame strictly depends on interface conditions between the panel and the surrounding elements. In non-integral infilled frames, due to shrinkage of the mortar or to constructive problems, there is a lack of contact between the two elements, thus leading to high reduction in the initial stiffness (Crisafulli, 1997). On the contrary, in integral infilled frames the initial response is given by a monolithic behaviour of the whole composite system, ensured by bond capacities at the interface between the panel and the frame (see Figure 56b).

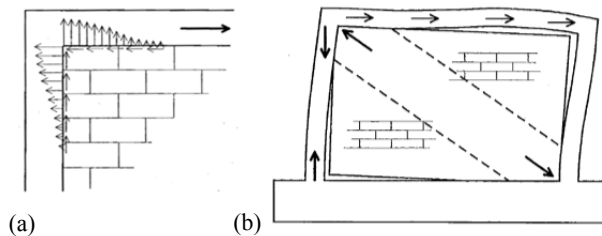


Figure 57: Normal and shear stresses acting on a loaded corner (a); and increase in the stress state along the diagonal of the panel (b) (from Crisafulli, 1997)

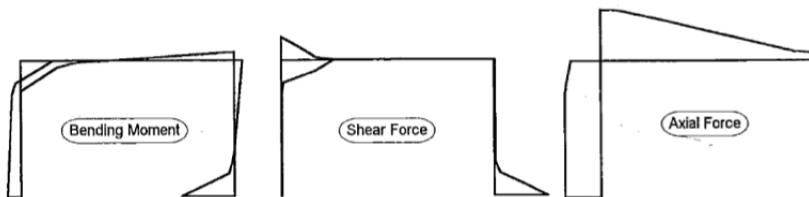


Figure 58: Bending moment, shear and axial force diagrams for a typical infilled RC frame (from Crisafulli, 1997)

As far as integral infilled frames are concerned, with increase in lateral load differences in deformational characteristics between the panel and the RC frame cause cracking and separation at the interface between the two materials, leading to

a first stiffness decrease in the force-displacement response. This separation occurs for variable load levels, depending also on the interface conditions; however, it is expected to take place for very low drift values. Afterwards, an increase in the stress state narrowed in the opposite compression angles and along the diagonal of the panel takes place, together with a diagonal cracking; contact areas between the frame and the panel further decrease (Figure 57).

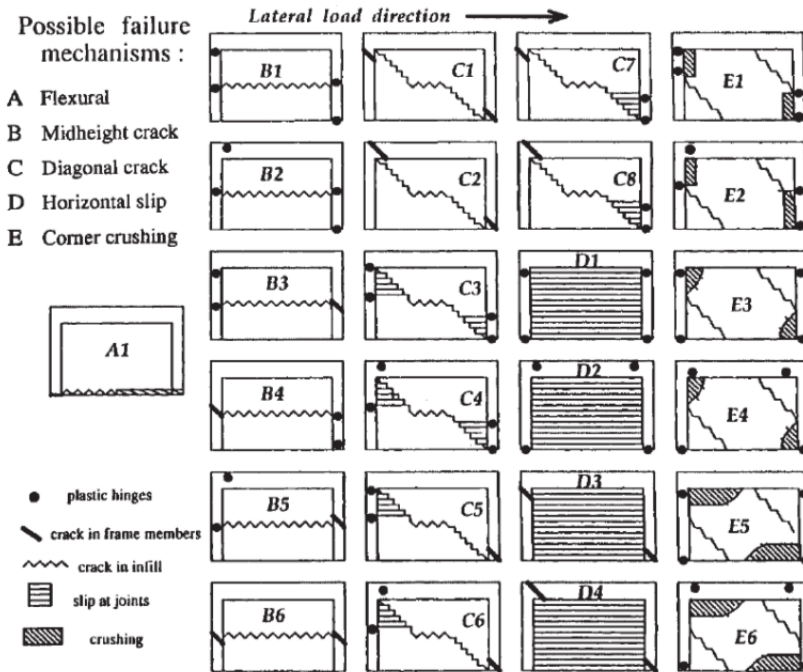


Figure 59: Failure mechanisms of infilled frames (from Shing and Mehrabi, 2002)

As the lateral load further increases, cracking and damage in the panel gradually increase up to the attainment of the maximum lateral strength of the infilled frame. This mechanism is usually referred to as “truss mechanism”, due to the clear analogy between the diagonal of the panel, along which compression stresses concentrates, and a compressed diagonal truss. The interaction between the compressed truss and the surrounding RC members develops in corner contact

areas whose dimensions are mainly influenced by the ratio between the stiffness of the panel and the stiffness of the RC frame. This interaction strictly influences the distribution of forces in RC members (see Figure 58). Shear and axial force variation in columns are of particular importance. After the peak, the experimental curve shows a different softening behaviour depending on the type of the panel failure and on the post-elastic response of the frame.

Nevertheless, the above described truss mechanism – which initially develops after the separation between the infill panel and the RC frame – may or may not evolve into a primary load-resistance mechanism, mainly depending on the interaction between the panel and the surrounding RC frame. Different failure modes may take place, different from diagonal cracking of the panel, such as corner crushing or horizontal shear sliding. The failure mechanism of the infill panel may also influence the failure mechanism of the surrounding RC frame, for instance, by determining the location of plastic hinge in columns (Figure 59).

1.3.1.2 Global performance

A detailed state of the art of numerical investigation of seismic behaviour of infilled RC buildings is carried out in Ricci (2010). Main conclusions are:

- an irregular distribution of infills (soft-storey effect) results in a worse seismic performance through a detrimental localization of inelastic displacement demand in the storey where infills are not present;
- a regular distribution of infills may lead to a beneficial reduction in displacement demand compared with the bare structure, especially if the seismic demand intensity does not overcome a certain threshold (e.g., for Damage Limitation Limit State);
- as the seismic demand intensity increases (e.g., for Collapse Limit State), a detrimental localization of inelastic displacement demand takes place also in the case of uniform infill distribution since the displacement demand tends to concentrate in one storey, thus resulting in a worse seismic performance compared with the bare structure;
- previous considerations are strongly dependent (i) on the design of the bare structure, both in terms of strength (e.g., base shear coefficient) and

application of Capacity Design principles such as weak beam/strong column condition, and (ii) on the strength of infills.

1.3.2 Mechanic properties of infill panels

1.3.2.1 Strength and stiffness

Shear resistance corresponding to the maximum strength of the infill (τ_{max}) panel assuming diagonal-strut mechanism is usually related to the cracking resistance (τ_{cr}) by a factor a_w , as shown in Equation (27). Proposed values for a_w are: 1.3 (Fardis, 1997) or 1.65 (Dolšek and Fajfar, 2008a).

$$\tau_{max} = a_w \cdot \tau_{cr} \quad (27)$$

The relative area of infills in plan in the i^{th} storey ($\rho_{w,i}$) is defined as the ratio between the area of infill panels ($A_{w,i}$) and the plan of the storey ($A_{b,i}$), see Equation (28a). Thus, for similar storey areas ($A_{b,i}=A_b$), the maximum shear force developed by infills in the first storey ($V_{w,max}$) is defined as in Equation (28b).

$$\rho_{w,i} = \frac{A_{w,i}}{A_b} \quad ; \quad V_{w,max} = \tau_{max} \cdot A_{w,1} = \tau_{max} \cdot \rho_{w,1} \cdot A_b \quad (28a,b)$$

Regarding stiffness, shear stiffness of a single element j in the storey i ($K_{w,ij}$) is defined as in Equation (29a), being G_w the shear modulus of elasticity. Then, assuming that all the infill panels in the building present similar composition and characteristics, the stiffness of infills corresponding to the storey i ($K_{w,i}$) is obtained as in Equation (29b) as function of $\rho_{w,i}$.

$$K_{w,ij} = \frac{G_{w,ij} \cdot A_{w,ij}}{h_{w,ij}} \quad ; \quad K_{w,i} = \frac{G_w}{h_i} \sum_j A_{w,ij} = \frac{G_w \cdot A_{w,i}}{h_i} = \frac{G_w \cdot \rho_{w,i}}{h_i} \cdot A_b \quad (29a,b)$$

1.3.2.2 Correlation between non-structural damage states and IDR of infills

Correlating damage levels in infill panels with interstorey drifts (IDR) is not an easy issue, given the huge variability of properties of single materials (bricks and mortar) and the resulting panels. Still, some authors have presented diverse correlations based in probabilistic approaches. Rossetto and Elnashai (2003)

propose a correlation based in HRC-scale (Figure 60). Colangelo (2012) propose correlations of damage levels in HAZUS scale with single infill panels from a fuzzy-probabilistic point of view (Figure 61), and an extensive comparison of those results with other works is carried out in Colangelo (2013), see Figure 62a and Figure 62b. In the last figure it is possible to appreciate the great dispersion of values inherent to this kind of evaluations. In general, damage states corresponding to low damages in infills are concentrated in a very short range of IDR values, because they are very sensitive to slight variations.

ISD _{max} (%) limits for HRC-scale				
HRC damage state	All	N-D MRF	Infilled MRF	Shear-walls
None	0.00	0.00	0.00	0.00
Slight	0.13	0.32	0.05	0.26
Light	0.19	0.43	0.08	0.34
Moderate	0.56	1.02	0.30	0.72
Extensive	1.63	2.41	1.15	1.54
Part. Coll.	3.34	4.27	2.80	2.56
Collapse	>4.78	>5.68	>4.36	>3.31

Figure 60: Correlation between damage levels in HRC-scale and IDR for different structural types (from Rossetto and Elnashai, 2003)

Parameter	Damage state			
	Slight (S)	Moderate (M)	Extensive (E)	Complete (C)
μ_R	0.03%	0.4%	0.8%	1.6%
σ_R	0.02%	0.3%	0.4%	0.4%
δ_R	67%	75%	50%	25%
$r_{\min}-r_{\max}^a$	0.0073–0.085%	0.085–0.45%	0.45–1.09%	1.09–2.22%
λ	0.24	0.21	0.56	0.68
γ	0.95	0.97	0.91	0.70

^aDrift values at the intersection of the probability density functions, or proper percentiles.

Figure 61: Fuzzy-probabilistic correlation between damage levels in HAZUS-scale and IDR of infills (from Colangelo, 2012)

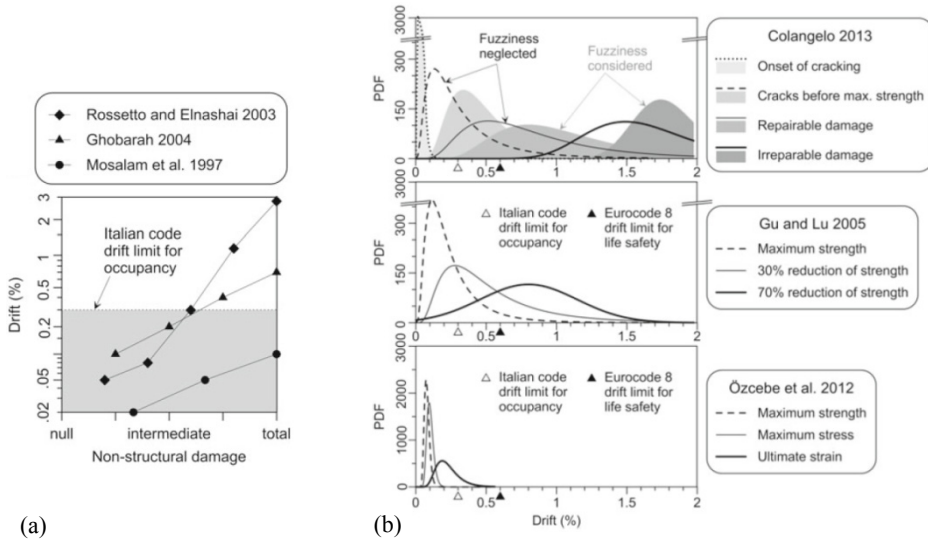


Figure 62: Correlation between damage levels IDR for infilled frames (a) and probability density functions of different correlation between damage levels and IDR proposed by different authors (b) (from Colangelo, 2013)

1.3.3 Distribution and geometry of infills in Mediterranean construction

All the precedent studies are based in the behaviour of frames with infill panels perfectly inserted within the space between columns and beams along the longitudinal axe of the frame. Only the possibility of existence of gaps between infill panel and frame is considered. However, the usual constructive practice is not only that one. Infill panels can be situated in several different positions and showing different geometry, as shown schematically in Figure 63:

- Position: Infill panels can be inserted into external frames (e.g. conforming façades) or internal frames, or also belonging to frames conforming cantilevered parts.
- Thickness: Some infills present very reduced thickness, e.g. internal layer of façade or partition walls.
- Completeness in plan: Infills can reach both columns, only one or none of them.

- Completeness in elevation: Infills can have complete interstorey height, framing both beams, or having lower height.
- Holes: Panels usually present holes, which can be internal (e.g. windows) or reaching borders (e.g. doors).
- Alignment: Infills can be aligned along the axe of columns or beams, or displaced from the axe but in contact with some of the columns or of the beams.
- Insertion: Infills can be inserted in frames or placed in the middle of a bay, being parallel or perpendicular to the direction of the joists.

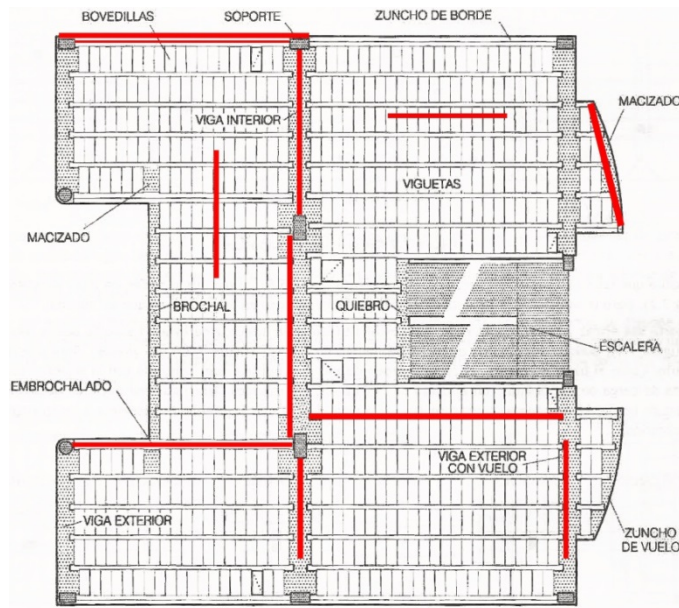


Figure 63: Different positions of infills within the RC frame in a representative Mediterranean layout

If it not clear which is the performance of infills in all of those particular cases. Strictly speaking, the position of infills may not change the performance: both exterior and interior panels may perform in similar way. Still, as internal infills usually present lower thickness and more uncertainty in their position,

authors (see Bal et al., 2008 or Ricci et al., 2011b) may assign lower reliability to internal panels. Infills in cantilevered parts of the frame should be also discarded. In the case of typical two-layered façades, it is not clear if internal layer should be considered or not. Regarding holes, some reductions of effective area can be considered (see Ricci, 2010).

If post-cracking diagonal-strut mechanism of infills is assumed, only infill panels in contact with two columns and two beams may be considered as full effective, i.e. able to develop post-cracking rising branch until maximum force. The rest of the infill panels may be characterised by an only equivalent elastic branch until cracking, following by a drop of resistance. In the case of infills at least in contact with one column, the transfer of forces from the structure to the infill panel is carried out through forces normal to the vertical face of the infill. Conversely, in the case of panels framing only beams, the transmission of forces is carried out by means of friction between beams and mortar, which in some cases cannot guarantee a full transmission because the interface may lose contact.

Hence, it is not possible to define accurately the effective area of infills in plan of a building; it is worth considering a wide range of values, aimed at representing lower and upper bounds of strength and stiffness provided by the panels as a whole.

Chapter 2

Spanish vs. European seismic codes

In this chapter, Spanish seismic codes and typical characteristics of the RC residential building stock in Lorca are studied, aimed at:

- understanding the feasible cause-effect relationship with the post-earthquake damage scenario, and
- defining the most representative input parameters for the application of FAST approach to the Lorca earthquake (see Chapter 6).

In the first section, a compared review of the past and present Spanish seismic codes is presented, in order to establish the demands requested to buildings corresponding to each period –which also determines the expected performances, as a code-based approach is assumed—. In the second section, main drawbacks of NCSE-02 in comparison with the common framework of modern seismic international codes –as Eurocode 8— are analysed in detail.

2.1 CRITICAL REVIEW OF SPANISH SEISMIC CODES

Modern international benchmark seismic codes, as European Eurocode 8 (CEN, 2004), American ACI 318-08 (ACI, 2008) or New Zealander NZS 3101 (NZS, 2006), establish such a restrictive set of provisions for RC buildings that

common “gravitational” structural solutions corresponding to non-seismic areas become almost impossible to be designed according to them.

However, this is not the case of Spanish seismic codes, even in the case of current one. It is still conceived as a set of provisions which compel the designer to make some modifications to the sections and reinforcement of the original “gravitational” outlines. These concepts are deeply studied in the next section.

Spanish codes containing provisions regarding seismic design are, cronologically:

- 1962: Chapter 7 of actions code MV-101 (MH, 1962)
- 1968: PGS-1 (CDSC, 1968)
- 1974: PDS-1 (CDSC, 1974)
- 1994: NCSR-94 (CDSC, 1994)
- 2002: NCSE-02 (CDSC, 2002)
- 2008: Annex 10 of RC code EHE-08 (PCSC, 2008)
- 2010: Proposed Spanish National Annex to Eurocode 8 (Alarcón et al., 2010)

Current one is NCSE-02 (2002), because the more recent ones are not mandatory: the penultimate is recommended and regards only RC structures, while the last one is optional. All of them can be grouped into four categories, depending on how “evolved” they are (see also Table 8):

- 1) Proto-code (MV-101): Very basic, do not understand buildings as oscillators.
- 2) Old-generation codes (PGS-1 and PDS-1): They set a common simplified static force method considering dynamic properties, but there is still no reference to ductility.
- 3) Medium-generation codes (NCSR-94 and NCSE-02): They incorporate modern probabilistic approach and ductility principles, but no complete capacity design is furnished.
- 4) New-generation codes (EHE-08 and EC8): Both capacity-design-based, but only the last one take worry about irregularities and stiffness.

Table 8: Progressive inclusion of prescriptions in the different Spanish seismic codes: included (pale grey), partially included (grey), not included (dark grey) and not susceptible to be regulated (white); in *italics*: not mandatory in Spain

Code	Proto-code	Old-generation		Medium-generation		<i>New-generation</i>	
	MV-101	PGS-1	PDS-1	NCSR-94	NCSE-02	<i>EHE-08</i>	<i>EC8</i>
Equivalent static forces analysis	Dark grey	Pale grey	Pale grey	Pale grey	Pale grey	White	Pale grey
Linear dynamic analysis	Dark grey	Dark grey	Dark grey	Pale grey	Pale grey	White	Pale grey
Probabilistic hazard	Dark grey	Dark grey	Dark grey	Pale grey	Pale grey	White	Pale grey
Explicit q -factor design	Dark grey	Dark grey	Dark grey	Pale grey	Pale grey	White	Pale grey
Hierarchy of resistances	Dark grey	Dark grey	Dark grey	Dark grey	Dark grey	Pale grey	Pale grey
RC reinforcement detailing	Dark grey	Dark grey	Dark grey	Dark grey	Dark grey	Pale grey	Pale grey
Second order effects	Dark grey	Dark grey	Dark grey	Dark grey	Dark grey	White	Pale grey
Limited columns compression	Dark grey	Dark grey	Dark grey	Dark grey	Dark grey	Pale grey	Pale grey
Complete capacity design	Dark grey	Dark grey	Dark grey	Dark grey	Dark grey	Pale grey	Pale grey
Limited deformability	Dark grey	Dark grey	Dark grey	Dark grey	Dark grey	Dark grey	Pale grey
Irregularity in elevation	Dark grey	Dark grey	Dark grey	Dark grey	Dark grey	Dark grey	Pale grey
Interaction with infills	Dark grey	Dark grey	Dark grey	Dark grey	Dark grey	Dark grey	Pale grey
RC squat columns design	Dark grey	Dark grey	Dark grey	Dark grey	Dark grey	Dark grey	Pale grey

Characteristics of the different codes are qualitatively presented herein, and a detailed quantitative comparison between all of them is carried out in section 2.1.5. Instead, characteristics of EC8 are described in section 2.2. Aimed at clarity, all the variables are expressed with the EC8 notation instead of using the specific variables of each code, whenever there is enough degree of correspondence.

2.1.1 Proto-code: MV-101 chapter 7 (1962)

Published only six years after the Albolote (Granada) earthquake (magnitude $M_{\bar{M}}=5.0$). It consists just on a brief chapter included in a general actions code. It

furnishes a hazard map of intensity which shows great influence of historic earthquakes (Cabañas et al., 2011), thus being very discrete, with a lot of isolated single areas of medium seismicity (Figure 65).

It does not consider buildings as oscillators with a different response depending on the vibration modes, but assigns constant spectral values that should be multiplied by the masses aimed at obtaining horizontal forces (or even vertical). Masses in the seismic situation corresponding to live loads are reduced (50% for residential use). Spectral values are obtained as discrete values shown in a table, which mix three different influences: hazard range (intensity), soil quality and type of structure. It is worth noting that, implicitly, a sort of behaviour factor $q=2$ is used for frames in comparison with masonry buildings.

2.1.2 Old-generation codes

Soon after the first consideration of seismic actions in design, PGS-1 (1968) and PDS-1 (1974) were published as exclusively seismic codes. The second one is just an upgrade of the first. Hazard map, similar for both (Figure 65), is more continuous, without so much influence of past events, and there is such a rough correlation between intensity and acceleration in probabilistic terms.

They consider buildings as oscillators, providing a simplified static-force method and simplified formulations for all the non-torsional periods of structures. Such method allows considering not only the fundamental mode, so equivalent forces corresponding to a modal superposition of several modes can be obtained. Linear or sinusoidal simplified deformed shapes are proposed. Vertical action is only required in particular situations, and it is largely reduced from horizontal.

The concept of response spectrum is not clearly shown: the spectral shape function is combined with the hazard parameter. Two branches are considered, with constant corner period: a first constant one and a second decreasing one; the maximum spectral amplification factor seems to be compensated by the behaviour factor, unless none of them are explicitly considered.

However, there is another coefficient (“response” factor) depending on the relative damping but also on the period. Thus, those two contributions of the

period can be considered together within a spectral amplification factor. The damping correction factor accounts for the presence of infill panels, intended to provide very high damping with respect to the critical (implicitly 10 or 13% depending on whether NCSE-02 or EC8 formulation is used, respectively).

There is not any explicit consideration of q . Instead, after a homogenisation within the rest of the codes (see section 2.1.5), a constant $q \approx 2.5$ for all the structural solutions comes out. It is worth noting that, contemporaneously, New Zealander seismic code of 1976, NZS 4203 (NZS, 1976), already had incorporate the q -factor design, while in Spain it appears 18 years later.

Aimed at defining of a soil correction factor, soil quality is classified attending to the velocity of compression waves instead of shear ones. Unlike most of international codes, the soil type of reference –to which a_g corresponds— is not rock but dense soil. Furthermore, also the type of foundation modifies the acceleration at the base of the building. There is no combination of effects between transversal directions. Masses corresponding to live loads in residential buildings are reduced in a 50% with respect to the non-accidental case.

Regarding formal design strategies, only some qualitative comments about symmetry are suggested. There are not any special detailing rules for reinforcement in RC structures except for some minor consideration about taking care of the disposition of reinforcement in joints.

Main modifications of PDS-1 with respect to PGS-1 are:

- it is mandatory in a much smaller area, corresponding to Intensity \geq VIII; this relaxation, together with the large period of time (20 years) in which this code was the current one, is one of the main causes of the high vulnerability of the Spanish RC building stock (Cabañas et al., 2011);
- fundamental period has a lower limit equal to corner period, allowing the first branch to remain horizontal –in fact, in the previous code the first branch is not constant because the “response” factor still depends on period, also within the first branch;
- also lower limits for periods corresponding to second and third mode are furnished;

- SRSS combination of modal effects is suggested instead of simple addition;
- polynomial deformed shape with vertical tangent at the base is also suggested;
- upper limit to the spectral acceleration is established;
- their risk factor values are more influenced by the hazard level;
- it presents higher upper limit of velocity for the poorest soil type but lower factor for such type;
- partial factors for materials are not reduced;
- some considerations about regularity of masses in height are indicated.

2.1.3 Medium-generation codes

After 20 years of use of PDS-1, not very restrictive, the first “modern” seismic code is promulgated in 1994: NCSR-94. Eight years later, it is upgraded by NCSE-02, both sharing the general framework.

They orient their procedures not only within a simplified static force method but also within a general linear dynamic (modal spectral) analysis –as they are contemporaneous to the generalisation of the use of computers in the structural analysis and design. They make explicit all the factors influencing the seismic action, including q and the ductility requirements associated to it.

Notwithstanding such an advance, they might not be considered as “new-generation” codes because they exhibit great lack of understanding of the modern strategies of capacity design and the principles of ductility; other than not providing quantitative rules for Damage Limitation State or for dealing with infill panels (see section 2.1).

Hazard maps (Figure 65) are based in probability concepts as life span and return period (T_R) –500 years instead of 475, as in EC8 and other benchmark codes. Only the south of Spain is considered as seismic-prone area, and a special factor K accounting for the influence of the Azores-Gibraltar fault both on the reference PGA in soil A and on the corner periods is used. Only two importance classes are considered (50 and 100 years of life span).

Soil quality is established as function of shear wave velocity, and soil factor can be obtained as combination of layers –unlike EC8, in which the combination is used to obtain the velocity of the ground. Thus, intermediate values of soil factor are likely obtained. Conversely from old-generation codes, no foundation factor is applied, but still reference soil is not rock but dense soil.

Spectral shape is explicitly defined: three branches (linear, constant and hyperbolic, respectively) divided by two periods, whose values are substantially higher than the EC8 equivalent ones. Horizontal action is combined with 30% in the perpendicular direction, and vertical action is 70% of the horizontal one.

Regarding behaviour factor (q), there is no explicit consideration of ductility classes, as in EC8. Only in the case of deep RC beams, it is possible to choose between two levels of q depending on the local detailing. In the rest of the cases, single values of q are associated to the different macro-structural arrangements, whatever the local design is: RC frames with wide beams, slabs, couple or uncoupled walls; steel frames with eccentric, diagonal or V-bracings, etc. Only 4 levels of q are provided, from 1.0 to 4.0. No explicit quantitative reduction of q due to irregularity is considered, although some qualitative suggestion is done.

Explicit formulations for the damping factor, compared with the reference of 5% of the critical, are also provided. Differently from EC8, this factor is not intended to be included in q but acts independently. Accidental eccentricity of masses of 5% is considered.

Regarding simplified static force method, sinusoidal deformed shape is suggested and more simplified formulations for the fundamental period of common buildings than in the old-generation codes are suggested. Both for simplified method and linear dynamic analysis, SRSS or CQC method for combination of modal effects are suggested.

Second order effects can be discarded in the analysis if the second to first order moment ratio is lower than 10%, as in EC8; but also if the total drift of the frame is lower than 2%.

Qualitative prescriptions aimed at classifying structures as regular are furnished. For RC frames, maximum eccentricity between members is established

and a battery of prescriptions regarding local detailing of members aimed at providing ductility is presented. However, complete capacity design is not ensured (see section 2.2.1). It is worth noting that the degree of severity of the detailing rules for RC columns in both codes does not depend on the ductility class but on the level of seismicity.

Main modifications of NCSE-02 with respect to NCSR-94 are:

- for common residential RC frames, the application of the code is not mandatory in a larger area;
- wide beams can be used as a structural system without any restriction based on the seismic hazard;
- soil factors are corrected in order to make them increase when the quality is poorer independently of the Azores-Gibraltar fault coefficient;
- soil factors converge in a value of to 1.0 for any soil type when seismicity is very high (see Figure 64), because in this situation the trend is not so clear and could also get inverted;
- spectral acceleration for $T=0$ accounts for soil factor;
- maximum spectral amplification factor is increased to a constant value of 2.5, which can be also interpreted as an increase of soil factors if an equivalent spectral factor of 2.5 is assumed for both codes;
- more conservative values of damping are suggested for RC frames;
- the fraction of live loads in seismic situation increases;
- it is possible to assume lower partial factor for materials corresponding to accidental situation;
- squat columns are qualitatively suggested to be capacity-designed.

2.1.4 New-generation codes

Only two years after the promulgation of NCSE-02, EC8 was published, although some preliminary versions were being divulged since 1998, also in Spanish –UNE-ENV 1998-1 (AENOR, 1998)—. Thus, it can be interpreted as Spanish current code was kind of obsolete since their promulgation.

Hence, perhaps in an attempt to compensate those lacks, some of the principles of EC8 were included in an annex of the first RC code promulgated after

2004, which is EHE-08 (2008). However, this annex is not compulsory, and regards only RC.

Main improvements with respect to NCSE-02 are:

- capacity design is explicitly presented as the target principle to which almost all the rest of the prescriptions are oriented;
- critical regions are explicitly defined;
- higher strength hierarchy factors are used;
- more restrictive detailing aimed at obtaining proper local ductility, especially in beams, is proposed;
- the degree of severity of reinforcement detailing of columns depend on the ductility class instead on the seismicity level;
- relative axial loads in columns are restricted;
- some rules for the reinforcement of joint panels are furnished;
- upper slab contribution to the strength of beams is established, and minimum thickness is set;
- partial factors of materials are suggested to not being reduced from not-accidental situation unless resistances accounting for cyclic degradation are contemporaneously used;
- the contribution of concrete to shear resistance is hardly reduced for high values of q , aimed at considering the degradation for large demands of ductility;
- it is possible to consider the increment of strength and ductility of concrete due to confinement;
- there is the possibility or consider some members as secondary elements.

Still, some important lacks can be observed if compared to EC8; they are widely analysed in section 2.2.

Finally, in 2010, a proposal for the promulgation of Spain National Annex to EC8 was elaborated. Main differences regarding RC frames with respect to the recommended values proposed in general EC8 are:

- no geographical limitations for the use of low-ductility structures;
- importance factor of 1.3 instead of 1.2 for relevant-importance buildings;
- minimum width of foundation beams of 0.40m instead of 0.25m.

Also, in an accompanying work, it is clarified that response spectrum type 2 should be used for the whole territory.

2.1.5 Comparison of codes

In this section, a comparison of the prescriptions given by the different codes is carried out. Thus, a homogenisation of values of coefficients must be carried out; EC8 is chosen as a benchmark, both for values and terminology.

Hence, a common homogeneous expression for design acceleration response spectrum (Equation (30)) is adopted for all the codes, being: $S_a(T)$, design spectral acceleration; T , fundamental period of the structure; a_{gR} , reference PGA in rock soil; γ_I , importance factor; S , soil amplification factor; α_{max} , maximum spectral amplification; $\alpha(T)$, spectral shape function; η , damping correction factor; and q , behaviour factor.

$$S_a(T) = (a_{gR} \cdot \gamma_I \cdot S) [\alpha_{max} \cdot \alpha(T)] \frac{\eta}{q} \quad (30)$$

In Table 13 to Table 17, all the prescriptions are compared, being: $a_g = a_{gR} \cdot S$; P_R , reference probability of the reference seismic action; T_L , reference life span of the building; V_S , velocity of the seismic shear waves through the soil; DCM, Medium Ductility Class; DCH, High Ductility Class; ξ , viscous damping ratio; λ_i , participating mass of the i^{th} mode expressed as a fraction of the total mass; H , building height; and L , length of the building plan in the considered direction.

In Figure 65, hazard maps proposed by the different codes are presented. They are homogenised as in NCSE-02, in which the hazard parameter is a_b : PGA corresponding to 9.5% of probability of exceedance in 50 years, measured in dense soil (intermediate between soil type A and B of EC8). Correcting all of them in order to be expressed in a_{gR} is a hard work out of the limits of this work.

Aimed at achieving homogenisation, maps values corresponding to proto-code and old-generation codes, expressed originally in terms of typical seismic intensity MSK (I_{MSK}), are transformed into a_b . It is considered to be equivalent to the product of the acceleration associated to each level of intensity and the “risk factor” intended to correct such primitive value in order to account for a constant

level of probability. Values of a_b associated to the different intensity degrees are shown in Table 9.

Furthermore, in Table 13 to Table 17, reference values of acceleration are all homogenised to a_{gR} as in EC8, corresponding to 10% of probability of exceedance in 50 years, measured in rock soil (type A). The transformation requires of two correction factors (Equation (31a)): c_{TR} and c_S , accounting for the differences in T_R and reference soil type, respectively.

The first factor c_{TR} would typically require of a probability distribution of acceleration, which is not easily available. Thus, simplified assumptions are necessary. A formula included in medium-generation Spanish codes (Equation (31b)) relating PGA reference values and T_R is used, so c_{TR} is obtained (Equation (31c)). The difference is only around 2%; in fact, Spanish National Annex suggest to not having it into account. However, in this work it is considered.

$$a_{gR} = a_b \cdot c_{T_R} \cdot c_S ; \frac{PGA_{T_{R1}}}{PGA_{T_{R2}}} = \left(\frac{T_{R1}}{T_{R2}} \right)^{0.37} = \left(\frac{T_{R1}}{T_{R2}} \right)^{\frac{1}{e}} ; c_{T_R} = \left(\frac{475}{500} \right)^{\frac{1}{e}} = 0.98 \quad (31a,b,c)$$

The second coefficient, c_S , may be coincident with the value of soil factor S corresponding to rock. Given that in NCSR-94 the expression of soil factor present some weaknesses (see previous section), a constant value of c_S obtained from NCSE-02 is applied to hazard values of both medium-generation codes.

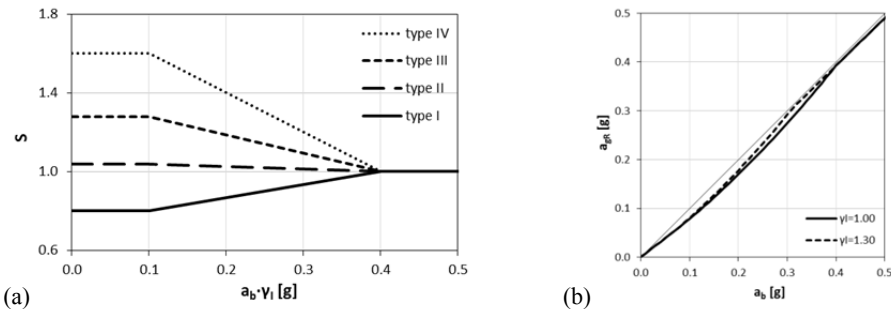


Figure 64: Soil factor S for the different types of soil depending on the seismicity, in NCSE-02 (a), and transformation of a_b into a_{gR} for the different importance classes of medium-generation Spanish codes, assuming variable $S_{NCSE-02,rock}$ (b)

However, in NCSE-02, S factors for the different soil types are not constant but converge into a common value of 1.0 for high seismicity levels (see Figure 64a). For rock, S adopts values between 0.8 and 1.0. Spanish National Annex suggest to adopt the value for low seismicity (0.8), as the subsequent increase to 1.0 may be rather understood as a possible amplification within a very conservative approach. In Equation (32), both options are presented.

$$c_S \equiv \begin{cases} S_{NCSE-02,rock,variable} = \min\{\max\{0.8; a_b \cdot \gamma_I\}; 1.0\} \\ or \\ S_{NCSE-02,rock|a_b \cdot \gamma_I \leq 0.1g} = 0.8 \end{cases} \quad (32)$$

If the upper expression in Equation (32) is adopted, the transformation of a_b into a_{gR} would depend both on the seismicity level and on the importance class, as shown in Figure 64b. Values of a_{gR} would range between 0.785 and 0.981 times a_b .

However, in this work, aimed at being coherent with Spanish National Annex, the lower expression in Equation (32) is adopted. In Table 9, some representative values of both parameters are shown for buildings of normal importance.

Hence, S factors in Table 13 to Table 17 are inversely corrected, i.e. divided by c_S . For NCSR-94, also factor S must be normalised by assuming a constant maximum spectral amplification factor.

For old-generation codes, as S factors are constant, also a constant correction of 0.8 is assumed. Given that values are tabulated, influence of soil and influence of foundation has been disaggregated by considering values corresponding to individual footings as reference ones. The last comes from the fact that soil factor corresponding to that foundation type assumes a value nearly to 1.0 (intermediate between 0.8 and 1.1) for the reference soil type, which has compression waves velocity of 1000m/s.

Furthermore, aimed at comparing soil factors and types of soil, such velocity of compression waves (V_P) should be correlated to velocity of shear waves (V_S). In Table 10, ratios V_S/V_P corresponding to the proposed lower and upper bounds of some soil types are obtained. Results are also congruent with the estimation proposed in Elnashai and Di Sarno (2008): ratios ranging between 0 and 0.53.

Ratios increase with both velocities, being higher for rock than for poorer soil. Those ratios are used in Table 11 in order to obtain the equivalent shear-waves velocities for old-generation codes.

Finally, in Table 12 a complete comparison of values regarding soil amplification is presented. Kind of similar thresholds might be identified for the different soil types.

Table 9: Relationship between different hazard scales for representative values used in Spanish codes, corresponding to normal-importance buildings

I_{MSK}	a_b	a_{gR}
-	[g]	[g]
V	0.020	0.016
VI	0.040	0.031
-	0.060	0.047
VII	0.080	0.063
-	0.120	0.094
VIII	0.135	0.106
-	0.160	0.126
IX	0.216	0.170

Table 10: Typical ranges of V_P and V_S for some soil types, and their corresponding ratios (from Bourbié et al., 1987)

	V_P [m/s]		V_S [m/s]		V_S/V_P	
	min	max	min	max		
Scree	300	700	100	300	0.33	0.43
Dry sands	400	1200	100	500	0.25	0.42
Wet sands	1500	2000	400	600	0.27	0.30
Saturated shales	1100	2500	200	800	0.18	0.32
Marls	2000	3000	750	1500	0.38	0.50
Saturated sand	1500	2200	500	750	0.33	0.34
Saturated sandstones	2000	3500	800	1800	0.40	0.51
Limestones	3500	6000	2000	3300	0.57	0.55
Chalk	2300	2600	1100	1300	0.48	0.50
Salt	4500	5500	2500	3100	0.56	0.56
Anhydrite	4000	5500	2200	3100	0.55	0.56
Dolomite	3500	6500	1900	3600	0.54	0.55
Granite	4500	6000	2500	3300	0.56	0.55
Basalt	5000	6000	2800	3400	0.56	0.57
Gneiss	4400	5200	2700	3200	0.61	0.62
Coal	2200	2700	1000	1400	0.45	0.52

Table 11: Proposed correlation between thresholds of velocity for the different soil types
for old- and medium-generation codes

Soil type	V_S/V_P (mean)	Medium- to old-generation codes				Old- to medium-generation codes			
		$V_{S,min}$ [m/s]	$V_{S,max}$ [m/s]	$V_{P,min}$ [m/s]	$V_{P,max}$ [m/s]	$V_{P,min}$ [m/s]	$V_{P,max}$ [m/s]	$V_{S,min}$ [m/s]	$V_{S,max}$ [m/s]
Rock	0.53	750	-	1732	-	2000	4000	866	2109
Dense	0.34	400	750	1242	1732	1000	2000	322	866
Medium	0.31	200	400	670	1242	500	1000	149	322
Loose	0.29	0	200	0	670	0	500	0	149

Table 12: Thresholds of V_S , homogenised values of S and reference soil for the different
Spanish seismic codes

PGS-1	PDS-1	NCSR-94	NCSE-02	EC8
ROCK S=0.50 $V_S=866\text{m/s}$	ROCK S=0.50 $V_S=866\text{m/s}$	ROCK S=1.13-1.25	ROCK S=1.00-1.25	ROCK S=1.00
		$V_S=750\text{m/s}$	$V_S=750\text{m/s}$	$V_S=800\text{m/s}$ Reference for a_{gr}
		Reference for a_{gr} ($V_S \approx 638\text{m/s}$)		
DENSE ⊕ S=1.00 $V_S=322\text{m/s}$	DENSE ⊕ S=1.00 $V_S=322\text{m/s}$	DENSE ⊕ S=1.10-1.16 $V_S=400\text{m/s}$	DENSE ⊕ S=1.25-1.30 $V_S=400\text{m/s}$	DENSE ⊕ S=1.35 $V_S=360\text{m/s}$
Reference for a_{gr}			MEDIUM ⊕ S=1.25-1.60 $V_S=200\text{m/s}$	MEDIUM ⊕ S=1.50 $V_S=180\text{m/s}$
MEDIUM ⊕ S=1.38 $V_S=90\text{m/s}$	MEDIUM ⊕ S=1.38 $V_S=149\text{m/s}$	MEDIUM-LOOSE ⊕ S=0.95-1.19	LOOSE ⊕ S=1.25-2.00	LOOSE ⊕ S=1.80
LOOSE ⊕ S=2.75	LOOSE ⊕ S=2.00			

In the same table, the velocity corresponding to the reference PGA for each code is estimated. For EC8, the minimum value furnishing $S=1.0$ is chosen. In old-generation codes, the velocity is explicitly indicated. Instead, for medium-generation codes, linear interpolation between velocities of soil types B and C is necessary, assuming that the nominal value of S for each soil type corresponds to an intermediate value of V_S between the bounds.

It is worth noting that reference soil for old-generation codes is poorer than for medium-generation codes, although both of them are classified as “dense”. In this case it is not necessary to homogenise reference PGA values, as for medium-generation codes with respect to EC8. The reason is that old-generation codes furnish their own hazard maps, while EC8 does not.

Anyway, PGA levels for a given site are not so different, e.g., for Lorca (Murcia), equivalent a_b in old-generation codes is $0.135g$, while for medium-generation ones it is $0.12g$. If the aforementioned conversion would be applied, ridiculous results are obtained: the equivalent a_b would be equal to the product of $0.135g$ and the not-homogenised soil factor for rock in old-generation codes, 0.4 , resulting in $0.054g$, which is lower than a half of the current PGA.

In old-generation codes, often values of factors are presented in tabulated form. Similar strategies of normalisation are followed: risk factor for different live span ratios are normalised to values corresponding to 50 years, and damping factors are normalised to values corresponding to bare frames.

Analogous procedure is also carried out for factors relating vertical to horizontal seismic action, which also depends on an assumption of a maximum spectral amplification and a behaviour factor. Behaviour factors of proto-code are normalised by assuming $q=1.0$ for masonry structures, as explicitly proposed in medium-generation codes. For vertical action in old-generation codes, also $q=1.0$ is assumed. In the case of EC8, ranges of q are obtained assuming different values of overstrength from the first yielding but without accounting with any reduction due to irregularity.

Regarding spectral shape, a common value of 2.5 for maximum spectral amplification factor is chosen for all the codes, thus being necessary a normalisation of some other parameters as S for NCSR-94 or η and q for old-generation codes. Aimed at obtaining explicit expressions for spectral shape in the case of such old-generation codes, the influence of “response factor”, which varies depending on the period, is joined together within $\alpha(T)$.

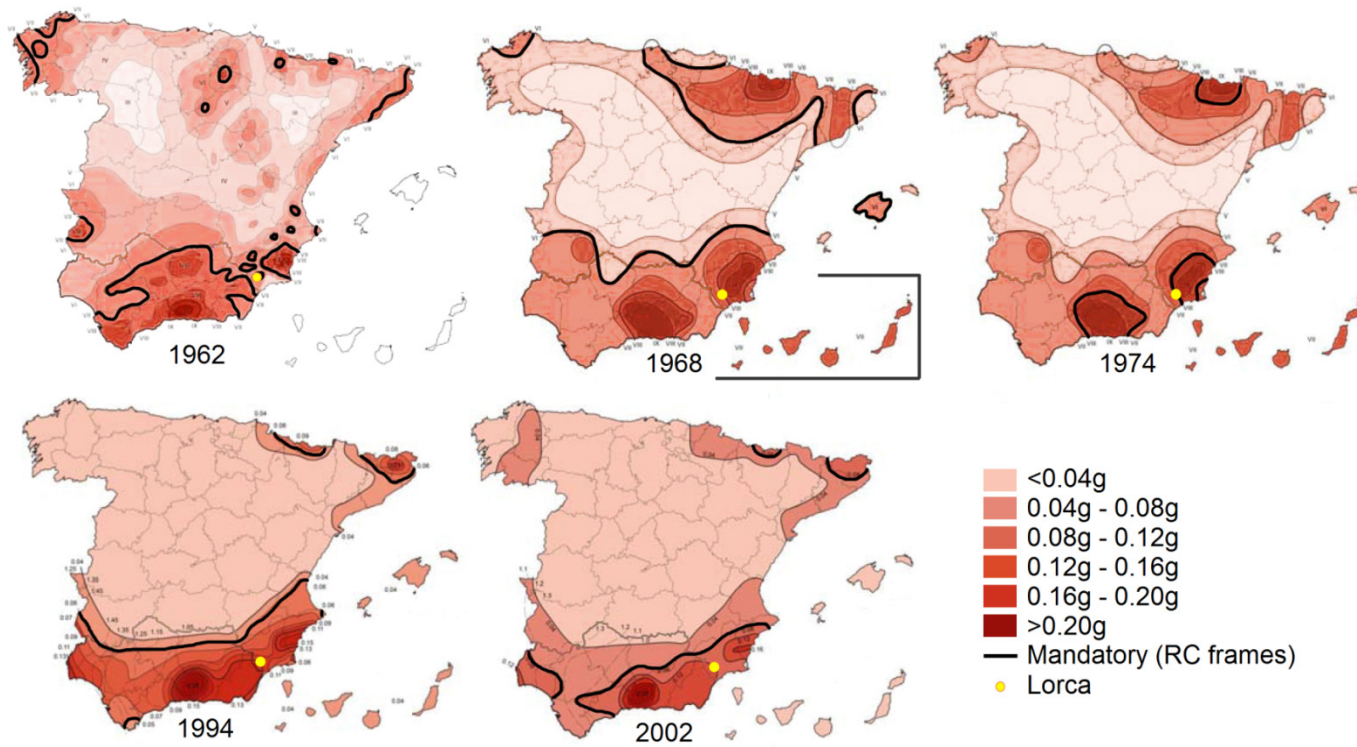


Figure 65: Hazard maps for each Spanish seismic code (adapted from Cabañas et al., 2011)

Table 13: Comparison of regulations of Spanish seismic codes (I) (*italics*: implicit)

Type of code		Proto-code	Old-generation		Medium-generation		New-generation	
Name		MV-101 (chapter 7)	PGS-1	PDS-1	NCSR-94	NCSE-02	EHE-08 (Annex 10)	EC8 (National Annex)
Year		1962	1968	1974	1994	2002	2008	2004/2010
Conditions for not mandatoriness		$a_{gR} < 0.063g$	Minor importance or $a_{gR} < 0.031g$	Minor importance; $a_{gR} < 0.031g$; or ordinary-importance frames when $a_{gR} < 0.106g$	Minor importance or $a_g < 0.047g$	Minor importance, $a_{gR} < 0.031g$, ordinary-importance 3D-frames when $a_{gR} < 0.063g$ unless both number of storeys ≥ 8 and $a_g \cdot S \geq 0.08$	-	$a_g \leq 0.045g$, RC DCL frames
Forbidden constructions		-	When $a_{gR} \geq 0.031g$, dry-stone masonry, concrete walls without fine aggregate, short masonry walls without ring RC beams or short masonry walls without RC confining frames	When $a_{gR} \geq 0.031g$, dry-stone masonry and relevant- and very-relevant-importance; when $0.063g \leq a_{gR} < 0.106g$, ordinary-importance concrete walls without fine aggregate, short masonry walls without ring RC beams or short masonry walls without RC confining frames; when $a_{gR} \geq 0.106g$, ordinary-importance masonry structures	Not-minor-importance masonry buildings when $a_g < 0.063g$; masonry buildings with more than 4 or 2 storeys when $0.063g \leq a_g < 0.094g$ or $a_g \geq 0.094g$, respectively; wide-beams RC frames when $a_g \geq 0.126g$	Not-minor-importance masonry buildings when $a_{gR} < 0.031g$; masonry buildings with more than 4 or 2 storeys when $0.063g \leq a_{gR} < 0.094g$ or $a_{gR} \geq 0.094g$, respectively	-	unreinforced masonry buildings when $a_g \cdot S \leq 0.20g$
Hazard	ULS	Mercalli modified with Wood-Newman	MSK transformed to non-explicit probability in $T_L=50$ years		$P_R=9.5\%$ in $T_L=50$ years $\equiv T_R=500$ years		-	$P_R=10\%$ in $T_L=50$ years $\equiv T_R=475$ years
	DLS	-						$P_R=10\%$ in $T_L=10$ years $\equiv T_R=95$ years
Azores-Gibraltar fault influence <i>K</i>		-	-		1.0-1.3		-	-

Table 14: Comparison of regulations of Spanish seismic codes (II) (*italics*: implicit)

Type of code		Proto-code	Old-generation		Medium-generation		New-generation	
Name		MV-101 (chapter 7)	PGS-1	PDS-1	NCSR-94	NCSE-02	EHE-08 (Annex 10)	EC8 (National Annex)
Year		1962	1968	1974	1994	2002	2008	2010
Risk factor γ_1 (T_L)	Minor importance	-	$(T_L+100)/1$ 50 (-)	1.0 (50)	$(T_L/50)^{(1/e)}$	1.0 (50)	-	0.8 (25)
	Ordinary importance			1.10-1.47 (100)		1.3 (100)		1.0 (50)
	Relevant importance			1.11-1.79 (200)		1.3 (100)		1.3 (100)
	Very relevant importance					1.3 (100)		1.4 (125)
Soil factor S (V_S range [m/s])	Hard rock	1.25 (-,-)	0.38 (>2109)		1.13-1.25 (>750)	1.00-1.25 (>750)	-	1.00 (>800)
	Rock		0.50 (866-2109)					1.25-1.30 (400-750)
	Dense	1.00 (322-866)		1.10-1.16 (400-750)	1.25-1.60 (200-400)	1.35 (360-800)		
	Medium	1.88 (-,-)	1.38 (90-322)	1.38 (149-322)	0.95-1.19 (<400)	1.25-1.60 (200-400)		1.50 (180-360)
	Loose	2.50 (-,-)	2.75 (<90)	2.00 (<149)		1.25-2.00 (<200)		1.80 (<180)
Reference soil type (V_S [m/s])			Medium-dense (322)		Dense (614)			Rock (800)
Foundation factor	Individual footings	-	1.1		-			
	Strip footings		1.0					
	Foundation slab		0.7					
	End bearing piling		0.9					
	Friction piling		1.0					
Shape of spectrum branches $\alpha(T)$ (range of periods at the end of each branch)	1 st (increasing)	-	-		Linear from $1.25a_g$ (0.15-0.31s)	Linear from $a_g \cdot S$ (0.10-0.26s)	-	Linear from $(2/3) \cdot a_g \cdot S$ (0.05-0.10s)
	2 ^o (Plateau)		$\sim T^{0.33}$ (0.5s)	Constant (0.5s)	Constant (0.34-0.94s)	Constant (0.40-1.04s)		Constant (0.25-0.30s)
	3 rd (decreasing)		$\sim T^{1.33}$		$\sim T^{-1}$			$\sim T^{-1}$ (1.2s)
	4 th (decreasing)		-	$\sim T^{-1}$	-			$\sim T^{-2}$
	5 th (residual)		-		-			Constant, being $S_d(T) \geq 0.2a_g$
Max. spectral amplification factor $\alpha_{max}=\alpha(T_C)$			2.5 (for comparison)		2.5 (for comparison)	2.5		2.5
Maximum design spectral acceleration [g]			-	0.20	-			
Combination of modal effects			Addition	SRSS	SRSS or CQC		-	SRSS or CQC

Table 15: Comparison of regulations of Spanish seismic codes (III) (*italics*: implicit)

Type of code		Proto-code	Old-generation		Medium-generation		New-generation	
Name		MV-101 (chapter 7)	PGS-1	PDS-1	NCSR-94	NCSE-02	EHE-08 (Annex 10)	EC8 (National Annex)
Year		1962	1968	1974	1994	2002	2008	2010
Behaviour factor q	Reduction coefficient for irregularity		-		Qualitative	-	-	0.88-1.00 (plan), 0.80 (elevation)
	Masonry (regular)	Unreinforced	<i>1.0</i>	<i>2.5</i>	1.0	-	1.50-2.50	
		Confined			2.00-3.00			
		Reinforced			2.50-3.00			
	RC (regular)	Joists one-way slab	<i>2.0</i>	<i>2.5</i>	2.0	-	-	
		Solid or waffle slab					1.50	
		Wide-beam MRF DCM			3.30-3.90			
		Wide-beam MRF DCH			4.95-5.85			
		Deep-beam MRF DCM			3.30-3.90			
		Deep-beam MRF DCH			4.95-5.85			
		Coupled walls DCM			4.0		1.50-3.60	
		Coupled walls DCH			2.25-5.40			
		Uncoupled walls DCM			3.0		1.50-3.00	
		Uncoupled walls DCH			2.00-4.80			
		Inverted pendulum DCM			2.0		1.50	
		Inverted pendulum DCH			2.00			
		Torsionally flexible DCM			-		2.00	
		Torsionally flexible DCH			3.00			
	Steel (regular)	MRF DCM	<i>2.0</i>	<i>2.5</i>	4.0	-	4.00	
		MRF DCH			5.50-6.50			
		Diagonal bracing			3.0		4.00	
		V-bracings DCM			2.0		2.00	
		V-bracings DCH			2.50			
		Eccentric bracings DCM			4.0		4.00	
		Eccentric bracings DCH			6.00			
		Inverted pendulum DCM			2.00			
		Inverted pendulum DCH			2.00		2.00-2.20	
MRF + concentric bracing DCM		3.0			4.00			
MRF + concentric bracing DCH		4.80						
Infilled MRF	4.0	2.00						
Vertical direction		-	<i>1.0</i>	1.0	-	1.50		

Table 16: Comparison of regulations of Spanish seismic codes (IV) (*italics*: implicit)

Type of code		Proto-code	Old-generation		Medium-generation		New-generation			
Name		MV-101 (chapter 7)	PGS-1	PDS-1	NCSR-94	NCSE-02	EHE-08 (Annex 10)	EC8 (National Annex)		
Year		1962	1968	1974	1994	2002	2008	2010		
Damping factor η (damping ratio ξ)	No partition walls	-	1 (-)		$(5/\xi)^{0.4}$	0.93 (6%)	$(5/\xi)^{0.4}$	1.09 (4%)	-	1.0, because $\eta=[10/(5+\xi)]^{0.5} \geq 0.55$ (5%) is actually included in q
	Many partition walls		0.75 (-)			0.87 (7%)		1.00 (5%)		
Conditions of applicability of simplified static force method		-	-		$n < 20$, $H < 60$ m, regularity in plan and elevation and continuous columns	$n < 20$, $H < 60$ m, regularity in plan and elevation and continuous columns; or $n < 4$ and normal importance	-	$T \leq \min\{4T_c, 2s\}$ and regular in elevation (spatial model); also regular in plan for planar models		
Minimum number of modes considered k		-	1 or 3, for $T < 1$ s or $T \geq 1$ s, respectively	1, 2 or 3 for $T \leq 0.75$ s, $0.75 < T \leq 1.25$ s or $T \geq 1.25$ s, respectively	All i whose $T_i > T_B$, $i \geq 4$; or satisfying $\sum_1^k \lambda_i \geq 0.9$		-	All i satisfying $\sum_1^k \lambda_i \geq 0.9$ and all i whose $\lambda_i \geq 0.0$; or $k=3 \cdot (\text{number of storeys})^{0.5}$ and $T_k \leq 0.20$ s		
Assumed simplified deformed shape			Linear ($T < 1$ s), Sinusoidal ($T \geq 1$ s)	Linear, sinusoidal or base-vertical-tangent-polynomic	Sinusoidal			-		
Simplified fundamental period T	RC frames		$0.09H/L^{0.5}$	$0.09H/L^{0.5} \geq 0.5$ s	$0.09n$			$0.075H^{0.75}$, $H \leq 40$ m		
	Steel frames		$0.10H/L^{0.5}$	$0.10H/L^{0.5} \geq 0.5$ s	$0.11n$			$0.085H^{0.75}$, $H \leq 40$ m		
	Masonry		$0.06 \cdot [H^3/(2L^2+HL)]^{0.5}$	$0.06[H^3/(2L^2+HL)]^{0.5} \geq 0.5$ s	$0.06[H/(2L+H)]^{0.5}H/L^{0.5} \leq 0.5$ s			$0.050H^{0.75}$, $H \leq 40$ m		
	RC wall			$0.85[1/(1+L/H)]^{0.5} \geq 0.5$ s	$0.070n[H/(L+H)]^{0.5}$					
Steel wall	$0.085n[H/(L+H)]^{0.5}$									
Simplified i^{th} period T_i		$T/(2i-1)$	$T/(2i-1)$; $T_2, T_3 \geq 0.25$ s	$T/(2i-1)$		-				
Vertical action	Negligible except	Cantilever	Cantilever or large-span beams, not-framed structures		-	Cantilever or large-span beams, beams supporting columns	If $a_g \leq 0.11g$: beams ≥ 20 m, cantilevers ≥ 5 m, pre-stressed beams, beams supporting columns, base-isolated structures			
	% of horizontal	100%	32-80%	40-80%	70%		45%			

Table 17: Comparison of regulations of Spanish seismic codes (V) (italics: implicit)

Type of code		Proto-code	Old-generation		Medium-generation		New-generation				
Name		MV-101 (chapter 7)	PGS-1	PDS-1	NCSR-94	NCSE-02	EHE-08 (Annex 10)	EC8 (National Annex)			
Year		1962	1968	1974	1994	2002	2008	2010			
Maximum IDR for DLS	Brittle infill panels		-	-	-	-	-	5.0‰			
	Ductile infill panels							7.5‰			
	Isolated or inexistent infill panels							10.0‰			
2 nd order effects	Discard if	2 nd to 1 st ord. moment ≤	-	-	10%		-	10%			
		Total drift ≤			2‰			-			
	Correction				-			-		Quantitative until ratio=30%	
Reduction factor for gravitational loads	Live	Residential	0.5	0.5	0.3	0.5	0.3 or 0.5				
		Office	0.7	0.6	0.6		0.3 or 0.6				
		Commercial					0.6				
		Public spaces	1.0	0.8		0.6		0.6			
		Storage	1.0	-		1.0		1.0			
	Snow	Low	1.0	0.5	0.0	0.0	0.0	0.0			
		High			1.5	0.3	0.5	0.2 or 0.5			
Accidental eccentricity of masses		-	-	-	5%		-	5%			
Consideration of effects in the transversal direction [%]		-			30%		-	30%			
Reduction in material partial factor for accidental situation with respect to persistent&transient		-	-30%	-	-	-15%	-0% (cyclic consideration) or -15%				
Conditions for regularity of	Geometry		-	Qualitative		Quantitative		-	Quantitative		
	Masses			-	Qualitative	Quantitative			Quantitative		
	Stiffnesses			-		Qualitative			Quantitative		
	Resistances			-		Qualitative			Qualitative		
Non-structural elements consideration		-	-	Qualitative	Qualitative		-	Quantitative			
Maximum column-beam eccentricity					25% column section base		-	25% column section base			
Overstrength factor for hierarchy of resistances in RC frames	Shear > Moment	Columns	-	-	-	1.10 (see section 2.2.1)	1.2 ($q < 3$) or 1.35 ($q \geq 3$)		1.10 (DCM) or 1.30 (DCH)		
		Beams			1.00 (see section 2.2.1)		1.35		1.00 (DCM) or 1.20 (DCH)		
	Columns > Beams				-		1.35		1.30		
	Joint > Member				-		1.35		1.20 (DCH)		
Maximum relative axial in columns		-	-	-		0.65	0.65 (DCM) or 0.55 (DCH)				
Contribution of upper slab to beams		-	-	-		Quantitative					
Specific design of squat columns		-	-	-	Qualitative	<i>Quantitative</i>	Quantitative (assessment)				

FAST simplified vulnerability approach for seismic assessment of infilled RC MRF buildings
and its application to the 2011 Lorca (Spain) earthquake

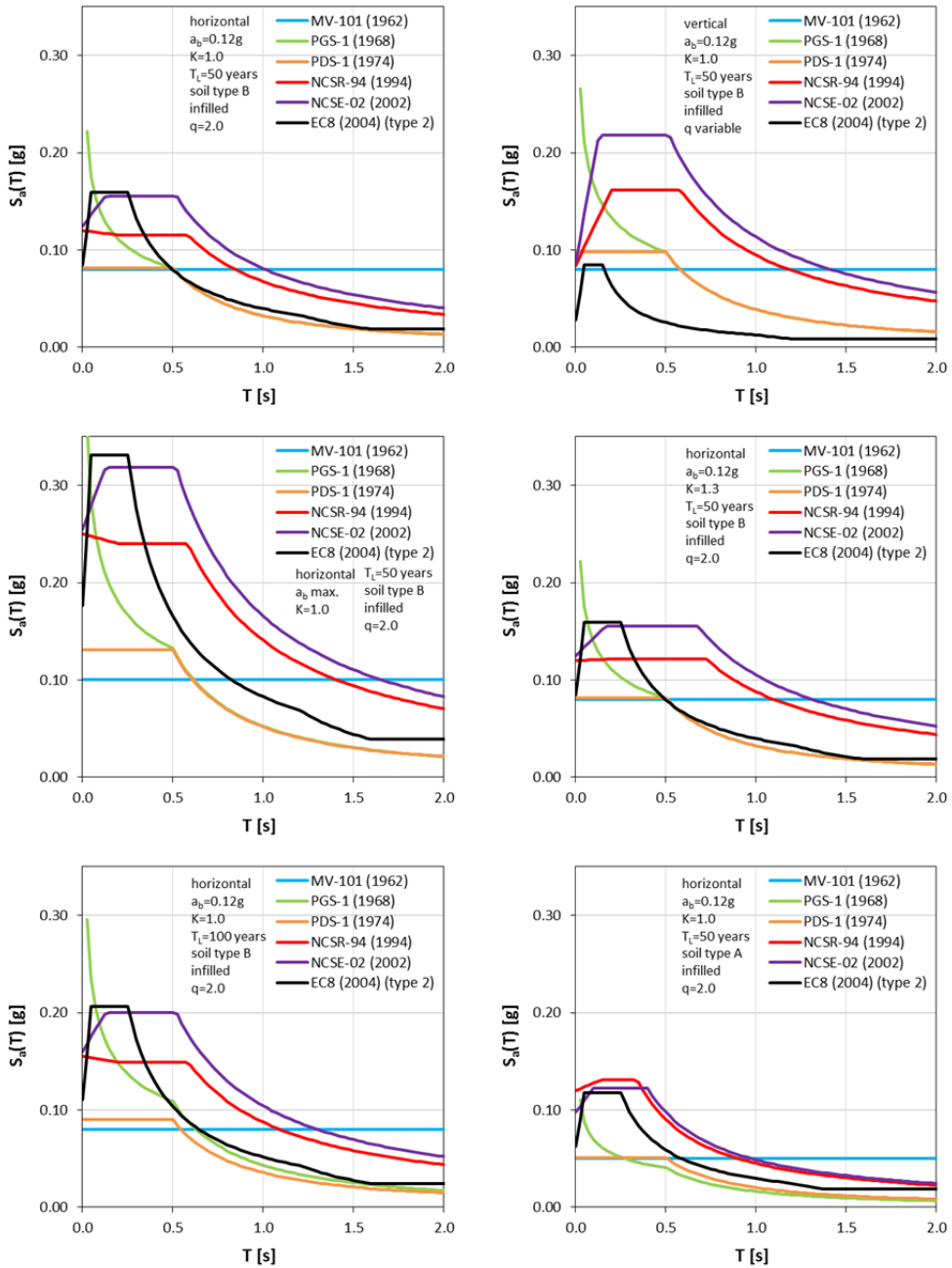


Figure 66: Design response spectra for all the codes for different assumptions (I)

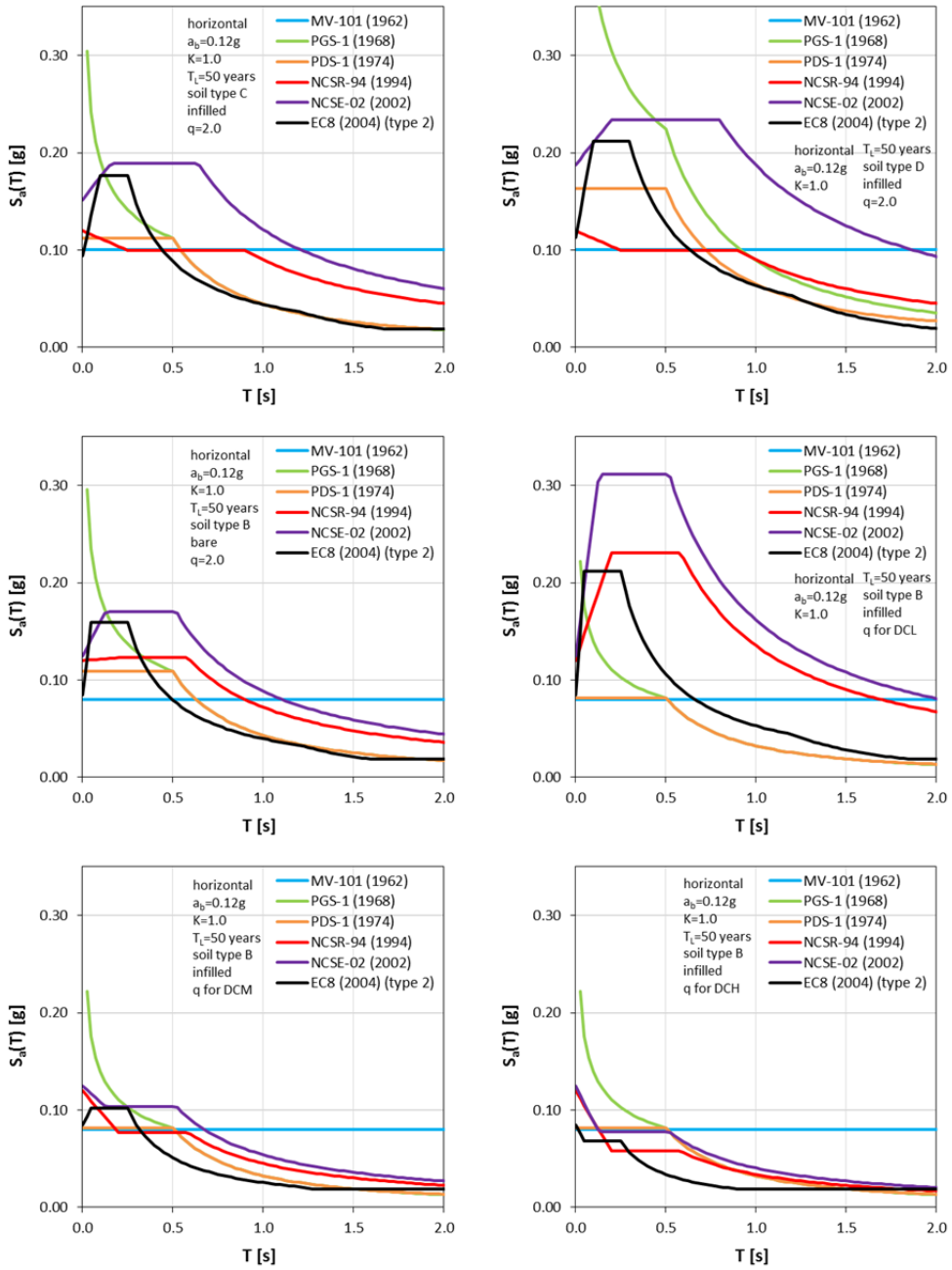


Figure 67: Design response spectra for all the codes for different assumptions (II)

In Figure 66 and Figure 67, design acceleration response spectra considering different situations, for all the codes, are compared. In each graphic, a single input value is modified, in order to understand the influence of each coefficient. The reference scenario is a RC infilled residential building in the city of Lorca (Murcia), on medium soil, analysed in the horizontal direction. In order to make the comparison evident, similar values of q are assumed –except for the cases in which the single modified value is the behaviour factor itself.

In the first graphic, main trend of the differences can be observed:

- MV-101 is always constant;
- PGS-1 shows clearly the important mistake in its first branch, being in the rest similar to PDS-1
- maximum $S_a(T)$ increase “chronologically”, being not so different for the current Spanish code than for EC8;
- the “plateau” is much longer for all the codes than for EC8, e.g. leading to half spectral acceleration values EC8 than for NCSE-02 for the medium range of periods;
- the incongruent values of S for NCSR-94 lead to smaller $S_a(T)$ than NCSE-02, together with very high suggested values of damping.

From the observation of the rest of the cases, the following ideas may be pointed out:

- vertical action is much more reduced for EC8, both for the decrease of corresponding PGA and for the assumption of larger q ;
- decrease of S due to the increase of seismicity is not very important as a_b is not higher than 0.25g in all the territory;
- larger K values exaggerate the difference of length between the “plateaus” of medium-generation codes and EC8;
- increase of demand for relevant-importance buildings is lower for PDS-1 than for the rest of codes;
- soil factors act similarly except for NCSE-94, which furnishes spectral values almost 2.5 times lower than NCSE-02 for loose soil;
- damping reduction for bare frames is very high for old-generation codes in comparison with the rest;

- considering $q=1$ as the representative value of DCL in Spanish codes – although it is not clear if such assumption could allow designers to omit all the specific local detailing imposed by seismic codes—, higher demand values than EC8 can be observed;
- assuming irregularity in elevation –likely due to higher interstorey height of ground floor together with a reduction of the infills area in plan—, roughly similar spectral values are obtained for DCM or DCH.

2.2 DIFFERENCES BETWEEN SPANISH AND EUROPEAN CURRENT CODES

In this section, main drawbacks of NCSE-02 in comparison with the common framework of main modern seismic international codes are analysed in detail.

2.2.1 Hierarchy of resistances

Capacity design is the main instrument of control of the performance of the building during an earthquake by ensuring that the maximum strength of members is only reached in the points of the structure that are able to develop adequate inelastic response, thus presenting large ductility capacities and not compromising the stability of other elements or the whole –or being easier to repair (Fardis, 2009).

Hence, capacity design consists of two procedures:

- 1) Hierarchy of resistances: a hierarchy of elements (and types of failures) must be established in order to “protect” some important elements, by providing more resistance than the capacities of the neighbouring elements, less important.
- 2) Local detailing: in order to provide sufficient chord rotation capacity and ductility, suitable local detailing of such elements selected to incursion into the inelastic range must be provided.

Then, it is necessary to define which elements are chosen to eventually experiment inelastic incursion. Theoretically, any set of elements could be selected

if they are accordingly detailed afterwards. However, the arrangement may be chosen in order to maximize the seismic global capacity, which is equivalent to maximizing the global displacement capacity.

The last is achieved when columns rotate as a rigid body from their bases, thus plastic hinges are formed in such bases and all beam ends, which is called “beam-sway” mechanism (Figure 68a). Consequently, inelastic deformation demand is spread throughout the beams of the entire structure, in every single storey, thus a mechanism of all the storeys is carried out.

On the other hand, the most unfavourable set of plastic hinges, causing minimum displacement capacity, would be a mechanism in which both ends (top and bottom) of every column of a storey form plastic hinges, which is called “soft-storey” mechanism (Figure 68b). Not only this mechanism furnishes the lowest displacement capacity but it is also more difficult to ensure proper local ductility in columns than in beams, because compressed sections must be very well confined for not suffering concrete failure.

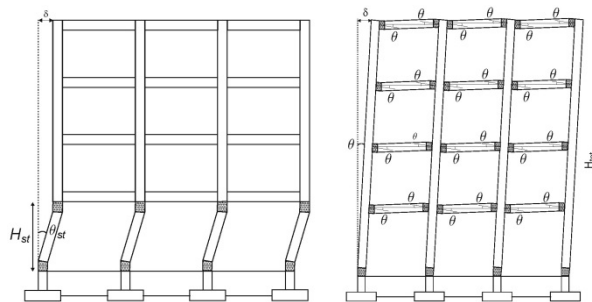


Figure 68: Soft-storey (a) and beam-sway (b) plastic mechanism of frames (from Fardis, 2009)

Hence, seismic codes establish three types of provisions regarding hierarchy of resistances aimed at obtaining structures able to carry out beam-sway mechanisms, i.e. with plastic hinges in beam ends:

- 1) Joint-beam hierarchy (or capacity design of joints): Joints shear resistance must be higher than shear demand consistent with flexural capacities of beam ends framing into the joint in the corresponding direction.
- 2) Column-beam hierarchy (or flexure capacity design of columns): Moment resistance of column ends framing into a joint must be higher than flexural capacities of beam ends framing into the same joint in the corresponding direction.
- 3) Shear-moment hierarchy (or shear capacity design of members): In each member end, shear resistance must be higher than shear demand consistent with maximum flexural forces able to be developed in such ends.

All of these rules are regulated by expressions with the generic form shown in Equation (31), being: R_i , resistance of the element –or type of force— i , which is the prevalent one; E_j , maximum force able to be developed by the element –or type of force— j , which is the not-prevalent one; and γ_R , the so-called “overstrength” factor, which furnish some conservativeness regarding the possibility that the demands of the not-prevalent element –or type of force— is higher than expected due to material overstrength.

$$R_i \geq \gamma_R \cdot E_j \quad (33)$$

There are some variations regarding the characterisation of each parameter depending on the code:

- most of them compel to use design values for resistances of materials, while other codes use nominal ones;
- the magnitude of γ_R sometimes depend on the design ductility class and other times it is independent (e.g. see Table 17);
- maximum capacities of not-prevalent elements –or type of forces— are obtained by considering different combinations of actions;
- sometimes the whole expression is assumed to be satisfied if some geometric conditions are fulfilled.

Both joint-beam and shear-moment hierarchy come from the consideration of shear failure as inherently brittle, i.e. avoidable. In fact, in shear diagonal mechanism reinforcement is not able to develop effective inelastic action

contemporaneously with proper confinement and control of cracking in concrete (Fardis, 2009).

Integrity of joints is ensured by making them more resistant than the beams; in fact, it is not necessary to compare them with columns because the column-beam hierarchy already warrants that the maximum shear demand in joint cannot be higher than the shear in correspondence with the flexural capacity of beams.

Usually codes provide similar formulations for shear demand in the centre of the joint panel for exterior and interior connections, and also explicit expressions for their shear resistances with empirical basis but consistent with strut-and-tie mechanical behaviour. Effective dimensions of joint panels vary within codes (see Table 30)

Joint-beam hierarchy is only explicitly required in EC8 for DCH; for DCM it is assumed that confinement furnished by hoops –more relaxed provision when panels receive members in almost all of their faces— is enough to satisfy requirements.

Shear-moment hierarchy is usually considered separately for columns and beams because the calculation of the shear demand is different. In columns, shear demand in each end comes from the consideration of moment capacities acting in both ends with different sign. Almost always it is not necessary to consider reversal of forces because columns present symmetric reinforcement, thus moment capacities are similar for both directions.

However, in beams not only moment capacities in ends act but also gravitational action, and reversal of forces must be considered. In Italian code NTC, not only the typical gravitational long-term action is considered but also it is suggested to assume that only dead loads act.

It is worth noting that some codes, as EC8, relax the provision for columns by assuming that the actual shear demand in each end is not the shear consistent with the moment capacity but consistent with the maximum moment able to be developed by the connection, thus ruled by the capacity of beams framing each column end rather than the column itself.

In the following, some considerations regarding the different types of hierarchy of resistances and their correspondent provisions in seismic codes are discussed. Later, NCSE-02 provisions regarding this issue are analysed in order to show their deficiencies.

2.2.1.1 Capacity design of columns: formulations

Regarding column-beam hierarchy, quite interesting considerations could be done. The general scope of this provision is to avoid plastic hinges in columns. However, the common proposed formulation aimed at this purpose is kind of an “indirect” solution, which has demonstrated to somehow show a good performance (Fardis, 2009) but still is not able to completely warrant that a complete global mechanism involving all the storeys of the building is carried out.

The usual formulation adopted by codes is in the form of Equation (33) with $R_j = \Sigma M_{Rc}$ and $E_j = \Sigma M_{Rb}$, being ΣM_{Rc} and ΣM_{Rb} the summation of moment resistances of columns above and below the joint and of moment resistances of beams at both sides of the joint, respectively. It is worth noting that capacity design principles are not applied to each single column but to the global contribution of columns framing a joint, conversely to the case of the other two capacity design rules (shear-moment and joint-beam). Hence, it is possible that one of the columns possesses much less overstrength (i.e. the ratio between capacity and demand in terms of bending moment) than the other column or even less than some or all the beams framing the joint, thus not being protected against yielding.

In fact, the scope of Equation (33) is only to avoid, within a reasonable degree of security, the simultaneous formation of plastic hinges in both ends of all the columns of a storey (soft-storey); it do not prevent the formation of any plastic hinge in columns. If plastic hinges in the rest of the corresponding column ends placed at the same height, a collapse mechanism of few storeys can be developed (see Figure 129). Moreover, the probability of developing soft-storey mechanism is not zero; however, it has been proved to not causing global instability in a real event (Panagiotakos and Fardis, 1998).

In the following, special diagrams (whose legend is shown in Figure 69) are used aimed at representing the evolution or flexural demand in the four members

framing into a joint. In the quadrant placed near each member in the counterclockwise sense, the shadowed area represents the magnitude of its moment overstrength (M_{Rb}/M_{db}), and the radius corresponding to the end of this area represents its maximum moment resistance. Overstrength can be represented graphically only if resistance and design values have the same sign. Thus, any angle between the member and the maximum moment symbolise a feasible flexural demand in the member, normalised to the demand corresponding to the seismic situation. Moment overstrengths are represented as α_c and α_b for columns and beams, respectively.

Maximum global flexural demand in the connection due to horizontal loads is equal to $\min\{\sum M_{Rb}, M_{Rc}\} = \sum M_{Rb}$, which corresponds to a global overstrength $\alpha_b = \sum M_{Rb} / \sum M_{db}$; in the graphics, α_b would not necessarily correspond to the mean value of the overstrengths of both beams, but could be a good approximation in some cases. Thus, a parameter α varying between 0 (corresponding to no horizontal load) and α_b (corresponding to maximum horizontal load) can be defined in order to represent the evolution of flexural demand in members due to seismic loading. It is symbolised in the graphics with a thick line in each quadrant, always within the shadowed area (i.e. the moment in each member is always lower than the resistance). They form a thick “cross”, overlapped to the members, that starts to rotate in the counterclockwise sense.

The angles between the branches of the “cross” remain all equal to 90° (referred herein as being “synchronised”), which means that moments in members increase proportionally (homothetically) to their demand in the seismic situation (M_{di}), respectively; it means that the ratios between stiffnesses of members remain similar than if elastic values are considered, because cracking is not taken into account. In a first step, also moments in members due to gravitational load in seismic situation are discarded, as they may be small enough when compared with moment resistances of members.

When any of the branches of the “cross” reaches the end of the corresponding shadowed area, it means that the member has consumed its resistance and thus a plastic hinge is formed in such member end. From this point forward, that branch stays still as it cannot increase its demand, while the opposite member (which

belongs to the same type: beam or column) increases its demand more quickly than the other two elements in order to compensate the absence of increment in the plastic hinge and thus satisfying the equilibrium in the connection. The other two elements of the “cross” remain with the same angle, always if constant stiffness ratio is considered.

Then, a second plastic hinge is formed in the next element attaining its capacity. If this element is opposite to the first yielded one, the global moment cannot increase anymore and thus the connection flexural demand remains constant from then on. Conversely, if the second plastic hinge is formed in an adjacent member, the process can continue until a third hinge is created.

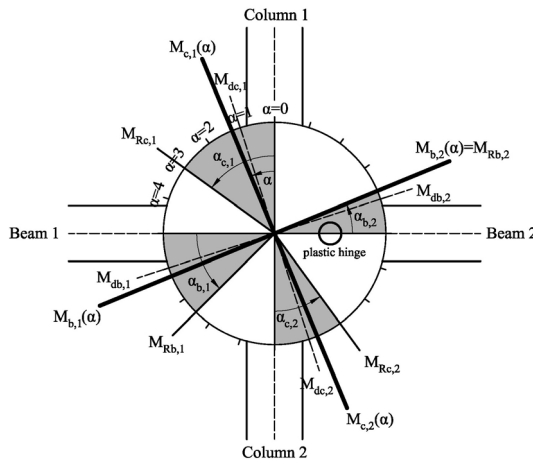


Figure 69: Legend for diagrams shown in the present section

However, the real evolution of flexural demand can be “not synchronised”, i.e. that relative increments of moment can be different (or even being a decrease, instead) between members due to cracking and post-elastic redistribution, so the flexural demand is not proportional to the elastic distribution. In the graphics, it is symbolised by a different “velocity” of each branch.

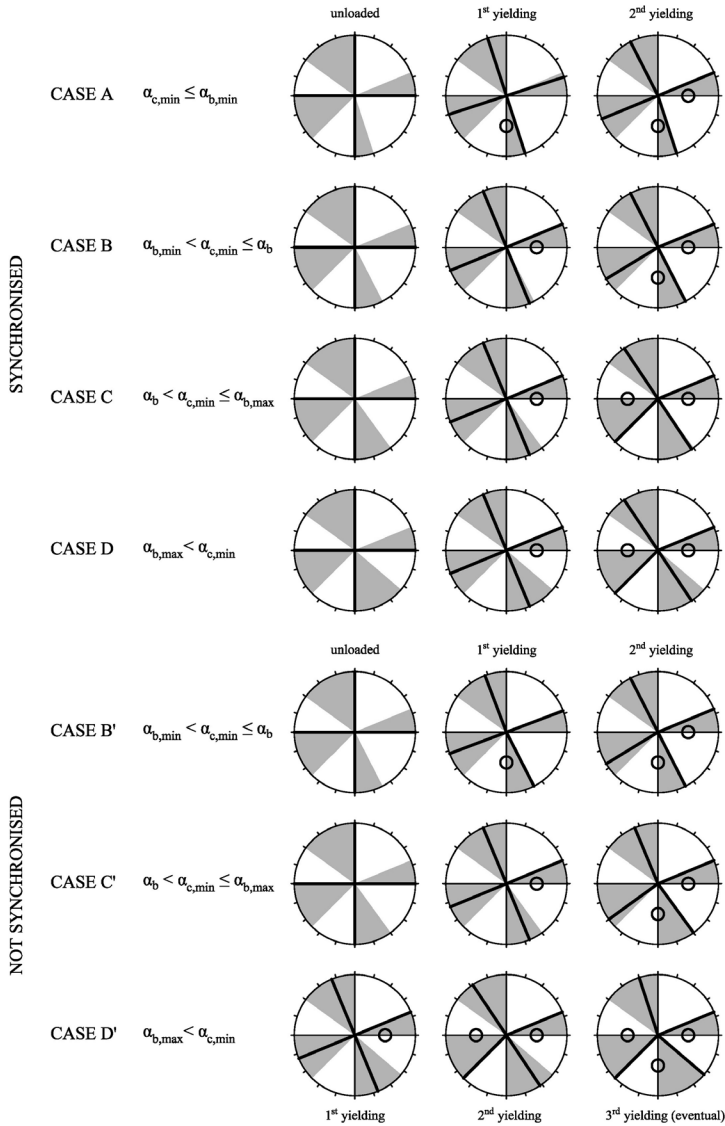


Figure 70: Diagrams representing different scenarios of evolution of moment demand in members framing into a joint, depending on their relative overstrength values

Within a connection, if each column's moment overstrength is compared to each beam's moment overstrength, four cases can be defined, depending on the

value of minimum column overstrength ($\alpha_{c,min}$) in relation with minimum ($\alpha_{b,min}$), maximum ($\alpha_{b,max}$) and global (α_b) overstrength of beams. In Figure 70, the evolution of moment demand and formation of plastic hinges corresponding to those four cases is shown; cases are named as A, B, C and D for the “synchronised” scenario, while for the “not synchronised” scenario, cases B’, C’ and D’ are considered –as an eventual case A’ would be similar to A.

Case A represents the most unfavourable situation: one of the columns presents less overstrength than both beams. In this case, the first plastic hinge is formed in that column. In case B, that column has an overstrength that is higher than the minimum overstrength of beams but lower than the global one. In this case, the first plastic hinge is formed in the beam with minimum overstrength; from that instant, the opposite beam increase its “velocity” of moment assumption, but it is not high enough to reach its resistance before than the column. In case C, the process is similar but the second beam reaches its maximum before than the column, which has overstrength higher than the global overstrength of beams. Finally, case D is trivial: if both columns have higher overstrength than each beam, only plastic hinges in beams are formed.

Conversely, considering the “not synchronised” scenario, in case B’ the first plastic hinge can be formed in a column, because of post-cracking moment redistribution; similarly, in case C’ a plastic hinge in column could be formed before than in the second beam. Furthermore, in case D’, even when both beams have yielded and thus the total flexural demand in the connection cannot increase, one of the columns can transfer its moment demand to the other, leading to the formation of a plastic hinge in such column (see Figure 129). One possible reason for explaining such behaviour may be that if a plastic hinge is formed in a column top for any reason, the rest of the columns in the same storey must increase their shear demand when subjected to a global increment of lateral loads, which could lead to a transfer of moment from the column bases placed above that storey. Thus, the adoption of formulations aimed at preventing formation of single plastic hinges in columns may be an issue, as it could induce the yielding of other column ends placed at the same height

“Synchronised” behaviour seems to be in agreement with the alternative formulation proposed in Italian seismic code NTC (CS.LL.PP, 2009), which is shown in Equation (34) with a different aspect, being: subscripts c and b referred to column and beam, respectively; subscripts i and j , the identifier of each column and beam, respectively; n_c and n_b , number of columns and beams, respectively, framing to the joint; M_d , moment demand in the seismic situation; and α refers to any moment overstrength of members.

$$\frac{\alpha_{c,i}}{\gamma_R} = \frac{M_{Rc,i}}{M_{dc,i}} \geq \frac{\sum_{j=1}^{n_b} M_{Rb,j}}{\sum_{i=1}^{n_c} M_{dc,i}} = \frac{\sum M_{Rb,j}}{\sum M_{db,j}} = \alpha_b \quad (34)$$

It is possible to demonstrate that, if “synchronisation” is assumed, this expression prevents columns from yielding on the condition that the summation of moments in columns due to gravitational loads in seismic situation is negligible with respect to moments of design and resistance.

A generic interior connection, with two columns and two beams (corresponding to subscripts 1 and 2 in each case), is considered. It is supposed to belong to case C, and beam with identifier 2 is supposed to have higher overstrength than beam 1. Parameter α increases from 0 until α_b , and increasing demand in each member is expressed as $M_{c,i}(\alpha)$ and $M_{b,i}(\alpha)$ for columns and beams, respectively. Their initial expressions, before the creation of the first plastic hinge in beam 1 (corresponding to a value of $\alpha = \alpha_{y,b1}$), are those shown in Equations (35) and (36), respectively, being M_g the moment caused by the gravitational load in the seismic situation, and M_h the moment caused by the horizontal action alone. In all the demonstration, values of moments are positive if they are consistent with the moments caused by lateral loading, i.e. opposite for columns and beams. Given that $M_{gb,1}$ and $M_{gb,2}$ have usually different sign, their summation is not expressed as a summatory but as a difference of absolute values, as shown in Equation (37).

$$M_{c,i}(\alpha \leq \alpha_{y,b1}) = (M_{dc,i} - M_{gc,i})\alpha + M_{gc,i} = M_{hc,i} \cdot \alpha + M_{gc,i} \quad (35)$$

$$M_{b,j}(\alpha \leq \alpha_{y,b1}) = (M_{db,j} - M_{gb,j})\alpha + M_{gb,j} = M_{hb,j} \cdot \alpha + M_{gb,j} \quad (36)$$

$$\Delta |M_{gb}| = M_{gb,1} + M_{gb,2} = M_{gc,1} + M_{gc,2} = \sum M_{gc,i} \Rightarrow M_{gc,i} \leq \Delta |M_{gb}| \quad (37)$$

Then, $\alpha_{y,b1}$ can be obtained by replacing $M_{b,1}(\alpha)$ by $M_{Rb,1}$ in Equation (36), resulting in Equation (38). For higher values of α , the evolution of moment demand in beam 2 (shown in Equation (39)) must include the aliquot of moment that beam 1 is not able to resist anymore, while columns remain governed by the same expression, because their stiffness ratio remain constant. Consequently, plastic hinge in beam 2 is created for a value of $\alpha = \alpha_{y,b2}$ as in Equation (40), obtained by replacing $M_{b,2}(\alpha)$ by $M_{Rb,2}$ in Equation (39).

$$\alpha_{y,b1} = \frac{M_{Rb,1} - M_{gb,1}}{M_{db,1} - M_{gb,1}} \quad (38)$$

$$\begin{aligned} M_{b,2}(\alpha > \alpha_{y,b1}) &= (M_{db,2} - M_{gb,2})\alpha + M_{gb,2} + \\ &\quad + (M_{db,1} - M_{gb,1})\alpha + M_{gb,1} - M_{Rb,1} = \\ &= \left[(M_{db,1} + M_{db,2}) - (M_{gb,1} + M_{gb,2}) \right] \alpha + (M_{gb,1} + M_{gb,2}) - M_{Rb,1} = \end{aligned} \quad (39)$$

$$\begin{aligned} &= \left(\sum M_{db,j} - \Delta |M_{gb}| \right) \alpha + \Delta |M_{gb}| - M_{Rb,1} \\ &= \left(\sum M_{db,j} - \sum M_{gc,i} \right) \alpha + \sum M_{gc,i} - M_{Rb,1} \\ M_{Rb,2} &= \left(\sum M_{db,j} - \sum M_{gc,i} \right) \cdot \alpha_{y,b2} + \sum M_{gc,i} - M_{Rb,1} \Rightarrow \\ &\Rightarrow \alpha_{y,b2} = \frac{\sum M_{Rb,j} - \sum M_{gc,i}}{\sum M_{db,j} - \sum M_{gc,i}} \end{aligned} \quad (40)$$

Hence, the condition that both columns must satisfy aimed at being considered of belonging to case C and thus at not experimenting yielding during lateral loading is that their resistance must be higher than the demand corresponding to a

global value of $\alpha_{y,b2}$, as shown in Equation (42), obtained from Equation (41). Finally, if $\Sigma M_{gc,i}$ is negligible with respect to moment of design and resistance, then each $M_{gc,i}$ and also $\Delta|M_{gb}|$ are negligible too (see Equation (37)), so $\alpha_{y,b2} = \Sigma M_{Rb,j} / \Sigma M_{db,j}$ in Equation (40). Thus, overstrength required to each column in order to not yield is expressed as in Equation (43), which is similar to the formulation suggested in Italian code (Equation (34)), without accounting with γ_R .

$$M_{Rc,i} \geq M_{c,i}(\alpha_{y,b2}) = (M_{dc,i} - M_{gc,i})\alpha_{y,b2} + M_{gc,i} \quad (41)$$

$$\begin{aligned} \alpha_{c,i} &= \frac{M_{Rc,i}}{M_{dc,i}} = \alpha_{y,b2} \left(1 - \frac{M_{gc,i}}{M_{dc,i}} \right) + \frac{M_{gc,i}}{M_{dc,i}} = \\ &= \left(\frac{\sum M_{Rb,j} - \sum M_{gc,i}}{\sum M_{db,j} - \sum M_{gc,i}} \right) \left(1 - \frac{M_{gc,i}}{M_{dc,i}} \right) + \frac{M_{gc,i}}{M_{dc,i}} \end{aligned} \quad (42)$$

$$\alpha_{c,i} \approx \frac{\sum M_{Rb,j}}{\sum M_{db,j}} = \alpha_b \quad (43)$$

Hence, if moments due to gravitational load in beams are quite high but similar in both beams, the formulation of NTC still works. In Figure 72 a and b, scenarios corresponding to negligible and no negligible but similar $M_{gb,j}$, respectively, are shown. The graphic consequence of gravitational moment is that branches start to rotate from an initial angle. Still, the safety factor for columns remains the same in both cases.

In Figure 71 a and b, columns of an interior connection are capacity designed following EC8 and alternative NTC prescriptions, respectively, in order to evaluate whether the last choice leads to much higher column dimensions than the first one. Design moments of all members and moment of resistance in beams are similar in both cases; only resistances of columns change depending on the method. Columns are designed strictly to satisfy hierarchy formulations, regardless of other issues as homogenisation of dimensions within the same storey or within the same column alignment. Gravitational moments in columns are considered to be negligible.

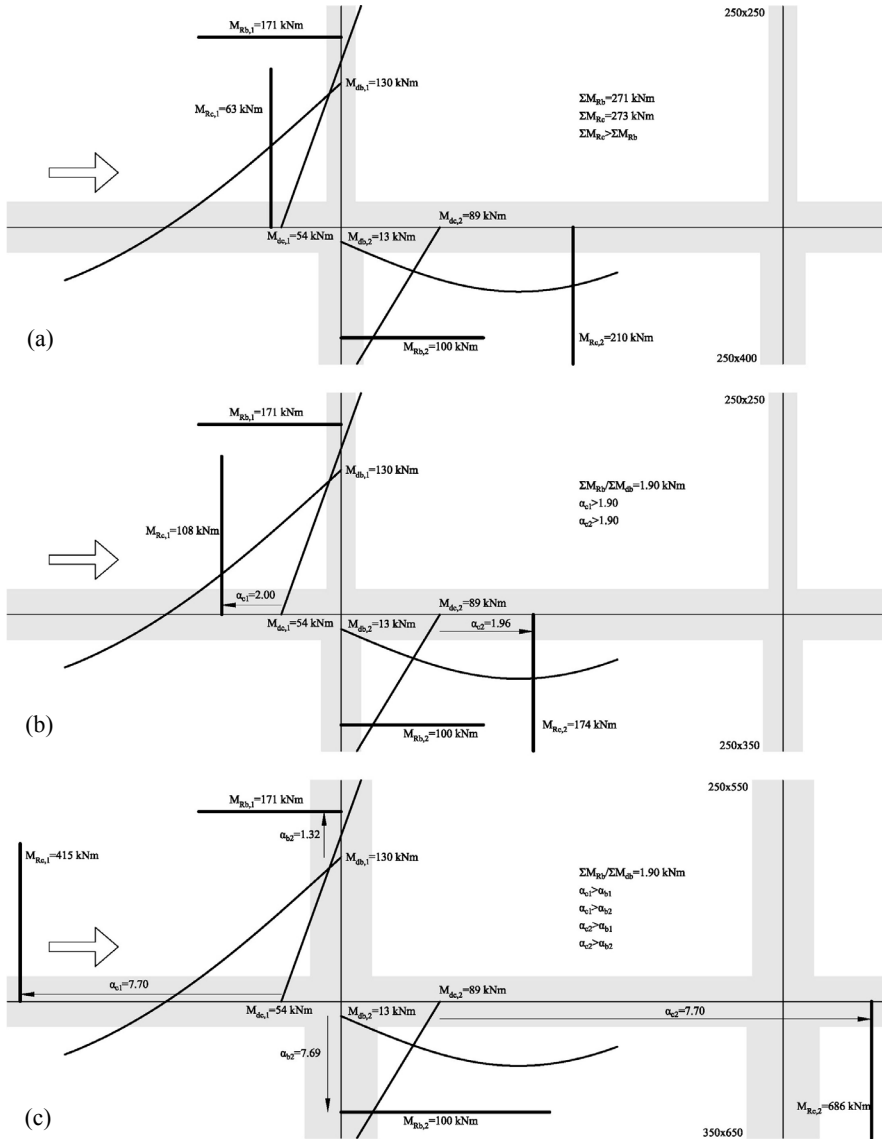


Figure 71: Example of capacity design of columns of interior connection, regardless of γ_R , following the procedure of EC8 (a), NTC –alternative– (b) and NCSE-02 (c)

In the first case (EC8), multiple solutions are possible if $\Sigma M_{Rc} \geq 271$ kNm. In the specific solution shown in Figure 71a, overstrength of upper column is only 1.17,

lower than the minimum overstrength in any beam (1.32), thus a plastic hinge in that end may be formed. In the second case (NTC), overstrength of both columns must be higher than the global overstrength of beams, leading to more similar values between them. Required global resistance in columns is 282kNm in this case, which is slightly higher than in the first case (271kNm). It suggests that application of alternative formulation of NTC is not necessarily more “expensive” in terms of material (related to the required resistance): it requires only a higher level of homogeneity between columns.

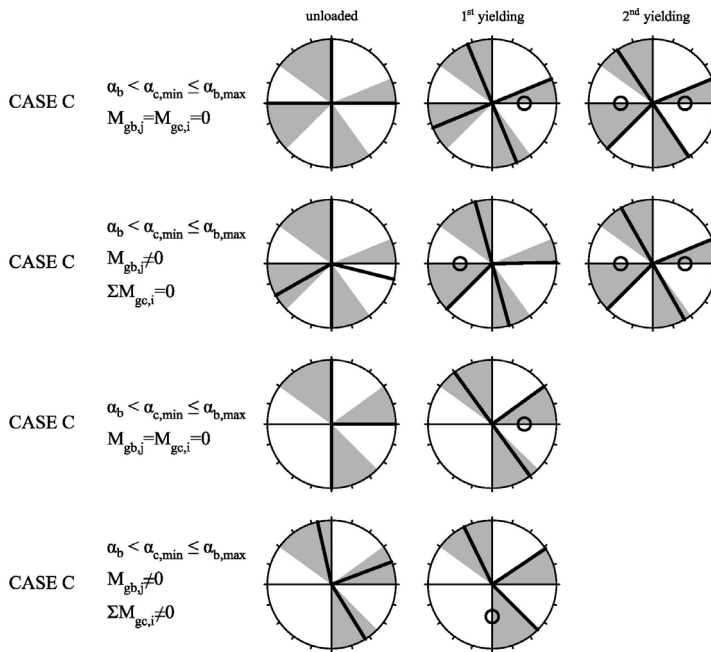


Figure 72: Diagrams of moment evolution in members framing into a joint for different assumptions of initial moments due to gravitational load in seismic situation

However, sometimes $\Sigma M_{gc,i}$ may not be negligible. This is the case of exterior connections belonging to the penultimate storey—as capacity design is not required in the last storey—, especially when span of beams is large and seismic design forces are reduced (due to low seismicity or to high values of q). In this case, the

real overstrength of columns can be lower than for the beam, as shown in Figure 72d with respect to Figure 72c, so columns may not be protected against yielding.

If negative gravitational moment in a beam is higher than design moment due to the only horizontal load ($M_{hb,j}$), then $M_{db,j}$ is negative. Thus, it should be introduced in Equation (43) with such different sign. Aimed at avoiding such concern, NTC replace $\Sigma M_{db,j}$ by $\Sigma M_{dc,i}$ because in interior connections gravitational moments in columns are usually low, so $M_{gc,i} \leq M_{hc,i}$ and then $M_{dc,i}$ and $M_{Rc,i}$ have likely the same sign.

Still, columns above and below the joint can have design moments with different sign. In this case, EC8 suggest to consider every $M_{Rc,i}$ as positive, thus assuming that the evolution of moments may be in both cases towards the conventional behaviour. Instead, NTC suggests that the alternative formulation (Equation (34)) should be transformed into Equation (44), thus moving the design moment with different sign (assumed to correspond to subscript 2) from denominator to numerator.

$$\frac{\alpha_{c,i}}{\gamma_R} = \frac{\sum M_{Rb,j} + M_{db,2}}{M_{db,1}} \quad (44)$$

Two typical scenarios are representative of this situation: i) bottom of exterior columns at last storey, in which gravitational moment is larger than moment due to horizontal loading and has different sign; and ii) top of columns at ground storey belonging to frames with high “cantilever behaviour” (see Table 33), in which $M_{hc,i} < 0$.

In case i), the assumption of EC8 seems to make sense as the evolution of moments tends to change the sign of such negative gravitational moment. Instead, proposal of NTC (Equation (44)) may not be justified; similarly to the case in which one of the beams have negative $M_{db,j}$, it is only necessary to introduce both design moments with their corresponding sign in Equation (43). If both columns have negative $M_{db,j}$, then it is impossible to use the NTC formulation, and also it would not make any sense as gravitational moments would not be negligible. Thus, suggested formulation in this work (Equation (42)) would be required.

Regarding case ii), it is not possible to know in advance which would be the evolution of moments in such column top with negative design moment. Assuming linear evolution, moment would remain negative, increasing its absolute value, as shown symbolically in Figure 73. However, between the instant in which a plastic hinge in column base is formed and the instants in which plastic hinges in beams beside column top, it is not possible to know if moment would change to positive, which could happen if upper column have less overstrength than the beams and yields prematurely. Anyway, the assumption of EC8 is always valid thanks to the similar resistance of columns in both directions –regardless of any variation of axial load. Again, NTC formulation for this case (Equation (44)) may not be justified, as it would be only necessary to introduce both design moments with their corresponding sign.

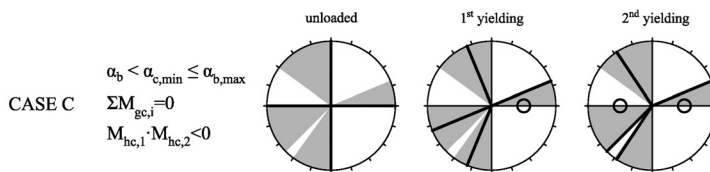


Figure 73: Diagrams of moment evolution in members framing into a joint when inferior column presents negative moment due to only horizontal loading

2.2.1.2 Capacity design of columns: equilibrium

Another important issue is where should be verified the equilibrium of resistances. Theoretically, it should be done in the virtual intersection of the beam-column axes, so the ratio $\Sigma M_{Rc}/\Sigma M_{Rb}$ –where the resistances are referred to the face of the joint panel— would get multiplied by $(1+h_b/H_{cl})/(1+h_c/L_{cl})$, where h_b and h_c are the mean cross-sectional depth of beams and columns framing into the joint, respectively, and H_{cl} and L_{cl} are the mean clear height of columns and span of beams of the same elements. This factor is usually higher than 1.00 (Fardis, 2009), thus the assumption of account with the resistances at faces may be conservative.

Besides, such factor is very sensitive to H_{cl} and especially to h_b . For instance, assuming default values of $H_{cl}=3\text{m}$, $L_{cl}=5\text{m}$, $h_c=400\text{mm}$ and $h_b=500\text{mm}$, similar reduction of the factor is obtained:

- when H_{cl} increase until 3.5m (+17%) or when L_{cl} decrease until 2m (-60%);
- when h_b decrease until 300mm (-40%) or when h_c increase until 2000mm (+500%, obviously not feasible).

The last enlightens that such a simplification of the procedure –not having into account the dimensions of the joint panel— could derive into very different capacity-design ratios for wide-beam frames than for deep-beam ones. In Table 18 to Table 21, a parametric study of the magnitude of the factor $(1+h_b/H_{cl})/(1+h_c/L_{cl})$ is carried out for representative ranges of values for the different variables: H_{cl} (2.5, 3.0, 3.5, 4.0 and 4.5m); L_{cl} (3, 4, 5, 6 and 7m); h_c (300, 400, 500, 600 and 700mm) and h_b (270, 300, 350, 400, 450, 500, 550, 600, 650 and 700mm). Regarding beam depth, the first three values ($\leq 350\text{mm}$) are considered to represent wide beams, while the rest are identified as deep beams.

Results show that mean (and median) values of the factor in the case of deep beams is 1.14, while for wide beams is 1.07 (in both cases with standard deviation lower than 5%). This represents a decrease of 6.2%, which could appear to be insignificant; however, it means that an overstrength factor $\gamma_R=1.39$ instead of 1.30 (if EC8 is assumed) should be applied to wide-beam frames in order to provide similar conservativeness, which might be hard to achieve in some situations. Furthermore, if it is considered that wide-beam frames designed to DLS in medium-to-high seismicity areas usually present larger column sections than deep-beam frames –in order to compensate the lower stiffness of beams aimed at satisfying the deformability limitations—, overstrength factor for wide-beam frames may be even larger.

Table 21: Amplification of flexural capacity-design factor when expressed in the centre of the joint panel (IV)

H_{cl} [m]	L_{cl} [m]	h_c [mm]	h_b [mm]	fact.	H_{cl} [m]	L_{cl} [m]	h_c [mm]	h_b [mm]	fact.	H_{cl} [m]	L_{cl} [m]	h_c [mm]	h_b [mm]	fact.	H_{cl} [m]	L_{cl} [m]	h_c [mm]	h_b [mm]	fact.
3.5	3	300	300	1.06	4.5	3	300	300	1.05	3.0	3	300	350	1.09	4.0	3	300	350	1.07
3.5	3	400	300	1.06	4.5	3	400	300	1.04	3.0	3	400	350	1.09	4.0	3	400	350	1.06
3.5	3	500	300	1.05	4.5	3	500	300	1.03	3.0	3	500	350	1.08	4.0	3	500	350	1.05
3.5	3	600	300	1.04	4.5	3	600	300	1.03	3.0	3	600	350	1.07	4.0	3	600	350	1.05
3.5	3	700	300	1.04	4.5	3	700	300	1.02	3.0	3	700	350	1.07	4.0	3	700	350	1.04
3.5	4	300	300	1.07	4.5	4	300	300	1.05	3.0	4	300	350	1.10	4.0	4	300	350	1.07
3.5	4	400	300	1.06	4.5	4	400	300	1.05	3.0	4	400	350	1.09	4.0	4	400	350	1.07
3.5	4	500	300	1.06	4.5	4	500	300	1.04	3.0	4	500	350	1.09	4.0	4	500	350	1.06
3.5	4	600	300	1.05	4.5	4	600	300	1.04	3.0	4	600	350	1.08	4.0	4	600	350	1.06
3.5	4	700	300	1.05	4.5	4	700	300	1.03	3.0	4	700	350	1.08	4.0	4	700	350	1.05
3.5	5	300	300	1.07	4.5	5	300	300	1.05	3.0	5	300	350	1.10	4.0	5	300	350	1.07
3.5	5	400	300	1.07	4.5	5	400	300	1.05	3.0	5	400	350	1.10	4.0	5	400	350	1.07
3.5	5	500	300	1.06	4.5	5	500	300	1.05	3.0	5	500	350	1.09	4.0	5	500	350	1.07
3.5	5	600	300	1.06	4.5	5	600	300	1.04	3.0	5	600	350	1.09	4.0	5	600	350	1.06
3.5	5	700	300	1.06	4.5	5	700	300	1.04	3.0	5	700	350	1.09	4.0	5	700	350	1.06
3.5	6	300	300	1.07	4.5	6	300	300	1.06	3.0	6	300	350	1.11	4.0	6	300	350	1.08
3.5	6	400	300	1.07	4.5	6	400	300	1.05	3.0	6	400	350	1.10	4.0	6	400	350	1.07
3.5	6	500	300	1.07	4.5	6	500	300	1.05	3.0	6	500	350	1.10	4.0	6	500	350	1.07
3.5	6	600	300	1.06	4.5	6	600	300	1.05	3.0	6	600	350	1.09	4.0	6	600	350	1.07
3.5	6	700	300	1.06	4.5	6	700	300	1.04	3.0	6	700	350	1.09	4.0	6	700	350	1.06
3.5	7	300	300	1.08	4.5	7	300	300	1.06	3.0	7	300	350	1.11	4.0	7	300	350	1.08
3.5	7	400	300	1.07	4.5	7	400	300	1.05	3.0	7	400	350	1.10	4.0	7	400	350	1.08
3.5	7	500	300	1.07	4.5	7	500	300	1.05	3.0	7	500	350	1.10	4.0	7	500	350	1.07
3.5	7	600	300	1.07	4.5	7	600	300	1.05	3.0	7	600	350	1.10	4.0	7	600	350	1.07
3.5	7	700	300	1.06	4.5	7	700	300	1.05	3.0	7	700	350	1.09	4.0	7	700	350	1.07
4.0	3	300	300	1.05	2.5	3	300	350	1.12	3.5	3	300	350	1.08	4.5	3	300	350	1.06
4.0	3	400	300	1.05	2.5	3	400	350	1.11	3.5	3	400	350	1.07	4.5	3	400	350	1.05
4.0	3	500	300	1.04	2.5	3	500	350	1.10	3.5	3	500	350	1.06	4.5	3	500	350	1.04
4.0	3	600	300	1.03	2.5	3	600	350	1.10	3.5	3	600	350	1.06	4.5	3	600	350	1.04
4.0	3	700	300	1.03	2.5	3	700	350	1.09	3.5	3	700	350	1.05	4.5	3	700	350	1.03
4.0	4	300	300	1.06	2.5	4	300	350	1.12	3.5	4	300	350	1.08	4.5	4	300	350	1.06
4.0	4	400	300	1.05	2.5	4	400	350	1.12	3.5	4	400	350	1.08	4.5	4	400	350	1.06
4.0	4	500	300	1.05	2.5	4	500	350	1.11	3.5	4	500	350	1.07	4.5	4	500	350	1.05
4.0	4	600	300	1.04	2.5	4	600	350	1.11	3.5	4	600	350	1.07	4.5	4	600	350	1.05
4.0	4	700	300	1.04	2.5	4	700	350	1.10	3.5	4	700	350	1.06	4.5	4	700	350	1.04
4.0	5	300	300	1.06	2.5	5	300	350	1.13	3.5	5	300	350	1.09	4.5	5	300	350	1.06
4.0	5	400	300	1.06	2.5	5	400	350	1.12	3.5	5	400	350	1.08	4.5	5	400	350	1.06
4.0	5	500	300	1.05	2.5	5	500	350	1.12	3.5	5	500	350	1.08	4.5	5	500	350	1.06
4.0	5	600	300	1.05	2.5	5	600	350	1.11	3.5	5	600	350	1.07	4.5	5	600	350	1.05
4.0	5	700	300	1.05	2.5	5	700	350	1.11	3.5	5	700	350	1.07	4.5	5	700	350	1.05
4.0	6	300	300	1.06	2.5	6	300	350	1.13	3.5	6	300	350	1.09	4.5	6	300	350	1.07
4.0	6	400	300	1.06	2.5	6	400	350	1.13	3.5	6	400	350	1.09	4.5	6	400	350	1.06
4.0	6	500	300	1.06	2.5	6	500	350	1.12	3.5	6	500	350	1.08	4.5	6	500	350	1.06
4.0	6	600	300	1.05	2.5	6	600	350	1.12	3.5	6	600	350	1.08	4.5	6	600	350	1.06
4.0	6	700	300	1.05	2.5	6	700	350	1.11	3.5	6	700	350	1.07	4.5	6	700	350	1.05
4.0	7	300	300	1.07	2.5	7	300	350	1.13	3.5	7	300	350	1.09	4.5	7	300	350	1.07
4.0	7	400	300	1.06	2.5	7	400	350	1.13	3.5	7	400	350	1.09	4.5	7	400	350	1.07
4.0	7	500	300	1.06	2.5	7	500	350	1.12	3.5	7	500	350	1.08	4.5	7	500	350	1.06
4.0	7	600	300	1.06	2.5	7	600	350	1.12	3.5	7	600	350	1.08	4.5	7	600	350	1.06
4.0	7	700	300	1.05	2.5	7	700	350	1.12	3.5	7	700	350	1.08	4.5	7	700	350	1.06

2.2.1.3 *Axial load in columns*

Regarding not only the column flexural capacity design but also the other two types of hierarchy, seismic codes show kind of vagueness concerning the specification of which combination of actions belonging to the seismic situation should be considered aimed at defining the axial load in columns. In fact, this force determines:

- moment of resistance for flexural capacity design of columns;
- both maximum moment able to be developed in column ends and shear resistance for shear capacity design of columns;
- shear resistance of joint panel for capacity design of joints.

Aimed at providing proper performance during a seismic event without requiring complex nonlinear dynamic (time-history) analysis, codes usually establish that in frames regular in plan, column-beam and joint-beam hierarchy can be evaluated in two orthogonal planes, in both directions. On the other hand, 32 different combinations of actions may belong to the “seismic situation” $-(4 \text{ directions for the main seismic action}) \times (2 \text{ directions for the secondary transverse seismic action}) \times (4 \text{ different positions of the barycentre of masses in each storey due to accidental eccentricity}) = 32$ —. Thus, 4 different seismic combinations can be ascribed to each direction of evaluation of hierarchy.

Sometimes codes seem to say that the most conservative value of axial of those 4 combinations may be taken, by using the expression “within the range of values”, which it is not clear whether refers to choose one of those four discrete values or conversely a value contained in the continuous range—note that, as the interaction diagram moment-axial is pseudo-parabolic, the most conservative value could not be neither the maximum nor the minimum—. Moreover, it is not clear whether an additional combination should be considered corresponding to only gravitational seismic load. Conversely, in other cases codes seem to say that axial load should be chosen from all the seismic combinations, independently of the direction. Also, other times it seems that it is suggested to adopt four new combinations, in addition to the other 32, without accidental eccentricity and without combining with transverse action, from which axial load is directly taken. Furthermore, some codes propose to obtain axial load as an addition of the force

coming from seismic gravitational load and the increment or decrease produced by the global frame action when maximum admissible horizontal loading is acting, i.e. the variation of axial consistent with maximum shear forces in all beam ends.

Analogously, it is not explicitly clarify whether the moment of resistance in the relevant direction should be obtained in presence of any transverse moment, corresponding to any of the seismic combinations, consistent or not with the direction, from specific combination for capacity design (without combining with transverse action) or even from seismic gravitational combination.

A summary of those different criteria is shown in Table 22; note that it is not the literal text found in bodies of codes but an interpretation of those provisions in a more explicit way.

Table 22: Interpretation of the different criteria for the election of the value of axial load in columns adopted for the calculation of bending moment of resistance for capacity-design purposes

Source	Column-beam hierarchy	Shear-to-moment hierarchy
EC8	Value, within the range corresponding to all seismic combinations, causing minimum moment resistances	Value corresponding to a/the seismic combination consistent with the considered direction
NTC		Value, within the range corresponding to all seismic combinations, causing maximum moment resistances
Fardis (2009)	-	Value, within the range corresponding to all seismic combinations (and only gravitational forces in the seismic situation), causing maximum moment actions
ACI 318-08	Value corresponding to a seismic combination consistent with the considered direction, causing minimum moment resistances	Value, within the range corresponding to all seismic combinations, causing maximum moment resistances
NZS 3101	Value, reduced proportionally to the number of storeys until a maximum of 30%, consistent with the achievement of overstrengthened flexural resistances in the beams in presence of gravitational loads corresponding to the seismic situation	

Capacity design provisions may be somehow understood as a set of simple rules that are intended to provide quite degree of conservativeness against undesirable behaviour. Obviously, they come from an agreement between accuracy, simplicity and feasibility.

However, regarding the assumption of axial loads in columns aimed at calculating the moment of resistance, some non-conservative scenarios could eventually take place. Exterior columns of frames can experiment significant variation of axial demand when subjected to horizontal loads if compared with the initial (default) state, only subjected to vertical loads in the seismic situation. Theoretically, it is not clear whether the most unfavourable situation is an increase or a decrease of axial load. However, in capacity-designed buildings the relative axial load may be medium-low, thus a decrease of axial load may be the most unfavourable scenario.

This evolution of axial load in columns may be understood within the behaviour of the frame when subjected to an incremental monotonic pattern of lateral forces pattern from the initial situation –under only gravitational loads in the seismic situation— until each one of the seismic situations, when the whole design seismic forces are acting. In a real earthquake, without accounting with overstrength sources, it can be assumed that if a global demand q times lower than design PGA is required, the structure may remain elastic, so the evolution of axial load until those levels may be proportional to the global demand.

Still, axial load in any of those situations is consistent with bending moments acting in all member ends that are lower than the respective maximum flexural capacities, thanks to overstrength and capacity design. The scope would be to calculate moment resistances of columns in presence of axial loads actually consistent with such maximum values of moment instead of being consistent with design moments, i.e. axial loads consistent with global maximum frame action. Within the linear incremental lateral-force framework, axial loads in exterior columns would proportionally decrease from the “design state” (design moments in both ends) until the “capacity state” (maximum moments in both ends, with in time depend of the level of axial load attained).

It may be possible that positive (tension) values are attained, especially in frames designed to DLS in medium-high seismicity areas, because large cross-sections are demanded because of stiffness requirements (see Table 38) and thus they present low relative axial loads also at the initial situation (under seismic gravitational loads). For the same reason, also those frames present low

reinforcement ratios, usually based on minimum required values. In this case, a substantial reduction of axial load may cause an important decrease of flexural capacity. For instance, in a column with minimum reinforcement ratio (1%) regularly distributed in the perimeter, a decrease of relative axial load from 0.4 to 0.0 entails a loss of flexural capacity of 35-40%, while for a column with high reinforcement ratio (3%) the loss is only about 10-15%.

Hence, in exterior columns of frames presenting higher overstrength of members, non-conservative scenarios of column-beam hierarchy could take place.

Herein, a variation of the usual procedures of codes, based in the previous considerations, is proposed and illustrated by a representative example of a generic exterior column with square cross-section and minimum reinforcement. In Figure 74, the 3D axial-moment interaction envelope representing the resistance of the column end is shown, consisting in a surface generated by the 90°-revolution of the plane curve, which is similar to a parabola.

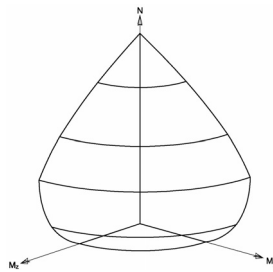


Figure 74: Typical N - M_x - M_y interaction resistance envelope of a generic column with square cross-section

In Figure 75, a typical non-seismic design procedure is shown. The thick line joining the origin with the surface is a vector representing in this case the linear evolution of the internal forces (axial N , longitudinal bending moment M_x and transversal bending moment M_y) in the column caused by gravitational actions. The intermediate points symbolized by letter E with different subscripts represent different design situations, while the points symbolized by the letter R represent the resistance of the columns when subjected to forces increased proportionally

with respect to the design situations. The ratio between lengths of vectors reaching R and reaching E represents the “safety factor” of the column in each design situation.

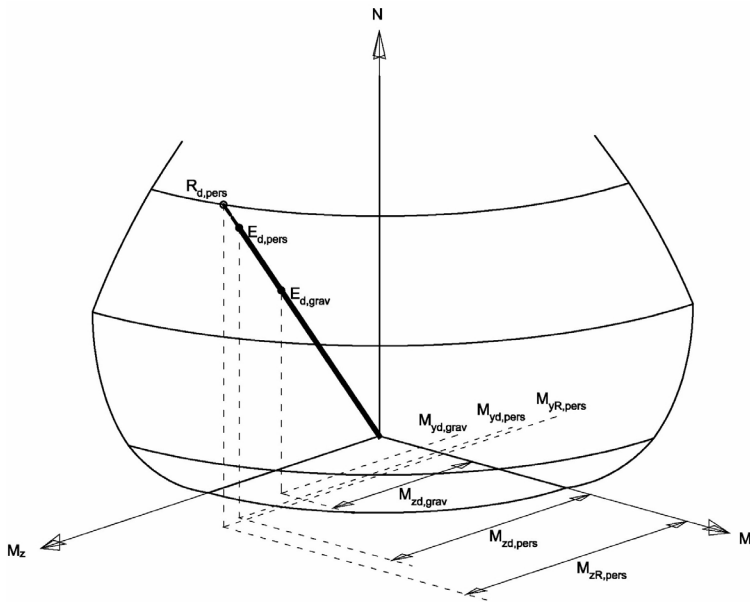


Figure 75: Alternative consideration of column axial loads for moment resistances calculation for columns-to-beams capacity-design purposes: definition of initial seismic state

In the same figure, both $E_{d,pers}$ and $R_{d,pers}$ refers to persistent/transient situation of design, while $E_{d,grav}$ refers to the state of the column only subjected to gravitational loads in the seismic situation. The last point can be obtained graphically by multiplying the vector modulus by $(1.35G+1.50Q)/(G+0.5Q)$, being G and Q the permanent and live loads, respectively. That vector is aligned with the previous one only if the forces caused by wind loads are lower than those caused by gravitational loads in the persistent/transient situation. Each one of those 3 points is related to values of M_z and M_y , identified in the figure with the corresponding subscripts. As values of M_y are relatively small, the vector is almost

parallel to the plane M_z-N . The relative axial load corresponding to seismic gravitational loading in this case is about 0.4.

In Figure 76, vector representing the evolution of forces when the frame is laterally loaded is represented. Its origin is $E_{d,grav}$, and its direction is oriented to the point $E_{d,seis,hie,c>b}$, which represents the tensional state of the column in the specific seismic combination (subscript *seis*) for column-beam hierarchy (*hie,c>b*), i.e. without accidental eccentricity of masses and without combining main horizontal action with 30% in the perpendicular direction. This point is characterised by a lower axial load (because the column is exterior) and a transverse moment insignificantly different from that of $E_{d,grav}$. In the figure, the vertical section of the resistance envelop, plotted with thick line, contains $E_{d,seis,hie,c>b}$ and represents the resistance curve assuming constant M_y .

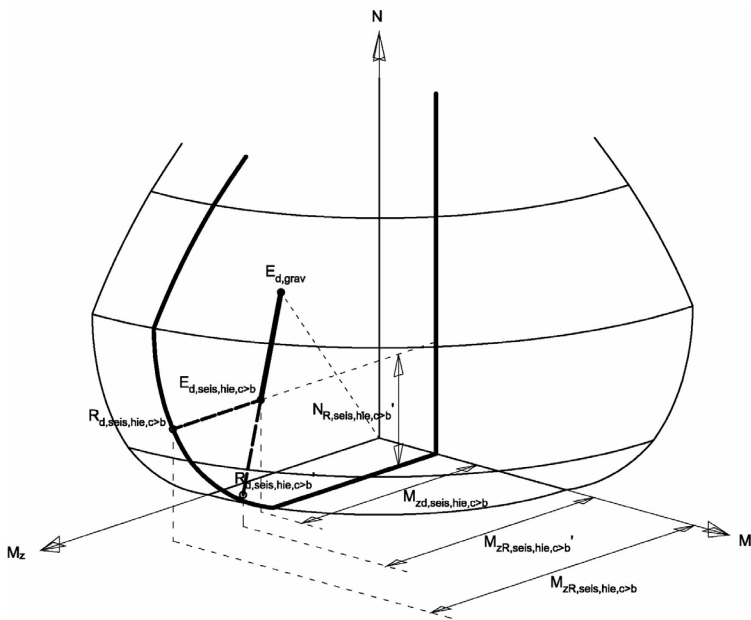


Figure 76: Alternative consideration of column axial loads for moment resistances calculation for columns-to-beams capacity-design purposes: obtaining of moment resistance

Usually, codes suggest to obtain M_z of resistance by assuming constant N , which is equivalent in the diagram to move horizontally from $E_{d,seis,hie,c>b}$ until reaching the envelop in the point $R_{d,seis,hie,c>b}$, corresponding to a moment of resistance $M_{zR,seis,hie,c>b}$. Actually, some codes suggest to do this “horizontal itinerary” starting from different axial values and choosing the lower M_{zR} , as seen before.

Instead, the alternative procedure proposed in this work is based in the proportionality of forces: it is assumed that the increment of the three internal forces must be proportional, so the maximum flexural capacity of a column end must be consistent with the direction of the vector matching the gravitational situation with the seismic one. It is represented in Figure 76 as $R_{d,seis,hie,c>b}'$, being $M_{zR,seis,hie,c>b}'$ the alternative moment resistance associated to this state. It corresponds graphically to the intersection of the resistance surface with the vector whose direction is determined by $E_{d,grav}$ and $E_{d,seis,hie,c>b}$. It is worth noting that the alternative flexural resistance can be substantially lower than the value obtained by the classic method, especially for low-reinforced columns in which the seismic situation is not so much more demanding than the persistent/transient one.

Nevertheless, the axial corresponding to the development of full flexural capacities in columns is actually never acting, because such capacities are not able to be attained. In fact, the column-beam hierarchy causes maximum moments in column ends that are reduced by a factor $\Sigma M_{Rb}/\Sigma M_{Rc}$. When such reduction is applied, an intermediate state between $E_{d,seis,hie,c>b}$ and $R_{d,seis,hie,c>b}'$ may be reached, as shown in Figure 77.

EC8 allows using this reduction when the flexural demand in column ends is needed aimed at capacity-designing of columns to shear. Thus, an axial load $N_{d,seis,hie,V>M}'$, consistent with this intermediate state $E_{d,seis,hie,V>M}$, could be used for the estimation both of the shear demand based on the maximum moment developed by column ends and the shear capacity.

Either way, this alternative procedure may have a high degree of robustness because:

- it is deterministic;

- could become unconservative for columns whose compression increases when the frame is subjected to seismic action;
- the evolution of moments in member ends is not proportional after the first yielding in any element;
- maximum capacities in columns cannot be attained.

Hence, it may be understood as an alternative procedure that adds one more value of moment resistance to the range from which the minimum value should be chosen.

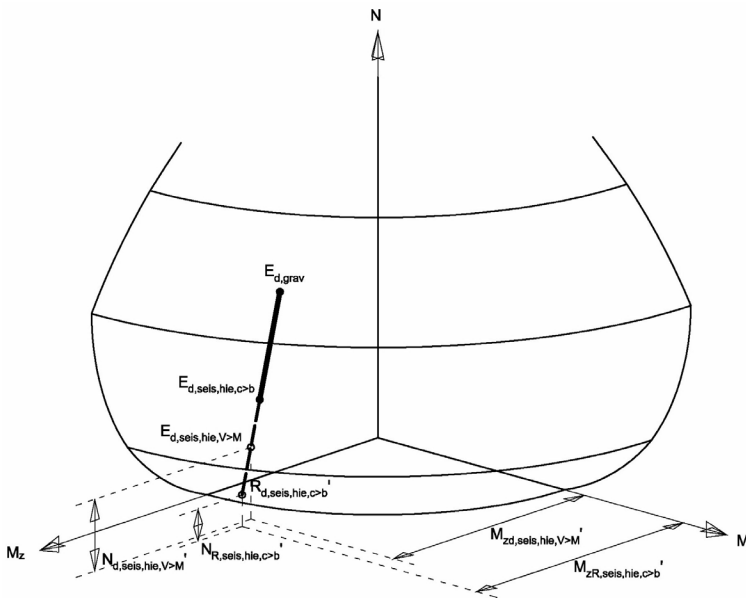


Figure 77: Alternative consideration of column axial loads for moment resistances calculation for columns-to-beams capacity-design purposes: obtaining of more realistic moment resistances by accounting with different overstrength between beams and columns

Actually, the most precise approach for the evaluation of the moment of resistance for flexural capacity design of columns can be found in New Zealander seismic code NZS 3101 (NZS, 2006). It evaluates the axial load in a column corresponding to the maximum horizontal action in the frame by assuming that all

beam ends develop maximum flexural capacities accounting with the overstrength factor (see Table 22). Thus, axial load in a single column results from the addition of the compression due to gravitational load in seismic situation plus the maximum shear forces of all beam ends framing into joints placed above the column in its same vertical. Note that, in this case, overstrength factor is considered twice: for the evaluation of axial load and also for the “a-posteriori” evaluation of the degree of hierarchy.

In Figure 78, the demand point in agreement to the attainment of maximum capacities of beam ends is plotted as $E_{d,seis,hie,c>b}$, and their corresponding resistance point and flexural capacity are expressed as $R_{d,seis,hie,c>b}$ and $M_{zR,seis,hie,c>b}$, respectively. This method furnish similar values to the alternative method proposed in the present work only if all the ratios $\Sigma M_{Rb}/\Sigma M_{Rc}$ above the evaluated column end are equal to the overstrength factor employed.

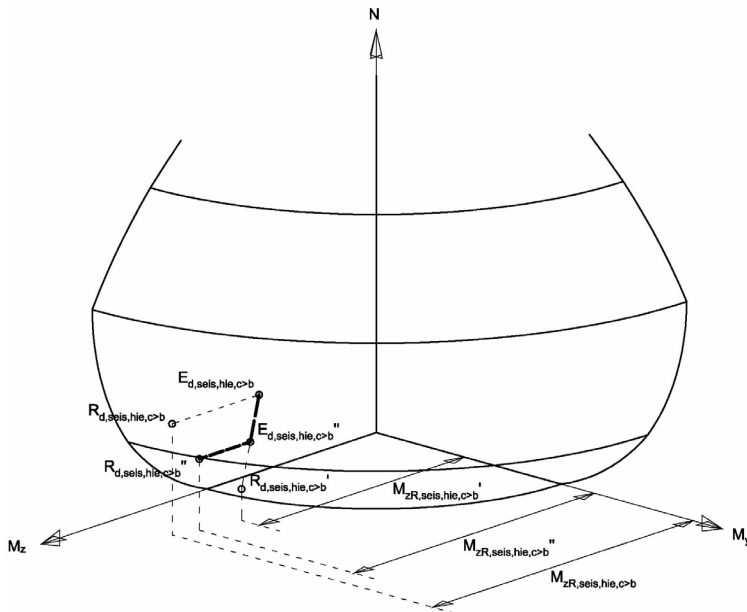


Figure 78: Alternative consideration of column axial loads for moment resistances calculation for shear-to-moment capacity-design purposes

Notwithstanding its great accuracy and coherence, the main shortcoming of the last method is that the evaluation of two many members (all the beams framing to joints placed above the evaluated connection) is required aimed at designing each column end, instead of referring only to the capacities of the beams framing to the same joint. Also, such axial load corresponds to the formation of the last plastic hinge in beams of all the storeys above the column, which may be different from the axial load corresponding only to the yielding of beam ends framing the actual joint.

All the precedent disquisitions lead to consider that in moment-to-beam hierarchy framework, γ_R may be understood as a global “safety factor” which not only has into account the possible overstrength of materials but also represents the degree of robustness of the structure against all of those weaknesses that could case yielding of column ends in some situations.

2.2.1.4 Hierarchy of resistances in NCSE-02

Notwithstanding the discussion on the accuracy of some specific statements of different seismic codes, general prescriptions in the form of Equation (33) may be appropriate in order to ensure capacity design to structures within a reasonable level of conservativeness, given the multiple uncertainties associated to the behaviour, other than material hardening: upper slab contribution to flexural capacity of beams, biaxial bending of columns, etc. (Panagiotakos and Fardis, 1998).

However, current Spanish seismic code NCSE-02 does not adopt such framework (Gómez-Martínez et al., 2015a and 2015d). In order to warrant hierarchy of resistances, it provides different rules that present some defficiencies if studied in detail: sometimes are impossible to be applied, other times can be unefficient or conversely can compel to design members with excessive overstrength. Also, they do not provide quantitative formulations for calculating some resistances, they provide very low values of γ_R even for high ductility and, in general, they do not provide proper guidelines for the application of such rules in order to face all the possible particularities. All of those deficiencies are shown in Table 23.

Table 23: Defficiencies (grey) detected in capacity-design provisions of NCSE-02

Type of hierarchy provision	Sometimes unefficient	Sometimes impossible to be applied	Sometimes leading to excessive overstrength	Quantitative formulations not provided	Including unnecessary rules	Low γ_R for high ductility
Joint-beam						
Column-beam						
Shear-to-moment						

Old-generation Spanish codes present some qualitative prescriptions related to the issue of hierarchy of resistances. Both PGS-1 and PDS-1 suggest that joints should be protected against failure, and the first one also establish that longitudinal bars should not experiment buckling, which could be interpreted as an encouragement to detail kind of critical regions by increasing the transversal reinforcement ratio.

Medium-generation codes, regarding any type of structure –not only RC frames—, compel to provide higher overstrength to column than to beams (without specifying any relation of contiguity), and, only in beams, higher overstrength for shear than for moment. Then, only for RC structures, the last provision extends also for columns, and it is clarified that plastic hinges in members should correspond to yielding of steel; the last may not correspond to any hierarchy provision but to a consequence of proper local detailing. NCSR-94 does not consider any γ_R , while current NCSE-02 recommends adopting a constant value of 1.10 for any structural type and ductility class. Also, this code clarify that hierarchy of resistances must be provided to members with respect to contiguous ones.

Still, capacity-design rules of NCSE-02 consist just on four paragraphs of text written in a very general sense, without any equation, quantitative expression or clarifying figure. It may reflect a not very deep understanding of the phenomenon. It contains only general proposals but it actually does not furnish enough tools to the designer in order to solve a wide range of possible scenarios. Actually, the most widespread commercial software for structural analysis and design in Spain

(CYPE Ingenieros®, <http://www.cype.com/>), has not incorporated those prescriptions until 2013 (<http://cypecad.cype.es/#sismico>), and it is not clear whether they have followed NCSE-02 or other principles.

The key of the drawbacks of provisions in NCSE-02 is that they are based in the concept of overstrength instead of capacity, i.e. it compels the prevalent member (or type of force) to possess higher overstrength than the not-prevalent one, instead of designing the prevalent member (or type of force) to the maximum force in agreement with the development of maximum capacities of the non-prevalent one. Paradoxally, such framework based in overstrength causes inefficiency when applied to shear-to-moment design but conversely causes excessive –likely impossible to manage— overstrength when applied to joints' and columns' capacity design.

Moreover, unlike EC8 or other benchmark codes (Gómez-Martínez et al., 2015a and 2015d), it does not specify lots of practical issues:

- in how many vertical plans and directions of loading should hierarchy be satisfied;
- which axial load in columns should be considered in order to evaluate flexural resistance;
- where to set the equilibrium of forces for column-beam hierarchy: in faces or in axe of joint panels;
- how to consider overstrength factor when demand and resistance have different sign;
- which elements or structural types are suitable to be exent of capacity design;
- how to account for the contribution of upper slab to capacity of beams;
- how to account for the cyclic degradation of resistances or confinement improvement;
- how to calculate demand and capacity in joint panels, and how to account for confinement provided by beams;
- how to improve capacity of joints with stirrups.

In the following, prescriptions of NCSE-02 regarding capacity design are deeply discussed.

This code sets that capacity design of columns is attained when “overstrength of each force in each column is higher than corresponding overstrength of each force in all beams” framing into the joint between columns. First of all, “each force” may be understood as “each type of force”, i.e. bending moment in both axes, shear in both axes, axial and torsion. It may be also understood that each resistance value associated to each design force may be evaluated assuming that the rest of the forces remain constant. Establishing hierarchy between types of forces different from vertical bending moment is not only unnecessary and absurd but also counter-productive. It is absurd because the physical principle that is pursued is the formation of plastic hinges in beams rather than in columns, and this is only possible for bending moment action (in presence of other types of forces with lower magnitude). It is not possible to form plastic hinges with only axial, shear or torsion forces. Moreover, it is unnecessary because capacity design of members prevent shear failure, thus shear overstrength indicative of any safety factor. It seems that each capacity design rule does not consider the consequences of the other ones. Finally, it is counter-productive because those secondary types of forces (axial load in beams, perpendicular moment and shear, torsion) are usually very low in comparison with resistances, thus overstrength values can reach extremely large values that can be very difficult to be superated by the corresponding overstrength in columns.

Identical problem can be individuated in the prescription for capacity design of joints: “overstrength of each force of each beam or column framing the joint is higher than each strut or tie within the joint”. Also, including columns in the prescription is not in agreement with capacity design of columns: they cannot develop their full resistance because beams yield prematurely.

Apart from those negligible deficiencies, the main problem of “overstrength framework” is that comparison is done between single values instead of couple of values. In Figure 71c, an example of capacity design of columns as established in NCSE-02 is shown. Bottom reinforcement of beams is usually constant in the full length of the member. Thus, if positive moment due to horizontal loading is quite different in both ends, the end with lower moment would have much higher overstrength. Also, if gravitational moment is high in comparison with seismic demand, higher positive moment would be reached at middle-span than in ends. In

both cases, it is possible that one of the beams framing the joint has very high overstrength (7.69 in this case), thus leading to each column to have at least that overstrength. Instead, if the connection is designed to EC8 (Figure 71a), global overstrength required to both columns is only 1.90, and if NTC is followed (Figure 71b), such value is required to each single column. The reason of this decrease is that demand in columns depend on two values (resistances of beams at both sides) instead of only one; they “compense” each other. Required dimensions for columns are extremely large in the case of NCSE-02. Moreover, as overstrength of beams may increase in upper storeys (because minimum reinforcement and gravitational forces may determine design), it could be possible that higher dimensions are required to upper storeys than in bottom storeys, which is absurd.

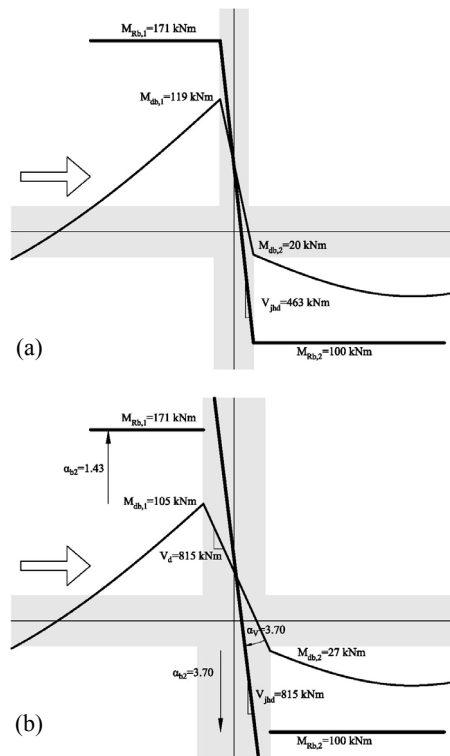


Figure 79: Example of capacity design of joints of interior connection, following the procedure of EC8 (a) and NCSE-02 (b)

Analogous problem can be observed for capacity design of joints. In the case of EC8 (Figure 79a), demand on joints depend of resistances of both beams, while in NCSE-02 approach (Figure 79b), joint must be designed to reach the maximum overstrength of the two beams.

Actually, the mathematical problem of “overstrength framework” is that overstrength is a ratio, i.e. it is based on multiplication, while “capacity framework” is based on addition. When design values are very little, overstrength ratios grow without any control, while the decrease in global capacities is more controlled by the addition.

Regarding shear capacity design of members, NCSE-02 compels “each section to have more shear overstrength than moment overstrength”. Imposing such rule to sections placed in the intermediate part of the member would lead to enormous required shear overstrength values around the point of the member where design moment is zero.

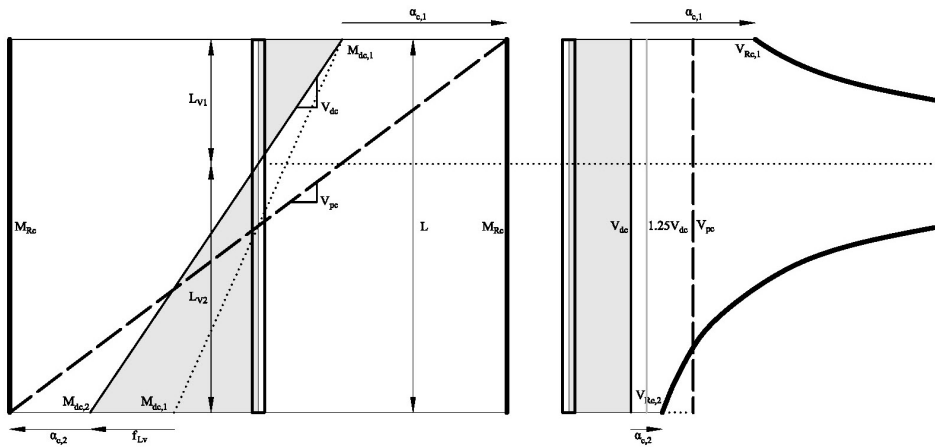


Figure 80: Shear capacity design of columns as in NCSE-02

For a better understanding of the problem shown by this capacity-design rule, in the following development the specific case of columns is considered (constant values for design and resistant shear forces), and γ_R is not taken into account.

Conversely to joints' and columns' capacity design, in this case the strategy of comparing single overstrengths do not lead to excessive overstrengths in both ends but only in the end with lower moment overstrength.

In Figure 80, procedure suggested by NCSE-02 is shown. A generic column is considered, whose linear distribution of design moments is not symmetric, being $M_{dc,2} \geq M_{dc,1}$. Thus, shear span lengths (L_{Vi}) are different and can be related by a factor f_{Lv} as in Equation (45) and also with total height of column (L) as in Equation (46).

$$f_{Lv} (\geq 1) = \frac{L_{V2}}{L_{V1}} = \frac{M_{dc,2}/V_{dc}}{M_{dc,1}/V_{dc}} = \frac{M_{dc,2}}{M_{dc,1}} \quad (45)$$

$$L = L_{V1} + L_{V2} = L_{V2} \left(\frac{1}{f_{Lv}} + 1 \right) = L_{V2} \left(\frac{f_{Lv} + 1}{f_{Lv}} \right) \Rightarrow L_{V2} = \frac{f_{Lv} \cdot L}{f_{Lv} + 1} \quad (46)$$

Each member end present a moment overstrength $\alpha_{c,i}$ as defined in Equation (47a); shear overstrength must be equal or higher than this value in each end. On the other hand, “plastic shear”, i.e. shear force obtained from the application of opposite moments of resistances at column ends (V_{pc}), is considered to be the target shear resistance in order to warrant hierarchy. Hence, target shear overstrength (α_{Vdc}) is defined as in Equation (47b).

$$\alpha_{c,i} = \frac{M_{Rc}}{M_{dc,i}} \leq \frac{V_{Rc,i}}{V_{dc}} \quad ; \quad \alpha_{Vdc} = \frac{V_{pc}}{V_{dc}} \quad (47a,b)$$

Design shear is the ratio between design moment in any end and its corresponding shear span. In Equation (48), L_{V2} is replaced by expression shown in Equation (46) and ratio between maximum design moment ($M_{dc,2}$) and L is isolated. Similar isolation is carried out in Equation (49) for the expression of plastic shear, in which moment of resistance is expressed as dependent on $M_{dc,2}$. Then, in Equation (50), both expressions of $M_{dc,2}/L$ in previous equations (48) and (49) are equalised.

Equation (50) relates target (plastic) shear with design shear. Target shear overstrength can be expressed (Equation (51)) as function of the “shape” of design

moments (reflected in the shear span factor f_{Lv}) and the minimum moment overstrength (corresponding to end 2) or conversely to maximum moment overstrength (end 1). Thus, at each end of the column, the ratio between shear overstrength required by NCSE-02 –which must be at least equal to moment overstrength— and target shear overstrength depends only on f_{Lv} (Equation (51)).

$$V_{dc} = \frac{M_{dc,2}}{L_{v2}} = M_{dc,2} \frac{f_{Lv} + 1}{f_{Lv} \cdot L} \Rightarrow \frac{M_{dc,2}}{L} = \frac{V_{dc} \cdot f_{Lv}}{f_{Lv} + 1} \quad (48)$$

$$V_{pc} = \frac{M_{Rc}}{L/2} = \frac{2 \cdot \alpha_{c,2} \cdot M_{dc,2}}{L} \Rightarrow \frac{M_{dc,2}}{L} = \frac{V_{pc}}{2 \cdot \alpha_{c,2}} \quad (49)$$

$$\frac{V_{dc} \cdot f_{Lv}}{f_{Lv} + 1} = \frac{V_{pc}}{2 \cdot \alpha_{c,2}} \quad (50)$$

$$\frac{V_{pc}}{V_{dc}} = \alpha_{Vdc} = \alpha_{c,2} \frac{2 \cdot f_{Lv}}{f_{Lv} + 1} = \alpha_{c,1} \frac{2}{f_{Lv} + 1} \Rightarrow \begin{cases} \alpha_{c,1} = \frac{f_{Lv} + 1}{2} \\ \alpha_{Vdc} \\ \alpha_{c,2} = \frac{f_{Lv} + 1}{2 \cdot f_{Lv}} \\ \alpha_{Vdc} \end{cases} \quad (51)$$

Hence, in order to evaluate the reliability of the rule in NCSE-02, i.e. if such rule results in shear resistances higher than target values, in Equation (52) values of f_{Lv} necessary to warrant conservativeness for each column end are obtained. For the end whose design moment is the minimum (end 1), any value of f_{Lv} satisfies the condition (because it is always higher than 1, see Equation (45)), thus shear design is always conservative. Conversely, for column end whose design moment is the maximum (end 2), only a value of $f_{Lv}=1$ derives in conservativeness. Hence, it is demonstrated that NCSE-02 rule is not conservative for columns in which design moments are different in both ends.

In Figure 81a, safety factors (i.e. ratio between shear resistance imposed by the code and target shear intended to provide hierarchy) of both ends for different shapes of design moments are shown. It is worth noting that not only the rule is not conservative for one of the ends, but for the other end the required overstrength can

reach values which may make impossible to be provided to the section. This may be representative, for example, of 1st storey columns of wide-beam frames, in which design moments at the base may be much higher than moments at the top due to cantilever behaviour (see Table 33).

$$V_{Rc,i} \geq V_{pl} \Leftrightarrow \left\{ \begin{array}{l} \alpha_{c,1} \geq \alpha_{Vdc} \Leftrightarrow \frac{f_{Lv} + 1}{2} \geq 1 \Leftrightarrow f_{Lv} \geq 1 \\ \alpha_{c,2} \geq \alpha_{Vdc} \Leftrightarrow \frac{f_{Lv} + 1}{2 \cdot f_{Lv}} \geq 1 \Leftrightarrow f_{Lv} \leq 1 \end{array} \right\} \Rightarrow f_{Lv} = 1 \quad (52)$$

Still, NCSE-02 establish that in the case that $a_g \cdot S \geq 0.12g$ (following the hazard framework of Spanish codes), $V_{Rc} \geq 1.25V_{dc}$ in all the length of the column. Thus, it could be possible that the weakness of the hierarchy rule in the unfavourable end gets overshadowed by that 25% amplification.

In Equation (53) it is evaluated in which case a shear resistance equal to the 25%-amplified shear demand is higher than target shear; Equation (51) is replaced into this expression. It is concluded that design may be conservative only for quite reduced values of overstrength in the unfavourable column and very symmetric (in absolute values) distribution of design moments. In Figure 81b, this tiny sub-space is indicated in soft grey. Moreover, if it is considered that moment overstrength must be at least 1.10 aimed at satisfying column-beam hierarchy (except for base of columns in ground storey), such sub-space is even more reduced (marked in dark grey).

$$1.25 \cdot V_{dc} \geq V_{pl} \Leftrightarrow 1.25 \geq \alpha_{Vdc} = \alpha_{c,2} \frac{2 \cdot f_{Lv}}{f_{Lv} + 1} \Rightarrow \alpha_{c,2} \leq 0.625 \frac{f_{Lv} + 1}{f_{Lv}} \quad (53)$$

In columns, very often similar arrangements of stirrups are placed on top and bottom ends; thus, in practice the weakness of capacity-design rule for shear of NCSE-02 may be overcome. However, both ends should be designed for shear values that can be extremely high. It is not clear in which cases such high values get overshadowed by local detailing provisions on minimum stirrups in critical regions, but still the hierarchy rule may not be acceptable. In beams it is not so easy to individuate the not-conservative scenarios, because moments of resistance

and target plastic shear neither are similar in both ends nor in the two directions, and vertical load changes both values.

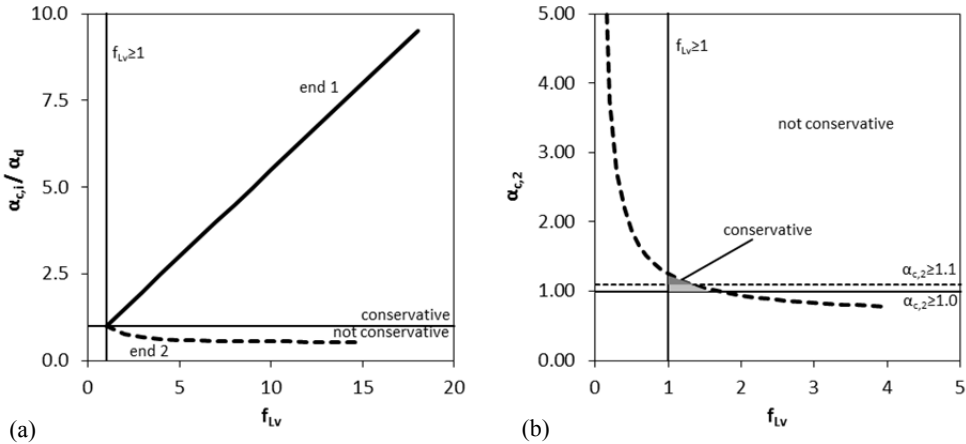


Figure 81: Conservativeness of shear capacity design of columns depending on shear span proportion, without (a) and with (b) consideration of the increment of 25% to shear of design suggested by NCSE-02

Besides, it is worth noting that NCSE-02, in its comments, says that “it is easier to provide capacity design of columns with deep beams than with wide ones”. In fact, contribution of upper slab could be higher for wide beams (see Figure 106), and also gross width could be uncertain. Also, previously it has been stated that geometry of joint panel can be slightly unfavourable for wide-beam frames. Anyway, it is not clear if NCSE-02 refers to those phenomena.

Annex 10 of EHE-08 is the first Spanish seismic code that operates with framework similar to EC8; however, it concerns only RC structures and it is not mandatory. Moreover, it establishes values of γ_R quite higher than EC8 and also not relaxed for DCM in most of the cases (see Table 17). Also, contribution of upper slab is taken into account. However, some issues remain without clear provisions:

- in capacity design of columns: which sign of resistance should be adopted when design moments of members have opposite sign to the common scenario;
- in capacity design of joints: demand is not explicitly stated, thus designer may doubt on whether demand consistent with capacities of beams or columns should be adopted; neither capacity is explicitly stated, sending designer to the general strut-and-tie formulations, thus one of the load path inside joint panel (truss mechanism) is ignored, providing only minimum amount of stirrups; and particularities of lateral confinement provided by beams is not taken into account.

2.2.2 Local detailing of members

Appart from strength hierarchy, capacity design requires sufficient local ductility in non-prevalent elements, i.e. critical regions (member ends experimenting inelastic incursion). Seismic codes provisions are oriented to maximise ultimate chord rotation of those regions through the following strategies: (i) high density of stirrups, aimed at confinement of the concrete core; (ii) in beams, lower ratio between tensioned and compressed reinforcement, in order to avoid concrete failure; (iii) in columns, lower axial load. Usually, those limitations are more severe for higher classes of ductility.

Prescriptions of NCSE-02 show important weaknesses. Although local detailing of columns seems to be quite similar to EC8, prescriptions depend on the seismicity level instead on the ductility class. Thus, columns can be designed to DCH without enough density of transverse reinforcement, likely leading to brittle failures. Also, there is not any limitation of axial load; this restriction is included in Annex 10 of EHE-08.

Instead, prescriptions for beams do depend on the ductility class. Rules regarding transverse reinforcement are rather similar to EC8. Restrictions of ρ_{max}/ρ_{min} are also similar for low total reinforcement, but it is more permissive for high reinforced sections (see Figure 82). In EHE-08, same formulations than in EC8 are suggested.

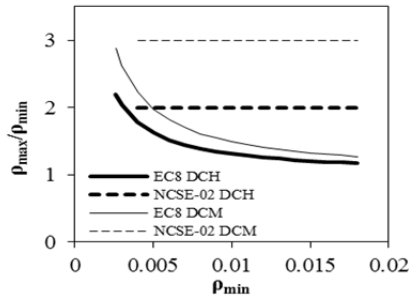


Figure 82: Maximum allowed ratio between reinforcement in both sides of beam sections correspond to DCH and DCM, for EC8 and NCSE-02

2.2.3 Restrictions of lateral deformability

Most of modern codes compel to design not only to ULS but also to SLS, typically Damage State Limitation, aimed at minimising damages in non-structural elements. They establish maximum lateral deformability to frames when subjected to seismic demands which are lower than those employed to ULS, thus corresponding to lower T_R (typically 95 years). Typical values of maximum IDR is 0.5%, which would cause cracks in infill panels (Colangelo, 2012 and 2013; see also section 5.1.3.1). Also, some codes suggest considering that the effective stiffness of members is lower than the elastic uncracked one (see section 3.3.3). Hence, in some cases this requirement is such restrictive that it becomes the critical condition of section design of columns and sometimes of beams. Furthermore, the resulting RC frame is so stiff that the relative influence of infills get substantially reduced, thus they do not jeopardise the global behaviour of the building, but still remain as a “second line of defense” against earthquake (Fardis, 2009). Also, it is demonstrated that the lower is the relative influence of infills, the more distributed is the collapse mechanism (Dolšek and Fajfar, 2001).

However, the Spanish framework does not establish any restriction to lateral deformability in the seismic case. Generic code CTE-DB-SE (MPW, 2006) furnishes restrictions of the total drift (0.2%) and IDR (0.4%), but they are not applicable for accidental situation (i.e. seismic case). Neither NCSE-02 suggest any quantitative limitation (Table 25): it just establishes vague and generic statements as: “small events should not cause significative damages to non-

structural elements” or “it is recommended that the structure is the most rigid part of the building”. In Figure 83a it is shown a typical NCSE-02 building, in which infills are the main contributors to global stiffness. Thus, it is clear that such qualitative provisions are not generally applied in design phase.

Moreover, it states that structural deformation can compromise the stability of infills “especially for high ductility”, which reflects ignorance regarding equal-displacement principle: high ductility may cause higher structural damage than low ductility, but the induced deformation to non-structural elements is the same.



Figure 83: Examples of NCSE-02 typical buildings; likely high contribution of infills to the global strength and stiffness (a) and no compensation of infills reduction at 1st storey by any increase of resistance of columns (b)

On the other hand, codes usually establish maximum values of IDR aimed at discarding second order effects (i.e. $P-\Delta$) by means of a limitation of the second- to first-order moment in the whole storey. EC8 discard such effects until a ratio of 10%, while for ratios between 10% and 30% suggest a simplification consisting in an increase of the seismic action in the corresponding storey. NCSE-02 suggest the same ratio for discarding second order effects (10%), but it do not furnish any

simplified correction of the action for larger values, thus making it impossible to design buildings with usual linear approach. It is worth noting that NCSE-02 establishes a second condition for discarding second order effects: total drift must be lower than 0.2%, which is quite restrictive if compared to the typical IDR limitation of EC8 and other seismic codes, which is 10‰ if expressed in ULS terms (assuming $ULS \approx 2$ times SLS, as in EC8). However, a total drift of 2‰ may be reached contemporaneously with greater values of IDR in lower storeys (see Figure 129).

2.2.4 Interaction with masonry infills

RC sub-standard buildings regularly infilled in elevation are likely to show mechanism of collapse of few storeys. Furthermore, if there is a substantial reduction of infills in ground storey (which is very typical, see Gómez-Martínez et al., 2015a), a soft-storey mechanism is likely to occur (Dolšek and Fajfar, 2001). Aimed at avoiding this behaviour, EC8 establish two provisions: (i) a 20% reduction of q factor if irregularity in elevation is confirmed, and (ii) an increase of demand in columns of the storey in which reduction of infills is observed, proportional to the decrease of strength provided by infills with respect to contiguous storeys. None of those prescriptions are suggested by NCSE-02, other than similar vague and qualitative statements (see previous section). In Figure 83b, an example of new building showing those characteristics is shown.

Regarding local interaction of columns with infills, EC8 compel to consider as critical regions not only the column ends but also the following zones (Table 25):

- the whole length of columns at ground storey, in order to avoid shear failures in the central part of the member due to the development of mechanism of failure in the infill panel that could be different from the diagonal-strut one, i.e. sliding shear (see Figure 59)
- end of members until a length which is approximately equal to the contact surface of the equivalent diagonal strut
- clear length of captive columns (with a little extension through the infilled part)

- “unbalanced” columns, i.e. those with infill panels only in one side, as corner columns.

Again, NCSE-02 only furnish qualitative suggestions: “infills able to develop stiffness and strength enough to modify the conditions in the structure, should be considered in the structural model”

2.2.5 Squat columns

Strictly speaking, EC8 part 1 does not explicitly regulates the design of squat columns. Fardis (2009) interpretes that they may be designed as coupling beams, with diagonal reinforcement in every direction in which the column acts as a squat one; if it is squat in both directions, the disposition of reinforcement may be impossible. Still, EC8 part 3 (CEN, 2005) adopts the formulation suggested by Biskinis et al. (2004) for the shear strength of squat columns, thus it could be used also for designing. This formulation does not depend on transverse reinforcement ratio, because when $L_v/h \leq 2$, stirrups may not prevent for the failure of the compressed concrete strut.

NCSE-02 only compels to provide shear capacity design to squat columns, and suggest to be “particular cautious”, thus it does not prevent from brittle failure.

2.2.6 Moment inversion

When bending moment has different signs at both faces of the joint panel, a strut-and-tie mechanism must be developed aimed at ensuring proper equilibrium of force paths. As seen in section 2.2.1, NCSE-02 does not provide any formulation aimed at evaluating demand and capacity of joint panels in such case.

On the other hand, when there is moment inversion, bond of longitudinal reinforcement of beams may be developed in a quite reduced length, lower than the depth of the column. EC8 and other codes furnish severe limitations to the ratio between the diameter of longitudinal bars of beams and column depth (see Table 30). Conversely, NCSE-02 does not provide any specific rule.

However, NCSE-02 states that design to DCH cannot be carried out if there is moment inversion. So, instead of providing precise rules aimed at dealing with very specific problems, NCSE-02 increase in a 33% the seismic demand, which may reflect some ignorance and fear about how to resolve well-known issues, as it suggest too conservative measures.

2.2.7 Reliability and cost-effectiveness of NCSE-02

In all the precedent, it is shown that current Spanish seismic code is not a modern performance- and capacity-design-based code. It is still conceived as a set of provisions which compel the designer to make some modifications to the sections and reinforcement of the original “gravitational” outlines, without alter substantially the structural typology, thanks to the absence of some important provisions as capacity design rules, limitation of lateral deformability or provisions aimed at minimising the influence of infill panels. All of this would provoke so high levels of stiffness, strength and ductility that larger sections, very regular distribution of elements and often shear walls would be required, resulting in substantially different structural typologies (Fardis, 2009). Hence, it is difficult to find some specific seismic structural global arrangement in Spain.

As a consequence of those different approaches, the expected damages after an earthquake in buildings designed to NCSE-02 or EC8 (or any other new-generation code) may also be different. In Table 24 and Table 25, a synopsis of the generic relation cause-effect between the absence of those prescriptions and the resulting characteristics of the frames is shown.

Based on the analysis shown in section 3.6.3 and Figure 135b, it can be stated that global safety factor of bare structures in high seismicity zones is roughly 50% higher for EC8 than for NCSE-02; if infills are taken into account, the difference may be higher due to global and local interaction (i.e. less distributed collapse mechanism and brittle failures).

This could be also interpreted in economical terms: buildings designed to EC8 may be more expensive than NCSE-02 ones. Still, the choice of global security for buildings is not only based on construction cost but also in post-earthquake

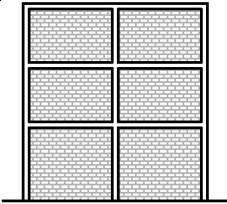
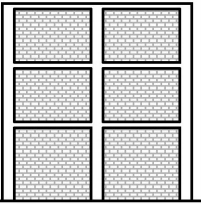
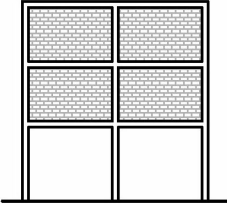
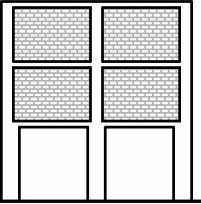
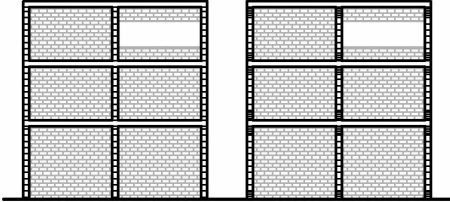
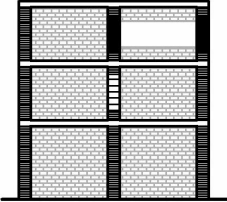
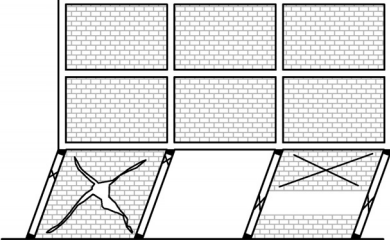
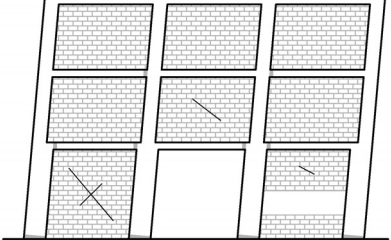
retrofitting and human costs, always from a statistical and probabilistic point of view.

Table 24: Generic consequences of the lack of prescriptions in NCSE-02 on the characteristics of the average RC residential building stock

Lack of prescription in seismic codes	Derived constructive characteristic	Potential damages
Damage limitation	Absence of shear walls	Lower stiffness, performance ruled by infills rather than by structure, more brittle global behaviour, high structural and non-structural damage level
Quantitative 2nd-order corrections	Reduced section of columns	
Maximum ratio column depth to beam reinforcement bar diameter		
Maximum axial load in columns		
Capacity design of joints	Low shear capacity of joints	Failure of nodes (whenever there is not any preemptive brittle failure of columns)
Corrections for irregularity of infills in elevation	Low flexural capacity of columns	Soft-storey mechanism
Capacity design of columns		
Local detailing of critical regions	Low ductility of beams	Lower displacement capacity
Shear capacity design	Low shear capacity of columns	Brittle shear failure in columns
Squat columns proper design		
Corrections for local interaction with masonry infills		

Damages provoked by NCSE-02 are typically concentrated in 1st storey: soft-storey mechanisms, brittle failures in columns, captive columns and destruction of infills panels. Instead, typical damages provoked by EC8 may be: incipient yielding in column bases at ground floor and maybe only in beams of lower storeys, while some splitting may be observed in other beam ends; and damage in infills may be much lower: cracking in first storey and few slight cracks in adjacent storeys (Table 25). For EC8, even in the case of design to DCH, overstrength is so high that inelastic incursion for ELU is quite low (see Figure 133 and Figure 134). However, while damages caused by old- and medium-generation codes have been extensively observed in the last decades, new-generation codes are so recent that there are not sufficient examples.

Table 25: NCSE-02 vs. EC8 regarding infills, and typical damages induced

	NCSE-02	EC8
Lateral deformability		 IDR $\leq 5\%$ with stiffness reduced in a 50% from the elastic one
Corrections for irregularity in elevation due to masonry infills		 20% reduction on q ; Columns overstrengthened as much as interstorey reduction of infills' resistance
Transverse reinforcement in columns aimed at avoiding local interaction with infills	 Low seismicity Medium-high seismicity (Only local detailing of critic regions)	 Higher stirrups density in columns at ground storey, with infills only at one side and in captive columns
Typical pattern of damages	 Soft storey, brittle failures in 1 st storey column, captive columns and destruction of 1 st storey infills	 Cracking of column bases and some beam ends in lower storeys with some splitting, cracking of 1 st storey infills and minor cracking in adjacent storeys

Hence, NCSE-02 damages are not only more important than in EC8 but also less predictable (because of the higher relative influence of infills), more dangerous (because 1st storey columns compromise the whole stability) and more expensive to repair (because they include large cracks in concrete and buckling of reinforcement). Conversely, having almost all the damages concentrated in columns and infills of ground floor may be an advantage for NCSE-02, because it is easy to achieve all the faces of those elements and it is not necessary to make retrofitting works inside private houses (De Miguel, 2011). However, the last may not decrease the final costs of retrofitting, because the severity of damages may make it necessary to evacuate and underpin the whole building.

Instead, the fact that EC8 damages are more widespread across the building than NCSE-02 ones may not make it much less cost-effective, because:

- It may not be necessary to remove flooring for repair beams. Incipient yielding in beams may cause only splitting on the bottom of the section – due to proper confinement—, which is easy to achieve.
- Damages in beams may not endanger the serviceability against gravitational forces –although perhaps they could experiment larger deflections. They do not lose negative bending capacity; they just use some of their ductility, which may not be so relevant for a following earthquake as ductility of columns may be more important (see Table 38).

2.2.8 Regulation of assessment and retrofitting

In the Spanish framework, there is not any specific code oriented to the regulation of assessment and retrofitting. In the case of post-earthquake interventions of buildings, codes of design (NCSE-02 and CTE-DB-SE) may be used instead, which is considered not to be actually a suitable strategy (Fardis, 2009).

CTE-DB-SE (a generalistic code) furnish some qualitative and vague guidelines for assessment and retrofitting, transferring almost all the responsibility to the designer. It states that “the use of current codes for the assessment of existing buildings, constructed according to previous codes, is not appropriate”, but “the new elements used in the retrofitting must be designed according to

them”. Regarding the safety factor required for the retrofitted buildings, it establish that “partial coefficients may be less strict [that for design of new buildings]”, but it does not provide any quantitative magnitude for such a relaxation of safety. It is neither reasonable nor sometimes feasible to require similar safety factors to new buildings and sub-standard buildings.

The main issue is the evaluation of seismic demand for assessment. Design codes are usually force-based instead of displacement-based, i.e. they replace the displacement capacity due to inelastic incursion by an equivalent reduction of the force demand (behaviour factor q). It is not coherent to assess an existing building considering that the force demand is obtained by means of a behaviour factor, which it is not clear whether it should be 1.0 (no ductility, extremely conservative), 1.5 (value proposed by EC8 part 3 for existing buildings, which is supposed to have into account only the building overstrength), the value of q in the original code (which can be inexistent, because some old-generation codes do not specify explicit q) or the value of the current code (which has no sense). Furthermore: q factors of design are established to be used together with design (reduced) resistances instead of mean real values. Moreover, the absence of shear capacity design can cause brittle failures in members if the retrofitting solution increases local or global stiffness, thus increasing seismic demand.

Instead, some modern codes propose specific parts oriented to the assessment and retrofitting of existing structures for seismic action, as EC8 part 3 or Italian NTC (CS.LL.PP, 2009). They propose different partial factors depending on the degree of knowledge of the building and they provide several formulations for the assessment of resistance and chord rotations of elements. Also infill panels are considered, given that sometimes could be necessary to take them into account in order to achieve the required safety factor in sub-standard buildings, otherwise it could be necessary to rebuild them. Those codes are displacement-based, and require a non-linear model and analysis (likely pushover). Thus, it is possible to assess the global security factor and the local shear capacity design, thus knowing exactly which are the critical points of the structure. The procedure may be more demanding than a simple linear dynamic analysis with q factor, but it may provide more reliable results.

2.2.9 Other relevant prescriptions included in RC codes

Within the period of time from 1962 to nowadays, 7 different RC codes have been promulgated in Spain: EH-68, (PCSC, 1968), EH-73, (PCSC, 1973), EH-80, (PCSC, 1980), EH-88, (PCSC, 1988), EH-91, (PCSC, 1991), EHE-99, (PCSC, 1999) and EHE-08, (PCSC, 2008). The analysis of all of them is relevant because they furnish some relevant information for the application of FAST approach regarding three aspects:

- 1) partial factors for actions in the accidental seismic situation;
- 2) minimum required amount of stirrups for end of columns;
- 3) degree of severity of the limitation for vertical deflections in beams due to gravitational load in persistent-transient situations.

2.2.9.1 *Partial factors for actions in the accidental seismic situation*

Except for the current Spanish RC code EHE-08, all of the aforementioned RC codes also regulated the way in which actions should be combined in each situation. Not only RC codes did it: different combinations were proposed in each code regulating design of structures in steel, wood, masonry... Instead, in 2006, CTE-DB-SE (MPW, 2006) established common prescriptions for combination of actions for all the structures, regardless of the material.

The differences between codes concerning partial factors for seismic action in the accidental seismic combination actually modifies the assumed base shear demand on the building. As FAST method is a code-based approach, also the base shear capacity is assumed to be dependent on those partial factors established by the different codes.

The influence of the rest of the partial factors –corresponding to permanent, live, snow and wind loads in accidental and permanent/transient situations— may have less influence in the resulting seismic capacity of the building, especially for high seismicity. It can increase the structural overstrength R_S (see section 1.2.1.3); such increase may be specifically classified within the source corresponding to gravitational design or contribution of gravitational loads in the seismic situation. Anyway, it may not be easy to have it into account in a simplified way; for beams, larger partial factors lead to higher sections, but in columns the correlation is not

so simple, as for different magnitudes of increment of axial loads the influence can be different.

It is worth noting that, sometimes, both types of codes –seismic and RC codes— regulate the same partial factors and provide their own values, which often are different; however, sometimes they cite each other in order to not cause “overlapping”. Furthermore, often the masses established by seismic codes for the calculation of seismic forces are not coincident with the quasi-permanent values of gravitational loads suggested by RC codes.

It is not clear which one is dominant in case of overlapping. In this work, it is assumed that an average designer may follow seismic codes for the evaluation of masses aimed at obtaining seismic action, and RC codes for combining the actions.

In Table 26, a detailed comparison between all these factors corresponding to the different seismic and RC codes is presented. They are again homogenised to be conforming to an assumed generic expression of the accidental seismic combination of actions with the form shown in Equation (54). The different variables are:

- 1) actions: G , Q , N , W and S are permanent, live, snow, wind and seismic loads, respectively;
- 2) partial factors for actions: γ_G , γ_Q , γ_N and γ_S , for the corresponding actions depending on the subscript;
- 3) quasi-permanent coefficients of combination: ψ_Q , ψ_N , ψ_W , for the corresponding actions depending on the subscript, being *res*, *off*, *com*, *pub* and *sto* the subscripts associated to the different uses (residential, office, commercial, public concurrence and storage), and *I* and *II* the subscripts associated to the degree of exposition (low or high, respectively) to the snow and wind.

$$\gamma_G G + \gamma_Q \sum \psi_{Q,i} Q_i + \gamma_N \psi_N N + \psi_W W + \gamma_S S \quad (54)$$

From the observation of Table 26, some general issues may be highlighted:

- 1) coefficients decrease chronologically, being more relaxed in the last codes;

- 2) RC codes are usually more conservative than seismic codes;
- 3) partial factors for gravitational loads G and Q have been higher than 1.0 from 1973 until 1999;
- 4) snow and wind loads have not been always discarded for seismic combination.

Table 26: Chronological comparison of partial factors for actions and combination coefficients between the different seismic and RC Spanish codes (“-“: not proposed; “=”: similar to the contemporaneous seismic code)

	1960	1970	1980	1990	2000	2010		
seismic	MV-101	PGS-1	PDS-1			NCSR-94	NCSE-02	
RC/actions		EH-68	EH-73	EH-80	EH-88	EH-91	EHE-99	CTE
γ_G	-	1.00	1.00			-	-	
		1.00	1.28	1.28	1.28	1.28	1.00	1.00
γ_Q	-	1.00	1.00			-	-	
		1.00	1.28	1.28	1.28	1.28	1.00	1.00
γ_N	-	1.00	1.00			-	-	
		1.00	1.28	1.28	1.28	1.28	1.00	1.00
γ_S	-	1.00	-	-	-	-	-	
		1.00	1.10	1.00	1.00	1.00	1.00	1.00
$\psi_{Q,res}$	0.50	0.50	0.50			0.30	0.50	
		=	1.00	=	=	=	0.30	0.30
$\psi_{Q,off}$	0.70	0.60	0.60			0.60	0.60	
		=	1.00	=	=	=	0.30	0.30
$\psi_{Q,com}$	0.70	0.60	0.60			0.60	0.60	
		=	1.00	=	=	=	0.60	0.60
$\psi_{Q,pub}$	1.00	0.80	0.80			0.60	0.60	
		=	1.00	=	=	=	0.60	0.60
$\psi_{Q,sto}$	1.00	-	-	-	-	1.00	1.00	
		=	1.00	=	=	=	0.80	-
$\psi_{N,I}$	1.00	0.50	0.00			0.00	0.00	
		=	0.80	=	=	=	0.00	0.00
$\psi_{N,II}$	1.00	0.50	0.50			0.30	0.50	
		=	1.00	=	=	=	0.00	0.20
$\psi_{W,I}$	-	0.50	0.00			0.00	0.00	
		=	=	=	=	0.00	0.00	0.00
$\psi_{W,II}$	-	0.50	0.25			0.25	=	
		=	=	=	=	0.25	0.00	0.00

In the previous comparative study, the influence of the different partial factor for materials (see Table 17) is not considered. In fact, for PGS-1 and NCSE-02, all the values could be multiplied by the ratio between partial factors in the accidental situation to those in the persistent-transient one.

The reasons for such discard are that designers probably have not taken profit of this advantage, aimed at conservativeness and simplicity (Fardis, 2009). Actually, considering different resistances of materials for the diverse situations would make impossible to design beams with the strategy of “envelop” of forces, i.e. to overlap graphically the graphics of forces (bending moment or shear) coming from the different combinations. Furthermore, more widespread Spanish commercial pieces of software for structural design, do not consider any reduction in the partial factor for materials (De Miguel, 2008).

Notwithstanding the observed trend of those coefficients –less conservative in more recent codes—, it is worth noting that the characteristic values for actions assumed in the design have been conversely increased in the studied period of time (see section 5.1.1.1). The causes of this increase could be the higher conservativeness of codes, the use of heavier constructive or structural solutions, or the use of computer in the design process (which permits to have into account the self weight of columns and beams).

2.2.9.2 Minimum required amount of stirrups at column ends

Aimed at evaluating, within FAST framework, the susceptibility of first storey columns of suffering brittle failure because of interaction with infill panels, it is important to know which are the minimum transversal reinforcement established by RC codes for columns.

As seen in section 2.2.2, medium- and new-generation seismic codes somehow warrant implicitly that brittle interaction failure does not occur thanks to the local detailing of column ends –at least in the case of diagonal strut behaviour of infill panels—. Thus, only prescriptions belonging to RC codes current before 1994 are of interest. These limitations are:

- 1) longitudinal spacing of stirrups $s_L \leq \min\{15d_{bL}; 300\text{mm}; 0.85d; 3b_c\}$, being d_{bL} the minimum longitudinal compressed reinforcement bar, d the effective depth and b_c the column section width;
- 2) internal legs linking at least one of two longitudinal compressed reinforcement bars within a maximum distance of 30cm

2.2.9.3 Severity of deflection limitation in beams

It is important to study the different degree of severity of the limitation for vertical deflections in beams due to gravitational load in persistent-transient situations within the different RC codes because:

- 3) its influence on the structural overstrength R_S could be relevant;
- 4) hierarchy of resistances between columns and beams could be not reached for codes in which it is not explicitly and quantitatively regulated.

Very severe deflection limitations could lead to the assumption of larger depth of beams. For gravitational design, this solution may not necessarily increase the overstrength so much, because the reinforcement may decrease proportionally in order to furnish just the demanded flexural strength, considering that the minimum required reinforcement is not so high to interfere with this procedure.

However, in seismic design, rules for local detailing of critical regions of beams lead to reinforcement patterns actually different from the “gravitational” one. Thus, in this case larger depths may lead to higher flexural overstrengths, which could compromise the column-beam strength hierarchy old- and medium-generation codes.

Furthermore, if wide beams are used together with one-way slabs (see Chapter 3), the thickness of the slab should be similar to the beam depth. Unless length of the joists is much bigger than beams one, overstrength in slabs may be even so higher than in beams. As seen in Figure 108, joists flexural contribution to beams parallel to them is very important, thus leading to very high overall overstrengths and so compromising even more the acquisition of strength hierarchy.

Given that the deflection in RC beams is an intricate phenomenon –due to nonlinear behaviour of both concrete and steel, slip of steel, cracking of

concrete...—, RC codes usually furnish some simplified conditions of minimum beam depth (h_b) that allows to avoid any deflection calculation.

In Equations (55), (56) and (57), expressions of the different codes for such minimum h_b are presented, being: f_{ck} , concrete compressive strength; f_{yk} , yield strength of steel; G and Q , permanent and live loads on the beam, respectively; c_L , coefficient of length relating the distance between two inflection points of the deflected line of the beam to the real length (presented in Table 27 for all the codes); L , beam length; d' , distance from the beam tensioned border to the centreline of the tension reinforcement bars; ε_y , yield strain of steel; and ρ and ρ' , tension and compression geometric reinforcement ratio.

$$h_{b,EH-68} = \frac{10f_{ck} + f_{yk}}{6000} \frac{G}{G+Q} c_L L \quad (55)$$

$$h_{b,EH-68,73,80,88,91} = d' + \varepsilon_y c_L L \cdot \max \left(30; 50 \frac{G}{G+Q} \right) \quad (56)$$

$$h_{b,EHE-99,08} = d' + \frac{c_L L}{11 + \left\{ \begin{array}{l} \frac{0.0015f_{ck}}{\rho} + 3.2 \sqrt{f_{ck} \left(\frac{\sqrt{f_{ck}}}{1000\rho} - 1 \right)^3}, \text{ if } \rho \leq \frac{\sqrt{f_{ck}}}{1000} \\ \frac{0.0015f_{ck}}{\rho - \rho'} + \frac{1}{12} \sqrt{f_{ck} \frac{1000\rho'}{\sqrt{f_{ck}}}}, \text{ if } \rho > \frac{\sqrt{f_{ck}}}{1000} \end{array} \right\}} \quad (57)$$

In Table 28, those formulations are applied to some particular usual cases of beams. It can be observed that the restrictiveness of the two last RC codes is not higher than the precedent if intermediate values of ρ are considered. Anyway, it is worth noting that for some cases in which L is on the upper bound —considering residential use—, depths of wide beams and joist must be almost 40cm, leading to not only higher overstrengths but also higher masses and base shear demand. Such long spans might be required sometimes in garages, or in specific points of the construction. Unfortunately, often an exceptional geometric constraint may condition the overall structural solution.

Table 27: Values of c_L for each RC code

RC code	Beam end conditions					Fixed
	Cantilever	Pin-pin	Half fixed-pin	Half fixed	Fixed-pin	
EH-68 (1968)						
EH-73 (1973)						
EH-80/82 (1980/82)	2.00	1.00	0.85		0.70	0.50
EH-88 (1988)						
EH-91 (1991)						
EHE-99 (1999)	2.50		1.00		0.76	0.66
EHE-08 (2008)						

Table 28: Minimum beam effective depth aimed at avoiding any deflection calculation for each RC Spanish code, considering different assumptions

RC code	Situation	Extreme beam				Cantilever beam			
	L [m]	4.00		6.50		1.00		2.00	
	ρ [%]	1.5	0.5	1.5	0.5	1.5	0.5	1.5	0.5
EH-68 (1968)		193		313		138		275	
EH-73 (1973)									
EH-80/82 (1980/82)		230		355		173		316	
EH-88 (1988)									
EH-91 (1991)									
EHE-99 (1999)		252	184	391	280	197	155	363	280
EHE-08 (2008)									

Table 29: Maximum deflection in beams for each RC Spanish code

RC code	Total load	Permanent load	Active load for infills
EH-68 (1968)	-	-	-
EH-73 (1973)			
EH-80/82 (1980/82)	$L/300$	$L/500$	-
EH-88 (1988)			
EH-91 (1991)			
EHE-99 (1999)	$L/250$		$\min\{L/400; 1\text{cm}\}$
EHE-08 (2008)	$\min\{L/250; L/500+1\text{cm}\}$	-	$L/400$

Furthermore, if the designer decides, in order to minimise beam depths, not to apply the simplified condition for avoiding the deflection calculation, sometimes the resulting demand of depth could be even higher.

In Table 29, the limitations of deflection for the different codes are shown. The restriction for total load within an infinite period of time may be somehow common to all of them and kind of reasonable. However, the limitation for active deflection with respect to infill panels in EHE-99 of 1cm seems to be so much restrictive.

Aimed at illustrating it, a specific example is considered: $b_w=650\text{mm}$, $h_b=300\text{mm}$, $G=7\text{kN/m}^2$, $Q=2\text{kN/m}^2$, $b_{trib}=4\text{m}$, being b_w the beam section width and b_{trib} the loads tributary transverse distance. The flooring is assumed to be placed after the construction of infill panels. The active deflection of this beam is within the limits if EHE-08 is considered. However, if EHE-99 is considered, b_w should be increased until 900mm –which is almost unfeasible unless very large columns are placed, see section 3.2.4.1— or conversely h_b should be increase until 330mm. The last could increase the flexural strength of the member end in a 10% (proportional to the increase of depth) if reinforcement pattern is ruled by local detailing prescriptions or also by the flexural demand in the mid-span region.

Chapter 3

Seismic performance of wide-beam frames

In the previous chapter, Spanish seismic codes have been reviewed in order to achieve enough knowledge about the characteristics of the Spanish RC residential building stock derived from those codes, in order to define the input parameters required by FAST approach (see Chapter 5). Still, some other typical characteristics of Spanish buildings may be understood as territorial peculiarities of construction that are not influenced or “corrected” by the codes; this is the case of the use of wide beams. In this chapter, the prescription of lower behaviour factors for wide-beam frames with respect to deep-beam frames proposed only by Spanish and Italian seismic codes is discussed, and relative performances between wide- and deep-beam frames designed to high ductility are assessed through different approaches.

3.1 INTRODUCTION

It is worth noting that almost all the Spanish territory corresponds to low or very-low seismicity (see Figure 65). According to current Spanish seismic code, 88% of the territory can be considered as low seismicity zones, and also 67% as very low seismicity areas –following the EC8 criteria for defining seismicity zones—. Thus, there is a high influence of “gravitational” design practice of such

88% in the seismic prone areas, some of them with high levels of hazard, e.g. $a_{gR} > 0.20g$. In these areas it is still usual to find some of these solutions:

- 1) masonry staircases supporting stair landings, which often suffer easily out-of-plane failure;
- 2) reduction of infills in ground floor;
- 3) bidirectional (flat-solid or waffle) slabs, whose behaviour against important earthquakes is still not well-known (Fardis, 2009), and whose thickness and overstrength could be excessive due to deflection limitations (see section 2.2.9.3).
- 4) one-way slabs with wide beams, which is the main structural solution for slabs in Spain (Feriche et al., 2012). However, its behaviour may not be similar to bidirectional slabs, although it might not be completely similar to that of deep-beam frames.



Figure 84: Construction of typical wide-beam frame in Spain

Regarding the last point, in this chapter a profound study of the specific case of wide beams reinforced concrete moment resisting frame (WBF, see Figure 84) is carried out, aimed at understanding its behaviour in comparison with common

deep-beam frames (DBF) and also at finding out the real behaviour factor (q) provided by those frames –needed for the simplified assessment of bare frames, see section 5.1.1—, given that Spanish codes compel to reduce q of design with respect to DBF without any further justification.

In Mediterranean countries, such as Spain or Italy, WBF constitute a common structural solution for earlier gravity-load designed (“sub-standard”) buildings, and also for lateral-load designed buildings in low-to-moderate seismic prone areas. Wide beams (WB) are those whose width is larger than its depth, being usually also larger than the column width. Their depth is designed to be equal to the thickness of the one-way slab in which they are included together with joists and upper slab, being typically in the range of 20-30cm; if thicker, they may not be cost-effective. Thus, wide beams present usually a width 2 or 3 times bigger than the depth. Sub-standard buildings did not used to present internal transverse beam (Verderame et al., 2010a), while modern frames designed to seismic action in both directions do. However, they are usually narrower than main girders due to their lower gravitational action.

The advantages of wide-beam construction are mainly related to architectonic, constructive or economic reasons rather than to their structural performance, at least in origin. These benefits have been amply described (Gentry and Wight, 1992; Quintero-Febres and Wight, 1997): possible reduction of interstorey height, simplicity and reduction of the formwork, straightforwardness in the itinerary of the facilities behind the slab, freedom for the layout of partitions or eventual modifications, lower cost and time of construction, and plain ceiling appearance.

However, its progressive use for seismic resistance purposes is not a result of a broad understanding of its behaviour but comes merely as an adaptation of a common “gravitational” system. Its behaviour may be considered as intermediate between that of a common frame and that of a flat-slab system when subjected to lateral loading (Benavent-Climent, 2007), and has not been completely investigated.

Thus, given the multiple uncertainties concerning its performance if compared with the better-known behaviour of deep beams (DB), the consecutive seismic codes have been quite cautious in the acquiescence to use WB with the same

design rules. Typical restrictions imposed by the codes to this structural system have been the impossibility of considering it as a high-ductility system by imposing a reduction of the behaviour factor of design, or even to forbid its use in seismic-prone areas. Currently, main international benchmark seismic codes as European Eurocode 8 –EC8— (CEN 2004), American ACI 318-08 (ACI, 2008) or New Zealand NZS 3101 (NZS, 2006) do not present any of those restrictions. However, some national seismic codes in the Mediterranean area still do, as the Spanish NCSE-02 (CDSC, 2002), the Italian NTC (CS.LL.PP, 2009) or the Greek EAK 2000 (MEPP, 2000a).

Contemporaneously, different experimental and analytical studies regarding wide beam-column (WB-C) exterior and interior connections performance have been carried out (Gentry and Wight, 1992; LaFave and Wight, 1997; Quintero-Febres and Wight, 1997; Siah et al., 2003; Benavent-Climent, 2007; Benavent-Climent et al., 2009 and 2010; Li and Kulkarni 2010, Masi et al. 2013). These experiments show different geometry, loading and reinforcement of the subassemblages. Main issues analysed in these tests are: stiffness of the system, plastic hinge development, ductility of the sections, upper slab participation, joint behaviour, hysteretic loops, bond development and especially the effective width of the beam in relation with the torsional behaviour of the transverse beam. Quite similar conclusions are extracted: if some parameters of design –not so restrictive— are taken into account, local performance of these arrangements may be satisfactory as much as deep beam systems.

The scope of this chapter is: firstly, to give a suitable mechanical interpretation to the restrictions of those codes, attempting to evaluate their pertinence by means of both an examination of the experimental background and some generic analytical considerations; secondly, to assess, through a case study, the global seismic performance of WBF in comparison with DBF, both designed to high ductility. The last is carried out by means of several spectral pushover-based seismic analyses of a 5-storey building model designed according both to Eurocode 8 and Spanish seismic code NCSE-02, assuming different hypotheses. The contributions of this work with respect to other case-study analytical studies present in literature are: (i) pure DBF and pure WBF 3D buildings with similar geometry and structural arrangement -and not containing disturbing elements as

shear walls— are compared; (ii) models are designed to European seismic codes instead of American ones; (iii) generic experimental-based expressions for yielding and ultimate chord rotations are employed within a lumped plasticity framework instead of using fibre models only fitted to some particular tests. Also, some generic spectral considerations are proposed, in order to extrapolate the analytical results to any case.

The whole chapter is based on Gómez-Martínez et al. (2015b, 2015c)

3.2 REVIEW OF CODE PROVISIONS

First national seismic codes used to present vast differences between them due to the high local influence –site earthquakes and construction practice. However, in the last decades they have converged to several common considerations. In particular, in the European sphere, the appearance of the EC8 has standardise the rest of the national codes or even driven to adopting it through the corresponding National Annex. Still, as wide-beam construction is mainly widespread in the Mediterranean area, some differences regarding the use of this system can be found in the current codes of Spain (NCSE-02), Italy (NTC) or Greece (EAK 2000).

Concerning the use of WBF as proper lateral resisting systems, three types of limitations can be identified in the different current seismic codes. They are, ordered by significance: (i) impossibility of using WBF as the only lateral resisting system in the building; (ii) impossibility of considering it as a high-ductility system; and (iii) geometric and mechanical restrictions for the connections. Types (i) and (ii) are seldom included in current codes; however, it is worth noting that similar restrictions are often imposed to flat-slab solutions.

Sometimes code requirements are not consistent or even divergent when compared between themselves. However, underlying reasons for these limitations are not always evidently specified. Thus, it is not clear whether they respond to assumed mechanical models based in theory or experimental results, or conversely they are just vague conservative legacies –sometimes coming from flat-slab similar requirements—, not matching accurately into a framework of cause-effect relationships.

In the following, an overview of those requirements is presented, referring to some Mediterranean seismic codes –the three aforementioned plus the Turkish one (TSI, 2007)— in comparison with some prestigious international codes –EC8, ACI 318-08 (complemented with ACI 352R-02 (ACI-ASCE, 2002) and ASCE/SEI 7-10 (ASCE, 2010)), and NZS 3101 (complemented with NZS 1170.5 (NZS, 2004))—, mentioning occasionally some other past codes that showed particular restrictions. Previously, some code considerations regarding flat-slab structures are described, in order to enlighten eventually underlying causes for further restriction regarding WBF.

A resume of this compared analysis is shown in Table 30, where codes are ordered by restrictiveness degree, approximately; geometric nomenclature used from now on is also specified. Graphic description of variables is shown in Figure 85.

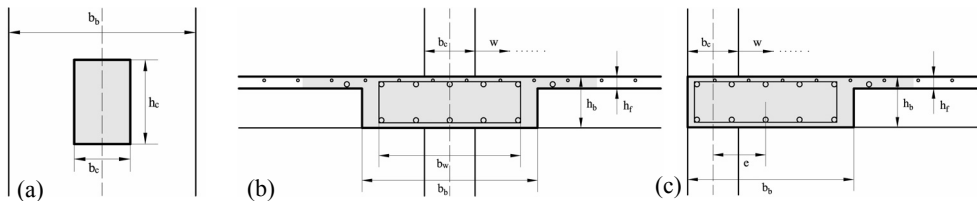


Figure 85: Graphic description of variables used in Table 1, corresponding to: plan of interior connection (a), and elevation of connection belonging to central (b) and edge (c) frame

3.2.1 Code provisions on flat-slab structures

Some of the past seismic codes recommended or compelled to avoid flat slabs as the only lateral resisting system in seismic situation, e.g. the American ACI 318-89 (ACI, 1989), which required to complement them with shear walls. Current codes still present severe restrictions to their use, which can be classified in three types: site-hazard, deformability and ductility limitations.

Table 30: Prescriptions regarding flat-slab and wide-beam frames according to different codes

CODE (seismic, RC, connections)	Max. IDR ⁽¹⁾ [%]	BEAMLESS TWO-WAY FLAT SLAB			WIDE BEAMS									
		Max. α_g [g]	Deforma- -bility restrictions	Max duct. class (q reduction from DCH)	Min. h_b [cm]	Max. duct. class (q reduction from H)	Min. h_c [cm]	Max. w from effective width for					% upper reinf. within column core	
							Member web	Reinf. (both sides)	Edge beam h_b from max. e	Joint shear	Upper slab tension flange reinforcement	Beam shear		
Greece: EAK (2000), EKOS (2000)	1.25	-	stiffness required ⁽⁵⁾	DCH ($q=3.5$)	stiffness required ⁽⁵⁾	DCH ($q=3.5$)	(25)	$\min\{0.25h_c;$ $0.5b_c\}$ ⁽⁶⁾⁽⁷⁾	-	$0.66b_c$	-	$h_f \{0; 2; 2.5; 4\}$ ⁽¹⁷⁾	- ⁽²¹⁾	-
New Zealand: NZS 1170.5 (2004), NZS 3101 (2006)	2.5 ⁽²⁾	-	IDR ≤ 0.9 %	DCL ($q=1.25$; -79%)	$\approx 27\phi_w \approx$ $43\phi_w$ ⁽⁷⁾	DCH ($q=3.5$)	$\approx 30\phi_w$ $\approx 48\phi_w$ ⁽⁷⁾	-	$0.25h_c$ ⁽¹¹⁾	$0.25h_c$ ⁽¹⁶⁾	$\min\{L/8; 8h_f/h_c;$ $h_c \{0.5; 0.75\}$ ⁽⁸⁾⁽⁹⁾ ; $\min\{L/8; 8h_c/3h_f\}$ ⁽¹⁹⁾	$(0.25h_c$ ⁽²³⁾)	90% ⁽²⁴⁾	
Spain: NCSE-02 (2002), EHE-08 (2008)*	-	-	-	DCL ($q=2$; -50%)	-	DCL ($q=2$; -50%)	(25)	-	$0.0; 0.5h_c$ ⁽¹²⁾	$0.5b_c$	-	$h_f \{0; 2; 2; 4\}$ ⁽¹⁷⁾	0.0 ⁽²³⁾	-
Italy: NTC (2008)	≈ 1.3 ⁽³⁾	-	-	DCH ($q=5.85$)	-	DCM ($q=3.9$; -33%)	$\approx 36\phi_w$ $\approx 55\phi_w$ ⁽⁷⁾	$\min\{0.5h_c;$ $0.5b_c\}$ ⁽⁶⁾⁽⁹⁾	-	$0.5b_c$ ⁽¹⁴⁾	$0.25h_c$ ⁽⁸⁾	$h_f \{0; 2; 0; 2\}$ ⁽¹⁷⁾	- ⁽²¹⁾	75%
Europe: EC8 (2004)	1.0	$\min\{0.08; 0$ $1/8\}$	-	DCL ($q=1.5$; -74%)	-	DCH ($q=5.85$)	$\approx 36\phi_w$ $\approx 55\phi_w$ ⁽⁷⁾	-	$\min\{0.5h_c;$ $0.5b_c\}$ ⁽⁶⁾⁽¹³⁾	$0.5b_c$	$0.25h_c$ ⁽⁸⁾	$h_f \{0; 2; 2; 4\}$ ⁽¹⁷⁾	-	-
Turkey: (2007)	2.0	0.24	H $\leq 13m$	DCM ($q=4$; -50%)	-	DCH ($q=8$)	(25)	$0.5h_c$ ⁽⁸⁾⁽⁹⁾	-	-	0.0	-	- ⁽²¹⁾	-
USA: ASCE/SEI 7-10 (2010), ACI 318-08 (2008), ACI 352R-02 (2002)*	1.0- 2.5 ⁽⁴⁾	-	-	DCM ($q=4$; -38%)	-	DCH ($q=8$)	$20\phi_w$ $\approx 32\phi_w$ ⁽⁷⁾	$\min\{0.75h_c;$ $b_c\}$ ⁽⁹⁾	-	- ⁽⁴⁾	0.0	$\min\{L/20; b_w/2; 8h_f\};$ $\min\{L/8; b_w/2; 8h_f;$ $h_c \geq 2b_c\}$ ⁽¹⁹⁾⁽²⁰⁾	- ⁽²¹⁾	33%
* Recommendations, not mandatory					⁽¹⁰⁾									
⁽¹⁾ For DLS but obtained from ULS displacements														
⁽²⁾ Specific for ULS														
⁽³⁾ Obtained from specific DLS demand spectrum														
⁽⁴⁾ Depending on α_g and number of storeys														
⁽⁵⁾ Sufficient stiffness to ensure frame –not cantilever– behaviour in all columns														
⁽⁶⁾ Formulation depending in most of the cases on ductility class, material strengths, axial load, reinforcement ratios and location of the joint														
⁽⁷⁾ Considering $\phi_w = 16mm$														
⁽⁸⁾ Edge beams not explicitly considered														
⁽⁹⁾ Not for low-ductility design														
⁽¹⁰⁾ Referred to gross section, not to web														
⁽¹¹⁾ Referred to the 90% of the required flexural reinforcement; remaining 10% within (19)														
⁽¹²⁾ Required transverse beam for external connections or internal connections with moment inversion														
⁽¹³⁾ Not mandatory, only for taking advantage of the column compression on the bond behaviour														
⁽¹⁴⁾ Higher values only if proper perpendicular reinforcement is placed														
⁽¹⁵⁾ Further research is needed														
⁽¹⁶⁾ Also reciprocal requirement for columns in the case of wide column – narrow beam connection														
⁽¹⁷⁾ Exterior connection with and without transverse beam, and analogous for interior connection, respectively														
⁽¹⁸⁾ Exterior connection with and without transverse beam, respectively														
⁽¹⁹⁾ For beam flexural designing and for overstrength evaluation for column and joint designing, respectively														
⁽²⁰⁾ Torsional evaluation of spandrel beam in external connections required														
⁽²¹⁾ Maximum h_c limitation may control both flexural and shear behaviour														
⁽²²⁾ Uncertain, not explicitly indicated														
⁽²³⁾ Value at the column face; $0.5h_c$ at distance of higher than $0.5h_c$ from the column face; intermediate values from linear interpolation														
⁽²⁴⁾ Not column core but joint effective width; strut-and-tie analysis required for lower values														
α_g Design ground acceleration		DCH	High Ductility Class			b_c	Beam gross section width		h_f	Upper slab tension flange thickness				
S Soil amplification factor		DCM	Medium Ductility Class			b_w	Beam web width		e	Beam - column eccentricity				
H Building height		DCL	Low Ductility Class			h_b	Beam depth		ϕ_c	Maximum column bar diameter				
L Beam span		q	Behaviour factor			b_c	Column width		ϕ_w	Maximum beam bar diameter passing through the joint				
IDR Interstorey drift		w	Outer cantilevered beam width respect to narrower column core			h_c	Column depth		$\phi_{w,c}$	Maximum beam bar diameter passing outside the joint				

3.2.1.1 *Deformability restrictions*

Most of modern codes set limitations for interstorey drift (IDR) whatever it is the structural system, oriented mainly to prevent non-structural damages in Serviceability (Damage) Limit State (DLS). Those values range typically between 1 and 2.5% if transformed into equivalent values corresponding to demand at Ultimate Limit State (ULS), as shown in Table 30.

However, some current codes establish specific deformability restrictions to flat-slab structures. New Zealand NZS 3101 allows using flat-slab as primary seismic elements only for IDR not higher than 0.9%. This value is much lower than the required 2.5% for any structural type, which is also higher than the thresholds shown in the rest of the studied codes. It is worth noting that NZS 3101 is the only code to limit IDR for ULS.

Instead, other codes present qualitative conditions for the deformed shape, as Greek EAK 2000. It settles that “substantial frame action for most of the columns [...] with beams of sufficient stiffness [must be ensured]. Wherever this is not possible (e.g. flat or ribbed slabs), it is necessary to provide for sufficient structural walls”. In this context, “frame action for columns” might be understood as columns presenting opposite moments in both extremes (Fardis, 2009). It is not clear whether the code obliges to assess such behaviour in each case or simply establishes that those structural types do not satisfy the requirement of stiffness for horizontal members by default. However, ensuring not-cantilevered behaviour for ground floor columns is sometimes difficult even for deep-beams structures when they are designed to high ductility class (Fardis, 2009). Thus, this restriction would lead to slab depths that may not be economically reasonable.

Besides, other codes limit the overall height of the building when flat slab is the only resisting system: 13m for the Turkish one and 10m or three storeys for the Iranian seismic code (BHRC, 2004), “unless resisted by shear walls or braced frames”.

3.2.1.2 *Ductility restrictions*

Most of codes do not consider flat-slab system able to be designed to high ductility class (DCH). EC8, NCSE-02, NZS 3101 compel to design as low ductility

class (DCL), while for ACI-318-08 and Turkish code they can be designed as kind of medium ductility class (DCM). Thus, reductions of behaviour factors (q) from DCH range between 38% and 79% (see Table 30). EAK 2000 and NTC do not explicitly mention any ductility restriction. In the first case it may not matter as the deformability restriction makes it difficult to use flat-beam structures. In the second case it could be a lapse, because no reference is made to flat slabs in all the text. In (CS.LL.PP, 2011), flat slab are confirmed to be able to be designed to DCH but no further specification for design is made.

In fact, if flat slabs are allowed to be designed to some ductility, some specific rules to ensure the local ductility of the connections are usually furnished, similar to those concerning beams. ACI-318-08 defines the equivalent width of “column strips”, which indirectly make it possible to evaluate the moments of resistance in the slab in order to carry out the capacity design of connections. Also give some specific rules for the placement of reinforcement within a certain width, smaller than the “column strip” width.

3.2.2 Impossibility of using wide-beam frames as the only lateral resisting system

Similarly to flat-slab structures, the American ACI 352R-91 (ACI-ASCE, 1991) recommended not to use this system to inelastically dissipate energy in seismic situation; these impossibility remained until the appearance of ACI 318-95 (ACI, 1995), which allowed it with some geometric restrictions. Likewise, the previous Spanish national seismic code NCSR-94 (CDSC, 1994) prevented for their use for values of design ground acceleration higher than 0.16g. Currently, almost all the codes have removed those limitations.

However, same stiffness requirement in EAK 2000 for flat slabs may rule also for WBF, although they are not explicitly mentioned. WB may be assumed to have similar performance –regarding initial stiffness— because their gross flexural stiffness is lower than that of a flat slab, given that their thicknesses are similar. Similar condition is required in current Iranian seismic code: “if beams depths are less than 30cm [...] shall be considered as flat slab type”. In this case, a depth

threshold is given for estimating the “sufficient stiffness” requirement, in such a way that it is still reasonably possible to use WBF.

It is worth noting that severe restrictions for the depth of WB likely force to use another structural system –unlike restriction regarding maximum beam width or column dimensions, which can be assumed. This is the case of NZS 3101, whose condition of minimum ratio between beam height and maximum column bar diameter –aimed at ensuring adequate bond behaviour inside the joint— is so restrictive to usually require beam depths around 40-45cm (see Table 30), which clearly preclude the use of WB. In fact, the only way to use WB of nearly 30cm deep would be to place longitudinal bars of 12mm diameter.

3.2.3 Impossibility of considering wide-beam frames as high-ductility systems

Spanish and Italian national codes do not permit designing WBF as systems of high ductility. The Spanish NCSE-02 reduces the behaviour factor (q) in a 50% – from $q=4.0$ for high-ductility systems to $q=2.0$ for WBF, corresponding this behaviour factor to Low Ductility Class (DCL)—. So does the Italian NTC in a 33%, from a value of 5.85 to 3.90 for WBF –corresponding to Medium Ductility Class (DCM)—. Greek EAK 2000 reduces q in a 14% –from $q=3.5$ to 3.0— for “walls acting as cantilevers”, which may not apply to WBF notwithstanding the considerations made in the previous section.

The fact that Italian code still settles this distinction for WBF is more unexpected than in the Spanish case. In fact, the NTC is intended to be kind of a local arrangement of EC8, following the same principles and organization and sharing almost all the requirements, while NCSE-02 is far away of the philosophy of EC8 (Gómez-Martínez et al., 2015a and 2015d). Furthermore, the last RC Spanish code EHE-08 (PCC, 2008), which include some recommendations regarding seismic design close to the EC8 principles, still limit behaviour factor to $q=2.0$.

It is worth noting that EC8, as most of the codes, does not relate any Ductility Class to the general typology of the frame system (DBF or WBF) but to the specific characteristics of the design: minimum dimensions and reinforcements

(longitudinal and transverse), local ductility, axial limitation in columns, capacity design rank, and eventual modifications depending on the regularity in plan or elevation. In the Italian case, as in EC8, the reduction of the behaviour factor is followed by a reasonable relaxation of those requirements. However, in the Spanish case—whose assumption of $q=2.0$ for WBF may be assimilate to the DCL in EC8 ($q=1.5$)—the limitations are more severe than those habitually required for low-ductility systems, usually quite relaxed because the resistance to the lateral action is assumed to come only from the overstrength given by a gravitational design (Fardis, 2009).

3.2.4 Geometrical restrictions for connections of wide-beam frames

Aimed at ensuring the equilibrium effectiveness of WB-C connections, most of the codes agree in the necessity of establish some restrictions to the section geometry of members framing the joint. These limitations constitute prerequisites for the application of the usual design procedure for section dimensions and reinforcement; otherwise, it may not be possible to account with their full capacities.

The main limitation regards the effective width of beams, i.e. the fraction of the beam section intended to be able to satisfy the flexural equilibrium with the column, whose width is narrower. Also, the same principle is underneath other prescriptions, as some limits for the amount of top reinforcement placed within the width of the beam or in the upper slab flange, or some other effective widths as those for shear behaviour of beam and joint. Besides, other restrictions for depths of members are oriented to ensure adequate bond behaviour of the longitudinal reinforcement. All of them are described herein and listed in Table 30, specifying the reason employed by the codes when existing.

3.2.4.1 *Beam effective width for flexural equilibrium*

The different code prescriptions regarding the restriction of the beam width can be classified attending to four aspects:

- 1) Mandatory nature: some codes forbid to design beams whose width is larger than the settled limit, while other ones permit any width whenever

the required reinforcement is placed within a certain distance (NZS 3101, NCSE-02 and somehow EC8).

- 2) Ductility class in which it rules: in most of the cases restrictions are required only for medium or high ductility, with some exceptions in which they also apply for low ductility (NCSE-02 and NTC).
- 3) Element of reference: codes can be grouped in those whose beam width (b_w) limitation depends on the column depth (h_c) (EKOS 2000 (MEPP, 2000b), NZS 3101 and ACI 318-08) or on the beam depth (h_b) (the rest); some codes of both groups also relate the limitation to the column width (b_c).
- 4) Consideration of edge beams: in some cases, the particular case of edge beams—in which the cantilevered part of the section with respect to the narrow column is larger than for internal beams, assuming equal widths—is explicitly regulated (NZS 3101, NCSE-02 and ACI 318-08); in the rest of the cases, it may be understood in a similar way.

It is worth noting that, except NTC, which is the only one that limits the gross section width (b_b), the rest of the codes limit the web width (b_w). A particular interpretation of this requirement could lead to include, both for elastic stiffness and for negative flexure, the contribution of the concrete placed outside of the web, given that the first clay element between joists is usually moved 10-15cm away from the end of the joist and the beam web (Figure 86b); also, in the proximity to the columns, sometimes an additional clay element is removed (Figure 86a). This is actually not possible for DB, as their bottom is not within the depth of the slab.

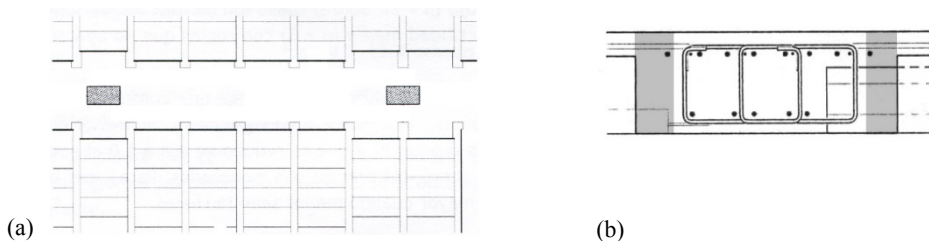


Figure 86: Typical distribution of elements in a one-way joist slab (a) and detail of joist-wide beam connection (b, from De Andrés and CSCAE, 2009; in grey, gross section concrete outside the beam web)

In NZS 3101, not only the gross width is allowed to overcome the limits, but also the web of stirrups and the upper and lower reinforcement. Although the effective width is assumed to be quite reduced (cantilevered part (w) 3 times lower than the established by ACI 318-08), the code only establishes that the reinforcement “that shall be assumed to resist the forces transmitted by the column” must be placed within this distance. It is worth noting that it is the only code which furnishes reciprocal limitation for columns in the case of wide column-narrow beam connections.

Maybe the most severe restriction is given by the NCSE-02, which states that all the upper and bottom reinforcement must be placed within the column core unless transverse beams are present. Also, it states that the improvement in the bond behaviour due to the axial load of the column only affects to the column core. Conversely, the most permissive code seems to be EC8, whose limitation is only a condition “to take advantage of the favourable effect of column compression on the bond of horizontal bars passing through the joint”. Herein, “joint” might be interpreted not as the column core but as the connection, i.e. all the effective width shall take advantage of the compression.

3.2.4.2 *Reinforcement placed inside the column core*

Other than limiting the effective width for placing the reinforcement, some codes also compel to warrant that a minimum aliquot of the upper reinforcement passes through the width of the column. It is referred only to upper bars because in this side it is usual to place reinforcement not only in the internal part of the beam web located outside of column core but also outside of the beam web, in the upper slab flange (Figure 86b). Large dispersion of values within codes is observed. It is worth noting that NZS 3101 requirement is referred not to the column core but to the effective width, so it may be inferred that the remaining 10% of the upper reinforcement could be place outside of this distance but within the upper slab effective width.

3.2.4.3 *Edge beam effective width from eccentricity limitations*

Most of codes limit the eccentricity between the axis of beams and columns in order to ensure an adequate equilibrium, being those axes referred to the gross

section of concrete. In the case of edge beams (see Table 30), this requirement indirectly limits the beam width, being in most of the cases consistent with the effective width limitation. NTC is the only code that allows higher eccentricities if proper reinforcement is placed in the perpendicular direction; a suitable solution is shown in Figure 87. Anyway, larger values of eccentricity would lead to an exceedance of the common width limitation.

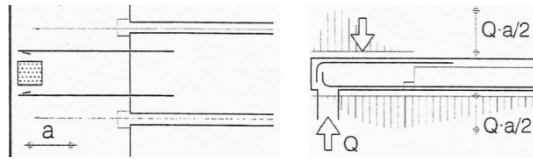


Figure 87: Perpendicular reinforcement in eccentric edge beams (from De Andrés and CSCAE, 2009)

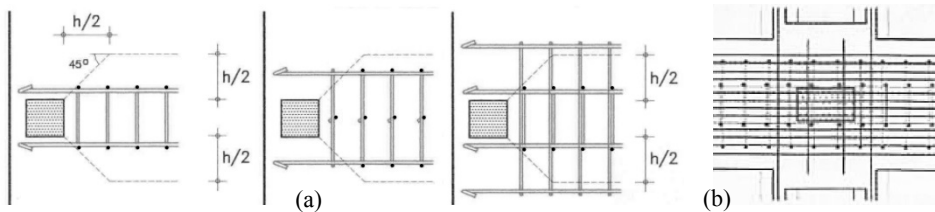


Figure 88: Effective stirrup legs (in black) (a) and arrangement of stirrups within the connection (b) according to NCSE-02 (b from De Andrés and CSCAE, 2009)

3.2.4.4 Beam effective width for shear equilibrium

Codes whose beam width limitation is referred to the web or to the gross section do not need to establish any other requirement for stirrups, assuming implicitly this width to be effective both for flexion and shear forces. Conversely, some of the codes whose limitation for beam width is not referred to the web but to the longitudinal reinforcement settle also values for the width in which stirrups are effective. This is the case of NCSE-02, which considers that the shear is able to be equilibrated only within the column core; the effective width opens following a plan-45° spread until reaching a magnitude similar to the flexural effective width (Figure 88a).

NZS 3101, despite referring its width limitation to the reinforcement, do not settle any further requirement for the effectiveness of stirrups. Such limitation could be understood as common to flexion and shear –given that the main text refers generically to “forces transmitted by the column”– but the comments only refers to longitudinal reinforcement.

Nevertheless, any reduction of the effectiveness of stirrup legs placed outside the column core may not difficult the design of beams to shear. In fact, both limitations of longitudinal spacing between stirrups and transversal spacing between legs within the member section – $0.75d$ for Eurocode 2 (BSI, 2004) or d for Spanish EHE-08; no limitation in ACI 318-08— are so restrictive to rule the design in most of the cases.

Besides, it is important to examine which member’s stirrups should pass through the connection according to the codes. All the codes establish that the column stirrups are those which must not be interrupted, except for Spanish NCSE-02, which recommends not to interrupt wide beam stirrups especially with deep columns and also encourage to place vertical legs close to the column lateral faces ((Figure 88b). However, Spanish EHE-08 recommends not interrupting column hoops. Besides, ACI 318-08 states that, although column stirrups should run uninterrupted, beam longitudinal reinforcement passing outside the column core must be linked by hoops (Figure 89 a and b). However, for connections with beams framing from both directions, in which it is not easy to organize the reinforcement, ACI 352R-02 shows examples in which wide beam stirrups are interrupted not only within the joint but at the intersection with the transverse beam (Figure 89 c and d).

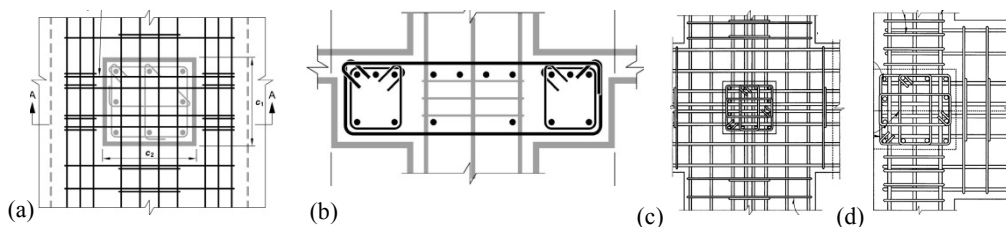


Figure 89: Arrangement of stirrups within wide beam-column connection according to ACI 318-08 (a, b) and ACI 352R-02 (c, d)

3.2.4.5 Upper slab effective width

Regarding the contribution of the upper slab to the flexural performance of the wide beam acting as a T-beam (Figure 90a), code restrictions can be organized in two types: those which only depends on the local geometry of the connections, and those which also depend on the span on the beam –which derive from the evaluation of the compressive contribution at middle-span in gravitational situation. Also, some codes propose different magnitudes depending on the purpose of the evaluation, aimed to conservativeness: lower values for flexural designing of the beam and higher values for assessing its maximum flexural capacity aimed to the capacity design of columns and joints. It is worth noting that they always refer to the effectiveness of tensioned reinforcement; there is no mention to the compressive behaviour.

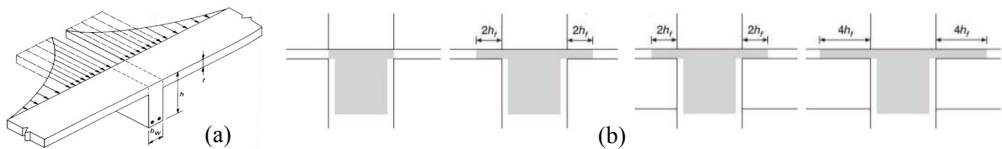


Figure 90: Upper slab flexural contribution in a T-beam (a) and typical limitations for effective width of the upper slab tensioned flange for some codes (b)

EC8, NTC, NCSE-02 and EKOS belong to the first group. Proposed magnitudes of the effective upper slab from the column face range between 0 and 4 times the depth of the flange, depending on the situation of the connection (interior or exterior) and on the eventual presence of transverse beams. As all the sketches are referred to deep beam-column connections (Figure 90b), it is not clear how to account for the contribution in the case of WB. In fact, when no transverse beam is present, wide beam web or reinforcement can be wider than column but paradoxically none of the upper reinforcement placed outside the column core may be effective according to the upper slab tensioned flange restriction. Spanish EHE-08 specifies that this overstrength may only be considered for capacity design of other elements, while the rest also consider it to rule for beam design purposes.

On the other hand, ACI 318-08 and NZS 3101 belong to the second group; both also propose diverse requirements for design or overstrength evaluation. Limitations depend, other than on flange depth, on the beam span and depth and on the column depth, resulting typically in higher effective widths than those corresponding to the codes of the first group. Values for beam flexural design are practically not useful for WB, as magnitudes result to be lower than maximum allowed beam width. ACI 352R-02 is the only one requiring torsional evaluation of the spandrel beam corresponding to the upper slab bars within the effective slab width.

3.2.4.6 *Joint effective width*

Besides, some codes establish that the effective width of the joint for shear behaviour can be higher than the strict volume contained within the beam-column intersection. Generally, codes allow considering enlargements up to $0.25h_c$ (Figure 91). They do not specify whether this magnitude is related or not to the beam effective width, although in some cases they are coincident. This effective width rules both for concrete resistance and for the placement of stirrups.

In the case of WB, although the effective width is larger than for DB – considering similar columns—, capacity design of joints is likely difficult to achieve because of the reduced beam depth (Benavent et al., 2010), especially for edge beams.

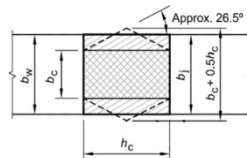


Figure 91: Joint effective width for NZS 3101

3.2.4.7 *Member depths for bond development*

Geometric restrictions of codes sometimes involve member depths compared to diameters of longitudinal bars –as in NZS 3101, NTC, EC8 or ACI 318-08—,

aimed to ensure proper bond behaviour in the connection. Such restriction usually regards only column depth, but in NZS 3101 also beam depth is also strongly limited by a similar expression. Similar restrictions for beam depth are present in previous codes as ACI 352-85 (ACI-ASCE, 1985).

Requirements for column depth-bar diameter ratio depend usually on different aspects as: ductility class, strengths of materials, axial load in columns, reinforcement ratios and location on the joint, resulting in values of h_c/ϕ ranging from 20 (ACI 318-08) to 36 (EC8), which leads to column depths around 32-48cm, respectively, considering the use of longitudinal bars of 16mm of diameter. This is actually a very strong limitation for column dimensions of upper floors, in which it may rule above other restrictions.

3.2.5 One-way slab as the only lateral resisting system in its direction

One-way slab made of RC joists, also called “banded floor”, is the most typical solution of slab to be used in conjunction with WB, in order to take advantage of the continuous formwork. In sub-standard buildings, designed only to gravitational loads, it was not usual to place beams in the transverse direction –i.e. parallel to the joists— except for edge members (Verderame et al., 2010a). Also, some Spanish recommendations (De Andrés and CSCAE, 2009) allow using double joist instead of beams for edge members.

Actually, one of the main reasons for choosing one-way joists slabs for common residential buildings is their flexibility in the organization of elements aimed to deal with typical plan irregularities –due to the necessity of saving space—. In these cases, sometimes it is even difficult to align columns in the transverse direction (Figure 92). Thus, the most profitable solution may be to not use transverse beams, trusting in one-way joist slab for resist lateral loads as primary seismic element. However, codes do not establish clearly whether this “beamless one-way slab” solution for the transverse direction is possible or not and which ductility class must be eventually assumed.

When subjected to lateral loads, codes do not clearly assume one-way slabs to be understandable to flat two-way slabs or to WB. Neither is it determined whether the same effective widths are required for the placement of reinforcement near the

column; anyway, most of codes do not prescribe any effective width for low ductility class, which is in some cases the only one permitted.



Figure 92: Typical wide-beam one-way joist slab system solution for common residential building (from De Andrés and CSCAE, 2009)

Furthermore, some codes as ACI 318-08 or NZS 3101 do not distinguish between one-way joist slab and solid slab acting only in one direction –because of high ratio between spans in both directions or because of support or boundary conditions—. In fact, the local behaviour around the connection with the column could not be similar for both cases due to the behaviour in the transverse direction.

According to EAK 2000, same stiffness requirement than for flat slabs and WB would be necessary, with the same ulterior uncertainty about the corresponding ductility class. In NZS 3101, one-way slabs are recognize as belonging to the same category as beams, and also some reference to one-way slabs for ductility design in earthquake is done, but no further specification is made. No reference is done in NTC and Turkish seismic code. Conversely, in EC8, the rules for DCM and DCH are referred specifically to beams, but only two-way flat slabs are forced to be designed to DCL, with no explicit reference to banded floors. ACI 318-08 states that requirements for the design of two-way slabs for DCM are not applicable to one-way slabs, but still does not make any other requirement.

NCSE-02 is the only one who explicitly establishes that one-way joist slabs, waffle slabs and flat solid slabs shall be treated similarly to beams concerning all the prescriptions referred to geometry and reinforcement. Thus, it may be possible to consider one-way joist slab as the only primary seismic element just in the case that transverse beams are not required by the main beams: for interior connections without moment inversion for beams or when beam width is not larger than the column width.

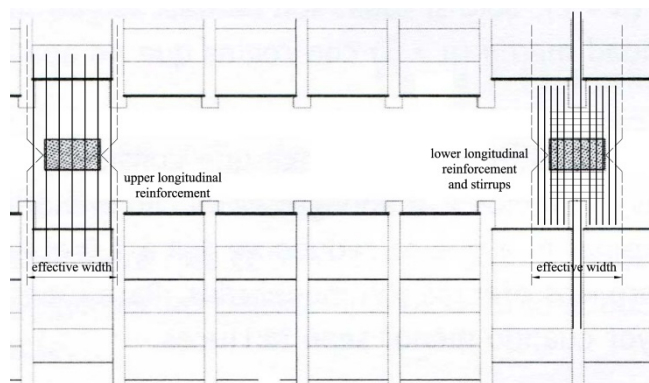


Figure 93: Suitable arrangement of reinforcement within effective width in joists-column connections

However, the main difficulty would be to place the required reinforcement within the effective width –required in NCSE and NTC also for DCL—, which is usually not higher than the lateral distance between joists. For the upper reinforcement it would not be difficult because it can be placed in the upper slab (Figure 93). Instead, the lower reinforcement may be contained within the gross width of the main wide beam –except for a couple of bars eventually placed along the sides of the joists—, being it necessary to use lower diameters in order to not require high anchorage lengths. It is worth noting that lower reinforcement in seismic situation is more relevant for joists than for beams given its low gravitational negative moment at the ends of members. Also stirrups could be placed in this portion, aimed to fulfil the requirements corresponding to the critical

regions, although it may be hard to lead with the congestion in the intersection with the main beam stirrups.

Aimed at the evaluation of the required reinforcement, codes often provide values for width of “column strips” considered to be effective in the transmission of loads in each direction, within an “equivalent-frame” framework. Some codes, as ACI 318-08 or EHE-08 also establish the aliquot of reinforcement corresponding to that strip which should be placed near the column within an effective width. Anyway, codes do not provide clear rules to satisfy those requirements when the analysis comes from a physical model or a plastic approach instead of from an approximate method.

3.3 EXPERIMENTAL BEHAVIOUR AND ANALYTICAL MODELS OF WBF

Experimental tests on WB and WBF have been representing the benchmark for changes and improvements to codes in the last decades. Several cyclic tests on subassemblages representing external and internal WB–C connections have been carried out (Gentry and Wight, 1992; LaFave and Wight, 1997; Quintero-Febres and Wight, 1997, see Figure 94; Siah et al., 2003; Benavent-Climent, 2007; Benavent-Climent et al., 2009 and 2010; Li and Kulkarni, 2010, Masi et al., 2013a and 2013b). All these studies capture different conditions (e.g., presence of upper slab, axial load on columns, vertical load on beams, or transverse DB). Furthermore, post-earthquake damage scenarios in the Mediterranean area have shown different in-field performance of WBF with respect to that of DBF. For instance, plastic hinges in beams and damage in joints are quite rarely observed (Gómez Martínez et al., 2015a).

3.3.1 Equilibrium of forces in wide beam-column connections

On the topic of local behaviour of WB–C connections, most of the aforementioned works have enlightened that the portion of forces (moment and shear) corresponding to the fraction of beam section passing outside the column core (called herein “outer” part of the section) can be equilibrated only if the

transverse beam develops sufficient torsional behaviour; otherwise, full beam section capacities are not attained. Moreover, if longitudinal bars passing outside the column core are not adequately bonded, not even maximum flexural capacities of WB are transmitted to the transverse beam. On the other hand, WB–C connections generally show higher contribution of the upper slab and better shear performance of joints and beam ends than deep beam-column (DB–C) connections (LaFave and Wight, 1997).



Fig. 6—Specimen IWB1 in testing rig and IWB2 on casting platform.

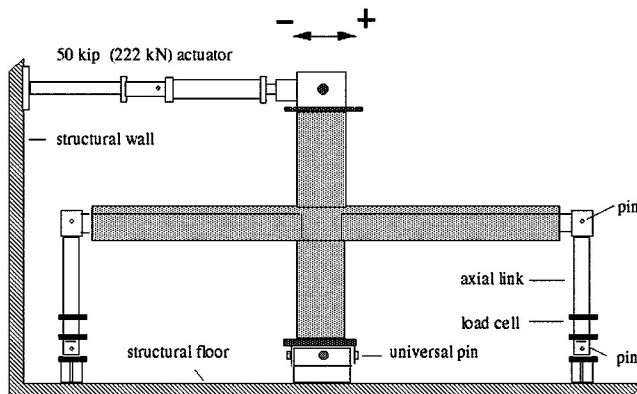


Figure 94: WB-C subassemblage tested in Quintero-Febres and Wight (1997)

Most of these phenomena can be reproduced with different strut-and-tie mechanisms, as shown for a typical 3D sub-assembly of interior WB–C connection with upper slab and transverse beam in Figure 95. Herein, the strut-and-tie model in Figure 95 is the basis of authors' theoretical interpretation of experimental behaviour of WB–C connections.

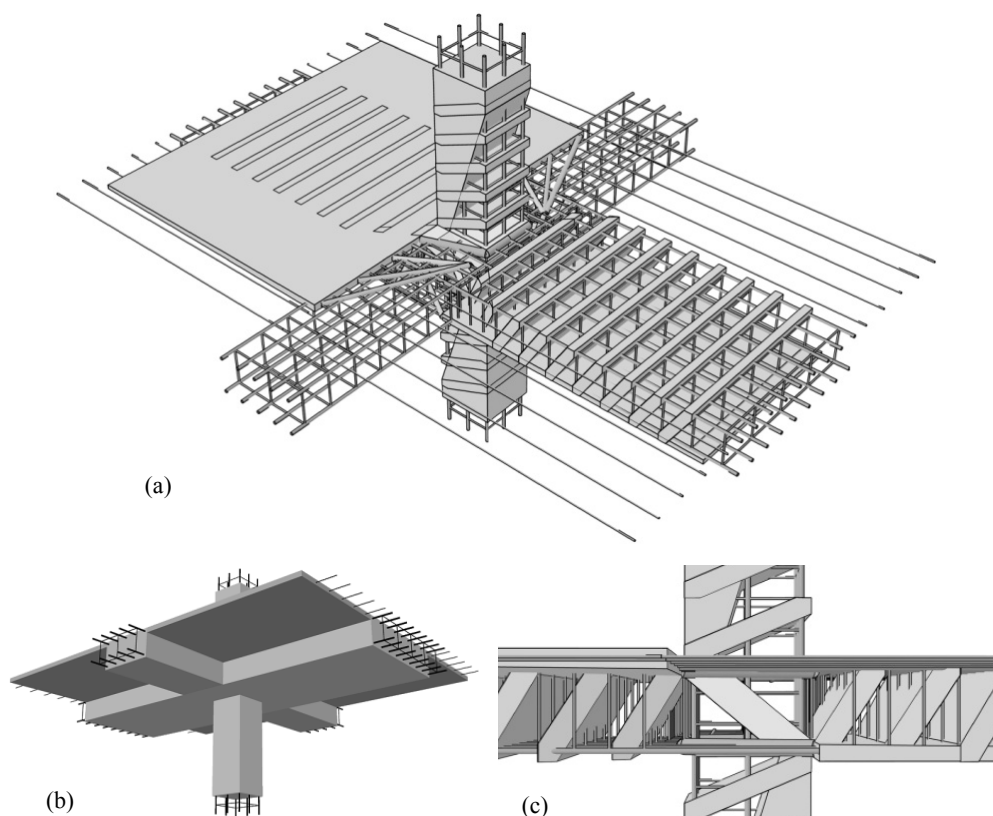


Figure 95: 3D subassembly of typical WB-C connection: solid view (a) and strut-and-tie scheme (b and c)

3.3.1.1 Effective width and torsional behaviour of transverse beam

Both upper and lower faces of the lateral parts of the section of the wide beam passing outside the column core transmit opposite horizontal forces (due to

flexural action) that must be transferred to the joint in order to reach the complete flexural capacity of the section. This transmission is carried out through the torsion of the transverse beam, if present. This behaviour does not occur in internal connections without moment inversion.

However, all the experimental works have enlightened that a fraction of the outer part of the section –corresponding to the “effective width” estimated by the codes— is able to transfer the couple of horizontal forces to the core through both horizontal compressed struts tied by the reinforcement in the transverse direction (Figure 96), even if no explicit transverse beam is present. In fact, it has been experimentally proved that the effective width is more related to the column depth than to the beam depth (Gentry and Wight, 1994), which supports the assumption of a horizontal strut-and-tie mechanism. Large values for the effective width suggested by ACI 318-08 are founded in several experimental works (Gentry and Wight, 1992, LaFave and Wight, 1997, Quintero-Febres and Wight, 1997); the rest of the codes seem to not having such large experimental background.

Alternative interpretations for the strut-and-tie mechanism within the effective width have been proposed. In (Gentry and Wight, 1992), it is proposed that the fusiform joint diagonal strut may flow between both stress blocks of column and beam, likely holding the horizontal tie inside the wider extreme of the strut, as if it was composed of several contiguous oblique struts (Figure 97a). Although it is not indicated, this mechanism may be assumed to perform in both directions, resulting in a superposition of two trapezoidal struts (Figure 96c and Figure 97b). It is worth noting that the parts of the struts placed outside the column core do not have their own vertical ties, thus being equilibrated by the longitudinal reinforcement of the columns. This model could be ascribed to EC8, given that it explicitly considers the column compression to flow within all the effective width and not only in the column core.

Outside of this “effective width”, torsion is required in the transverse beam (Figure 98a), thus complete strut-and-tie mechanism in its 4 faces is carried out (Figure 98b). For a complete development of the flexural capacity of the wide beam, sufficient torsional capacity is required, thus the maximum bending moment developed outside the effective width is the minimum between the yielding

moment corresponding to the reinforcement placed in the outer parts and the maximum torque of the transverse beam (Benavent-Climent et al., 2010).

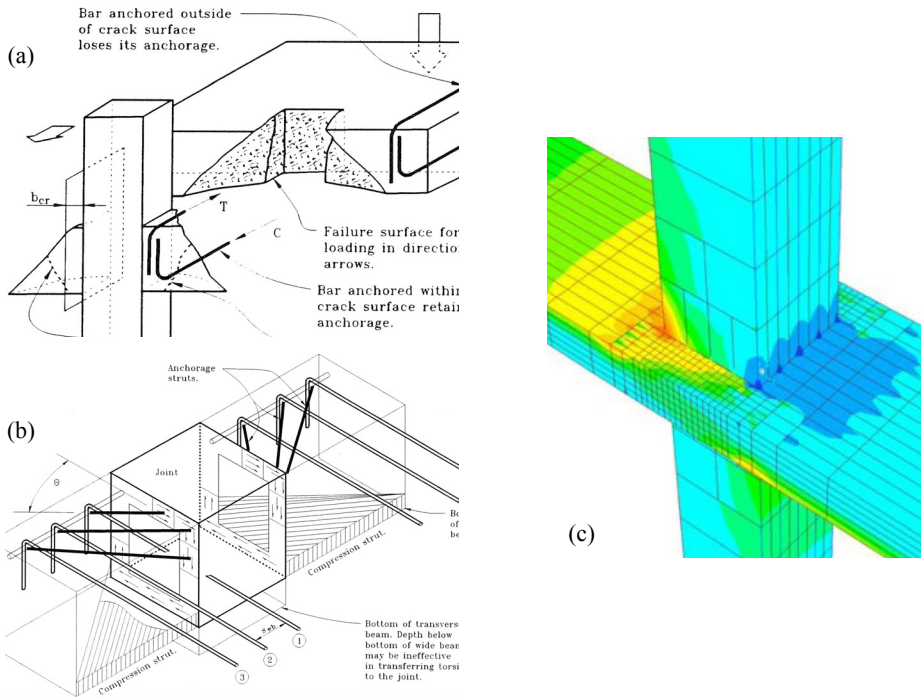


Figure 96: Effective width from failure surface interpretation (a), strut-and-tie interpretation (b, from Gentry and Wight, 1992) and non-linear finite element analysis of connection (c, from Benavent-Climent et al., 2010)

If there is not enough torsional resistance, no yielding of the outer bars takes place and incomplete plastic hinges are developed (Gentry and Wight, 1994). The brittle behaviour of the torsional failure with respect to the complete formation of a flexural plastic hinge may provoke poorer cyclic performance, other than the obvious decrease in the beam strength. Still, if the torsional demand exceeds the cracking torque, large drifts are needed to reach the yielding of the longitudinal reinforcement, which results in lower equivalent stiffness and pinching of the hysteresis loops.

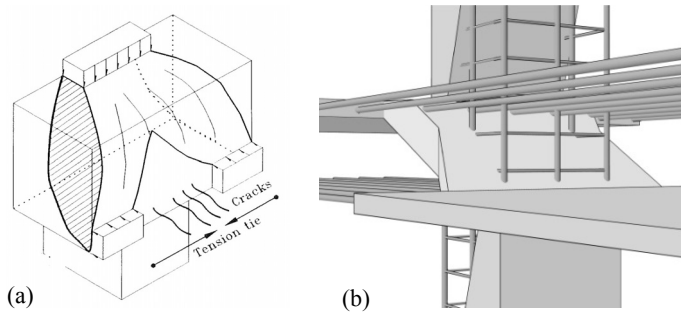


Figure 97: Alternative solutions for compressed diagonal strut within the beam effective width: trapezoidal (a) (from Gentry and Wight, 1992) and bi-trapezoidal (b)

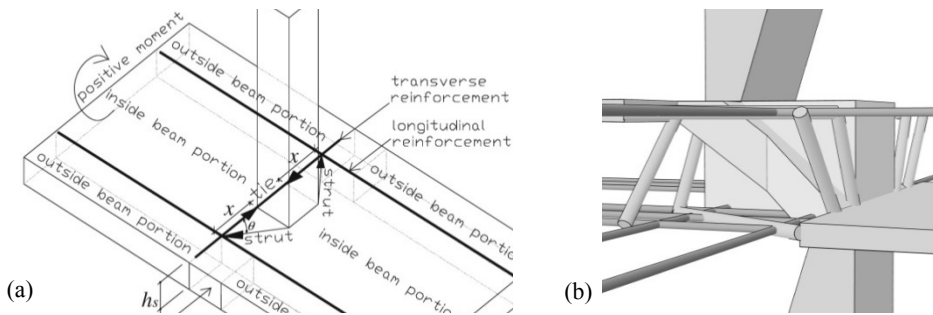


Figure 98: Two flexural transfer paths (strut-and-tie and torsional) (a, from Benavent-Climent et al., 2010), and strut-and-tie model of the torsional mechanism outside effective width (b)

Concerning the placement of stirrups at both sides of the column in main beams, their vertical legs may also contribute to the torsional strength in the transverse direction even though they are not conventionally part of a closed stirrup of the transverse beam. Hence, vertical legs may improve strength capacity of the connection for both directions of the seismic action.

In interior connections with moment inversion, although torsional demand is approximately twice the torque on exterior connections, torsional performance may not be the critical point because the upper slab contribution to the torsion increases the strength so much to overcome the problem (Gentry and Wight, 1992) (Figure 99). In fact, ACI 352R-02 is more cautious for exterior connections, requiring

torsional evaluation corresponding to the upper slab bars within the effective slab width.

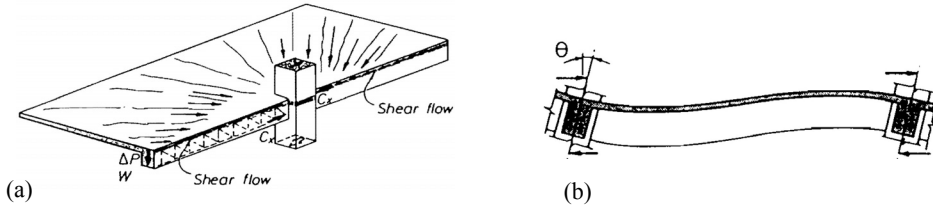


Figure 99: Slab contribution to the torsional behaviour of transverse beam (from Cheung et al., 1991)

Most of codes do not require any torsional evaluation because they intend to remove the problem simply by limiting the width of the beam to the effective width. Only NCSE-02 requires both provisions simultaneously –width limitation and transverse beams—, also for DCL, which may highlight its lower faith in the efficiency of the connection.

3.3.1.2 *Joint effective width*

Experimental results agree with code prescription in assuming that the joint diagonal concrete strut extends to both sides, thus enlarging the joint effective shear area (Figure 100); this assumption is also coherent with the alternative bi-trapezoidal model (Figure 97b). Some authors (Gentry and Wight, 1992) have proposed that the whole width of the beam could be effective (Figure 101a), but subsequent works and codes agree in set limits to the lateral expansion of the strut.

However, experimental results (LaFave and Wight, 1997) have demonstrated that such strut expansion is higher for WB than for DB, resulting in a lower joint cracking and thus in a lower stiffness deterioration. One of the causes could be that, in WBF, the joint panel is totally included within the thickness of the slab, which may act as a more effective confining diaphragm.

The improvement of the joint strength has been also attributed (Paulay and Priestley, 1992) to the better shear truss mechanism (Figure 101b) due to the

favourable bond conditions of beam bars when passing through a deeper column – which often occurs in WBF due to severe lateral stiffness requirements. The eventual placement of stirrups in the outer part of the beam might increase the confinement of the joint enlarged strut (Quintero-Febres and Wight, 2001).

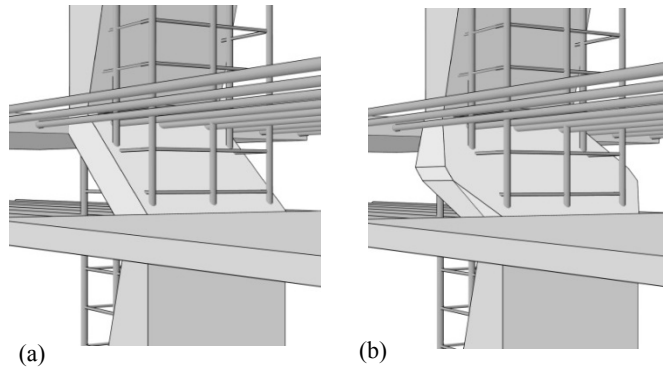


Figure 100: ACI 318-08 (a) and NZS 3101 (b) models for joint compressed strut

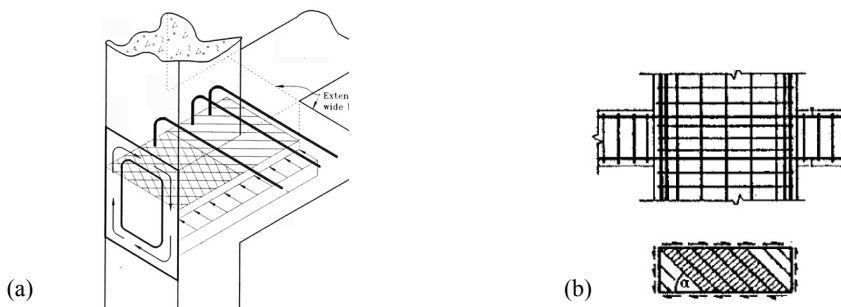


Figure 101: Effective area according to Gentry and Wight, 1992 (a); and joint mechanism for shallow beam-very deep column (b, from Paulay and Priestley, 1992)

3.3.1.3 *Bond development*

In the case of moment inversion, interior connections of both DB and WB with columns must deal with bond deficiencies because of the “push-pull” behaviour of the longitudinal bars, which must provide inverse forces at opposite

faces of the joint. However, the entity of the problem is more severe in the case of WB, because the available development length for column bars is very small and beam bars placed further from the column core may not get clamped by the column compression. Although beam to column capacity design prevent column bars from yielding, the reduced depth of the wide beam could be insufficient for ensure that no bond deterioration occurs (LaFave and Wight, 2001).

Deficient bond development causes slippage of bars, which do not contribute to the section flexural strength and stiffness, being the main responsible of the incomplete formation of plastic hinges in beams with lower yielding moment, and also of the pinching on the hysteresis loops (LaFave and Wight, 2001). Most of the experimental works (Gentry and Wight, 1992; LaFave and Wight, 1997; Quintero-Febres and Wight, 1997) suggest slippage is more likely to occur in bars passing outside the column core (Figure 102b). However, other authors (Benavent-Climent et al., 2010) have observed slippage also in internal bars (Figure 102a).

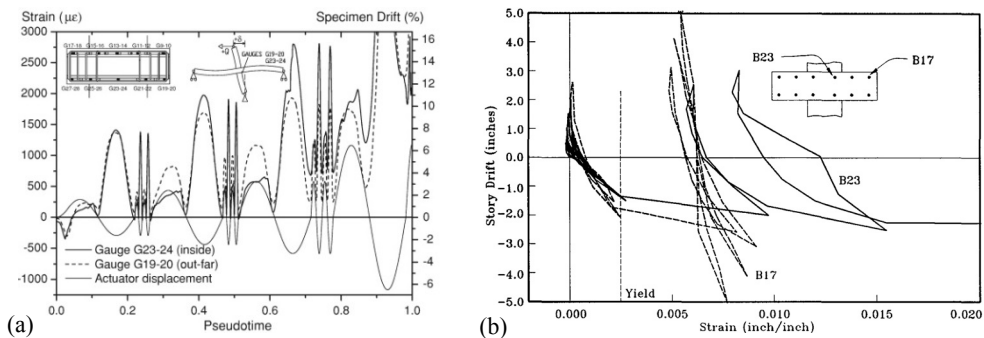


Figure 102: Bond behaviour of beam longitudinal bars placed inside and outside column core (a, from Benavent-Climent et al., 2010; b, from Gentry and Wight, 1994)

The same author suggests poorer bond behaviour may be expected in WB than in DB because the higher initial cracking due to the gravitational loads. In fact, the cracking moment, proportional to the resistance modulus, is usually lower for WB given their reduced depth. On the other hand, it is not clear whether the perpendicular cracking in the upper face due to the transversal gravitational loads

on the joist and transverse beam would be relevant and neither is clear its relative importance for WB or DB.

Some alternatives for avoiding slippage have been proposed:

- anchoring all the bars within the joint, being really hard in the practice due to the concentration of bars coming from three directions in a reduced space (Paulay and Priestley, 1992) (Figure 103a), being recommended by NZS-3101 only for bottom reinforcement when positive moment is very different at both faces of the column;
- debonding the outer bars in a certain length close to the connection (Siah et al., 2003) (Figure 103b).

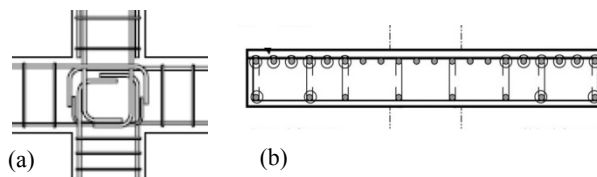


Figure 103: Anchorage within the joint (a, from De Andrés and CSCAE, 2009); and debonding strategy (b, from Siah et al., 2003)

3.3.1.4 *Upper slab contribution*

The contribution of the upper slab shall be also interpreted within a strut-and-tie framework (Figure 104). However, determination of the effective width of the upper slab is not trivial, because there is no agreement in its definition and also because it depends on the demand, as it increases with the interstorey drift.

Codes allow accounting for the whole strength of the reinforcement placed within the upper slab effective width, assuming implicitly that this capacity is equivalent to the decreasing strength provided by a larger amount of slab (Figure 90a). Thus, theoretically, the portion of slab experimenting axial forces within a T-beam section with the beam may be larger than the effective width. Furthermore, such definition may proceed from the evaluation of the compression contribution in positive bending moment situation, in which the potential compression capacity of the slab is constant. In fact, for negative bending moment, the potential capacity

is not uniform, as almost all the reinforcement is placed within the slab effective width, near the beam; thus, accounting for the whole capacity may be not conservative for flexural purposes and conservative for capacity design purposes.

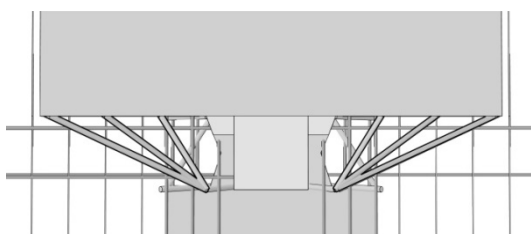


Figure 104: Strut-and-tie model representing upper slab contribution

In tests of (Lafave and Wight, 1997; and Quintero-Febres and Wight, 1997), effective width is evaluated from a visual inspection as the width in which the flexural cracks in the lower face do not close alternatively, which may not be a very feasible methodology given that the transition from pure axial to pure bending behaviour is very gradual. Hence, limits of the effective width shall be very fuzzy.

Earlier experimental works (Cheung et al., 1991; Kurose et al., 1991), as well as the aforementioned tests, have clearly shown how the larger is the drift demand, the higher is the slab portion involved in flexural regime (Figure 105), being necessary the torsional contribution of the transverse beam. ACI 352R-02 affirms that proposed values for the effective width correspond to an approximate drift of 2%.

Results presented in (LaFave and Wight, 1997) show values of effective width 40% higher or conversely 26% lower for WB than for DB, if measured from the lateral face of the column or from the beam axe, respectively (Figure 106). It seems that the upper slab contribution may be similar if measured from the end of the beam effective width, thus equalising the part of the slab corresponding to the strut-and-tie mechanism outside the bi-trapezoidal joint strut. The increase of effective reinforcement belonging to the slab in the case of WBF may not be relevant. Nevertheless, upper slab belonging to most of the tested subassemblages

have depths of around 10cm, which is usually two times the thickness used in the Mediterranean area.

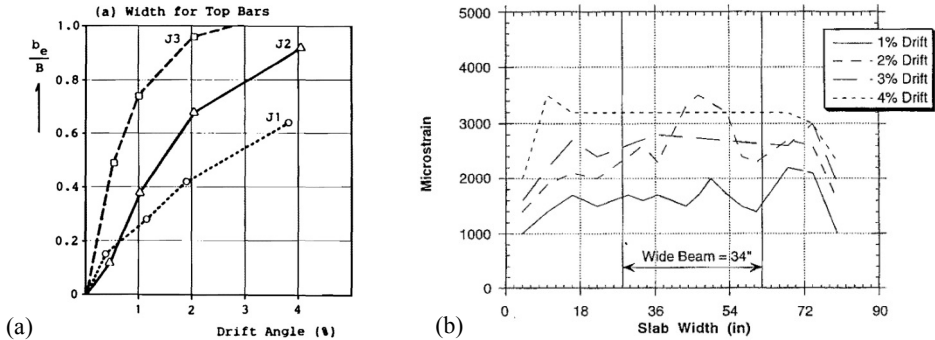


Figure 105: Increase of upper slab effective width for larger drifts (a, from Kurose et al., 1991; b, from LaFave and Wight, 1999)

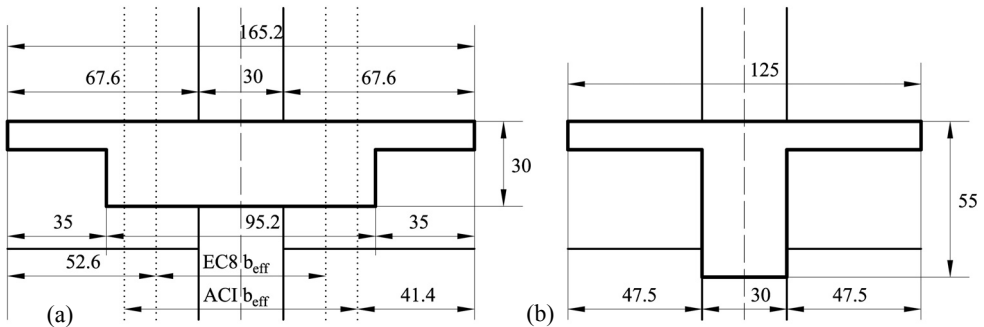


Figure 106: Upper slab effective width in WB (a) and DB (b) specimens (adapted from LaFave and Wight, 2001)

It is worth noting that all the values for upper slab effective width given by codes and experimental works are referred to the strength for ULS design purposes. No value referred to the contribution of the upper slab to the initial uncracked stiffness of the structure for DLS purposes is furnished; only Fardis (2009) proposes that similar magnitudes might be considered for stiffness contribution.

3.3.1.5 *Joists contribution*

Similarly to upper slab, joists are also intended to provide stiffness and strength contribution to the transverse beams (intended herein as the beams perpendicular to the girders, thus parallel to the joists) when seismic loads act in their direction.

Unfortunately, almost none of the available experimental studies on WB-C connection subassemblages include joists (precast or casted in-situ). Only in the case of precast prestressed joists and floor units, some experimental works (Fenwick et al., 2005 and MacPherson, 2005, respectively) have enlightened their contribution to edge beams. Thus, there is no evidence of whether their contribution is higher for WB than for DB, and whether the contribution increases with the drift demand, as for upper slab.

In the case of flat slabs, to which joists banded floors can be compared –given that torsional transference of moments to the column through the main beams is feasible—, some experimental works have proposed different effective widths for positive and negative bending for ULS purposes (Figure 107).

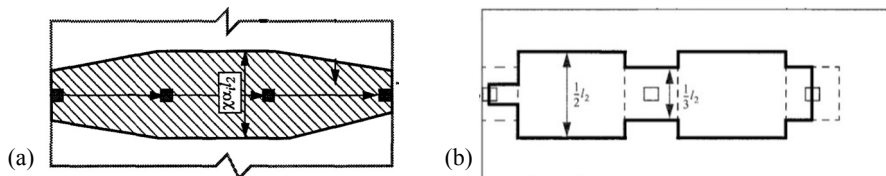


Figure 107: Strength effective width of flat slab according to Luo et al. (1994) (a) and Dovich and Wight (2005) (b)

Regarding specifically joists banded floors, some analytical results –as in (Nudo et al., 2004), based in 3D-FE models of complete subassemblages of DB, joists, upper slab and transverse beam— have shown that flexural strength of transverse beam can be increased more than 50%, involving a couple of joists at both sides (Figure 108), which could lead to a column-sway mechanism. Thus, this phenomenon seems to be of crucial importance regarding capacity design of frames.

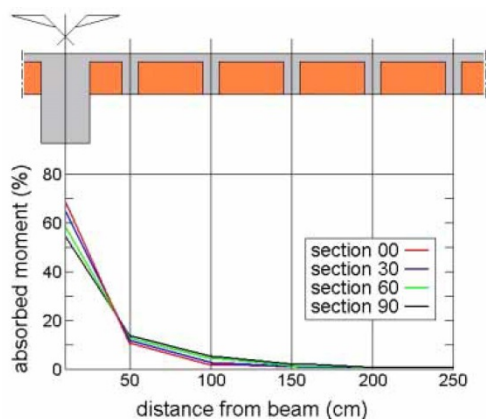


Figure 108: Flexural contribution of joists to transverse beams (from Nudo et al., 2004)

Furthermore, it may not be ventured to guess that, in the case of WBF, the contribution of joists to the flexural behaviour of transverse beams (when subjected to seismic action parallel to them) might be higher than in the case of DB, given that the torsional behaviour of longitudinal WB may be better than for DB, as their area is larger and the density of stirrups is usually similar.

On the other hand, when seismic loads act perpendicularly to the joists –i.e. parallel to the main beams—, it is not clear whether joists can improve the torsional contribution of the upper slab to the transverse beam.

3.3.1.6 *Shear equilibrium*

Other than bending moment, there must be equilibrium of shear and axial forces in the beam-column connection. At the column face, analogously to flexural behaviour, not the whole width of the beam may be effective in order to transfer the shear forces to the joint without requiring torsional strength of the transverse beam (Figure 109).

Some experimental works with WB-C subassemblages subjected to static gravitational loads (Serna-Ros et al., 2001; and Shuraim, 2012) have demonstrated that more regular distribution of stirrup legs within the width of the section results in an increase of shear strength. This can be interpreted as a confirmation of the fact that the effectiveness of stirrups legs decrease with the distance to the column

lateral face. Another cause that has nothing to do with the effective width is the fact that the higher is the amount of stirrup legs, the better is the vertical distributed equilibrium of the inclined shear struts, avoiding concentration of diagonal compression stresses.

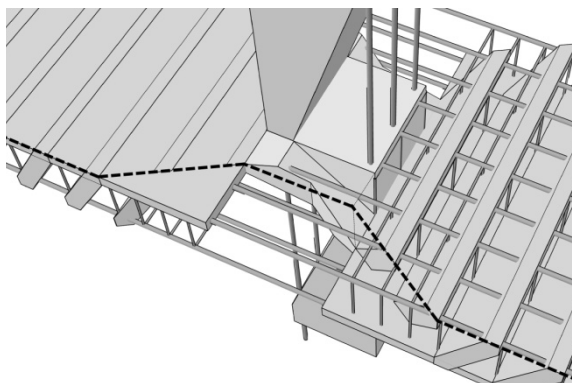


Figure 109: Proposed strut-and-tie model for shear equilibrium within the connection

Anyhow, (LaFave and Wight, 1997) concludes that much less shear cracking and shear deformation near the column is observed for WB specimens than for deep-beam ones, for similar stirrup concentration, which may be interpreted as a sign of larger shear effective width.

3.3.2 Ductility of wide beams

Lack of local ductility (i.e. low chord rotation ductility, μ_0 , for elements) and global ductility (i.e., impossibility to develop global collapse mechanism) is generally the reason for any q reductions in codes. In the light of the above statement, WBF case is analysed. Evaluation of local ductility of WB with respect to DB depend on relationships between ultimate (θ_u) and yielding (θ_y) chord rotation, which in turn depend on analogous curvatures (ϕ_u and ϕ_y , respectively). Herein a parametric study is provided for a straightforward comparison between WB and DB. Eight couples of DB and WB corresponding to similar flexural resistances are considered, varying geometry and reinforcements. Then, ϕ_y , ϕ_u , θ_y ,

θ_u , curvature ductility (μ_ϕ), and μ_θ are evaluated according to different formulations and then compared. Shear span length of 2.5m, concrete covering of 20mm and mean diameter of longitudinal bars of 14mm are assumed for all the beams. Mean resistances of materials ($f_{cm}=33\text{MPa}$ and $f_{ym}=630\text{MPa}$ for concrete and steel, respectively) correspond to characteristic values typical of Spanish building stock ($f_{ck}=25\text{MPa}$ and $f_{yk}=500\text{MPa}$ for concrete and steel, respectively).

Five parameters are assumed: (i) class (DB or WB); (ii) cross-sectional aspect ratio (types A and B, providing higher or lower bending moment resistances, respectively); (iii) top-to-bottom reinforcement ratio (1:1 or 3:2); (iv) total reinforcement ratio (high and low, which makes top and bottom reinforcement, respectively, correspond to code's upper and lower limit, when top-to-bottom ratio is 3:2); and (v) consideration of confinement (yes or no). Reinforcement arrangements are selected in order to obtain similar moment resistances between analogous deep and wide beams, resulting in total reinforcement ratios in WB approximately twice (1.9) the reinforcement in DB (almost similar to the ratio between effective depths). In each case, high reinforcement case provides approximately three times the flexural strength provided by low reinforcement case (mean value of such ratio is 2.92). Common stirrup arrangements, according to Eurocode 2 prescriptions (BSI, 2004), are considered. Characteristics of the different elements are shown in Table 30, being: ω , ω' and ω_{tot} , bottom, top and total mechanical reinforcement ratio; ρ_w , transverse reinforcement ratio; and M_y , yielding moment resistance.

Values of curvature and moments are obtained by means of a fibre model; mechanical model proposed by Mander et al. (1988) is adopted for concrete. Aimed at obtaining chord rotations, two different approaches are adopted, corresponding to the European –EC8 part 3 (CEN, 2005)— and American –ASCE/SEI 41 (ASCE, 2007)— codes regarding modelling strategies for assessment. In the first case, θ_y and θ_u are obtained through explicit formulations A.4 and A.1 in EC8 part 3, respectively. In the second case, θ_y is obtained indirectly as the addition of flexural and shear contributions both as ratios between resistance and effective stiffness, whose values are taken from Table 6-5 of ASCE/SEI 41; θ_u are obtained as the sum of θ_y and plastic part of ultimate chord rotation (θ_{pl}), which is taken from Table 6-7.

Table 31: Characteristics of the analysed set of beams

Class of beam	Geometry		Transverse reinforcement				Longitudinal reinforcement									
	Section type (A/B)	b_w [mm]	h_b [mm]	Hoops [mm]	ρ_w [%]	Low				High						
						ω_{tot}	$\omega'/\omega=1.5$		$\omega'/\omega=1$		ω_{tot}	$\omega'/\omega=1.5$		$\omega'/\omega=1$		
							Reinf. ratio [%]	M_y [kNm]	[%]	M_y [kNm]		Reinf. ratio [%]	M_y [kNm]	[%]	M_y [kNm]	
DB	A	300	600	2 ϕ 8/70	0.48	0.10	ρ'	0.30	-181	0.25	± 152	ρ'	0.90	-524	0.75	± 442
							ρ	0.20	+122			ρ	0.60	+357		
	B	300	500				ρ'	0.30	-124	0.25	± 104	ρ'	0.90	-357	0.75	± 301
							ρ	0.20	+84			ρ	0.60	+244		
WB	A	650	300	4 ϕ 8/70	0.44	0.19	ρ'	0.60	-177	0.50	± 149	ρ'	1.89	-513	1.50	± 446
							ρ	0.40	+120			ρ	1.26	+362		
	B	500	300				ρ'	0.54	-123	0.45	± 103	ρ'	1.65	-355	1.38	± 301
							ρ	0.36	+83			ρ	1.10	+244		

Figure 110 shows the detailed results of the parametric study. In Table 32, mean values of ratios between the same parameter (curvatures, rotations and ductilities) corresponding to WB and DB are shown. Ratios for any parameter A are indicated as $A_{W/D}$ (rather than using the heavier notation A_{WB}/A_{DB}), and analogously $A_{W-D} \equiv A_{WB} - A_{DB}$.

In general, when ρ' is higher than ρ better performances are achieved (i.e. lower yielding values and higher ultimate ones) for both DB and WB. It is worth noting that the two adopted approaches (EC8 and ASCE) return very different values of θ (sometimes more than 100%) in all the cases (Figure 110 d to h).

Regarding curvatures, $\phi_{y,W/D}$ (Table 32) seems to be approximately inversely proportional to ratio between the effective heights ($d_{W/D}$). In fact, given similar yielding strains at tensioned reinforcement in WB and DB, given $b_{w,W/D} \approx 1.92$ (Table 31) and given $\rho_{tot,W/D} \approx 1.9$, the compression zone depths may be similar and little in comparison with d due to the presence of compressed reinforcement. Thus, $\phi_{y,W/D} \approx 1/d_{W/D}$. Conversely, ϕ_u are quite similar for both WB and DB (Figure 110 b and c), because in this case not only the compression zone depth but also the concrete maximum stress are similar. Hence, WB show μ_ϕ lower than half the values for DB (Figure 110 i and j), because WB show similar ϕ_u but double ϕ_y . Confinement contribution almost triplicates ultimate curvatures and reduces the differences between high- and low-reinforced sections.

However, the decrease of μ_ϕ for WB does not imply significant decreases of μ_θ if EC8 is adopted (see Figure 110 i versus k and j versus l): while the yielding ratios remains similar ($\theta_{y,W/D} \approx \phi_{y,W/D}$), ultimate values are higher for WB than for DB. So, although ϕ_u are similar for both types, the length of the plastic hinge may be higher for WB.

Table 32: Mean wide-to-deep ratios (W/D) corresponding to different variables

Approach	$\phi_{y,W/D}$	$\phi_{u,W/D}$	$\mu_{\phi,W/D}$	Approach	$\theta_{y,W/D}$	$\theta_{pL,W/D}$	$\theta_{u,W/D}$	$\mu_{\theta,W/D}$
Mander	2.16	0.97	0.46	EC8	1.85	1.29	1.38	0.75
				ASCE	3.14	0.99	1.36	0.44

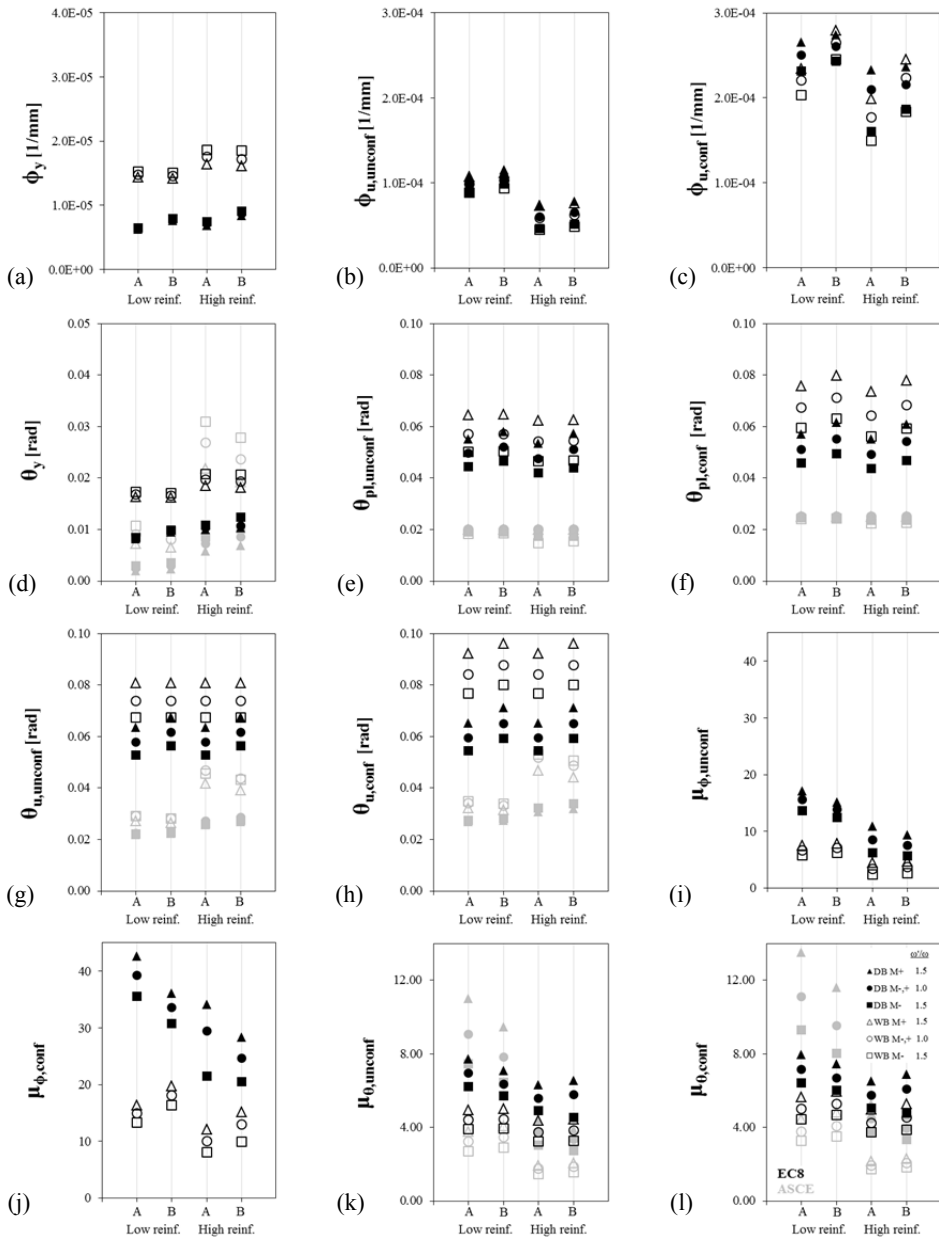


Figure 110: DB vs. WB local ductility parametric analysis: ϕ_y (a) and ϕ_u without (b) and with (c) confinement contribution; θ_y (d); θ_{pl} without (e) and with (f) confinement contribution; θ_u without (g) and with (h) confinement contribution; μ_ϕ without (i) and with (j) confinement contribution; and μ_θ without (g) and with (h) confinement contribution

EC8's results of θ_y reproduce the same trend than those of ϕ_y , because they are directly proportional –except for the shear experimental term in the expression, which is the less relevant. High-reinforced sections show mean values of θ_y only 18% higher than low-reinforced sections, which means that the increase of secant-to-yielding stiffness of beams may be almost proportional to the increase of ρ . Conversely, ASCE does not consider any influence of the reinforcement in the secant stiffness, which is approximately 0.3 times the elastic one; thus, θ_y and M_y are always proportional, and $\theta_{y,W/D} \approx 3$ (Table 32). Stiffness degradation (secant-to-elastic stiffness ratio) obtained with EC8 (mean 0.32) is similar to values proposed by ASCE, but very different values are obtained if results are disaggregated: 0.19 and 0.45 for low- and high-reinforced sections, respectively. Value corresponding to low-reinforced section is similar to the mean value suggested in Panagiotakos and Fardis (2001): 20%. However, WB show lower stiffness degradation than DB: the increase of secant-to-elastic ratio is 1.53, which is approximately 80% of $\rho_{tot,W/D}$.

Regarding θ_{pl} , values provided by EC8 are significantly larger (around 3 times) than those provided by ASCE (Figure 110 e and f). For EC8, WB present larger values than DB (around 30%, see Figure 110f and Table 32), while ASCE provide similar values for both types. Still, in both approaches all values are almost independent on aspect ratio variations or total reinforcement of the section. Hence, both EC8 and ASCE provide values of θ_u significantly higher for WB than for DB (mean 38% and 36%, respectively, see Table 32). In the first case this increase is a consequence of larger contributions of yielding and plastic chord rotation for WB than in the case of DB, due to lower h_b . Conversely, for ASCE only $\theta_{y,W/D}$ contributes to $\theta_{u,W/D}$. Notwithstanding the different origin of contributions, $\theta_{u,W/D}$ is quite similar for both approaches.

It is worth noting that mean confinement contributions (f_{conf}) are larger for ASCE (1.28) than for EC8 (1.10). In the last case, confinement contribution is bigger for WB than for DB (mean 12% larger) –because concrete core is divided in more regular rectangles— while ASCE return similar improvements. Finally, local ductility (μ_θ) is lower for WB than for DB: 25% for EC8 and 56% for ASCE (Table 32).

In the next section it is discussed whether these local values (i.e., element level) can be directly compared with q reductions (i.e., structure level) for WBF suggested by codes (e.g. 33% and 50% for Italian and Spanish seismic codes, respectively). This decrease of local ductility for WB with respect to DB seems to be one of the most important reasons for such code restrictions. In fact, this issue cannot be overcome by design rules, while deficient local equilibrium (see section 3.3.1) and lower lateral stiffness (see section 3.3.3) can be softened through specific provisions.

Another key aspect for local comparison of WB and DB is the hysteretic behaviour. Cyclic energy dissipation is poorer (i.e., higher pinching) in WB rather than in DB when sub-standard buildings (Benavent-Climent, 2007; Benavent-Climent et al., 2009, 2010) or seismic-designed frames with no fulfilment of EC8 width limitations (Gentry and Wight, 1992; LaFave and Wight, 1997; Quintero-Febres and Wight, 1997) are considered. Even in the case of EC8 conforming WB–C connections, pinching is still significant (Quintero-Febres and Wight, 1997; and Li and Kulkarni, 2010). LaFave and Wight (1997) quantify such hysteretic behaviour in terms of observed equivalent viscous damping, which is 20% lower for WB subassemblages than in DB (Figure 111). The causes may be the poorer bond behaviour and the poorer transverse beam torsional performances of WB specimens.

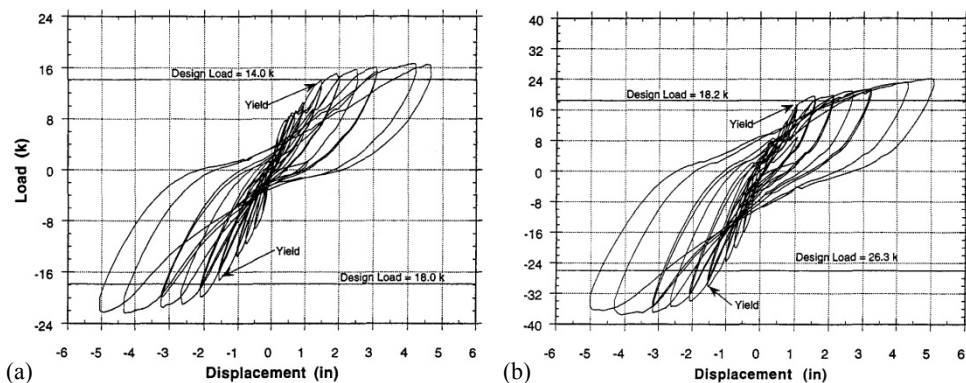


Figure 111: Cyclic behaviour of wide-beam (a) and deep-beam (b) subassemblages (from LaFave and Wight, 2001)

On the other hand, global ductility of frames (i.e. top displacement capacity of frames) depends not only on local ductility of members but also on the ability to develop global mechanisms, which requires capacity design of columns. Experimental results on sub-standard WBF (Benavent-Climent et al., 2010) show beam-sway mechanisms even without capacity design of columns, because torsional failure of transverse beams prevent the attainment of full flexural capacities in longitudinal beams so columns get “protected”. However, this is not an advantage in terms of frame top displacement capacity since torsional failure is not ductile. Besides, analytical studies regarding compared performances of seismic-designed WBF and DBF (Gentry and Wight, 1992; and Quintero-Febres and Wight, 1997) show quite similar performances (Figure 112), although those comparisons cannot be considered fulfilling (see section 3.5).

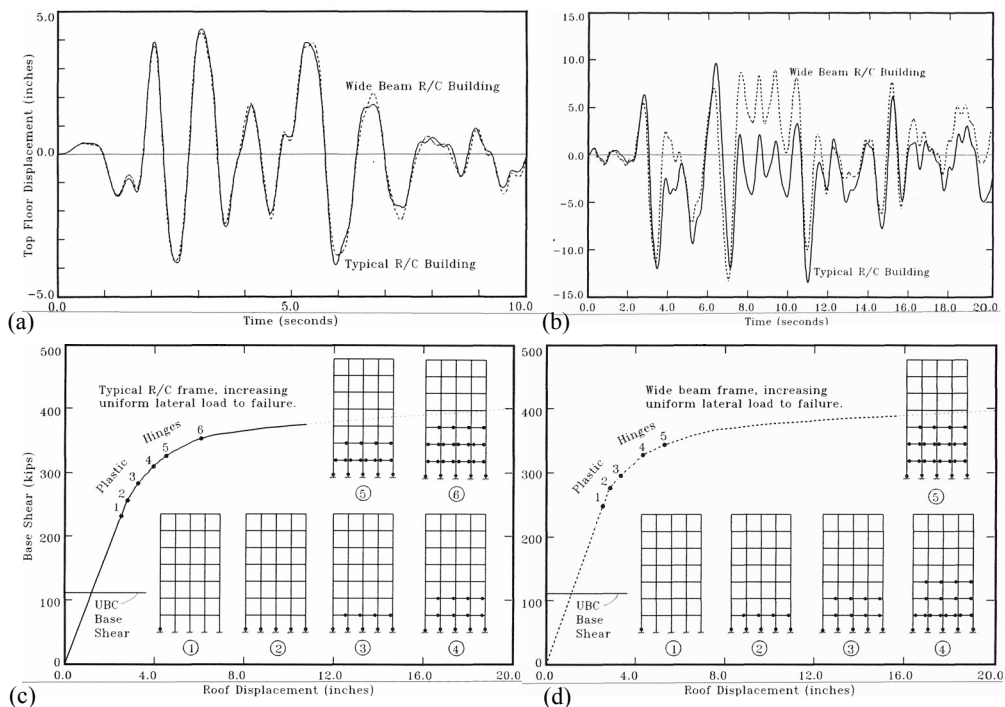


Figure 112: Two examples (a and b) of nonlinear time-history performance of deep- and wide-beam frames; and pushover curve and collapse mechanisms of deep- (c) and wide-beam (d) frames (from Gentry and Wight, 1992)

Concerning the type of collapse mechanism, in the case of wide-beam sub-standard buildings, in which column-sway mechanisms are expected, torsional failure of transverse beams (if present) may cause strong column-weak beam failures, but the ductility of the connection is very low due to the brittle nature of torsional failure (Benavent et al., 2010). However, for wide beams, as the contribution of the upper slab to the maximum strength seems to be higher than for DB, weak column-strong beam mechanisms could occur unless higher overstrength factors are used in the first case. None of these provisions are suggested by codes. Furthermore, joists strength contribution is also neglected in both cases.

3.3.3 Lateral stiffness

Usually, wide beams have substantial lower stiffness—both elastic and secant to yielding— than deep-beam ones, leading to higher deformability of WBF than DBF when similar columns are adopted. Similar behaviour may be expected from flat or waffle slabs. Although high deformability leads to larger fundamental and effective periods and thus to lower acceleration demands, severe disadvantages for lateral-load-resisting systems can be identified: higher non-structural damage and possibility of developing second order effects on columns (P- Δ effect).

This is the cause of the original preventions of codes regarding WBF. However, none of those preventions should remain after codes have incorporated IDR limitations and simplified consideration of P- Δ effects. Only in the case of codes with no drift limitation (as NCSE-02) it may have sense to provide indirectly higher stiffness to the frame through the use of very low behaviour factors, thus by increasing the strength demand and likely the dimensions of the members.

In other codes in which there are IDR limitations, deformability preventions seem to be just a legacy associated with flat slabs. In fact, for these structures, drift limitations should be more severe because strong cyclic degrading shear capacity due to increasing ductility demand have been observed, leading to brittle punching shear failures, as NZS 3101 suggests based in (Pan and Moehle, 1989; and Hawkins and Mitchell, 1979). However, no similar behaviour has been identified in wide-beam subassemblages with width limitation.

Besides, code preventions about the predominant component of the deformed shape –i.e. shear- or cantilever-type— have not any mechanical base. Shear-type deformation to horizontal loading is characterised by showing opposite bending moments in the ends of all the members, axial loads in edge columns and decreasing IDR with the height; conversely, cantilever-type deformation is defined by decreasing bending moments in the whole columns with no axial load and increasing IDR with the height. Frames rarely show pure shear-type deformation; the lower is the beam-to-column stiffness ratio, the higher is the cantilever-type contribution.

It is hard to define a threshold aimed to define the substantial entity of the cantilever-type contribution; two criteria could be: i) when a single member do not show opposite bending moments; and ii) when IDR of a single storey is higher than the immediately lower. It seems that code presume higher displacement to frames with high cantilever-type contribution; again this consideration lose their fundament when IDR limitations are provided. On the other hand, cantilever-type deformation could cause yielding of some column end over a connection when both columns have the same moment sign, even in the case of capacity-designed frames, but it still would not cause any soft-storey mechanism (Fardis 2009).

Notwithstanding all the preventions based in simplified analytical elastic evaluation of the stiffness of WBF by taking into account only the deformability of the members, experimental works (LaFave and Wight, 1997) have shown that real stiffness of WBF is much higher than expected. Results of three subassemblages show that the stiffness ratio between WBF and DBF increase from 0.58, corresponding to predicted analytical elastic stiffnesses, to 0.86, corresponding to measured secant-to-yielding stiffnesses; the increase is as high as 48%. Main causes are: i) higher slab participation; ii) much less cracking and deformability of the joint; iii) less shear cracking in plastic hinges; and iv) likely higher reinforcement ratios

However, upper slab –or eventually joists— contribution to the elastic stiffness is not explicitly suggested by codes. In the case of upper slab, the same effective width than for strength capacity is arbitrarily suggested for DLS purposes by some authors (Fardis, 2009). Neither the gross real inertia of wide beams taking

into account the lateral increment of concrete out of the web is considered. All of these contributions could likely be taken into account for stiffness and discarded for strength.

It is not clear whether factors multiplying the elastic stiffness of members aimed to account for the cracking and degradation up to the performance point corresponding to DLS assessment are calibrated having into account those contributions. It is worth noting that an adequate definition of the initial stiffness is very important because can influence both the deformability and deformed shape of the frame for DLS purposes and the elastic distribution of forces between the members for ULS design purposes.

Finally, it is worth noting that poorer cyclic bond behaviour in WBF, causing pinching of hysteresis loops characterised by lower reload stiffnesses, is a problem concerning only energy dissipation. It do not elongates the effective period nor modifies the global demand, and neither influences the non-structural damage – given that bond deterioration starts at larger drifts than those interested by DLS.

3.4 SIMPLIFIED SPECTRAL ESTIMATION OF RELATIVE PERFORMANCES BETWEEN DEEP- AND WIDE-BEAM FRAMES

The spectral approach provided herein is a simplified assessment of global seismic performances of WBF with respect to DBF, finally aimed at a fulfilling contextualization of code provisions regarding q reduction reviewed in section 3.2 and experimental and analytical observations provided in section 3.3.

In section 3.3.2 it is concluded that the lower μ_0 of WB with respect to DB may be the main reason for the reduction of q for WBF proposed by some codes (see Table 30 and Table 32). However, q is a global structural quantity and it cannot be straightforward related to μ_0 of beams, which is a proxy of single element performances. Furthermore, q not only depends on global ductility ductility (R_μ) but also on other two factors: overstrength (R_S), and demand reduction (R_D), i.e, the ratio between strength demands corresponding to design and effective periods (Borzi and Elnashai, 2000; Mwafy and Elnashai, 2002).

All those conditions should be satisfied in order to get a direct translation of $\mu_{\theta, W/D}$ of beams in the ratio between behaviour factors of WBF and DBF ($q_{W/D}$):

- 1) DBF and WBF show similar overstrength until first structural yielding and similar R_D .
- 2) DBF and WBF show similar height involved in the mechanism of collapse (H_{mec}).
- 3) Displacement corresponding to the strength at the first yielding of the structure is similar both for the pushover curve and the piecewise linear fit of the curve.
- 4) The first member end which yields is a beam.
- 5) The first member end which reaches θ_u is the same beam of point 4)
- 6) From the instant of first yielding on, all member ends, yielded or not, rotate at the same rate.

The first condition may be likely satisfied if similar strategies of design are employed. The second depends on the column-to-beam capacity design ratio, and these in turn depend on section design overstrengths, which can be very different (see section 3.4.2). The third condition could be discarded given the uncertainties of any procedure even if the same fitting rule is employed for the two structures (De Luca et al., 2013). Condition 4 is plausible because of capacity design of columns. However, condition 5 and 6 can seldom be achieved. The first element reaching θ_u can be a column (which is the most usual situation, see section 3.4.2); and even if it is not a column, it is quite likely that a different beam reaches θ_u . In fact, redistribution of bending moments between members is a very uncertain process, causing not proportional evolution of chord rotations. Hence, $\mu_{\theta} \neq R_{\mu} \neq q$, thus global performances of WBF are not necessarily poorer than DBF because of lower local ductility of beams.

3.4.1 Safety Factor ratio

Aimed at comparing the relative capacities of WBF and DBF, it is necessary to reformulate the problem in the acceleration-displacement response spectrum (ADRS) format, shifting the assessment from q to PGA (Peak Ground Acceleration corresponding to the site soil). This is only possible if spectra for different PGA

are homothetic. Global performance of a building could be represented by its safety factor $SF=PGA_c/PGA_d$, i.e. the ratio between capacity (PGA_c) and demand (PGA_d) in terms of PGA. Since PGA_d are equal for two WBF and DBF structures in the same site, to compare global performances it is necessary to evaluate $PGA_{c,W/D}$. The estimation of PGA_c through spectral procedures asks for the assumption of a strength reduction factor – ductility – period (R_μ - μ - T) relationship (e.g., Vidic et al. 1994; Miranda and Bertero, 1994; Vamvatsikos and Cornell, 2002), that is also the basis of behaviour factor definition.

Consequently, SF only depends on two variables: effective period (T_{eff}) and maximum displacement capacity (S_{dc}) of the equivalent single degree of freedom (SDOF), assuming that the response is controlled by a single mode. Equal-displacement rule, i.e. $T_{eff} > T_C$, can be assumed in all the cases, being T_C the period corresponding to the end of the constant-acceleration branch of the spectrum. In fact, if mean member stiffness degradation ratio from elastic to effective (0.20) proposed by Panagiotakos and Fardis (2001) is assumed to be also representative of the frame behaviour –which is confirmed in the case study, see section 3.6.3—, $T_{eff} > T_C$ is verified for buildings of at least 2 storeys designed to EC8 spectra types 1 and 2 for any soil type, assuming the design elastic period suggested by EC8 as lower bound value for “modern” capacity-designed and DLS-designed frames (Crowley and Pinho, 2010). Consequently, safety factor of buildings can be expressed as the ratio of spectral displacement capacity and demand: $SF=S_{dc}/S_{dd}$.

Spectral displacement capacity of the SDOF is obtained from top displacement capacity of the frame (D_u) as in Equation (58), being Γ the first mode participation factor, and $\theta_{u,min}$ the minimum ultimate chord rotation between column bases, column tops at a height of H_{mec} (both θ_{uc}) and beam ends under H_{mec} (θ_{ub}) (Fardis, 2009), as shown in Figure 113. Thus, a “rigid” mechanism of n storeys is assumed, without any pre-yielding contribution neither of the $(n-1)$ upper storeys nor of the intermediate column ends, and assuming similar evolution of chord rotations in all the member ends involved. Similar approaches have been already proposed in other studies (Cosenza et al., 2005).

On the other hand, S_{dd} can be obtained from the elastic spectral acceleration demand ($S_{ae,d}$), which is typically inversely proportional to the period for $T_{eff} > T_C$

(see Equation (59a)), being f_0 the spectral amplification for the constant branch, which may depend on the level of PGA. As spectral acceleration and displacement are related by the period as in Equation (59b), S_{dd} can be expressed as in Equation (59c).

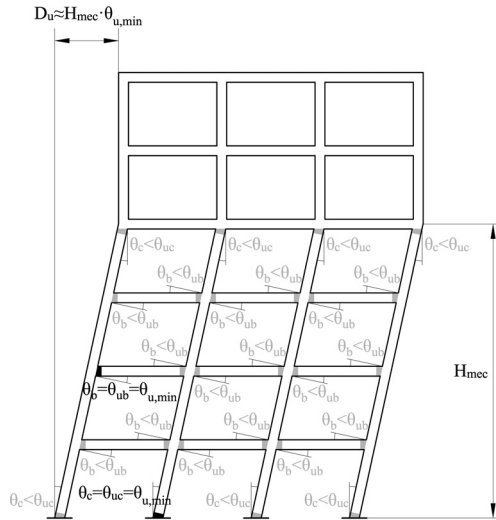


Figure 113: Simplified estimation of the top displacement capacity of a frame

Therefore, SF of a building can be expressed as in Equation (60), where the first term of the product is independent on the structural system. It is very important to note that there is no explicit influence of local ductility ($\mu_\theta = \theta_u / \theta_y$) of beams on the global capacity, and, moreover, it is also possible that there is not either implicit influence. In the numerator, $\theta_{u,min}$ do not necessarily refer to beams. In fact, if expression A.1 of EC8 part 3 (Equation (61)) is considered for θ_u of sections without diagonal reinforcement, in general lower values may be expected for columns than for beams because of: (i) the presence of axial load; (ii) lower L_v/h for medium-high span range (unless higher cantilever behaviour is shown); and (iii) slightly lower (ω'/ω) (assuming regular distribution of reinforcement bars in the perimeter of the column section and local detailing of reinforcement in beams). Thus, θ_u of beams may not be relevant in most cases. On the other hand, θ_y ,

of beams does have influence in the value of T_{eff} , but there is not a direct equivalence between effective stiffness of beam ends and that of the whole frame, which also depend on columns. Furthermore, if design to DLS is the most critical condition of design, θ_y of beams would not have any influence on T_{eff} because the lateral stiffness of the frame becomes a target, thus section of columns are designed accordingly.

$$S_{dc} = \frac{D_u}{\Gamma} \approx \frac{H_{mec} \cdot \theta_{u,\min}}{\Gamma} \quad (58)$$

$$S_{ae,d} = f_0 \cdot PGA_d \cdot \frac{T_C}{T_{eff}} ; \quad T = 2\pi \sqrt{\frac{S_d}{S_a}} ; \quad S_{dd} = \frac{f_0 \cdot PGA_d \cdot T_C}{4\pi^2} \cdot T_{eff} \quad (59a,b,c)$$

$$SF = \frac{PGA_c}{PGA_d} = \frac{S_{dc}}{S_{dd}} \approx \frac{4\pi^2}{f_0 \cdot PGA_d \cdot T_C} \cdot \frac{H_{mec} \cdot \theta_{u,\min}}{\Gamma \cdot T_{eff}} \quad (60)$$

$$\theta_u = 0.016 \cdot 0.3^v \cdot \left[\frac{\max(0.01; \omega')}{\max(0.01; \omega)} f_c \right]^{0.225} \cdot \left(\frac{L_V}{h} \right)^{0.35} \cdot f_{conf} \quad (61)$$

Finally, relative SF between WBF and DBF ($SF_{W/D}$) when designed to the same PGA_d is obtained as in Equation (62): similar performances are expected for WBF and DBF if the increase of T_{eff} is balanced by a similar increase of displacement capacity. It is illustrated in Figure 114 by means of a graphic example in the ADRS format. Figure 114 shows bilinear capacity curves, corresponding IN2 curves (Dolšek and Fajfar, 2004b), common demand spectrum, and scaled capacity spectrum with their corresponding values of PGA_c both for WBF and DBF.

$$SF_{W/D} = \frac{H_{mec,W/D} \cdot \theta_{u,\min,W/D}}{\Gamma_{W/D} \cdot T_{eff,W/D}} \quad (62)$$

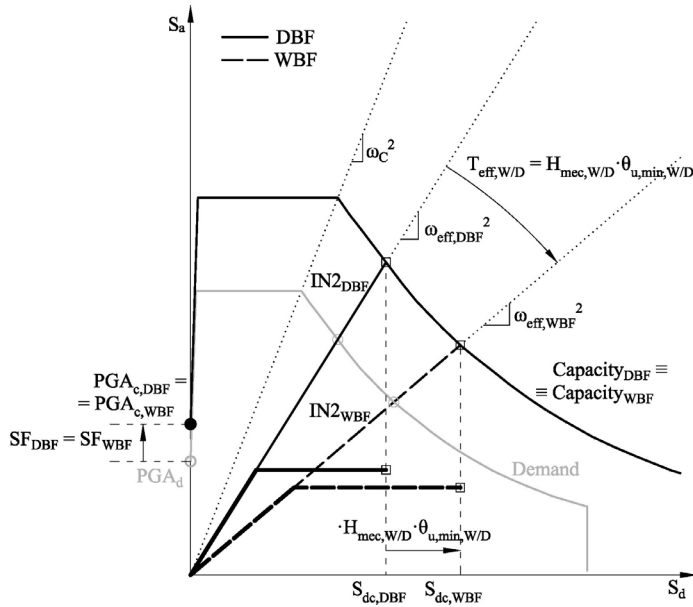


Figure 114: ADRS N2 simplified comparison between WBF and DBF showing similar performances, considering similar Γ for both types

3.4.2 Estimation of relative performances between WBF and DBF

In this section, an attempt to make a rough prediction of which could be representative values of $SF_{W/D}$ (Equation (62)), in most practical cases, is carried out. In order to understand which may be the relative influence of each design parameter, several simplified assumptions must be done. The scope herein is to evaluate whether WBF may provide similar capacities than DBF; thus, all the simplifications are assumed in order to be conservative from the point of view of WBF, i.e. unfavourable for WBF with respect to DBF. It is worth noting that the legitimacy of such simplified estimation is limited, because not only the assessment procedure, but also the parameters derived from design, are assumed “a priori”. In fact, a feasible assertion about the present issue should be supported by some specific cases of study where both design and assessment are carried out accurately, as it is made in the next section.

Some preliminary assumptions of design must be done: both structures are assumed to be designed adopting similar q , similar corrections due to second-order effects, similar ρ_{tot} between corresponding columns of both types, and similar (ω'/ω) between corresponding beams. It is also possible to assume that Γ may be similar for WBF and DBF, according to several codes that suggest values depending only on the number of storeys (as ASCE/SEI 41-06), thus $\Gamma_{W/D}=1.0$.

Regarding T_{eff} , WBF may show lower period elongation (T_{eff}/T_{el}) than DBF, if the experimental behaviour shown in Lafave and Wight (2001) for single connections (see section 3.3.3) is extrapolated to the whole frame. Thus, $T_{eff,W/B}$ can be estimated (Equation (63)) as the ratio between elastic periods ($T_{el,W/D}$) weighted by a factor $f_{K,sec}$, which can be estimated equal to 1.48 on the basis of the ratio between secant-to-1% stiffness and elastic stiffness for WBF with respect to DBF shown in Lafave and Wight (2001). Such variable is included in Equation (63) after being switched from stiffness-based to period-based as shown in Equation (64), assuming similar values of m^* (first mode participating mass of the equivalent SDOF) for both frame types. However, the experimental based value 1.48 for $f_{K,sec}$ is considered just as an upper-bound level. So, aimed at conservativeness, all the following simplified development are carried out assuming $f_{K,sec}=1$.

$$T_{eff,W/D} = T_{el,W/D} \cdot f_{K,sec}^{-0.5} \quad (63)$$

$$T = 2\pi\sqrt{\frac{m^*}{K}} \Rightarrow T_{W/D} \approx K_{W/D}^{-0.5} \quad (64)$$

Given that $SF_{W/D}$ depends on the balance between $T_{el,W/D}$ and $D_{u,W/D}$, in the following all the possible performance comparison are organised in different scenarios depending on the magnitude of these factors. Regarding $T_{el,W/D}$, two possible scenarios can be defined:

- Scenario I: similar T_{el} for both types ($T_{el,W/D} \approx 1$). It may correspond to a design situation in which the fulfilment of the IDR limitation becomes the most restrictive condition, thus leading to similar interstorey stiffnesses for WBF and DBF, and likely similar global stiffness and design period T , thanks to the use of larger column sections in WBF than in DBF, in order

to compensate the lower stiffness of WB). This scenario may be associated to structures designed in compliance with EC8 (Fardis, 2009).

- Scenario II: higher T_{el} for WBF ($T_{el,W/D} > 1$). It may correspond to situations in which the design to DLS is not the critical condition. It can depend on the adoption of different codes: consideration of a lower degradation of member stiffness (see section 3.3.3), higher maximum IDR (Table 30), higher stiffness of joint regions (Fardis, 2009) or larger effective width of upper slab (Table 30); or conversely it can just reflect situations in which the relevance of DLS is low due to small seismic demand or due to higher relative importance of gravity loads –e.g. very high number of storeys, see section 3.7—, regardless of the code adopted for design.

On the other hand, $D_{u,W/D} = H_{mec,W/D} \cdot \theta_{u,min,W/D}$. H_{mec} of a frame is not possible to be known beforehand, but it is feasible to assume that $H_{mec,W/D} \geq 1.0$. In general, the higher is the member overstrength ratio between columns and beams in a frame, the higher is H_{mec} . Considering that minimum ρ_{tot} is required for columns, in general larger column sections causes higher overstrength. For both scenarios, columns of upper storeys may present larger sections for WBF rather than DBF because of beam effective width limitation in WB (see Table 30), especially when large b_w are required for WB (i.e. high seismic demand or deflection limitation due to gravitational loads in large-span beams). Furthermore, for scenario I, larger column sections in all the building are required for WBF rather than for DBF in order to provide similar stiffness (see section 3.3.3). Hence, $H_{mec,W/D} > 1.0$ for scenario I and $H_{mec,W/D} \geq 1.0$ for scenario II.

Regarding $\theta_{u,min,W/D}$, in each structural type the critical member can be a beam (B) or a column (C). Thus four sub-scenarios of relative performances could be configured: CC, CB, BC and BB, the first letter corresponding to WBF, and the second one to DBF. However, sub-scenario BC may not be possible to occur. In fact, WB show greater values of θ_u than DB (1.38 times could be a representative value according to section 3.3.2), thus sub-scenario BC would require that columns of WBF have values of θ_u at least 1.38 times higher than those in DBF. In general, if constant L_V and axial loads are assumed in columns, values of θ_u may not vary substantially when different section dimensions and proportions are considered, as shown in Figure 115. The plot in Figure 115 is obtained assuming regular

distribution of reinforcement bars along the perimeter of the section, increasing slightly the density of bars in the sides corresponding to the effective flexural direction. In fact, when h_c increases, v and f_{conf} decrease, thus their corresponding contributions to θ_u are inverse and thus the result is similar θ_u . Hence, whether columns of WBF present larger sections (typical of scenario I) or not (typical of scenario II), $\theta_{uc,min,W/D}$ can be assumed to be only proportional to $L_V^{0.35}$, because similar axial loads act in analogous columns of both types. Consequently, sub-scenario BC would only take place for values of L_V 2.5 times higher for WBF than for DBF, which may not be usual. Thus, for WBF the probability for columns to be the first element to exhaust its rotation capacity may be higher than for DBF.

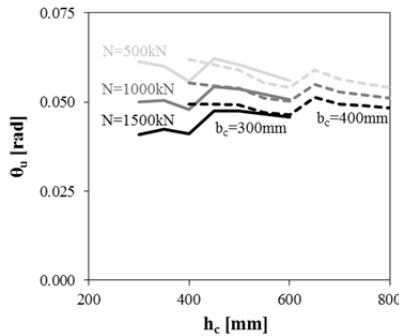


Figure 115: θ_u in columns for different cross-sections and axial loads, assuming constant $L_V=2m$ and typical distribution of reinforcement bars

Expressions for $\theta_{u,min,W/D}$ are shown in Equation (65a) (corresponding to sub-scenario CC) and Equation (65b) (sub-scenario BB), both obtained as ratios between (61) applied to WBF and DBF. Usually $\theta_{uc,min,W/D} < \theta_{ub,min,W/D}$, and intermediate values may be representative of sub-scenario CB. For scenario I, L_V may be larger for WBF, as column sections are larger and beams are more flexible, so relative stiffness between columns and beams is higher and thus cantilever behaviour is more important; conversely, for scenario II, such increment may be quite smaller. Consequently, $\theta_{uc,min,W/D} \geq 1.0$.

$$\theta_{uc,min,W/D} = \frac{0.3^{V_{c,W/D}} \cdot L_{V_{c,W/D}}^{0.35} \cdot f_{conf,c,W/D}}{h_{c,W/D}^{0.35}} ; \quad \theta_{ub,min,W/D} = \frac{f_{conf,W/D}}{h_{W/D}^{0.35}} \quad (65a,b)$$

In Figure 116, representative values for $SF_{W/D}$ corresponding to scenarios I and II in correspondence with sub-scenarios BB and CC are shown; all the influencing parameters assume rather conservative values: $f_{K,sec}=H_{mec,W/D}=L_{V_{c,W/D}}=1.0$. Intermediate values of $SF_{W/D}$ may be representative of sub-scenario CB. Results show: one situation evidently favourable to WBF (I-BB); two situations that suggest similar performances for WBF and DBF (I-CC and II-BB) and one situation (II-CC) unfavourable for WBF, conservatively.

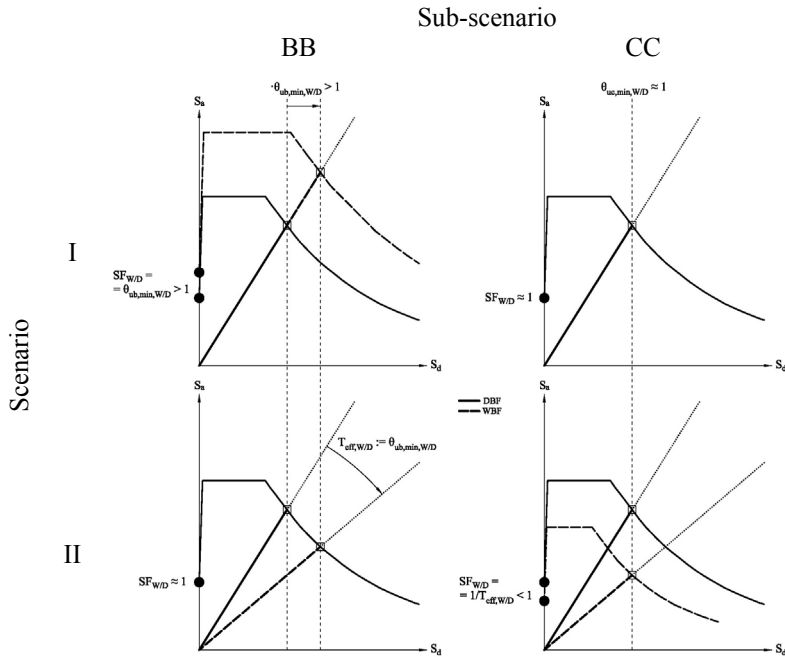


Figure 116: Graphic evaluation of $SF_{W/D}$ corresponding to four different situations, considering conservative assumptions ($f_{K,sec}=H_{mec,W/D}=L_{V_{c,W/D}}=1.0$)

Within the limits of this simplified approach it is not possible to know whether the combined favourable influence of $f_{K,sec}$, $H_{mec,W/D}$ and $L_{V_{c,W/D}}$ could increase the

capacity of WBF in the situation II-CC in order to get $SF_{W/D} \geq 1.0$. Neither it is possible to estimate the probability of occurrence of each situation, in order to know whether the most unfavourable scenario for WBF is more likely to occur than the others. However, for similar geometry of frames, it is feasible to hypothesise that sub-scenario BB may be more probable to occur in conjunction with scenario I, because columns of frames designed to DLS may present higher L_V and thus higher θ_u . Analogously, sub-scenario CC may be more related to scenario II. Probabilities of occurrence of sub-scenarios CC, CB and BB are related to the ratio between L_V of columns and beams (Figure 117). This ratio depends also on the geometry of the frame: large-span buildings may belong to sub-scenario CC and thus they may show poorer performance for WBF than medium/short-span ones.

Nevertheless, it is not clear how smaller $SF_{W/D}$ should be in order to justify a reduction of q for WBF. In fact, the level of tolerance inherent to q -based design is very high: quite large dispersion of results for SF can be observed between very similar structures, considering the very simplified nature of the q -based design and the non-negligible influence of personal choices of design (Mwafy and Elnashai, 2002).

Despite the limited scope of the simplified approach presented in this section, some relevant issues can be consequently remarked:

- Local ductility of beams may not be the most relevant parameter governing the relative performance of WBF and DBF.
- Instead, global stiffness of the frame and overstrength of columns may rule $SF_{W/D}$, thus the more restrictive is the code regarding design to DLS, the more favourable is WBF performance with respect to DBF one: EC8 may show higher $SF_{W/D}$ than NTC, and this in turn higher than NCSE-02. Only for EC8 certainly $SF_{W/D} > 1.0$.

Further statements about the appropriateness of the use of lower design values of q for WBF are proposed in next section, supported by some specific cases of study where both design and assessment are carried out, and thus representative values of $T_{el,W/D}$, $H_{mec,W/D}$ and $L_{Vc,W/D}$ are known and the probability of occurrence of each scenario can be estimated.

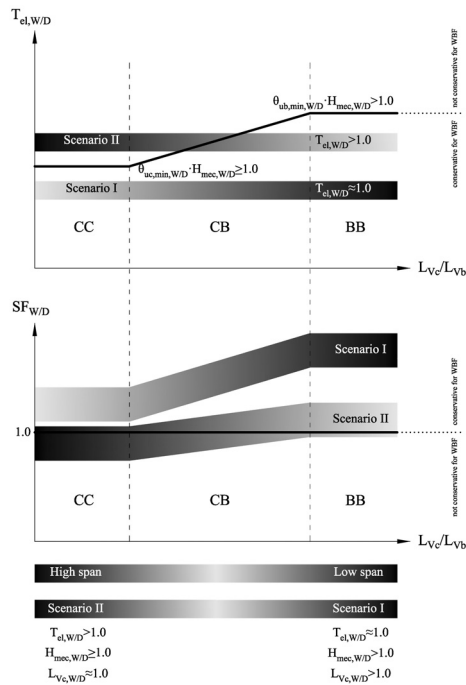


Figure 117: Schematic estimation of the probability of occurrence of each situation representing different relative performances between WBF and DBF, with expression of: boundary of $T_{el,W/D}$ for equal-performances (a) and estimated $SF_{W/D}$ (b); dark shadowed areas represent higher probabilities

3.5 CASE STUDY: DESIGN

Diverse analytical studies regarding the performance of WBF and their comparison with DBF (Gentry and Wight, 1992; and Quintero-Febres and Wight, 1997) show good performance of WBF, in some cases very similar to that of DBF. However, these studies cannot be yet defined neither systematic nor generalizable. Firstly, they have been carried out within the American framework of codes and construction practice. Gentry and Wight (1992) present planar frames, not buildings; and lower interstorey heights are used for WBF, resulting in fundamental design periods (T) only 9% higher than that of DBF. In Quintero-Febres and Wight (1997), the tested buildings have WB in internal frames, DB in external ones and intermediate shear walls; thus, the collapse mechanism is not

ruled by WB, making any comparison impossible. Moreover, both works use chord rotation values obtained from mix lumped plasticity and fibre models matching with their own experimental results, but not fitted to any larger database in accordance to the most common approach employed in the last ten years among the scientific community and adopted by recent codes. Conversely, other works (i.e., López-Almansa et al., 2013) suggest that WBF may provide poorer capacities than DBF; however, these studies are carried out on sub-standard RC buildings instead of frames designed to any ductility.

The scope herein is to provide a systematic and generalisable analytical comparison of WBF and DBF performances when both systems are designed in DCH. The latter is carried out by means of spectral pushover-based seismic analyses of a 5-storey building model designed alternatively with WB and DB, according both to Eurocode 8 –EC8– (CEN, 2004) and Spanish seismic code NCSE-02, assuming different design hypotheses based on the critical review of code and experimental data provided in previous sections, and evaluating the consequences of the design assumptions on the nonlinear performances. Finally, simplified assessment of a parametric set of 72 frames corresponding to different codes (EC8, NTC and NCSE-02) is carried out in order to extrapolate and generalise the results obtained for the specific case study.

In this section, a case study building is designed to medium-high seismic level according to different codes and assuming different modelling assumptions. Then, in next section, their respective performances are assessed.

3.5.1 Case study

In Figure 118, a typical Mediterranean 5-storey RC multi-family housing unit is presented. Different orientation and fix point for growth in columns are assumed. Design gravitational loads are similar for all the storeys: superficial dead loads (6.2kN/m^2), brick walls linear dead loads (7, 5 and 3kN/m) and live loads (2.0kN/m^2).

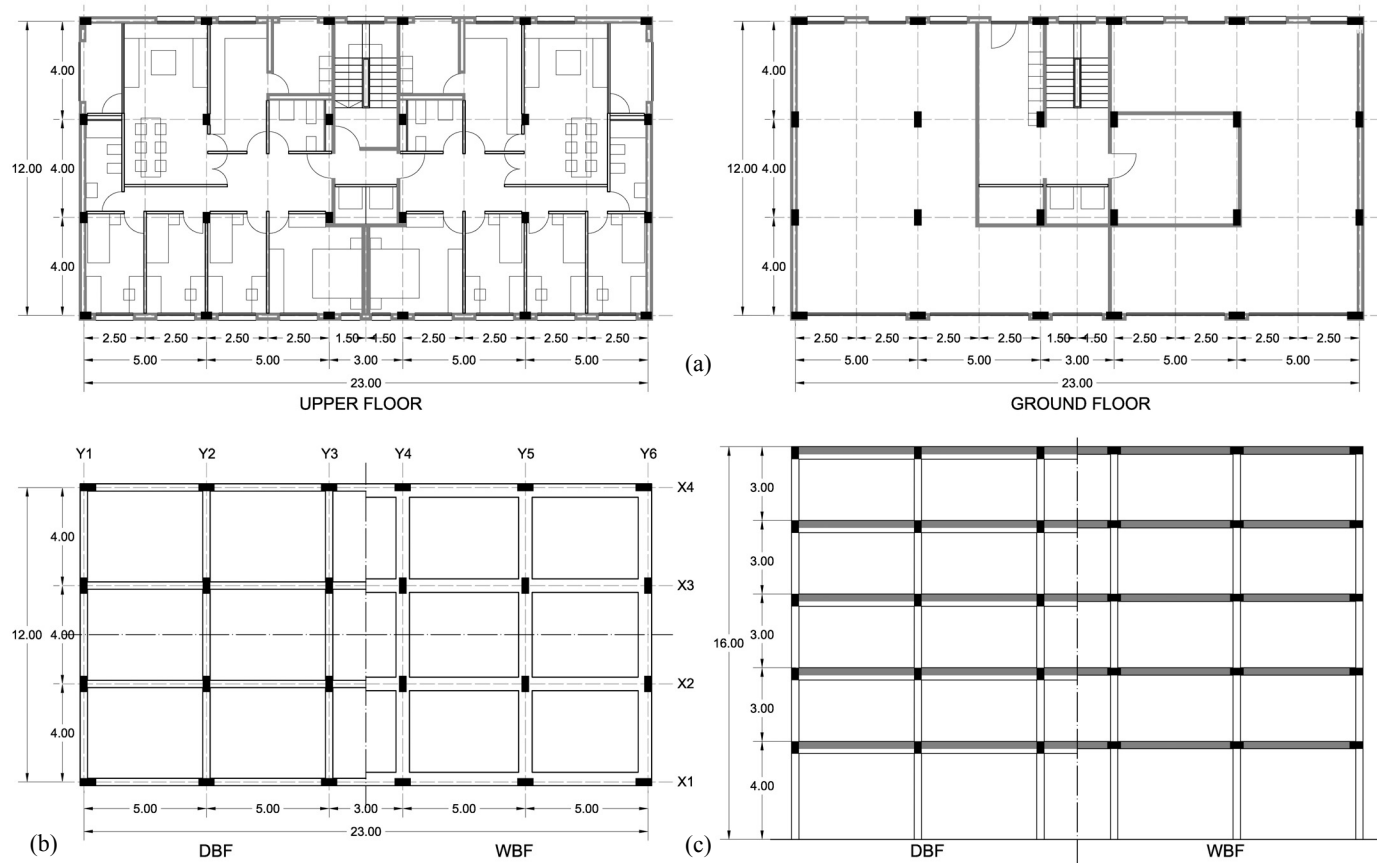


Figure 118: Case study; distribution (a) and structural arrangement in plan (b) and in elevation (c).

Regardless of which is the seismic code of design in each case, a NCSE-02 horizontal demand elastic spectrum is chosen for all the cases (Figure 119). Design ground acceleration (a_{gR}) is $0.25g$, average soil wave velocity is 300m/s . Finally, importance level of the building is normal, and 5% of the critical damping is assumed. The above assumptions results in a soil amplification factor $S=1.14$, importance factor $\gamma_I=1$, and damping spectral coefficient $\eta=1$.

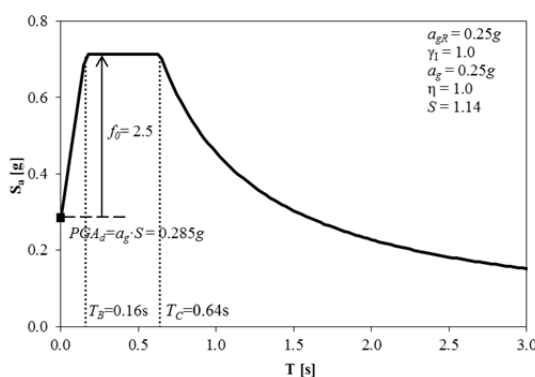


Figure 119: Elastic horizontal demand acceleration spectrum; parameters follow EC8 terminology

3.5.2 Three design alternatives: EC8₅₀₋₅₀, EC8₁₀₀₋₅₀ and NCSE-02

Two different seismic codes are chosen: EC8 and NCSE-02. The last one imposes a q reduction of 50% for WBF and it represent one of the most restrictive codes in Europe for WBF, while EC8 does not provide any specific limitation for WBF in terms of q .

As shown in sections 3.6 and 3.7, effective stiffness of WBF plays a very important role in their relative performance. Thus, the assumption of certain design stiffness for members is a crucial decision. EC8 suggests a reduction of 50%, while American ASCE/SEI 41-06 (ASCE, 2007) up to a 70% for beams and 30-70% for columns; Italian NTC from 0% to 50%; New Zealander NZS 3101 (NZS, 2006), 60-73% and 0-70% for beams and columns in Ultimate Limit State, respectively, and 0-65% for Serviceability Limit State (i.e. Damage Limitation State (DLS)).

In order to cover a wide range of design choices, two different versions of design for EC8 are considered. They correspond to two different assumption of elastic members' stiffness for DLS design. Design called “EC8₅₀₋₅₀” corresponds to the alternative in which both elastic stiffness at DLS and ULS is assumed as 50% of the uncracked one. “EC8₁₀₀₋₅₀” corresponds to the alternative in which 100% of uncracked stiffness is employed for DLS, and 50% for ULS. EC8₁₀₀₋₅₀ is expected to show lower influence of DLS limitation on columns' dimensions. Hence, EC8₁₀₀₋₅₀ is an “artificial” design version aimed at providing more robust conclusions. Results of the case EC8₁₀₀₋₅₀ can cover also other design alternatives characterised by higher stiffness: higher values of concrete modulus of elasticity, higher contribution of joint regions or higher effective width of upper slab to global stiffness. Furthermore, it could be representative of a design made according to Italian NTC, given that the rest of the prescriptions are similar to EC8. Conversely, in NCSE-02 models no reduction of stiffness is considered, according the typical assumption made for design of RC frames in Spain.

3.5.3 Mechanic properties and design strategies

Concrete C25/30 ($f_{ck}=25\text{MPa}$) and steel B500 ($f_{yk}=500\text{MPa}$) are used. Persistent-transient material partial factors (1.50 and 1.15, respectively) are conservatively assumed, instead of accidental ones. Factor accounting of long term effects on the compressive strength of concrete is assumed to be 1.0.

Members are modelled as linear frames, and rigid horizontal diaphragms at the level of slabs are considered. Neither stairs nor infill panels are modelled. Different contributions of joint regions to the stiffness of the building are considered. NCSE-02 does not suggest any strategy, thus no contribution is considered. Conversely, EC8 suggest considering it, but no clear modelling strategy is proposed. American ACI 369R-11 (ACI, 2011) proposes to consider as rigid a portion of member end within the joint region (“offsets”), depending on the column-to-beam capacity design ratio: only in columns (ratio >1.2), vice-versa (ratio <0.8), and half in beams and half in columns for the intermediate situation. Fardis (2009) suggests only rigid offsets in beams (conversely to ACI 369R-11 for the most likely situation), in order to indirectly accounting for the shear elastic deformability of the joint panel. The assumption of the latter hypothesis leads to a decrease of elastic stiffness with

respect to that of the corresponding structure with rigid joints. Such a decrease is proportional to beam depths, so it is higher for DBF rather than for WBF; it is also coherent with the behaviour observed in representative subassemblages (LaFave and Wight, 2001). Hence, given the more satisfactory matching with experimental results, Fardis' offset modelling approach is adopted in this work for EC8 structures. Upper slab contribution is only considered in terms of strength; on the contrary, its contribution to stiffness is discarded, as no specific rules are provided in codes. This assumption is conservative for DLS design.

Regarding seismic action, values of q adopted in design by EC8 are 5.85 or 4.68 for structures regular in elevation or not, respectively. The quantitative check of regularity in elevation is made through the criteria provided by NTC. In NCSE-02, q is 4.0 (DCH) and 2.0 (DCL). DCH is only allowed if there is no bending moment inversion. Such restriction, rather than being based on ductility considerations, seems to compensate the low confidence in the capacity of the joint to alternate bending moments reflected in the absence of joint detailing rules (Gómez Martínez et al., 2015a and 2015d). Thus, only within the scope of this paper, no reduction of q because of this cause is taken into account.

Two additional minor storey amplification of seismic action are adopted in EC8 buildings: due to reduction of masonry infills and due to P- Δ effect. Both codes EC8 and NCSE-02 provide thresholds of IDR that permit discarding P- Δ effects, but only the first one furnishes some quantitative increment of the action for greater values of IDR. The maximum storey factor is applied to the entire frame in each case. EC8 does not establish explicitly whether this amplification should be retroactively considered in the evaluation of IDR aimed to DLS design. Furthermore, if different member stiffnesses were chosen for DLS and ULS, P- Δ amplification factors to be multiplied by IDR values should be calculated using the stiffness corresponding to DLS.

Members are designed to the forces corresponding to the face of the joint panel. Flexural design of WB is carried out assuming full cyclic flexural and shear capacities, as for DB, provided that all the code prescriptions regarding geometric and mechanical restrictions in beam-column connections are satisfied.

Design redistribution of bending moments in beams, which is allowed by EC8, is not considered in this work, because it is not clear whether it is conservative or not for the assessment of WBF. It would eventually lead to the attainment of pre-emptive yielding in some beam end; however, it is intended to not reduce substantially the provided q of structures, as the evolution of chord rotation in all the hinges is not proportional and also better local ductility of beams is expected due to more symmetrical reinforcement (Fardis, 2009). Negative moments in WB are higher than in DB due to their lower relative stiffness when framing similar columns, thus higher redistribution would be needed in order to equalise negative hogging and sagging moments.

Linear dynamic analyses are carried out for all the models. Masses of elements are weighted in such a way that their centre of mass is placed alternatively in four symmetric points corresponding to the accidental eccentricity established by codes ($\pm 5\%$). Different masses corresponding to the fraction of live loads are considered: factors of 0.3 and 0.5 are used for EC8 and NCSE-02, respectively, while such factor is 0.3 in both cases for the combination of effects of loads. Seismic action in one direction is combined with 30% in the transversal direction.

Regarding homogenisation of members, both symmetry axes are observed also for geometry of sections and reinforcements. In the X-direction, lateral frames are stiffer than central ones, thus rule the design. Most critical beams are the lower central short ones belonging to those frames. In the Y-direction the distribution of stiffness is more homogeneous; still, frames Y2 and Y5 are highly demanded due to larger tributary areas. All section dimensions are multiple of 50mm. Beam section dimensions are assumed to be similar in all the building. Depth of DB is assumed to not be lower than 500mm, due to constructive reasons. Column dimensions are assumed to be similar in each storey. They cannot be reduced considerably within two consecutive storeys, especially for WBF, because spliced bars from the lower column cannot separate significantly from the vertical configuration when passing through the joint. Sizing of columns in WBF is influenced also by beams width limitation and maximum eccentricity requirements in edge beams. Proportions between sides of column sections are not larger than 2:1.

NCSE-02 capacity design rules are not effectively aimed at their target, and it does not either evaluate shear capacity of joints (Gómez Martínez et al., 2015a and 2015d). Thus, the same quantitative expressions established by EC8 for column-to-beam and shear-to-bending capacity design are taken into account, and no joint-to-member capacity design is considered. Capacity design factors are: 1.2-1.3 for EC8 and 1.1 for NCSE-02.

3.5.4 Results of design

In Table 33, Table 34 and Table 35, characteristics of the 6 design versions are summarised. Geometry of section is often more related to beam-to-column width limitation, IDR limitation or capacity design ratio rather than force-based design. Also, higher global cantilever behaviour of WBF determines results in most cases.

Essentially, EC8₅₀₋₅₀ buildings are very stiff ones in which DLS design is the critical condition. Especially for WBF, very large sections are required, so minimum reinforcement is enough to satisfy ULS prescriptions with high section overstrengths. Important cantilever behaviour is observed. Conversely, in EC8₁₀₀₋₅₀ buildings, design to DLS is not so relevant especially in DBF, resulting in smaller sections with reinforcement ratios slightly higher than the minimum. In this case, DBF and WBF present similar columns. On the other hand, NCSE-02 buildings are mainly force-based, so small sections and high reinforcement ratios are shown also in WBF design to DCL. In Figure 120, deformed shapes of all the models (obtained after a homogenisation of parameters influencing stiffness for comparison) are compared.

DBF are always resolved with similar moderate dimensions, while WBF present different beam widths depending on the design alternative (Table 33; being i the storey; L the member length; b_c and h_c the width and height of column sections; and b_w and h_b the width and height of beam sections). Columns ρ_{tot} and v are quite low for EC8 structures, especially for WBF, in which dimensions of columns are more oversized than for DBF in order to compensate the lower stiffness of beams. In EC8₅₀₋₅₀ buildings, huge section dimensions of first and also second storey columns may constitute a great shortcoming regarding architectural functionality (see Figure 121).

Table 33: Geometric design properties of each model (*mean)

MODEL	Columns										Beams						
	<i>i</i>	<i>b_c</i> [mm]	<i>h_c</i> [mm]	$(L_v/L)_X$ -	$(L_v/L)_Y$ -	$(L_v/h_c)_{min}$ -	$v^{(*)}$ -	$\rho_{tot}^{(*)}$ [%]	$\rho_{w,b}$ [%]	$\rho_{w,h}$ [%]	<i>b_w</i> [mm]	<i>h_b</i> [mm]	$\rho^{(*)}$ [%]	$\rho^{(*)}$ [%]	$\rho_{max}/\rho_{min}^{(*)}$ -	ρ_w [%]	
EC8 ₅₀₋₅₀	DBF	5	300	300			10.0	0.08	1.8	0.67	0.67			0.28	0.37	1.37	
		4	300	300			10.0	0.11	1.4	0.67	0.57			0.32	0.37	1.24	
		3	400	350	≈0.50		7.5	0.14	1.1	0.54	0.57	300	500	0.43	0.38	1.13	0.48
		2	500	350			6.0	0.15	1.0	0.56	0.57			0.50	0.47	1.14	
		1	600	400	0.75	0.75	6.7	0.17	1.3	0.56	0.67			0.57	0.53	1.21	
	WBF	5	500	500			7.5	0.03	1.0	0.54	0.54			0.30	0.23	1.29	
		4	600	550	≈0.50		6.0	0.06	1.1	0.67	0.54			0.45	0.26	1.77	
		3	700	550			5.0	0.07	1.0	0.67	0.61	650	300	0.58	0.39	1.53	0.44
		2	800	550			4.4	0.08	1.0	0.67	0.61			0.62	0.45	1.41	
		1	800	550	0.95	0.97	5.0	0.11	1.0	0.67	0.61			0.59	0.41	1.47	
EC8 ₁₀₀₋₅₀	DBF	5	400	350			7.7	0.05	1.4	0.67	0.57			0.28	0.37	1.36	
		4	450	350	≈0.50		6.7	0.10	1.3	0.60	0.57			0.33	0.37	1.24	
		3	500	350			6.0	0.14	1.1	0.54	0.57	300	500	0.44	0.45	1.26	0.48
		2	550	350			5.5	0.17	1.3	0.61	0.57			0.57	0.54	1.19	
		1	600	350	0.55	0.60	6.7	0.20	1.1	0.56	0.57			0.64	0.63	1.14	
	WBF	5	400	350			7.7	0.05	1.4	0.67	0.57			0.33	0.25	1.34	
		4	450	350	≈0.50		6.7	0.10	1.3	0.60	0.57			0.50	0.31	1.59	
		3	500	350			6.0	0.14	1.1	0.54	0.57	500	300	0.61	0.42	1.46	0.53
		2	550	350			5.5	0.17	1.3	0.61	0.57			0.73	0.56	1.32	
		1	600	350	0.69	0.83	6.7	0.20	1.1	0.56	0.57			0.78	0.56	1.40	
NCSE-02	DBF	5	300	300			10.0	0.08	1.9	0.45	0.45			0.31	0.41	1.32	
		4	300	300	≈0.50		10.0	0.17	2.8	0.45	0.45			0.34	0.41	1.21	
		3	350	300			8.6	0.22	2.4	0.38	0.45	300	500	0.43	0.41	1.12	0.48
		2	400	300			7.5	0.27	2.1	0.50	0.45			0.49	0.46	1.20	
		1	450	300	0.53	0.55	8.9	0.30	2.3	0.45	0.45			0.61	0.57	1.22	
	WBF	5	300	300			10.0	0.08	2.8	0.48	0.48			0.54	0.50	1.11	
		4	350	300	≈0.50		8.6	0.14	3.0	0.38	0.67			0.94	0.68	1.42	
		3	400	300			7.5	0.19	3.1	0.50	0.67	450	300	1.36	1.02	1.41	0.45
		2	500	300			6.0	0.21	2.5	0.40	0.67			1.61	1.28	1.30	
		1	600	300	0.75	0.78	6.7	0.22	3.5	0.45	0.67			1.56	1.30	1.22	

Table 34: Mechanic design properties of each model (^(*)mean)

MODEL	IDR limitation		P-Δ amplification		Capacity design ratio		Regularity in elevation							
	<i>i</i>	IDR_X	IDR_Y	$C_{P-\Delta X}$	$C_{P-\Delta Y}$	$(\Sigma M_{Rc}/\Sigma M_{Rb})_X^{(*)}$	$(\Sigma M_{Rc}/\Sigma M_{Rb})_Y^{(*)}$	Δm	ΔK_X	ΔK_Y	$(V_R/V_d)_X$	$(V_R/V_d)_Y$	q_d	
	-	[%]	[%]	-	-	-	-	[%]	[%]	[%]	-	-	-	
EC8 ₅₀₋₅₀	DBF	5	0.45	0.47	1.00	1.00	-	-	-	-	-	(3.73)	(3.61)	
		4	0.46	0.46	1.00	1.00	1.48	1.77	11.3	41.2	43.0	3.71	3.61	
		3	0.48	0.45	1.00	1.00	1.89	2.20	1.6	22.5	26.1	3.50	3.46	4.68
		2	0.49	0.45	1.00	1.00	2.19	2.28	1.5	14.8	17.6	3.99	3.97	
		1	0.44	0.42	1.11	1.00	2.67	2.68	5.2	-7.7	-13.9	3.43	3.40	
	WBF	5	0.30	0.30	1.00	1.00	-	-	-	-	-	(10.29)	(10.17)	
		4	0.45	0.44	1.00	1.00	4.50	5.93	10.1	17.4	17.0	8.69	8.56	
		3	0.50	0.50	1.12	1.11	5.39	6.23	3.5	15.7	15.7	9.51	9.37	5.85
		2	0.50	0.50	1.14	1.13	6.66	7.19	2.2	15.9	15.9	9.84	9.72	
		1	0.32	0.32	1.00	1.00	8.03	8.54	6.1	24.5	23.0	7.07	7.00	
EC8 ₁₀₀₋₅₀	DBF	5	0.17	0.18	1.00	1.00	-	-	-	-	-	(6.42)	(6.25)	
		4	0.30	0.29	1.00	1.00	1.81	2.21	9.7	13.8	15.8	4.07	3.97	
		3	0.36	0.35	1.00	1.00	1.89	1.90	0.8	7.3	10.0	3.50	3.43	4.68
		2	0.41	0.38	1.12	1.00	1.92	2.03	0.8	9.0	10.0	3.71	3.65	
		1	0.38	0.37	1.14	1.13	1.96	1.98	4.2	-15.8	-20.1	2.91	2.82	
	WBF	5	0.25	0.24	1.00	1.00	-	-	-	-	-	(9.29)	(9.14)	
		4	0.40	0.39	1.15	1.15	2.55	3.34	9.7	8.0	7.6	6.27	6.16	
		3	0.49	0.48	1.24	1.23	2.38	3.09	0.8	3.3	4.7	5.57	5.48	5.85
		2	0.50	0.50	1.32	1.29	2.51	3.01	0.8	7.7	8.8	5.97	5.89	
		1	0.40	0.40	1.26	1.25	2.97	3.38	4.2	10.1	8.8	4.56	4.53	
NCSE-02	DBF	5	0.21	0.22			-	-						
		4	0.40	0.42			1.36	1.72						
		3	0.56	0.57		-	1.39	1.71						4.00
		2	0.57	0.55			1.56	1.61						
		1	0.63	0.62			1.62	1.63						
	WBF	5	0.33	0.34			-	-						
		4	0.53	0.52			1.52	1.71						
		3	0.65	0.63		-	1.47	1.45						2.00
		2	0.64	0.62			1.53	1.57						
		1	0.43	0.42			2.32	2.25						

In NCSE-02 structures, in which the increment of strength of WBF with respect to DBF is obtained through a mix strategy of increasing both the sections and the reinforcements, ρ_{tot} and v are triple or double, respectively, than for EC8₅₀₋₅₀ buildings. In all the versions, minimum ρ_w are enough both to resist the shear demand and to fulfil the shear-to-bending capacity design requirements. However, $\rho_{w,h}$ is 30% higher for EC8 buildings (Table 33).

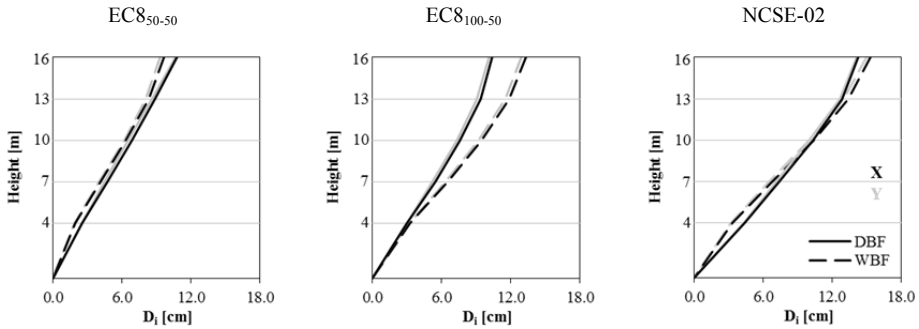


Figure 120: Lateral deformed shape in both directions for all the models (adapted for comparison)



Figure 121: Distribution (a) and structural arrangement (b) of case-study version EC8₅₀₋₅₀ with DB and WB

Larger oversizing of column sections of WBF, together with the adoption of minimum longitudinal reinforcement ratios, leads to storey shear overstrengths (V_R/V_d) and column-to-beam capacity design ratios ($\Sigma M_{Rc}/\Sigma M_{Rb}$) much higher for

WBF than for DBF in the case of EC8 (Table 34). Capacity design ratios are also higher for the Y-direction rather than for the X-direction, because in the first case beams have lower section overstrengths due to better exploitation of positive flexural capacity as those beams support almost no gravitational loads. For NCSE-02, in which design of columns is essentially force-based, the asymmetry of bending moment diagrams in first-storey columns is the only cause of the slightly higher $\Sigma M_{Rc}/\Sigma M_{Rb}$ of this storey in comparison with the rest. Flexural capacity is ruled by the large demand at the base section of columns, while the connection corresponding to their heads have substantially lower demands.

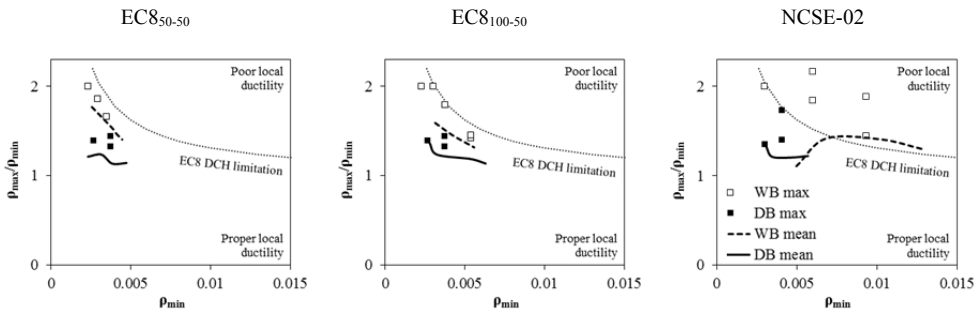


Figure 122: Mean and maximum storey values of ρ_{max}/ρ_{min} in relation with the EC8 limitation for design to DCH, for all the cases

Actually, design results confirm the severity of the requirements of EC8 not related to the force-based design: resulting dimensions and base shear capacities are always larger than NCSE-02 ones even for higher q . Reinforcement ratios of beams are generally low: around 0.3-0.6% and 0.3-0.8% for DBF and WBF, respectively, except for NCSE-02 WBF, in which are much higher. In those buildings, lower ductilities are expected compared with the rest of them, given that local ductility of members may be smaller: in columns, due to higher v and lower confinement contribution; and in beams, due to higher ratio between reinforcements in both sides (ρ_{max}/ρ_{min} , see Figure 122). It is worth noting that beams of NCSE-02 DBF show quite similar mean values of ρ_{max}/ρ_{min} to both EC8 DBF, despite the differences between prescriptions (Figure 82), because total reinforcement is low.

Ratios between global flexural capacities of WB and corresponding spectral demand acceleration ($S_{ad}(T)$, see Table 35) are lower than those of DB, i.e., WBF induce lower relative demand to beams that DBF especially in higher and lower storeys –assuming similar design section overstrengths— (Figure 123). In top storeys section design overstrengths furnished by minimum reinforcement ratios are proportional to h_b , so higher for DB. Conversely, in lower storeys the cause is the cantilever behaviour, which also increase shear span (L_V) of first-storey columns from what is suggested by EC8 part 3 (CEN, 2005): approximately $0.5 \cdot L$. Thus, L_V for column bases in WBF are 25-42% higher than in DBF (Table 33). Cantilever effect also causes lower IDR in first storey with respect to the second one, especially for WBF, which is the cause of their regularity in elevation notwithstanding the greater interstorey height (Table 34, being Δm and ΔK the relative interstorey differences regarding storey mass and stiffness, respectively). Different strength contribution of masonry infills in first storey with respect to the second one does not exceed the limits, because internal thin infill panels are not taken into account (Gómez-Martínez et al., 2013).

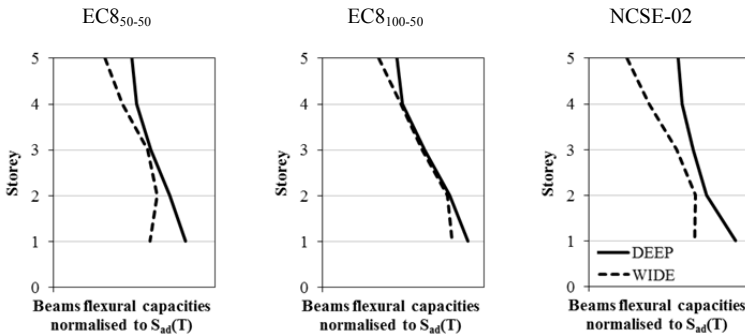


Figure 123: Mean storey flexural capacity of beams, normalised to spectral design demand acceleration, for all the cases

Design periods ($T_{50\%EI}$ or $T_{100\%EI}$, corresponding to EC8₅₀₋₅₀ and EC8₁₀₀₋₅₀, respectively) are quite higher than those suggested by codes (T_{code}) (Table 35, Figure 124). However, T_{code} shows proper agreement with $T_{100\%EI}$ for EC8₅₀₋₅₀; the last confirms that simplified code-based periods may constitute good

approximations to elastic periods of “modern” capacity-designed and DLS-designed frames (Crowley and Pinho, 2010). In EC8₅₀₋₅₀ and NCSE-02, stiffnesses of both structural types are similar. For NCSE-02, the last is an indirect consequence of the higher strength required for WBF. Still, global stiffnesses of NCSE-02 buildings are quite lower than for EC8 ones: IDR of NCSE-02 versions are up to 15% higher than the EC8 requirement (Table 34). Conversely, in EC8₅₀₋₅₀ buildings, the reason for the similarity between periods of DBF and WBF is that IDR limitation is the most restrictive design requirement. In each storey, if similar IDR are required for both types, storey stiffnesses must be also similar and likely global stiffness and elastic period (T_{el}) too. Moreover, for EC8₅₀₋₅₀ frames, periods of design are even 7% lower for WBF, because column sections in upper storeys are slightly oversized with respect to the maximum IDR, due to limitation in the interstorey reduction of column sections and beam effective width requirements. Regarding first mode participation factor (Γ), higher values are obtained for EC8₅₀₋₅₀ rather than in the other two alternatives. In these cases, columns of top storeys present larger sections aimed at fulfilling capacity design, which is not necessary in EC8₅₀₋₅₀ because penultimate storeys already furnish sufficient strength; thus, IDR is higher in last storey of EC8₅₀₋₅₀, causing larger Γ .

Table 35: Dynamic properties for each model (bold: design to ULS; italics: design to ELS)

MODEL		Modal properties					Spectral demand acceleration			
		T_{code} [s]	$T_{100\%EI}$ [s]	$T_{50\%EI}$ [s]	Γ -	λ -	$S_{ae}(T)$ [g]	$S_{ae}(T)'$ [g]	$S_{ad}(T)$ [g]	
EC8 ₅₀₋₅₀	DBF	X	0.69	0.98	1.36	0.83	0.466	0.597	0.128	
		Y	0.60	0.67	0.95	1.39	0.82	0.480	0.552	0.118
	WBF	X	0.60	0.64	0.90	1.34	0.80	0.505	0.659	0.113
		Y	0.60	0.63	0.89	1.34	0.80	0.515	0.669	0.114
EC8 ₁₀₀₋₅₀	DBF	X	0.60	0.71	1.00	1.29	0.87	0.456	0.596	0.127
		Y	0.60	0.69	0.97	1.29	0.87	0.471	0.611	0.131
	WBF	X	0.60	0.90	1.28	1.30	0.85	0.357	0.544	0.093
		Y	0.60	0.88	1.24	1.30	0.85	0.368	0.548	0.094
NCSE-02	DBF	X	0.45	1.00	-	1.26	0.89	0.454	0.454	0.114
		Y	0.45	0.99	-	1.27	0.89	0.461	0.461	0.115
	WBF	X	0.45	1.11	-	1.31	0.83	0.412	0.412	0.206
		Y	0.45	1.09	-	1.32	0.83	0.419	0.419	0.210

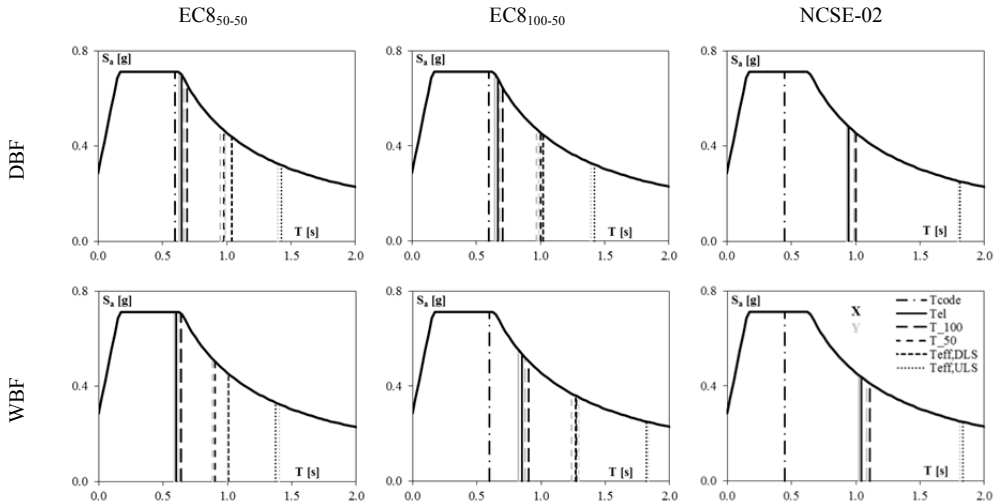


Figure 124: Different fundamental periods for each model: code-based (T_{code}), elastic (T_{el}), design to 100%EI ($T_{100\%EI}$), design to 50%EI ($T_{50\%EI}$) and effective (T_{eff})

Furthermore, in EC8₅₀₋₅₀ buildings the assumption of lower member stiffness permits the design to DLS fulfilling P- Δ requirements too (through amplification factors $C_{P-\Delta}$, see Table 34). On the contrary, in EC8₁₀₀₋₅₀ buildings such factors are considerably higher, being in some case beyond the suggested limit of EC8 for the use of the simplified approach (1.25), but always within the allowed range (not higher than 1.43). $C_{P-\Delta}$, together with another factor corresponding to the equivalent amplification due to the accidental eccentricity of masses, are needed in order to define the equivalent real elastic spectral acceleration of design ($S_{ae}(T)'$) from the original value ($S_{ae}(T)$), see Table 35. Higher values of $C_{P-\Delta}$ for WBF rather than for DBF partially compensate the differences between q of design in the case of EC8, leading to almost equivalent demands.

On the other hand, the modelling strategy of joint panels produces mean values of elastic stiffness of DBF 17% lower with respect to the same model with rigid joint panels; in literature, experimental values of this decrease are around 29% in sub-standard buildings and likely lower for modern ones (De Risi et al., 2014). In WBF models such decrease is lower (5%), which is consistent with LaFave and Wight (2001).

3.6 CASE STUDY: N2 ASSESSMENT

In this section, performances and capacities of all the models are assessed by means of nonlinear static analysis (“pushover”, SPO) and spectral N2 method (Fajfar and Gaspersic, 1996; Fajfar, 1999).

3.6.1 Nonlinear local behaviour

Plastic hinges at member ends are modelled following lumped plasticity approach. Only flexural inelasticity is considered: three-linear bending moment-chord rotation envelopes are assumed, defined by cracking, yielding and maximum ULS capacity, being the last branch horizontal. Bending moment values and corresponding curvatures are obtained through fibre models. Chord rotation values are obtained through the expressions suggested by EC8 part 3, whose reliability is supposed to be higher than any physical model, since they have been selected to fit with a large experimental database (Biskinis, 2007). Other formulations with experimental basis, as in ASCE SEI/41-06 (ASCE, 2007), do not provide such different values for DB and WB as L_V/h is considered to not influence the capacities. Maximum chord rotation capacity (θ_{ULS}) is assumed to correspond to the Limit State of Significant Damage, which EC8 part 3 considers equal to 75% of ultimate chord rotation capacity (θ_u). θ_u is calculated by assuming constant column v corresponding to the gravitational load in the seismic situation, which in this case provides capacities not more than $\pm 5\%$ different than real values in first-storey columns.

Regarding L_V , in this work spans between axes are considered instead of clear span, in order to somehow compensate that shear deformation of joint panels is not taken into account; this assumption is conservative for assessment of WBF. Consistently with the design assumptions, rigid offsets are only placed in beam ends, and plastic hinges are placed at the faces of joint panels. Values of L_V equal $0.5 \cdot L$ are assumed for all the members except for first storey columns (Table 33), in which they correspond to the design bending moment diagrams.

Mean values for material properties are adopted. For concrete, an increment of 8MPa with respect to the characteristic compressive strength is adopted, and modulus of elasticity is considered in all the cases: 31476MPa, as suggested by

Eurocode 2 (BSI, 2004). For steel, typical factors of around 1.26 between mean and characteristic yield strengths are observed (Galasso et al., 2011a), which is equivalent to a factor 1.45 between mean and design values.

In Figure 125 and Figure 126, ranges of values θ_y and θ_{ULS} of all the buildings are presented; in first-storey columns, values correspond only to bases. Chord rotations of columns increase with the storeys, because of their higher flexibility and lower v . However, rotations in first storeys are higher with respect to other elements, especially for WBF, due to their larger L_v . At higher storeys, similar capacities are obtained for columns of DBF and WBF, given that v , ρ_{tot} and bars distribution in corresponding sections are similar. Analogous results are observed in both directions, thanks to the similarity of sections and reinforcements. Much higher variability is observed for beams in the X-direction than in the Y-direction, because in the first one beams present different spans.

Higher θ_y , lower θ_{ULS} and, in turn, lower μ_θ are shown for NCSE-02 (Figure 127), because of the poorer local ductility requirements if compared with EC8: worse disposition of reinforcement in beams (Figure 82 and Figure 123) and higher v in columns. θ_{ULS} of WB are on average 38% higher than DB ones (Figure 128a), the same value obtained in the parametric study presented in section 3.3.2. Higher ratios are obtained for EC8₁₀₀₋₅₀ than for EC8₅₀₋₅₀, because of lower stiffness of columns in the first case, resulting in higher positive bending moments in beams and almost symmetric sectional reinforcement. , lower μ_θ for WB are obtained with respect to DB (Figure 128b): 13% and 28% lower for EC8 and NCSE-02, respectively, consistent with 27% obtained in the parametric analysis.

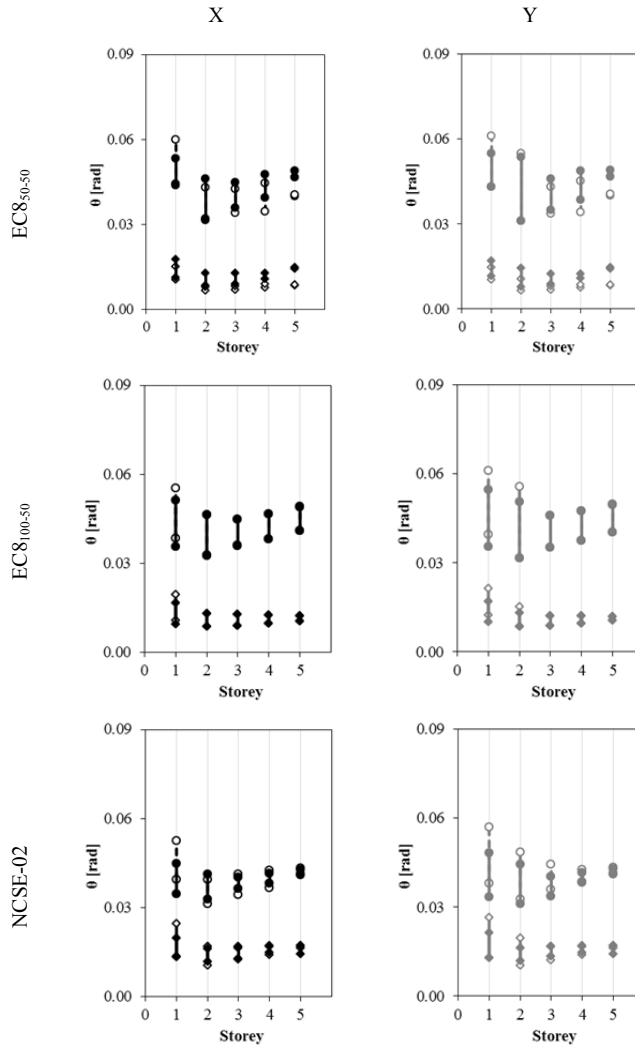


Figure 125: θ_y and θ_u ranges in columns in each storey

FAST simplified vulnerability approach for seismic assessment of infilled RC MRF buildings and its application to the 2011 Lorca (Spain) earthquake

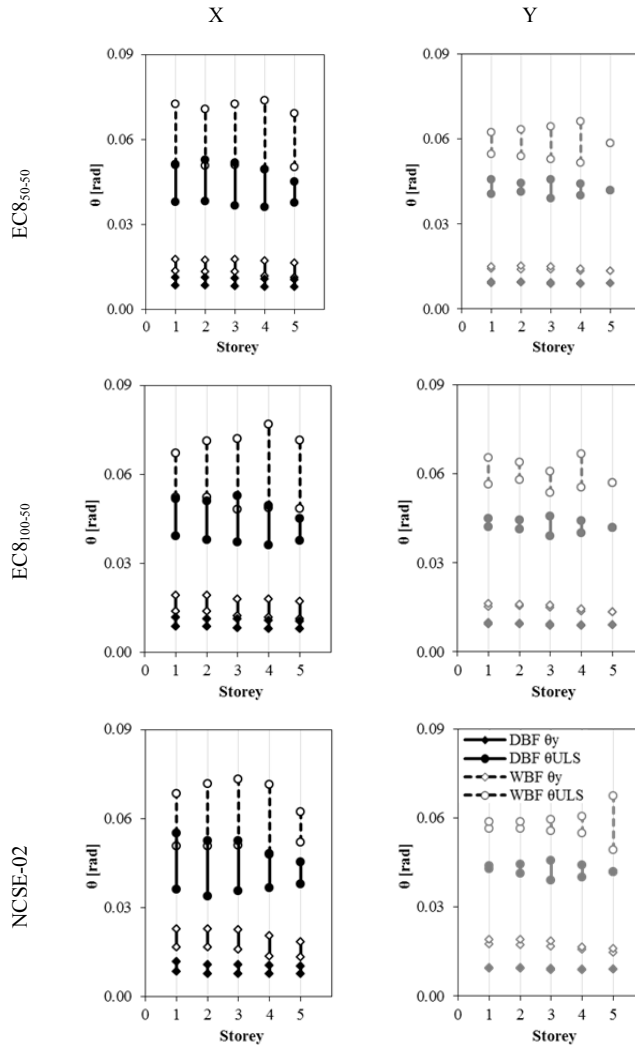


Figure 126: θ_y and θ_{UL} ranges in beams in each storey

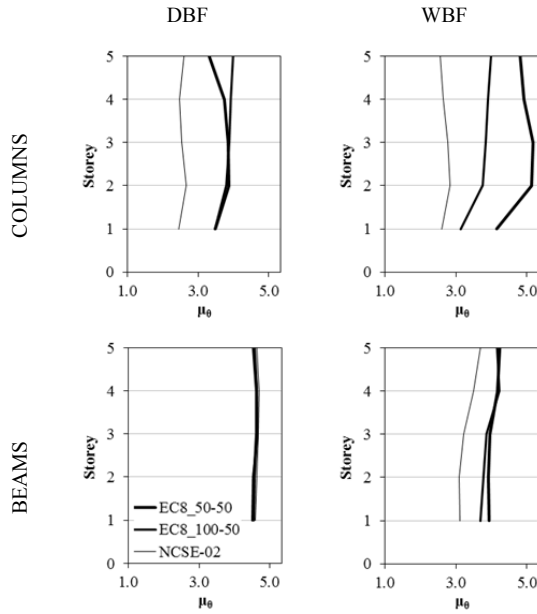


Figure 127: Mean storey μ_0 for columns and beams in all the models

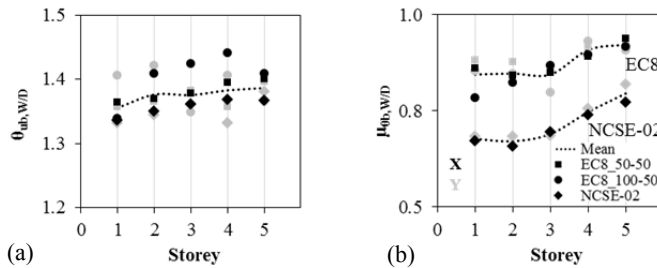


Figure 128: Mean ratios between WB and DB regarding ultimate θ_u (a) and μ_0 (b) capacities, depending on the design code

3.6.2 SPO analyses

As suggested by EC8, two different lateral load patterns are considered for SPO: one proportional to modal displacement and masses (“MODE”), and another one only proportional to masses (“MASS”). Maximum lateral displacement capacity of structures is considered to be attained when the first plastic hinge get a

chord rotation equal to θ_{ULS} . In Figure 129, “MODE” mechanisms and displacement capacities (D_u) of all the models are shown. The height involved in the mechanism (H_{mec}) depends mainly on column-to-beam capacity design ratios (Table 34), which is higher for WBF than for DBF especially for DLS-ruled frames (EC8₅₀₋₅₀). Hence, H_{mec} is higher for WBF with respect to DBF in all the cases. H_{mec} is higher in the Y-direction with respect to the X-direction. EC8₅₀₋₅₀, EC8₁₀₀₋₅₀, and NCSE-02 buildings have decreasing H_{mec} , showing the influence of design alternative on this parameter.

WBF often show mechanisms involving all the storeys, while it only happens once for DBF. It is worth noting that, even in the case in which capacity design ratios are quite similar for both WBF and DBF (e.g. NCSE-02 buildings, see Table 34), a difference of one or two storeys favourable to WBF is observed. This effect is caused by different redistribution of moments and chord rotation demands characterising the two types of frame. Estimated values of ultimate displacement ($D_{u,pred}$), calculated by means of the simplified approach proposed in section 3.4, are only 5% (on average) lower than real ones (D_u). The lower is H_{mec} , the higher is the underestimation of the displacement, because the deformation of the upper storeys not involved in the mechanism (sometimes including plastic hinges) is not taken into account. Conversely, overestimation occurs typically in frames with all the storeys involved in the mechanism, in which the first hinge attaining θ_{ULS} is a beam end, whose chord rotation evolution rate is not “faster” than the others.

In EC8₅₀₋₅₀ buildings, first yielding occurs only in a beam end, while in the rest of the cases yielding is attained simultaneously at some columns bases and in those beams. Beams usually present lower design section overstrength with respect to columns, especially in EC8₅₀₋₅₀. Still, column bases, which are fixed to the foundation, increase their chord rotation demand more quickly than the surrounding hinges (also X-direction shorter bay beams experiment such behaviour). When this occurs, those column bases are also the first in attaining θ_{ULS} (i.e., elements limiting structural capacity). However, in most cases, first member ends attaining yielding are not the same that attain ULS; mainly because of moment redistribution. Regarding columns, most demanded elements are usually central columns, so usually the last plastic hinges forms in lateral columns heads of last storey of the plastic mechanism.

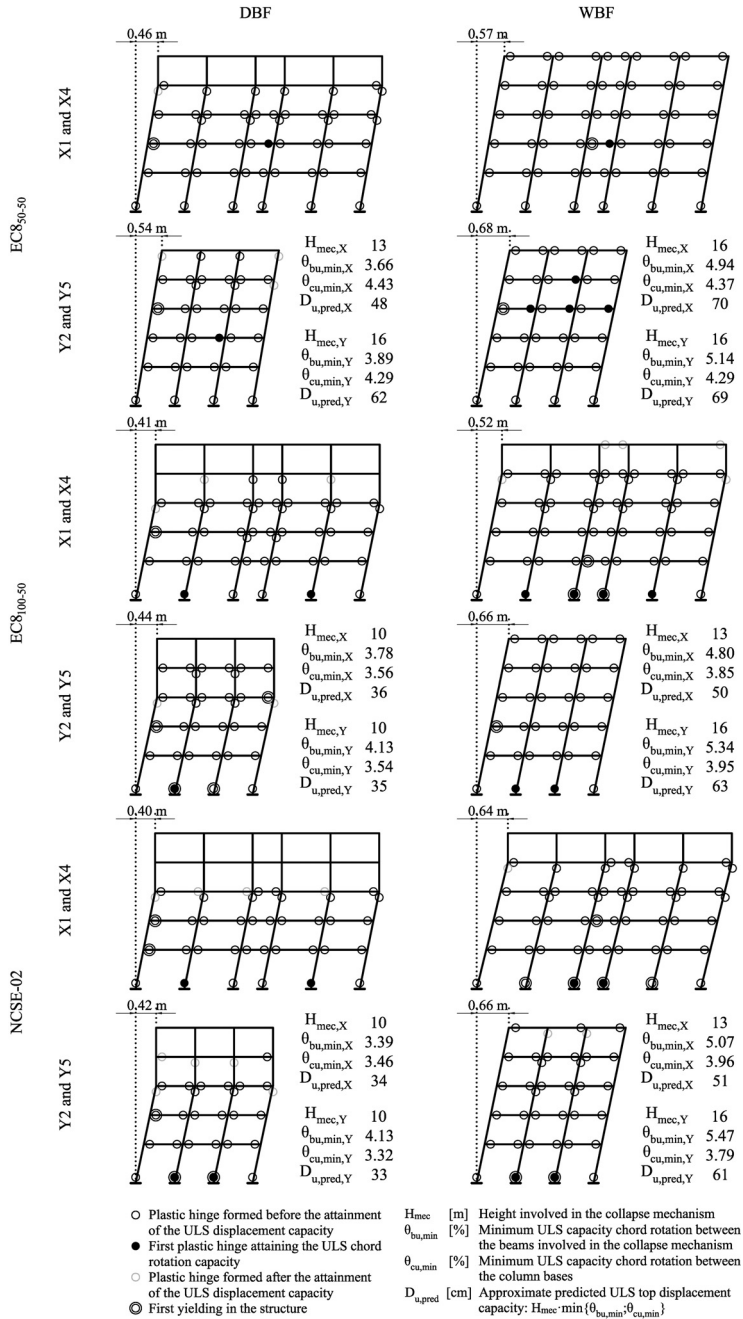


Figure 129: Mechanisms of collapse for “MODE” lateral load distribution

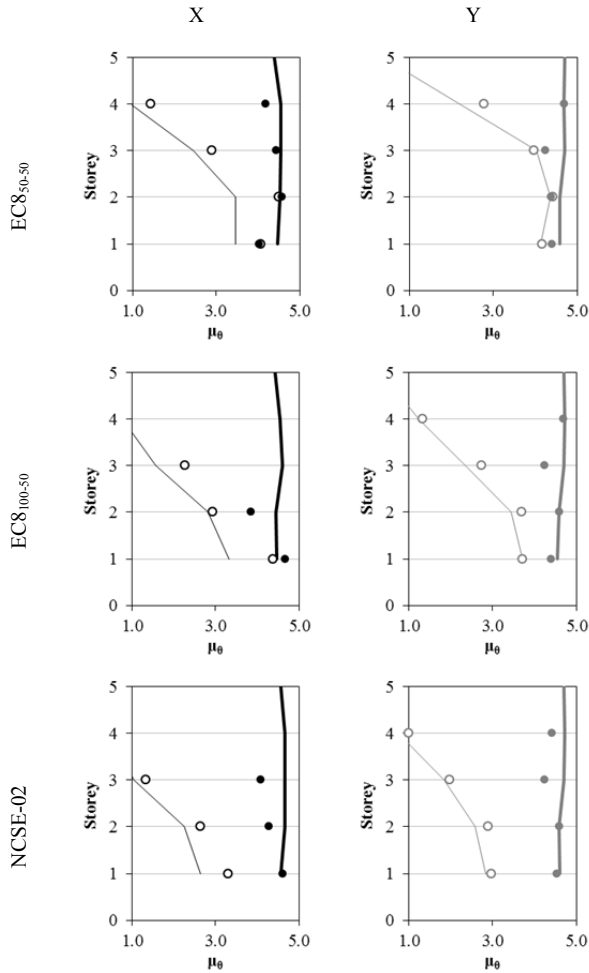


Figure 130: Mean ductility exploitation and capacity of beams in each storey of EC8 models at collapse, for DBF

In Figure 130 and Figure 131, the different degrees to which local ductility of beams are exploited in the collapse mechanism are plotted. It can be observed how far the beams from their ULS capacities are, and which design alternative is more likely to cause higher exploitation. In all the cases, the use of beam ductilities is lower in the X-direction, due to the presence of short-span beams which reach their capacities faster than the rest. In general, WBF show higher mean values of

exploited ductility with respect to DBF, because larger section of columns lead to higher θ_{ULS} .

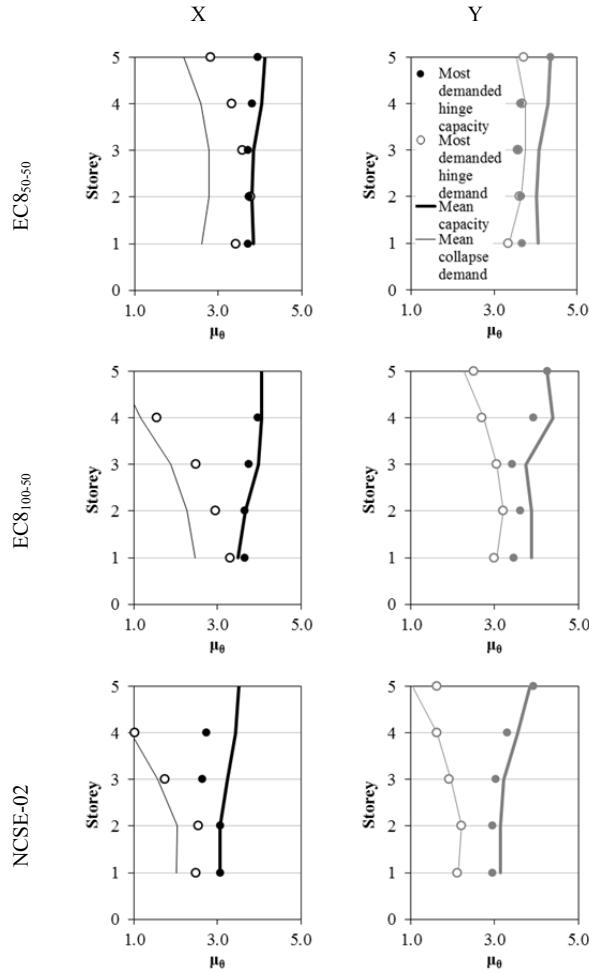


Figure 131: Mean ductility exploitation and capacity of beams in each storey of EC8 models at collapse, for WBF

In Figure 132, pushover curves are plotted. All of them are substantially tri-linear, like direct transposition of bending moment-chord rotation local envelopes,

because singular attainments of the hinges (cracking and to a lesser extent yielding) occur at similar steps, given the similar design overstrengths of the sections. This is also the cause of the proximity of first yielding corresponding to both directions. In most cases, ULS capacity of frames is attained before the complete formation of the collapse mechanism. Although most of the attainments of yielding are concentrated in the time –the transition from the “cracked” slope to the quasi-horizontal one is very quick—, the last hinges necessary to form the mechanism are created with a significant delay, even if in these cases the base shear increase is non-significant. So, local ductility capacity is exhausted beforehand. Pushover curves are transformed into bilinear ones by means of the procedure suggested by EC8, considering the ULS capacity point as the target one (Figure 132).

3.6.3 Assessment of capacities

Spectral N2 method is used in order to assess performances and peak ground acceleration capacities (PGA_c) of all the structures. Bilinear pushover curves are expressed as capacity curves in the acceleration-displacement response spectrum (ADRS) format. Only “MODE” distribution results are considered, as rather similar relative capacities between both structural types are obtained for “MASS” cases. Results are shown in Table 36 and ADRS graphical format in Figure 133 and Figure 134. Effective periods (T_{eff}) and their corresponding spectral effective acceleration demand ($S_a(T_{eff})$) are obtained. This demand is compared with the real elastic spectral acceleration of design ($S_{ae}(T)$, see Table 35) in order to obtain the contribution (R_D) of stiffness degradation to behaviour factor of capacity.

Capacity curves (plotted together in Figure 135a) are defined by their maximum spectral acceleration capacity (C_s) and yielding and maximum spectral displacement capacity (S_{dy} and S_{du} , respectively). Spectral acceleration corresponding to first structural yielding and C_s , together with the spectral acceleration of design ($S_{ad}(T)$, see Table 35), are necessary to obtain overstrength ($R_S = R_a \cdot R_o$, being the first factor the ratio between C_s and the acceleration corresponding to first structural yielding, and the second factor the ratio between the last magnitude and $S_{ae}(T)$). Ductility contribution (R_μ) is obtained by means of the R_μ - μ - T relationship suggested in EC8, and IN2 curves are obtained (Dolšek and

Fajfar, 2004b). Then, capacity values of $q=R_w \cdot R_a \cdot R_\mu \cdot R_D$ are obtained. Finally, PGA_c is calculated as the “anchorage” acceleration value of the spectrum passing through the spectral acceleration capacity at T_{eff} . Finally, safety factors $SF=PGA_c/PGA_d$ (Figure 135b) can be obtained for each design alternative.

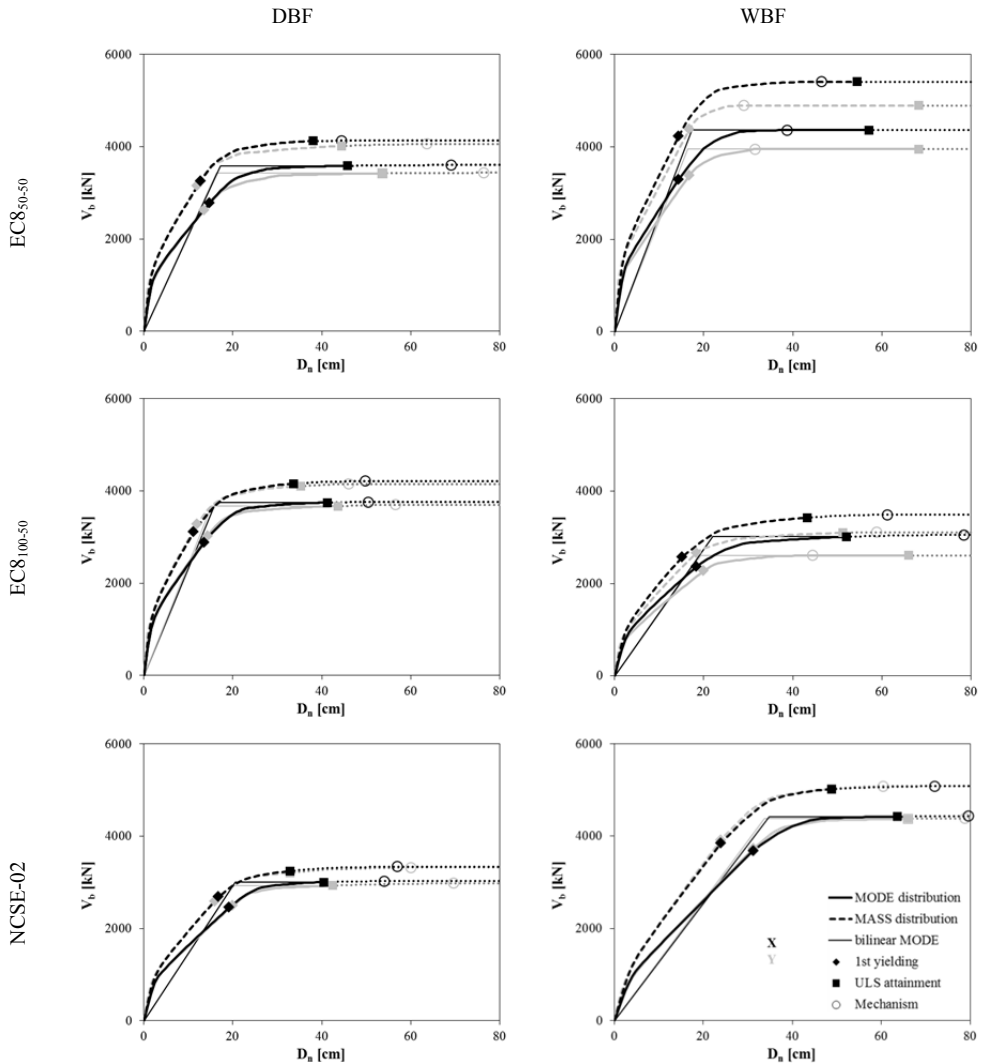


Figure 132: Pushover curves of each model

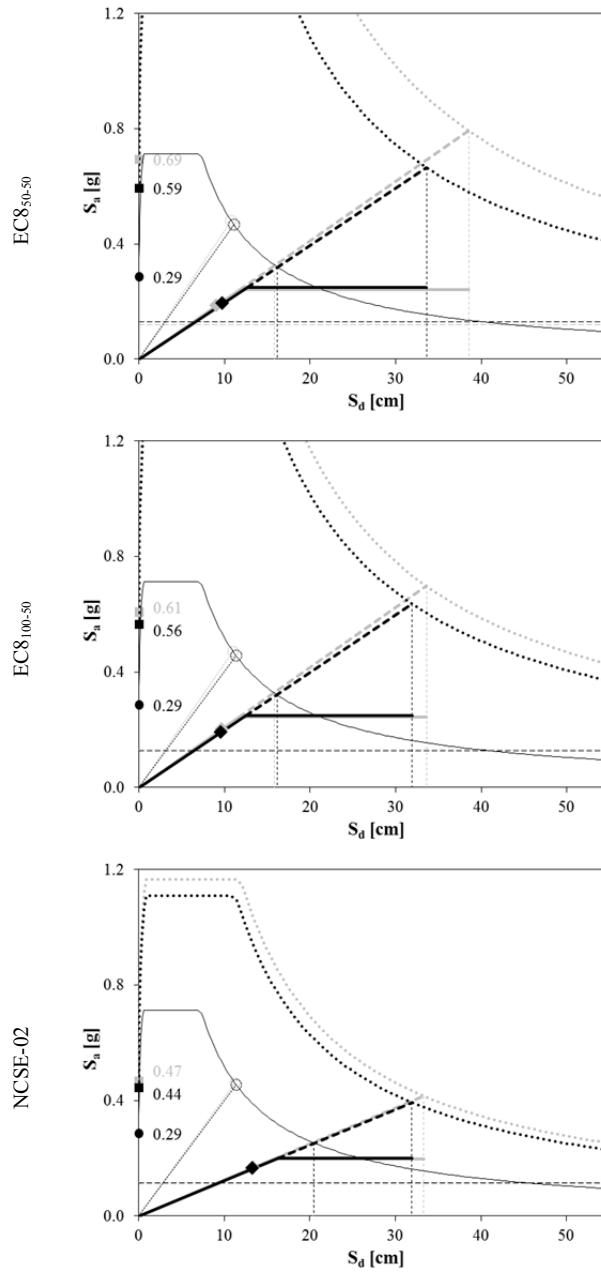


Figure 133: ULS spectral performance and maximum capacity of each model, obtained with N2 method, for DBF

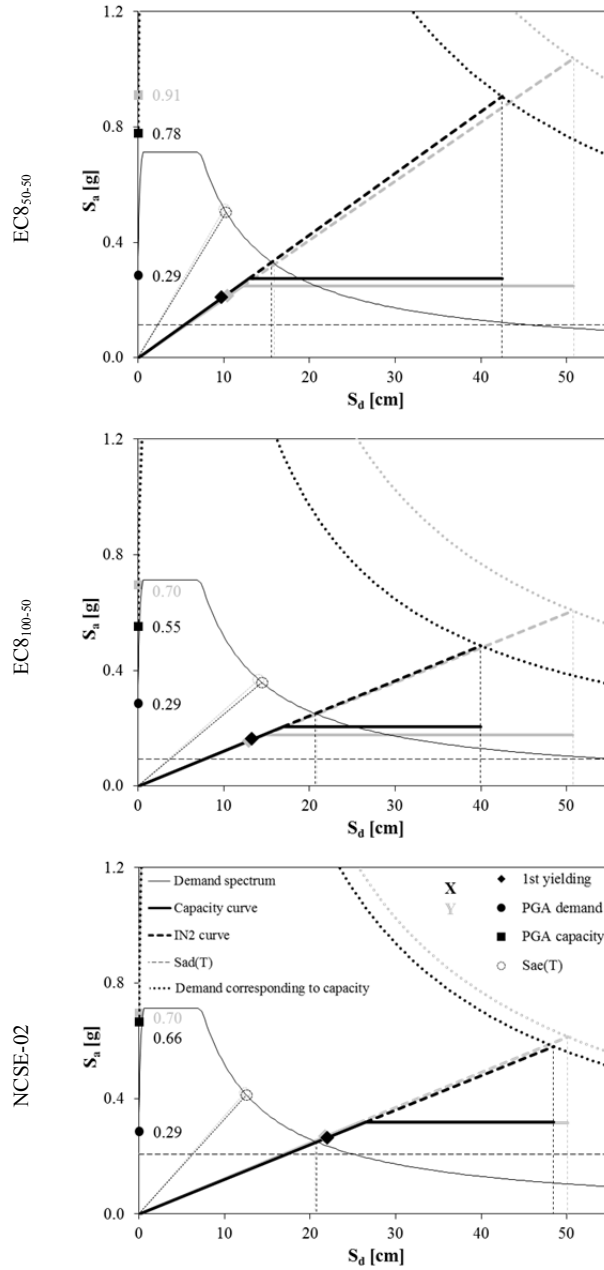


Figure 134: ULS spectral performance and maximum capacity of each model, obtained with N2 method, for WBF

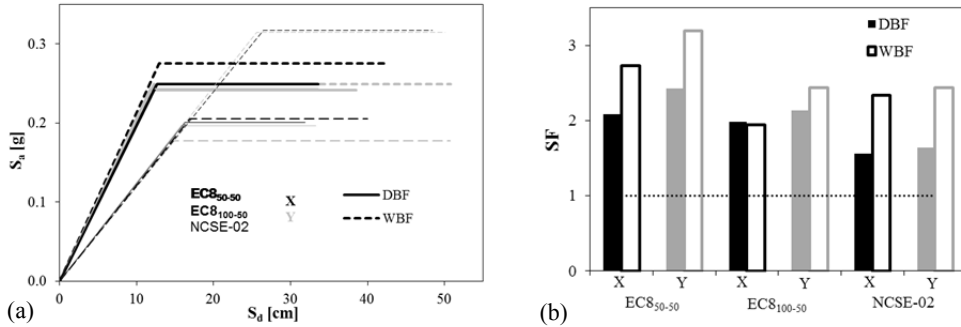


Figure 135: Bilinear capacity curves (a) and global safety factor (b) of all the models

Table 36: Performance properties for each model

MODEL	Bilinear capacity curve										Overstrength					
	T_{el} [s]	T_{eff} [s]	T_{eff}/T_{el} -	C_s [g]	S_{dy} [cm]	S_{du} [cm]	$S_d(T_{eff})$ [g]	R_w -	R_α -	R_D -	q -	PGA_c [g]	SF -			
EC8 ₅₀₋₅₀	DBF	X	0.65	1.43	2.19	0.249	12.6	33.6	0.320	1.51	1.29	2.67	1.87	9.73	0.59	2.08
		Y	0.63	1.40	2.21	0.242	11.8	38.6	0.326	1.57	1.30	3.28	1.69	11.38	0.69	2.43
	WBF	X	0.60	1.37	2.28	0.275	12.9	42.5	0.332	1.84	1.32	3.30	1.99	15.96	0.78	2.73
		Y	0.59	1.40	2.38	0.249	12.2	50.8	0.325	1.87	1.17	4.17	2.06	18.69	0.91	3.19
EC8 ₁₀₀₋₅₀	DBF	X	0.67	1.42	2.13	0.248	12.5	31.9	0.321	1.50	1.30	2.56	1.86	9.27	0.57	1.98
		Y	0.65	1.39	2.16	0.243	11.7	33.6	0.328	1.54	1.21	2.87	1.87	9.97	0.61	2.13
	WBF	X	0.85	1.82	2.14	0.205	16.9	40.0	0.250	1.73	1.27	3.27	2.17	11.33	0.55	1.94
		Y	0.83	1.84	2.22	0.177	14.9	50.8	0.248	1.65	1.15	3.42	2.21	14.27	0.70	2.44
NCSE-02	DBF	X	0.95	1.81	1.91	0.200	16.3	31.9	0.252	1.44	1.22	1.96	1.80	6.23	0.44	1.56
		Y	0.93	1.80	1.92	0.196	15.7	33.3	0.254	1.45	1.17	2.12	1.82	6.55	0.47	1.64
	WBF	X	1.05	1.83	1.75	0.317	26.5	48.5	0.249	1.28	1.20	1.83	1.65	4.67	0.67	2.33
		Y	1.03	1.81	1.77	0.314	25.6	50.1	0.252	1.28	1.17	1.96	1.66	4.88	0.70	2.44

Similar overstrengths (Table 36) are obtained for all the cases, while NCSE-02 frames show lower ductility. In general, low inelastic penetration in ULS is required to all the buildings (Figure 133 and Figure 134), especially in NCSE-02 WBF, which remain in equivalent elastic field. Magnitudes of the different sources of overstrength are coherent with the design assumptions and literature. R_w is 1.56 on average, slightly higher with respect to the steel overstrength of 1.45, while R_α is mean 1.23, slightly lower than $\alpha_u/\alpha_1=1.30$ proposed by EC8. R_D (mean 1.89) corresponds to mean period elongation T_{eff}/T_{el} equal to 2.21 for EC8 frames and 1.84 for NCSE-02 ones; such difference is caused by the higher reinforcement ratio of sections of NCSE-02 frames (Table 33). Thus, mean K_{eff}/K_{el} is 0.20 (EC8) and 0.30 (NCSE-02), which in both cases is lower than the assumed value for ULS design (50%). It is worth noting that 0.20 is also the mean value for secant-to-

elastic stiffness ratio for members suggested in Panagiotakos and Fardis (2001), thus in this particular case the extrapolation from local to global may be possible.

Regarding the relative performances of WBF and DBF, WBF show similar or even greater capacities with respect to DBF in all the cases (Table 36, Figure 133 and Figure 134): SF of WBF are 31%, 6% and 49% higher than those for DBF on average, in the case of EC8₅₀₋₅₀, EC8₁₀₀₋₅₀ and NCSE-02, respectively. Moreover, if no reduction of q due to irregularity in EC8-DBF had been adopted, still better relative performances would have been expected for WBF. The causes of such good performances of WBF are: (i) $H_{mec,W/D} \geq 1$ (see Figure 132); (ii) higher $\theta_{u,min,W/D} \geq 1$ (Figure 125 and Figure 126), due to $h_{b,W/D} \leq 1$ and $L_{Vc,W/D} \geq 1$ (see Table 33); (iii) sufficient stiffness of WBF; and, only for NCSE-02 frames, (iv) higher elastic displacement capacity due to design q lower than DBF.

T_{eff} of WBF (Table 36 and Figure 135a) show similar values than DBF for EC8₅₀₋₅₀ and NCSE-02. In EC8 buildings it is an expected result, since DLS design is the critical condition; while for NCSE-02, such low difference in periods is likely a coincidence, because the increment of stiffness is not a target, but a secondary consequence of the increment of strength, in turn depending on whether such increment is achieved by means of bigger sections of higher reinforcements. Conversely, EC8₁₀₀₋₅₀ WBF show higher T_{eff} with respect to DBF.

Such values of T_{eff} correspond to mean values of K_{eff} 16% lower than those obtained assuming rigid joints, which is very close to the experimental value of secant-to-1% stiffness (17%) observed in DBF (De Risi et al., 2014). On the other hand, the strategy of modelling employed herein returns values of K_{eff}/K_{el} 11% higher for WBF rather than for DBF, which is able to represent the lower stiffness degradation of WBF due to lower shear deformability (LaFave and Wight, 2001), given that the contribution of reinforcement is explicitly modelled. This contribution may be the cause of the different period elongation of WBF and DBF: 6% and 2% higher for EC8₅₀₋₅₀ and EC8₁₀₀₋₅₀, respectively, and conversely 8% lower for NCSE-02. Those results are consistent with relative reinforcement ratios of sections between WBF and DBF (Table 33). In EC8 frames, lower reinforcements in WBF are caused by higher q due to regularity, overstrength of columns due to DLS design and lower flexural demand on beams due to cantilever

behaviour (Figure 123); conversely, in NCSE-02, higher reinforcements in WBF are caused by lower q together with the absence of DLS design.

Concerning deformed shape of buildings corresponding to the performance point of ULS demand, in comparison with the design deformed shape, higher “cantilever behaviour” is observed in EC8₅₀₋₅₀ frames because of the presence of fix-end bases (Figure 136). In the rest of the cases similar behaviour is observed between linear design and nonlinear performance except for NCSE-02 wide-beam frames. The last is consequence of the very high reinforcement ratio of first storey columns in comparison with the rest of the storeys.

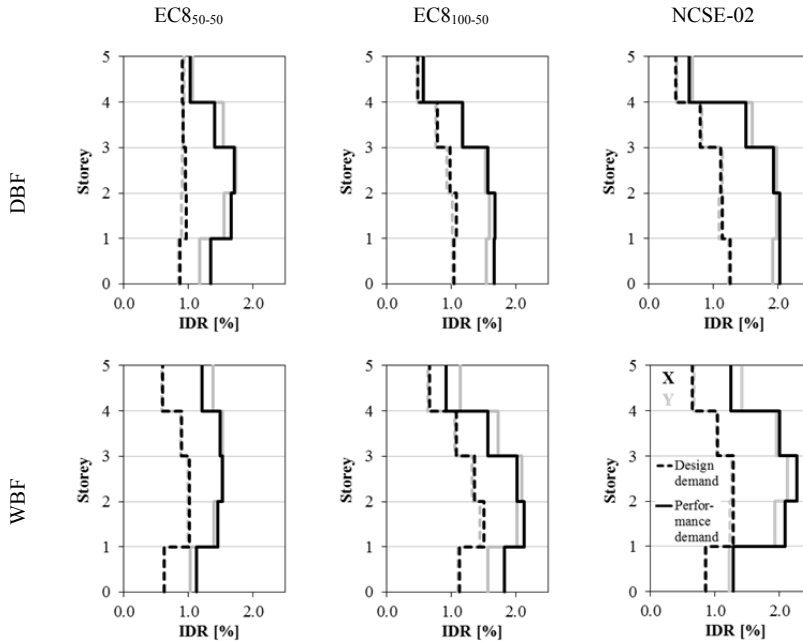


Figure 136: Interstorey drifts demands corresponding to design to ULS and performance corresponding to the design demand, for each model

On the other hand, assessment of DLS performance of EC8 frames –by adopting bilinear capacity curves until first structural yielding– (Figure 137) suggest that, at least in this particular case study, assuming 100% of the gross

elastic stiffness for members might not be appropriate. Mean value for stiffness degradation is 55%, which is slightly higher than 50% assumed in EC8₅₀₋₅₀ structures but much higher than 0% assumed in EC8₁₀₀₋₅₀ ones. In fact, in all the cases DLS is not satisfied but in EC8₅₀₋₅₀ buildings the capacity is very close to the demand.

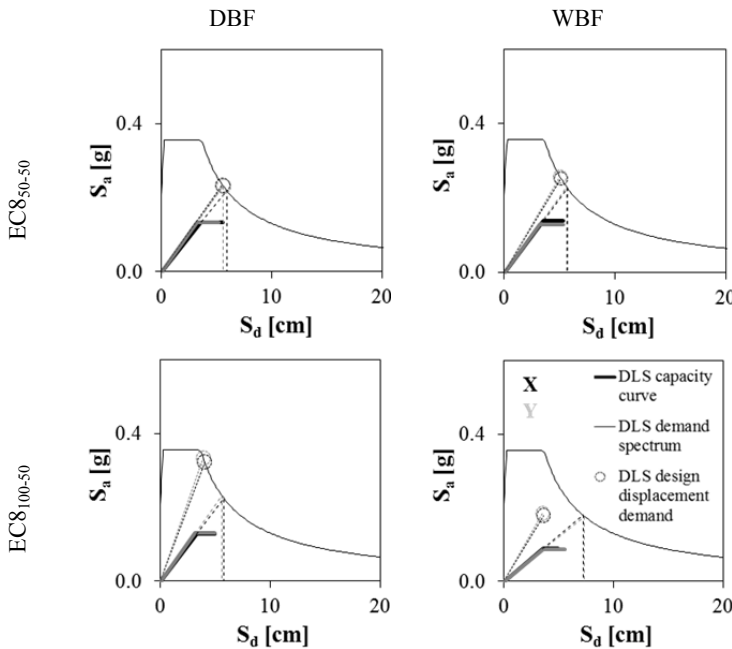


Figure 137: DLS spectral performance of EC8 models

Besides, structures with infill panels could also present some yielded hinge when subjected to demand assigned to DLS, which is half of the demand corresponding to ULS for EC8. In general, IDR limitation is intended to provide structures which remain in pre-yielding regime when performing to DLS. However, this is hard to achieve in structures designed to DCH because the behaviour factors of design (usually greater than 4.0) are much higher than the decrease of demand for DLS with respect to ULS (2.0).

Hence, the difference between those factors must be overcome by the overstrength sources R_o (ratio between first yielding and design spectral accelerations) and $R_{D,y}$ (ratio between demands corresponding to design period and effective period corresponding to a bilinearisation until the first yielding), as seen in Figure 138. This period may be intermediate between $T_{eff,DLS}$ and T_{eff} . In the case study, mean values for the safety factor regarding yielding are 0.79 and 1.23 corresponding to $T_{eff,DLS}$ and T_{eff} , respectively; thus, yielding might occur.

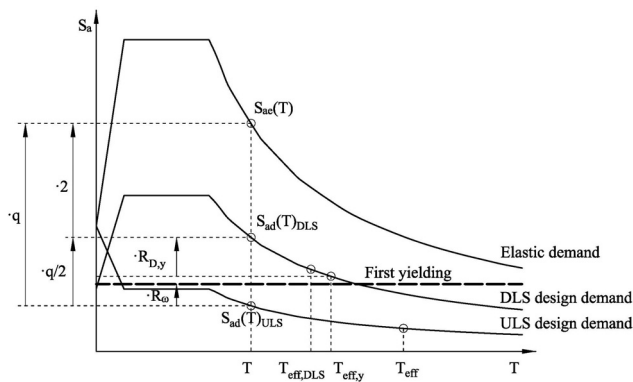


Figure 138: Scheme of pre-emptive yielding occurrence when performing to DLS demand

3.7 COMPLEMENTARY ASSESSMENT OF PARAMETRIC SET OF FRAMES

The previous results, corresponding to three different design alternatives and two directions of analysis, suggest that: (i) WBF designed to DCH, adopting similar q than DBF and satisfying different DLS limitations, may provide similar capacities than DBF; and (ii) WBF designed to DCL, adopting much lower q than DBF and without satisfying any DLS limitations, may provide larger capacities than DCL. Thus, code limitations of q for WBF could not be justified in some cases. In order to evaluate whether such conclusion could be generalised to RC-MRF residential building stock designed according to different codes, a higher set of case studies may be evaluated.

Hence, a parametric design is carried out, resulting in 72 different planar frames, corresponding to 12 couples of WBF and DBF with different geometry and designed to low and high seismicity complying three different codes: EC8, NTC and NCSE-02. In each code, q corresponding to DCH is assumed also for WBF. EC8 represents the most favourable code for WBF due to its strict reduction of member stiffness ($E_c I_c$) for DLS design (50% of the elastic one). Frames corresponding to NTC are designed assuming uncracked stiffness of members (thus rather equivalent to design EC8₁₀₀₋₅₀, see section 3.5.2), in order to ensure that, even in the most unfavourable situation for WBF allowed by the code, they are able to perform satisfactorily. Frames corresponding to NCSE-02 have no design to DLS but in this case similar q are adopted for WBF and DBF, in order to check if also codes with no IDR limitation are able to remove the prevention for WBF regarding q .

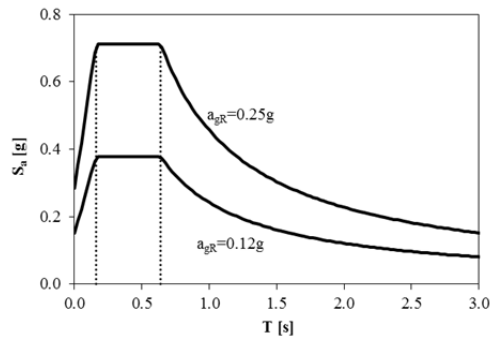


Figure 139: Elastic horizontal demand acceleration spectrum corresponding to both levels of a_{gR}

Aimed at covering the widest possible range of situations of design, a parametric study based on relevant design features is carried out, assuming different realisations for each parameter; number of storeys (n): 3, 6 and 9; spans (L): 3.5 and 5.5m, i.e. a representative range for residential buildings in the Mediterranean area (Cosenza et al., 2005); and two design PGA on rock (a_{gR}): 0.12g and 0.25g. Elastic spectra (Figure 139) are obtained in analogy with that in section 3.5.1, and similar material mechanic properties and design strategies are

adopted. Geometry of the frames is shown in Figure 140; all of them have four bays with similar spans, and interstorey heights are 3m except for ground storey, which is 4m.

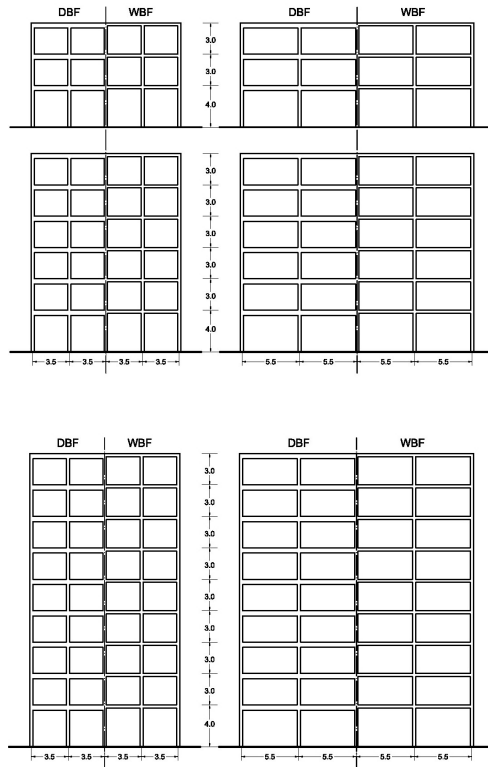


Figure 140: Geometry of the different frames of the set

In this case, the assessment is carried out by means of the simplified approach proposed in section 3.4, aimed at a reduction of the computational demand. In Table 37, predicted values of $SF_{W/D} = H_{mec,W/D} \cdot \theta_{u,min,W/D} / (\Gamma_{W/D} \cdot T_{el,W/D})$ corresponding to the EC8 frames of the specific case study are compared with the real ones, considering similar H_{mec} for both typologies. Results show that underestimation of $SF_{W/D}$ with respect to real values is only 4% on average, which is conservative for the assessment of WBF.

Table 37: Estimated and real ratios between capacities of WBF and DBF for EC8 frames belonging to the specific case study, considering similar H_{mec} for both typologies

MODEL		$\theta_{u,min,W/D}$	$T_{el,W/D}$	$\Gamma_{W/D}$	$SF_{W/D,estimated}$	$SF_{W/D,real}$
EC8 ₅₀₋₅₀	X	1.20	0.92	0.99	1.31	1.19
	Y	1.10	0.93	0.97	1.22	1.31
EC8 ₁₀₀₋₅₀	X	1.08	1.28	1.01	0.84	0.91
	Y	1.12	1.28	1.00	0.87	0.97

Results of design are presented in Table 38, where: subscript l and n refer to the l^{th} storey; c and b refer to column and beam, respectively; $\theta_{u,min}$ is the minimum θ_u between members involved in the collapse mechanism; f_{conf} is the confinement contribution to θ_u ; and $f_{K,sec}$ is the ratio between the stiffness degradation of connections in WBF with respect to DBF. Results confirm the trends observed in the specific case studies. DLS is likely to be the critical condition of design for WBF rather than DBF. For frames designed according to EC8, this is the most frequent critical condition for both types, except for some cases of low seismicity. For NTC frames, the critical condition is DLS for high seismicity and gravitational situation for low seismicity. Conversely, for NCSE-02 frames, seismic situation is the critical one in most cases, due also to the lower q corresponding to DCH. In general, capacity design of columns in WBF does not often affect the dimensions because of the higher overstrength due to DLS design.

Beams dimensions are generally conditioned by gravitational deflection limitation in the case of large spans and by seismic situation for short spans. For frames with large spans designed to EC8 and NTC in high seismicity, high depths are required for WB: up to 350mm, which can be considered as a cost-effective limit for such beams. Moreover, in these frames very large depths of columns are required (up to 900mm), and it may not be possible to reduce them very much in higher storeys, because WB present also large width due to DLS limitation, and thus large widths of columns are required in order to satisfy width limitation of WB. The last condition not only determines depth of columns but also widths, so it may not be possible in most of cases to place “wall-type” columns along non-structural walls. Hence, WBF may not be a feasible cost-effective solution for such situations.

Regarding chord rotations, $\theta_{ub,min,W/B}$ (mean 1.29) is lower than value (1.38) obtained both in the specific case study and in the numeric analysis carried out in section 3.3.2. This is only due to lower values of $h_{b,W/D}$ (see Table 39), given that confinement contribution is 1.11 times higher for WB, similar in all three studies. Such lower $h_{b,W/D}$ is caused by the adoption in the actual procedure of small depths of DB for low spans, which is not possible to be pursued in buildings with different spans because h_b is usually similar for all the beams and depends on the largest span of the building. On the other hand, $\theta_{uc,min,W/B}$ (mean 1.07 for EC8 and NTC and 1.02 for NCSE-02) is almost only proportional to L_V , which is larger for WBF than for DBF (mean 1.25 times for EC8 and NTC, and only 1.09 times for NCSE-02). Still, such values correspond to limited favourable influence of L_V in the performance of WBF with respect to DBF (not higher than 8% on average). Contributions of h_c , v and $f_{conf,c}$ are limited and balanced between them (Table 39). Notwithstanding the large values of L_V in columns of WBF, the critical element is always a beam, while for DBF it occurs only in 6 cases of 36, all of them corresponding to EC8. The last is due to higher transverse reinforcement in columns rather than in NTC, causing larger $f_{conf,c}$ in EC8 (1.28) rather than in NTC (1.14), on average.

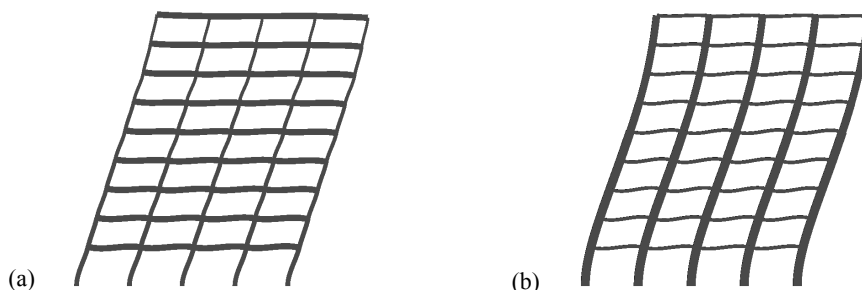


Figure 141: Deformed shape for seismic situation of DBF (a) and WBF (b) with $n=9$ and $L=5.5\text{m}$ designed to EC8 for $a_{gR}=0.25g$

With respect to T_{el} , WBF whose critical condition is DLS design not only can show similar T_{el} than DBF but also lower, especially in the case of high seismicity. Again, the reason is the greater cantilever behaviour and the required high

dimensions in upper storeys, as it is shown in previous specific case study EC8₅₀₋₅₀ and in Figure 141: DBF can be designed to show almost linear deformed shape, thus each storey show similar IDR, slightly lower than the limit; conversely, in WBF the storeys in the central part rules completely the design, thus top and bottom storeys show higher stiffness than corresponding storeys of DBF. The above effect causes lower T_{el} but not as much as it would correspond to the increment of global stiffness, because the requirement of greater structural members can increment total mass up to 25%. Hence, almost all the couples designed according to EC8 and NTC show $T_{el,W/D} \approx 1$ (with an upper-bound tolerance of 5%), even for some cases in which DLS design is not the critical condition. Only two out of 12 couples for each code show periods up to 25% higher for WBF than DBF. Conversely, most NCSE-02 couples (nine out of 12) show $T_{el,W/D} > 1$ (1.14 on average) (Table 39). On the other hand, such different deformed shape implies values of Γ slightly lower for WBF than for DBF, as observed in the specific case study.

Finally, assessment of relative performance between WBF and DBF –i.e. values of $SF_{W/D}$ — are carried out by means of the simplified approach presented in section 3.4. Two several unfavourable assumptions for WBF are considered: neither the likely higher number of storeys involved in the mechanism nor the lower stiffness degradation of connections are taken into account. Hence, favourable results for WBF can be considered so by a significant safety margin, while unfavourable ones may not be classified as unfavourable with a detailed analysis.

Results are presented in Figure 142. EC8 and NTC show mean values of $SF_{W/D}$ favourable to WBF (1.08 and 1.02, respectively, see Table 39), while for NCSE-02 mean performance is poorer for WBF than for DBF (mean 0.91). In EC8, only two cases with $T_{el,W/D} > 1.0$ show $SF_{W/D} < 1.0$, thus in 83% of the cases WBF show better performance than DBF. For NTC the ratio decrease until 50%, because some couples with $T_{el,W/D} > 1.0$ show $SF_{W/D} < 1.0$. Conversely, every single couple designed to NCSE-02 show $SF_{W/D} < 1.0$. It is worth noting that dispersion of values is very low (coefficients of variation are 10% for EC8 and NTC and only 5% for NCSE-02), thus likely correlations between q adopted in design and the use of one or another structural typology could be suitable.

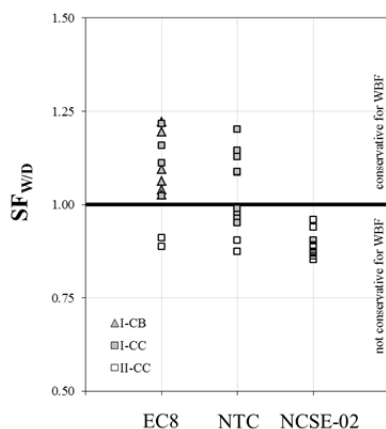


Figure 142: Estimated relative performance between WBF and DBF ($SF_{W/D}$) for each code considering $H_{mec,W/D} = f_{k,sec} = 1.0$

The cause of the satisfactory performance of WBF in EC8 and NTC (also without any consideration of the contribution of $H_{mec,W/D}$) is that they almost always show sufficient stiffness, and whenever it is lower than stiffness of DBF, the difference is so small that it gets largely overcome by the combination of the other minor contributions. Thus, it could be concluded that, within the actual framework of Italian NTC, the design of WBF to DCH, adopting the corresponding q , could be allowed without any further prevention than local geometric limitations in connections. Regarding NCSE-02, it is not possible to state with enough confidence that q limitations for WBF can be removed within the actual framework, which does not provide any DLS design. Anyway, such conclusions may not be considered as demonstrated statements, because they are based in a limited number of analysis and also because the strategies of design reflect always personal choices.

Notwithstanding the mean satisfactory performance of WBF, even better than DBF, it is worth noting that in some cases they may not be cost-effective or even feasible. However, the adoption of one or another system should be a decision of the designer, without any further penalisation of the code as lower q .

3.8 ULTIMATE CHORD ROTATION OF WIDE BEAMS

In the previous sections, it is shown that wide beams (WB) usually show greater ultimate chord rotation than deep beams (DB). Also, it is proved that, in some cases (e.g. frames designed to EC8 or frames with very short spans), such increment can be very favourable to wide-beam frames (WBF), likely causing higher global capacities for WBF than for deep-beam frames (DBF).

Still, those conclusions are based in several assessment carried out by means of nonlinear models with lumped plasticity, in which ultimate chord rotation of all members (columns and beams) are obtained through the empirical formulation proposed by EC8 part 3 (CEN, 2005), which is shown in Equation (66).

That formulation, as well as the rest of the formulations of EC8 part 3 regarding curvatures and chord rotations, are obtained as regressions of empirical tests on a database of more than 1500 specimens present in past literature, available in Biskinis (2007) and Biskinis and Fardis (2010a, 2010b). This database is an extension of the one used in Panagiotakos and Fardis (2001), which only includes rectangular full sections, resulting in 1012 specimens. In order to classify specimens as columns or beams, authors consider as columns the elements that satisfy one of those requirements: some axial load, symmetric reinforcement or square cross section. Thus, database is composed of 266 beams and 746 columns. Instead, if specimens with no axial load are considered as beams, the number of beams increase until 314. Anyway, reliability of the formulations may be likely lower for beams than for columns.

$$\theta_{u,EC8} = 0.016 \cdot 0.3^v \cdot \left[\frac{\max(0.01; \omega')}{\max(0.01; \omega)} f_c \right]^{0.225} \cdot \left(\frac{L_V}{h} \right)^{0.35} \cdot 25^{\alpha_{\omega_{sx}}} \cdot 1.25^{100\rho_d} \quad (66)$$

However, it is very important to note that, in almost all the cases, specimens are tested in the direction in which cross sections present higher stiffness, i.e. oriented as “deep” sections instead of “wide” ones. Only 11 columns and 37 beams show $h < b$, which is less than a 5% of the total database. Thus, the reliability of the formulations regarding wide sections could be questionable, and the

aforementioned conclusions regarding relative performances of WBF vs. DBF could not be supported anymore.

Aimed at evaluating if formulations are appropriate for WB, the beams of the database are disaggregated in two groups: DB (277, 88%) and WB (37, 12%). Then, experimental results corresponding to yielding curvature (ϕ_y), yielding and ultimate chord rotations (θ_y and θ_u , respectively) and chord rotation ductility (μ_θ) are compared with the predicted values given by the experimental-based formulations of: Panagiotakos and Fardis (2001), indicated with subscript *P&F*; Biskinis and Fardis (2010a, 2010b), indicated with subscript *B&F*. In order to extend the comparison, also formulations suggested by American code for existing buildings ASCE/SEI 41-06 are used, although their expressions have been extrapolated from a different database. Values of ϕ_y are also calculated by means of a fibre model which accounts for cracking of concrete, indicated with subscript *fib*. All the expressions are presented herein (Equations (67) to (73) and Table 40).

$$\phi_{y,P\&F} = \phi_{y,pred} = \phi_{y,s} = \frac{f_y}{E_s(1-\xi_y)d}; \quad \xi_y = \sqrt{n^2 A^2 + 2nB} - nA; \quad (67)$$

$$\begin{cases} A = \rho + \rho' + \rho_v \\ B = \rho + \rho' \frac{d'}{d} + 0.5\rho_v \left(1 + \frac{d'}{d}\right) \end{cases}$$

$$\theta_{y,P\&F} = \phi_y \frac{L_V}{3} + 0.0025 + a_{st} \frac{0.25\varepsilon_y d_{bL} f_y}{(d-d')\sqrt{f_c}} \quad (68)$$

$$\theta_{y,B\&F} = \phi_y \frac{L_V + a_v z}{3} + 0.0014 \left(1 + 1.15 \frac{h}{L_V}\right) + a_{st} \phi_y \frac{d_{bL} f_y}{8\sqrt{f_c}} \quad (69)$$

$$\theta_{y,ASCE} = \frac{M_y L_V}{3(0.3E_c I)} \quad (70)$$

$$\theta_{u,P\&F,emp1} = 0.01\alpha_{st}\alpha_{cyc} \left(1 + \frac{a_{sl}}{2.3}\right) \left[\frac{\max(0.01;\omega')}{\max(0.01;\omega)} f_c\right]^{0.275} \cdot \left(\frac{L_V}{h}\right)^{0.45} \cdot 1.1^{100\alpha_{\omega_{xx}}} \cdot 1.3^{100\rho_d} \quad (71)$$

$$\theta_{u,B\&F,emp1} = a_{st} \left[1 - \frac{a_{old}a_{cy}}{6}(1 - 0.05a_{pl})\right] (1 - 0.43a_{cy}) \left(1 + \frac{a_{sl}}{2}\right) \cdot \left[\frac{\max(0.01;\omega')}{\max(0.01;\omega)} f_c\right]^{0.225} \cdot \left[\min\left(9; \frac{L_V}{h}\right)\right]^{0.35} \cdot 25^{\alpha_{\omega_{xx}}} \cdot 1.25^{100\rho_d} \quad (72)$$

$$\theta_{u,ASCE} = \theta_{y,ASCE} + \theta_{pl,ASCE} \quad (\text{Values of } \theta_{pl,ASCE} \text{ from Table 40}) \quad (73)$$

Table 40: Values of θ_{pl} in ASCE/SEI 41-06

$s_i < d/3$ and $V_s > 0.75V_{pl}$ [Y/N]	$\frac{\rho - \rho'}{\rho_{bal}}$ -	$\frac{V_{pl}}{bd\sqrt{f_c}}$ -	$\theta_{pl,ASCE}$ [rad]
Y	≤ 0.0	≤ 3	0.025
		≥ 6	0.020
	≥ 0.5	≤ 3	0.020
		≥ 6	0.015
N	≤ 0.0	≤ 3	0.020
		≥ 6	0.010
	≥ 0.5	≤ 3	0.010
		≥ 6	0.005

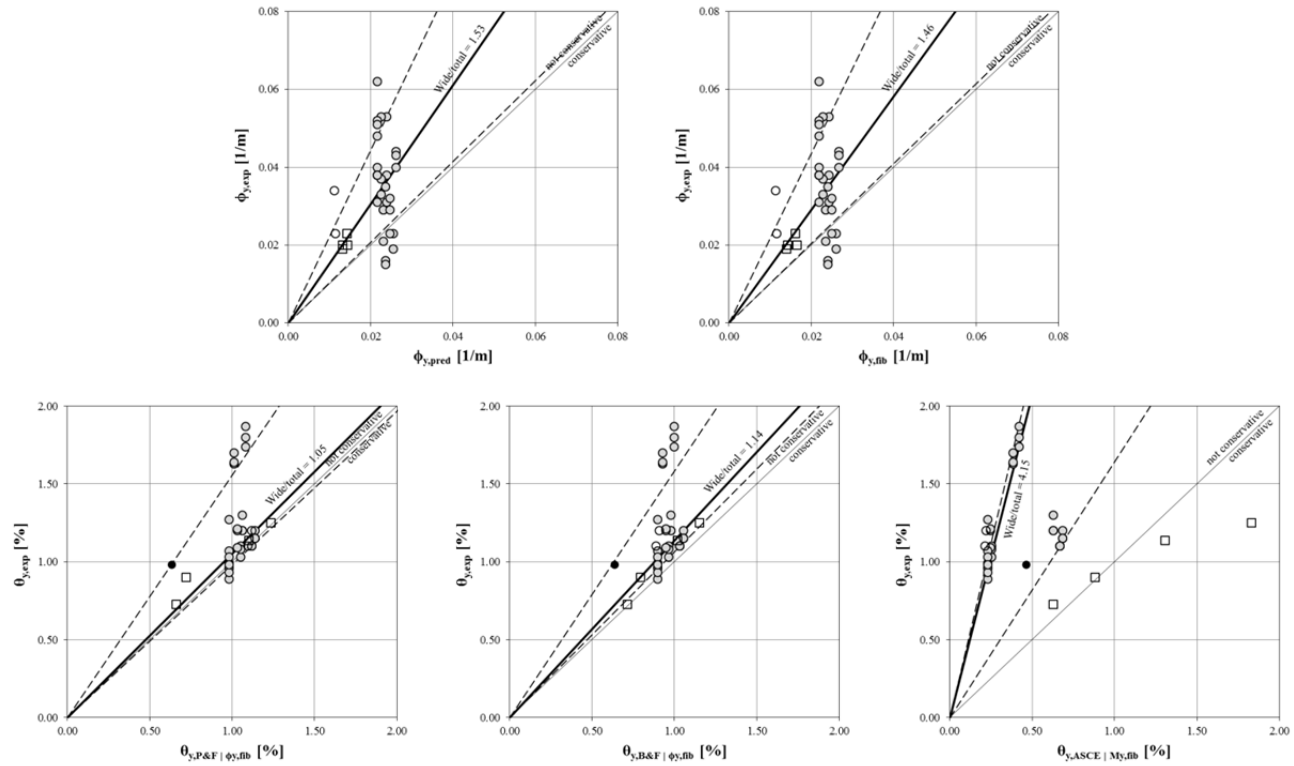


Figure 143: Predicted vs. experimental values of ϕ_y and θ_y for WB

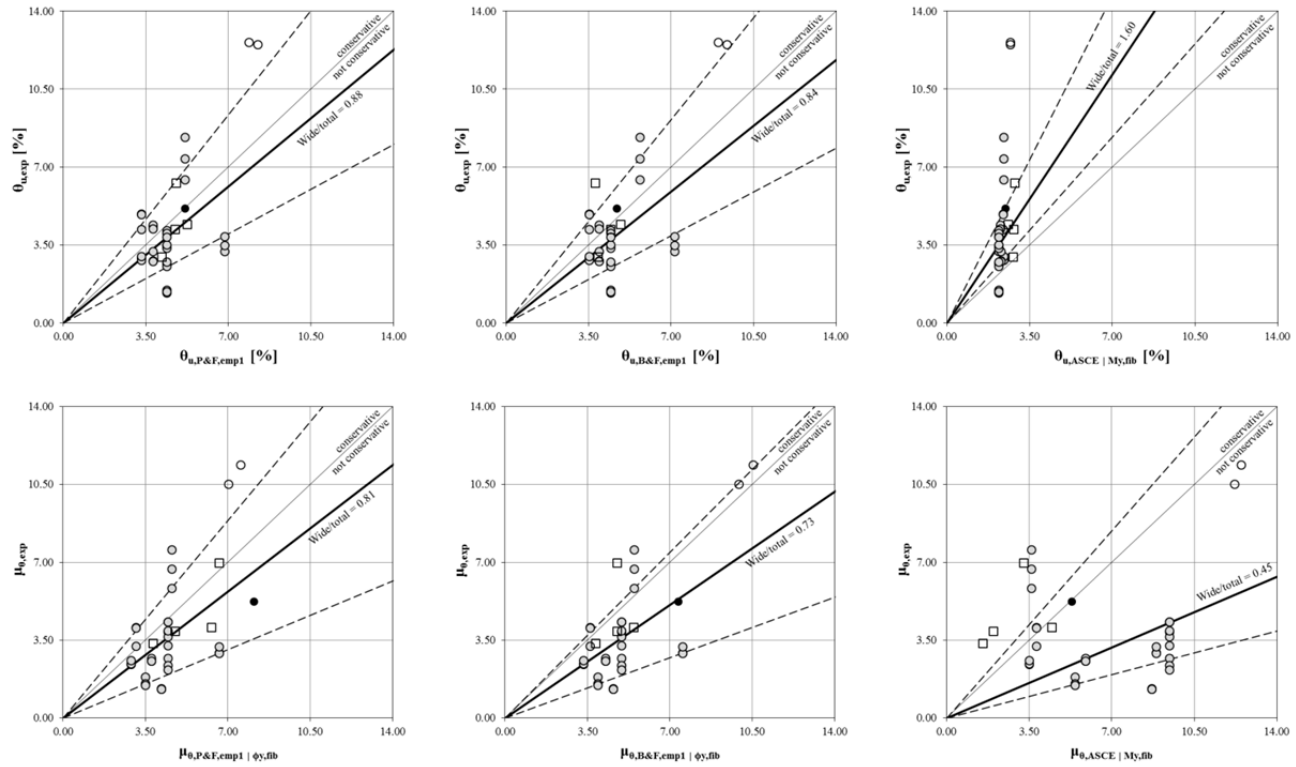


Figure 144: Predicted vs. experimental values of θ_u and μ_0 for WB

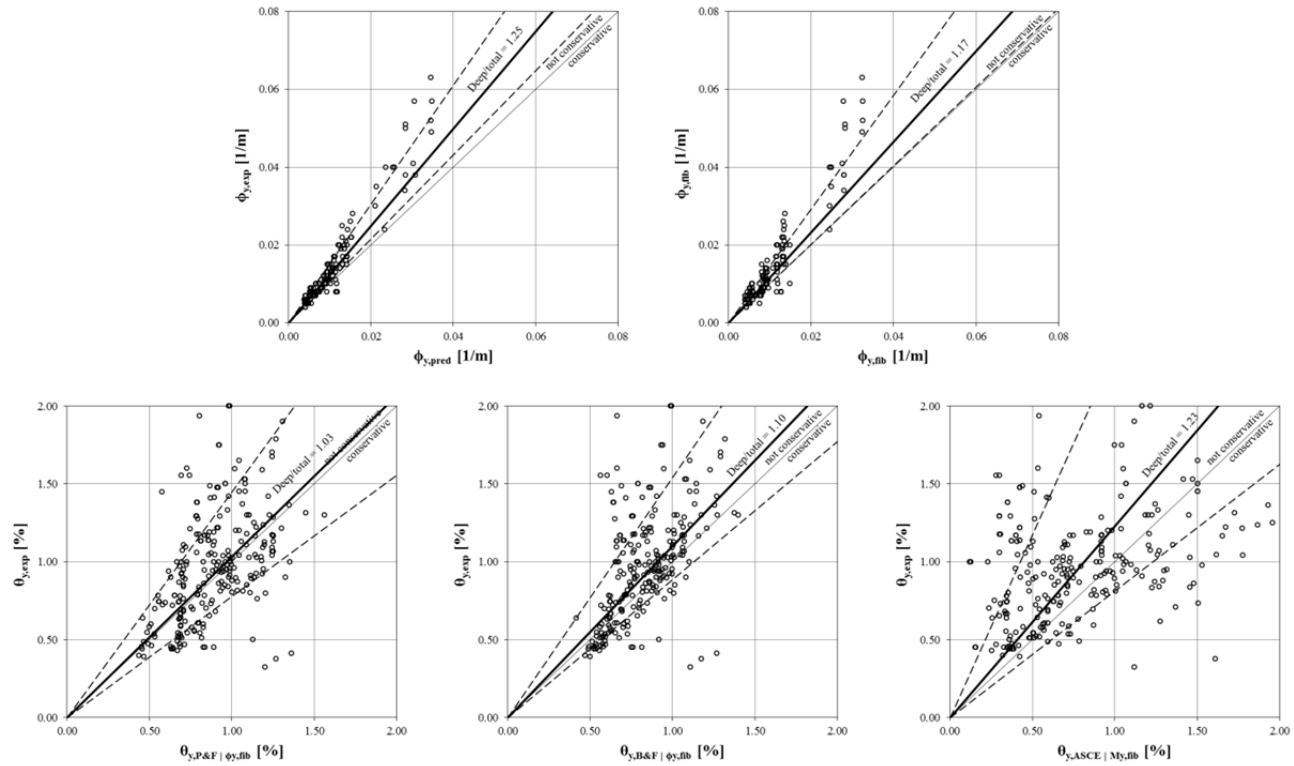


Figure 145: Predicted vs. experimental values of ϕ_y and θ_y for DB

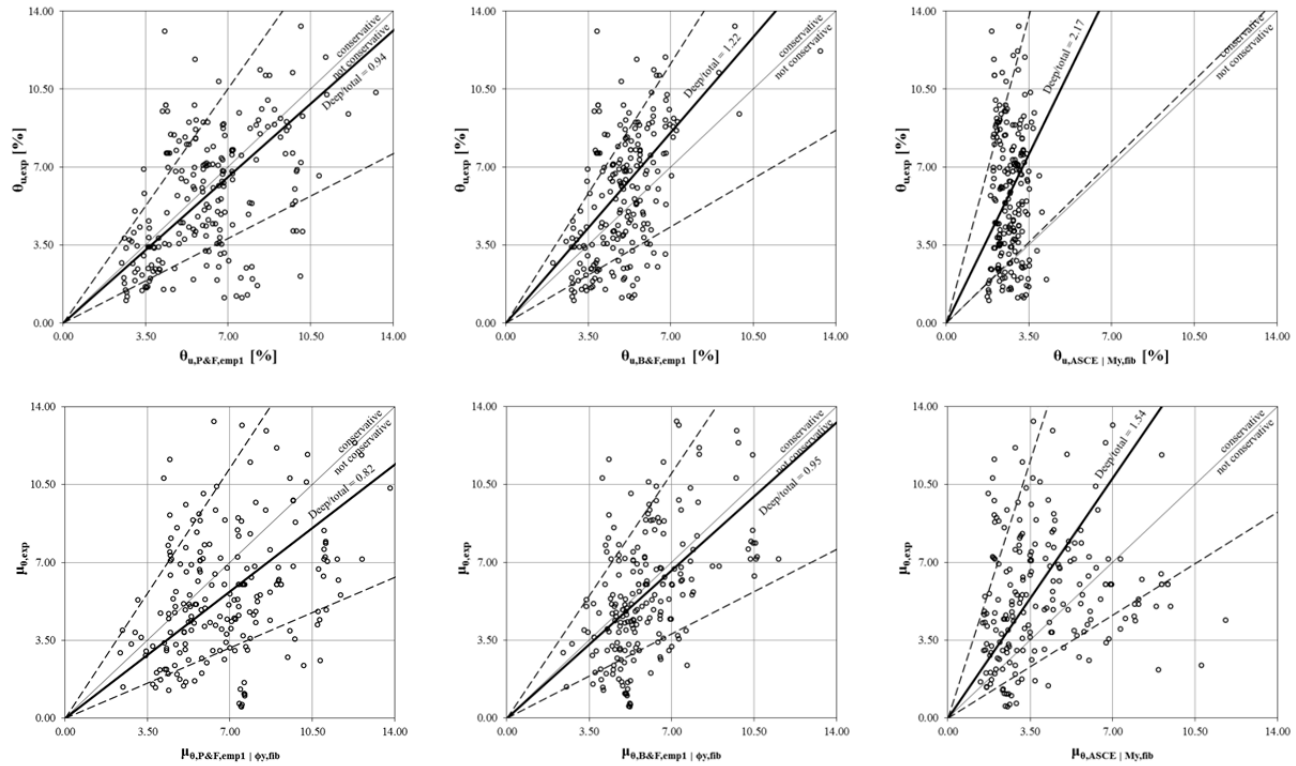


Figure 146: Predicted vs. experimental values of θ_u and μ_0 for DB

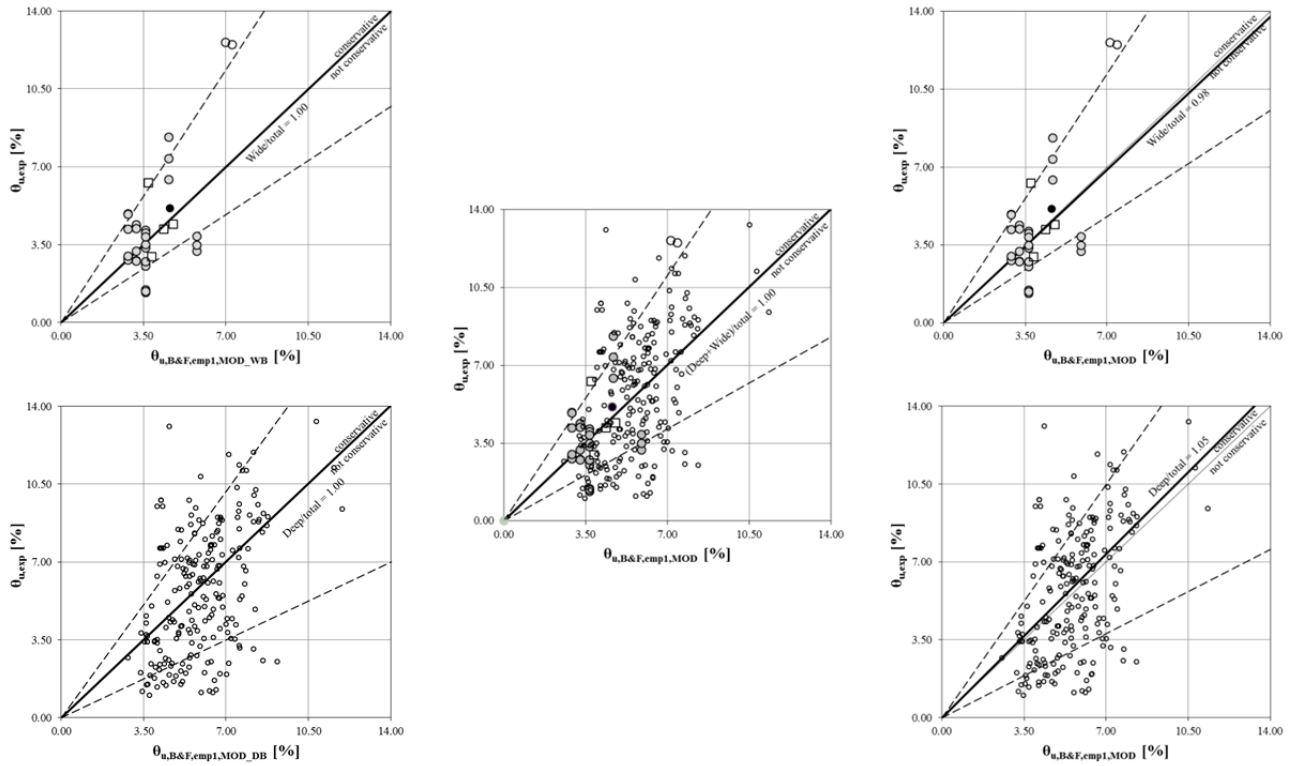


Figure 147: Corrected-predicted vs. experimental values of θ_u and μ_0 for WB and DB

Results for WB are presented in Figure 143 and Figure 144, and results for DB in Figure 145 and Figure 146. In all the graphics, the trend (thick line) corresponds to the median value instead of mean, as suggested in Panagiotakos and Fardis (2001) for larger databases. Dotted lines, representing dispersions, correspond to fractiles 16% and 84% of the probabilistic distribution.

Both simplified formulations and values obtained by means of the fibre model return values of ϕ_y , quite lower than experimental values, especially for WB (Figure 143). As fibre model values are slightly lower (less than 7%) than simplified formulations, the error is lower, so those values are used for the obtaining of θ_y . Despite the large error in ϕ_y , the underestimation of θ_y in the simplified expressions is much lower. It is worth noting that it is not conservative for beams, as it means that the real secant stiffness may be lower than predicted. Formulations P&F return more accurate values than more recent B&F formulations: the ratio between experimental to predicted θ_y is 1.05 (WB) and 1.03 (DB) for P&F, while for B&F those ratios are 1.14 and 1.10, respectively. On the other hand, values provided by ASCE furnish higher underestimation, especially for WB (ratio experimental-to-predicted equal to 4.15).

Regarding θ_u , both P&F and B&F formulations furnish overestimation of values for WB, which is also unconservative: ratios 0.88 and 0.84, respectively. In the case of DB, P&F overestimates (0.94) but B&F underestimates (1.22), which is conservative. If only B&F predictions are considered –as their use is more extended because they are in the base of expressions contained in EC8 part 3—, the ratio $\theta_{u,W/D} \approx 1.38$ proposed in section 3.3.2 should be divided by $(1.22/0.84=1.45)$, resulting in $\theta_{u,W/D,corrected} \approx 0.95$, thus WB would have typically lower rotation capacity than DB. In this case, ASCE formulations return very conservative values, especially for DB (ratio 2.17). Finally, predicted values of μ_θ are quite accurate (but still unconservative) for DB in the case of B&F formulations (ratio 0.95), while for WB the conservativeness is quite lower (ratio 0.73).

Hence, the aspect ratio h/b may have some influence on θ_u in beams. Consequently, a factor $(h/b)^{exp}$ might provide better agreement to B&F formulations. Value of exp is firstly sought separately for WB and DB, indicated by

subscripts *MOD,WB* and *MOD,DB*, respectively (see Figure 147). It is considered that optimal values of *exp* are those for which median trend of ratio experimental-to-predicted is 1.00. Those values are 0.21 and 0.27 for WB and DB, respectively. Then, a value of *exp* able to be applied both for WB and DB with low error is sought: 0.19, which causes errors of 2% and 5% for WB and DB, respectively, which may be accurate enough. Thus, formulations for θ_u of B&F and EC8 part 3 could be corrected as shown in Equations (74) and (75), respectively; the added factor is remarked in blue.

$$\theta_{u,B\&F,emp1,beams} = a_{st} \left[1 - \frac{a_{old} a_{cy}}{6} (1 - 0.05 a_{pl}) \right] (1 - 0.43 a_{cy}) \left(1 + \frac{a_{st}}{2} \right) \cdot \left[\frac{\max(0.01; \omega')}{\max(0.01; \omega)} f_c \right]^{0.225} \cdot \left[\min\left(9; \frac{L_V}{h}\right) \right]^{0.35} \cdot \left(\frac{h}{b}\right)^{0.19} \cdot 25^{\alpha\omega_{sx}} \cdot 1.25^{100\rho_d} \quad (74)$$

$$\theta_{u,EC8,beams} = 0.016 \cdot \left[\frac{\max(0.01; \omega')}{\max(0.01; \omega)} f_c \right]^{0.225} \cdot \left(\frac{L_V}{h}\right)^{0.35} \cdot \left(\frac{h}{b}\right)^{0.19} \cdot 25^{\alpha\omega_{sx}} \cdot 1.25^{100\rho_d} \quad (75)$$

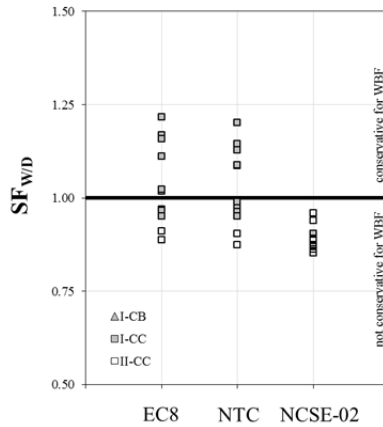


Figure 148: Correction of Figure 142 based on the new expressions proposed for θ_u of beams

If this correction is applied to the parametric assessment carried out in 3.7, new results of relative performances of WBF vs. DBF are obtained (see Figure 148). Only 7 couples of 36 (all belonging to EC8 frames) register a reduction of $SF_{W/D}$: the only six couples belonging to sub-scenario CB, which changes to CC, and one couple originally belonging to sub-scenario CC, which changes to BC. Hence, mean $SF_{W/D}$ for EC8 decreases from 1.08 to 1.05, while the rest of the codes (NTC and NCSE-02) do not get influenced.

It is worth noting that this analysis may not be conclusive, as it is based on a very limited number of cases, and also almost all of them belong to the same set of experimental tests –carried out in Calvi et al. (1993)—.

3.9 CONCLUSIONS

Prescriptions of three benchmark international seismic codes –Europe, USA, and New Zealand— and four Mediterranean codes –Spanish, Italian, Greek and Turkish ones— regarding wide beams are compared in detail are reviewed and analysed in their structural and historical genesis. Furthermore, limitations regarding flat slabs are examined in order to understand whether codes are homologating wide beams to flat slabs. Then, experimental behaviour is analysed in light of code provisions. Strut-and-tie micro-models for connections are suggested, and detailed parametrical analyses of local performance of beams based in different experimental formulations are carried out. Finally, an estimation of the trends for relative performance of wide-beam frames with respect to deep-beam frames is suggested by means of a simplified spectral analytical approach.

No current code suggests any reduction of behaviour factor (q) for wide-beam frames except Spanish and Italian ones. Any possible justification should be related to the three main shortcomings of wide-beam frames with respect to deep-beam frames: deficient local equilibrium, higher deformability and lower local ductility of beams. However, recent codes actually provide specific limitations aimed at avoiding the first two issues. In fact, geometric limitations in connections minimise transverse torsional path and slip of bars, while minimum lateral stiffness is required in design to DLS and second-order effects. Hence, the only justified

reason for the reduction of q may be the last one, regardless of any likely improper homologation with flat slabs.

However, the extrapolation from local ductility to q is not appropriate, because q refers to global capacity and not only depends on global ductility, and neither global ductility depends only on local ductility of beams. Instead, the most relevant parameters governing the relative performance of wide- and deep-beam frames are global stiffness of the frame and overstrength of columns. Thus, the more restrictive is the code regarding design to DLS, the more favourable is performance of wide-beam frames with respect to deep-beam frames, because DLS becomes the critical condition of design and likely similar stiffnesses are expected for both frames, while displacement capacities may be larger for wide-beam frames due to larger column overstrengths. Hence, based on general consideration and likely approximations, it is only possible to state a priori that no reduction of q is necessary for design of wide-beam frames to DCH for codes in which design to DLS is the critical condition in most cases, as in EC8.

Next, different assessments of typical Mediterranean 5-storey RC housing unit are carried out in order to evaluate the relative performance of wide-beam frames with respect to deep-beam frames. Different design alternatives are considered: Eurocode 8 (EC8, assuming diverse stiffness modelling approaches) and Spanish seismic code NCSE-02. The first code allows designing wide-beam frames in high ductility class, without any reduction of behaviour factor (q) with respect to deep-beam frames, while the Spanish code prescribes half values of q for wide-beam frames. Assessments are carried out by means of the N2 method. Finally, results are generalized through simplified assessment of a set of 72 high ductility frames corresponding to both wide and deep-beam frames designed according to Eurocode 8, Italian seismic code NTC, and NCSE-02 adopting similar q for both lateral load carrying systems.

Notwithstanding the lower local ductility of wide beams with respect to deep beams, global capacity of wide-beam frames get substantially improved thanks to some causes that increase both their effective stiffness and their maximum deformation capacity. These causes can be organised in three groups:

- 1) mechanical causes: higher ultimate chord rotation in beams (which is subsequently demonstrated, through a comparison between formulations and experimental results, to be under discussion) and also in column bases (due to higher cantilever behaviour), thus higher displacement capacity; and lower shear deformability of joints results in higher effective stiffness;
- 2) code limitations: beam-to-column width limitation makes hard to reduce column sections at upper storeys, and both design to Damage Limitation State (DLS) and corrections due to second order effects lead to greater column sections in the mid-low part of the building; these provisions cause higher stiffness and higher overstrength in columns, which leads to mechanisms involving higher number of storeys;
- 3) constructive causes: as larger column sections are required in lower storeys, it is not possible for spliced bars to make important reduction of column sections when rising to the upper storeys.

Hence, high-ductility wide-beam frames may provide similar or better performances with respect to deep-beam frames when Damage State Limitation is among design criteria. Hence, within the limitations of this work, it is suggested that design of wide-beam frames in high ductility class, adopting the corresponding q , could be allowed within the actual framework of NTC without any additional provision than local geometric limitations in connections. Regarding NCSE-02, it is not possible to state with sufficient confidence that q limitations for wide-beam frames can be removed within the actual framework, which does not provide any serviceability limit state (i.e. damage limitation).

Chapter 4

The 2011 Lorca (Spain) earthquake

This chapter is dedicated to the case study: the 2011 Lorca earthquake. The special characteristics of the seismic event are analysed, as the directivity effects. Then, the statistics of damage are interpreted and treated in order to obtain a clear damage scenario for RC buildings, which is also analysed in the light of the deficiencies of Spanish code provisions studied in the previous chapter. Real damage scenario is aimed to be used afterwards as a benchmark for being compared with the simulated damage scenario obtained with FAST.

Very detailed information about the event can be found in several post-earthquake reports (Cabañas et al., 2011; Goula et al., 2011; Vidal et al., 2011; De Miguel, 2011; Regalado and Lloret, 2011). Some other works focus in the dynamics of the strong motion (Benito et al., 2011; Rueda et al., 2011; Alguacil et al., 2013; Cabañas et al., 2013); and further studies regarding damages in buildings are also available (Benavent-Climent et al., 2013; Romao et al., 2013; De Luca et al., 2014; Hermanns et al., 2014; Vidal et al., 2014). Hence, given that the issue has been sufficiently studied, in this chapter only the subjects which are necessary for the subsequent application of FAST approach are presented.

4.1 CHARACTERISTICS OF THE EVENT

On 11th May 2011 at 16:47:25 an earthquake of magnitude $M_W=5.1$ struck Murcia region (Spain); the epicenter was 2km far from the city of Lorca (3km from the seismic station). This was the third largest earthquake recorded by strong-motion instruments in Spain since 1951. The mainshock was preceded by an important foreshock of magnitude $M_W=4.5$, occurred at 15:05:13, nearly in the same place (3.5km from Lorca seismic station, see Figure 149). Focal mechanism was strike slip with low inverse influence. Proximity to the epicenter and low hypocenter depth (2-4km for both events), caused very high macro seismic intensities in Lorca for such moderate event. Macrosesimic intensities were VI for the foreshock and VII for the mainshock, respectively.

4.1.1 General considerations

The main earthquake was registered by 17 stations located from 3 to 185km from the epicenter. Lorca station (LOR) was the nearest one. At this station maximum PGA was equal to 0.367g for mainshock NS component, and the same component was equal to 0.289g for the foreshock. Furthermore, it is worth to observe that the event was characterized by a significant attenuation of PGA and PGV with the distance, as shown in Figure 150 a and Figure 150b.

Horizontal elastic spectra of the foreshock and the mainshock are shown in Figure 151 for the three closest stations –Lorca (LOR), Zarcilla de Ramos (ZAR) and Alhama de Murcia (AM2). LOR, ZAR and AM2 stations were characterized, in the case of mainshock event, by increasing epicentral distance, 3.0, 24.6 and 25.9km, respectively, see Figure 149. Signals have been filtered and corrected according to the same criteria employed in Chioccarelli et al. (2009).

Main ground motion characteristics in Lorca station (Table 41) show a significant difference between NS and EW components. Low depth of the event and near fault location of LOR station are the causes of the high values of peak strong motion parameters (PGA and PGV) compared with the relative low values of integral strong motion parameters, such as 5-95% significant duration (S_D), Arias Intensity (I_A), Housner Intensity, and the so called Cosenza and Manfredi index (I_D). Small values for I_D are typical for impulsive earthquakes (Manfredi,

2001). In fact, I_D index can be assumed as an indicator of the cyclic demand of earthquakes (Manfredi, 2001; Iervolino et al., 2010), and low values indicate that most of the energy of earthquakes is dissipated by structures in a small number of cycles.



Figure 149: Lorca: river Guadalentín (discontinuous blue line), limit of the constructed area (green-black line), limits of different soil types (EC8 classification, black dotted line), LOR seismic station (green triangle), mainshock and foreshock epicenter (big and small beach balls, respectively), high (red) and medium (yellow) damaged buildings as classified in the on-site damage survey

FAST simplified vulnerability approach for seismic assessment of infilled RC MRF buildings and its application to the 2011 Lorca (Spain) earthquake

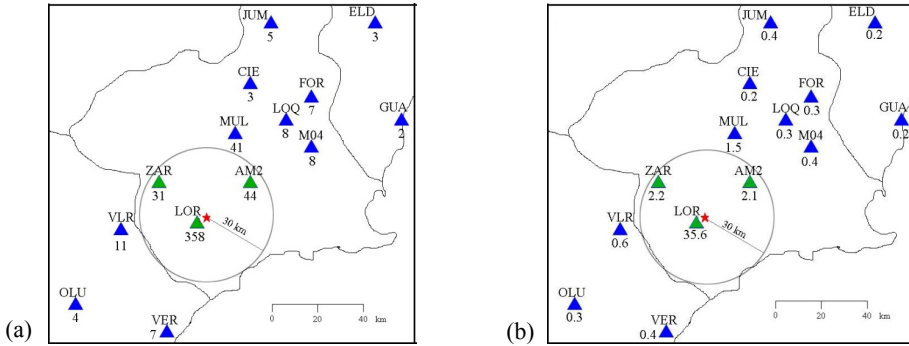


Figure 150: PGA in cm/s^2 (a) and PGV in cm/s (b) measured at the different stations

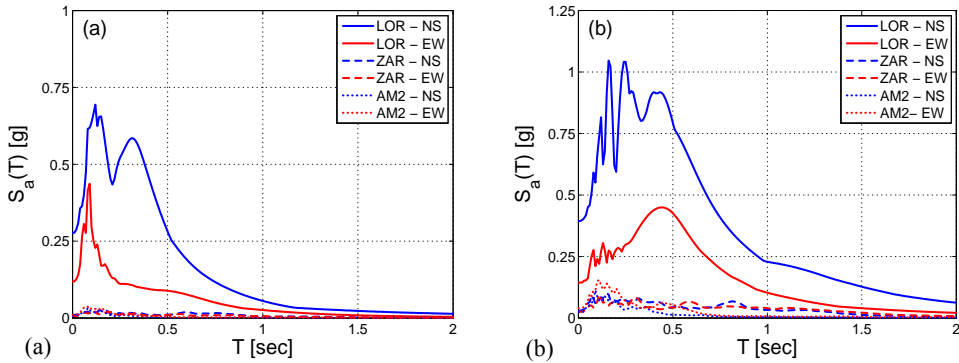


Figure 151: Elastic response spectra from the signals registered in LOR, ZAR and AM2 stations, closer than 30km to the epicenter, for foreshock (a) and mainshock (b)

Before any discussion regarding the relationship between the PGA registered in LOR station and the values of PGA to which the buildings in Lorca are designed, it is necessary to evaluate which are the soil types in the city. In Figure 149, soil types following EC8 classification are obtained from the soil distribution following NCSE-02 suggested in Cabañas et al. (2011), see Figure 152; transformation is done as shown in Table 12. A more accurate distribution is presented in Navarro et al. (2012), see Figure 153; in this case, it is classified according to EC8 and distinguishing two different classes of soil type B.

Table 41: Foreshock and mainshock peak and integral strong motion parameters at Lorca station (LOR).

Direction	Foreshock (LOR)			Mainshock LOR		
	N-S	E-W	V	N-S	E-W	V
PGA [g]	0.289	0.128	0.075	0.367	0.153	0.117
PGV [cm/s]	12.9	4.1	2.3	35.6	14.2	8.0
I_A [cm/s]	14.0	2.5	1.6	52.7	10.9	4.5
S_D [s]	0.535	1.85	1.82	1.01	3.395	3.28
I_D	2.403	3.123	5.882	2.571	3.208	3.081
Housner intensity [m]	22.941	7.598	5.757	78.012	31.698	24.537

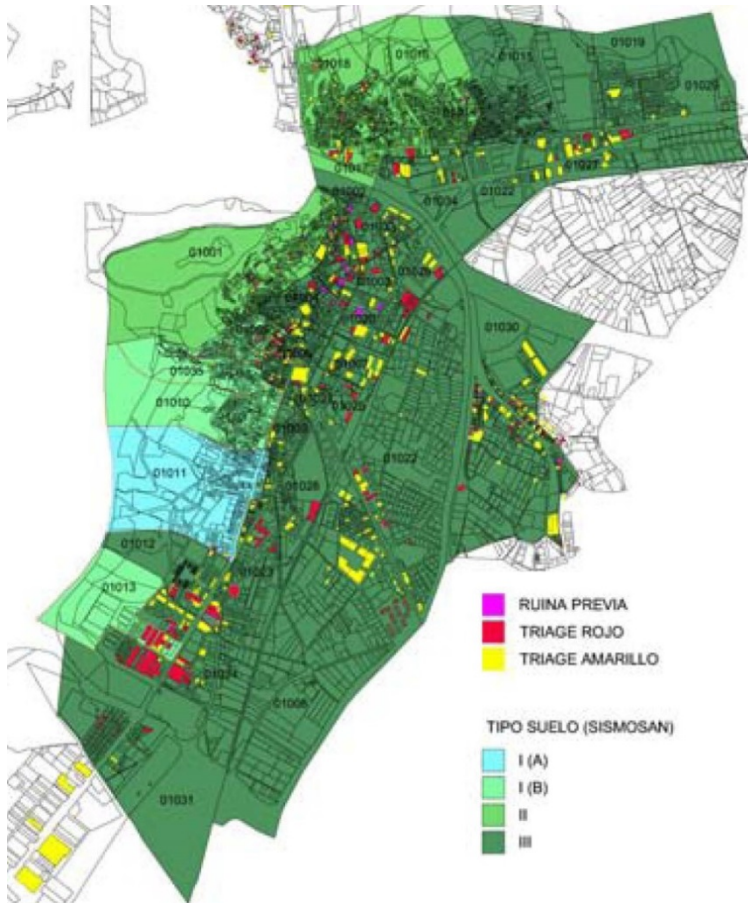


Figure 152: Soil classification of Lorca according to Cabañas et al. (2011) and damage level on buildings

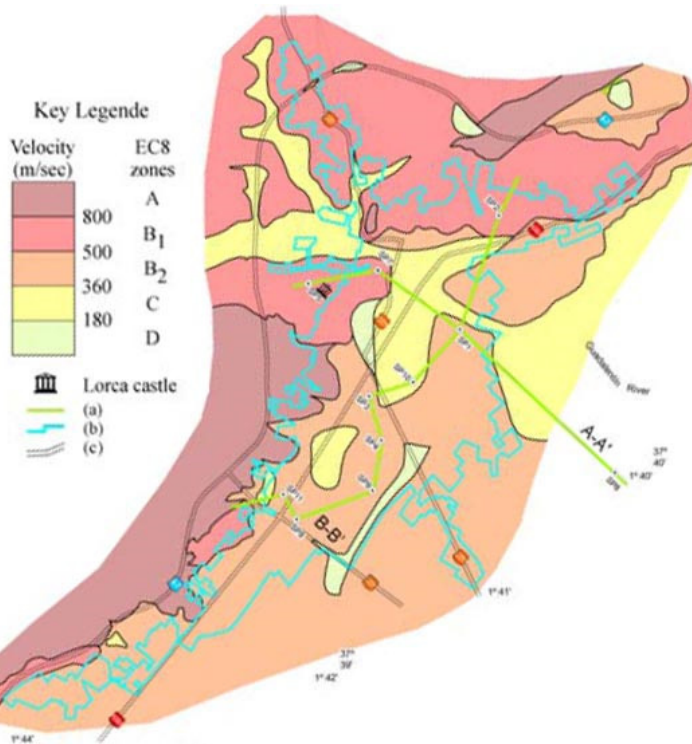


Figure 153: Soil classification of Lorca according to Navarro et al. (2012)

It the last option is considered as more reliable, it is worth noting that LOR station is placed in a soil whose velocity of shear waves is between 500 and 800m/s, thus likely corresponding to soil type II according to NCSE-02 (which ranges between 400 and 750m/s). Moreover, LOR station may correspond to “hard soil” (see Table 12), which is likely the reference soil used for the definition of seismic hazard in Spain. Thus, any comparison between event and design values regarding PGA or spectra should be considered as in soil type II. Also, it is possible to affirm that the more generalised soil type in the city is also type II, which is necessary for FAST approach.

In Figure 154, elastic response spectra of the mainshock in both directions are compared with the spectrum proposed by the code. The maximum PGA value

registered during the mainshock is more than three times higher than the typical design PGA provided by codes (equal to 0.124g for most usual characteristics, see section 6.1) and has 0.01% probability of being exceeded in 50 years (VV.AA., 2006); 1000 times lower than the conventional, code based, 10%. On the other hand, according to new probabilistic seismic hazard study, performed before the 11th May event, an increment from 0.12g to 0.19g was suggested for Lorca code acceleration (on hard soil type) (Mezcua et al. 2011). It is worth noting that the shape of the NS spectrum of the mainshock is rather proportional to the code-based shape for medium-low period range (<0.5s), but spectral acceleration decrease more quickly in the spectrum of the earthquake. Thus, the ratio PGA_d/PGA_c may be lower (i.e. more favourable) for flexible (e.g. taller) buildings.

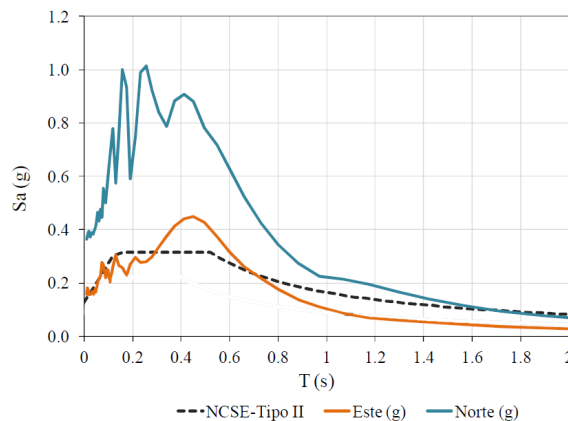


Figure 154: Comparison between elastic response spectra registered in LOR station and elastic response spectra proposed by NCSE-02 for Lorca on soil type II (adapted from Goula et al., 2011)

4.1.2 Directivity effects

Aimed at the quantitative classification of directivity effects, the record registered at Lorca station during the mainshock event was rotated according to parallel (FP) and normal (FN) directions of Alhama fault (strike=230°). In Figure 155, acceleration, velocity and absolute and relative energy input elastic spectra of the rotated components are shown for $\xi=0.05$, where ξ is the fraction of critical

damping. The energy input spectra in Figure 155 c and f are expressed in form of equivalent velocity (V_E) according to the same definition given in Uang and Bertero (1990). The significant difference between relative and absolute V_E represents a proxy for directivity effects. The presence of pulses generates smaller or larger relative energy magnitude in the short and long period ranges, respectively, with respect to absolute energy (Kalkan and Kunnath 2008).

The spectra in Figure 155 a and b, and Figure 155 d and e allow the evaluation of T_C and T_D periods delimiting the constant velocity branch of the spectra according to the procedure described in Lam et al. (2000). T_C and T_D periods are equal to 0.48s and 0.57s for FN component and equal to 0.24s and 0.88s for FP component. The pseudo velocity spectrum for the normal-fault component of the record shows a very short stretch of constant velocity value (see Figure 155b), typical of the impulsive motions (Chopra, 2007).

Indeed, the quantitative method by Baker (2007), based on wavelet analysis, confirmed the near-fault impulsive characteristics already suggested by the spectra in Figure 155. The period of the velocity pulse is an important parameter for structural engineers. No well-defined concept of periods exists for wavelets such as there is for sine waves in Fourier analysis, but the period associated with the maximum Fourier amplitude of a wavelet can be used to define a pseudo period (T_p). According to Baker's classification a pulse-like record meets all the following three criteria:

1. The pulse indicator value is greater than 0.85.
2. The pulse arrives early in the time history.
3. The original ground motion has a PGV of greater than 30 cm/sec.

For FN component at Lorca station, Baker's pulse indicator is equal to 0.99, T_p is equal to 0.68s and the component is classified as pulse-like (see Figure 156a); while for FP components pulse indicator is equal to 0.03, PGV is 9.97 cm/s and the record is not classified as pulse-like (see Figure 156b).

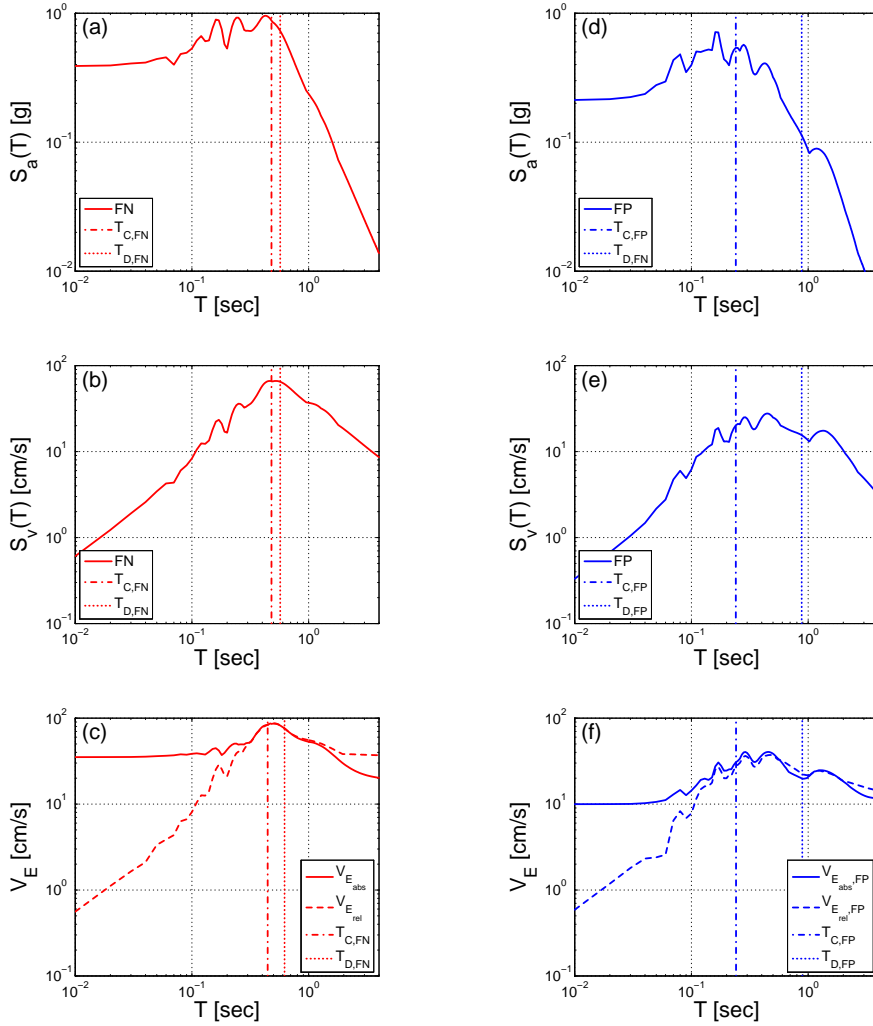


Figure 155: Acceleration, velocity, and relative and absolute energy in terms of equivalent velocity spectra for fault normal FN (a), (b), (c), and fault parallel FP, (d), (e), (f) mainshock signals registered in Lorca (LOR) station with the evaluation of T_C and T_D

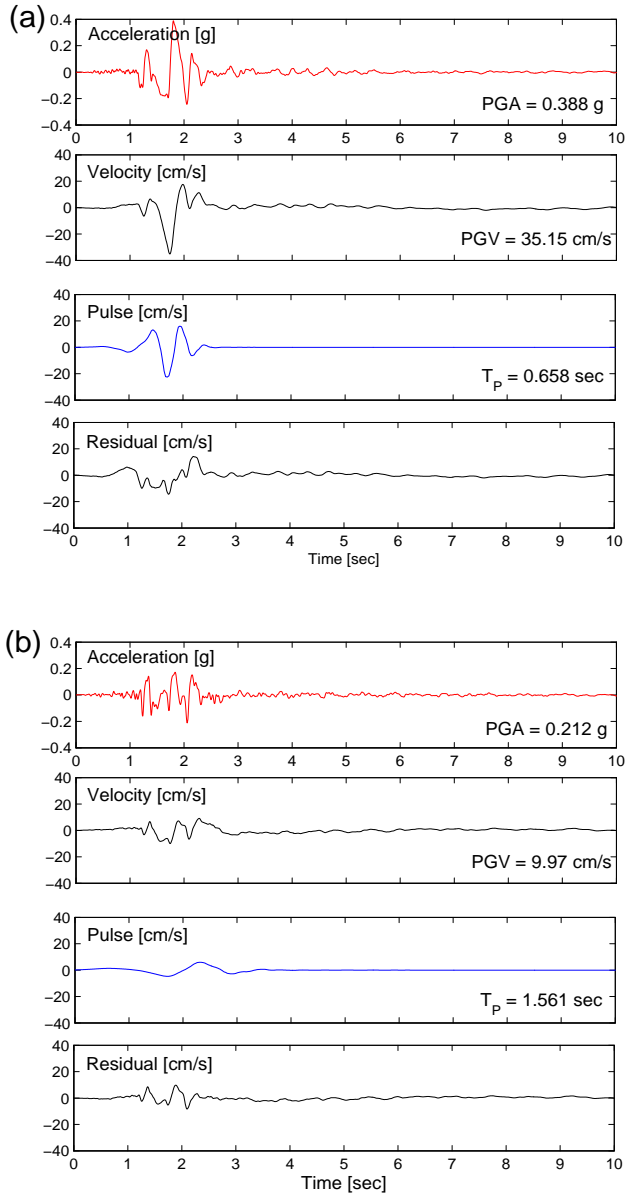


Figure 156: Baker (2007) quantitative classification of fault normal (FN) (a), and fault parallel (FP) (b) mainshock signals registered at Lorca (LOR) station, characterized by pulse indicators equal to 0.99 and 0.03, respectively

4.2 CHARACTERISTICS OF RC BUILDING STOCK IN LORCA

In Chapter 2, typical qualitative characteristics of RC MRF buildings in Spain are discussed. They could be generally classified as sub-standard (for old-generation codes) or at least non-capacity-designed buildings (medium-generation codes, including current one). Aimed at the application of FAST approach to the specific case of RC buildings subjected to the Lorca earthquake, it is necessary to know, about those buildings:

- 1) which are the typical number of storeys;
- 2) which are the typical seismic codes;
- 3) which is the typical interstorey height;
- 4) which is the typical superficial ratio of infills.

In order to answer to questions 1) and 2), data from Feriche et al. (2012) and Cabañas et al. (2011) are crossed. Results show that 77% of the buildings are masonry structures and the other 23% are modern frames (Cabañas et al., 2011), mainly RC. In Figure 157a, the distribution in terms of number of storeys is shown. Storeys' data are not specialized for structural typology (e.g., masonry, RC...). Therefore, it has been made the assumption that buildings with no more than three storeys are all masonry, so covering 68% of the total building stock, while three storey buildings are equally distributed between masonry and RC, dealing to the above 77% of masonry structures on the whole building stock, (see Figure 157a). According to the above assumptions it can be inferred that RC buildings in Lorca are mainly characterized by a number of storeys between 3 and 6. In Figure 157b, data on the age of construction are crossed with the year in which the different seismic codes have been released in Spain. Assuming that masonry buildings have been realized before RC buildings, it can be inferred that most of RC buildings had been designed according to codes PDS-1 (CDSO, 1974), NCSR-94 (CDSO, 1994) and NCSE-02 (CDSO, 2002).

Regarding interstorey height, most of vulnerability approaches in the Mediterranean framework (see section 1.1) generally adopt 3.0m for housing storeys, i.e. in all the storeys except first one, which can be exploited by other use (e.g. commercial or garage). In-field observations, together with Lorca local

regulation on minimum clear height from sidewalk to the bottom of cantilevered parts of the buildings (see <http://www.urbanismo.lorca.es/TomoII.asp>), suggest that 3.5m could be a feasible average value for 1st storey height of housing units in Lorca. Also, aimed at the application of generalised FAST, it is necessary to define a typical value for tributary area of columns (A_{trib}). In-field observation is coherent with usual assumptions made for spans of sub-standard buildings (as in Verderame et al., 2010a): spans ranging 3.5-5.5m, thus typical A_{trib} could be 20m².

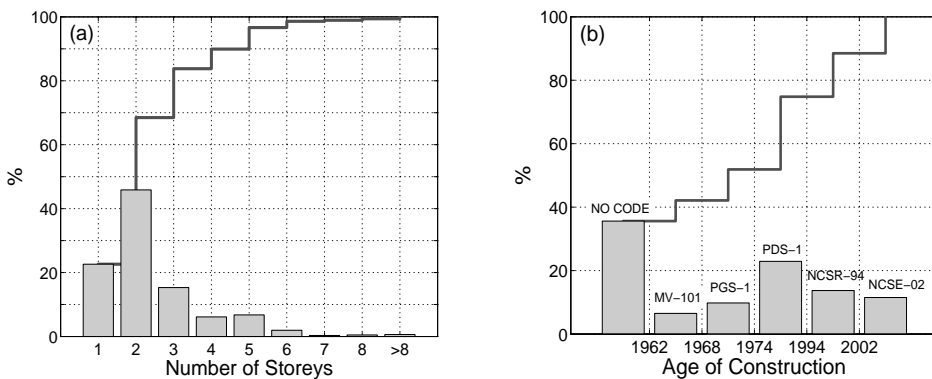


Figure 157: Frequency and cumulative distributions in Lorca building stock for: number of storeys (a), age of construction and applied code provision for the design of the building stock (b) (adapted from Feriche et al., 2012)

In the matter of infills ratio (see section 1.3), Crowley and Pinho (2010) suggest $\rho_w=2.5\%$ as a representative value for Mediterranean buildings; such ratio should be intended as an average of the different storeys. On the other hand, aimed at searching which could be representative values for infill ratio in 1st floor vs. rest of the storeys, local buildings should be analysed. In Figure 158, distributions of infills in two representative buildings are shown. As explained in section 1.3.3, there is some controversial about the effectiveness of infill panels depending on their geometric characteristics. Infills can be divided in: external (*ex*), which are facades or separation walls thicker than 15cm, placed into a RC frame; internal aligned (*al*), thin walls of usually 10cm placed into a RC frame; and internal not aligned (*in*), that include all the partitions not placed in any RC frame. Usually

only (*ex*) are considered as effective, since the other could not reach the upper slab and are characterized by high uncertainties on their position and characteristics. On the other hand, (*al*) in many cases may be as effective as (*ex*), even in the case in which no beams are located above and simply longitudinal joists close the contour structural frame. Finally, (*in*) are usually neglected, as they are supposed not to be able to develop post-cracking diagonal-strut behaviour. However, (*in*) can develop their elastic shear resistance (τ_{cr} instead of τ_{max}), which could be lower than the demand for any event in a non-uniformly infilled frame (see section 2.2.5). Also, they may influence the value of the elastic period.

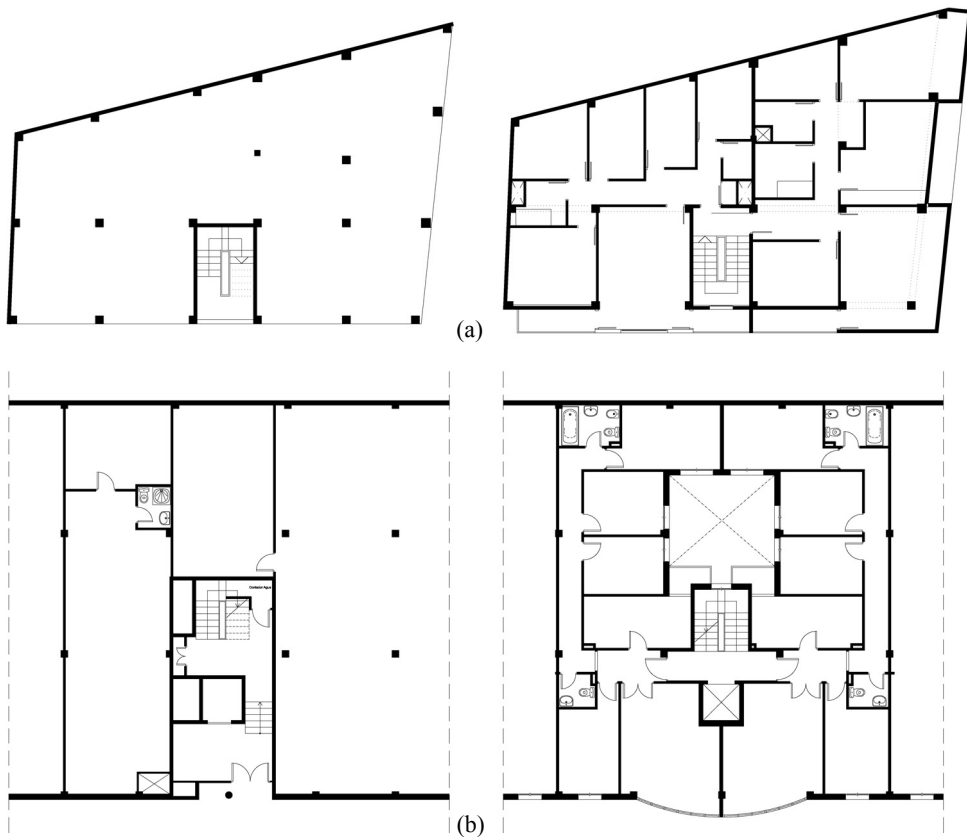


Figure 158: 1st (left) and upper (right) floors of two representative infilled RC buildings of Lorca; buildings I (a) and II (b)

Table 42: Infills ratios for building I and II

Building	Direction	$\rho_{w,l}$ [%]			$\rho_{w,s}$ [%]		
		<i>ex</i>	<i>ex+al</i>	<i>ex+al+in</i>	<i>ex</i>	<i>ex+al</i>	<i>ex+al+in</i>
I	X	1.3	1.5	1.5	2.1	2.8	4.5
	Y	0.8	1.4	1.4	2.1	3.1	4.6
II	X	0.8	1.0	1.3	1.6	2.1	3.9
	Y	1.1	1.4	1.8	1.9	2.3	3.9
average		1.1	1.3	1.5	1.9	2.6	4.2
				$\rho_{w,l}/\rho_{w,s}$	0.52	0.51	0.36

According to these observations, three different cases are considered: only the external infills are effective [ex]; also the interior aligned do [ex+al]; and that all the infills are effective [ex+al+in]. Openings and double layers (when present) are considered. For the evaluation of $\rho_{w,i}$, only infills oriented in the considered direction are taken into account. According to results shown in Table 2, it can be observed that hypothesis [ex] leads to very low $\rho_{w,i}$ values, while in the case of hypothesis [ex+al] the average value is 2.6% in upper storeys, consistent with Crowley and Pinho (2010), having the ground floor approximately half of the amount. When hypothesis [ex+al+in] is considered, the amount of upper walls increases to 4.2% resulting in a ratio of 0.36 between ground and upper storeys.

4.3 DAMAGE SCENARIO

In this section, level, type and distribution of damage are shown. The level of damage, classified according to the EMS-98 damage scale (Grünthal, 1998) is shown as function of number of storeys and age of construction. Such data are then integrated with some photographic examples of structural and nonstructural damage, aimed at highlighting local features of building practice and their consequences in terms of damage observed.

According to on-site damage survey after the earthquake, buildings were preliminary classified according to the scale ATC-21 or EPPO (Figure 4), consisting in three “colours”: green, yellow and red, corresponding to light, moderate and severe damages; more details can be found in Cabañas et al. (2011). Damage was not homogeneous between similar and contiguous structures. The

latter can be an effect explained by directivity effects characterizing the event (see previous section). On the other hand, according to data available, it is not possible to recognize whether the strong foreshock already damaged structures or induced preliminary residual drifts.

4.3.1 Soil influence on damages

The distribution of damages in relation with soil type is shown graphically in Figure 152 and numerically in Figure 159. Those data are then normalised for diverse groups of buildings regarding type of construction or damage level, in order to analyse the influence of soil type on the observed vulnerability. Results are shown in Table 43 and Figure 160. They show that:

- RC buildings are more frequent in new parts of the city, characterised by poorer soil type, while masonry buildings are more frequent in old parts, characterised by better soil type.
- Damage is quite higher for buildings on poorer soil type.

Table 43: Normalised damages depending on soil type for different cases

Soil type	IA	IB	II	IA+IB+II	III	Total
Number of buildings	369 (5.5%)	1006 (14.9%)	2013 (29.8%)	3388 (50.1%)	3374 (49.9%)	6762 (100%)
Number of masonry buildings	228 (3.4%)	855 (12.6%)	1800 (26.6%)	2883 (42.6%)	2272 (33.6%)	5155 (76.2%)
Number of RC buildings	141 (2.1%)	151 (2.2%)	213 (3.1%)	505 (7.5%)	1102 (16.3%)	1607 (23.8%)
Damaged buildings	23 (6.2%)	73 (7.3%)	125 (6.2%)	221 (6.5%)	655 (19.4%)	876 (13%)
“Red” buildings	13 (3.5%)	32 (3.2%)	75 (3.7%)	120 (3.5%)	430 (12.7%)	550 (8.1%)
“Yellow” buildings	10 (2.7%)	41 (4.1%)	50 (2.5%)	101 (3.0%)	225 (6.7%)	326 (4.8%)
Probable masonry damaged buildings	14	62	111	188	416	604 (11.7%)
Probable RC damaged buildings	9	11	14	33	239	272 (16.94%)

Theoretically, seismic codes do have into account soil influence, thus buildings should show similar performance whichever the soil type is. However, it

is worth noting that most of buildings are not designed to any seismic code; and those designed to seismic codes show such a great influence of infills in their strength and stiffness (see section 2.2) that soil factor get jeopardised.

distrito censal	Triage		Edificios Demolidos	Total Dañados	Tipo Suelo	Nº Edif. Tradicionales	Nº Edif. Tecnológicos	Total Edificios	% daños sobre total
	Amarillo	Rojo							
1001	28	26	1	55	II	527	57	584	9,4%
1002	33	29		62	III	164	56	220	28,2%
1003	9	6	1	16	III	25	37	62	25,8%
1004	21	19		40	III	201	48	249	16,1%
1005	22	29		51	IB	304	48	352	14,5%
1006	38	21		59	III	161	83	244	24,2%
1007	14	5		19	III	17	28	45	42,2%
1008	28	10		38	III	93	43	136	27,9%
1009	12	3		15	III	67	76	143	10,5%
1010	2	3	1	6	IB	333	57	390	1,5%
1011	13	10	1	24	IA	228	141	369	6,5%
1012	35	9	1	45	III	177	31	208	21,6%
1013	14	3	2	19	IB y III	21	25	46	41,3%
1014	0	1		1	II	318	26	344	0,3%
1015	1	7		8	III	376	34	410	2,0%
1016	5	3		8	II	315	46	361	2,2%
1017	21	6		27	II	275	50	325	8,3%
1018	21	14	1	36	II	365	34	399	9,0%
1019	8	0		8	III	19	56	75	10,7%
1020	10	1		11	III	25	26	51	21,6%
1021	8			8	III	6	26	32	25,0%
1022	18	5		23	III	129	73	202	11,4%
1023	14	13		27	III	45	71	116	23,3%
1024	22	8	3	33	III	31	50	81	40,7%
1025	3	5		8	III	14	24	38	21,1%
1026	7	6		13	III	25	32	57	22,8%
1027	17	11		28	III	20	50	70	40,0%
1028	4	4		8	III	38	23	61	13,1%
1029	5	5		10	III	28	23	51	19,6%
1030	70	32	1	103	III	277	57	334	30,8%
1031	14	7	1	22	III	177	38	215	10,2%
1032	4	2		6	III	42	32	74	8,1%
1033	12	10		22	III	44	27	71	31,0%
1034	9	4		13	III	50	33	83	15,7%
1035	8	9		17	IB	218	46	264	6,4%
Total	550	326	13	889		5155	1607	6762	13,1%

Figure 159: Damage level in Lorca buildings and soil type for each district (from Cabañas et al., 2011)

4.3.2 Disaggregation for RC building stock

Original survey data must be treated in order to obtain damages in RC buildings. In all the following, as well as in the rest of the work, EMS-98 damage scale (see Figure 6b) is adopted; colour code identifying each Damage State (DS)

is shown in Figure 161. Original survey data expressed according to EMS-98 are collected from Feriche et al. (2012).

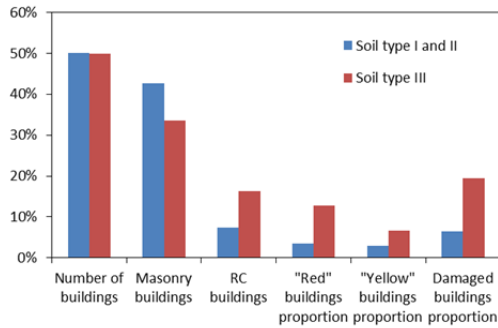


Figure 160: Normalised damages depending on soil type for different cases



Figure 161: Colour code used for each DS of EMS-98

In Figure 162, damage data according to EMS-98 for all the buildings from Feriche et al. (2012) is shown. According to EMS-98 scale, damage can be classified in five grades, increasing with damage (see Figure 6b). The description of each damage state depends on the type of structure considered (e.g., masonry, reinforced concrete). In most practical cases RC frames are realized with

nonstructural masonry infills. Thus, damage states refer to both structural and nonstructural damage up to grade 3. Grade 4 and 5 are characterized by heavy and very heavy structural damage.

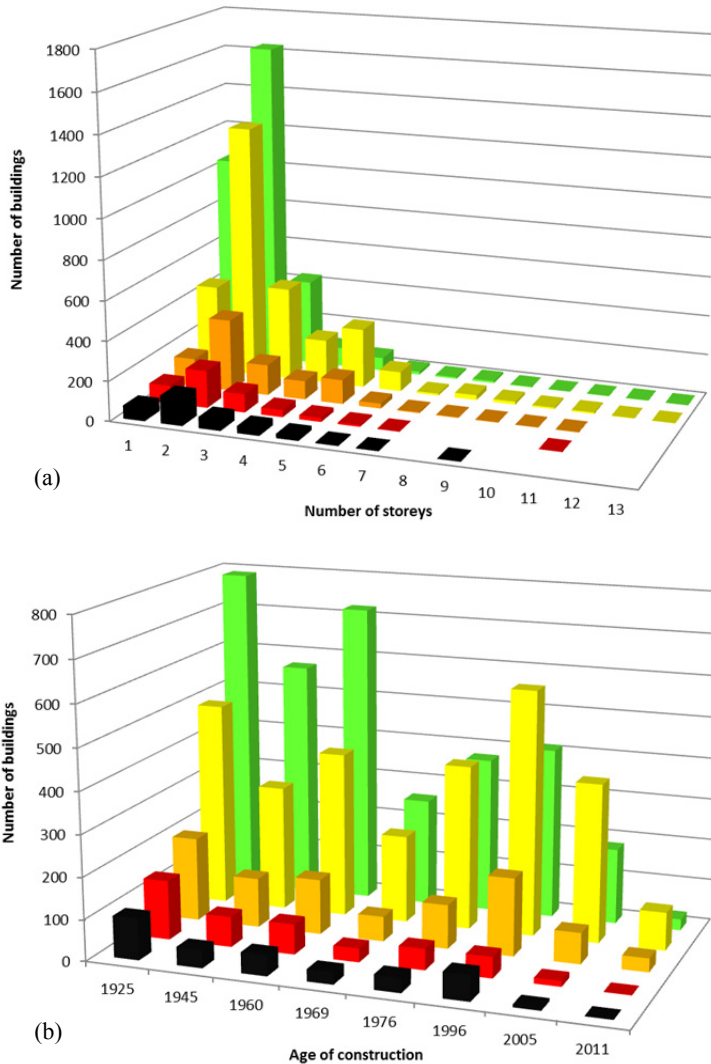


Figure 162: Damage survey data according to EMS-98 disaggregated by number of storeys (a) and age of construction (b) for all the buildings (adapted from Feriche et al., 2012)

In the following, statistics concerning RC structures are obtained by a disaggregation of the general data, according to assumptions made in section 4.2: RC buildings have been assumed to have three or more storeys and to be designed according to PDS-1 and subsequent codes released. Figure 163 shows the damage statistics for the total building stock and RC structures. Severe structural damage was not so frequent: only 8.53% of the RC structures were classified in grade 4 and 5, while grade 2 was very frequent. Moreover, severe structural damage in RC buildings was mainly induced by local or brittle failures, making hard to achieve the aim of a general, large scale explanation of the damage observed. Thus, in the following, only the trend of damage grade up to 3 will be considered. It is worth to note that buildings that showed no damage at all had been included in damage grade 1 in the following statistics.

According to data available in Cabañas et al. (2011), and the frequency distributions shown in Figure 163, it can be observed that 28.5% of RC buildings were characterized by damage grades between 3 and 5, while only 19.3% of masonry structures showed damage in the same range.

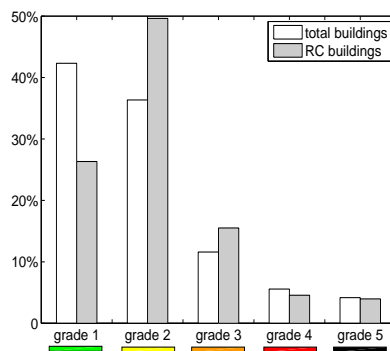


Figure 163: Frequency distribution of EMS-98 damage levels in Lorca

In Figure 164, data for RC structures are shown as function of the number of storeys, and age of construction. Storey data are shown from 3 to 6, since only 1.4% of the building stock has 7 or more storeys (Figure 162a). Results show that

high nonstructural and low structural damage increase with the number of storeys, being the median included in the middle range of DS2. Also, severe structural damage (DS4 and DS5) is reduced in more recent buildings designed to medium-generation codes, especially in the case of NCSE-02. The cause could be the likely reduction of brittle shear failures in column ends due to the local detailing of member ends required by medium-generation codes (see section 2.2.2).

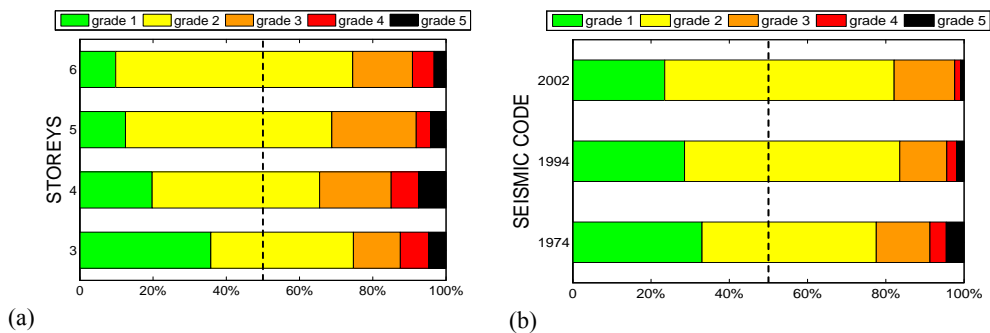


Figure 164: Frequency distribution of damage levels for RC structures depending on the number of storeys (a) and seismic code (b)

From a large-scale point of view, performance of Lorca RC buildings may be qualified as quite satisfactory, given that an earthquake whose demand is more than three times the design capacity provided to the more recent buildings (and much more to older ones) caused very few collapses or buildings with very severe structural damages. However, few troubling issues can be inferred from Figure 163 and Figure 164:

- 1) RC buildings show higher non-structural vulnerability (i.e. DS2 and DS3) than the average (Figure 163);
- 2) there is very slight reduction of structural damage (i.e. $DS \geq 3$) for medium-generation codes (NCSR-94 and NCSE-02) than for old-generation codes (PDS-1), see Figure 164;
- 3) proportion of buildings with almost no damage (i.e. DS1) is lower for medium generation codes than for old-generation codes (Figure 164)

First issue may be caused by soil influence (see previous section). However, second issue may suggest that effectiveness of code provisions aimed at avoiding structural damage and especially brittle failures is limited. Also, third issue may suggest that better performance is observed in buildings with less number of storeys and more infill panels (which is likely more usual in older buildings), thus relative influence of infill panels is much higher than any code prescription.

4.3.3 Observed typology of damages

Notwithstanding the satisfactory performance of Lorca from the large-scale point of view, if damages in buildings are analysed from a medium- and short-scale point of view, they are not so satisfactory. In fact, the damage scenario is typical of sub-standard buildings, also in recent RC buildings. This is coherent with the critical analysis of NCSE-02 carried out in section 2.2 and summarised in Table 24.

4.3.3.1 *Structural damage and collapses*

Structural damage observed during Lorca earthquake was not so frequent. However, structural damage was often a result of the lacks in code regulations. Mainly pre-emptive brittle failures at the ground floor columns, no relevant damages in beams, slabs or beam-column joints, and absence of significant residual drifts can be observed. The design approach, with no capacity design and frequent irregularity in elevation, did not allow the development of plastic deformations because of the occurrence of pre-emptive brittle failures or limited ductility failures (Sezen and Moehle, 2004, Biskinis et al., 2004).

Shear-axial failures in columns were frequent. Stirrups are characterized by low diameters, not proper spacing, and 90° hooks that do not confine the concrete core and reduce the effectiveness of the transversal reinforcement (Biskinis et al., 2004). Such shear design weaknesses accompanied by high longitudinal percentage ratios increases significantly the occurrence of brittle failures or limited ductility failures (De Luca and Verderame, 2013) that end up in typical shear diagonal cracking (Figure 165a) or buckling of the longitudinal reinforcement and consequent axial load collapse. When transverse reinforcement is not so scarce, plastic hinges in columns with limited ductility are observed (Figure 165b).

Another frequent cause of damage was the brittle failure of compressed diagonal concrete strut of “squat” (Figure 166a) or “captive” (Figure 166b) columns, due to the presence of RC basement walls or masonry infilling panels limiting shear span ratio. Other brittle failures observed were produced by squat columns in staircases.



Figure 165: Damages in RC columns due to lack of shear-to-column (a) and column-to-beam (b) hierarchy of resistances

In-plane behaviour of infills can lead sometimes to brittle failures into critical regions of RC columns because of the concentration of shear demand due to the interaction with the compressed diagonal of the panel, finally leading to undesirable progressive collapse mechanisms (Verderame et al., 2011), as seen in Figure 166c. Beam-column joint failures were scarce (Figure 167), especially if compared to other post earthquake reconnaissance reports in the Mediterranean area (e.g., Ricci et al., 2011a).

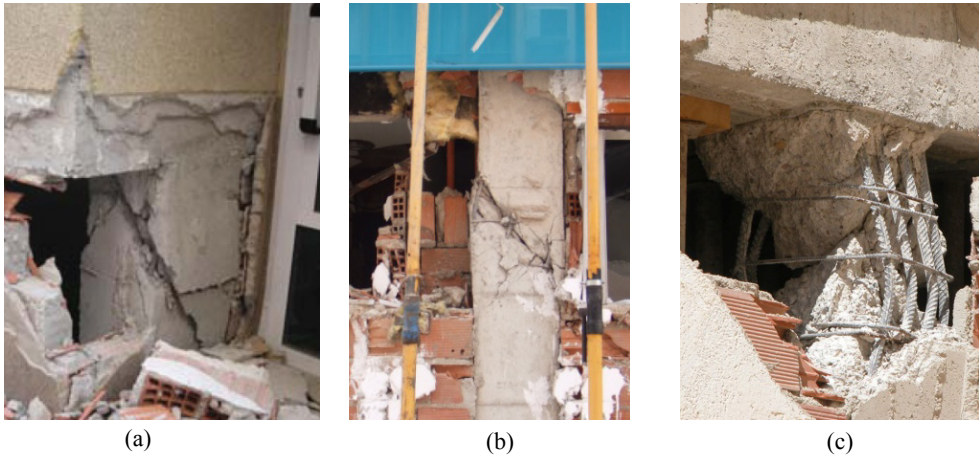


Figure 166: Brittle shear failures in RC squat (a) and captive (b) columns, and local interaction with diagonal strut of infills (c)

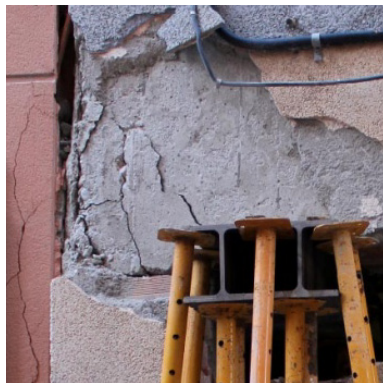


Figure 167: Brittle shear failures of RC beam-column joint

Only one building collapsed due to the earthquake (Figure 168). Its structural arrangement was characterized by RC waffle-flat plates supported by columns, with squat columns in two consecutive façades (Figure 168a) that failed and led to collapse all columns in the building (Figure 168 a and b), as described in Feriche et al. (2011). No relevant damage was found in the thick waffle-slab (Figure 168b).



Figure 168: The only building collapsed due to the Lorca earthquake, before (a, from Google Street View) and after the event (b and c)

4.3.3.2 Non-structural damage

Despite most of casualties and general damage were caused by out-of-plane behavior of nonstructural elements as facades or balustrades, in this section only in-plane failure of masonry infill panels of RC frames and their interaction is analyzed. The three typical in-plane failures for infill walls were recognized during in-field surveys: (i) diagonal cracking in one or two directions due to tensile stress in the central zone of the panel (Figure 169a); (ii) horizontal sliding (Figure 169b);

and (iii) corner crushing in the contact zone with the surrounding frame, because of local compression stresses (Figure 169c).



Figure 169: In-plane failures in masonry infill panels: shear diagonal cracking (a), horizontal sliding (b) and corner crushing (c)

Chapter 5

FAST approach for seismic assessment of infilled RC-MRF buildings

In this chapter, FAST method is presented, its theoretical framework is developed and its assumptions –based in literature or experimental works— are detailed. After a preliminary approach for code-based assessment of bare frames, two different versions of FAST are presented. The first one, “simplified FAST” (section 5.1), only considers uniformly infilled frames, while the second version, “generalised FAST” (section 5.2), allows accounting for any reduction of infills ratio at 1st storey, i.e. all the intermediate states between the uniformly infilled and the “pilotis” frame. Finally, some suitable complementary tools conforming “extended FAST” are exposed in section 5.3.

5.1 “FAST”: SIMPLIFIED APPROACH FOR UNIFORMLY INFILLED RC-MRF BUILDINGS

FAST is an approach for the estimation of large-scale vulnerability of RC MRF buildings accounting with the structural contribution of infills in terms of strength and stiffness. It allows predicting approximately the average level of damage state for each generic class of building when subjected to a certain event.

FAST is conceived for rapid decision making environments, such as the basic damage mapping in the phase of emergency management right after seismic events or in post-emergency priority analyses for preliminary interventions. Aimed at this “quick” behaviour, it adopts higher level of simplification: arrangement of RC building stock into classes is carried out depending on very few parameters, and simulated design only provides global dynamic and mechanical properties.

FAST framework is based in:

- a simplified definition of capacity curves (CC) for infilled frames;
- an approximate mechanical interpretation of damage states (DS) according to the EMS-98 scale in terms of interstorey drift (IDR).

According to the classification made in section 1.1, FAST is an analytical vulnerability approach. Aimed at a general comparison with the rest of the analytical methods presented in section 1.1.2 and resumed in Figure 3, the general characteristics followed by this methodology are:

- the general framework in which it is set is the capacity spectrum one;
- it is a code-based method, requiring a simulated design, but no specific model is constructed;
- the characteristic parameter defining the damage state thresholds is the interstorey drift;
- only one mechanism of collapse is considered: that of the bottom storey;
- periods evaluated are the effective ones;
- approximate capacity curves provided are bilinear;
- aimed at a probabilistic approach, uncertainties of the parameters are considered individually;
- this method takes into account explicitly the infill panels;
- it does not consider brittle failures in the RC members;
- results are compared with real case studies.

FAST belongs to a family of risk assessment methodologies developed for a decade in the University of Naples Federico II (see Cosenza et al., 2005; Iervolino et al., 2007; and Ricci, 2010). Actually, FAST can be considered as a simplification of POST, “PushOver on Shear Type models” (see section 1.1.2). The simplified characteristics are:

- Input: Only location, number of storeys, age of construction and ratio of infills in plan are needed. The rest of the geometric and mechanic properties are inferred from these four parameters or they assume fix values (see Table 44).
- Simulated design: Only global dynamic and mechanical properties are obtained (stiffness, periods, strength, ductility, etc.); specific structural member definition (dimensions and reinforcement) and storey pushover curves are not calculated.

It is important to remark that the scope of this method is to provide quick preliminary damage scenarios of the RC building stock of large areas; thus, a compromise between accurateness and quickness is needed. FAST tip the scales slightly to the quickness: the input is very simplified, as very few parameters are needed to be given, and the computational effort is not high in comparison with other approaches. Hence, some simplifications are assumed concerning the geometry and mechanic properties of the buildings (stiffnesses, strengths, infill ratios, etc). Thus, buildings (conforming building classes, i.e. not taken individually but considering average properties) are supposed to:

- have residential use;
- constitute RC frame systems –not wall nor dual systems— with moderate horizontal spans;
- have continuous vertical elements (columns) running without interruption from the foundation to the top;
- present similar interstorey height except only for the ground floor;
- not have substantial setbacks in elevation;
- present two main directions in plan;
- own kind of homogeneity (at least symmetry or compensation) in the distribution of stiffness, masses and resistances in each storey;
- present similar storey masses
- have similar infill ratios in all the storeys except for the ground floor;

Unfortunately, like most of large-scale methods with similar level of simplicity, there are some particularities that FAST is not able to have into account:

- brittle failures in RC elements are not considered;
- high structural damage states DS4 and DS5 are not considered;
- it cannot account for important torsion effects;
- out-of-plane behaviour of infills is not considered;
- it cannot evaluate the behaviour of buildings designed only to gravitational loads, without any seismic design;
- it is not fully adaptive: the dynamic properties are based in the elastic deformed shape;
- it does not consider the cumulative damage, not being able to evaluate the damage scenario caused by an event on a building stock which has previously been subjected to a damaging foreshock;

Along this chapter, the relevance of the consequences of these limitations is analysed, and justifications about the reliability of this simplification are offered. Anyway, in section 5.3 some guidelines regarding the implementation of several complementary algorithms aimed at the resolution of these problems are offered.

All in all, it can be stated that the method reaches a reasonable level of feasibility, given that the predicted scenarios when applied to real case study match quite accurately. In fact, FAST has been satisfactorily tested with the real damage scenarios of the earthquakes of: L'Aquila, Italy, 2009 (De Luca et al., 2013d); Lorca, Spain, 2011 (Gómez-Martínez et al., 2012; De Luca et al., 2013c and 2014; Gómez-Martínez et al., 2013, 2015a and 2015d); and Emilia, Italy, 2012 (Manfredi et al., 2013). Also, the last earthquake has been used in order to carry out a compared analysis between three methods representing such different steps of accuracy in the approach: exact pushover analysis, POST approach (see section 1.1.2) and FAST method. Results of this comparison confirm the satisfactory behaviour of the last one.

The general behaviour of FAST is resumed in the steps listed herein (see also Figure 1):

- 1) Parameters corresponding to a hypothetical simulated design of the whole class are collected: masses, period, spectral acceleration and level of overstrength.

- 2) Thanks to the assumption of values for the mechanical properties of infills and their ratio of area in plan, approximate CC and IN2 curve in terms of Peak Ground Acceleration (PGA) for the equivalent Single Degree of Freedom (SDOF) of the building are obtained.
- 3) Interstorey drift of the infills corresponding to the thresholds of the non-structural DS are stated through an empirical-mechanical interpretation.
- 4) Assuming shear-type behaviour of the frames, with a mechanism of collapse involving only the ground floor, thresholds of top displacement of the SDOF corresponding to the attainment of each DS at ground floor are carried out.
- 5) These SDOF displacement thresholds (obtained in (4)) are switched into PGA values through the IN2 curve (obtained in (2)), thus representing the PGA of the exceedance of each DS.

It is important to remark that FAST does not work with specific case study buildings but with general “classes” or categories of infilled RC buildings, being each class characterised only by: i) its number of storeys and ii) its age of construction. The rest of the input parameters (geometric and mechanical properties of buildings), as well as the internal variables and procedures governing the method (R - μ - T relation, deformed shape, dynamic properties and mechanism of collapse), are obtained from different sources:

- specific literature;
- seismic codes;
- experimental tests;
- in-situ collected data;

Given that each source provides data corresponding to different probabilistic fractiles, an effort has been done in order to uniform them to a constant level of conservativeness. Anyway, the assumptions are in most of the cases balanced to conservativeness.

Another important objective in the elaboration of FAST approach is to reach homogeneity within the level of accuracy of the assumptions of variables and the internal procedures. In general, it does not make sense to waste too much effort

hunting some values or formulations since most of the other assumptions defining the capacity and demand could be extremely approximate, based in theoretical assumptions or in few experimental or numerical examples. Furthermore, not only the definition of the capacity and demand associated to each class of building is approximate; also the benchmark for the comparison of the results –the Damage State classification— is too vague in its definition, difficult in its application for assessment and very sensitive to the expert opinion (see section 5.1.3.1).

However, concerning the level of accuracy of the assumption, it is necessary to difference between variables and algorithms which are applied to all the classes of buildings and those parameters that can make the difference between the performance of diverse classes. The last is important because can influence the trend of the results, the variability of the damage for the different basic input variables defining classes: age, number of storeys, etc. Thus, those parameters may be considered with higher accuracy, at least in their relative behaviour for each class of building.

It is worth noting that, as the role of each variable and each procedure are shown explicitly and their origin is detailed, different values or assumptions can easily be assumed within the same theoretical framework. Actually, the flexibility of the approach is based on this capacity of customisation, being the method able to be oriented towards a more theoretical or empirical point of view, or even varying its conservativeness, depending on the source of origin of the variables.

In Table 44, all the variables of input are presented and classified. In all the following, only the variables not included herein are described. The first three groups of variables are particularities of the specific building stock at the considered location, depending on the basic variables; the assumed values corresponding to the case study considered on this Thesis are detailed in section 6.1. On the other hand, the last two groups of variables do not depend on the particular application; suggested values for these parameters are provided in this chapter.

Table 44: Input variables of FAST

BASIC VARIABLES DEFINING CLASSES		
n	[storeys]	Number of storeys
age	-	Age of construction
lc	-	Location of the class of buildings
CODE SIMULATED DESIGN VARIABLES		
T	[s]	Fundamental period of design
$S_a(T, \text{age}, \text{lc})$	[g]	Spectral acceleration of design
$m_d(\text{age})$	[t/m ²]	Superficial storey mass of design
$\lambda_d(\text{age})^\dagger$	-	Relative MDOF 1 st mode participating mass of design
$\gamma_d(\text{age})$	-	Design seismic combination factor
$f_{cd}(\text{age})^\ddagger$	[N/mm ²]	Design value of concrete compressive stress
$f_{yd}(\text{age})^\ddagger$	[N/mm ²]	Design value of steel yield stress
$(L_V/h)_1(\text{age})^\ddagger$	-	Relative shear span at column ends of 1 st storey
GEOMETRIC VARIABLES FROM OBSERVATION		
$h_1(\text{lc})$	[m]	Ground floor interstorey height
$h_s(\text{lc})$	[m]	Upper floors interstorey height
$\rho_{w,i}(\text{lc})$	-	Ground floor infills ratio in plan
$\rho_{w,s}^\ddagger(\text{lc})$	-	Upper floors infills ratio in plan
$A_{trib}^\ddagger(\text{lc})$	[m ²]	Average tributary area of loads for columns
$\rho_s^\ddagger(\text{lc})$	-	Average reinforcement ratio of 1 st storey RC columns
$\lambda_g^\S(\text{lc})$	-	Average geometric slenderness of buildings
DYNAMIC VARIABLES		
T_1	[s]	Assumed real fundamental period of design
m_r	[t/m ²]	Assumed real superficial storey mass
λ_r	-	Assumed real relative MDOF 1 st mode participating mass
κ	-	Factor switching from elastic to effective period
MECHANIC VARIABLES		
R_ω	-	Overstrength factor up to the 1 st yielding
R_α	-	Overstrength factor from the 1 st yielding up to the structural yielding
τ_{max}	[N/mm ²]	Maximum masonry shear strength
μ_s	-	Ductility up to the infills' strength degradation start
α	-	Relative RC contribution to the maximum strength of the infilled frame
β	-	Relative infills contribution to the residual strength of the infilled frame
IDR_{DSj}	-	Interstorey drift of infill panels causing DSj
Ω_{sec}	-	Relative infills secant stiffness degradation at the attainment of DS2
G_w^\ddagger	[N/mm ²]	Masonry shear modulus
E_w^\S	[N/mm ²]	Masonry elastic modulus
[†] Only for simplified FAST [‡] Only for generalised FAST [§] Only for extended FAST		

It is worth noting that the location (classified as a basic variable) plays a triple role:

- it defines, directly, the real demand used in the vulnerability assessment, both in the case of a real earthquake or derived of a generic hazard estimation;
- it defines, indirectly, the assumed capacity of the assessed building stock, as this is evaluated as depending on the current code demand for that location when the considered class of building was designed;
- it influences the parameters representing the local characteristics of the building stock.

In this section, the first version of FAST, applicable only to uniformly infilled RC frames, is presented. In all the following it is called “simplified FAST”, while the extension of the method for non-uniformly infilled frames (exposed in section 5.2) is called “generalised FAST”, and the algorithms presented in section 5.3 conform the “extended FAST”.

5.1.1 Code-based assessment of bare frames

In this section, a preliminary version of FAST, corresponding to the assessment of the performance of bare frames, is presented. This is a code-based approach, i.e., it presupposes that both the characteristics of the building and its performance are those assumed in the process of design. Thus, it assumes that:

- i) there are not any infills or their structural contribution is intentionally discarded;
- ii) the strength of the bare frame is equivalent to the base shear of design, having only into account the sources of overstrength not depending of the design choices;
- iii) the spectral acceleration of design may correspond to a period of code rather than a period of physical model;
- iv) the ductility of the bare frame may be equivalent to the behaviour factor assumed in the design.

The resulting approach is too conservative. In fact, the assumption i) reduces the capacity largely, especially for poor-seismic-designed frames (see section 2.2); also the assumption iv) can be very conservative, as seen in section 3.6. Although iii) may be non-conservative, the combination with ii) becomes conservative, as explained in 1.2.2. Actually, this former approach, more than representing a real tool for the assessment of bare frames, can be useful in order to evaluate the maximum capacity of the RC frame aimed at being combined with the strength of the infills (see section 5.1.2).

It is worth noting that assumption ii) presupposes that the building has been designed to a seismic demand, and that this seismic demand rules the design. This hypothesis is conservative anyway: if the seismic demand is so insignificant that other actions –gravitational, wind, etc.— rule the design, the lack of assumed capacity would be a source of overstrength (see section 1.2.1.3). However, the first hypothesis prevents to assess the vulnerability of buildings designed only to gravitational loads, as no base shear of design can be considered. Actually, given that usually higher geographical extension of application are provided by more recent seismic codes, lots of cities characterized by a medium level of seismic hazard present RC building stock with “gravitational” design (Ricci et al., 2011a). Some alternatives aimed at dealing with this issue are proposed in 5.3.1.

5.1.1.1 *Strength capacity*

Aimed at defining the approximate bilinear CC of the bare frame, the maximum strength capacity (V_y) is obtained as function of the design base shear (V_d). It is calculated (see Equation (76)) as the product of spectral acceleration of design ($S_d(T)$, being T the period used in the hypothetical design) and the total mass of design corresponding to the seismic situation (M_d , expressed as a product of the number of storeys, the area of the storey A_b and the superficial storey mass considered in design), weighted by two factors:

- Relative MDOF first mode participating mass of design (λ_d), which represents the expected ratio between the effective mass of the MDOF to the total mass of design. This factor is usually suggested by codes in a conservative way or assuming a predetermined deformed shape (see section 1.2.1.4).

- Design seismic combination factor (γ_d), which is an amplification factor to be used at the combination with gravitational actions in the accidental situation that can be found in some codes (see section 2.2.9.1).

$$V_d \equiv V_d(T) = S_a(T) \cdot M_d \cdot \lambda_d \cdot \gamma_d = S_a(T) (n \cdot A_b \cdot m_d) \cdot \lambda_d \cdot \gamma_d \quad (76)$$

$$V_y = V_d \cdot R_s = [S_a(T) (n \cdot A_b \cdot m_d) \cdot \lambda_d \cdot \gamma_d] (R_\omega \cdot R_\alpha) \quad (77)$$

Then, V_y is obtained as the design base shear (V_d) amplified by the overstrength factor (R_s) decomposed in its two constituents R_ω and R_α , as shown in Equation (77) and Figure 24.

As widely explained in section 1.2.1.3, the only contribution completely traceable within R_ω is the relation between the mean and nominal strength capacity for materials. They have been stated as $f_y/f_{y,nom}=1.27$ and $f_c/f_{c,nom}=1.24$. For RC elements mainly in bending, it can be stated that the steel strength is the one which rules the behaviour, being its influence larger than that of the concrete[†]. Hence, conservatively, only this contribution is assumed to constitute R_ω . However, as the value of 1.27 corresponds to the switching from nominal (characteristic) to mean, if partial factors of materials corresponding to persistent-transient situations are used, it may be multiplied for the factor switching from design to characteristic value, called partial factor of design for steel (γ_s).

In fact, new codes, as Eurocode 2 (BSI, 2004), different values of γ_s for seismic (accidental in general) situations than for persistent and transient ones are suggested. However, for existing buildings, in general, common design practice (not extremely accurate) may have been to use the same partial factor for all the

[†] The moment of resistance of a RC section in a state of simple bending (no axial force) without compression reinforcement can be expressed as $M_r = \rho \cdot b \cdot d \cdot f_y (d - \rho \cdot d \cdot f_y / 2f_c)$, being ρ , b , d , f_y and f_c the reinforcement ratio, base and effective depth of the section, steel design yielding strength and concrete design maximum strength, respectively. When the same overstrength factor k is applied alternatively to steel and concrete, moments of resistance $M_{r,s}$ and $M_{r,c}$ are obtained, respectively, resulting in a factor relating the increments expressed as $(M_{r,s} - 1)/(M_{r,c} - 1) = 2kf_c / \rho f_y - k - k^2$, which ranges between 2 and 10 for common values of resistances and reinforcements. This factor also increases with the existence of compression reinforcement.

situations. Thus, in this work, although it is slightly non-conservative, γ_s is assumed to be 1.15, the typical value for persistent and transient situations. Thus, $R_\omega = 1.27 \cdot 1.15 \approx 1.45$. Anyway, any other assumption can be done.

Besides, for R_α , a very conservative value of 1.0 is suggested, thus discarding the contributions B2 to B9 in the whole ensemble of R_S . This assumption may not have a clear correlation with the hypothetical assumption of a storey mechanism of collapse (see section 1.2.1.3). Again, any other suitable value can be assumed.

Then, the maximum spectral acceleration capacity of the equivalent SDOF ($C_{s,RC}$, see Figure 170) is obtained by dividing the base shear capacity by the real participating mass of the MDOF, expressed as a fraction of the real total mass in the seismic situation M_r , which is function of the real superficial storey mass (see Equation (78)). In the last step of the equation, the whole second factor (between brackets) is simplified into R_D , the “reduced demand contribution” of the behaviour factor (see section 1.2.1.3). The two first fractions in the brackets represents somehow the contribution C1 (overestimation of dynamic properties and masses), while the third factor is ascribable to C2 (corrections of design).

$$\begin{aligned}
 C_{s,RC} \equiv C_{s,RC}(T) &= \frac{V_y}{\Gamma \cdot m^*} = \frac{V_y}{M_r \cdot \lambda_r} = \frac{[S_a(T)(n \cdot A_b \cdot m_d) \lambda_d \cdot \gamma_d](R_\omega \cdot R_\alpha)}{(n \cdot A_b \cdot m_r) \lambda_r} = \\
 &= S_a(T) \left(\frac{\lambda_d}{\lambda_r} \frac{m_d}{m_r} \gamma_d \right) (R_\omega \cdot R_\alpha) \equiv S_a(T) \cdot R_D \cdot R_S
 \end{aligned} \tag{78}$$

It is worth noting that in this expression, the variables contained in the numerator refers to assumptions of design (period, mass, deformed shape...) depending on the corresponding seismic code, while those contained in the denominator are intended to represent the real characteristics of the building. The variables in the numerator depend on the basic input parameters (n , age and location) defining the classes of buildings (see Table 44), thus changing for every case study. However, the variables in the denominator can be assumed to be more or less constant for all the classes of building belonging to a given location, if it is assumed that both the real mass of the buildings and the deformed shape are common.

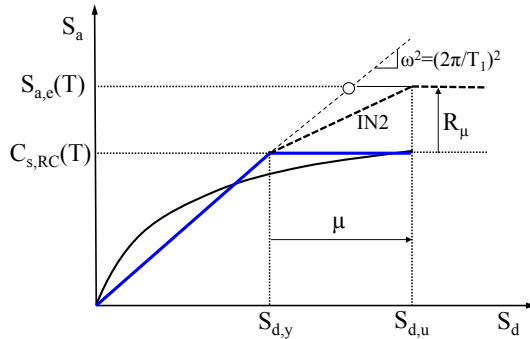


Figure 170: Approximate capacity curve of a RC bare frame

The values adopted by each one of the variables in the numerator refers to an hypothetical simulated design, so depend on the current codes –seismic and generic— at the age of the design and construction of the buildings representing the class, and also depend on the usual methods of design at that age. These parameters should be chosen attending to the following considerations, always having into account that the higher are the values, the lower is the conservativeness of the assessment:

- $S_a(T)$. It depends on general characteristics of the case study (soil conditions, importance of the building, assumed damping, behaviour factor and spectral shape, see Equation (30)) and, almost all, on the elastic period assumed in design. Unlike the general characteristics, settled by codes, the period can be chosen both from simplified code formulations or from a modal analysis (see section 1.2.2.1). It is worth noting that FAST need to reproduce a hypothetical simulated design aimed only to know the value of the base shear of design. Thus, assuming that the structure has been designed with a conservative estimation of the elastic period (i.e., with a code formulation providing lower values of period), results in an overestimation of the base shear of the structure, which is non-conservative. It may be reasonable to consider the age of the class of building in relation with the time thereafter the use of computer for structural analysis became widespread. In fact, before this moment, obtaining the period from a modal analysis was almost impossible, so the

assumption of a code-based period is right. For structures whose age of construction is posterior, some estimation of the period provided by modal analysis could be done. Anyway, as explained in section 1.2.2.1 and shown in Figure 35, elastic periods obtained from modal analyses carried out on frames designed with modern seismic regulation are similar to the formulations proposed by some of the codes.

- λ_d . It is suggested by the seismic codes, explicitly or indirectly –by proposing a deformed shape or a static equivalent load pattern, see section 1.2.1.4–. Again, it might be possible for modern classes of buildings to estimate its value based on a hypothetical modal analysis, but the effort may not worth it.
- m_d . The estimation of the mass assumed in the hypothetical design may be done by considering the following characteristics, depending on the age of construction:
 - i) differences in the real masses of the constructive elements for each class of building, i.e. thickness of the partitions, thickness of the flooring, section of the structural members, thickness of the slab, etc;
 - ii) different values proposed by the action codes for the evaluation of the loads coming from the same actions;
 - iii) different reduction coefficient provided by the seismic codes to be applied to the live loads in the seismic situation.
 - iv) the explicit consideration of the weight of the structural members (columns and primary and secondary beams), usually discarded in a manual calculation and having into account in a computerised analysis, even considering that the values for the weight of the slab provided by the codes actually accounts for the primary and secondary beams.

Regarding the variables in the denominator, they can be assumed to be more or less constant throughout the years:

- λ_r . It depends on the “concavity” of the deformed shape, which in turn depends on the distribution of stiffness along the height (see section

1.2.1.4). As it corresponds only to the bare frame, any eventual difference would be only a consequence of differences in the relative sections of the columns. It can be stated that the increment of the minimum resistance of concrete within years, together with the existence of code limitations for the minimum dimensions for the RC columns, cause that minimum columns can resist the seismic forces in almost all the storeys except for the lower ones, in the case of medium-low seismic demand. That means that the deformed shape would be more “concave”, similar to a sinusoidal curve, providing higher values of λ_r . However, within years also the site hazard has been usually increased; also in modern codes columns dimensions do not depend any more on the flexural demand but on drift limitations or capacity design rules. So, it is not easy at all to simplify the choice of λ_r . For the simplified FAST, values suggested by EC8 part 1 (CEN, 2004) for the evaluation of the equivalent static forces are used (see Equation (79); in a simplified way, it is assumed that always $T \leq 2 \cdot T_C$). Those values are conservative if a linear deformation is considered, but they are non-conservative for $4 \leq n \leq 8$ in the case of a sinusoidal deformation. Also, it is worth noting that λ_r is used in this case to switch into SDOF a pushover curve corresponding to a bare frame, so only the distribution of stiffness of the RC frame should be taken into account. However, the maximum spectral acceleration capacity of the frame, $C_{s,RC}$, is also used to estimate its partial or total contribution when combined with infill panels (see section 5.1.2.1). In this case, λ_r must correspond to the distribution of stiffness of the infilled frame, which can be constant in the case of uniformly infilled or reduced in the first storey, resulting in a very “concave” deformed shape, for pilotis frame (see Table 2). So, given the high variability of possible situations, the choice of EC8 values seems to be in accordance with the approximate framework of FAST. In the generalised method, exact values are used (see section 5.2.3). It is also important to note that λ_r is intended to represent the initial elastic deformed shape. Thus, analogously to that stated in section 5.1.3.7 for Γ , its value may be less precise for higher DS, considering that the assumed deformed shape, corresponding to a mechanism of the first storey, would furnish higher values of λ_r (see Table 2).

$$\lambda_r = \begin{cases} 0.85 & , \text{ if } n \geq 3 \text{ and } T \leq 2T_C \\ 1.00 & , \text{ otherwise} \end{cases} \quad (79)$$

- m_r . Different examples of differences in the real mass of the buildings depending on the age are indicated in point i) of the paragraph corresponding to the estimation of m_d . It is not easy to identify a trend in the dimensions of structural members, as explained in the precedent. Regarding the slabs, their thickness depends not only on the span, loads and seismic demand but also on the type of beams (deep or wide, being thicker in the last case to adapt to the beam height), on the deflection limitations provided by the RC codes and also on the limitation of impact noise. The common spans have increased within years; loads are more or less constant; seismic demand has increased; the use of deep beams depends on the site (see Chapter 3); and the deflection limitations tend to decrease in last years (at least in Spain, see section 2.2.9.3). Having every contribution into account, the thickness might be a bit higher for modern structures, but it should be supported by feasible literature. Regarding the rest of dead loads: thickness of the flooring seems to increase for modern buildings; brick partition walls, internal and external, are thicker and higher in modern buildings –given that the interstorey height may be higher too—, being its superficial density apparently similar. Live loads in residential buildings may be similar throughout years. So, real mass of modern building may be higher than for older ones. However, again considering both the approximate philosophy of the method and the difficulty of finding some feasible approach to evaluate these differences, a constant superficial storey mass of 0.8t/m^2 is assumed. This value comes from a conventional consideration of:

- i) a 1-directional slab of 25-30cm with primary and secondary beams $\rightarrow 4\text{kN/m}^2$;
- ii) equivalent superficial weight of RC columns $\rightarrow 0.4\text{kN/m}^2$;
- iii) terrazzo or ceramic flooring of less than 10cm $\rightarrow 1\text{kN/m}^2$;
- iv) equivalent superficial weight of internal brick partitions $\rightarrow 1\text{kN/m}^2$;

- v) equivalent superficial weight of internal external double-layered brick facades 1kN/m^2 ;
- vi) live loads in the seismic situation $\rightarrow 2 \cdot 0.3 = 0.6\text{kN/m}^2$.

Anyway, different values can be assumed if a consistent study is carried out, always considering that the higher are the values, the higher is the conservativeness of the assessment.

The other parameter representing the strength capacity of the hypothetic bare frame is the elastic spectral acceleration capacity, $S_{a,el}$ (see Figure 170). It is obtained by multiplying the inelastic capacity by the ductility contribution (R_μ), equivalent to multiply the spectral acceleration of design by the behaviour factor q assumed in the hypothetical design –proposed by seismic codes—, as seen in Equation (80). The last is consistent with the definition of q as in Equation (1a). If q is calculated as in Equation (1b) instead, then the expression for $S_{a,el}$ may be that on Equation (81), resulting in a larger elastic capacity.

$$S_{a,e} \equiv S_{a,e}(T) = C_{s,RC} \cdot R_\mu = S_a(T) \cdot (R_D \cdot R_S \cdot R_\mu) = S_a(T) \cdot q \quad (80)$$

$$S_{a,e} = S_a(T) \cdot q \cdot (R_w \cdot R_D) \quad (81)$$

The code-based assumption of q has been widely proved to be conservative (Fardis, 1999); in fact, the principle of codes is to furnish conservative design. In section 3.6.3, estimations of conservativeness for typical Spanish buildings are shown. More disquisitions about the conservativeness of the assumption of a code-based q are developed in section 5.1.1.3.

5.1.1.2 Fundamental period

The fundamental period defining the slope of the first branch of the capacity curve of the bare frames (T_1) is intended to represent their real effective period. It is worth noting that it has nothing to do with the elastic period of the hypothetical simulated design aimed at the evaluation of the strength capacity (T), considered in the previous section. Thus, it has no sense to consider for each seismic code a different code-based period.

However, similarly to the case of the real masses or the real distribution of stiffness, it is very hard to estimate the effective period of bare frames (see section 1.2.2.4) and even more its variation within years. For this reason, and consistently with the level of accuracy of the rest of the assumptions, constant values of the period for all the ages of construction are assumed.

Hence, an approximate formulation for the elastic period of bare frames is chosen in this work in order to represent the effective period. As seen in section 1.2.2.1, all those formulations underestimate the elastic period; also, no factor κ is used to have into account the switching from elastic to effective. This assumption is highly conservative from the point of view of the demand estimation, which is usually inversely proportional to the period; but it is slightly non-conservative for the evaluation of the ductility and the capacity of displacement of the frame, given that for the medium-low range of periods, $\mu \geq R_\mu$ for most of the R - μ - T relations (see section 1.2.3.4). Still, both influences result in conservativeness.

In this work, the conventional formulation proposed by EC8 (CEN, 2004), which was firstly proposed in SEAOC-88 (1988, see Table 4) is assumed. Any other simplified formulation and κ value is suitable.

5.1.1.3 *Displacement capacity*

Aimed at defining of the CC, the yielding and maximum spectral displacement capacity of the structure must be sought (see Figure 170). The yielding spectral displacement $S_{d,y}$ is obtained geometrically from the strength capacity and the effective period (see Equation (82a)), while the maximum spectral displacement $S_{d,u}$ is obtained by multiplying the yielding capacity by the assumed ductility (see Equation (82a)).

$$S_{d,y} = C_{s,RC} \left(\frac{T_1}{2\pi} \right)^2 ; \quad S_{d,u} = \mu \cdot S_{d,y} \quad (82a,b)$$

The value of the ductility μ comes from the assumption of a R - μ - T relation (see section 1.2.3.4). In this work, the simplified relation proposed in (Fajfar, 1999), based in the work of (Vidic et al., 1994), is assumed; any other assumption may be possible. The input value of R_μ can be chosen to be consistent with the

expression of q compatible with Equations (1a) and (80), as shown in Equation (83a), or conversely with the expression of q compatible with Equations (1b) and (81), as shown in Equation (83b). In this work, the second option is chosen, unless it is less conservative than the first one; anyway, the high conservativeness provided by all the rest of the assumptions –especially by the election of the effective period— rules the assessment. It is worth noting that R - μ - T requires a value of “corner” period (T_C) which must come from the considered event or generic demand.

$$R_\mu = \frac{q}{R_w \cdot R_\alpha \cdot R_D} \quad ; \quad R_\mu = \frac{q}{R_\alpha} \quad (83a,b)$$

5.1.1.4 Demand curve and IN2 curve

As seen in section 1.2.3.4, the maximum capacity of a structure is not independent of the event to which it is subjected. The real strength capacity is actually independent, but the displacement capacity associated with this strength is not. In fact, PGA capacity depends on the spectral elastic acceleration capacity and it in turn depends on the displacement capacity.

Aimed at obtaining of the PGA capacity of a structure, the IN2 curve (see section 1.2.3.5) must be constructed from the CC through the assumed R - μ - T , which needs to be given a value for T_C belonging to the demand (see section 1.2.3.2). This value depends on whether the considered demand spectra come from a real earthquake or they are smooth ones (from code or from a real event), but it is not possible to state which choice provide larger values for T_C . In this work, response spectra from real accelerograms are used directly; the other possibility would be also feasible.

Larger values of T_C result in lower slopes of the second branch of the IN2 curves corresponding to bare frames, and similarly for the second and third branch of those corresponding to infilled frames. Lower slopes involve lower PGA capacities for a given displacement demand; hence, larger values of T_C results in conservativeness. This fact is relevant for the FAST method for infilled frames; for the preliminary assessment of bare frame it has not any influence, as the estimation

of the capacities is done by assuming constant values for q and R_u , thus the PGA capacity of bare frames with T_1 higher or lower than T_C is the same.

5.1.1.5 *Assessment of the performance*

Finally, the performance of the bare frame when subjected to an event is suggested to be evaluated by means of the N2 method (see section 1.2.4.2 and Figure 55). The proposed assessment only returns a “yes/no” answer for the possibility of a complete collapse of the structure. Aimed at an assessment of the intermediate Damage States of Damage Levels, the corresponding thresholds of top displacement should be defined and transformed in intermediate PGA levels through the IN2 curves. This procedure is actually implemented for the simplified and generalised FAST for the assessment of infilled frames, which are explained in the following. For bare frames, it has not been included as the scope of this approach is to be a preliminary estimation of the relevance of the event in comparison with the hypothetical strength of bare frames.

5.1.2 Capacity curve of uniformly infilled frames

In the following three sections, the simplified FAST for infilled RC frames is developed. They are organised consistently with the conceptual diagram of FAST (see Figure 1):

- in the actual section, tools aimed at the evaluation of the PGA capacity of the buildings are furnished (left column of Figure 1);
- in section 5.1.3, expressions for the definition of top displacement thresholds for the different non-structural damage states (DS) are provided (right column of Figure 1);
- in section 5.1.4, the methodology of assessment is presented (last step of Figure 1).

In all the following, the subscript “ w ” refers to features related to the infill panels, while the subscript “ inf ” concerns the infilled frame as a whole.

5.1.2.1 *Maximum and residual strength capacities*

The conceptual generation of simplified CC from real pushover curves and their theoretical decomposition in bare frame and infills has been already explained in detail in section 1.2.1.5 and in Figure 28a. FAST propose directly the quadrilinear CC shown in Figure 171b, by an hypothetical switching from MDOF to SDOF from the pushover curve shown in Figure 171a. In this figure, both single pushover curves corresponding to the bare frame and to the infills are shown, being V_y and $V_{w,max}$ their maximum base shears, respectively. The conceptual addition of both curves results in the curve of the infilled frame, characterized by a maximum base shear (V_{max}), attained approximately at the same displacement than $V_{w,max}$, and a minimum residual base shear (V_{min}), attained after the collapse of the infills. As the maximums of the components V_y and $V_{w,max}$ are not attained at the same displacement level, the maximum of the combination (V_{max}) must be defined as a weighted addition of both values. Thus, two weighting factors, ranging between 0 and 1, are defined (see Figure 171a):

- α , which represents the strength –as a fraction of V_y – of the bare frame at the displacement corresponding to the attainment of $V_{w,max}$ by the curve of the infills, to be added to it;
- β , which represents the residual strength –as a fraction of $V_{w,max}$ – of the infills after their collapse, to be combined with the maximum strength of the bare frame V_y .

It would be possible to particularize the calculation of α for each single case, proceeding by iterations, as follows:

- i) a preliminary value of $\alpha=\alpha_0$ is assumed;
- ii) V_{max} is obtained with this value;
- iii) knowing $T_{eff,inf}$ (see section 5.1.2.2), the displacement corresponding to the attainment of V_{max} is obtained as $D_1=V_{max}/(2\pi/T_{eff,inf})^2$
- iv) knowing μ_s (see section 5.1.2.2), the displacement corresponding to the end of the “plateau” is calculated as $D_2=D_1 \cdot \mu_s$;
- v) the displacement corresponding to the midpoint of the “plateau” is calculated as the arithmetic mean $D_m=(D_1+D_2)/2$;

- vi) knowing the assumed effective period of the bare frame (T_1) and its yielding strength (V_y), the strength corresponding to the midpoint-plateau displacement is calculated as $V_{Dm} = \min\{(2\pi/T_1)^2 \cdot D_m; V_y\}$;
- vii) a new factor α is calculated as $\alpha_1 = V_{Dm}/V_y$, which is again introduced into the step i) of the algorithm until the target error is reached in the j^{th} iteration.

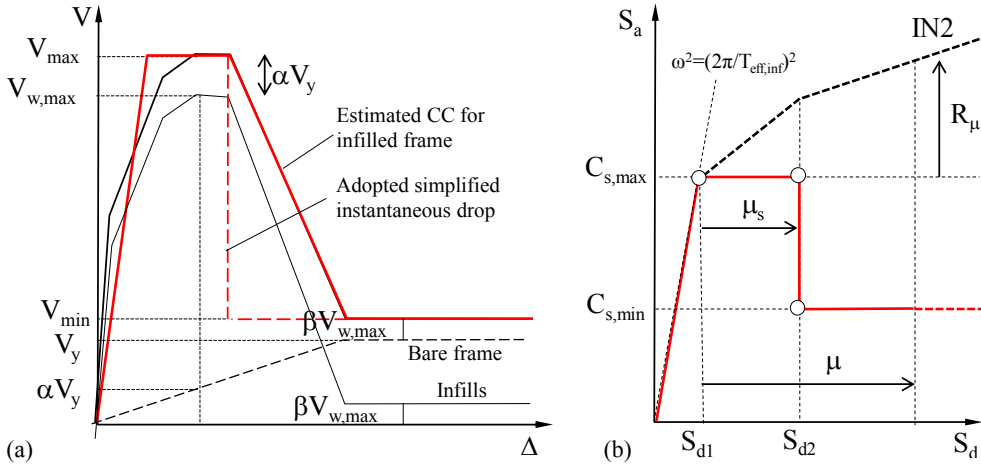


Figure 171: Conceptual generation of the pushover curve of infilled frame in FAST method (a) and variables defining the corresponding CC and IN2 (b)

However, in this approach, it is considered that it does not worth to carry out this procedure but assuming a constant value of α . This decision lays on the awareness of the high variability and difficulty of estimation of $V_{w,max}$, which is the main “contributor” to V_{max} . Thus, it do not seem reasonable to introduce a time-consuming algorithm only aimed at having into account a little contribution that would be anyway jeopardised by the error on the evaluation of the bigger contribution of the infills. Hence, a constant value of 0.5 is assumed.

On the other hand, the evaluation of β do not require any iterative procedure, as it is assumed that the residual strength of the infilled frame ($V_{w,max}$) is reached just after the instantaneous drop, even in the case that at that displacement level the bare frame has not reached yet its maximum strength capacity. Conservatively, a

constant value of 0.0 is assumed for β . Again, any other suitable value can be adopted.

The whole procedure results in the obtaining of the maximum ($C_{s,max}$) and minimum ($C_{s,min}$) acceleration of the equivalent SDOF, as shown in Equations (84a) and (84b), respectively, being the maximum strength of the bare frame and infills represented by $C_{s,RC}$ and $C_{s,w}$, respectively (see Figure 171b). As explained in section 1.3, the relative contribution of the infills is higher for sub-standard buildings than for capacity-designed ones. In the last case, it is also possible to obtain a residual strength of the infilled frame even higher than its maximum strength (ruled by the infills). As the CC is only defined by those two levels of strength, aimed at avoiding an “inverse drop” –i.e., a sudden increase of the strength at the displacement level when the infills are supposed to be collapsed—, the maximum spectral acceleration capacity of the infilled frame is stated to be at least as the residual one (see Equation (84c)).

$$C_{s,max} = \alpha \cdot C_{s,RC} + C_{s,w} \quad ; \quad C_{s,min} = C_{s,RC} + \beta \cdot C_{s,w} \quad ; \quad C_{s,max} \geq C_{s,min} \quad (84a,b,c)$$

$$C_{s,w} = \frac{V_{w,max}}{\Gamma m^*} = \frac{\tau_{max} \cdot A_{w,1}}{\lambda_r \cdot M} = \frac{\tau_{max} \cdot \rho_{w,1} \cdot A_b}{\lambda_r \cdot n \cdot A_b \cdot m_r} = \frac{\tau_{max} \cdot \rho_{w,1}}{\lambda_r \cdot n \cdot m_r} \quad (85)$$

The maximum spectral acceleration capacity of the infills ($C_{s,w}$) is obtained in a similar way to that of the bare frame: switching from MDOF to SDOF in ADRS format by dividing the maximum strength by the first mode participating mass of the MDOF (see Equation (85)). The transformation of the denominator is analogous to that in Equation (78), and the same considerations already done in section 5.1.1.1 about the different parameters contained in that denominator may be done.

The maximum shear resistance of the infills is obtained from the cracking one (τ_{cr}) through an amplification factor (a_w), as shown in Equation (27). In this work, the assumption in (Fardis, 1997) for a_w to be equal to 1.3 is chosen; concerning, τ_{cr} , a code-based –conservative— value is used: 0.35N/mm^2 , as suggested by the Italian current general construction code (CS. LL. PP., 2009). The last decision lays on the awareness of the high variability and difficulty of estimation of both two members defining $V_{w,max}$, especially $\rho_{w,1}$. Thus, it do not seem reasonable to use

very specific or particular values for τ_{cr} , given that its influence would be jeopardised by the error on the evaluation of $\rho_{w,1}$.

5.1.2.2 *Effective period and ductility*

Aimed at defining of the CC and IN2 curve, and having already the values for the maximum and minimum spectral acceleration capacity, only two more parameters are needed: the effective period of the infilled frame ($T_{eff,inf}$) and the ductility up to the beginning of the degradation of the infills (μ_s), see Figure 171b.

Regarding the period of the infilled frame, it is obtained as the elastic one $T_{el,inf}$ amplified by a factor κ (see section 1.2.2.4). Several empirical-based and numerical expressions have been presented in Table 5 and Figure 37 for the estimation of $T_{el,inf}$. In this work, the expression corresponding to Equation (17) is used, becoming into Equation (86) when switching from elastic to effective is carried out. On the other hand, κ is assumed to be equal to 1.3, consistently with the data of Table 7. Concerning to μ_s , a constant value of 2.5 for all the cases is suggested in this work for Mediterranean buildings, according to the literature cited in section 1.2.1.5. Any other suitable expressions and values can be taken instead.

$$T_{eff,inf} = \kappa \cdot T_{el,inf} = \kappa \cdot 0.0023 \frac{H_T}{\sqrt{\rho_{w,1}}} \quad (86)$$

As a result of the evaluation of $T_{eff,inf}$ and μ_s , the CC and IN2 curve can be completely defined, being the spectral displacements corresponding to the beginning and end of the second branch (S_{d1} and S_{d2} , respectively) calculated as in Equations a) and b), respectively. The IN2 must be expressed in PGA units instead on $S_a(T)$ by following the procedure already exposed in section 1.2.4.2 and shown in Figure 55.

$$S_{d1} = C_{s,max} \left/ \left(\frac{2\pi}{T_{eff,inf}} \right)^2 \right. ; \quad S_{d2} = S_{d1} \cdot \mu_s \quad (87a,b)$$

It is worth noting that both curves (CC and IN2) do not have any “ending”, i.e., the ultimate displacement capacity of the infilled frame is not defined; in

Figure 171b, both curves are extended with a dashed line. As explained in detail in the following section, in this work only the non-structural damage ($DS \leq 3$) is considered. Thus, the collapse of the building (equivalent to a DS5) is not defined: no spectral displacement –coming from an interstorey drift interpretation of DS5— is associated to it. Collapse of infilled frames is decided to not even being defined by a ductility capacity consistent with a code-based assumed behaviour factor, as for the preliminary methodology for the assessment of bare frames (see section 5.1.1.3). In fact, the excessive level of conservativeness of this assumption could generate improbable situations as to characterise the collapse of a building (DS5) with a level of displacement lower than that corresponding to the collapse of the infills (DS3).

5.1.3 Damage States displacement thresholds for uniformly infilled frames

As a result of the application of the first part of the methodology, presented in the previous section, the IN2 curves for each class of building, representing the spectral displacement demand for each PGA demand, are available.

Aimed at the assessment of the Damage State (DS) reached by each class of building when subjected to an event, it is necessary to know in each case the PGA demand for which each single DS is attained. The last is carried out through 3 steps:

- 1) values of interstorey drift (IDR) of the infills corresponding to the attainment of each non-structural DS are stated through an empirical-mechanical interpretation;
- 2) assuming shear-type behaviour of the frames, with a mechanism of collapse in the ground floor, thresholds of top displacement of the SDOF corresponding to each DS' interstorey drift at ground floor are carried out;
- 3) these SDOF displacement thresholds are switched into PGA values through the IN2 curve, thus representing the PGA of the exceedance of each DS.


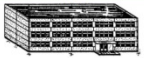


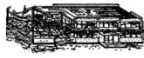
In the following, these three steps are developed in detail.

5.1.3.1 Correlation between interstorey drifts and Damage States

EMS-98 proposes 5 Damage States (DS). As seen in Table 45, each DS is characterised by a higher level of damage for non-structural elements than for structural members; thus, non-structural and structural damages are “stepped” by one DS. Any correlation between displacements and damage levels is a very hard process. Four causes are:

- 1) The consubstantial vagueness of the text of the EMS-98 classification:
 - the description of the damages is qualitative, not quantitative, and some adjectives –“fine”, “large”, “few”— are very imprecise;
 - it is not clear whether the described damages are enough to be appreciated in a single element or in a certain amount of similar ones;
 - based in the last assumption, neither it is clearly stated whether a certain amount of damaged elements of the same type (RC frame, RC walls or infill panels) is needed to be able to determine the damage, in the case that it is the higher one.
- 2) As a consequence of both the source 1) and the inherent difficulty of the in-situ assessment of damaged buildings, the variability due to the influence of the expert is very high.
- 3) The association of a mechanical phenomenon to every description of damage is a controversial issue; several interpretations are plausible.
- 4) Once assumed a mechanical phenomenon, it is also hard to represent its characteristic interstorey drift by a single fix value, or at least by a value which depend on a few input parameters.

Table 45: Proposal for correlation between *IDR* and DS

DS		DS1			DS2			DS3			DS4			DS5			
Scheme																	
Level of damage	General	Negligible to slight			Moderate			Substantial to heavy			Very heavy			Destruction			
	Non-str.	Slight			Moderate			Heavy			Very heavy			[Destruction]			
	Structural	[invisible]			Slight			Moderate			Heavy			Very heavy			
Element	Literal description of damage	Mechanical interpretation	IDR [%]	Literal description of damage	Mechanical interpretation	IDR [%]	Literal description of damage	Mechanical interpretation	IDR [%]	Literal description of damage	Mechanical interpretation	IDR [%]	Literal description of damage	Mechanical interpretation	IDR [%]		
Infill panels	Fine cracks	End of elastic phase, attainment of τ_c (Fardis, 1997)	$IDR_{cr}^{RC} \approx 0.03$ (Colangelo, 2012, 2013)	Cracks, fall of brittle cladding and plaster, falling mortar from the joints	Attainment of τ_{max} (Fardis, 1997)	$IDR_{max}^{RC} = 0.2$ (Dolsek and Fajfar, 2008; Colangelo, 2012)	Large cracks, failure of individual panels	Maximum strength degradation, residual strength (Fardis, 1997)	$IDR_{dr}^{RC} = 1.2$ (Colangelo, 2012, 2013)	-	-	-	-	-	-		
RC frame	Fine cracks in plaster over members	Cracking in the concrete, attainment of M_{cr} (Verderame et al., 2014)	$IDR_{cr}^{RC} \approx 0.3$ (Gómez-Martínez et al., 2014)	Cracks in columns and beams	Yielding in the steel bars, attainment of M_f (Verderame et al., 2014)	$IDR_{pl}^{RC} \approx 0.8$ (Gómez-Martínez et al., 2014)	Spalling of cover	-	$IDR_{sp}^{RC} = 1.5$ (Berry and Eberhard, 2003)	Large cracks in members, compression failure of concrete, fracture of rebars, bond failure of beam rods, tilting of columns; collapse of a few columns or of a single upper floor	Attainment of ultimate state for every failure, degradation of 20% (Panagiotakos and Fardis, 2001)	$IDR_{dr}^{RC} \approx 3.0$ (Elwood et al., 2007)	Opening of shear cracks	Collapse of ground floor or parts (e.g. wings)	-	IDR_{coll}^{RC}	
							Buckling of rods	-	$IDR_{br}^{RC} \approx 3.0$ (Berry and Eberhard, 2003)								
							Cracks in columns (only structures susceptible to brittle failures)	Shear failure without interaction	-								-
								Shear failure of squat column	-								-
								Shear failure with interaction	-								-
							Cracks in joints at the base	Diagonal cracking, principal tensile stress of $0.29\sqrt{f_c}$ (Priestley, 1997)	-								-
Shear walls	Fine cracks at the base	-	-	Cracks	-	-	Cracks at joints of coupled ones	-	-	-	-	-	-	-			

In this study, the definition of IDR characterizing each DS (IDR_{DSj}) is made for the only damage states characterized by a specific infill damage level (see Table 45 and Figure 172). In particular such procedure can be pursued up to DS3; values are mainly based on the studies shown in Figure 62:

- DS1: Fine cracks in partitions and infills. This DS is defined by the end of the phase in which infills are characterized by an elastic, uncracked stiffness. IDR_{DS1} could be evaluated as the drift characterizing the attainment of the cracking shear in the infill backbone (Fardis, 1997). Notwithstanding the value of a pure mechanical approach, in this approximate framework the IDR of the first storey at the specific damage level has been defined on experimental basis (Colangelo, 2012). Thus IDR_{DS1} is assumed equal to 0.0003. It is worth to note that such experimental value is similar to that computed on pure mechanical basis assuming typical infill characteristics of residential buildings (e.g., clay hollow bricks).
- DS2: Cracks in partition and infill walls, fall of brittle cladding and plaster. Crack pattern of the infill is typical of their theoretical post-cracking behavior up to the attainment of the peak strength. In a pure mechanical approach, IDR_{DS2} could be evaluated as the drift corresponding to the peak of the backbone according to Fardis' model (1997). The stiffness at this point can be computed according to the secant formulation by Mainstone (1970). On the other hand, in this case, again, the experimental basis for the evaluation of the IDR of the first storey was preferred and the value assumed is equal to 0.002 (Colangelo, 2012).
- DS3: Large cracks in partition and infill walls, failure of individual infill panels. At this stage the generic infill panel shows a significant strength drop with a consequent likely collapse of it. According to Fardis' backbone, the drift at this stage is strictly dependant on the softening stiffness of the infill. On the other hand the softening stiffness is characterized by a large variability depending on the specific kind of infill (mechanical properties, type of bricks,...). In such situation the experimental basis is the most reliable solution (Colangelo, 2012). Furthermore, it is worth to note that experimental data by Colangelo refer

to the typical infills employed in residential buildings of the Mediterranean area. Hence, in this case IDR_{DS3} is assumed equal to 0.012.

In Table 45, no definition of IDR characterising brittle failures in RC members is specified; simplified FAST is based only in damage states in relation with infill panels. Further research aimed at developing tools for accounting with brittle failures in RC members is presented in section 5.3.2. Notwithstanding this matter, it seems to be reasonable to define IDR_{DSj} by means of damages in infills, given that thresholds of IDR are lower than those corresponding to ductile failures in RC frame.

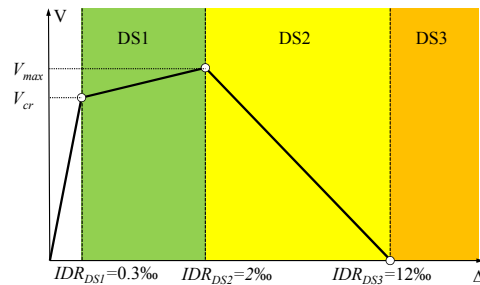


Figure 172: Correlation between IDR and DS based on the typical backbone of diagonal-strut masonry infill

It is worth noting that those values of IDR_{DSj} cannot be directly compared to the corresponding values associated with the CC of the frame (end of the equivalent-elastic branch, start of the drop and achievement of residual capacity). In fact, IDR_{DSj} may be lower, because the attainment of DS corresponds to the first damage of that level in a single element.

5.1.3.2 Deformed shape

Values of IDR_{DSj} are assumed to correspond to ground storey, where the maximum demand is concentrated; thus, mechanism of collapse of 1st storey is considered (Dolce et al., 2005). However, as FAST is based in ADRS framework, displacement of the equivalent SDOF must be obtained. Top displacement of the generic building corresponding to the attainment of each DS can be related to the

IDR_{DSj} of first storey by means of an “a-priori” deformed shape of the building for each DS.

Before any assumption, it is necessary to establish the basis of the formulations of FAST. In all the next, parameters representing mean values of any parameter A are expressed as \bar{A} , and the symbol Δ preceding a variable means the increment of that variable. Also, the following subscripts are adopted:

- i : indicates a generic storey level;
- n : top of the building, i.e. last storey level;
- 1 : first storey;
- s : mean value within upper storeys (all storeys except first).

Generic interstorey displacement (Δd_i) and that of 1st storey are expressed in Equation (88). Then, top displacement (d_n) is obtained as the accumulation of them (Equation (89)).

$$\Delta d_i = d_i - d_{i-1} \quad ; \quad \Delta d_1 = d_1 \quad (88a,b)$$

$$d_n = \sum \Delta d_i = \Delta d_1 + \sum_2^n \Delta d_i \quad (89)$$

IDR are expressed as in Equation (90a), depending on each interstorey height h_i , which is called h_s for $i > 1$. The total height (H_n) is trivially calculated from the basic input variables h_1 and h_s (see Table 44) as shown in Equation (90b). In most of the works regarding vulnerability, assessment, simulated design, estimation of the period or large-scale databases, usually constant interstorey height of 3m is considered, in a very simplified way. In this work, an exception is done by considering different interstorey height for the first storey, given the fact that usually it is dedicated to a different activity from the residential use and so needs a larger height, typically ranging from 3.0 to 5.0m. Then, top displacement is expressed as in Equation (91) by replacing Equation (90a) into Equation (89), thus as function of geometry and IDR.

$$IDR_i = \frac{\Delta d_i}{h_i} \quad ; \quad H_n = h_1 + (n-1) \cdot h_s \quad (90a,b)$$

$$\begin{aligned}
 d_n &= \Delta d_1 + \sum_2^n \Delta d_i = IDR_1 \cdot h_1 + \sum_2^n IDR_i h_s = \\
 &= IDR_1 \cdot h_1 \left(1 + \frac{1}{IDR_1 \cdot h_1} h_s \sum_2^n IDR_i \right) = IDR_1 \cdot h_1 \left(1 + \frac{h_s}{h_1} \cdot \frac{\sum_2^n IDR_i}{IDR_1} \right) \quad (91)
 \end{aligned}$$

Aimed at relating values of IDR with the lateral action, it is necessary to define the approximate mechanical behaviour of the infilled building. If shear-type behaviour is assumed (i.e. IDR only depends on shear forces, neglecting the flexural contribution), interstorey displacements for any DS is obtained as in Equation (92a), where V_i is the storey shear and $K_{sec,i}$ is the secant shear stiffness of the storey corresponding to any DS. Secant stiffness can be related to the elastic stiffness (K_i) through a factor Ω_i (Equation (92b)). Hence, storey shear is expressed as in Equation (93) by replacing Equations (92a) and (92b) into Equation (90a). Then, if Equation (93) is replaced into Equation (91), top displacement is expressed as in Equation (94).

$$\Delta d_i = \frac{V_i}{K_{sec,i}} \quad ; \quad K_{sec,i} = \Omega_i \cdot K_i \quad (92a,b)$$

$$V_i = IDR_i \cdot h_i \cdot \Omega_i \cdot K_i \quad (93)$$

$$\begin{aligned}
 d_n &= IDR_1 \cdot h_1 \cdot \left(1 + \frac{h_s}{h_1} \frac{\sum_2^n \frac{V_i}{h_s \cdot \Omega_i \cdot K_i}}{\frac{V_1}{h_1 \cdot \Omega_1 \cdot K_1}} \right) = \\
 &= IDR_1 \cdot h_1 \cdot \left(1 + \frac{h_s}{h_1} \cdot \frac{h_1 \cdot \Omega_1 \cdot K_1}{V_1} \cdot \frac{1}{h_s} \sum_2^n \frac{V_i}{\Omega_i \cdot K_i} \right) = \\
 &= IDR_1 \cdot h_1 \cdot \left(1 + \frac{\Omega_1 \cdot K_1}{V_1} \sum_2^n \frac{V_i}{\Omega_i \cdot K_i} \right) \quad (94)
 \end{aligned}$$

In sub-standard buildings or in buildings with poor capacity design or no design to DLS, shear stiffness of the RC frame may be neglectable when compared to the stiffness of the infills (Fardis, 2009; Dolšek and Fajfar, 2001). If similar infills ratio is assumed for all the upper storeys ($i > 1$) and also the stiffness degradation of such storeys is expressed as an average, Equation (94) can be transformed in Equation (95). If the rest of summations within upper storeys are expressed also as function of the average values, top displacement is obtained as in Equation (96).

$$d_n = IDR_1 \cdot h_1 \cdot \left(1 + \frac{\Omega_1 \cdot K_1}{V_1 \cdot K_s} \sum_2^n \frac{V_i}{\Omega_i} \right) = IDR_1 \cdot h_1 \cdot \left[1 + \frac{K_1}{K_s} \cdot \frac{\Omega_1}{V_1} \sum_2^n \frac{V_i}{\Omega_i} \right] \approx$$

$$\approx IDR_1 \cdot h_1 \left[1 + \frac{K_1}{K_s} \cdot \frac{\Omega_1}{\Omega_s} \cdot \frac{\sum_2^n V_i}{V_1} \right] \quad (95)$$

$$d_n = IDR_1 \cdot h_1 \left[1 + \frac{K_1}{K_s} \cdot \frac{\Omega_1}{V_1} \cdot \frac{\bar{V}_s \cdot (n-1)}{\Omega_s} \right] = IDR_1 \cdot h_1 \left[1 + \left(\frac{K_1}{K_s} \right) \left(\frac{\bar{V}_s}{V_1} \right) \left(\frac{\Omega_1}{\Omega_s} \right) (n-1) \right] \quad (96)$$

The meaning of the last equation is that the contribution of the upper part of the building to the total displacement can be related to the displacement of 1st storey through three contribution factors. Those factors account for the different characteristics that make upper part more rigid than 1st storey for any DS:

- Elastic stiffness contribution factor (χ): Upper storeys have higher stiffness than 1st storey
- Shear contribution factor (ζ): Upper storeys have lower shear demand than 1st storey
- Stiffness degradation contribution factor (γ): Upper storeys have higher stiffness degradation than 1st storey

Any “a priori” deformed shape can be adopted within the framework of the method. For simplified FAST, deformed shape is not defined explicitly but obtained through an “a priori” linear pattern of forces, which is commonly adopted

by vulnerability approaches for shear-type frames. In Figure 173, graphic interpretation of those three factors, together with a layout of the framework of simplified FAST regarding the definition of thresholds of top displacement for each DS, are shown. Variable H_i refers to the height from the base of the building until storey i .

It is worth noting that all the following developments are referred to frames which are physically intended as composed of storeys which are concentrated at points. Hence, 1st storey is not theoretically placed at the base of the building but at a height of h_1 . For very high number of storeys, the differences between discrete and continuous models would be lower.

5.1.3.3 *Elastic stiffness contribution factor (χ)*

Factor χ is in a general sense defined as shown in Equation (97a). For simplified FAST it is assumed that: (i) the building is uniformly infilled, i.e. $\rho_{w,1}=\rho_{w,s}$; and (ii) the stiffness of the RC frame is neglectible (less than 5-10%, see section 5.2.1.1) if compared with stiffness of infills. Thus, χ for simplified FAST only depends on the ratio between interstorey heights of upper and 1st storey (Equation (97b)).

$$\chi = \frac{K_1}{K_s} ; \quad \chi = \frac{K_{w,1}}{K_{w,s}} = \frac{\frac{G_w \cdot \rho_{w,1} \cdot A_b}{h_1}}{\frac{G_w \cdot \rho_{w,s} \cdot A_b}{h_s}} = \frac{\rho_{w,1}}{\rho_{w,s}} \cdot \frac{h_s}{h_1} = \frac{h_s}{h_1} \quad (97a,b)$$

5.1.3.4 *Shear contribution factor (ζ)*

General expression for factor ζ is shown in Equation (98) for similar interstorey heights in the upper part of the building. This factor can be understood in a graphic sense as the the area of the shear force diagram in the upper part of the building (A_{V_s}) divided by the rectangular area whose base is the shear force in 1st storey and its height is that of the upper part of the building (A_{V_1}) (see Figure 177). That assumption is demonstrated in Equation (99).

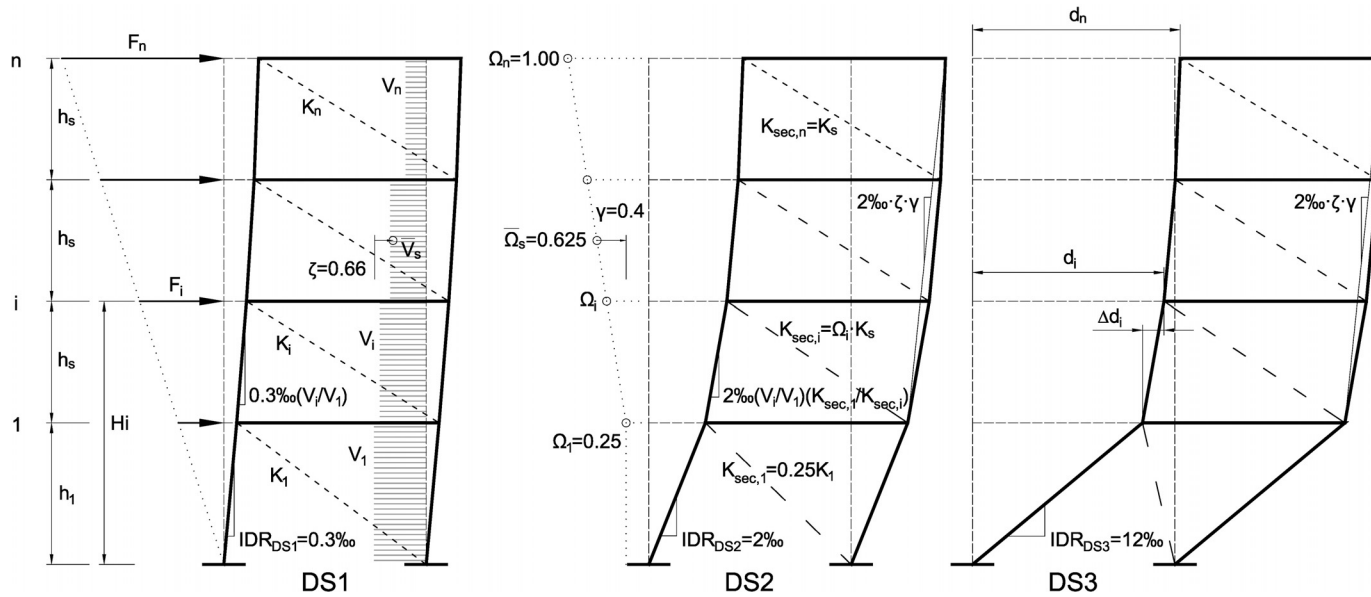


Figure 173: Framework of simplified FAST regarding deformed shape for the different DS: geometry, storey stiffnesses, lateral load pattern, shear diagram, contribution factors, IDR_{DSj} and lateral displacements

$$\zeta = \frac{\bar{V}_s}{V_1} = \frac{\sum_2^n V_i / (n-1)}{V_1} = \frac{\sum_2^n V_i}{(n-1) \cdot V_1} \quad (98)$$

$$\zeta = \frac{\sum_2^n V_i}{(n-1)V_1} \cdot \frac{(H_T - h_1)}{(H_T - h_1)} = \frac{\sum_2^n V_i}{(n-1)V_1} \cdot \frac{(n-1) \cdot h_s}{(H_T - h_1)} = \frac{h_s \sum_2^n V_i}{V_1(H_T - h_1)} = \quad (99)$$

$$= \frac{h_s \sum_2^n V_i}{V_1(H_T - h_1)} = \frac{\sum_2^n V_i h_s}{V_1(H_T - h_1)} = \frac{A_{V_s}}{A_{V_1}}$$

In simplified FAST, shear diagram is pseudo-parabolic from the level of the 1st storey, consequently with a linear pattern of forces. In a continuous model, factor ζ would be equal to the ratio between the area of the parabola with respect to the circumscript rectangle, thus $\zeta=2/3$. In discrete models this is only true when $h_1=h_s$, but, considering the simplified philosophy of FAST, this value can be assumed in all the cases. For instance, in the case of $h_1=4\text{m}$ and $h_s=3\text{m}$, $\zeta=0.65 \approx 2/3$.

5.1.3.5 Stiffness degradation contribution factor (γ)

General expression for factor Ω is shown in Equation (100a). Factor γ only has sense in the case of attainment of DS2 (see Figure 172), because for DS1 the secant stiffness is the equivalent-elastic one. Secant stiffness to DS2 of infill panels is estimated approximately as 25% of the elastic stiffness (Ricci et al., 2011b; Colangelo, 2013), thus $\Omega_1=0.25$. In simplified FAST, distribution of Ω along the height of the building is considered as being linear from a value of 0.25 at 1st storey to 1.00 (no degradation) at the top of the building, resulting in a degradation factor $\gamma=0.4$ (see Equation (100b))

$$\gamma = \frac{\Omega_1}{\Omega_s} \quad ; \quad \gamma = \frac{0.25}{\frac{0.25+1}{2}} = 0.4 \quad (100a,b)$$

5.1.3.6 Top displacement for each DS

If Equation (96) is particularised for DS1 and DS2, the first two expressions in Equation (101) are obtained. DS3 is attained in agreement with a drop of resistances in the infills, thus with a decrease on the demanded shear. While 1st storey infills increase their deformation (see Figure 173), the upper part may experiment a recession. Still, aimed at simplicity, an infinite unloading stiffness is assumed for the upper part, as if it was a perfectly-rigid body; this assumption is slightly unconservative. Thus, displacement for DS3 is obtained from DS2 by adding only the contribution of 1st storey.

In Equation (96), values of IDR_{DSj} shown in Figure 172 and values of χ , ζ and γ obtained in the previous sections shall be adopted.

$$d_{n|DSj} = \begin{cases} d_{n|DS1} = IDR_{DS1} \cdot h_1 [1 + \chi \cdot \zeta (n-1)] & , \quad j = 1 \\ d_{n|DS2} = IDR_{DS2} \cdot h_1 [1 + \chi \cdot \zeta \cdot \gamma (n-1)] & , \quad j = 2 \\ d_{n|DS3} = d_{n|DS2} + h_1 (IDR_{DS3} - IDR_{DS2}) & , \quad j = 3 \end{cases} \quad (101)$$

5.1.3.7 Switching into ADRS and into PGA

All the top displacement thresholds ($d_{n|DSj}$) must be transformed into spectral displacement of the equivalent SDOF ($S_{d|DSj}$) through the factor Γ (see Equation (102)). As FAST is a procedure based in a non-adaptive pushover framework, values of the participation factor corresponding to the initial elastic deformed shape are adopted (see section 1.2.1.1); this assumption is consistent with the consideration of a constant level of λ_r for the evaluation of the capacity (see section 5.1.1.1).

$$S_{d|DSj} = \frac{d_{n|DSj}}{\Gamma} \quad (102)$$

These values may be less precise for higher DS, considering that the assumed deformed shape, corresponding to a mechanism of the first storey, would furnish lower values of Γ (see Table 2). Anyway, the assumption of larger values of Γ only for the obtaining of the spectral displacement thresholds for the attainment of the DS may be a conservative choice. Some other suitable considerations regarding

pseudo-adaptive strategies aimed at the calibration of Γ and λ_r are discussed in section 5.3.5.

In the simplified FAST approach, other than considering always the dynamic characteristics corresponding to the elastic initial behaviour, fix values of Γ are assumed depending only on the number of storeys. This assumption lays in the fact that the frames have almost constant stiffness in height, being $\chi \approx 1.0$ (only influenced by the different interstorey height of the ground floor). So, it is possible to use pre-established values.

In this work, those suggested by the American code ASCE-SEI 41-06 (ASCE, 2007) for the seismic rehabilitation of existing buildings are adopted (see Table 46). The three options given by this code are shown: “shear building” subjected to triangular or uniform load pattern, and “other” buildings. As the footnote of the table states, the definition of “shear building” is based only in the final deformed shape (“concave”) instead of in the origin of the lateral deformation (shear or cantilever). “Other buildings” may serve for wall or dual frames, with “convex” deformed shape.

Values correspond to frames whose stiffness is constant in height; in fact, the “exact” values would be intermediate between triangular and uniform, thus corresponding to a load pattern proportional to the displacements (see section 1.2.1.4). In the simplified FAST, values of the first column (“triangular load pattern”) are suggested, consistently with the assumed forces (see section 5.1.3.2).

Table 46: Values for Γ (C_0) suggested by ASCE-SEI 41-06 (ASCE, 2007)

Number of Stories	Shear Buildings ²	
	Triangular Load Pattern (1.1, 1.2, 1.3)	Uniform Load Pattern (2.1)
1	1.0	1.0
2	1.2	1.15
3	1.2	1.2
5	1.3	1.2
10+	1.3	1.2

¹Linear interpolation shall be used to calculate intermediate values.

²Buildings in which, for all stories, story drift decreases with increasing height.

Finally, ordinates of the IN2 curve must be transformed from spectral displacement into PGA values, as shown in Equation (25).

5.1.4 Assessment of the performance

Once the IN2 curves and the thresholds of spectral displacement for each DS are obtained, they are used together as shown in Figure 174 in order to obtain equivalent PGA thresholds (PGA_{DSj}), i.e. the level of PGA for the attainment of each DS in the class of building considered. Hence, given a level of PGA (from a real or simulated earthquake), it is possible to predict which DS is expected for each class.

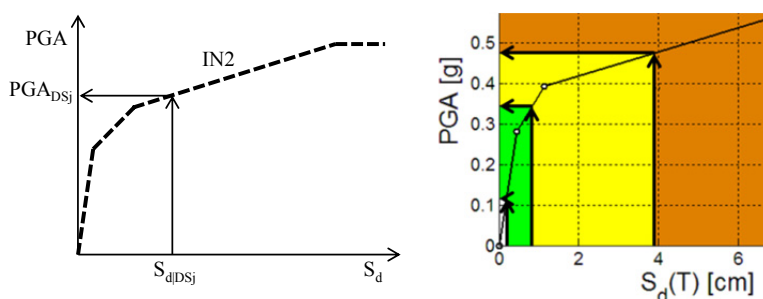


Figure 174: Expression of DS thresholds in PGA units through the IN2 curve of an infilled frame

It is worth noting that such PGA should correspond, for each class of building, to the level of acceleration measured in each specific soil type. If FAST is used aimed at estimating the vulnerability of a city from a code-based point of view, i.e. in order to elaborate vulnerability maps assuming homogeneous values of PGA in rock, code-based amplifications for soil type (factor S) may be considered. Conversely, if FAST is used in order to simulate the damage scenario after a real earthquake, knowing the PGA in each soil is not possible in most cases, because there are not so many seismic stations placed in every soil type within a single city. Hence, PGA corresponding to the closest station (or to the inter- or extrapolation in the case that several stations are available) may be adopted, whatever is the soil

type in which the station is placed. If the most common soil of the city is very different from the soil under the seismic station, unfortunately the assessment would have lower reliability.

Finally, it is possible to carry out fragility functions (see X). According to the approach provided in Porter et al. (2007), fragility functions (F_{ds}) are defined according to Equation (103). $F_{dsj}(PGA)$ denotes the fragility function for DS_j , defined as the probability that the building reaches or exceeds DS_j , given a particular PGA value, and idealized by a lognormal distribution, see Equation (104). Φ denotes the standard normal (Gaussian) cumulative distribution, μ denotes the median value of the distribution, and β denotes the logarithmic standard deviation, in this case assumed equal to 0.4 (see Porter et al., 2006).

$$F_{dsj}(pga) = P[DS \geq ds | PGA = pga] \quad (103)$$

$$F_{dsj}(pga) = \Phi \left[\frac{\ln(pga/PGA_{DSj})}{\beta} \right] \quad (104)$$

5.2 GENERALISED FAST APPROACH FOR NON-UNIFORMLY INFILLED RC-MRF BUILDINGS

In section 1.3, particularities regarding “pilotis” frames (i.e. infilled frames in which masonry walls in ground floor are almost inexistent) are presented. In section 4.2 it is pointed out that this typology is quite usual in Spain, as well as in Mediterranean countries. On the other hand, in section 2.2.4 it is concluded that all Spanish seismic codes (including the current one) do not balance the reduction of stiffness and strength in 1st storeys of these buildings. However, simplified FAST is not able to account for any reduction of infills in 1st storey: it considers that the whole storey stiffness comes from the infills, which are assumed to be uniformly distributed in elevation.

In this section, an evolved version of the vulnerability method, called “generalised FAST”, is carried out aimed at accounting for possible reduction of

infills in 1st storey. The main goal of the new approach is that it is able to consider any magnitude of reduction, thus all the intermediate situations from uniformly infilled frames to pilotis frames can be assessed by generalised FAST.

In the previous section, the general framework of FAST is presented. Generalised FAST uses also the same general formulations, but some parameters must be redefined. Regarding the framework for the calculation of capacity curves, parameter λ_r (see Equation (85)) cannot be based on codes anymore, as deformed shape of sub-standard pilotis frames would likely be constant rather than linear or sinusoidal (see Table 2). Also $T_{el,inf}$ (see Equation (86)) must be re-evaluated, given that there are not reliable simplified formulations corresponding to pilotis frames; moreover, given that any intermediate situation between uniformly infilled and pilotis can be considered, even an eventual explicit formulation for pilotis frames would not be appropriated. Hence, generalised FAST proposes an evaluation of those variables in closed form, i.e. through theoretical developments of formulations in which empirical or numerical variables are used, instead of using explicit formulations.

Regarding the framework for the calculation of displacements, contribution factors need also to be re-proposed (see Equation (101)), because: contribution of RC columns to the stiffness of 1st storey may not be neglectable; shear diagrams may change their shape; and upper storeys' infills may experiment less degradation of stiffness. Finally, factor Γ could be taken from the second column of Table 46, corresponding to constant load pattern, considering that any intermediate situation could be interpolable. However, Γ needs to be calculated in close form as an intermediate step of the calculation of λ_r .

5.2.1 Non-uniformity of infills: from uniform to pilotis

In Figure 175, different schemes of frames depending on the relationship between the infills ratio in 1st storey and in the rest of the storeys are shown. Pure uniformly infilled frame and pure pilotis frame correspond to upper and lower bound of the range that generalised FAST is able to consider. They are characterised by stiffness contribution factor χ (see Equation (97b)) tending towards 1 and 0, respectively. For pure uniformly infilled frames, $\chi=1$ for similar

interstorey height across the building. Instead, for pure pilotis frames, $\chi=0$ if stiffness provided by RC columns is neglected. However, the last is not a suitable approach anymore, because the lower is $\rho_{w,1}$, the higher is the relative contribution of RC frame. Hence, first of all, it is necessary to redefine factor χ aimed at accounting with RC contribution at 1st storey.

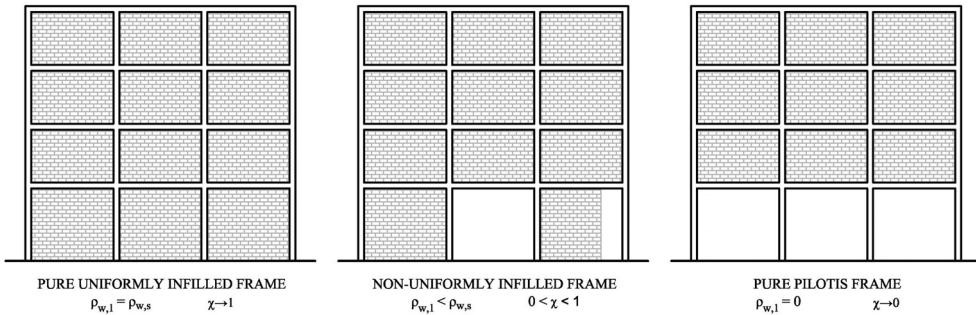


Figure 175: Characterisation of frames depending on the different 1st storey infills ratio vs. upper storeys

5.2.1.1 Generalised elastic stiffness contribution factor (χ)

Generic expression of χ considering contribution of infills and RC frame is shown in Equation (105), being K_{RC} the last contribution; only columns are considered to provide stiffness to the storey, given that high infill ratios in 2nd storey make it behave as a rigid body (Fardis, 2009).

In Equation (106a), formulation for translational (shear) stiffness of column j at storey i is shown, being E_c and I the modulus of elasticity and the moment of inertia of the section, respectively. Then, tributary area of each column (A_{trib}) is defined as the total area (A_b) divided by the number of columns of the storey (n_c), assuming that they are homogeneously distributed in plan (see Equation (106b)). Considering the simplified approach of FAST, cross section of columns is considered to be square, being b_c the side; similar columns within each storey are assumed; and eventual contribution of the stair is neglected. Then, stiffness of columns in a storey can be expressed as in Equation (107)).

$$\chi = \frac{K_1}{K_s} = \frac{(K_w + K_{RC})_1}{(K_w + K_{RC})_s} \quad (105)$$

$$K_{RC,ij} = \frac{12 \cdot E_{c,ij} \cdot I_{ij}}{h_i^3} \quad ; \quad A_{trib} = \frac{A_b}{n_c} \quad (106a,b)$$

$$\begin{aligned} K_{RC,i} &= \sum_{j=1}^{n_c} K_{RC,ij} = \sum_{j=1}^{n_c} \frac{12 \cdot E_c \cdot I_{c,ij}}{h_i^3} = \frac{12 \cdot E_c}{h_i^3} \sum_{j=1}^{n_c} \frac{b_{c,i}^4}{12} = \frac{E_c \cdot b_{c,i}^4}{h_i^3} \sum_{j=1}^{n_c} 1 = \\ &= \frac{E_c \cdot b_{c,i}^4}{h_i^3} n_c = \frac{E_c \cdot b_{c,i}^4}{h_i^3} \frac{A_b}{A_{trib}} \end{aligned} \quad (107)$$

A parameter $\rho_{RC,i}$ (analogously to $\rho_{w,i}$ for infills), representing a sort of “RC area ratio”, can be defined as in Equation (108). Then, $K_{RD,i}$ can be expressed as in Equation (109). Then, a factor $c_{\chi,i}$, which represents the relative contribution of RC with respect to infills, is defined as in Equation (110). Note that such factor depends on the relationships of modulus of deformability and area ratios between both elements (RC columns and infills).

$$\rho_{RC,i} = \frac{A_{c,i}}{A_b} = \frac{n_p \cdot A_{c,ij}}{n_p \cdot A_{trib}} = \frac{b_{c,i}^2}{A_{trib}} \quad (108)$$

$$K_{RC,i} = \frac{E_c (\rho_{RC,i} \cdot A_{trib})^2}{h_i^3} \frac{A_b}{A_{trib}} = \frac{E_c \cdot \rho_{RC,i}^2 \cdot A_{trib}}{h_i^3} A_b \quad (109)$$

$$c_{\chi,i} = \frac{K_{RC,i}}{K_{w,i}} = \frac{\frac{E_c \cdot \rho_{RC,i}^2 \cdot A_{trib}}{h_i^3} A_b}{\frac{G_w \cdot \rho_{w,i}}{h_i} A_b} = \frac{E_c \cdot \rho_{RC,i}^2 \cdot A_{trib}}{G_w \cdot \rho_{w,i} \cdot h_i^2} \quad (110)$$

Then, if Equation (110) is replaced into Equation (105), a detailed expression of χ is obtained (Equation (111)), which in turn can be simplified as depending on three different ratios relating characteristics of 1st storey with upper storeys: χ_h , χ_ρ and χ_c , corresponding to interstorey heights (Equation (112a)), infills ratios (Equation (112b)) and relative contributions of RC with respect to infills (Equation

(112c)). The last ratio may be similar to the numerator for sub-standard buildings, given that relative contribution of RC in upper storeys may be neglectable: $c_{\chi,s} \rightarrow 0$ thus $(1+c_{\chi,s}) \rightarrow 1$.

$$\chi = \frac{K_{w,1} + \overline{K}_{RC,1}}{K_{w,s} + \overline{K}_{RC,s}} = \frac{K_{w,1} \left(1 + \frac{K_{RC,1}}{K_{w,1}} \right)}{K_{w,s} \left(1 + \frac{\overline{K}_{RC,s}}{K_{w,s}} \right)} = \frac{\frac{G_w \cdot \rho_{w,1}}{h_1} A_b (1 + c_{\chi,1})}{\frac{G_w \cdot \rho_{w,s}}{h_s} A_b (1 + c_{\chi,s})} = \quad (111)$$

$$= \frac{h_s}{h_1} \cdot \frac{\rho_{w,1}}{\rho_{w,s}} \cdot \frac{(1 + c_{\chi,1})}{(1 + c_{\chi,s})} = \chi_h \cdot \chi_\rho \cdot \chi_c$$

$$\chi_h = \frac{h_s}{h_1} \quad ; \quad \chi_\rho = \frac{\rho_{w,1}}{\rho_{w,s}} \quad ; \quad \chi_c = \frac{(1 + c_{\chi,1})}{(1 + c_{\chi,s})} \approx 1 + c_{\chi,1} \quad (112a,b,c)$$

5.2.1.2 Estimation of dimensions of cross sections of RC columns at 1st storey

Aimed at defining of the influence of the RC columns of the first storey ($c_{\chi,1}$) to the elastic stiffness contribution factor, it is necessary to estimate the dimensions of the side (b_c) of the assumed square section. This estimation may come from a simplified simulated design, having into account the current seismic code and the construction practice at the corresponding age of construction of the class of building.

According with the level of accuracy of the rest of the method, very simplified expressions corresponding to the resistance of RC column sections are adopted from (De Andrés and CSCAE, 2009), which consist in some recommended guidelines to the design of RC structures for housing buildings in Spain.

In this code, two expressions for the assessment of the resistance are suggested: one corresponding to “low eccentricities” of the axial force (Equation (113)) and another one corresponding to “bending with axial load whose eccentricity is higher than one sixth of the height of the section, with reinforcement in two sides” (Equation (115)). Another usual expression for only compression

(Equation (114)) is used in addition. The variables in the expressions are: the minimum eccentricity of design (e_0); the base and height of the rectangular section (b_c and h_c , respectively); the maximum and yielding stress of concrete (f_{cd}) and steel (f_{yd}), respectively; the total ($A_{s,tot}$) and side (A_s) area of the reinforcement, respectively; the concrete stress block depth (y); the distance between the reinforcement of opposite sides (z); the axial load of design in the case of low eccentricity ($N_{d,g}$) and the bending moment of design in the case of high eccentricity ($M_{d,s}$).

$$N_{d,g} \left(1 + 2.5 \frac{e_0}{h_c} \right) = b_c \cdot h_c \cdot f_{cd} + A_{s,tot} \cdot f_{yd} \quad (113)$$

$$N_{d,g} = b_c \cdot h_c \cdot f_{cd} \quad (114)$$

$$M_{d,s} = b_c \cdot y \cdot f_{cd} \frac{h_c - y}{2} + A_s \cdot f_{yd} \cdot z \quad (115)$$

All the expressions are transformed into Equations (116), (117) and (118), respectively, by making the following simplifications:

- The case of low eccentricity may represent the gravitational phase of the design, and also the design to wind actions (see section 5.3.1); hence, $N_{d,g}$ represents the axial load corresponding to these combinations of actions, and the value for the base of the column sections obtained from these approach is called $b_{c,g}$. On the other hand, the case of high eccentricity may represent the seismic phase of the design; consequently, $M_{d,s}$ correspond to the bending moment caused by the seismic base shear V_d , and the value for the base of the column sections obtained from these approach is called $b_{c,s}$.
- Sections are square: $h_c = b_c$. Then, the total reinforcement area can be expressed as function of the area of the section through the reinforcement ratio ρ_s : $A_{s,tot} = \rho_s \cdot b_c^2$.
- The minimum eccentricity is usually defined by codes as $e_0 = \max \{ h_c / f_e; e_{min} \}$, being f_e equal to 20 in RC Spanish codes and 30 in Eurocode 2, and being $e_{min} = 20 \text{ mm}$ in both cases. Aimed at the simplicity

of the final expression of b_c , e_0 is assumed to be h_c/f_e , although this term is higher than 20mm only when h_c is higher than 400mm or 600mm in the Spanish or European case, respectively. In this work, f_e is assumed to be 20, as in Spanish codes.

- The distance between the reinforcement of opposite sides depends on the mechanic concrete cover (r_c), i.e. the distance from the border of the section to the axis of the longitudinal reinforcement: $z = h_c - 2 \cdot r_c$. The value of the cover is assumed to be 35mm, according to common RC codes and construction practice.
- In square sections, assuming that the longitudinal reinforcement is equitably distributed in the perimeter, the reinforcement corresponding to one side is function of the total reinforcement: $n_t = 4 \cdot n_s - 4$, being n_t and n_s the number of bars in the whole section and in one side, respectively. Thus, $A_s/A_{tot} = 1/n_t + 0.25$, which assume values of 0.38, 0.33 and 0.30 for 8, 12 and 20 bars in the whole section, respectively. A value of $A_s/A_{tot} = 0.35$ is assumed, consequently.
- The concrete stress block depth (y) is substituted by $N_{d,s}/(b \cdot f_{cd})$.
- The seismic moment of design $M_{d,s}$ can be expressed as $V_d \cdot L_{V1} = V_d \cdot h_1 \cdot (L_V/h)_1$, being V_d the shear base of design and $(L_V/h)_1$ the relative shear span of the columns of the first storey[†] (shear span divided by the total span, i.e. the first interstorey height), which depends on the general deformed shape of the frame.

$$N_{d,g} \left(1 + 2.5 \frac{b_{c,g1}/20}{b_{c,g1}} \right) = b_{c,g1}^2 (f_{cd} + \rho_s \cdot f_{yd}) \Rightarrow \quad (116)$$

$$b_{c,g1} = \sqrt{\frac{N_{d,g} (1 + 0.125)}{f_{cd} + \rho_s \cdot f_{yd}}} = \sqrt{\frac{1.125 \cdot N_{d,g}}{f_{cd} + \rho_s \cdot f_{yd}}}$$

[†] It is important not to mislead with L_V/h where h is the height of the section of the RC column

$$b_{c,g2} = \sqrt{\frac{N_{d,g}}{f_{cd}}} \quad (117)$$

$$\begin{aligned} M_{d,s} - b_{c,s} \cdot \frac{N_{d,s}}{b_{c,s} \cdot f_{cd}} \cdot f_{cd} \frac{b_{c,s} - \frac{N_{d,s}}{b_{c,s} \cdot f_{cd}}}{2} - 0.35 \cdot \rho_s \cdot b_{c,s}^2 \cdot f_{yd} (b - 70) = 0 \Rightarrow \\ \Rightarrow \dots \Rightarrow (0.35 \cdot \rho_s \cdot f_{yd}) b_{c,s}^4 - (24.5 \cdot \rho_s \cdot f_{yd}) b_{c,s}^3 + \left(\frac{N_{d,s}}{2} \right) b_{c,s}^2 - \\ - \left[V_d \cdot h_1 \cdot \left(\frac{L_V}{h} \right)_1 \right] b_{c,s} - \left(\frac{N_{d,s}^2}{2 \cdot f_{cd}} \right) = 0 \end{aligned} \quad (118)$$

Values for the average reinforcement ratio (ρ_s) should be proposed according both to general construction practice and minimum values of current seismic code at the age of construction of the building class.

Then, the final value of b_c is obtained (Equation (119)) as the maximum between those obtained in gravitational and seismic situations (Equations (116), (117) and (118)) and the minimum value suggested by the RC and seismic codes, usually 25cm or 30cm. In a real design, values for b_c would be rounded upwards in order to be multiple of 5cm; aimed at having into account this source of overstrength, an amplification factor c_{hom} is added to the expression of b_c instead of applying the same procedure that in a real design. This decision make possible to show a continuous trend in the stiffness of the first floor as function of the height; otherwise, big “steps” would appear.

$$b_c = c_{hom} \cdot \max \{ b_{c,g1}; b_{c,g2}; b_{c,s}; b_{c,min} \} \quad (119)$$

The assumption of axial loads corresponding to both situations (gravitational and seismic) is carried out according to Equations (120) and (121), respectively. G and Q are dead and live loads, respectively; γ_G and γ_Q are the partial factors for G and Q in persistent and transient situation, i.e. for design to gravitational loads; and Ψ_2 is the combination factor for Q corresponding to the quasi-permanent situation.

All of these values must be evaluated according to the corresponding codes at the age of construction of the selected class of building.

$$N_{d,g} = n \cdot A_{trib} (G \cdot \gamma_G + Q \cdot \gamma_Q) \quad (120)$$

$$N_{d,s} = n \cdot A_{trib} (G + \psi_2 \cdot Q) \quad (121)$$

5.2.2 Generalised Damage States displacement thresholds for non-uniformly infilled frames

Once that factor χ has been defined for any type of non-uniformly infilled frame, it is necessary to reconsider the choice of “a priori” linear lateral load pattern. In fact, typical deformation of pure pilotis building may be more likely to be coherent with a quasi-constant load pattern (see Table 2).

As seen in section 1.2.1.1, pushover-based approaches are based on using “a priori” lateral load patterns that would cause lateral deformations homotetic to the forces. In generalised FAST, two lateral load patterns are considered: linear (suitable for pure uniformly infilled frames) and constant (suitable for pilotis frames). For intermediate situations, it is necessary to analyse which is the error committed when each load pattern (linear or constant) is applied to frames with different factors χ , in order to find out a “corner value” which would allow recognising any infilled frame as similar to uniformly infilled or conversely similar to pilotis frame. The error is intended as the cumulated differences between the storey lateral displacements and the displacement corresponding to a deformed shape homotetic to the lateral load pattern and normalised to the top displacement. Aimed at that target, a parametric analysis, varying χ from 1 to 0 (not included), returns a suitable corner value of $\chi=0.5$, which may correspond to any suitable combination of χ_h , χ_p and χ_c (see Equation (111)). Aimed at simplicity, similar corner value is defined for χ_p , thus all the buildings with any reduction of infills in 1st storey can be assigned to one of two types depending on whether $\rho_{w,1} \geq 0.5 \cdot \rho_{w,s}$ (called in all the following “uniformly infilled frames”, UIF) or conversely $\rho_{w,1} < 0.5 \cdot \rho_{w,s}$ (called in all the following “non-uniformly infilled frames”, NIF), as seen in Figure 176.

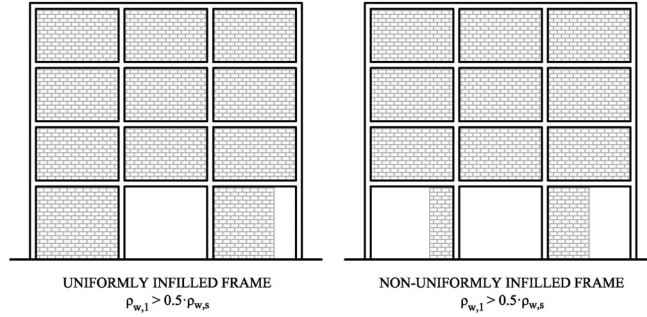


Figure 176: Definition of the two classes of infilled frames adopted in generalised FAST framework

All the subsequent formulations are developed in parallel for both types UIF and NIF; they are all referred to Figure 177, in which the whole framework of displacement of generalised FAST is shown. All the formulations are referred to the generic case of $h_1 \neq h_s$; if $h_1 = h_s$, it is possible to simplify equations by replacing H_i by i .

5.2.2.1 Generalised shear contribution factor (ζ)

Firstly, analytical expressions for lateral load patterns (lineal and constant) depending on the geometry of the frame are shown in Equations (122a) and (122b), respectively, being a and a' generic parameters simulating hypothetic monotonic increment. Then, corresponding distributions of shear (V_i) are obtained (Equations (123a) and (123b), respectively). If $i=1$, base shear (V_1) is obtained (Equations (124a) and (124b)). Regarding notation of summatories, $\sum A_i = \sum_{i=1}^n A_i$ for any parameter A .

$$F_{i,UIF} = a \cdot H_i \quad ; \quad F_{i,NIF} = a' \quad (122a,b)$$

$$V_{i,UIF} = a \cdot \sum_i^n H_i \quad ; \quad V_{i,NIF} = a' \cdot (n + 1 - i) \quad (123a,b)$$

$$V_{1,UIF} = a \cdot \sum H_i \quad ; \quad V_{1,NIF} = a' \cdot n \quad (124a,b)$$

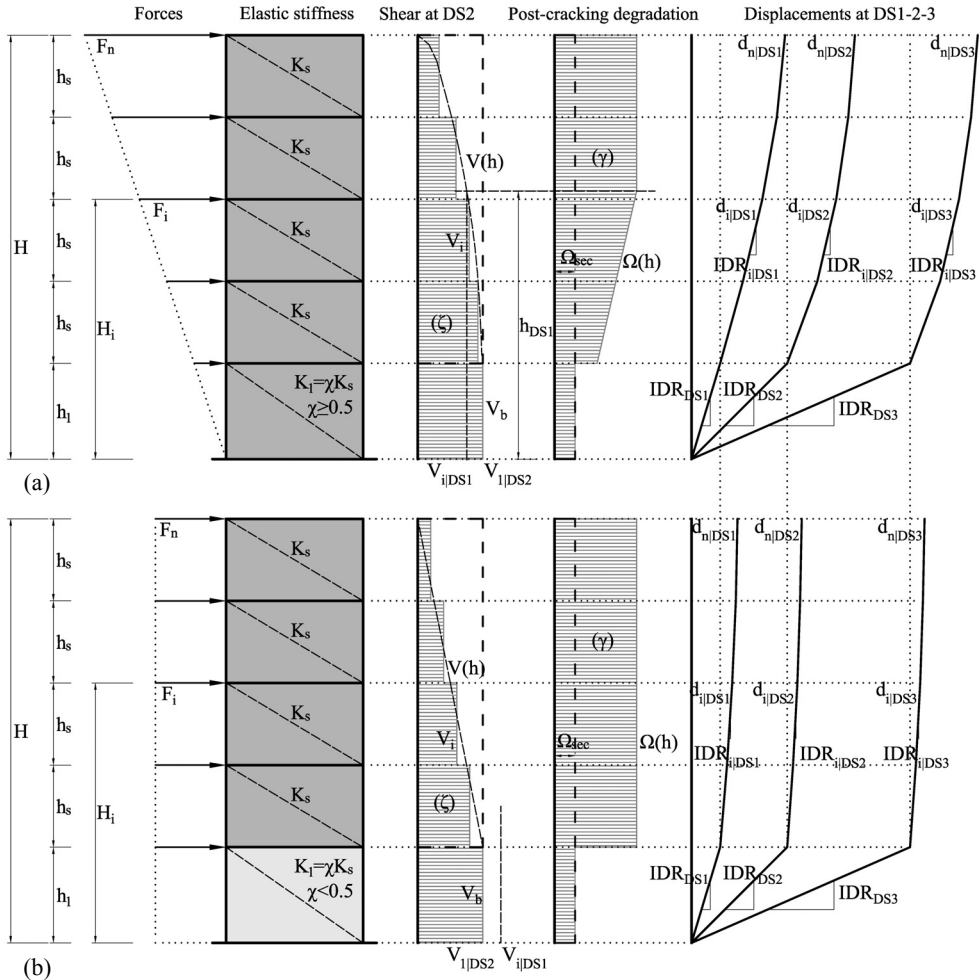


Figure 177: Framework of generalised FAST regarding deformed shape for the different DS: geometry, storey stiffnesses, lateral load pattern, shear diagram, contribution factors, IDR_{DSj} and displacements for uniformly infilled (a) and non-uniformly infilled (b) frames

Then, if Equations (123a) and (124a), or conversely (123b), and (124b), are replaced into Equation (98), both expressions for the shear contribution factor ζ are obtained for UIF and NIF, respectively (see Equations (125a) and (125b)). As demonstrated in Equation (99) and represented graphically in Figure 177, both values represent the ratio between the area of the shear diagram with respect to the

circumscribed rectangle whose base is placed at 1st storey level. Final values (2/3 and 1/2, respectively) correspond to a parabola and a triangle, respectively.

$$\zeta_{UIF} = \frac{\sum_2^n \sum_i^n H_i}{(n-1) \cdot \sum H_i} \approx \frac{2}{3} \quad ; \quad \zeta_{NIF} = \frac{\sum_2^n (n+1-i)}{n \cdot (n-1)} = \frac{\sum_1^{n-1} i}{n \cdot (n-1)} = \frac{1}{2} \quad (125a,b)$$

5.2.2.2 Generalised stiffness degradation contribution factor (γ)

Finally, in order to calculate the factor γ , it is necessary to evaluate the level of stiffness degradation, if any, of the infills at the upper storeys when the first storey attains the threshold interstorey drift characterising DS2 (IDR_{DS2}). Thus, it is necessary to Ω_i of each storey i .

First of all, it is necessary to obtain: (i) which is the shear force that causes the attainment of DS2 threshold at ground floor ($V_{1|DS2}$), and which is the shear force that causes the DS1 at any upper storey ($V_{i|DS1}$). Both values (see Equations (126a) and (126b)) as particularisations of Equation (93).

$$V_{1|DS2} = IDR_{DS2} \cdot h_1 \cdot \Omega_{DS2} \cdot K_1 \quad ; \quad V_{i|DS1} = IDR_{DS1} \cdot h_i \cdot \Omega_{DS1} \cdot K_s \quad (126a,b)$$

Then, the shear force distribution corresponding to the attainment of DS2 at the first storey is built up by increasing homothetically the initial shape (see Figure 2). The infills corresponding to upper storeys having a current shear force higher than that corresponding to the DS1 are supposed to be beyond cracking. Unfortunately, the employment of a discrete expression of storey shears results in a difficult evaluation of the number of storeys belonging to the “cracked part”. Thus, a continuous functional expression for shear force distribution ($V(H)$), depending on the height and matching with the discrete shape, must be assumed (see Figure 177). Functions for UIF and NIF (parabolic and linear, respectively) are shown in Equations a) and b), respectively, being a and a' generic parameters representing theoretical monotonic increment. As explained previously, functions are assumed to start from 1st storey level instead of the base of the building. Base shear (Equation (128)) is then obtained by making $H=0$.

$$V_{UIF}(H) = \frac{a}{2} \cdot (H_n^2 - H^2) \quad ; \quad V_{NIF}(H) = a' \cdot (H_n - H) \quad (127a,b)$$

$$V_{b,UIF}(H) = \frac{a \cdot H_n^2}{2} \quad ; \quad V_{NIF}(H) = a' \cdot H_n \quad (128a,b)$$

Thus, the “cracked part” of the building is placed below the height at which shear force attains the value corresponding to DS1 drift threshold, called “cracked height” (H_{DS1}). The cracked part can be expressed as a normalised height, H_{DS1}/H_n . Aimed at obtaining the last parameter, generic expressions for H/H_n must be obtained as in Equations (129) and Equation (130).

$$\frac{V_{UIF}(H)}{V_{b,UIF}} = 1 - \left(\frac{H}{H_n} \right)^2 \Rightarrow \left(\frac{H}{H_n} \right)_{UIF} = \sqrt{1 - \frac{V_{UIF}(H)}{V_{b,UIF}}} \quad (129)$$

$$\frac{V_{NIF}(H)}{V_{b,NIF}} = 1 - \frac{H}{H_n} \Rightarrow \left(\frac{H}{H_n} \right)_{NIF} = 1 - \frac{V_{NIF}(H)}{V_{b,NIF}} \quad (130)$$

Then, H_{DS1}/H_n is obtained for each case in Equations (131a) and (132b) by making $V_b = V_{i|DS2}$ and $V(H) = V_{i|DS1}$.

$$\left(\frac{H_{DS1}}{H_n} \right)_{UIF} = \sqrt{1 - \frac{1}{\chi \cdot \Omega_{DS2}} \cdot \frac{IDR_{DS1}}{IDR_{DS2}} \cdot \frac{h_s}{h_1}} \geq 0 \quad (131)$$

$$\left(\frac{H_{DS1}}{H_n} \right)_{NIF} = 1 - \frac{1}{\chi \cdot \Omega_{DS2}} \cdot \frac{IDR_{DS1}}{IDR_{DS2}} \cdot \frac{h_s}{h_1} \geq 0 \quad (132)$$

The analytical expression for H_{DS1} could in some cases provide unreal negative values. It would mean that the shear force necessary to make the upper storeys exceed DS1 is higher than the shear force corresponding to the DS2 in the ground floor. This situation is representative of non-uniformly infilled frames: as the infills ratio is very low at ground floor, quite low shear force makes it attain the DS2, while upper storeys are still characterized by uncracked stiffness (see Figure 2). On the other hand, for uniformly infilled frames, a typical value for the relative “cracked height” –normalised to the total one— is approximately 0.65: two thirds

of the height are depicted by a cracked stiffness. Thus, Ω_i is equal to 1 in the upper “elastic” part or the building, while it is expressed in the “cracked part” as a continuous function inversely proportional to the shear force (Equation (133)).

$$\Omega(H) = \begin{cases} \Omega_{DS2} + H_n \cdot H \frac{1 - \Omega_{DS2}}{(H_{DS1}/H_n)} & , H < H_{DS1} \\ 1 & , H \geq H_{DS1} \end{cases} \quad (133)$$

Then, γ is obtained (Equation (134)) as a relationship between the areas of the diagram of the degradation function (see Figure 177). Typical values of γ are 0.35 and 0.25 for uniformly and non-uniformly infilled frames, respectively, if applied for some case study shown in 4.2.

$$\gamma = \frac{\Omega_{DS1} \cdot H_n}{\int_0^{H_n} \Omega(H) dH} = \dots = \frac{2 \cdot \Omega_{DS1}}{\frac{H_{DS1}}{H_n} \cdot (\Omega_{DS1} - 1) + 2} \quad (134)$$

5.2.3 Generalised capacity curves for non-uniformly infilled frames

Aimed at defining CC for generalised FAST, values of λ_r and $T_{el,inf}$ must be redefined in closed form. For the first variable, it is necessary to develop the expressions for the relative first mode participating mass of the SDOF (m^*/M) and Γ ; the second variable is obtained as function of (m^*/M) and K_g (global elastic stiffness of the frame).

5.2.3.1 *Global elastic stiffness*

Global elastic stiffness of the frame is defined in general as in Equation (135).

$$K_g = \frac{V_1}{d_n} \quad (135)$$

The expression for d_n presented in Equation (136) is developed from Equation (89) by replacing the increments of displacement with Equation (92a), assuming elastic phase of infills ($\Omega_i=1$) and also assuming stiffnesses accounting with RC contribution (see Equation (105)). The summatory of V_i is replaced by cleared

expression from Equation (98), and K_1 is expressed as function of K_s through factor χ (see Equation (105)). Then, if Equation (136) is replaced into Equation (135), K_g adopts the form in Equation (137a). And if expression for K_s in Equation (105) is assumed, contribution of RC in upper floors is discarded and stiffness of infills is obtained from Equation (29b), then the global stiffness, normalised to the building area in plan, is obtained in Equation (137b).

$$d_n = \frac{V_1}{K_1} + \sum_2^n \frac{V_i}{K_s} = \frac{V_1}{\chi \cdot K_s} + \frac{\zeta \cdot (n-1) \cdot V_1}{K_s} = \frac{V_1}{K_s} \left[\frac{1}{\chi} + \zeta \cdot (n-1) \right] \quad (136)$$

$$K_g = \frac{K_s}{\left[\frac{1}{\chi} + \zeta \cdot (n-1) \right]} \quad ; \quad \frac{K_g}{A_b} = \frac{G_w \cdot \rho_{w,s}}{h_s \cdot \left[\frac{1}{\chi} + \zeta \cdot (n-1) \right]} \quad (137a,b)$$

5.2.3.2 *Relative first mode participating mass of the SDOF*

In section 1.2.1.4, a graphic interpretation of (m^*/M) is proposed, in which it is expressed in terms of the ratio between the area of the deformed shape of the MDOF with respect to the total rectangle (see Figure 26). Hence, Equation (11) is developed in Equation (138) by normalising displacement to the top one.

$$\frac{m^*}{M} = \frac{\sum \varphi_i}{n} = \frac{1}{n} \sum \frac{d_i}{d_n} = \frac{1}{n \cdot d_n} \sum d_i \quad (138)$$

In Equation (139), summatory of displacements is expressed as an accumulation of interstorey displacements; afterwards, contributions of 1st storey and upper storeys are isolated, increments of displacement are replaced by means of Equation (92a) and K_1 is expressed as function of K_s through factor χ (see Equation (105)). Hence, if Equations (139) and (136) are replaced into Equation (138), general expression of (m^*/M) is obtained in Equation (140). That expression is particularised for both types (UIF and NIF) in Equations (141) and (142), by means of a replacement of shear forces with Equations (123a), (123b), (124a) and (124b), and also replacing shear contribution factors by Equations (125a) and (125b).

$$\begin{aligned} \sum d_i &= n \cdot \Delta d_1 + (n-1) \cdot \Delta d_2 + \dots + (n-i+1) \cdot \Delta d_i = \\ &= n \cdot \Delta d_1 + \sum_2^n [(n-i+1) \cdot \Delta d_i] = n \cdot \frac{V_1}{K_1} + \sum_2^n \left[(n-i+1) \cdot \frac{V_i}{K_s} \right] = \end{aligned} \quad (139)$$

$$\begin{aligned} &= \frac{n \cdot V_1}{\chi \cdot K_s} + \frac{1}{K_s} \sum_2^n [(n-i+1) \cdot V_i] = \frac{\frac{n}{\chi} \cdot V_1 + \sum_2^n [(n-i+1) \cdot V_i]}{K_s} \\ \frac{m^*}{M} &= \frac{\frac{n}{\chi} \cdot V_1 + \sum_2^n [(n-i+1) \cdot V_i]}{n \cdot d_n \cdot K_s} = \frac{\frac{n}{\chi} \cdot V_1 + \sum_2^n [(n-i+1) \cdot V_i]}{n \cdot \frac{V_1}{K_s} \cdot \left[\frac{1}{\chi} + \zeta \cdot (n-1) \right] \cdot K_s} = \end{aligned} \quad (140)$$

$$= \frac{\frac{n}{\chi} \cdot V_1 + \sum_2^n [(n-i+1) \cdot V_i]}{n \cdot V_1 \cdot \left[\frac{1}{\chi} + \zeta \cdot (n-1) \right]}$$

$$\left(\frac{m^*}{M} \right)_{UIF} = \frac{\frac{3}{2} \cdot n \cdot \sum H_i + \sum_2^n [(n+1-i) \cdot \sum H_i]}{n \cdot \left[\frac{1}{\chi} + \frac{2}{3} \cdot (n-1) \right] \cdot \sum H_i} \quad (141)$$

$$\left(\frac{m^*}{M} \right)_{NIF} = \frac{\frac{n^2}{\chi} + \sum_1^{n-1} i^2}{n^2 \cdot \left[\frac{1}{\chi} + \frac{(n-1)}{2} \right]} \quad (142)$$

5.2.3.3 *First mode participation factor*

Equation (143) is developed by replacing Equations (136) and (139) into Equation (11). Then, $\sum d_i^2$ in the denominator is developed in Equation (144);

similar assumptions made for the development of (m^*/M) are adopted. Finally, general expression of Γ is presented in Equation (145), and particularised formulations for both types (UIF and NIF) are obtained in Equations (146) and (147).

$$\Gamma = \frac{\sum \varphi_i}{\sum \varphi_i^2} = \frac{\frac{1}{d_n} \cdot \sum d_i}{\frac{1}{d_n^2} \cdot \sum d_i^2} = d_n \cdot \frac{\sum d_i}{\sum d_i^2} = \quad (143)$$

$$= \frac{V_1}{K_s} \left[\frac{1}{\chi} + \zeta \cdot (n-1) \right] \cdot \frac{\frac{n}{2} \cdot V_1 + \sum_2^n [(n-i+1) \cdot V_i]}{K_s \cdot \sum d_i^2}$$

$$\begin{aligned} \sum d_i^2 &= \Delta d_1^2 + \sum_2^n d_i^2 = \Delta d_1^2 + \sum_2^n \left(d_1 + \sum_2^i \Delta d_i \right)^2 = \\ &= \frac{V_1^2}{K_1^2} + \sum_2^n \left(\frac{V_1}{K_1} + \sum_2^i \frac{V_i}{K_s} \right)^2 = \frac{V_1^2}{\chi^2 \cdot K_s^2} + \sum_2^n \left(\frac{V_1}{\chi \cdot K_s} + \frac{1}{K_s} \sum_2^i V_s \right)^2 = \end{aligned} \quad (144)$$

$$\begin{aligned} &= \frac{V_1^2}{K_1^2} + \sum_2^n \left(\frac{V_1}{K_1} + \sum_2^i \frac{V_i}{K_s} \right)^2 = \frac{V_1^2}{\chi^2 \cdot K_s^2} + \sum_2^n \left(\frac{V_1}{\chi \cdot K_s} + \frac{1}{K_s} \sum_2^i V_s \right)^2 = \\ &= \frac{V_1^2}{\chi^2 \cdot K_s^2} + \frac{1}{K_s^2} \cdot \sum_2^n \left(\frac{V_1}{\chi} + \sum_2^i V_s \right)^2 = \frac{1}{K_s^2} \cdot \left[\frac{V_1^2}{\chi^2} + \sum_2^n \left(\frac{V_1}{\chi} + \sum_2^i V_s \right)^2 \right] \end{aligned}$$

$$\Gamma = \frac{V_1 \left[\frac{1}{\chi} + \zeta \cdot (n-1) \right] \cdot \left[\frac{n}{2} \cdot V_1 + \sum_2^n [(n-i+1) \cdot V_i] \right]}{\frac{V_1^2}{\chi^2} + \sum_2^n \left(\frac{V_1}{\chi} + \sum_2^i V_s \right)^2} \quad (145)$$

$$\Gamma_{UIF} = \frac{\sum H_i \cdot \left[\frac{1}{\chi} + \zeta \cdot (n-1) \right] \left[\frac{n \cdot \sum H_i}{\chi} + \sum_2^n \cdot [(n+1-i) \cdot \sum H_i] \right]}{\frac{(\sum H_i)^2}{\chi^2} + \sum_2^n \left[\frac{\sum H_i}{\chi} + (i-1) \cdot \sum H_i - \sum_2^i \sum_1^{j-1} H_j \right]^2} \quad (146)$$

$$\Gamma_{NIF} = \frac{n \cdot \left[\frac{1}{\chi} + \frac{1}{2} \cdot (n-1) \right] \left[\frac{n^2}{\chi} + \sum_2^n (n+1-i)^2 \right]}{\frac{n^2}{\chi^2} + \sum_2^n \left[\frac{n}{\chi} + (i-1) \cdot (n+1) - \sum_2^i i \right]^2} \quad (147)$$

In Table 47, some examples of (m^*/M), Γ and λ_r for different UIF and NIF are presented. Results seem to be reasonable, as they follow the trends shown in Table 2.

Table 47: Modal properties for some examples of 4- and 8-storey UIF and NIF

χ	n	UIF			χ	n	NIF		
		m^*/M	Γ	λ_r			m^*/M	Γ	λ_r
1.0	4	0.71	1.25	0.89	0.3	4	0.86	1.13	0.98
	8	0.67	1.28	0.85		8	0.80	1.19	0.95

5.2.3.4 *Elastic period of non-uniformly infilled frames*

Finally, the elastic period of a generic non-uniformly infilled (Equation (148)) is obtained in closed form by replacing the general expression for elastic period of the SDOF into Equation (86). Afterwards, the formulation is re-arranged in such a way that the variables contained are those previously calculated in closed form: (m^*/M) and K_g/A_b .

$$\begin{aligned} T_{eff,inf} &= \kappa \cdot T_{el,inf} = \kappa \cdot 2\pi \sqrt{\frac{m^*}{K^*}} = \kappa \cdot 2\pi \sqrt{\left(\frac{m^*}{M}\right) \cdot \frac{M}{K_g}} \\ &= \kappa \cdot 2\pi \sqrt{\left(\frac{m^*}{M}\right) \cdot \frac{n \cdot m_r \cdot A_b}{K_g}} = \kappa \cdot 2\pi \sqrt{\left(\frac{m^*}{M}\right) \cdot \frac{n \cdot m_r}{(K_g/A_b)}} \end{aligned} \quad (148)$$

In Figure 178, the last expression is applied to different non-uniformly infilled frames depending on the number of storeys, adopting different degrees of non-uniformity (i.e. different χ for similar $\rho_{w,s}$, see Figure 178a) and different degree on infilling (i.e. different $\rho_{w,s}$ for similar χ , see Figure 178b). Results show that generally, unless the reduction of infills in 1st storey is really important, elastic period is not much high than period of uniformly infilled frame. For some case studies of Lorca (see section 4.2), non-uniformly infilled buildings may not have values of χ lower than 0.30, because RC columns balance the reduction. Thus, increase of $T_{eff,inf}$ for typical non-uniformly infilled frames in this case may not be greater than 15% with respect to pure uniformly infilled frames. Also, results for $\chi=1$ are in quite good agreement with the numerical-based formulation proposed in Ricci et al. (2011), which is used in simplified FAST for uniformly infilled frames (see Equation (86)).

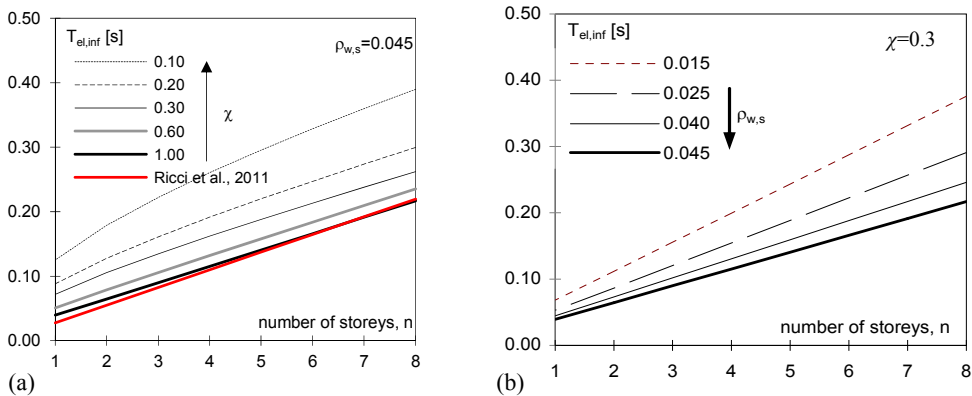


Figure 178: Elastic fundamental period of different non-uniformly infilled frames depending on χ (a) and $\rho_{w,s}$ (b)

5.3 SUITABLE EXTENSIONS OF FAST APPROACH

If both simplicity and skills of FAST are considered, it is possible to conclude that it is an efficient method of assessment of the vulnerability. However, if an absolute comparison of the capabilities with other not so simplified method is

carried out, obviously FAST fails to reach their level of feasibility, as seen in section 5.1.

The main limitation of FAST regarding the inclusion of those skills is that it does not consider specific geometric and mechanic characteristics of the structural and non-structural elements. Thus, in order to overcome this limitation, lots of generalisations with geometric, empiric or mechanic origin may be done, similarly to the assumption of IDR representing the non-structural DS.

In this chapter, some guidelines regarding the implementation of several complementary algorithms aimed at the resolution of these problems are offered. Some of them consist in an extension of the global simulated design presented in section 5.2.1.2. However, keeping in mind the simple nature of FAST, too few new input parameters are required by these new approaches; they are shown in Table 44 as belonging to the “extended FAST”, which is the name given to these group of procedures.

Unfortunately, they have not been tested with any real damage scenario as a benchmark; this test and other eventual corrections would be possible further developments.

5.3.1 Assessment of “gravitational” buildings

Regarding the estimation of the strength capacity of buildings, FAST method is not a mechanical-based approach but a code-based one, i.e. the capacity is not evaluated from any knowledge of the characteristics of the elements but simply from the assumption that building satisfies spectral acceleration seismic code requirements.

This approach is not able to estimate the seismic capacity of sub-standard RC frames designed only to gravitational loads. Thus, some simulated design procedure may be carried out. In (Verderame et al., 2010a), a detailed methodology is presented aimed at this scope; but it may not be coherent with the level of simplification of FAST because it work with specific dimensions of case study buildings.

In this work, the same methodology proposed in section 5.2.1.2 for the estimation of the dimensions of sections of first storey RC columns is used in order to assess the base shear of design of gravitational buildings. It is possible to assume that these frames have been designed by using Equation (113), corresponding to sections of columns subjected to axial loads with no tension in any border (low eccentricity). Thus, the dimension of the square section ($b_{c,g}$) is obtained from Equation (116), assuming a suitable value for the average reinforcement ratio ρ_s . Then, Equation (118) can be used for the estimation of the resistance of the same sections when the regime is not simple compression but bending caused by a diverse axial load (corresponding to the seismic situation) with a higher eccentricity. The “equivalent” base shear of design –in the sense that it is not the real capacity because would correspond to design assumptions— can be cleared up, replacing $b_{c,s}$ by the value of $b_{c,g}$ obtained previously and using the same value of ρ_s . The resulting base shear of design is called $V_{d,g}$, and the associated spectral acceleration capacity $C_{s,RC,g}$ is calculated as in Equation (149), which is similar to Equation (78). The values for overstrength may be the same.

$$C_{s,RC,g} = \frac{V_y}{\Gamma \cdot m^*} = \frac{V_y}{M_r \cdot \lambda_r} = \frac{V_{d,g} (R_w \cdot R_\alpha)}{(n \cdot A_b \cdot m_r) \lambda_r} \quad (149)$$

For gravitational tall buildings, the design to wind loads may not be negligible. It would be necessary to furnish a code-based value of base shear capacity ($V_{d,wn}$), in order to be compared with the gravitational base shear of design.

The wind base shear ($V_{d,wn}$) is the total lateral action, shown in Equation (150) as the product of the wind pressure (q_{wn}) and the lateral area of the building; $L_{x,y}$ represents alternatively L_x and L_y . In Equation (151), the expression corresponding to the associated value of spectral acceleration capacity ($C_{s,RC,wn}$) is shown. In this case, it is also necessary to assume a value for the geometric slenderness of the building (λ_g). Finally, the spectral acceleration capacity of the gravitational building would be the maximum of both values $C_{s,RC,g}$ and $C_{s,RC,wn}$.

$$V_{d,wn} = q_{wn} \cdot L_{x,y} \cdot H \quad (150)$$

$$\begin{aligned}
C_{s,RC,wn} &= \frac{V_y}{\Gamma \cdot m^*} = \frac{V_{d,wn} \cdot (R_\omega \cdot R_\alpha)}{M_r \cdot \lambda_r} = \frac{q_{wn} \cdot L_{x,y} \cdot H \cdot (R_\omega \cdot R_\alpha)}{(n \cdot A_b \cdot m_r) \cdot \lambda_r} = \\
&= \frac{q_{wn} \cdot H}{n \cdot L_{x,y} \cdot m_r \cdot \lambda_r} (R_\omega \cdot R_\alpha) = \frac{q_{wn}}{n \cdot m_r \cdot \lambda_r} (R_\omega \cdot R_\alpha) \lambda_g
\end{aligned} \tag{151}$$

5.3.2 DS related to the RC frame

In section 5.1.3.1, DS referred to non-structural damage (DS1 to DS3) are related to IDR of infills, because they are considered to be lower than those corresponding to RC columns, thus ruling the behaviour.

However, DS4 and DS5 are referred to structural elements, not being able to be defined through the state of the infills. Hence, it is necessary to assume some values of IDR for these DS, based on theoretical, empirical or mechanical interpretations. Furthermore, also for DS1 to DS3, IDR referred to the RC frame are assumed, thus being possible to evaluate in each case whether the infills or the RC frame rule the behaviour. Also, an effort to solve the particular case of the brittle failures of RC columns is carried out.

In Table 48, mechanical interpretations of the different DS and values for IDR corresponding to the RC frame are presented. The cells corresponding to brittle failures are highlighted in grey. Those values are obtained thanks to: (i) the adoption of typical relative displacements in columns proposed in Elwood et al. (2007) and adopted by ASCE/SEI 41-06; (ii) the assumption of suitable sections of 1st storey columns as proposed in 5.2.1.2; and (iii) assuming common geometric layouts columns regarding different constraints and interaction with infill panels. A graphic comparison is shown in Figure 179. It is worth noting that, previously to the use of extended FAST, classes of buildings may be classified into susceptible or non-susceptible to suffer brittle failures.

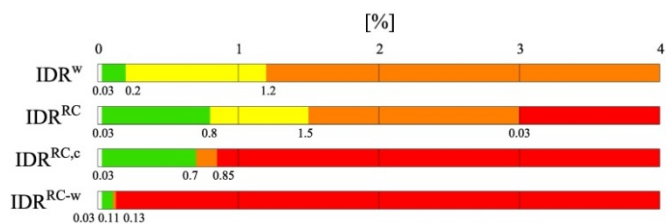


Figure 179: Comparison of IDR characterising the attainment of different DS proposed in Table 48

5.3.3 Irregularity of infills in plan

FAST method assumes that buildings present uniformity of stiffness in plan, or at least kind of symmetry that prevent them for general torsional behaviour. Although this is a suitable approximation for most of the cases, the amount of buildings not belonging to this type is not negligible. In this section, a procedure for the consideration of larger demands due to torsion is proposed.

As seen in Chapter 4 for the specific case of Lorca, Mediterranean urban design corresponding to the second half of 20th century –period corresponding to most of the RC building stock— still presents city blocks. Thus, buildings are not usually isolated from the others but presenting contiguity in their organization and continuous facades without holes in their interfaces.

The last is considered in section 5.2 as the main reason of the inexistence of pure “pilotis” frames, being more common the intermediate situations between uniformly infilled and pilotis case. In this case (non-uniformly infilled buildings), some considerations must be done regarding possible torsional behaviour:

- i) buildings belonging to a city block present usually medium-thick walls in the shared limits with the other buildings;
- ii) in common city blocks, corner buildings share two contiguous sides while the rest of buildings share three –or two if there is a block courtyard—;
- iii) if there is some reduction of the amount of (effective) infills in the ground floor, this reduction operates only on the internal infills or the external ones belonging to the “free” sides, or both of them;

- iv) as seen in section 5.2.1.1, also for common non-uniformly infilled frames, the translational stiffness of the infills is much higher than the columns contribution for most of the cases;
- v) common buildings present infill walls conforming the staircase, whose position and relevance in comparison with the rest of the plan is variable.

This scenario causes that most of the non-uniformly infilled corner buildings – and also some of the other buildings, if there are not infills in the main façade— may have torsional behaviour due to their irregularity of infills in plan. In fact, in past earthquakes poorer performance of corner buildings have been observed, although sometimes this could be attributed to pounding or to the lower subsoil strength because of smaller overburden (Fardis, 2009).

As shown in Figure 180, the response of this kind of plan-irregular buildings when subjected to lateral loads can be interpreted as the addition of a translation due to the lateral action plus a torsion because of the eccentricity between that action (placed in the centre of mass, marked in all the figures with a circle) and the centre of torsion, which is always closer to the side of the plan where there are more infills. Consequently, the “flexible” part of the building experiments larger deformation demands than the “rigid” one –but usually not larger than those corresponding to the bare frame (Fardis et al., 1999)—.

5.3.3.1 *Torsion in multi-storey buildings*

First of all, it is important to clarify some concepts about the differences between torsional behaviour in multi-storey framed buildings in comparison with single-storey ones, always considered into a framework of equivalent-static-force-method in shear-type frames with rigid diaphragms. In this section, terminology associated to torsion in (Tso, 1990) is adopted:

- Floor vs. storey: the different effects of the action can be referred to the “floor” or to the “storey”. In the first case, they correspond to the isolated single floor as free body. In the second case, they include the influence of the upper rest of the building.
 - floor force vs. storey shear;

- floor torque vs. storey torsional moment;
- floor centre of rigidity vs. storey shear centre;
- floor eccentricity vs. storey eccentricity.
- Centres: different centres corresponding to diverse properties can be considered:
 - centre of rigidity: point where application of a lateral force do not cause rotation of the floor (marked in all the figures with an “X”);
 - shear centre: point where the shear reacts when there is not rotation of the floor (marked in all the figures with a square);
 - centre of twist or decoupling: centre of rotation of the floor;
 - centre of stiffness: obtained from a weighted sum of stiffness of the parts of the floor.

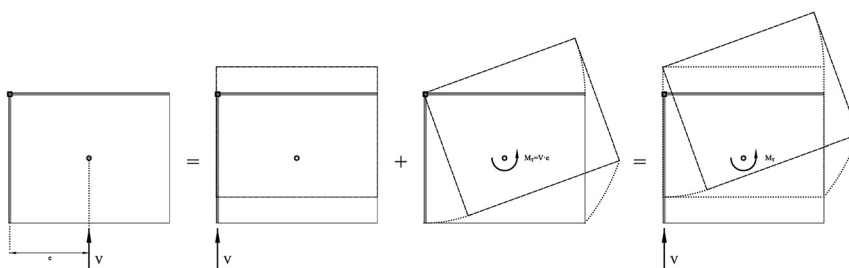


Figure 180: Decomposition of torsional behaviour due to lateral loading

All of these centres are at the same location and are load-distribution independent only for single-storey frames. For multi-storey frames, the first one is different from all the rest. Thus, two eccentricities are associated to those two positions of the centre: floor and storey eccentricity, corresponding to centre of rigidity and shear, respectively. Based on this difference, two different procedures can be followed aimed at the calculation of the storey torsional moments (Tso, 1990):

- 1) sum of the torques above the floor, considering floor eccentricities;
- 2) product of shear and storey eccentricities.

In Figure 181, these two procedures are illustrated for a bare frame whose columns are similar within each floor, being F_i , V_i , T_i , M_{Ti} , e_i and e_i^* the floor forces, storey shears, floor torques, storey torsional moments, floor eccentricities and storey eccentricities, respectively. In this case, although the centres of masses are coincident with the shear centres at each floor, their different position in plan within storeys is the cause of the torsion in the lower part.

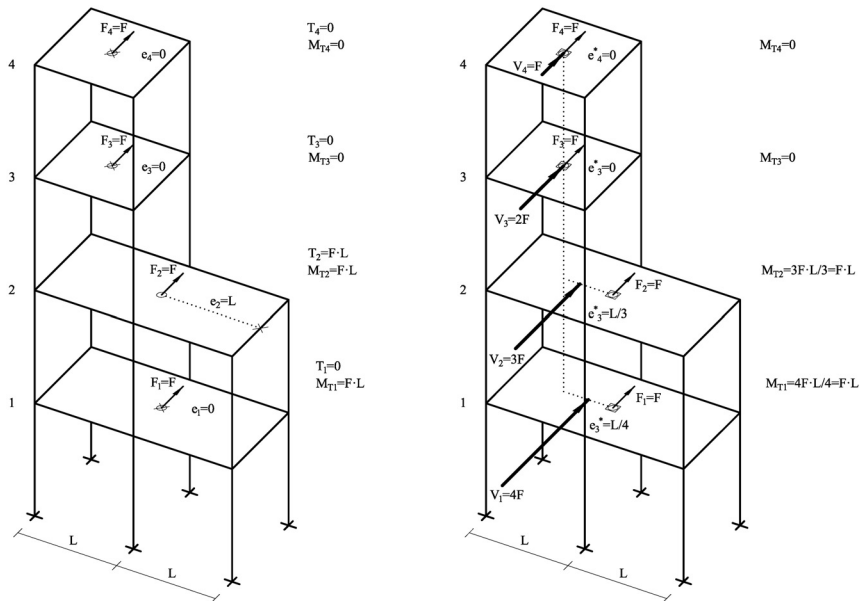


Figure 181: Two different approaches for the calculation of storey torsional moments: bare frames (adapted from Tso, 1990)

The two procedures are applied in Figure 182 to a non-uniformly infilled frame, which is the structural typology considered in this section. In this case, all the centres of mass are vertically aligned, and they are coincident with the shear centres in all the floors except for the bottom one.

The first approach requires obtaining the centres of rigidity, which depend on the vertical distribution of forces; a suitable method aimed at their calculation is presented in (Cheung and Tso, 1986). The second procedure needs to be given the

shear centres, which are independent on the load pattern, instead; distribution of forces only influences the value of the storey shear, not the eccentricity. For this reason, if the second approach is followed, the calculation of the torsional moment in the first storey is completely independent of the load pattern, as the storey shear is actually the total force applied to the building. In the extension of FAST method presented in this section, the second procedure is used, as there is only torsion in the first storey.

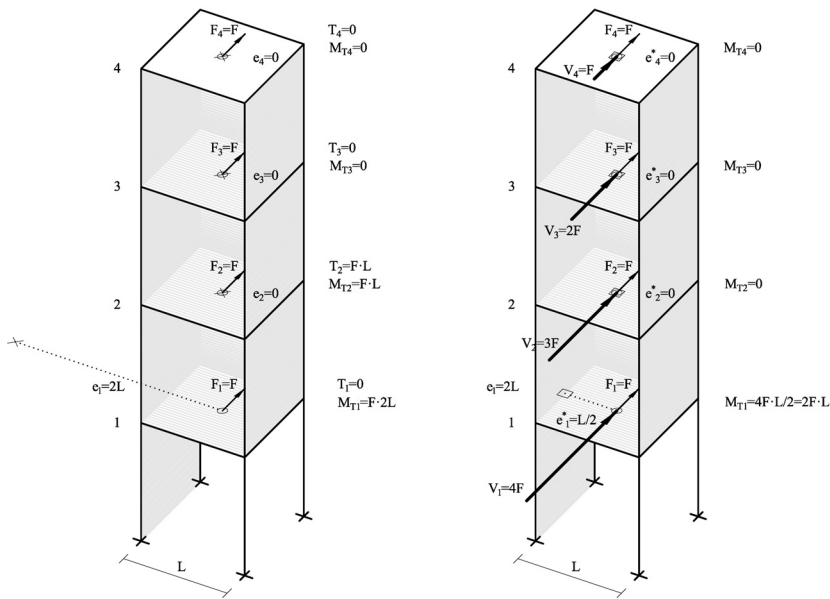


Figure 182: Two different approaches for the calculation of storey torsional moments: non-uniformly infilled frames

Coordinates of shear centres –which are also centres of twist— are calculated as shown in Equations (152a) and (152b), as relationships between rotations caused by unit loads (θ_{F_y} and θ_{F_x} , respectively) and rotation caused by a unit torsional moment (θ_{MT}), being the coordinates expressed from a reference system placed at the point of application of the unit loads.

In the case of storeys composed by individual vertical elements as walls or columns, the centre of shear can be calculated as the centre of stiffness only having into account the stiffnesses in the considered direction, as a weighted sum of their coordinates; see Equations (153a) and (153b), being $K_{x,i}$ and $K_{y,i}$ the stiffnesses of the different elements and $x_{CM,i}$ and $y_{CM,i}$ their centres of mass.

$$x_{SC} = -\frac{\theta_{Fy}}{\theta_{MT}} \quad ; \quad y_{SC} = \frac{\theta_{Fx}}{\theta_{MT}} \quad (152a,b)$$

$$x_{SC} \approx \frac{\sum K_{y,i} x_{CM,i}}{\sum K_{y,i}} \quad ; \quad y_{SC} \approx \frac{\sum K_{x,i} y_{CM,i}}{\sum K_{x,i}} \quad (153a,b)$$

It is worth noting that in this case, although both shear-type behaviour of the frame and rigid diaphragm behaviour of the slab are considered, the phenomenon of distribution of shear forces into the resisting elements of a storey is not able to be extrapolated from the analogous behaviour of a member section. As shown in Figure 183, the flux of tangential stresses in the section (equivalent to the shear forces in the storey) involves also the parts perpendicular to the external action[†]. So, the situation of the shear centre is not similar for a storey than for a section of a member.

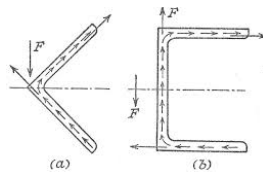


Figure 183: Distribution of tangential stresses and location of shear centre for two thin-wall sections

[†] This is consequence of the application of the Cauchy's stress theorem to a differential element of a thin wall: there must be symmetry in the tensor representing the tensional state of the element, so both tangential stress components (longitudinal and transversal to the normal direction of the section) are similar. As the longitudinal tangential component is not zero in flexional behaviour (except for the neutral axis), neither does the transversal tangential component.

5.3.3.2 *Simplified estimation of the displacement increase due to the torsion*

The scope of this development is to make FAST able to predict the DS in torsional-sensitive buildings when subjected to a certain level of PGA. Again, it is important to remark that the difficulty lays in the assumptions of simplifications in order not to need more input parameters to define building classes.

As explained in section 5.1, if a single case study was considered and all its elements (infills and columns) and their locations were known, it would be easy to reproduce exactly the torsional behaviour, obtaining the displacement demands of each element and monitoring their attainment of the different DS.

However, given that FAST method does not deal with specific case studies, and aimed at the consideration of new classes of building suitable to torsional behaviour inside the actual framework of FAST method, without changing the main input parameters (age of construction, number of storeys and infills ratio), some simplified assumptions may be done:

- few “torsionable” simple distribution of infills in ground floor, able to be applied to any class of building, should be proposed according to the observed building stock;
- the position of the centre of twist may be estimated in a simplified way, considering some translational stiffnesses as negligible when compared to other ones;
- the rotation of the building also may be estimated in a simplified way, considering some torsional stiffnesses as negligible when compared to other ones;
- a constant proportion for the plan of buildings may be assumed;
- a type of element (infill or column) and its location in plan may be assumed as being the one ruling the attainment of the different DS

As explained in the introduction of this section, two frequent types of buildings with irregular ground floor can be considered:

- i) “Corner buildings”: they have two consecutive infilled sides and two free ones (main façades). If they are also non-uniformly infilled in height, probably these infilled sides constitute almost all the infilling

of the ground floor. In this work, they are represented by a prototype with ground floor “L” infill distribution (see Figure 184a).

- ii) “Side buildings”: they have three infilled sides and one free one (main façade). If they are also non-uniformly infilled in height, probably these infilled sides constitute almost all the infilling of the ground floor. In this work, they are represented by a prototype with ground floor “C” infill distribution (see Figure 184b).

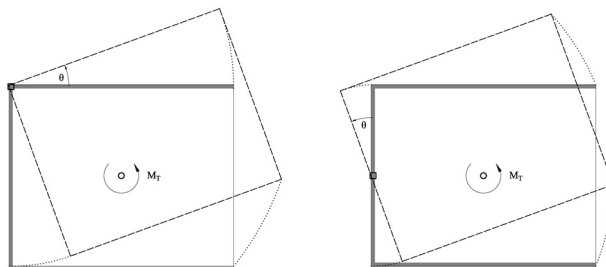


Figure 184: The two “torsionable” prototypes, without RC structure: “L” (a) and “C” (b)

For both prototypes “L” and “C”, if only the infill walls are taken into account, i.e. neglecting the influence of the RC columns, the locations of the centres of twist calculated with Equation (153) are approximately those marked with a square in Figure 184: at the intersection of the axes of both infills for “L” and at the centre of mass of the intermediate wall for “C”. This approximation arises from the consideration of the out-of-plane (plate) infills stiffness as negligible when compared with the in-plane (membrane) infills translational stiffness. Furthermore, aimed at gaining simplicity in later developments, it is possible to assume that both centres of twist are located in the external edge of the wall—which is also the edge of the building plan— instead of being in the axe.

When RC columns are taken into account, the centres of twist in both cases experiment a slight movement towards the centre of mass. However, in section 5.2.1.1 it is highlighted how the contribution of the ensemble of columns to the storey translational stiffness is almost negligible when compared to that of the infills, even in the case of a reduced amount of infills in the ground floor. So, it is

possible to assume that the centre of twist remain in the same position described previously for both prototypes, being independent from the characteristics (density and dimensions) of the columns, and also from the contribution of other neglected elements as the stairs.

In Figure 185a and Figure 185b, torsional behaviour of both prototypes including the RC structure is shown. General geometry, torsional moment caused by base shear (V) and eccentricity (e), rotation (θ) and translation due to the rotation (δ) are described. In all the following, the eccentricity between the shear and the centre of twist is not anymore designated as e^* (like in Figure 181 and Figure 182, following the nomenclature of (Tso, 1990)) but as e .

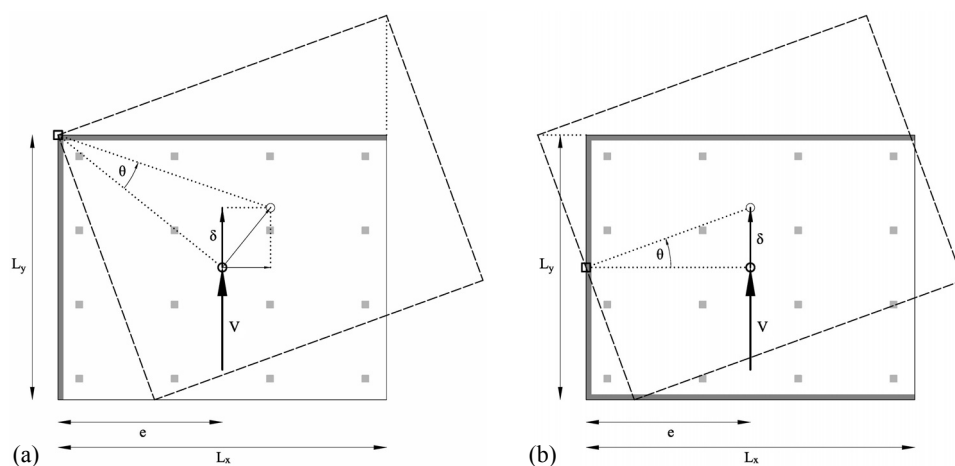


Figure 185: Torsional behaviour of prototypes “L” (a) and “C” (b)

Next, aimed at obtaining the global torsional stiffness of the whole floor, it is necessary to calculate the partial torsional stiffnesses of the elements j of the storey with respect to the centre of twist. Then, the global torsional stiffness (K_T) is obtained as a sum (in parallel) of all the partial values (Equation (154a)). Each torsional stiffness is calculated as the relationship between the torsional moment and the rotation that provokes that moment (Equation (154b)). In all the following,

regarding the relationships between rotations and displacements, the principle of small deformations rules, so $\sin\theta \approx \tan\theta \approx \theta$ and $\cos\theta \approx 1$.

Again, it is important to remark that the procedure used to calculate the torsional stiffness of the storey cannot be extrapolated from the expression corresponding to the linear members (Equation (155), being G the shear modulus, I_T the torsional inertia and L the length of the member).

$$K_T = \sum K_{Tj} \quad ; \quad K_{Tj} = \frac{M_{Tj}}{\theta} \quad (154a,b)$$

$$K_{T,member} = \frac{GI_T}{L} \quad (155)$$

Hence, each element j (wall or ensemble of columns) can be considered from a double prospective: “macro” and “micro”. From the “macro” point of view, they can be considered as members whose translational stiffness is known. From the “micro” point of view, they can be intended to be composed of a string of members acting individually.

The common procedure for the calculation of the torsional stiffness of an element j with a length l_j placed at a distance d_j from the centre of twist is:

- 1) Impose a “rigid” rotation θ to the upper end of the element, remaining the base fixed and considering each section of the element as rigid in its own plane. This “rigid” rotation provokes a triangular pattern of displacements in all the distance d_j , reaching a maximum value (δ_j) in the further extreme (Equation (156a)).
- 2) The distribution of shear forces inside the element caused by this rotation is calculated in each case as proportional to the translational stiffness of the “micro-elements” forming the element.
- 3) This distribution corresponds to a resultant force F_j placed at the barycentre of the shear diagram, thus with an eccentricity e_j with respect to the centre of twist.
- 4) The torsional moment resisted by the element is obtained as the product of the resultant force and the eccentricity (Equation (156b)).

$$\delta_j = d_j \cdot \theta \quad ; \quad M_{Tj} = F_j \cdot e_j \Rightarrow F_j = \frac{M_{Tj}}{e_j} \quad (156a,b)$$

- 5) On the other hand, the “translational stiffness in torsional regime” (K_{VTj}) – the relationship between the maximum displacement δ_j caused by the rotation θ and the resultant force F_j generated— can be obtained as a fraction of the common translational stiffness of the element (K_{Vj}) –the same relationship when the whole element experiments the maximum displacement δ_j , generating a resultant force F_j' —. This fraction corresponds to the relationship between resultant forces (see Equation (157a)), being also equivalent to the relationship between the areas of the different shear diagrams (A_{Vj} and A_{Vj}'), resulting in the factor a_{Vj} .
- 6) Also, by definition, K_{VTj} can be expressed as the relation between the force and maximum displacement (Equation (157b)).
- 7) The two expressions of K_{VTj} corresponding to points 5) and 6) are equalised, clearing up in one member the relationship between the torsional moment and the rotation, which is actually the torsional stiffness of the element (see Equation (158)).

$$K_{VTj} = \frac{F_j}{F_j'} K_{Vj} = \frac{A_{Vj}'}{A_{Vj}} K_{Vj} = a_{Vj} \cdot K_{Vj} \quad ; \quad K_{VTj} = \frac{F_j}{\delta_j} \quad (157a,b)$$

$$a_{Vj} \cdot K_{Vj} = \frac{F_j}{\delta_j} \Rightarrow a_{Vj} \cdot K_{Vj} = \frac{\frac{M_{Tj}}{e_j}}{d_j \cdot \theta} = \frac{\frac{M_{Tj}}{\theta}}{d_j \cdot e_j} = \frac{K_{Tj}}{d_j \cdot e_j} \Rightarrow \quad (158)$$

$$\Rightarrow K_{Tj} = a_{Vj} \cdot d_j \cdot e_j \cdot K_{Vj}$$

Two different torsional stiffnesses must be obtained: the out-of-plane one (plate behaviour) and the in-plane one (membrane behaviour. In all the following, the interstorey height of the ground floor is represented by h instead of h_1 as in the rest of the work, and all the infill walls are supposed to have the same interstorey height, material and thickness t_w .

In the first case (out-of-plane), as shown in Figure 186a, the triangular displacement pattern causes also a triangular shear diagram, given the homogeneous distribution of stiffness in the infill panel due to its similar thickness in all the length. Thus, the corresponding terms in Equation (158) are $e_j=2/3 \cdot l_j$ and $d_j=l_j$. The shear diagram in the case of a translation instead of a rotation is rectangular, so $a_{Vj}=1/2$.

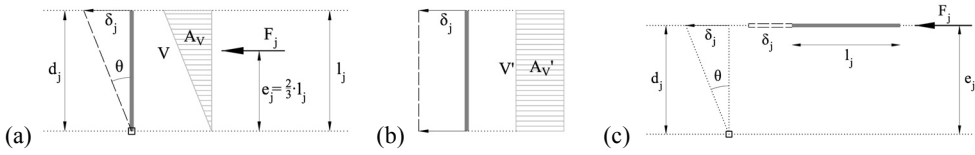


Figure 186: Torsional out-of-plane behaviour of infill walls (a) and its corresponding translational behaviour (b); and torsional in-plane behaviour of infill walls (c)

The translational stiffness to be substituted in Equation (158) corresponds to the shear stiffness of the member, as shown in Equation (159). Hence, Equation (158) transforms into Equation (160).

$$K_{wp,Vj} = \frac{12E_w \cdot I_j}{h^3} = \frac{12E_w \cdot l_j \cdot t_w^3}{h^3 \cdot 12} = \frac{E_w \cdot l_j \cdot t_w^3}{h^3} \quad (159)$$

$$K_{wp,Tj} = \frac{1}{2} \cdot l_j \cdot \frac{2}{3} l_j \cdot \frac{E_w \cdot l_j \cdot t_w^3}{h^3} = \frac{E_w \cdot l_j^3 \cdot t_w^3}{3 \cdot h^3} \quad (160)$$

In the second case, as shown in Figure 186c, the rotation around the centre of twist of an element perpendicular to the radius causes a homogeneous displacement of the whole element, so $e_j=d_j$ and the translational stiffness in torsional regime is equal to the common in-plane shear stiffness of infill walls (Equation (161)), i.e. $a_{Vj}=1$. Hence, Equation (158) transforms into Equation (162).

The case of the RC columns should be treated in a different way. It is not possible to proceed in a similar way as with the infill walls, because in that case their number and location are known. Conversely, for columns, only the density (expressed as function of the input parameter “tributary area”, A_{trib} , which is

equivalent to define the number of columns –distributed kind of homogeneously— in the storey, n_c (see Equation (106)) and the dimension of the section b_c – assuming square section— are known.

$$K_{wm,lj} = \frac{G_w \cdot A_w}{h} = \frac{G_w \cdot l_j \cdot t_w}{h} \quad (161)$$

$$K_{wm,Tj} = 1 \cdot d_j \cdot d_j \cdot \frac{G_w \cdot l_j \cdot t_w}{h} = \frac{G_w \cdot l_j \cdot t_w \cdot d_j^2}{h} \quad (162)$$

Thus, the most suitable strategy is to proceed by assuming a “fuzzy” homogeneous distribution of the stiffness of the ensemble of columns within the rectangular plan. The first simplification to be done is to assume that the behaviour of such rectangular plan is equivalent to a circular plan whose area is similar to the original rectangle, through the definition of an equivalent square whose side L is the arithmetic mean of the sides of the rectangle (L_x and L_y). Hence, the radius of the circle is equal to $L/\sqrt{\pi}$.

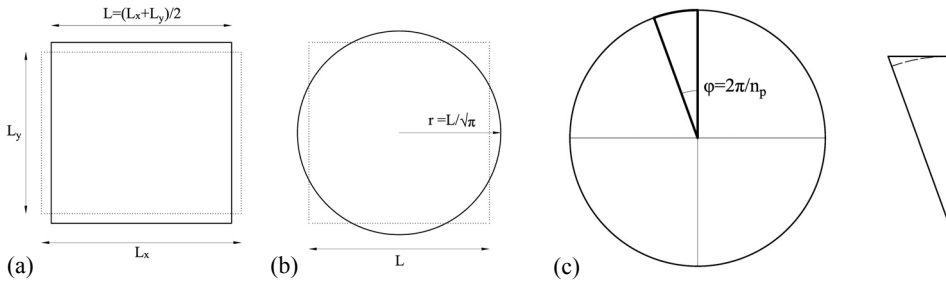


Figure 187: Transformation of a rectangle into a square (a) and this into a circle (b); and circular sector chosen as element representing a part of the ensemble of RC columns (c)

Consequently, the element whose torsional stiffness must be evaluated is a circular sector. Arbitrarily, a sector of equivalent area corresponding to one column is chosen, so its angle ϕ is equal to $2\pi/n_p$ (see Figure 187a). The shape of the sector is simplified as that of a rectangular triangle (see Figure 187b), with length $l_j = L/2$.

In Figure 188a, the torsional behaviour of the circular sector is represented. In this case, the application of a rotation generates a parabolic shear diagram. This is because the distribution of stiffness is triangular – a linear function proportional to the height of the triangle at each point, which represents the “amount of columns” acting in parallel at that point. Thus, the corresponding terms in Equation (158) are $e_j=3/4 \cdot l_j$ and $d_j=l_j$. The shear diagram in the case of a translation instead of a rotation is triangular, so $a_{vj}=(1/3)/(1/2)=2/3$

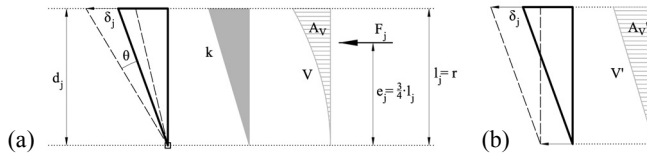


Figure 188: Torsional behaviour of a part of the ensemble of columns (a) and its corresponding translational behaviour (b)

The translational stiffness to be substituted in Equation (158) corresponds to the shear stiffness of one column, as shown in Equation (163). Hence, Equation (158) transforms into Equation (162).

$$K_{RC,vj} = \frac{12E_c \cdot I_j}{h^3} = \frac{12E_c \cdot b_c^4}{h^3 \cdot 12} = \frac{E_c \cdot b_c^4}{h^3} \quad (163)$$

$$K_{RC,tj} = \frac{2}{3} \cdot \frac{L}{\sqrt{\pi}} \cdot \frac{3}{4} \cdot \frac{L}{\sqrt{\pi}} \cdot \frac{E_c \cdot b_c^4}{h^3} = \frac{E_c \cdot L^2 \cdot b_c^4}{2\pi \cdot h^3} \quad (164)$$

Once calculated the single torsional stiffness of the components of both prototypes “L” and “C”, the torsional stiffness of the whole ground storey is calculated as sum of the corresponding elements in each case, adapting the magnitudes when necessary.

For the “L” prototype, the torsional stiffness corresponding to the infills, $K_{wp,T,L}$ is obtained by summing the out-of-plane torsional stiffness of the infills in both wings, corresponding to $l_j=L_x$ and L_y (Equation (165)).

$$\begin{aligned}
 K_{wp,T,L} &= \sum K_{wp,Tj} = K_{wp,T,x} + K_{wp,T,y} = \frac{E_w \cdot L_x^3 \cdot t_w^3}{3 \cdot h^3} + \frac{E_w \cdot L_y^3 \cdot t_w^3}{3 \cdot h^3} = \\
 &= \frac{E_w \cdot t_w^3}{3 \cdot h^3} (L_x^3 + L_y^3)
 \end{aligned}
 \tag{165}$$

Assuming it to be similar to that of the equivalent square plan, the expression in Equation (166) is obtained.

$$K_{wp,T,L} = \frac{2 \cdot E_w \cdot t_w^3 \cdot L^3}{3 \cdot h^3}
 \tag{166}$$

The other contribution to the global torsional stiffness is that of the columns. For the “L” prototype, considering that the centre of twist is located in a corner of the rectangle representing the plan, the expression for the aliquot (Equation (162)) may be transformed into another one corresponding to a plan whose L_x and L_y are two times the original, being the centre of twist in the barycentre of this new rectangle (see Figure 189).

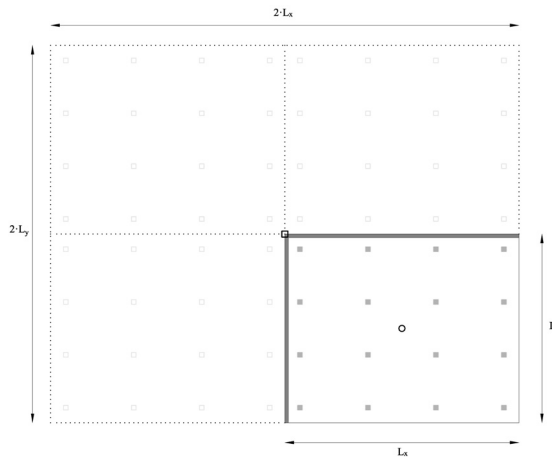


Figure 189: Hypothetical rectangular plan corresponding to the real centre of twist placed in his barycentre for the “L” prototype

Thus, the contribution of the ensemble of columns can be evaluated as a quarter of the hypothetical big rectangle, as shown in Equation (167). Assuming it to be similar to that of the equivalent square plan, the expression in Equation (168) is obtained.

$$K_{RC,T,L} = \frac{1}{4} \sum_{j=1}^{4 \cdot n_p} K_{RC,Tj} = \frac{1}{4} \cdot 4 \cdot n_c \frac{E_c \left(\frac{2 \cdot L_x + 2 \cdot L_y}{2} \right)^2 b_c^4}{2\pi \cdot h^3} = \frac{n_c \cdot E_c \cdot b_c^4 (L_x + L_y)^2}{2\pi \cdot h^3} \quad (167)$$

$$K_{RC,T,L} = \frac{n_c \cdot E_c \cdot b_c^4 (2 \cdot L)^2}{2\pi \cdot h^3} = \frac{2 \cdot n_c \cdot E_c \cdot b_c^4 \cdot L^2}{\pi \cdot h^3} \quad (168)$$

Then, the global torsional stiffness of the whole ground floor for the equivalent square plan is obtained as the sum of the two contributions, substituting L^2 by the plan area A_b (see Equation (169)). In the case of the “C” prototype, the torsional stiffness corresponding to the out-of-plane infills behaviour is obtained by summing the contributions of the infills in the three wings, $K_{wp,T,L}$, corresponding to 2 times $l_j=L_x$ and two times $l_j=L_y/2$ (Equation (170)). Assuming it to be similar to that of the equivalent square plan, the expression in Equation (171) is obtained.

$$K_{T,L} = K_{wp,T,L} + K_{RC,T,L} = \frac{2 \cdot E_w \cdot t_w^3 \cdot A_b \cdot L}{3 \cdot h^3} + \frac{2 \cdot n_c \cdot E_c \cdot b_c^4 \cdot A_b}{\pi \cdot h^3} = \frac{2 \cdot A_b}{h^3} \left(\frac{E_w \cdot t_w^3 \cdot L}{3} + \frac{n_c \cdot E_c \cdot b_c^4}{\pi} \right) \quad (169)$$

$$K_{wp,T,C} = \sum K_{wp,Tj} = 2 \cdot K_{wp,T,x} + 2 \cdot K_{wp,T,y/2} = \frac{2 \cdot E_w \cdot L_x^3 \cdot t_w^3}{3 \cdot h^3} + \frac{2 \cdot E_w (L_y/2)^3 \cdot t_w^3}{3 \cdot h^3} = \frac{2 \cdot E_w \cdot t_w^3}{3 \cdot h^3} \left(L_x^3 + \frac{L_y^3}{8} \right) \quad (170)$$

$$K_{wp,T,C} = \frac{2 \cdot E_w \cdot t_w^3}{3 \cdot h^3} \left(L^3 + \frac{L^3}{8} \right) = \frac{2 \cdot E_w \cdot t_w^3 \cdot 9 \cdot L^3}{3 \cdot h^3 \cdot 8} = \frac{3 \cdot E_w \cdot t_w^3 \cdot L^3}{4 \cdot h^3} \quad (171)$$

On the other hand, the torsional stiffness corresponding to the in-plane infills behaviour is obtained by summing the contributions of the infills in the wings along the y-direction, corresponding to $l_j=L_x$ and $d_j=L_y/2$ (Equation (172)). Assuming it to be similar to that of the equivalent square plan, the expression in Equation (173) is obtained.

$$K_{wm,T,C} = \sum K_{wm,T,j} = 2 \cdot K_{wm,T,x} = 2 \frac{G_w \cdot L_x \cdot t_w \cdot (L_y/2)^2}{h} = \frac{G_w \cdot t_w \cdot L_x \cdot L_y^2}{2 \cdot h} \quad (172)$$

$$K_{wm,T,C} = \frac{G_w \cdot t_w \cdot L^3}{2 \cdot h} \quad (173)$$

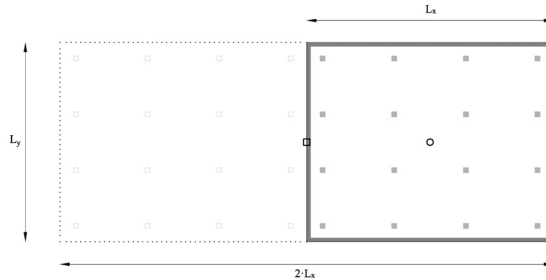


Figure 190: Hypothetical rectangular plan corresponding to the real centre of twist placed in his barycentre for the “C” prototype

The other contribution to the global torsional stiffness is that of the columns. For the “C” prototype, considering that the centre of twist is located in the middle of a side of the rectangle representing the plan, the expression for the aliquot (Equation (162)) may be transformed into another one corresponding to a plan whose L_x is two times the original, being the centre of twist in the barycentre of this new rectangle (see Figure 190).

Thus, the contribution of the ensemble of columns can be evaluated as a half of the hypothetical big rectangle, as shown in Equation (174). Assuming it to be similar to that of the equivalent square plan, the expression in Equation (175) is obtained.

$$K_{RC,T,C} = \frac{1}{2} \sum_{j=1}^{2 \cdot n_p} K_{RC,Tj} = \frac{1}{2} \cdot 2 \cdot n_p \frac{E_c \left(\frac{2 \cdot L_x + L_y}{2} \right)^2 b_c^4}{2\pi \cdot h^3} = \frac{n_p \cdot E_c \cdot b_c^4 (L_x + L_y/2)^2}{2\pi \cdot h^3} \quad (174)$$

$$\begin{aligned} K_{RC,T,C} &= \frac{n_c \cdot E_c \cdot b_c^4 (L + L/2)^2}{2\pi \cdot h^3} = \frac{n_c \cdot E_c \cdot b_c^4 \left(\frac{3 \cdot L}{2} \right)^2}{2\pi \cdot h^3} = \\ &= \frac{n_c \cdot E_c \cdot b_c^4 \cdot 9 \cdot L^2}{2\pi \cdot h^3 \cdot 4} = \frac{9 \cdot n_c \cdot E_c \cdot b_c^4 \cdot L^2}{8\pi \cdot h^3} \end{aligned} \quad (175)$$

Then, the global torsional stiffness of the whole ground floor for the equivalent square plan is obtained as the sum of the three contributions, substituting L^2 by the plan area A_b (see Equation (176)).

$$\begin{aligned} K_{T,C} &= K_{wp,T,C} + K_{wm,T,C} + K_{RC,T,C} = \\ &= \frac{3 \cdot E_w \cdot t_w^3 \cdot A_b \cdot L}{4 \cdot h^3} + \frac{G_w \cdot t_w \cdot A_b \cdot L}{2 \cdot h} + \frac{9 \cdot n_c \cdot E_c \cdot b_c^4 \cdot A_b}{8\pi \cdot h^3} \\ &= \frac{A_b}{2 \cdot h} \left(\frac{3 \cdot E_w \cdot t_w^3 \cdot L}{2 \cdot h^2} + G_w \cdot t_w \cdot L + \frac{9 \cdot n_c \cdot E_c \cdot b_c^4}{4\pi \cdot h^2} \right) \end{aligned} \quad (176)$$

The expressions of the torsional stiffness of both prototypes may contain only variables of input of FAST (see Table 44). For this reason, in Equations (169) and (176), n_c is substituted by A_b/A_{trib} and t_w by $\rho_w \cdot L$ (see Equation (177)), resulting in Equations (178) and (179).

$$\rho_w = \frac{A_w}{A_b} = \frac{t_w \cdot L}{L^2} = \frac{t_w}{L} \Rightarrow t_w = \rho_w \cdot L \quad (177)$$

$$K_{T,L} = \frac{2 \cdot A_b}{h^3} \left(\frac{E_w \cdot \rho_w^3 \cdot A_b^2}{3} + \frac{A_b \cdot E_c \cdot b_c^4}{\pi \cdot A_{trib}} \right) = \frac{2 \cdot A_b^2}{h^3} \left(\frac{E_w \cdot \rho_w^3 \cdot A_b}{3} + \frac{E_c \cdot b_c^4}{\pi \cdot A_{trib}} \right) \quad (178)$$

$$\begin{aligned} K_{T,C} &= \frac{A_b}{2 \cdot h} \left(\frac{3 \cdot E_w \cdot \rho_w^3 \cdot A_b^2}{2 \cdot h^2} + G_w \cdot \rho_w \cdot A_b + \frac{9 \cdot A_b \cdot E_c \cdot b_c^4}{4\pi \cdot h^2 \cdot A_{trib}} \right) = \\ &= \frac{A_b^2}{2 \cdot h} \left(\frac{3 \cdot E_w \cdot \rho_w^3 \cdot A_b}{2 \cdot h^2} + G_w \cdot \rho_w + \frac{9 \cdot E_c \cdot b_c^4}{4\pi \cdot h^2 \cdot A_{trib}} \right) \end{aligned} \quad (179)$$

Once the torsional stiffnesses of both prototypes have been obtained, it is necessary to express them in terms of translational stiffness of the representative point of the ground floor, which is the center of mass.

Hence, as shown in Figure 185, it is necessary to calculate the displacement of the centre of mass of the first storey (δ) when subjected to a torsional moment generated by the first storey shear force (V) and the eccentricity to the centre of twist (e). It is important to note that the magnitude of the displacement in relation with the rotation (θ) is the same for both cases “L” and “C”, as demonstrated in Equations (180a, b and c).

$$\sqrt{2}\delta_L = \theta \frac{L}{2} \sqrt{2} \Rightarrow \delta_L = \theta \frac{L}{2} \quad ; \quad \delta_C = \theta \frac{L}{2} \quad ; \quad \delta_L = \delta_C = \delta \quad (180a,b,c)$$

In Equation (181), the rotation is expressed as function of the geometry of the plan and the shear force. Then, if this equation is substituted into Equation (180b), the expression for the displacement as function of the torsional stiffness is obtained, again replacing L^2 by A_b (Equation (182)).

$$\theta = \frac{M_T}{K_T} = \frac{V \frac{L}{2}}{K_T} = \frac{V \cdot L}{2 \cdot K_T} \quad ; \quad (181)$$

$$\delta = \frac{V \cdot L}{2 \cdot K_T} \frac{L}{2} = \frac{V}{4 \cdot K_T} = \frac{V \cdot A_b}{4 \cdot K_T} \quad ; \quad (182)$$

Consequently, it is possible to define a translational stiffness due to the torsion (K_{VT}) as function of the torsional stiffness (K_T) by substituting the displacement (Equation (182)) into the general expression of a translational stiffness (Equation (183)).

$$K_{VT} = \frac{V}{\delta} = \frac{V}{\frac{V \cdot A_b}{4 \cdot K_T}} = \frac{4 \cdot K_T}{A_b} \quad (183)$$

Therefore, it is possible to replace in Equation (183) the variable K_T by the corresponding expressions for both prototypes “L” and “C” (Equations (169) and (176), respectively), resulting in Equations (184) and (185), respectively. These two formulations are presented in Equations (186) and (187) as normalised to the floor plan area A_b .

$$K_{VT,L} = \frac{4}{A_b} \frac{2 \cdot A_b^2}{h^3} \left(\frac{E_w \cdot \rho_w^3 \cdot A_b}{3} + \frac{E_c \cdot b_c^4}{\pi \cdot A_{trib}} \right) = \frac{8 \cdot A_b}{h^3} \left(\frac{E_w \cdot \rho_w^3 \cdot A_b}{3} + \frac{E_c \cdot b_c^4}{\pi \cdot A_{trib}} \right) \quad (184)$$

$$K_{VT,C} = \frac{4}{A_b} \frac{A_b^2}{2 \cdot h} \left(\frac{3 \cdot E_w \cdot \rho_w^3 \cdot A_b}{2 \cdot h^2} + G_w \cdot \rho_w + \frac{9 \cdot E_c \cdot b_c^4}{4\pi \cdot h^2 \cdot A_{trib}} \right) = \quad (185)$$

$$= \frac{2 \cdot A_b}{h} \left(\frac{3 \cdot E_w \cdot \rho_w^3 \cdot A_b}{2 \cdot h^2} + G_w \cdot \rho_w + \frac{9 \cdot E_c \cdot b_c^4}{4\pi \cdot h^2 \cdot A_{trib}} \right)$$

$$K_{VT,L}/A_b = \frac{8}{h^3} \left(\frac{E_w \cdot \rho_w^3 \cdot A_b}{3} + \frac{E_c \cdot b_c^4}{\pi \cdot A_{trib}} \right) \quad (186)$$

$$K_{VT,C}/A_b = \frac{2}{h} \left(\frac{3 \cdot E_w \cdot \rho_w^3 \cdot A_b}{2 \cdot h^2} + G_w \cdot \rho_w + \frac{9 \cdot E_c \cdot b_c^4}{4\pi \cdot h^2 \cdot A_{trib}} \right) \quad (187)$$

It is worth noting that, for both prototypes, the contribution of the out-of-plane torsional stiffness of the infills to the translational stiffness of the whole storey is proportional to the plan area A_b . As this variable is not into the input parameters of FAST, it would be impossible to assume that the class of buildings behaves independently of the dimensions.

However, it is possible to assume that the out-of-plane infills contribution is suitable to be neglected if compared both with the in-plane infills contribution and with the columns one. For example, a common simple case study is considered, assuming $h=3\text{m}$, $L_x=20\text{m}$, $L_y=16\text{m}$, $G_w=2916.7\text{N/mm}^2$, $E_w=7000\text{N/mm}^2$, $E_c=28000\text{N/mm}^2$ and $n_p=25$, and making ρ_w and b_c range between usual lower and upper bound values for non-uniformly infilled frames.

Results are shown in Table 49. The neglected contribution decreases with the increase of the section of columns but increases with the infills ratio. Only in the case of high infills ratio (1.5%, which is high for a non-uniformly infilled frame) and small RC sections (30x30cm) the error reaches unacceptable high values. Nevertheless, in most of the case the error do not exceed 10%, which can be assumed as an acceptable value considering the approximate philosophy of the whole procedure and all the rest of the simplifications carried out.

Table 49: Error committed when out-of-plane infill torsional contribution to the translational stiffness is neglected

ρ_w [%]	b_c [cm]	error	
		“L”	“C”
0.8	30	6%	1%
	50	1%	1%
1.5	30	34%	5%
	50	6%	3%

Accordingly, normalised translational stiffnesses in Equations (186) and (187) can be simplified into Equations (188a) and (188b) by neglecting the addends corresponding to out-of-plane infills contributions. It is worth noting that, paradoxically, the translational stiffness for the “L” prototype only depends of the RC columns, although the position of the centre of twist only depends of the in-plane stiffness of the infill walls.

$$K_{VT,L}/A_b = \frac{8 \cdot E_c \cdot b_c^4}{\pi \cdot h^3 \cdot A_{rib}} \quad ; \quad K_{VT,C}/A_b = \frac{2 \cdot G_w \cdot \rho_w}{h} + \frac{9 \cdot E_c \cdot b_c^4}{2\pi \cdot h^3 \cdot A_{rib}} \quad (188a,b)$$

Aimed at estimating the magnitude of those stiffness values, it is possible to relate them to the translational stiffness of in-plane walls and RC columns, presented in Equations (189a) and (189b) for “L” and “C” prototypes, respectively.

$$K_{VT,L} = \frac{8}{\pi} K_{RC} \quad ; \quad K_{VT,C} = 2 \cdot K_w + \frac{9}{2\pi} K_{RC} \quad (189a,b)$$

Finally, the translational stiffness of the ground floor in “torsionable” buildings (K_1') with respect to the lateral displacement of the centre of mass is obtained as the combination of the shear stiffness (K_1) and the translational stiffness due to the torsion (K_{VT}), as acting in series, i.e., imposing a shear force that activates both stiffnesses obtaining a displacement which is the sum of both deformations (Equation (190a)). Then, it is possible to define the factor χ_T (Equation (190b)) corresponding to the relation between the translational stiffness accounting with the torsional contribution and without accounting for it.

$$K_1' = \frac{1}{\frac{1}{K_1} + \frac{1}{K_{VT}}} \quad ; \quad \chi_T = \frac{K_1'}{K_1} \quad (190a,b)$$

This factor, other to be used to re-define the elastic stiffness contribution factor (see section 5.1.3.3), can be also representative of the differences between the displacement demand of the different points of the first floor plan. In fact, K_1 represents also the displacement of the “rigid” side of the plan, which contains the centre of twist and do not experiment an increase of the displacement demand due to the torsion. Conversely, K_1' represents the displacement of the centre of mass. Thus, χ_T represents the relation between the displacement of the “rigid” side and the centre of mass, while $(2-\chi_T)$ represents the relation between the displacement of the “flexible” side and the centre of mass.

Aimed at the evaluation of the appropriateness of all the expressions developed in this procedure, two simple specific case studies, corresponding with the two prototypes proposed, are analysed. They correspond to the properties used to obtain the values of Table 49 except for the ranging parameters ρ_w and b_c , which in this case adopt fix values of 0.8% and 30cm, respectively. These distributions are considered to be usual in accordance to the building construction practice

presented in section 4.2. Their aspect is shown in Figure 191. In Figure 192, the torsional behaviour of the infills without columns is presented, while in Figure 193, the real behaviour with columns is shown. It is possible to appreciate how the position of the centre of twist is in the last case slightly displaced towards the centre of mass, but still being possible to consider this change as negligible.



Figure 191: Zenithal perspectives of “L” (a) and “C” (b) case studies

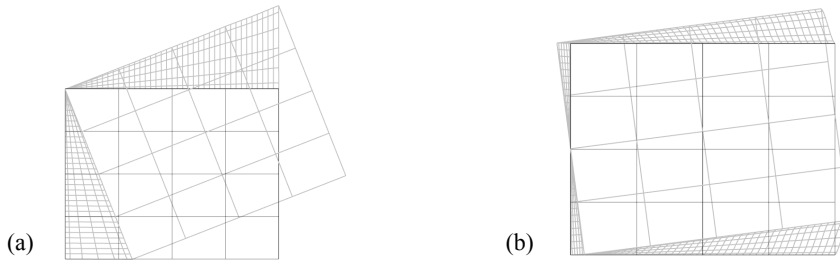


Figure 192: Deformed shape of “L” (a) and “C” (b) case studies without RC columns; the scale of the deformation is not the same in both cases

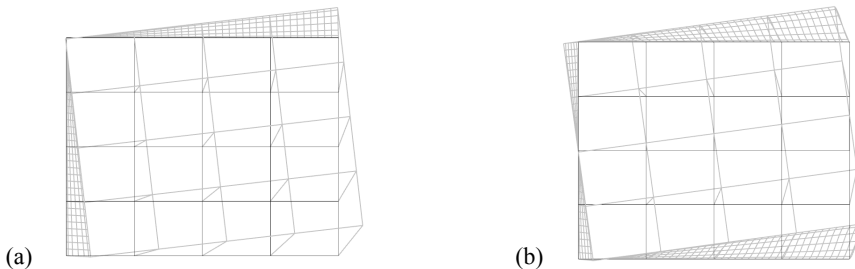


Figure 193: Deformed shape of “L” (a) and “C” (b) case studies with RC columns; the scale of the deformation is not the same in both cases

Results are in accordance with the proposed expressions with an error lower than 10% in both cases. It is worth noting that the displacement of the centre of mass is higher –approximately 5 times ($\chi_T=0.20$) for “L” prototype and 1.5 times ($\chi_T=0.66$) for “C” prototype— than that of the equivalent “non-torsionable” building –presenting the same infill ratio but not regularly distributed—, which shows the high impact on the vulnerability of those buildings.

5.3.3.3 *Influence of torsional behaviour on the vulnerability*

Aimed at an evaluation of the vulnerability of “torsionable” building classes inside the established framework of FAST, it is necessary to examine the influence of this behaviour in both parts of the method:

- dynamic behaviour: a new first storey translational stiffness may be used in all the expressions;
- DS thresholds: each representative IDR threshold for the different DS may be altered depending on the relative position of the control element in the ground floor.

The new translational stiffness of the first storey (K' , Equation (190)) must be replaced in all the expressions presented in Chapter 5. In Equation (191), the elastic stiffness contribution factor (χ) is re-defined as the relation between K_1' and the translational stiffness of the upper storeys. Then, it can be transformed in an expression similar to Equation (111), with an additional factor χ_T (Equation (190b)) corresponding to the relation between the translational stiffness accounting with the torsional contribution and without accounting for it.

$$\chi = \frac{K_1'}{K_s} = \frac{K_1 \frac{K_1'}{K_1}}{K_s} = (\chi_h \cdot \chi_p \cdot \chi_c) \chi_T \quad (191)$$

The dynamic consequences of this reduction regarding the vulnerability assessment of the “torsionable” buildings if compared with an equivalent regular-in-plan building are almost similar that those corresponding to the non-uniformly infilled frame when compared to the uniform one. The only difference is that the maximum spectral acceleration capacity $C_{s,max}$ (Equation (84a)) do not get reduced,

because in the “torsionable” case the decrease of χ do not come from a diminution of ρ_w . Thus, only the parameters containing χ in their expressions are affected:

- the first mode participating mass (m^*) increase slightly and the global stiffness (K_g) decrease a lot, so the fundamental ($T_{el,inf}$) and the effective period ($T_{eff,inf}$) increase;
- as a result, the elastic spectral acceleration demand ($S_{a,el}(T)$) usually decreases, so the IN2 curve in PGA units reaches relatively higher values of PGA_c (see Equation (25));
- the first mode participation factor (Γ) decrease slightly, so it makes the thresholds of spectral displacement for the different DS ($S_{d|DSj}$, Equation (102)) increase slightly;
- the contribution of the upper storeys to the displacement thresholds corresponding to the different DS ($d_{n|DSj}$, Equation (101)) is much lower; thus, the $S_{d|DSj}$ decrease, being this influence bigger than that of Γ .

These two last consequences of the torsional behaviour on the DS thresholds are made assuming that the IDR thresholds remains similar; in the next section, these argument is discussed.

As a result, the different DS are reached with substantial lower values of PGA, so the vulnerability is higher. All these differences can be appreciated in Figure 194.

Rotation of the first storey causes that each point of the plan experiment a different displacement demand. Global dynamic behaviour of the building, expressed in the factor χ_T and represented by the IN2 curve, is referred to the displacement of the centre of mass of the first storey. However, aimed at defining of IDR_{DSj} corresponding to the different elements, different points of the plan must be considered. Also, it is worth studying carefully whether the dynamic behaviour remains torsional beyond DS3.

In Table 48, IDR_{DSj} corresponding to infills, RC columns and their interaction are shown. Given that the DS is attained when the first element of any type attains the corresponding IDR, it is necessary to assume a fix position for the “candidate” element of each type.

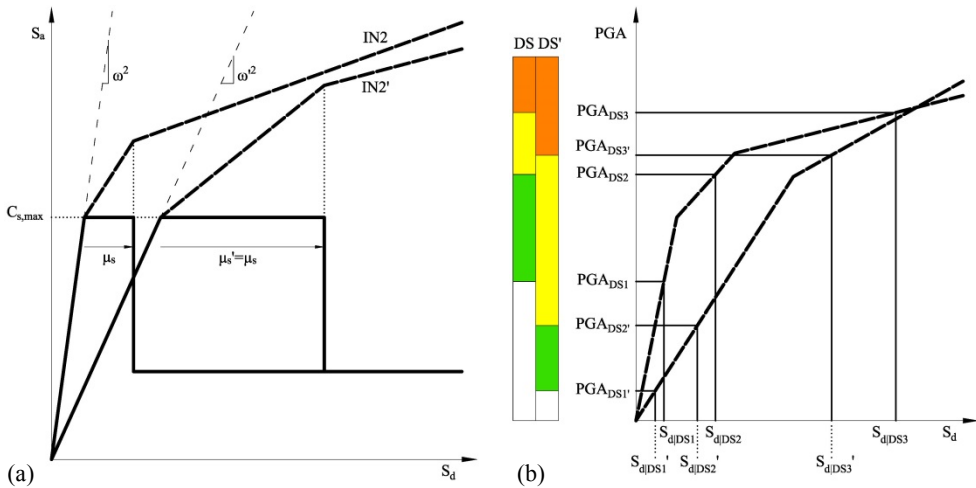


Figure 194: Hypothetical comparison between regular and “torsionable” equivalent building class: CC and IN2 (a) and DS thresholds (b)

Regarding the infills, in both assumptions (“L” and “C”) the effective panels are placed in the “rigid” side of the plan, aligned with the centre of twist, so they do not experiment an increment of the displacement demand if compared with the non-torsionable buildings. It is worth noting that in this case neglecting out-of-plane behaviour may be less accurate than in the non-torsionable case, considering the higher demand of the “flexible” side of the plan, where perpendicular infill panels are placed.

Nevertheless, as shown in section 4.2, almost all the buildings suitable to be classified into “L” or “C” prototype present a little amount of effective interior infills. It is quite usual to find ground floors with two or three sides closed with infills but presenting approximately in the middle on the plan some brick walls forming the staircase. If the dimensions of the staircase, its distribution of infills or their thickness are so relevant to make it impossible to be neglected when compared to the façades, then this building cannot be classified as “torsionable”. But if the stiffness of infills do not change the approximate torsional behaviour of the ground floor (mainly the position of the centre of twist), then it is possible to consider the building as belonging to one of the two “torsionable” prototypes.

Unfortunately, the uncertainty about its location is very high. Anyway, according with all the other important simplified assumptions considered in the whole procedure, it is possible to suppose that the probabilistic average position of the control element is the barycentre of the floor.

Thus, in this simplified approach one of those “probable” infills is assumed to be the control element ruling the attainment of the IDR_{DS_j} corresponding to infills in Table 48. As its position is coincident with the point defining IN2 curve (centre of mass), it is not necessary to correct the values for interstorey drift thresholds.

It is worth noting that in both cases (“L” and “C”), the behaviour remains torsional even beyond DS3. The secant stiffnesses at the attainment of DS1 and DS2 are 100% and 25% of the initial effective one ; but this state is attained by the control element at the centre of mass. The infills on the “rigid” side experiment a displacement demand χ_T times lower, which might be assumed to be represented by a DS($j-1$). Thus, at the attainment of DS3, the infills at the control point have almost no stiffness, but the “rigid” side of the plan may have still enough stiffness to maintain the torsional behaviour of the whole plan, conservatively.

This fact is important regarding the correction of IDR_{DS_j} corresponding to RC columns. In this case, the control elements are assumed to be placed in the “flexible” border of the plan, being its displacement demand ($2-\chi_T$) times higher than that of the centre of mass. So, values of interstorey drift thresholds on Table 48 must be divided by that quantity. As a consequence, DS1 and DS3 may be attained first by the RC columns than by the infills.

However, for DS4 it is not clear whether the same reduction factor should be applied for the IDR threshold of RC columns. Between the attainment of DS3 and DS4 by the columns of the “flexible” side, the torsional behaviour gets progressively “corrected”. In a hypothetical adaptive pushover, the increment of load would be applied progressively with a different eccentricity, having the increments of displacement an associated rotation gradually lower; actually, the cyclic behaviour is more complicated. Anyway, it is reasonable to assume that at a level of drift of 3-4% (representative of DS4 for RC columns), the displacement of the centre of mass is almost the same than that of the flexible side, so the IDR threshold may not be reduced.

Regarding brittle failures in RC columns due to the interaction with infill panels, corresponding values of IDR may be amplified by χ_T . This assumption derives from considering that only the effective infills on the “rigid” side are suitable to interact with the columns. Conversely to non-brittle failures, in this case torsional behaviour still rules for DS4, given that their corresponding IDR are not much higher than those for DS3; hence, infills still remain with considerable stiffness to provoke torsional behaviour.

Finally, it is worth noting that, as well as for non-uniformly infilled frame, the procedure is useful only in the case of having such detailed and disaggregated survey information: it is necessary to know not only the proportion of “torsionable” buildings with respect to the total RC building stock but also their particular level of damage. Also, in the case of buildings similar to “C” prototype, directional information must be required, given that it would belong to different classes of building in each direction.

5.3.4 Cumulative damage

Several works (Bazzurro et al., 2006, Luco et al., 2004, Bazzurro et al., 2004, Polese et al., 2013) focus in the analysis of the performance of RC structures previously damaged (i.e. a foreshock). Some typical issues are discussed, as the equivalent period to be used in each step.

Herein, a simplified approach is proposed within the general framework of FAST. It consist on assuming that the demand spectra may be introduced into the N2 procedure as if their ordinates cross the abscissa at the unloading point consistent with the previous damage level (see Figure 195).

Similar periods for loading and unloading are considered. However, different periods are assumed depending on the DS previously attained: if it is lower than DS2, the initial period of the infilled frame (uniformly or non-uniformly infilled) is assumed subsequently; if it is equal or higher than DS2, the period may correspond only to the value of χ accounting only for the RC columns at 1st storey, i.e. the period of the pure pilotis frame. In Figure 196 to Figure 199, graphic examples of attainment of the different DS are shown aimed at illustrating the procedure.

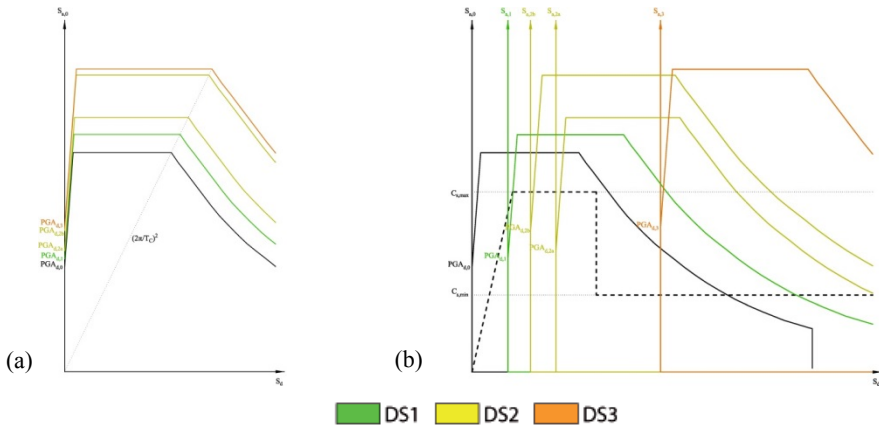


Figure 195: Four increasing demand spectra (0, 1, 2a-2b and 3) (a) causing the successive DS when acting consecutively on an infilled frame (b)

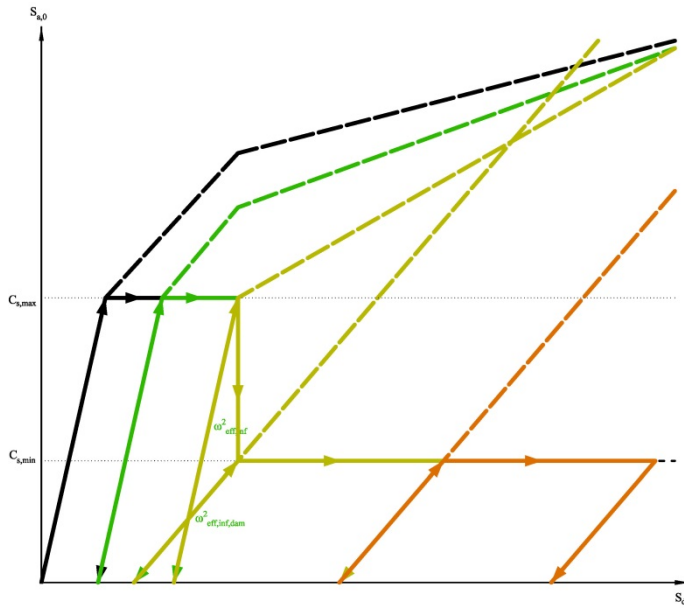


Figure 196: General backbone of the CC, load paths and IN2 of all the cases

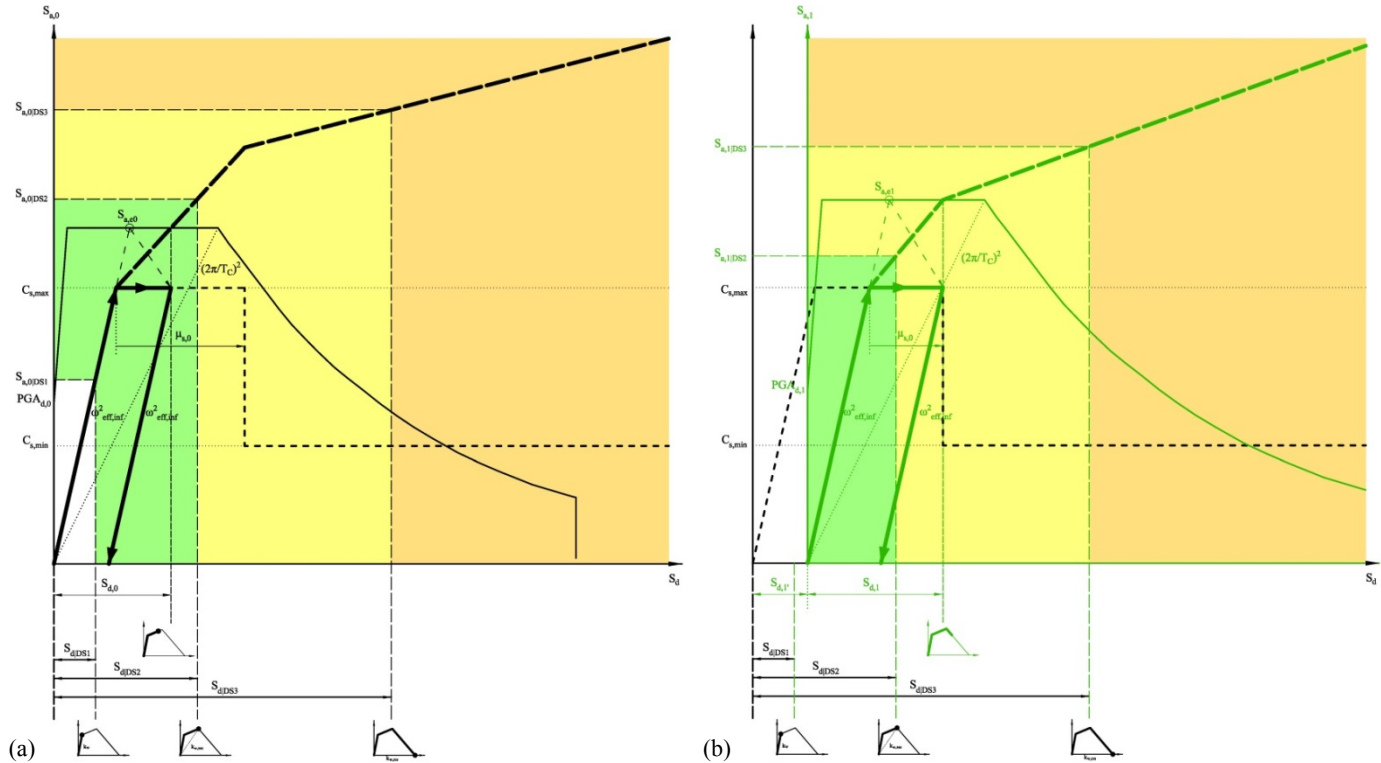


Figure 197: General CC backbone, load path, IN2 and DS thresholds of: a non-damaged infilled frame subjected to a demand causing DS1 beyond the beginning of the “plateau” (a) and a an infilled frame previously “DS1-beyond-plateau damaged” subjected to a demand causing DS2 scarcely before the drop (b)

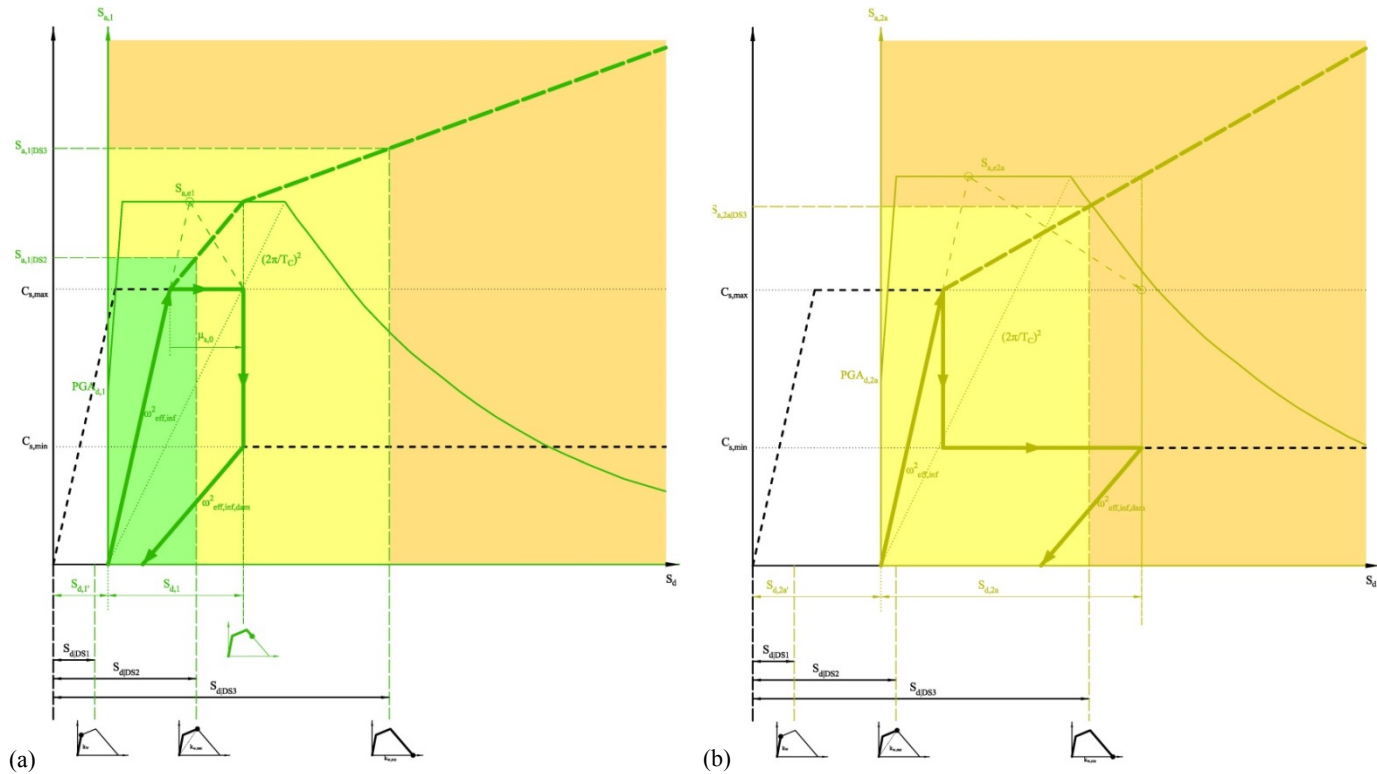


Figure 198: General CC backbone, load path, IN2 and DS thresholds of: an infilled frame previously “DS1-beyond-plateau damaged” subjected to a demand causing DS2 scarcely after the drop (a) and infilled frame previously “DS2-before-drop damaged” subjected to a demand causing DS3 (b)

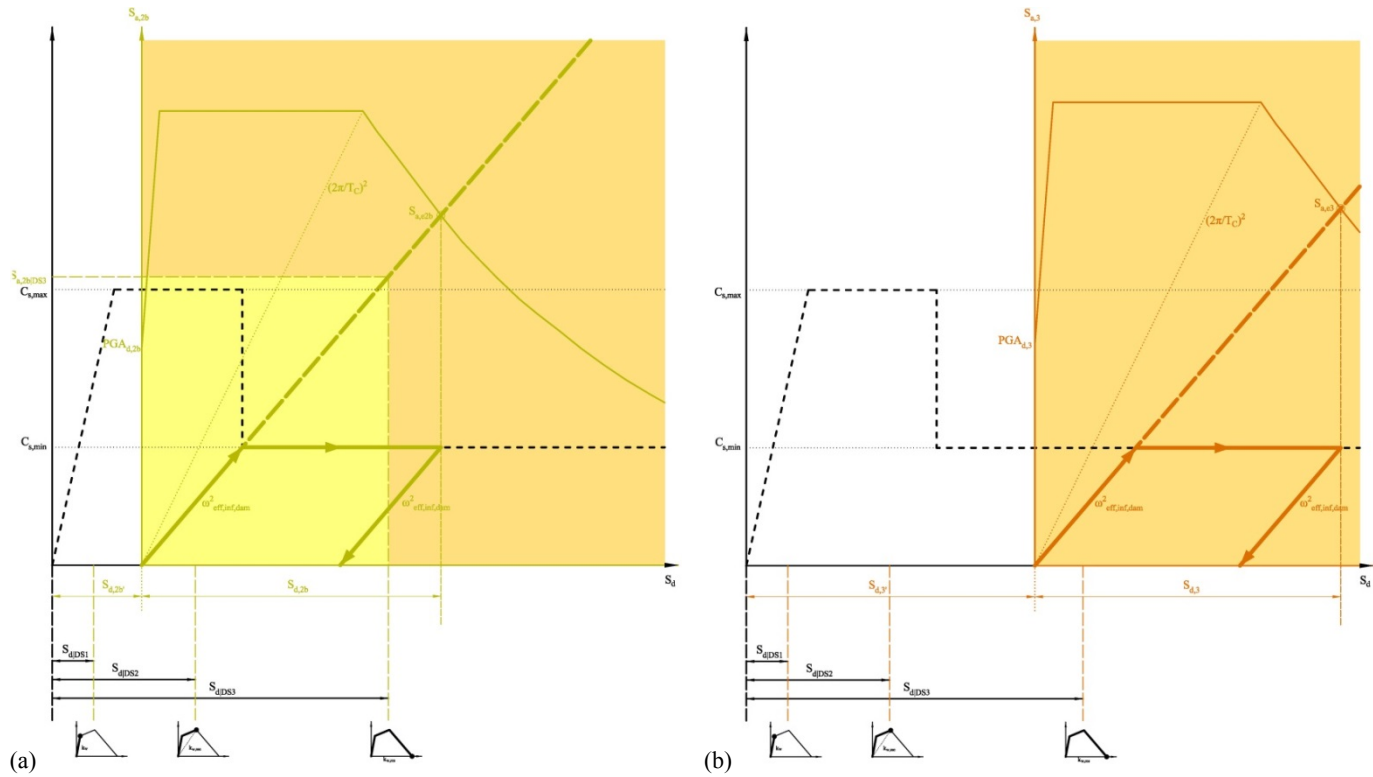


Figure 199: General CC backbone, load path, IN2 and DS thresholds of: infilled frame previously "DS2-after-drop damaged" subjected to a demand causing DS3 (a) infilled frame previously "DS3 damaged" (b)

5.3.5 Adaptive dynamic properties

Generalised FAST use values for $\lambda_r = \Gamma \cdot (m^*/M)$ not only depending on the number of storeys but also on the distribution of elastic stiffness (reflected in factor χ). Furthermore, notwithstanding that the whole FAST approach is based in a non-adaptive pushover framework, some specific strategies extracted from the adaptive methodology (see section 1.2.1.1) are suitable to be applied to the generalised method.

Considerations regarding the loss of precision for the evaluation of the capacity and damage thresholds corresponding to higher DS due to the use of initial elastic dynamic properties are carried out in sections 5.1.1.1 and 5.1.3.7, respectively. An adaptive pushover methodology would solve this problem by updating these values at each step.

As FAST is a discrete method, the translation of this principle would be to use two different values of (m^*/M) and Γ : the elastic ones for the first and second branches of the CC, and another couple of values corresponding to the last branch, which can be related to the attainment of the higher DS considered in this methodology: DS3. This last branch is defined by the residual capacity ($C_{s,min}$, see Equation (84b)). Thus, a reduced value ($C_{s,min}'$, see Equation (192)) may be used, resulting from the adoption of a new value of relative participating mass (λ_r) assumed to be equal to its upper bound (1.0), corresponding to a quasi-constant deformed shape, typical of a soft ground storey mechanism (see Table 2). This reduction would be typically of a 10-20%, causing a decreasing in the slope of the corresponding branch of the IN2 curve (see Figure 200b). Anyway, in this work, this modification is not applied.

$$C_{s,min}' = \frac{C_{s,min}}{\lambda_r' (=1.0)} = \lambda_r \cdot C_{s,min} \quad (192)$$

For the conversion of the DS thresholds from top displacement to spectral displacement unities, the same specific values of Γ for the obtaining of the maximum and minimum capacities of the CC must be used.

Following the same reasoning, it would be possible to consider, for the DS3 spectral displacement threshold, a value of $\Gamma'=1.0$, equivalent to the lower bound of this parameter, corresponding to a deformed shape closer to the constant one, typical of a soft first storey mechanism (see Table 2).

$$S_{d|DS3}' = \frac{S_{d|DS3}}{\Gamma' (=1.0)} = \Gamma \cdot C_{s,min} \quad (193)$$

This assumption would be feasible within the FAST framework due to its discrete philosophy and the high number of branches of the CC. In Figure 200a, the IN2 corresponding to the three assumptions of dynamic properties (shown in Figure 27) are plotted. Also, for a given top displacement of the original MDOF, the three corresponding spectral displacement and acceleration (S_d and S_a , respectively) are marked, being the values for the assumption of dynamic properties of the collapsed structure an upper and lower bound for S_d and S_a , respectively. In this case, it might not be feasible to apply this extreme hypothesis only to higher values of displacement because the whole horizontal branch should be moved down. Also, it is not clear which effective period should be used, circumstance that would provoke a change in the demand.

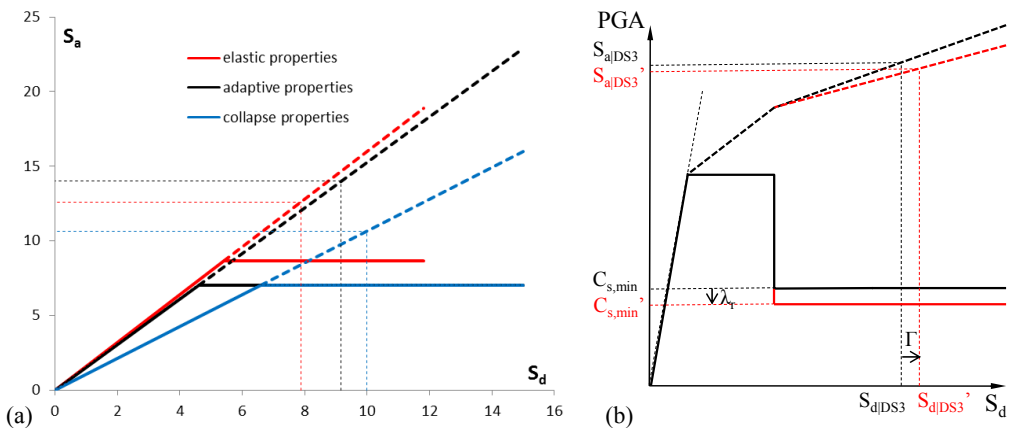


Figure 200: CC and IN2 obtained from the same pushover curve of a bare frame assuming three diverse hypotheses (a), and CC and IN2 curve of an infilled frame with modifications for higher DS

Conversely, for infilled frames, as the first two branches (defined by the effective period, maximum spectral acceleration capacity and ductility up to the start of the degradation) are associated to DS lower than DS3, it is clear that both the capacity and the displacement thresholds may be defined with the initial elastic dynamic properties, while for the rest of the curve and the displacement threshold corresponding to DS3, the modified values can be used (see Figure 200b).

The conservativeness of this procedure with respect to the original one depends on the relationship between the slope of the third branch of the IN2 curve and Γ . Anyway, in this work, this modification is not applied.

Chapter 6

Application of FAST to the Lorca earthquake

In this chapter, FAST is applied to the case study of Lorca earthquake: firstly to the bare frames, later to the uniformly infilled buildings and finally to the non-uniformly infilled frames. The input variables respond to the local characteristics analysed in the previous chapters. Hence, simulated damage scenarios are obtained and compared with the real observed damage statistics presented in Chapter 2.

6.1 SIMULATED DESIGN

In Chapter 5, the input parameters of FAST are presented (see Table 44). Some of them must be defined in accordance with the local characteristics of the case study to be assessed, but some others are likely independent; suggested values have been proposed in the previous Chapter. Those values (see Table 50) are used in the assessment carried out herein.

FAST requires to be given a value of design base shear (V_b) for each class of buildings. Such values must be obtained from a simulated design. Firstly, location and soil type must be defined: Lorca and type II, respectively (see section 4.3.1). Then, design spectra for each Spanish seismic code is defined for those parameters (see Figure 201a); the variables required for the construction of such spectra are

shown in Table 51. Typical wide-beam buildings are assumed to be the most frequent (see Chapter 3).

Table 50: Suggested values for some input parameters of FAST regardless of the specific case study

m_r	[t/m ²]	0.8	τ_{cr}	[N/mm ²]	0.35	α	-	0.5	IDR_{DS1}	[%]	0.03
λ_r	-	0.85	a_w	-	1.3	β	-	0.0	IDR_{DS2}	[%]	0.20
R_ω	-	1.45	G_w	[N/mm ²]	1350	κ	-	1.3	IDR_{DS3}	[%]	1.20
R_α	-	1.00	μ_s	-	2.5	T_1	[s]	$0.075H^{0.75}$	Ω_{DS2}	-	0.25

Table 51: Variables required for code-based simulated design of the different classes of buildings of Lorca, considering soil type II

Seismic code	MV-101	PGS-1	PDS-1	NCSR-94	NCSE-02
Intensity MSK (G)	VIII		VIII	-	-
PGA reference [g]	implicit	$C_{0.5} \cdot R = 0.15 \cdot 0.9 = 0.14$		$a_b = 0.12$	
Azores contribution (K)	-	-	-	1.0	
Soil factor	implicit		$\delta = 1.1$	$C = 1.4$ ($S = 1$)	$S = 1.04$
Risk factor	-		implicit	$\rho = 1.0$	
Damping factor	-		$B = 0.6$	$v = 0.87$	$v = 1.00$
Behaviour factor (μ)	implicit		implicit	2	
Response factor (β)	-		implicit	0.44	0.50
Max. spectral amplification (α)	implicit		1.0	2.2	2.5
Period for plateau start [s]	-		0.0	$T_0 = 0.20$	$T_A = 0.13$
Period for plateau end [s]	-		0.5	$T_1 = 0.59$	$T_B = 0.52$
Max. spectral value ($S_a(T)_{max}$) [g]	$s = 0.08$	(0.11)	0.11	0.12	0.16
Fundamental period T [s]	-		$0.09 \cdot H/L^{0.5}$		$0.09n$
Reduction coeff. for live loads	0.5		0.5	0.3	0.5
Superficial mass (m_d) [kN/m ²]		7		8.6	9
Accidental combination factor (γ_d)	1.0	1.0	1.1		1.0
MDOF relative participating mass (λ_d) (number of storeys)	-		0.86 (3), 0.83 (4), 0.82 (5), 0.81 (6)	0.93 (3), 0.91 (4), 0.89 (5), 0.88 (6)	

Spectral acceleration is obtained thanks to the adoption of fundamental period of design, assuming that simplified formulations have been used in that phase. Next, masses of design are assumed to be higher for modern buildings (see section 5.1.1.1), and different combination factors and participating mass factors are considered (see Table 51). Hence, normalized V_b are shown in Figure 201b. It is worth noting that the increment of design base shear for NCSE-02 respect to old-

generation codes is quite larger than the same increment in terms of spectral acceleration.

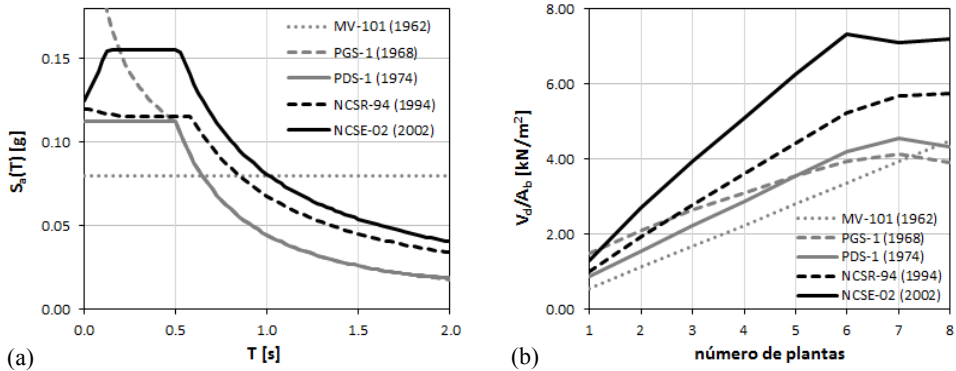


Figure 201: Design acceleration response spectra (a) and normalised base shear demand (b) for the city of Lorca for the different seismic codes

Then, it is necessary to define the representative classes of building of RC building stock in Lorca. In section 4.2 it is inferred that typical number of storeys are: 3, 4, 5 and 6; and typical seismic code of application (i.e. typical age of construction) are: 1974, 1994 and 2002. Finally, the rest of the input parameters described in Table 44 are particularised for the case study (see Table 52). Parameters regarding geometry (interstorey heights and infill ratios) are based on in-field observations described in section 4.2; nomenclature “ex”, “al” and “in” refer to external, aligned and internal infill panels. Aimed at the application of generalised FAST to the case study, other parameters should be defined: material properties and reinforcement ratios (based on the more frequent values according to the corresponding RC codes (see section 2.2.9.1)) and tributary areas for columns (see section 4.2).

In Figure 202a, spectra in ADRS format corresponding to the mainshock registered in LOR station (see section 4.1), according with a reference system depending on the fault directions (perpendicular (FN) and parallel (FP), are shown. It is worth noting that corner period for FN direction is larger, due to directivity

effects (see section 4.1.2). Thus, not only demand is larger in FN direction rather than for FP but also capacities are lower for infilled frames (see R - μ - T relationships in section 1.2.3.4). Real spectra are used instead of smoothed ones (see section 1.2.3.1). In the whole chapter, all the graphics follow the legend shown in Figure 202b.

Table 52: Input parameters for the specific case study of Lorca

h_1	[m]	3.5	f_{cd}	[N/mm ²]	15, 17.5, 25 (age<1974, 1974<age<1994, 1994<age)
h_s	[m]	3.0	f_{yd}	[N/mm ²]	400, 500 (age<2002, 2002<age)
A_{trib}	[m]	20	$\rho_{w,1}$	[%]	2.5 (simplified); 1.1, 1.3, 1.5 (ex, ex+al, ex+al+in)
ρ_s	[%]	2.0	$\rho_{w,s}$	[%]	2.5 (simplified); 1.9, 2.5, 4.2 (ex, ex+al, ex+al+in)

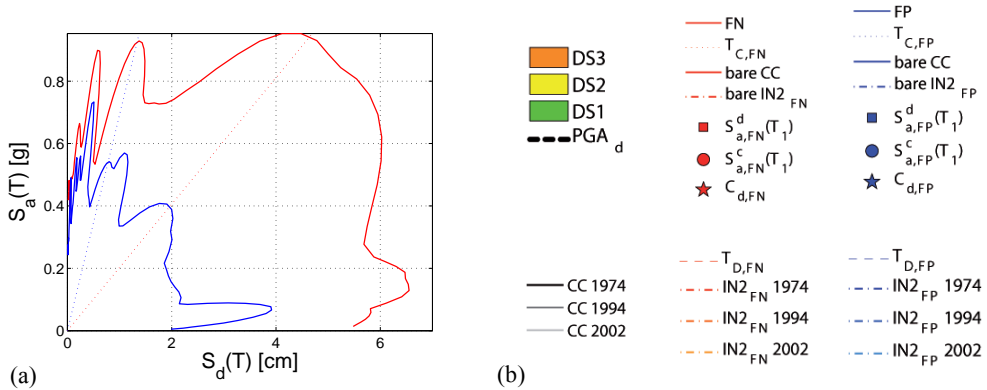


Figure 202: ADRS of Lorca mainshock for Fault Normal (FN, red) and Fault Parallel (FP, blue) directions (a); and legends for all the graphics of the chapter (b)

6.2 ASSESSMENT OF BARE FRAMES

Firstly, the preliminary procedure shown in section 5.1.1 for code-based assessment of bare frames is carried out. In Table 53, demand corresponding to 3- and 5-storey frames is calculated according to Figure 202a. Then, in Table 54, spectral capacities in terms of acceleration and displacement are obtained; Equations (78), (80) and (82b) are used.

Table 53: Demand estimation for 3- and 5-storey bare RC frames for FN and FP mainshock signals in LOR station

Number of storeys	3		5	
	$S_{a, FN}^D(T)$	$S_{a, FP}^D(T)$	$S_{a, FN}^D(T)$	$S_{a, FP}^D(T)$
Demand	[g]	[g]	[g]	[g]
PDS-1 (1974)	0.81	0.56	0.95	0.40
NCSR-94 (1994) & NCSE-02 (2002)	0.82	0.55	0.94	0.39

Table 54: Simplified code-based capacity estimation for 3- and 5-storey bare RC frames

Number of storeys	3						5					
	Heigh, H [m]						15.5					
	T	$S_a(T)$	$C_{s, RC}$	$S_{du, FN}$	$S_{du, FP}$	$S_{a, e}$	T	$S_a(T)$	$C_{s, RC}$	$S_{du, FN}$	$S_{du, FP}$	$S_{a, e}$
	[s]	[g]	[g]	[cm]	[cm]	[g]	[s]	[g]	[g]	[cm]	[cm]	[g]
PDS-1 (1974)	0.27	0.11	0.16	0.78	0.59	0.32	0.44	0.11	0.16	1.58	1.57	0.32
NCSR-94 (1994)	0.27	0.13	0.19	0.92	0.69	0.38	0.45	0.13	0.19	1.93	1.93	0.38
NCSE-02 (2002)	0.27	0.16	0.23	1.08	0.82	0.45	0.45	0.16	0.23	2.27	2.27	0.45

In Figure 203 and Figure 204, the procedure is applied to the 12 classes of buildings. In all the cases, the assessment in FN direction returns values of demand quite larger than capacity, while for FP only 3- and 4-storey 1974 frames would collapse. It is worth noting that, in all the cases, the higher is the number of storeys, the better is the performance. The reason is that the mainshock acceleration spectrum experiment a larger decrease for medium-high periods than the code-based spectrum (see section 4.1 and Figure 154). Better performances are expected for new buildings rather than for old ones, according to the design base shear distribution shown in Figure 201b.

According to the hypothesis of code-based performance of bare frames, all the RC buildings stock of Lorca should have collapsed; FN demand is sometimes twice the capacity. Only 6-storey NCSE-02 frames almost provide capacities similar to demand.

FAST simplified vulnerability approach for seismic assessment of infilled RC MRF buildings and its application to the 2011 Lorca (Spain) earthquake

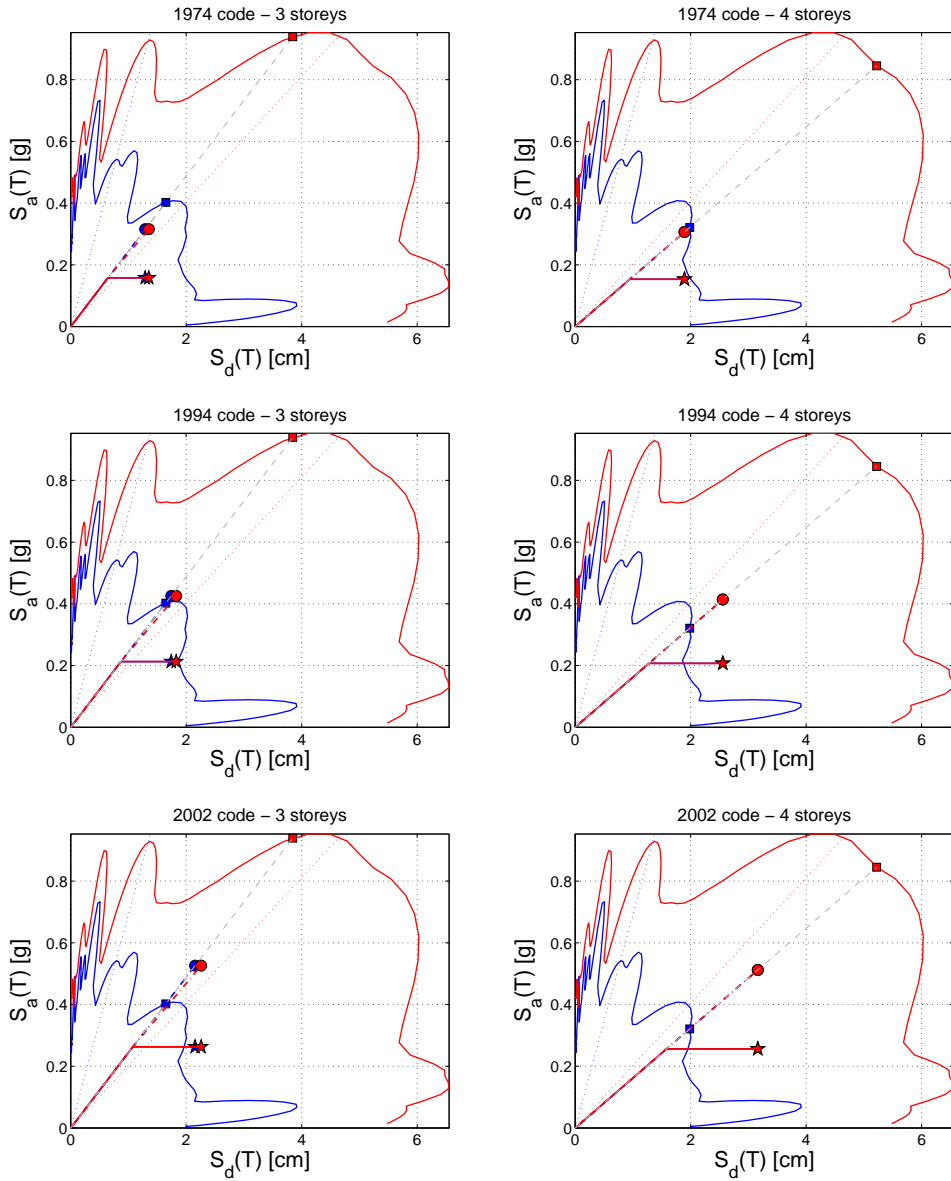


Figure 203: Preliminary code-base assessment of 3- and 4-storey bare RC frames subjected to mainshock in LOR station in FN and FP directions

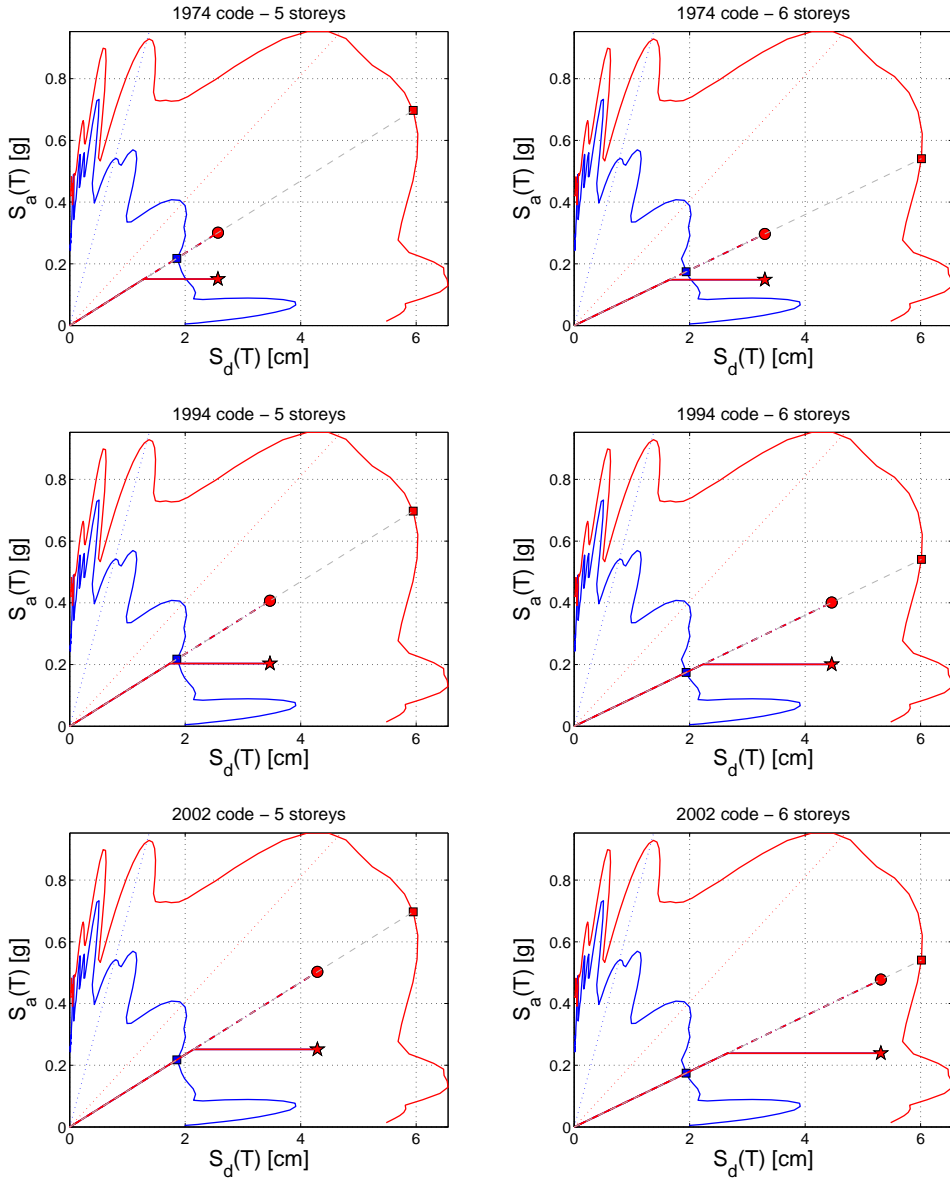


Figure 204: Preliminary code-base assessment of 5- and 6-storey bare RC frames subjected to mainshock in LOR station in FN and FP directions

As it is discussed in section 5.1.1, regardless of infills contribution, the assumption of behaviour factors of capacity similar to those adopted for design is a very conservative strategy. In chapter 3, results of a case study on NCSE-02 bare frames show typical average value of safety factors (SF) of 2.0, which already includes overstrength. Thus, a more realistic value of $S_{a,e}$ may be obtained by multiplying actual values by $2.0/1.45=1.38$. However, only for 5-storey NCSR94 and 5- and 6-storey NCSE-02 buildings it can balance the difference. Even in those cases, the damage level would be so high, as severe structural damage would take place.

It is evident that the real damage scenario is totally different than the scenario suggested by that preliminary code-based approach. Firstly, from a large-scale point of view, the number of collapses (or buildings with severe damage level, i.e. $DS \geq 4$) is very reduced (8.5%, see section 4.3.2). And secondly, from a short-scale point of view, damage scenario suggests that there is no use of ductility at all, i.e. inelastic penetration of buildings is scarce. Thus, any approach based on behaviour may not be suitable to be considered as fulfilling, because its philosophy is not coherent with reduced ductility performances.

6.3 ASSESSMENT OF UNIFORMLY INFILLED FRAMES: SIMPLIFIED FAST

In this section, simplified FAST approach (whose complete procedure is detailed in section 5.1) is applied to the case study. In Figure 205, CC and IN2 curves for all the classes of buildings in both directions are shown; higher capacities are obtained for FP direction thanks to lower corner period of the demand. For buildings with low number of storeys, higher relative contribution of infills is shown (in terms of equivalent elastic stiffness, maximum strength but also in terms of drop of resistance). It is worth noting that low increase of capacities are shown for new buildings than for old ones, as performance is almost ruled by infills.

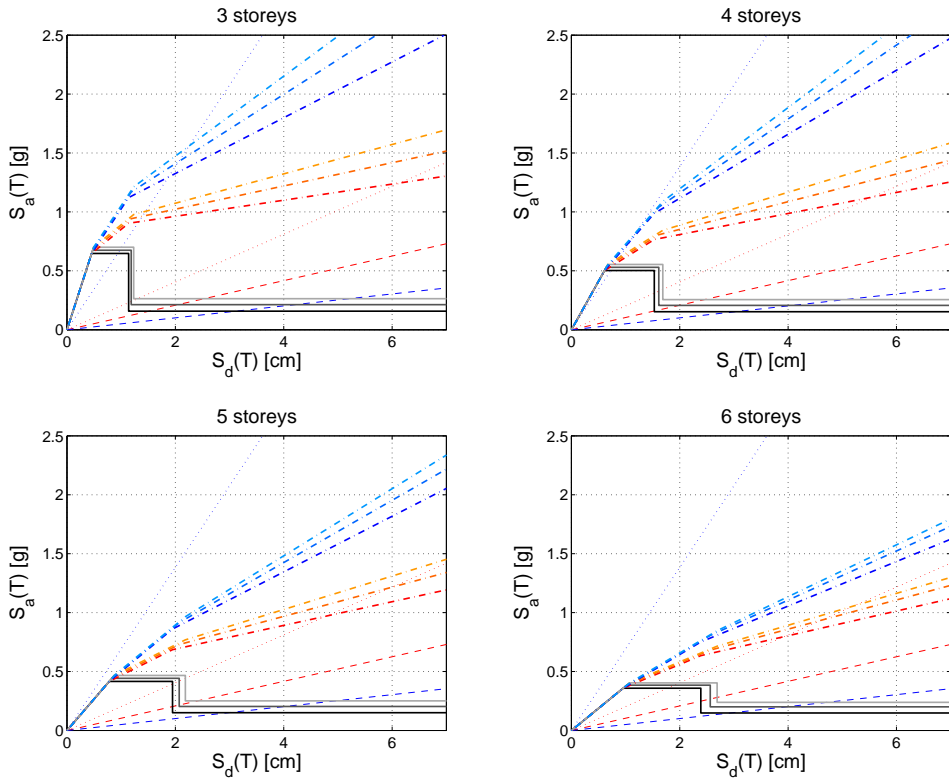


Figure 205: Approximate CC and IN2 curves for uniformly infilled frames subjected to mainshock in LOR station in FN and FP directions

Then, IN2 curves together with spectral displacement thresholds for each DS are shown in Figure 206 and Figure 207 for FN direction, and in Figure 208 and Figure 209 for FP direction. Thresholds do not depend on the code of design, as similar deformed shapes and 1st storey IDR are adopted for all of them (see section 5.1.3). It is worth noting that the displacement corresponding to the local attainment of each DS takes place before the IN2 curve attains the equivalent point (see section 5.1.3.1). Demand PGA corresponding to mainshock is also plotted; it would cause DS2 for FN in all the cases, while for FP, sometimes DS1 would be the typical damage of buildings.

FAST simplified vulnerability approach for seismic assessment of infilled RC MRF buildings
and its application to the 2011 Lorca (Spain) earthquake

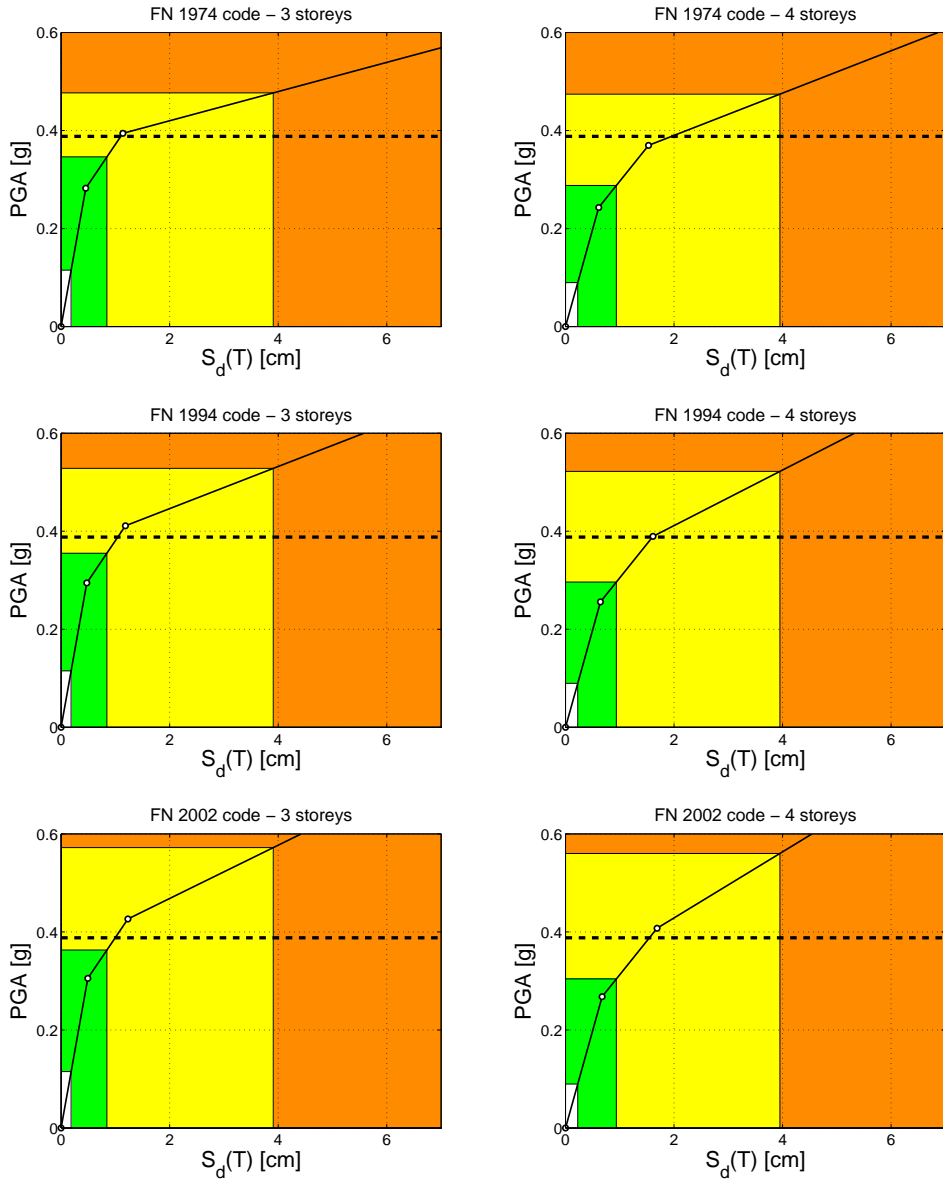


Figure 206: Damage assessment in terms of PGA for 3- and 4-storey uniformly infilled frames subjected to mainshock in LOR station in FN direction

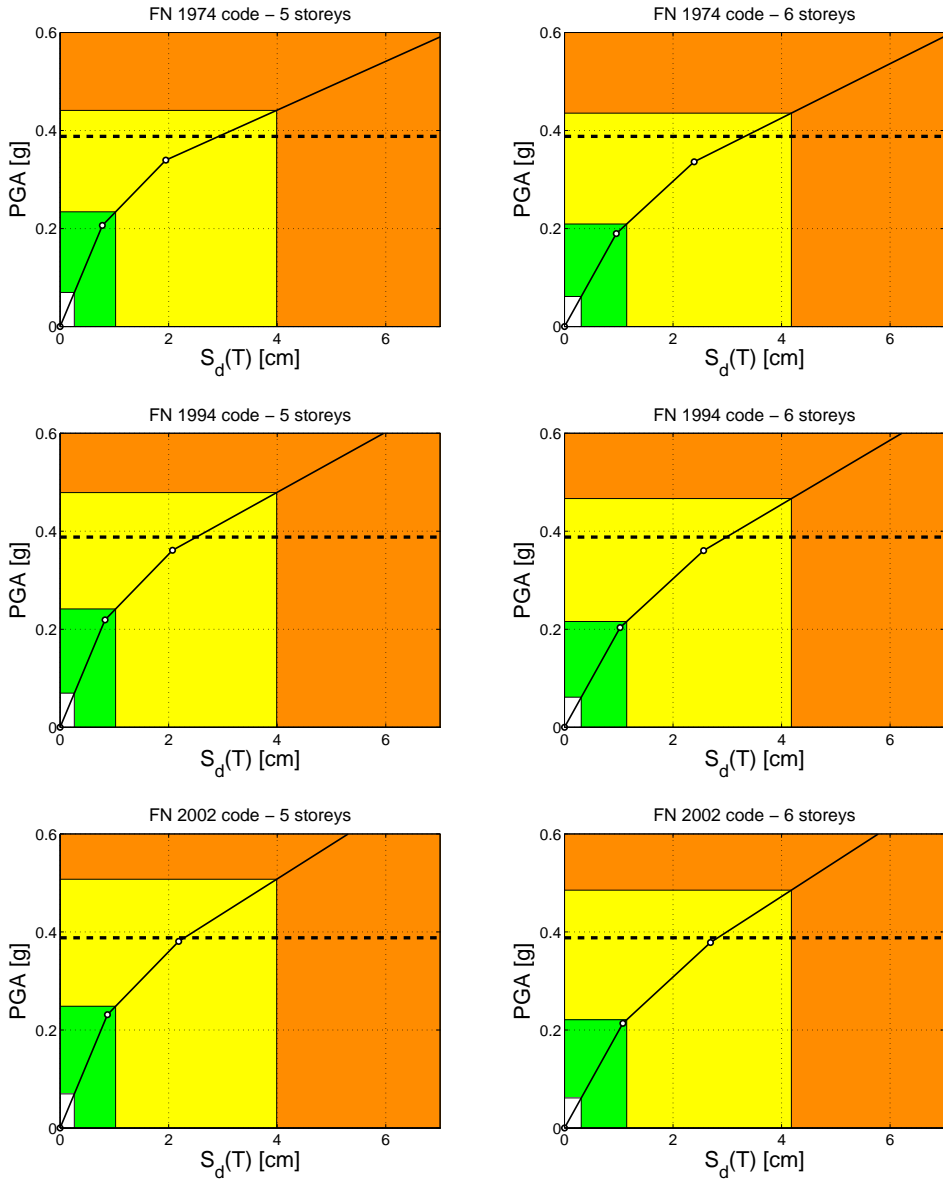


Figure 207: Damage assessment in terms of PGA for 5- and 6-storey uniformly infilled frames subjected to mainshock in LOR station in FN direction

FAST simplified vulnerability approach for seismic assessment of infilled RC MRF buildings and its application to the 2011 Lorca (Spain) earthquake

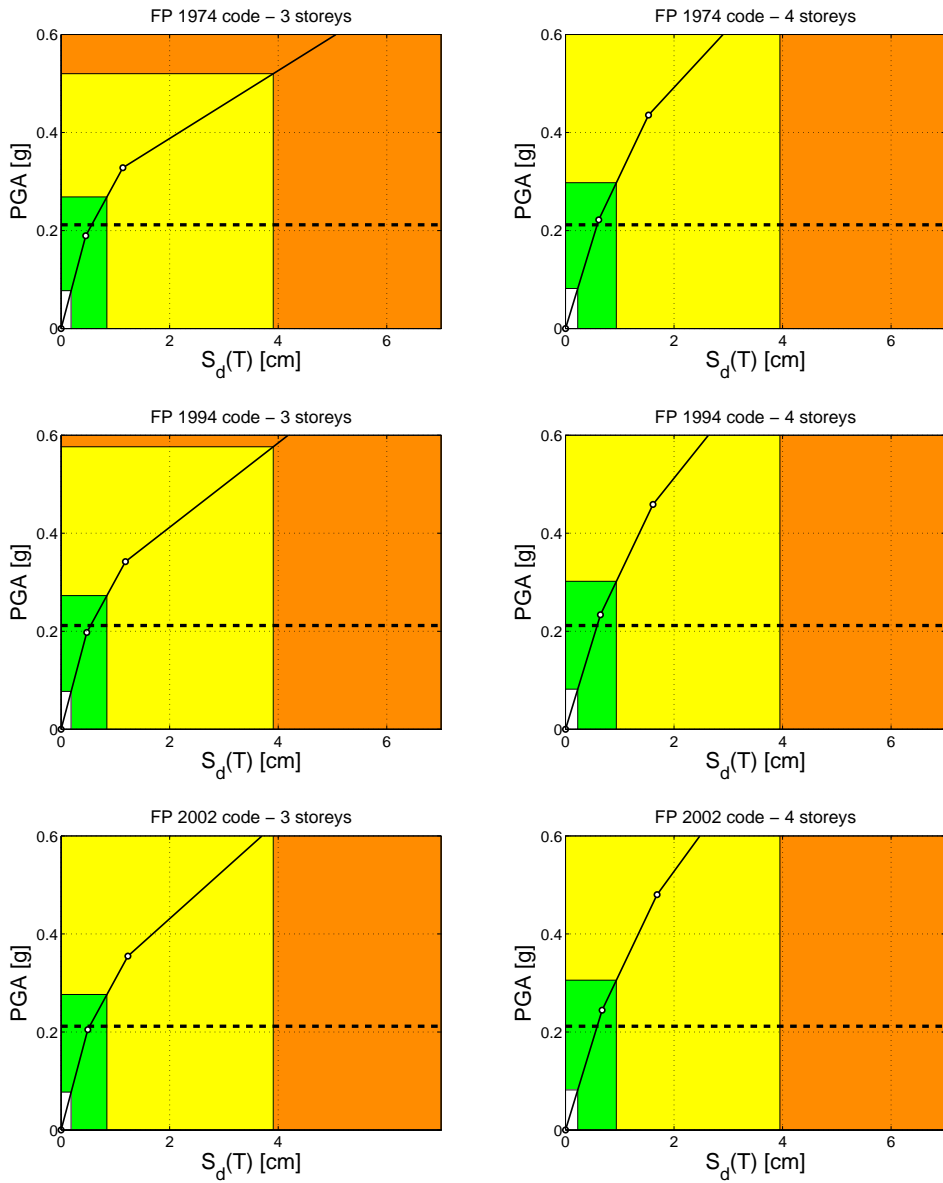


Figure 208: Damage assessment in terms of PGA for 3- and 4-storey uniformly infilled frames subjected to mains shock in LOR station in FP direction

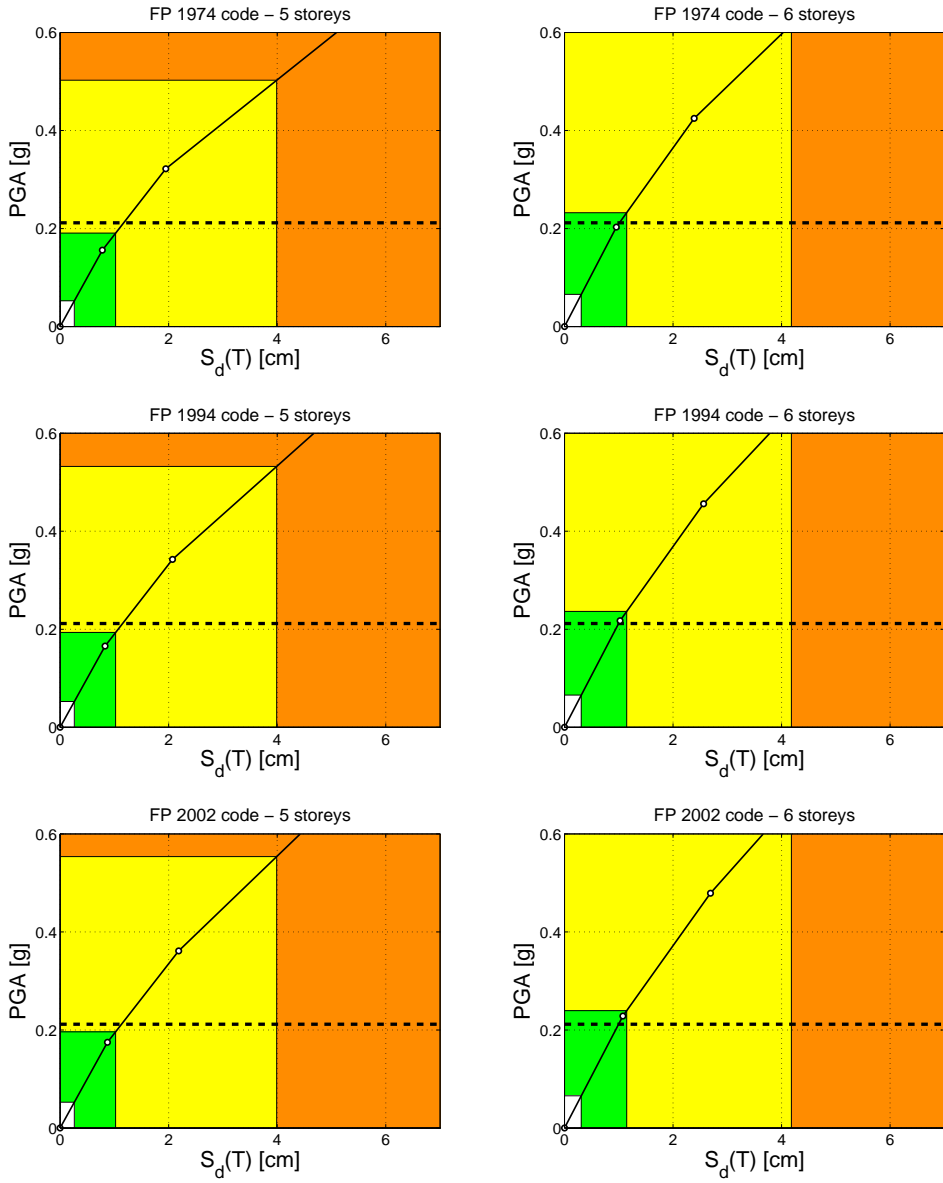


Figure 209: Damage assessment in terms of PGA for 5- and 6-storey uniformly infilled frames subjected to mainshock in LOR station in FP direction

Those graphics are summarised in Figure 210, where not only the predicted DS but also the trends of results can be observed. Furthermore, in Figure 211 and Figure 212, simplified fragility curves are obtained as established in section 5.1.4. Different considerations about the results can be done:

- more sever damages are expected in FN direction rather than for FP, thus FN may be the responsible of the DS classification;
- DS2 (cracks in infills) is predicted for all the classes of buildings
- in general, poorer performances are predicted for taller buildings rather than for shorter ones, as expected for sub-standard buildings;
- the assumption of real spectra instead of smoothed ones cause that the evolution of damages within number of storeys is not gradual, i.e. taller buildings not always present higher damages;
- the influence of age (i.e. the code of design) is minimum: similar trends and almost similar magnitudes of DS thresholds are observed;

If predicted damages are compared with real damage scenario (see Figure 164), fair to good agreement is observed: similar median DS and similar trend with number of storeys. The probabilities of exceeding of each DS shown in Figure 211 and Figure 212 match quite well with real damage scenario, showing in almost all the cases maximum probabilities for DS2.

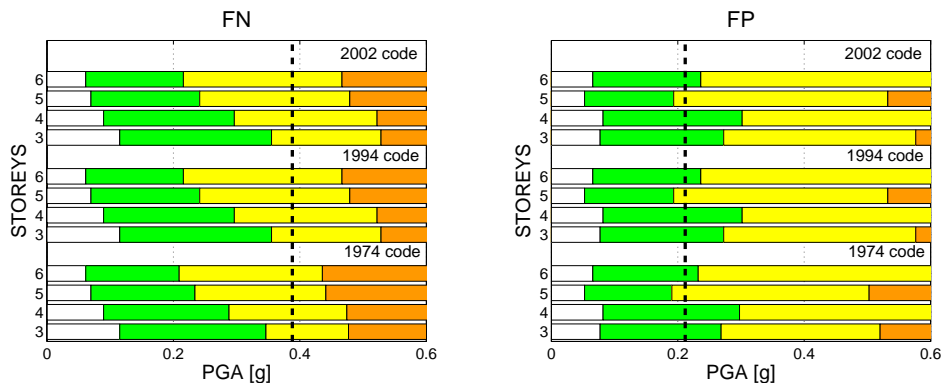


Figure 210: Damage assessment in terms of PGA for uniformly infilled frames subjected to mainshock in LOR station

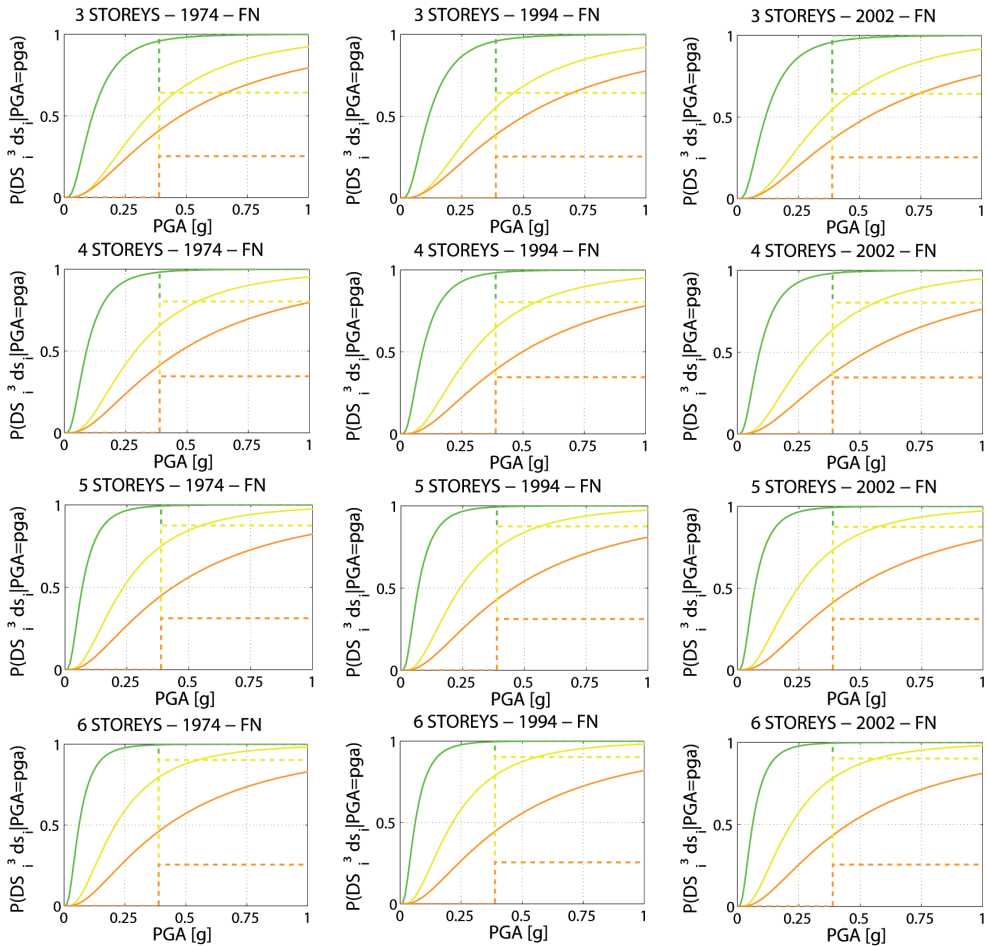


Figure 211: Fragility curves (solid line) in terms of PGA for uniformly infilled frames subjected to mainshock in LOR station in FN direction, and real damages (dashed line)

However, as explained in section 4.3.2, the real trend of damages depending on seismic code is not possible to be resembled by an approximate tool aimed at the estimation of vulnerability because there is influence of number of storeys within different seismic codes (i.e. the proportion of buildings corresponding to each number of storeys is not similar between codes). Unfortunately, real damage scenario is disaggregated independently by number of storeys and age of construction; data are not combined. Furthermore, the reduction of DS3 for new

buildings observed in predicted results is only related to non-structural damages; real damages show almost no reduction of DS3 because of brittle failures of the RC frame, which is not considered by simplified FAST.

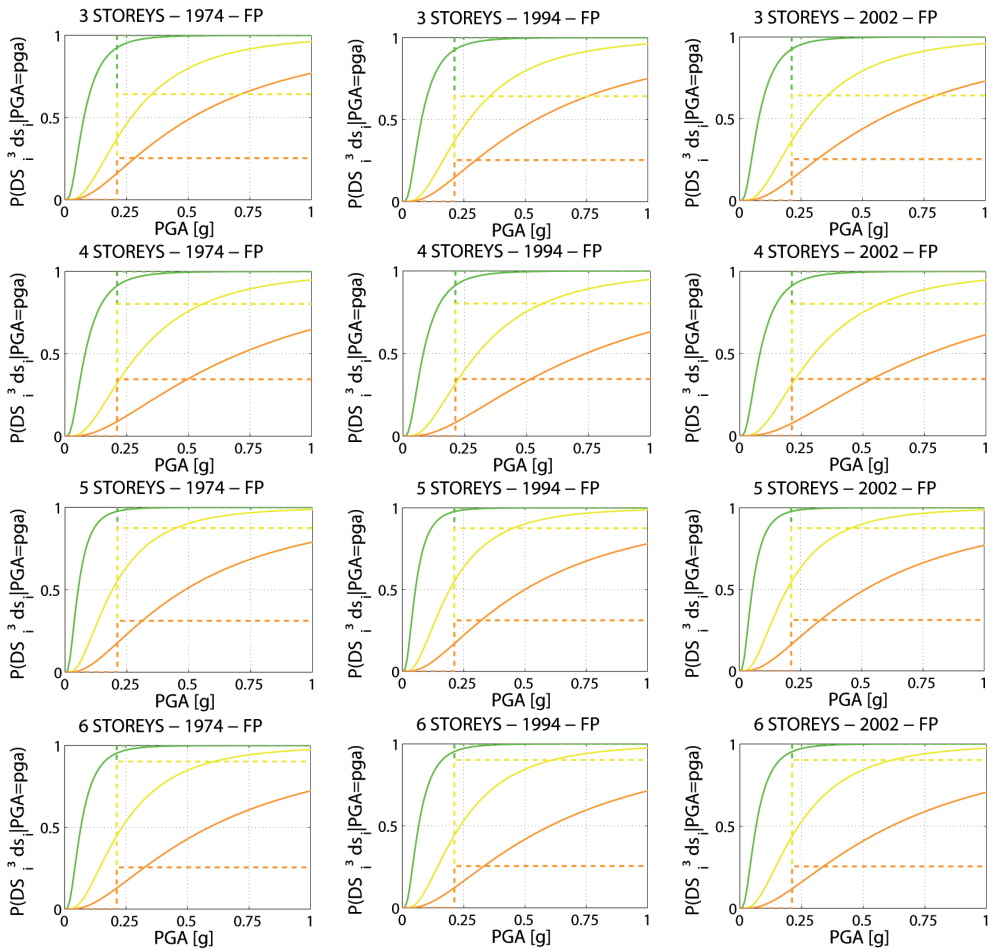


Figure 212: Fragility curves (solid line) in terms of PGA for uniformly infilled frames subjected to mainshock in LOR station in FP direction, and real damages (dashed line)

In order to make it even clearer that performance of buildings of Lorca are ruled mainly by infills instead of by RC frame, simplified FAST is applied to the

case study without considering any contribution of the RC frame before the degradation of infill panels. This is equivalent to make $\alpha=0$ into Equation (84a). Results are shown in Figure 213. Almost similar performances than for the orthodox hypothesis (see Figure 210) are observed: thresholds for DS are reduced in less than 8% in all the cases. It means that, regardless brittle failures in RC frame, the damage scenario in Lorca would have been rather similar to the real one if RC building stock was not designed to any seismic code.

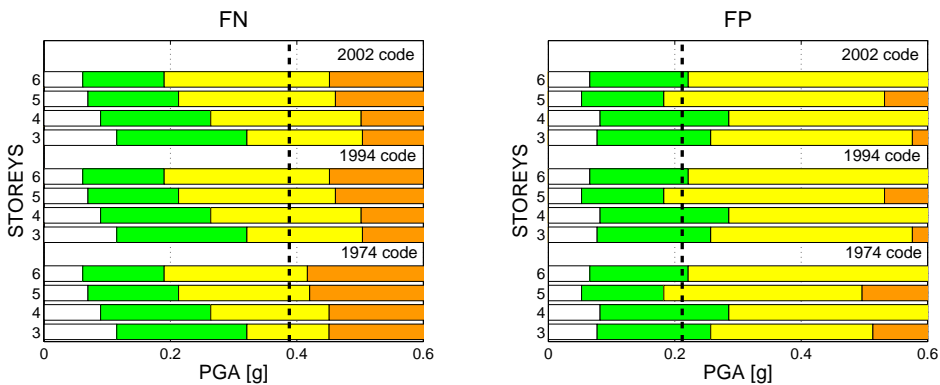


Figure 213: Damage assessment in terms of PGA for uniformly infilled frames subjected to mainshock in LOR station, without considering any contribution of the RC frame before infills degradation

Aimed at the estimation of the sensitivity of the method, some parameters (whose proposed values are based on statistic or probabilistic approach and thus whose reliability is not excessive) can be assumed to move within a range of values. This is the case of interstorey drift of attainment of DS (IDR_{DSj}), or also the considered infill ratios (ρ_w). Regarding the last issue, different strategies of accounting for infill panels depending on their effectiveness are discussed in section 4.2, resulting in three typical hypotheses:

- “ex”: accounting only with external infills, i.e. façades;
- “ex+al”: accounting also internal infill panels contained within frames;
- “ex+al+int”: accounting also with internal panels not contained in any frame.

Typical values for Lorca representing each hypothesis are shown in Table 52 ($\rho_{w,s}$). Results of lower- and upper-bound values of infills ratio are presented in Figure 214. FAST is very sensitive to this parameter; in fact, representative DS is DS2-3 for [ex] and DS1-2 for [ex+al+in]. On the other hand, sensitivity to IDR_{DSj} seems to be lower, as seen in Figure 215.

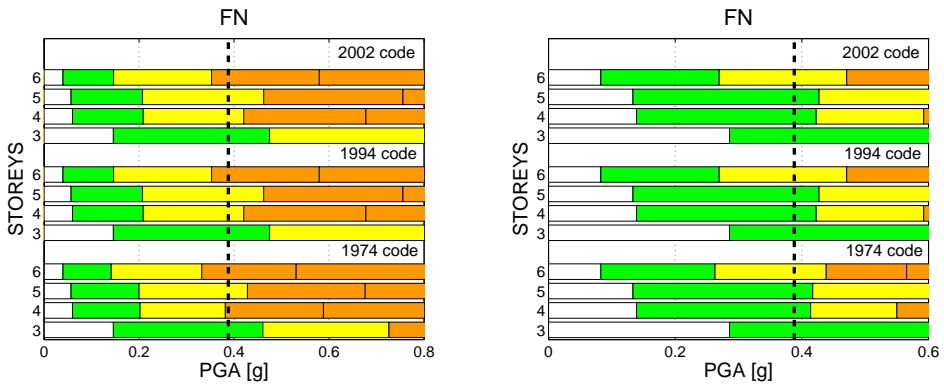


Figure 214: Damage assessment in terms of PGA for uniformly infilled frames subjected to mainshock in LOR station, for lower-bound [ex] (a) and upper-bound [ex+al+in] (b) infills ratios

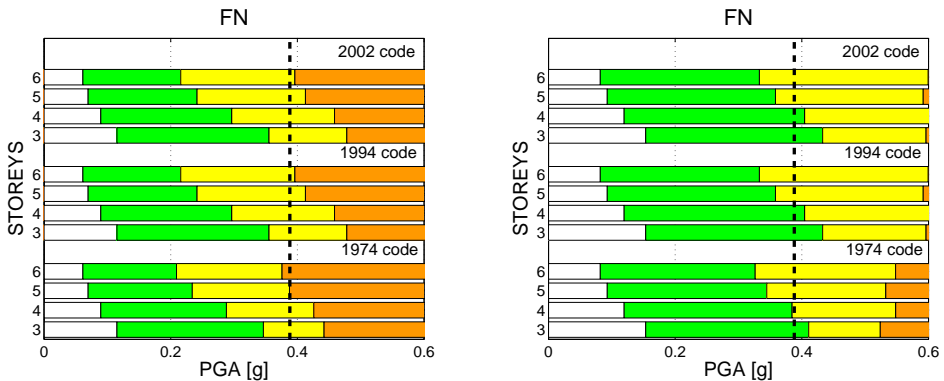


Figure 215: Damage assessment in terms of PGA for uniformly infilled frames subjected to mainshock in LOR station, for lower-bound (a) and upper-bound (b) for IDR_{DSj}

It is also possible to apply FAST to the foreshock (Figure 216). Results show that taller buildings ($n=6$) may have attained DS2 during foreshock, while the rest of the building remain with DS1. Notwithstanding the lower damages, they have had likely some influence in the performances during the mainshock, considering the high relative contribution of infills to the global behaviour. For a complete understanding of the phenomenon, cumulative strategies shown in section 5.3.4 should be carried out.

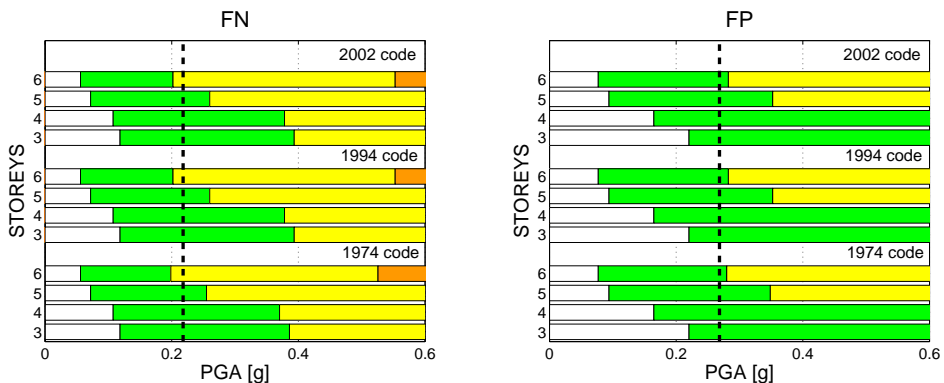


Figure 216: Damage assessment in terms of PGA for uniformly infilled frames subjected to foreshock in LOR station

6.4 ASSESSMENT OF NON-UNIFORMLY INFILLED FRAMES: GENERALISED FAST

FAST is a large-scale method: its scope is to provide global results, even from the point of view of complete cities. The application of generalised FAST (see section 5.2) or also extended FAST (see section 5.3) is conditioned to the inspection of singles buildings, in order to determine more classes of buildings, depending not only of number of storeys and age of construction but also depending on the reduction of 1st storey infills, location in corner of a city block (i.e. torsionable), etc. If this is not possible, it is suitable to use generalised FAST to provide alternative results to those obtained with simplified FAST, in order to evaluate which is the behaviour of most common non-uniformly infilled buildings.

Also, if this kind of buildings is considered to be more representative of the whole RC building stock of the city, generalised FAST can be used as the only tool.

In this section, typical non-uniformly infilled buildings of Lorca (see section 4.2) are assessed, considering similar hypotheses for the efficiency of infill panels than in last section: “ex”, “ex+al” and “ex+al+in”. For these hypotheses, different stiffness contribution values (χ , see sections 5.1.3.3 and 5.2.1.1) are obtained: 0.57, 0.49 and 0.34, respectively. Regarding simulated design of 1st storey RC columns (following the procedure detailed in 5.2.1.2), maximum values of $c\chi$ are 0.27 for 6-storey NCSE-02 building in the hypothesis [ex], which is not so high. Thus, in typical non-uniformly infilled buildings of Lorca, in the most unfavourable hypothesis of infills efficiency, still they rule the performance.

CC and IN2 curves of all the classes of buildings are shown in Figure 217 (“ex”), Figure 219 (“ex+al”) and Figure 221 (“ex+al+in”), while damage assessments are shown in Figure 218, Figure 220 and Figure 222, respectively.

If results of non-uniformly infilled frames are compared with those of uniformly infilled frames, four relevant differences are confirmed:

- 1) higher period (see section 5.2.3.4 and Figure 178)
- 2) lower maximum strength: in some cases, especially for modern buildings, the maximum strength provided by RC columns is higher than the maximum strength of infills, but they are not developed simultaneously (see section 5.1.2.1);
- 3) lower contribution of upper storeys to the displacement capacity (see Figure 177);
- 4) lower stiffness degradation of upper storeys (see Figure 177).

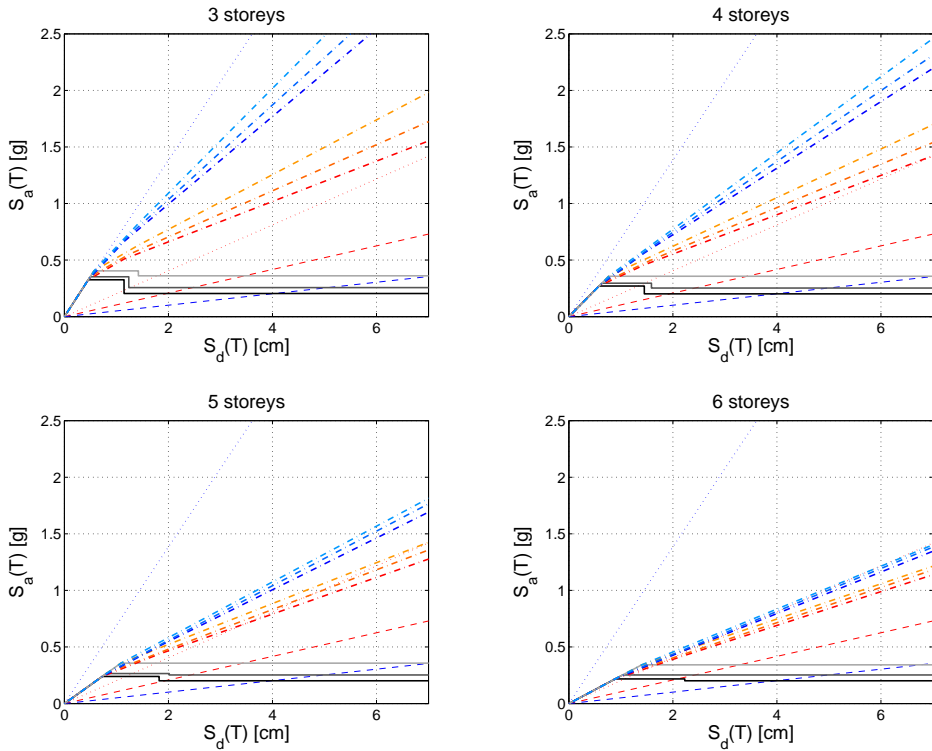


Figure 217: Approximate CC and IN2 curves for non-uniformly infilled frames subjected to mainshock in LOR station in FN and FP directions, assuming hypothesis [ex]

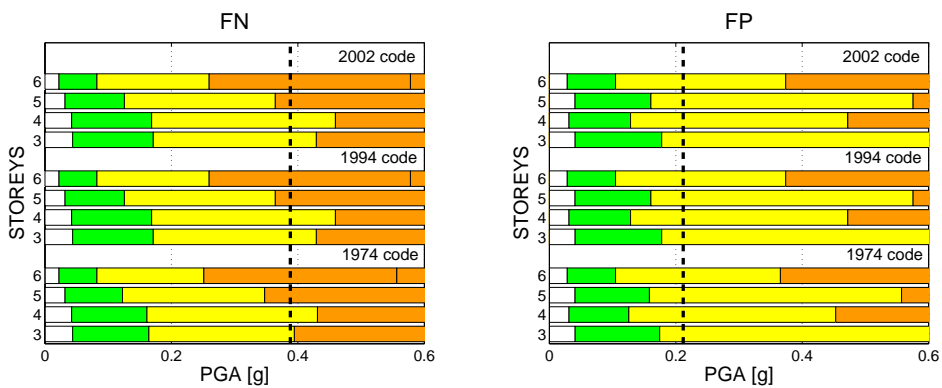


Figure 218: Damage assessment in terms of PGA for non-uniformly infilled frames subjected to mainshock in LOR station, assuming hypothesis [ex]

FAST simplified vulnerability approach for seismic assessment of infilled RC MRF buildings and its application to the 2011 Lorca (Spain) earthquake

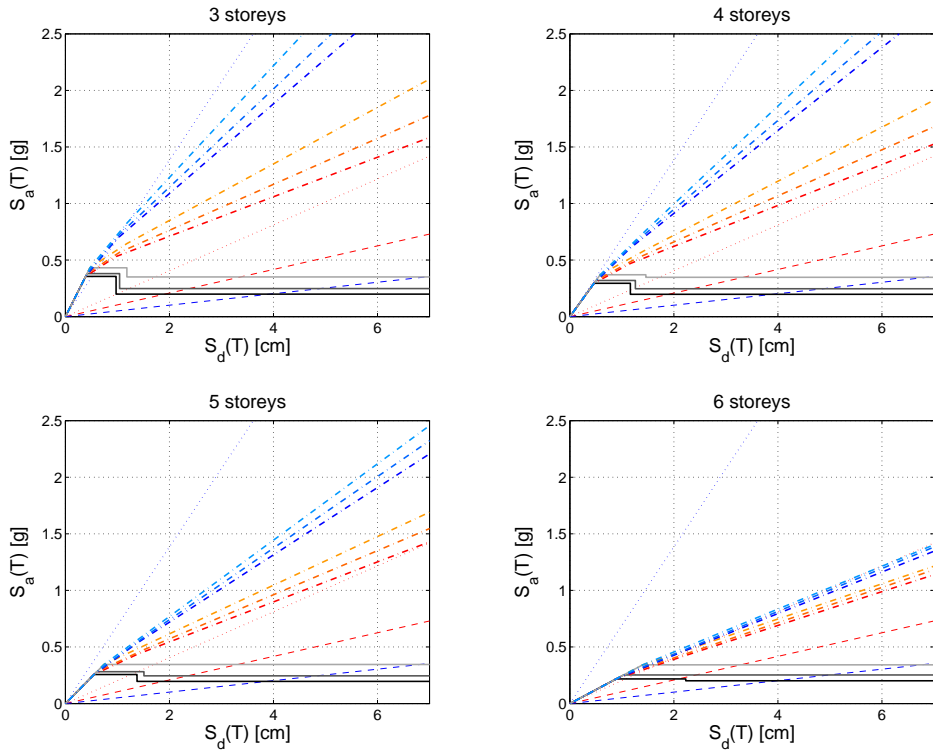


Figure 219: Approximate CC and IN2 curves for non-uniformly infilled frames subjected to mainshock in LOR station in FN and FP directions, assuming hypothesis [ex+al]

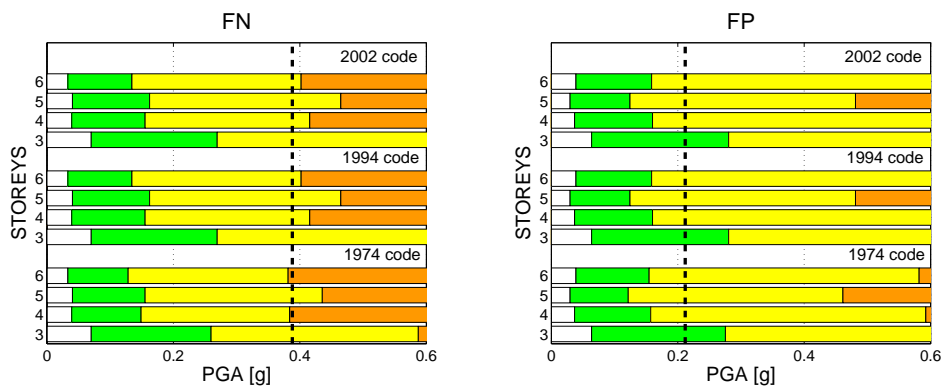


Figure 220: Damage assessment in terms of PGA for non-uniformly infilled frames subjected to mainshock in LOR station, assuming hypothesis [ex+al]

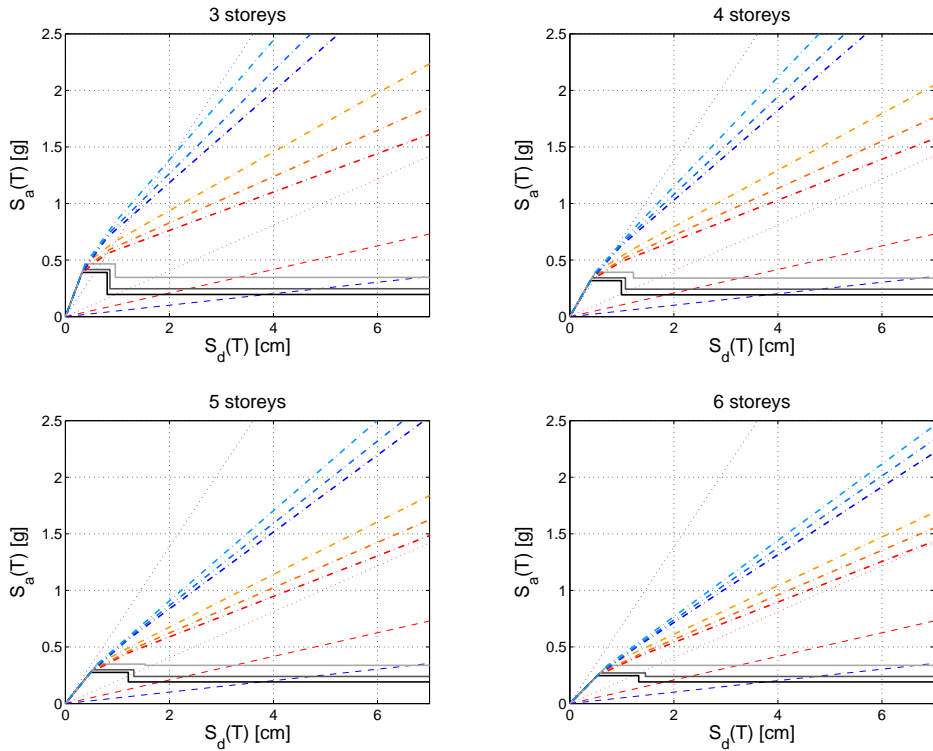


Figure 221: Approximate CC and IN2 curves for non-uniformly infilled frames subjected to mainshock in LOR station in FN and FP directions, assuming hypothesis [ex+al+in]

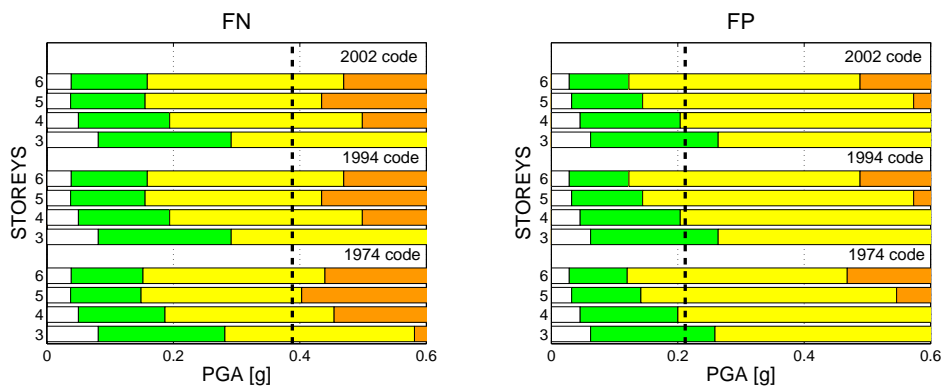


Figure 222: Damage assessment in terms of PGA for non-uniformly infilled frames subjected to mainshock in LOR station, assuming hypothesis [ex+al+in]

Damages are higher than for uniformly infilled frames; characteristic damage for the different hypotheses is: DS2-3, mostly DS3 [ex]; DS2-3, mostly DS2 [ex+al]; and DS2 [ex+al+in]. The last hypothesis may be the most representative of the behaviour of uniformly infilled frames. In fact, upper storeys remain elastic (as the cracked height does not exceed first storey, see section 5.2.2.2), thus all the infills, including internal not-aligned panels, are effective –given that no diagonal post-cracking action is required. Also, the equivalent elastic period is more representative in this case. There only would be a problem if the amount of internal not-aligned panels in 1st storey is very high compared with the rest of infills in that storey, because strength capacity would be oversized. However, this is not the case of typical non-uniformly buildings in Lorca (see section 4.2), thus hypothesis [ex+al+in] may be suitable. Hence, regardless of damages in the RC frame due to soft-storey ductile mechanisms, also in buildings with typical reduction of infills in 1st storey, the most representative damage level may be DS2.

6.5 DISCUSSION OF RESULTS

In this section, FAST approach is applied to the 2011 Lorca earthquake. Different hypotheses are considered. Firstly, a preliminary code-based assessment of buildings considered as bare frames, without any infill contribution and considering a behaviour factor of capacity consistent with that of design, is carried out. Secondly, simplified FAST is applied, considering buildings as uniformly infilled. Then, assessment corresponding to various assumptions are considered: buildings without contribution of RC frame before infills degradation, different infills ratio, lower- and upper-bound for IDR characterising DS, and also foreshock is simulated. Finally, generalised FAST is employed in order to assess non-uniformly infilled frames, considering diverse hypotheses.

The scope of the application of FAST approach, assuming different strategies, to the 2011 Lorca earthquake is double:

- 1) Validate the procedure (formulations and proposed values for parameters).
- 2) Allow proposing a suitable explanation to the real damage scenario in Lorca.

The test of the approach may be evaluated as positive: fair to good agreement is shown between predicted values and real damage scenario. Same characteristic Damage State (DS2), similar trend depending on the number of storeys and suitable distribution of probabilities for each DS are observed. Also, framework of FAST has also proved to be flexible and robust enough in order to assimilate the particularities of a case study. In fact, FAST has demonstrated to be able to have into account some characteristics as non-uniformity of infills in elevation, which also show damage scenarios quite similar to real ones.

However, as well as other accurate mechanical or numerical large-scale vulnerability approaches (e.g. Borzi et al., 2008), it may not be as valid as for Lorca earthquake if applied to another event in which brittle failures of RC members or higher characteristic average DS rules the scenario. Extension of FAST aimed at dealing with RC frame (see section 5.3.2) must be fully developed; otherwise, the appropriateness of case studies should be carefully analysed.

On the other hand, the application of FAST to the Lorca earthquake allowed proposing a suitable explanation to the damage scenario, which is characterised by: (i) generalised average satisfactory performances considering the disproportion between real demand and code-based demand; and (ii) unsatisfactory local performances, because of the brittle (global and local) nature of the small amount of structural damages. The last is due to the prescriptions of seismic codes, also the current one (as discussed in chapters 2 and 4). Furthermore, thanks to the employment of FAST in this chapter, it has been possible to prove that neither the average satisfactory performances can be attributable to the appropriate provisions of seismic codes. In fact, assessment of bare frames has demonstrated to be not representative at all, also when more realistic safety factors are considered. Then, when infills are taken into account, damage scenario matches with real one, thus infills may be the responsible of the proper behaviour of frames, also in the case in which there is a substantial reduction of infills in 1st storey. Those assertions are confirmed by the analysis in which no contribution of RC before degradation of infills is considered: almost similar damages are predicted, thus the influence of RC may be very small in comparison with infills. The last is considered by modern seismic codes as a serious issue, because the responsibility of proper performance cannot be delegate to elements whose reliability is uncertain.

Conclusions

FAST approach was presented in this Thesis: it is a simplified analytical method for the estimation of large-scale vulnerability of infilled RC frames. Then, FAST was applied to the 2011 Lorca earthquake, in order to compare observed damage with analytical results. FAST proved to be a powerful and simple tool, providing suitable explanation to the damage scenario observed after the Lorca earthquake, which is characterised by generalised average satisfactory performances given the disproportion between earthquake demand and code-based demand. Main conclusions are outlined:

- FAST must be intended as a large-scale tool, conceived for rapid decision such as basic damage mapping or for post-emergency priority analyses for preliminary interventions. It is suitable for all the situations asking for agreement between accuracy and simplicity of the procedures.
- Results obtained by FAST for Lorca earthquake showed in this case a fair to good agreement with respect to the benchmark of real damages. Appropriateness for other case studies in which structural damage is more frequent should be carefully studied.
- The satisfactory average large-scale performances of RC buildings in Lorca rely more to the presence of masonry infill panels –even when they

are reduced in 1st storey— than to the eventual improvements of current Spanish code NCSE-02 with respect to previous codes.

- The text of NCSE-02 is, in principle, based on modern concepts as performance-based framework or capacity design; on the other hand, its provisions are not always effective for that aim. NCSE-02's failing to meet Eurocode standard could be, to some extent, considered as one of the causes of predominance of local and global brittle mechanisms observed in Lorca.
- Some Mediterranean codes show very conservative approach on wide-beam frames as high ductility structural system. Notwithstanding the lower local ductility of wide beams with respect to deep beams, global capacity of wide-beam frames get substantially improved thanks to some causes that increase both their effective stiffness and their maximum deformation capacity. Thus, any reduction of behaviour factor prescribed for wide-beam frames as main lateral load system appears to be at least obsolete.

Further research in process is related to: (i) the experimental behaviour of wide-beam-slab-column subassemblages subjected to lateral loading, accounting with the stiffness and strength contribution of joists in their parallel direction; (ii) the reliability of the expressions in Eurocode 8 for chord rotations in the case of wide beams; (iii) reliability of different formulations for capacity design; and (iv) the phenomenon of period elongation and numerical expressions for elastic period of pilotis frames.

References

- ACI (1989). Building Code Requirements for Reinforced Concrete (ACI 318-89). ACI Committee 318, American Concrete Institute, Farmington Hills, Michigan, USA
- ACI (1995). Building Code Requirements for Structural Concrete (ACI 318-95) and Commentary (318-95). ACI Committee 318, American Concrete Institute, Farmington Hills, Michigan, USA
- ACI (2008). Building Code Requirements for Structural Concrete (ACI 318-08) and Commentary (318-08). ACI Committee 318, American Concrete Institute, Farmington Hills, Michigan, USA
- ACI (2011). Guide for Seismic Rehabilitation of Existing Concrete Frame Buildings (ACI 369R-11) and Commentary. ACI Committee 369, American Concrete Institute, Farmington Hills, Michigan, USA
- ACI-ASCE (1985). Recommendations for Design of Beam-Column Connections in Monolithic Reinforced Concrete Structures (ACI 352R-85). Joint ACI-ASCE Committee 352, American Concrete Institute, Farmington Hills, Michigan, USA
- ACI-ASCE (1991). Recommendations for Design of Beam-Column Connections in Monolithic Reinforced Concrete Structures (ACI 352R-91). Joint ACI-ASCE Committee 352, American Concrete Institute, Farmington Hills, Michigan, USA

- ACI-ASCE (2002). Recommendations for Design of Beam-Column Connections in Monolithic Reinforced Concrete Structures (ACI 352R-02). Joint ACI-ASCE Committee 352, American Concrete Institute, Farmington Hills, Michigan, USA
- AENOR (1998). Eurocódigo 8: Proyecto de estructuras sismorresistentes. UNE-ENV 1998-1-1:1998, Asociación Española de Normativa y Certificación, Madrid, Spain (in Spanish)
- Aguilar Falconi, R. (2007). Overstrength factor in reinforced concrete structures without shear walls. *Revista Internacional de Desastres Naturales, Accidentes e Infraestructura Civil* 7(2):197-212 (in Spanish)
- Alarcón, E., Astiz, M.A., Benito, M.B., Álvarez, R., Maeso, O., Bernal, A., Hermanns, L. (2010). Informe final sobre [...] la propuesta del anexo nacional español a la norma europea en 1998 (Eurocódigo 8), Ref: CMM_IGN_0210. Centro de Modelado en Ingeniería Mecánica.
- Albanesi, T., Nuti, C. (2007). Analisi statica non lineare (Pushover). Department of Structures, Università degli studi di Roma Tre, Roma, Italy
- Alguacil, G., Vidal, F., Navarro, M., García-Jerez, A., Pérez-Muelas, J. (2014). Characterization of earthquake shaking severity in the town of Lorca during the May 11, 2011 event. *Bulletin of Earthquake Engineering* 12:1889-1908
- American Society of Civil Engineers (ASCE), Seismic Rehabilitation of Existing Buildings, ASCE/SEI 41-06, Reston, Virginia, 2007.
- ASCE (2007). Seismic Rehabilitation of Existing Buildings, ASCE/SEI 41-06. American Society of Civil Engineers, Reston, Virginia, USA
- ASCE (2010). Minimum Design Loads for Building and Other Structures, ASCE/SEI 7-10. American Society of Civil Engineers, Reston, Virginia, USA
- Astiz, M.A., Marí, A., Perepérez, B. (2005). Conceptos específicos del proyecto de estructuras en zonas sísmicas. *Hormigón y acero* 237.
- ATC (1978). Tentative provisions for the development of seismic regulations for buildings. Report No. ATC3-06, Applied Technology Council, Palo Alto, CA, USA
- ATC (1982). An investigation of the correlation between earthquake ground motion and building performance. Report ATC-10, Applied Technology Council, Redwood City, California, USA

- ATC (1985). Earthquake damage evaluation data for California. Report ATC-13, Applied Technology Council, Redwood City, California, USA
- ATC (1995). A critical review of current approaches to earthquake resistant design. Rep. n° ATC-34, Redwood City, California, USA
- ATC (1996). Seismic evaluation and retrofit of concrete buildings. Report No. ATC-40, Applied Technology Council (ATC). Redwood City, California, USA
- ATC (1997). NEHRP guidelines for the seismic rehabilitation of buildings (FEMA 273), Building Seismic Safety Council for the Federal Emergency Management Agency, Washington, DC, USA
- Baker, J.W. (2007). Quantitative classification of near-fault ground motions using wavelet analysis. *Bulletin of the Seismological Society of America* 97, 1486-1501.
- Bal, I.E., Crowley, H., Pinho, R., Gülay, F.G. (2008). Detailed assessment of structural characteristics of Turkish RC building stock for loss assessment models. *Soild Dynamics and Earthquake Engineering* 28:914-932
- Bazzurro, P., Cornell, C.A., Menun, C., Motahari, M. (2004). Guidelines for seismic assessment of damaged buildings. *Proceedings of the 13th World Conference on Earthquake Engineering*, August 1-6, Vancouver, B.C., Canada. Paper n° 1708
- Bazzurro, P., Cornell, C.A., Menun, C., Motahari, M., Luco, N. (2006). *Advanced Seismic Assessment Guidelines*. Pacific Gas & Electric (PG&E)/PEER Lifelines Program Task 507, PEER 2006/05
- Benavent-Climent A. (2007). Seismic behavior of RC wide beam-column connections under dynamic loading, *Journal of Earthquake Engineering*, 11, 493-511.
- Benavent-Climent A., Akiyama H., Lopez-Almansa F., Pujades L.G. (2004). Prediction of ultimate earthquake resistance of gravity-load designed RC buildings. *Engineering Structures* 26, 1103-1113.
- Benavent-Climent A., Cahis X., Catalàn A. (2008). Seismic behavior of interior connections in existing waffle-flat-plate structures. *Engineering Structures*,30, 2510-2516.
- Benavent-Climent, A., Cahís, X., Vico, J.M. (2010). Interior wide beam-column connections in existing RC frames subjected to lateral earthquake loading. *Bulletin of Earthquake Engineering* 8:401-420.

- Benavent-Climent, A., Cahís, X., Zahran, R. (2009). Exterior wide beam-column connections in existing RC frames subjected to lateral earthquake loads. *Engineering Structures* 31:1414-1424
- Benavent-Climent, A., Escobedo, A., Donaire-Ávila, J., Oliver-Saiz, E., Ramírez-Márquez, A.L. (2014). Assessment of expected damage on buildings subjected to Lorca earthquake through an energy-based seismic index method and nonlinear dynamic response analyses. *Bulletin of Earthquake Engineering* 12:2049-2073
- Bendimerad, F.M., Shah, H.C., Hoskins, T. (1991). Extension of study on fundamental period of reinforced concrete moment-resisting frame structures (no. 96). John A. Blume Earthquake Engineering Center
- Benedetti, D., Petrini, V. (1984). Sulla vulnerabilità di edifici in muratura: proposta di un metodo di valutazione. *L'industria delle Costruzioni* 149(1):66-74 (in Italian)
- Benito, B., Rivas, A., Gaspar-Escribano, J.M., Murphy, P. (2012). El terremoto de Lorca (2011) en el contexto de la peligrosidad y el riesgo sísmico en Murcia. *Física de la Tierra* 24:255-287 (in Spanish)
- Bertero, V.V., Bendimerad, F.M., Shah, H.C. (1988). Fundamental period of reinforced concrete moment-resisting frame structures. Report n° 87, Department of Civil and Environmental Engineering, Stanford University, Stanford, California, USA
- BHRC (2004). Iranian Code of Practice for Seismic Resistant Design of Buildings. Standard N° 2800, 3rd edn. Building and Housing Research Center, Tehran, Iran
- Biskinis, D.E. (2007). Resistance and deformation capacity of concrete members with or without retrofitting. PhD Thesis. Civil Engineering Department, University of Patras, Patras, Greece (in Greek)
- Biskinis, D.E., Fardis, M.N. (2010a). Deformations at flexural yielding of members with continuous or lap-spliced bars. *Structural Concrete* 11(3):127-138
- Biskinis, D.E., Fardis, M.N. (2010b). Flexure-controlled ultimate deformations of members with continuous or lap-spliced bars. *Structural Concrete* 11(2):93-108
- Biskinis, D.E., Roupakias, G.K., Fardis, M.N. (2004). Degradation of shear strength of reinforced concrete members with inelastic cyclic displacement. *ACI Structural Journal*, 101, 773-783.

- Bonett Díaz, R.L. (2003). Vulnerabilidad y riesgo sísmico de edificios. Aplicación a entornos urbanos en zonas de amenaza alta y moderada. PhD Thesis. Universitat Politècnica de Catalunya, Barcelona, Spain (in Spanish)
- Borzi, B., Crowley, H., Pinho, R. (2008b). The influence of infill panels on vulnerability curves for RC buildings. Proceedings of the 14th World Conference on Earthquake Engineering, Beijing, China, October 12-17. Paper 09-01-0111
- Borzi, B., Elnashai, A.S. (2000). Refined force reduction factors for seismic design. *Engineering Structures* 22:1244-1260
- Borzi, B., Pinho, R., Crowley, H. (2008a). Simplified pushover-based vulnerability analysis for large scale assessment of RC buildings. *Engineering Structures* 30(3), 804-820.
- Bourbié, T., Coussy, O., Zinszner, B. (1987). *Acoustics of porous media*. Ed. Technip, Paris, France
- Braga, F., Dolce, M., Liberatore, D. (1982). A statistical study on damaged buildings and an ensuing review of the MSK-76 scale. Proceedings of the 7th European Conference on Earthquake Engineering, Athens, Greece: 431-450
- BSI (2004). Eurocode 2: Design of concrete structures: Part 1-1: General rules and rules for buildings. British Standards Institutions, London, UK
- Cabañas, L., Carreño, E., Izquierdo, A., Martínez, J.M., Capote, R., Martínez, J., Benito, B., Gaspar, J., Rivas, A., García, J., Pérez, R., Rodríguez, M.A., Murphy, P. (2011). Informe del sismo de Lorca del 11 de mayo de 2011. (in Spanish). Available in <http://www.ign.es/ign/resources/sismologia/Lorca.pdf>
- Cabañas, L., Alcalde, J.M., Carreño, E., Bravo, J.B. (2014). Characteristics of observed strong motion accelerograms from the 2011 Lorca (Spain) earthquake. *Bulletin of Earthquake Engineering* 12:1909-1932
- Calconsa XXI (2011). Photographic report of the building “Menorca”, Avda. de las Fuerzas Armadas, 28-30-32, 30800 Lorca (Murcia), Spain. www.calconsa.com
- Calvi, G.M. (1999). A displacement-based approach for vulnerability evaluation of classes of buildings. *Journal of Earthquake Engineering* 3(3):411-438

- Calvi, G.M., Cantu, E., Macchi, G., Magenes, G. (1993). Experimental investigation on the rotation capacity of concrete slab elements reinforced with welded wire meshes. Report n° 34, Department of Structural Mechanics, University of Pavia, Pavia, Italy
- Calvi, G.M., Pinho, R., Magenes, G., Bommer, J.J., Restrepo-Vélez, L.F., Crowley, H. (2006). The development of seismic vulnerability assessment methodologies for variable geographical scales over the past 30 years. ISET Journal of Earthquake Technology 43(3):75-104
- Cassis, J., Bonelli, P. (1992). Lessons learned from the March 3, 1985 Chile earthquake and related research. Proceedings of the 10th World Conference on Earthquake Engineering, A.A. Balkema, Rotterdam, Netherlands, Vol.X:5675-5680
- CDSC (1968). Seismic construction code, PGS-1 Parte A. Committee for the Development of Seismic Codes, BOE 1969 N° 30, Spanish Ministry of Construction, Madrid (in Spanish)
- CDSC (1974). Seismic construction code, PDS-1 Parte A. Committee for the Development of Seismic Codes, BOE 1974 N° 279, Spanish Ministry of Construction, Madrid (in Spanish)
- CDSC (1994). Seismic construction code, NCSR-94. Committee for the Development of Seismic Codes, BOE 1995 n° 33, Spanish Ministry of Construction, Madrid, Spain (in Spanish)
- CDSC (2002). Seismic construction code, NCSE-02. Committee for the Development of Seismic Codes, BOE 2002 N° 244, Spanish Ministry of Construction, Madrid, Spain (in Spanish)
- CEN (2004). Eurocode 8: design of structures for earthquake resistance – Part 1: general rules, seismic actions and rules for buildings. European Standard EN 1998-1:2003 – Comité Européen de Normalisation, Brussels, Belgium
- CEN (2005). Eurocode 8: design of structures for earthquake resistance – Part 3: assessment and retrofitting of buildings. European Standard EN 1998-1:2003 – Comité Européen de Normalisation, Brussels, Belgium
- Cheung, P.C., Paulay, T., Park, R. (1991). Mechanisms of slab contributions in beam-column subassemblages. ACI special publication(123)

- Cheung, V.W.T., Tso, W.K. (1986). Eccentricity in irregular multistory buildings. *Canadian Journal of Civil Engineering* 13:46-52
- Chioccarelli, E., De Luca, F., Iervolino, I. (2009). Preliminary study on L'Aquila earthquake ground motion records, V5.20. <http://www.reluis.it/>
- Chopra, A.K. (1995). *Dynamics of structures: theory and applications to earthquake engineering*. Prentice-Hall, Inc., Upper Saddle River, New Jersey, USA
- Chopra, A.K. (2007). *Dynamics of the Structures*, Prentice Hall, Upper Saddle River, New Jersey, 3rd edition.
- Chopra, A.K., Goel, R.K. (1999). Capacity-demand-diagram methods based on inelastic design spectrum. *Earthquake Spectra* 15(4):637-656
- CMLP (2009). Circolare del Ministero dei Lavori Pubblici n° 617 del 2/2/2009. Istruzioni per l'applicazione delle "Nuove norme tecniche per le costruzioni" di cui al D.M. 14 gennaio 2008. G.U. n° 47 del 26/2/2009 (in Italian)
- Colangelo, F. (2012). A simple model to include fuzziness in the seismic fragility curve and relevant effect compared with randomness. *Earthquake Engineering and Structural Dynamics*, 41, 969-986.
- Colangelo, F. (2013). Drift-sensitive non-structural damage to masonry-infilled RC frames designed to Eurocode 8. *Bulletin of Earthquake Engineering*:1-26. DOI 10.1007/s10518-013-9503-y
- Colombi, M., Borzi, B., Crowley, H., Onida, M., Meroni, F., Pinho, R. (2008). Deriving vulnerability curves using Italian earthquake damage data. *Bulletin of Earthquake Engineering* 6(3):485-504
- Cornell, C.A., Krawinkler, H. (2000). Progress and challenges in seismic performance assessment. *PEER News*, April
- Cosenza, E., Galasso, C., Maddaloni, G. (2009). Resistenza del calcestruzzo: modellazione probabilistica e risultati sperimentali. *Proceedings of the XXV Convegno Nazionale AICAP "La progettazione e l'esecuzione delle opere strutturali nell'ottica della sostenibilità"*, Pisa, Italy, May, 14-16 (in Italian)
- Cosenza, E., Manfredi, G., Polese, M., Verderame, G.M. (2005). A multi-level approach to the capacity assessment of existing RC buildings. *Journal of Earthquake Engineering* 9(1):1-22

- Crisafulli, F.J. (1997). Seismic behaviour of reinforced concrete structures with masonry infills. Ph.D. Thesis, University of Canterbury, Christchurch, New Zealand
- Crowley, H., Colombi, M., Borzi, B., Faravelli, M., Onida, M., López, M., Polli, D., Meroni, F., Pinho, R. (2009). A comparison of seismic risk maps for Italy. *Bulletin of Earthquake Engineering* 7(1):149-190
- Crowley, H., Pinho, R. (2004). Period-height relationship for existing European reinforced concrete buildings. *Journal of Earthquake Engineering* 8(Special issue 1):93-119
- Crowley, H., Pinho, R. (2006). Simplified equations for estimating the period of vibration of existing buildings. *Proceedings of the 1st European Conference on Earthquake Engineering and Seismology*, Geneva, Switzerland, September 3-8. Paper n° 1122
- Crowley, H., Pinho, R. (2010). Revisiting Eurocode 8 formulae for periods of vibration and their employment in linear seismic analysis. *Earthquake Engineering and Structural Dynamics*, 39(2), 223-235
- Crowley, H., Pinho, R., Bommer, J.J. (2004). A probabilistic displacement-based vulnerability assessment procedure for earthquake loss estimation. *Bulletin of Earthquake Engineering* 2(2):173-219
- Crowley, H., Pinho, R., Bommer, J.J., Bird, J.F. (2006). Development of a displacement-based method for earthquake loss assessment. ROSE Research Report n° 2006/01, IUSS Press, Pavia, Italy
- CS.LL.PP (2009). Instructions for the application of the Technique Code for the Constructions. *Official Gazette of the Italian Republic*, 47 (in Italian)
- CS.LL.PP (2011). Answer to the requests for clarification concerning the application of NTC, DM 14/01/2008, made by the Direction of Public Works, Land Protection, Mountain Economy and Forest of the Piedmont Region. Protocole 0000482-24/10/2011, Rome, Italy (in Italian). Available at http://www.rete.toscana.it/sett/pta/sismica/03normativa/norme/pareri/img_pareri/parere-llpp_53-11.pdf
- De Andrés Álvarez, F., CSCAE (2009). Documento de aplicación de la EHE-08 a edificación: DA-EHE, hormigón. Consejo Superior de los Colegios de Arquitectos de España (in Spanish)

- De Luca, F. (2012). Records, capacity curve fits and reinforced concrete damage states within a performance based earthquake engineering framework. Ph.D. Thesis. University of Naples Federico II, Naples, Italy. Available at <http://wpage.unina.it/flavia.deluca/outreach.htm>
- De Luca, F., Vamvatsikos, D., Iervolino, I. (2013). Near-optimal piecewise linear fits of static pushover capacity curves for equivalent SDOF analysis. *Earthquake Engineering and Structural Dynamics* 42:523-543
- De Luca, F., Verderame, G.M. (2013). A practice-oriented approach for the assessment of brittle failures in existing RC elements, *Engineering Structures* 48, 373-388.
- De Luca, F., Verderame, G.M., Gómez-Martínez, F. (2013c). FAST vulnerability approach: a simple solution for seismic reliability of RC infilled buildings. *Proceedings of ANIDIS 2013 – XV Convegno. Padova (Italy), June 30 – July 04, paper B7*
- De Luca, F., Verderame, G.M., Gómez-Martínez, F., Pérez-García, A. (2014). The structural role played by masonry infills on RC building performances after the 2011 Lorca, Spain, earthquake. *Bulletin of Earthquake Engineering* 12(5):1999-2026
- De Luca, F., Verderame, G.M., Manfredi, G. (2013d). FAST vulnerability approach: a simple solution for damage assessment of RC infilled buildings. *Proceedings of Vienna Congress on Recent Advances in Earthquake Engineering and Structural Dynamics 2013 (VEESD 2013), Vienna (Austria), August 28-30, paper n° XXX*
- De Miguel, J.L. (2008). Personal communication
- De Miguel, J.L. (2011). Lorca. Department of Structures, ETSAM, Madrid, Spain (in Spanish)
- De Risi, M.T., Ricci, P., Verderame, G.M., Manfredi, G. (2014). A nonlinear macromodel of exterior RC joints without transverse reinforcement under seismic loads. *Engineering Structures* (under review)
- Di Pasquale, G., Orsini, G. (1997). Proposta per la valutazione di scenari di danno conseguenti ad un evento sismico a partire dai dati ISTAT. *Proceedings of the VIII convegno ANIDIS “L’ingegneria sismica in Italia”, Taormina, Italy, September 21-24, (1):477-486 (in Italian)*

- Di Pasquale, G., Orsini, G., Romero, R.W. (2005). New developments in seismic risk assessment in Italy. *Bulletin of Earthquake Engineering* 3(1):101-128
- Dolce, M., Cardone, D., Ponzo, F.C., Valente, C. (2005). Shaking table tests on reinforced concrete frames without and with passive control systems. *Earthquake Engineering and Structural Dynamics*, 34:1687-1717.
- Dolce, M., Masi, A., Marino, M., Vona, M. (2003). Earthquake damage scenarios of the building stock of Potenza (southern Italy) including site effects. *Bulletin of Earthquake Engineering* 1(1):115-140
- Dolce, M., Moroni, C. (2005). La valutazione della vulnerabilità e del rischio sismico degli edifici pubblici mediante le procedure VC (vulnerabilità C.A.) e VM (vulnerabilità muratura), *Proceedings of the Department of Structures, Geotechnic, Geology applied to the Engineering n° 4/2005 (in Italian)*
- Dolšek, M., Fajfar, P. (2001). Soft storey effects in uniformly infilled reinforced concrete frames. *Journal of Earthquake Engineering* 5(1), 1-12.
- Dolšek, M., Fajfar, P. (2004a). Inelastic spectra for infilled reinforced concrete frames. *Earthquake Engineering and Structural Dynamics* 33:1395-1416
- Dolšek, M., Fajfar, P. (2004b). IN2 – A simple alternative for IDA. *Proceedings of the 13th World conference on Earthquake Engineering*, August 1-6, Vancouver, Canada. Paper n° 3353
- Dolšek, M., Fajfar, P. (2005). Simplified non-linear seismic analysis of infilled reinforced concrete frames. *Earthquake engineering and Structural Dynamics* 34,49-66.
- Dolšek, M., Fajfar, P. (2008a). The effect of masonry infills on the seismic response of a four-storey reinforced concrete frame – a deterministic assessment. *Engineering Structures* 30:1991-2001
- Dolšek, M., Fajfar, P. (2008b). The effect of masonry infills on the seismic response of a four-storey reinforced concrete frame – a probabilistic assessment. *Engineering Structures* 30:3186-3192
- Domínguez, D., López-Almansa, F., Benavent, A. (2014). Comportamiento, para el terremoto de Lorca de 11-05-2011, de edificios de vigas planas proyectados sin tener en cuenta la acción sísmica. *Informes de la Construcción*, 66(533): e008 (in Spanish)

- Dovich, L.M., Wight, J.K. (2005). Effective slab width model for seismic analysis of flat slab frames. *ACI Structural Journal* 102(6):868-875
- Dunand, F., Bard, P.Y., Chatelain, J.L., Guéguen, P. Vassail, T., Farsi, M.N. (2002). Damping and frequency from Randomdec method applied to in situ measurements of ambient vibrations. Evidence for effective soil structure interaction. Proceedings of the 12th European Conference on Earthquake Engineering, London, UK, 9th-13th September
- Dymiotis, C., Kappos, A.J., Chryssanthopoulos, M.K. (2001). Seismic reliability of masonry-infilled RC frames. *Journal of Structural Engineering (ASCE)* 127:296-305
- Elghadamsi, F.E., Mohraz, B. (1987). Inelastic earthquake spectra. *Earthquake Engineering and Structural Dynamics* 15:91-104
- Elnashai, A.S. (2001). Advanced inelastic static (pushover) analysis for earthquake applications. *Structural Engineering and Mechanics* 12(1):51-69
- Elnashai, A.S., Di Sarno, L. (2008). *Fundamentals of Earthquake Engineering*. Ed. Wiley, Chichester, UK
- Elwood, K.J., Matamoros, A.B., Wallace, J.W., Lehman, D.E., Heintz, J.A., Mitchell, A.D., Moore, M., Valley, M., Lowes, L.N., Comartin, C. and Moehle, J.P. (2007). Update to ASCE/SEI 41 concrete provisions. *Earthquake Spectra* 23(3):493-523
- Elwood, K.J., Moehle, J.P. (2005). Drift capacity of reinforced concrete columns with light transverse reinforcement. *Earthquake Spectra* 21(1):71-89
- Enomoto, T., Navarro, M., Sánchez, F.J., Vidal, F., Seo, K., Luzón, F., García, J.M., Martín, J., Romacho, M.D. (1999). Evaluación del coportamiento de los edificios en Almería mediante el análisis del ruido ambiental. Proceedings of the 1^a Asamblea Hispano-Lusa, Aguadulce, Almería, Spain, 9th-13th February 1998 (in Spanish)
- Enomoto, T., Schmitz, M., Abeki, N., Masaki, K., Navarro, M., Rocavado, V., Sanchez, A. (2000) Seismic risk assessment using soil dynamics in Caracas, Venezuela. Proceedings of the 12th World Conference on Earthquake Engineering, Auckland, New Zealand.
- Erdik M., Durukal E., Siyahi B., Fahjan Y., Sesetyan K., Demircioglu M., Akman H., (2004). Earthquake risk mitigation in Istanbul. Chapter 7. IN: Mulargia F. And Geller R.J. Editors, *Earthquake science and seismic risk reduction*. Kluwer.

- Faccioli, E., Pessina, V. (editors) (2000). The Catania project: earthquake damage scenarios for a high risk area in the Mediterranean. CNR-Gruppo Nazionale per la Difesa dai Terremoti, Rome, Italy
- Faccioli, E., Pessina, V., Calvi, G.M., Borzi, B. (1999). A study on damage scenarios for residential buildings in Catania city. *Journal of Seismology* 3(3):327-343
- Fajfar P. (1999). Capacity spectrum method based on inelastic demand spectra. *Earthquake Engineering and Structural Dynamics*, 28, 979-993.
- Fajfar, P. (2000). A nonlinear analysis method for performance based seismic design. *Earthquake Spectra* 16(3):573-592
- Fajfar, P. (2002). Structural analysis in earthquake engineering – A breakthrough of simplified non-linear methods. *Proceedings of the 12th European Conference on Earthquake Engineering*, London, UK, 9th-13th September, Paper n° 843
- Fajfar, P., Drobnič, D. (1998). Nonlinear seismic analyses of the “ELSA” buildings. *Proceedings of the 11th European Conference on Earthquake Engineering*, September 6-11, Paris, France
- Fajfar, P., Fischinger, M. (1988). N2 – A method for non-linear seismic analysis of regular buildings. *Proceedings of the 9th World Conference on Earthquake Engineering*. August 2-9, Tokyo-Kyoto, Japan, Vol. V:111-116
- Fajfar, P., Gaspersic, P. (1996). The N2 method for the seismic damage analysis of RC buildings. *Earthquake Engineering and Structural Dynamics* 25:31-46
- Fardis, M.N. (1997). Experimental and numerical investigations on the seismic response of RC infilled frames and recommendations for code provisions. Report ECOEST-PREC8 No. 6. Prenormative research in support of Eurocode 8
- Fardis, M.N. (2009) *Seismic Design, Assessment and Retrofitting of Concrete Buildings*. Ed. Springer, London
- Fardis, M.N., Bousias, S.N., Franchioni, G., Panagiotakos, T.B. (1999). Seismic response and design of RC structures with plan-eccentric masonry infills. *Earthquake Engineering and Structural Dynamics* 28:173-191
- FEMA (1994). NEHRP recommended provisions for seismic regulations for new buildings. FEMA 273, Federal Emergency management Agency, Washington, DC, USA

- FEMA (2001). HAZUS99 Technical Manual. Service Release 2. Federal Emergency Management Agency, Washington, D.C., USA
- Fenwick, R.C., Davidson, B.J., Lau, D.B.N. (2005). Interaction between ductile RC perimeter frames and floor slabs containing precast units. New Zealand Society for Earthquake Engineering Conference: 23-35
- Ferliche M., y Equipo de Trabajo del IAGPDS, (2011). Efectos del Terremoto de Lorca en las edificaciones (in Spanish). Available at http://www.ugr.es/~iag/lorca/Efecto_edificaciones.pdf
- Ferliche, M., Vidal, F., Alguacil, G., Navarro, M., Aranda, C. (2012). Vulnerabilidad y daño en el terremoto de Lorca de 2011. 7ª Asamblea hispano-portuguesa de Geodesia y Geofísica, San Sebastián, Spain, June 25-29 (in Spanish)
- Fischinger, M., Fajfar, P., Vidic, T. (1994). Factors contributing to the response reduction. Proceedings of the 5th U.S. National Conference on Earthquake Engineering, Earthquake Engineering Research Institute, Oakland, California, USA: 97-106
- Freeman, S.A. (1990). On the correlation of code forces to earthquake demands. Proceedings of the 4th U.S.-Japan Workshop on Improvement of Building Structural Design and Construction Practices, Applied Technology Council, Redwood City, California, USA.
- Freeman, S.A. (1998). The capacity spectrum method as a tool for seismic design. Proceedings of the 11th European Conference on Earthquake Engineering, Paris, France, 6-11 September
- Freeman, S.A., Nicoletti, J.P., Tyrell, J.V. (1975). Evaluations of existing buildings for seismic risk – A case study of Puget Sound Naval Shipyard, Bremerton, Washington. Proceeding of the 1st US National Conference on Earthquake Engineering, EERI, Berkeley, California, USA:113-122
- Freeman, S.A., Nicoletti, J.P., Tyrell, J.V. (1975). Evaluations of existing buildings for seismic risk – A case study of Puget Sound Naval Shipyard, Bremerton, Washington. Proceedings of the 1st US National Conference on Earthquake Engineering: 113-122
- Galasso C., Cosenza E., Maddaloni G. (2011a). Statistical analysis of reinforcing steel properties for seismic design of RC structures. Proceedings of the 14th European Conference on Earthquake Engineering, August 30-September 3, Ohrid, Republic of Macedonia.

- Galasso, C., Cosenza, E., Maddaloni, G. (2011b). Influence of seismic reinforcing steel properties on flexural overstrength of new designed RC beams. Proceedings of the XIV Convegno ANIDIS, Bari, Italy, September 18-22
- Gallipoli, M.R., Mucciarelli, M., Vona, M. (2009). Empirical estimate of fundamental frequencies and damping for Italian buildings. *Earthquake Engineering and Structural Dynamics* 38:973-988
- Gaspar-Escribano, J.M., Benito, B., García-Mayordomo, J. (2008). Hazard-consistent response spectra in the Region of Murcia (Southeast Spain): comparison to earthquake-resistant provisions. *Bulletin of earthquake engineering* 6,179-196.
- Gates, W.E., Foth, V.A. (1978). Building period correlation. Report to the Applied Technology Council. Applied Technology Council, Palo Alto, California, USA
- Gentry, T.R., Wight, J.K. (1992). Reinforced concrete wide beam-column connections under earthquake-type loading. Report n° UMCEE 92-12. Department of Civil and Environmental Engineering, University of Michigan, Ann Arbor, Michigan, USA
- Giovinazzi, S. (2005). The vulnerability assessment and the damage scenario in seismic risk analysis. PhD Thesis, Technical University Carolo-“ilhelmina at Braunschweig, Braunschweig, Germany and University of Florence, Florence, Italy
- Giovinazzi, S., Lagomarsino, S. (2004). A macroseismic method for the vulnerability assessment of buildings. Proceedings of the 13th World Conference on Earthquake Engineering, Vancouver, Canada, August 1-6. Paper n° 896
- Glaister, S., Pinho, R. (2003) Development of a simplified deformation-based method for seismic vulnerability assessment. *Journal of Earthquake Engineering* 7(S11):107-140
- GNDT (1993). Rischio sismico di edifice pubblici. Parte I: aspetti metodologici. CNR-Gruppo Nazionale per la Difesa dai Terremoti, Rome, Italy
- Goel, R.K., Chopra, A.K. (1997). Period formulas for moment-resisting frame buildings. *Journal of Structural Engineering (ASCE)* 123(11):1454-1461
- Goel, R.K., Chopra, A.K. (1998). Period formulas for concrete shear wall buildings. *Journal of Structural Engineering (ASCE)* 124(4):426-433

- Gómez Martínez, F., Pérez García, A., De Luca, F., Verderame, G.M. (2015a). Comportamiento de los edificios de HA con tabiquería durante el sismo de Lorca de 2011: aplicación del método FAST. *Informes de la Construcción* 67(537):e065 (in Spanish)
- Gómez-Martínez, F., Pérez-García, A., De Luca, F., Verderame, G.M. (2013). Generalized FAST approach for seismic assessment of infilled RC MRF buildings: application to the 2011 Lorca earthquake. 9th World Conference on Earthquake Resistant Engineering Structures, ERES 2013, July 8-10, La Coruña, Spain. In: *Proceedings of 13th International Conference on Structures Under Shock and Impact, SUSI 2014*
- Gómez Martínez, F, Pérez García, A., Alonso Durá, A., Martínez Boquera, A., Verderame, G.M. (2015d). Eficacia de la norma NCSE-02 a la luz de los daños e intervenciones tras el sismo de Lorca de 2011. *Proceedings of Congreso Internacional sobre Intervención en Obras Arquitectónicas tras Sismo: L'Aquila (2009), Lorca (2011) y Emilia Romagna (2012)*. 13-14 May, Murcia, Spain (in Spanish)
- Gómez-Martínez, F., Alonso Durá, A., De Luca, F., Verderame, G.M. (2015b). Ductility of wide-beam RC frames as lateral resisting system. *Bulletin of Earthquake Engineering* (under revision)
- Gómez-Martínez, F., Alonso Durá, A., De Luca, F., Verderame, G.M. (2015c). Seismic performance and behaviour factor of wide-beam and deep-beam RC frames. *Engineering Structures* (under revision)
- Gómez-Martínez, F., Pérez-García, A., De Luca, F., Verderame, G.M., Manfredi, G. (2012). Preliminary study of the structural role played by masonry infills on RC building performances after the 2011 Lorca, Spain, earthquake. *Proceedings of 15th World Conference on Earthquake Engineering*, 24-28 September, Lisbon, Portugal
- Goretti A., Di Pasquale G. (2006). Technical emergency management. In: Oliveira C.S., Roca A., and Goula X. (Editors); *Assessing and managing earthquake risk*, Springer, chapter 16
- Goula, X., Figueras, S., Irizarry, J., Macau, A., Barbat, A., Lantada, N., Carreño, M.L., Valcárcel, J., Combescure, D., Belvaux, M., Monfort, D., Bremond, S., Verrhiest, G., Camares, C., Bairrao, R. (2011). *Rapport de la mission AFPS du séisme de Lorca. France* (in French)

- Grant, D., Bommer, J.J., Pinho, R., Calvi, G.M. (2006). Defining priorities and timescales for seismic intervention in school buildings in Italy. ROSE Research Report n° 2006/03, IUSS Press, Pavia, Italy
- Grünthal, G. (editor) (1998). European Macroseismic Scale 1998. Cahiers du Centre Europeen de Geodynamique et de Seismologie, 7, Luxembourg, 99p.
- Hassan, A.F., Sozen, M.A. (1997). Seismic vulnerability assessment of low-rise buildings in regions with infrequent earthquakes. ACI Structural Journal 94(1):31-39
- Hawkins, N.M., Mitchell, D. (1979). Progressive collapse of flat plate structures. ACI Journal(7):775-808
- Hermanns, L., Fraile, A., Alarcón, E., Álvarez, R. (2013). Performance of buildings with masonry infill walls during the 2011 Lorca Earthquake. Bulletin of Earthquake Engineering 12:1977-1997
- Hidalgo, P.A., Arias, A. (1990). New Chilean code for earthquake-resistant design of buildings. Proceedings of the 4th US National Conference on Earthquake Engineering, Palm Springs, California, 1990, 2:927-936
- Hwang, H.H.M., Shinozuka, M. (1994). Effect of large earthquake on the design of buildings in eastern United States. Proceedings of the 5th U.S. National Conference on Earthquake Engineering, Earthquake Engineering Research Institute, Oakland, California, USA: 223-231
- Iervolino I., De Luca F., Cosenza E., (2010). Spectral shape-based assessment of SDOF nonlinear response to real, adjusted and artificial accelerograms, Engineering Structures 32, 2776-2792.
- Iervolino, I., Manfredi, G., Polese, M., Verderame, G.M., Fabbrocino, G. (2007). Seismic risk of RC building classes. Engineering Structures 29(5):813-820
- IGN (2011): Seismic catalog: database. Service of seismic information.
- INGV-DPC S1 (2007). Progetto S1. Proseguimento della assistenza al DPC per il completamento e la gestione della mappa di pericolosità sismica prevista dall'Ordinanza PCM 3274 e progettazione di ulteriori sviluppi. Istituto Nazionale di Geofisica e Vulcanologia – Dipartimento della Protezione Civile, <http://esse1.mi.ingv.it> (in Italian)

- Jain, S., Navin, R. (1995). Seismic overstrength in reinforced concrete frames. *Journal of Structural Engineering* 121(3):580-585
- JBDPA (1990). Standard for seismic capacity assessment of existing reinforced concrete buildings. Japanese Building Disaster Prevention Association, Ministry of Construction, Tokyo, Japan
- Jennings, P. (1974). Calculation of selected ordinates of Fourier spectra. *Earthquake Engineering and Structural Dynamics* 2:281-293
- Kadaş, K. (2006). Influence of idealized pushover curves on seismic response. Master Thesis. Middle East Technical University, Ankara, Turkey
- Kakaletsis, D.J., Karayannis, C.G., 2009. Experimental investigation of infilled reinforced concrete frames with openings. *ACI Structural Journal* 106(2):132-141
- Kalkan E., Kunnath S.K., (2008). Relevance of absolute and relative energy content in seismic evaluation of structures, *Advances in Structural Engineering*, 11, 1-18.
- Kappos, A.J., Ellul, F. (2000). Seismic design and performance assessment of masonry infilled R/C frames. *Proceedings of the 12th World conference on Earthquake Engineering*, Auckland, New Zealand, January 30-February 4. Paper n° 989.
- Kappos, A.J., Ptilakis, K., Stylianidis, K.C. (1995). Cost-benefit analysis for the seismic rehabilitation of buildings in Thessaloniki, based on a hybrid method of vulnerability assessment. *Proceedings of the 5th International Conference on Seismic Zonation*, Nice, France, October 17-19, (1):406-413
- Kappos, A.J., Stylianidis, K.C., Ptilakis, K. (1998). Development of seismic risk scenarios based on a hybrid method of vulnerability assessment. *Natural Hazards* 17(2):177-192
- Kircher C.A., Nassar A.A., Kutsu O., Holmes W.T., (1997). Development of building damage functions for earthquake loss estimation. *Earthquake Spectra*, 13(4), 663-681.
- Kircher, C.A., Reitherman, R.K., Whitman, R.V., Arnold, C. (1997). Estimation of earthquake losses to buildings. *Earthquake Spectra* 13(4):703-720
- Kobayashi H, Vidal F, Feriche D, Samano T, Alguacil G., (1996). Evaluation of dynamic behavior of building structures with microtremors for seismic microzonation mapping. *Proceedings of the 11th World Conference on Earthquake Engineering*, 23-28 june, Acapulco, Mexico. Paper 1769

- Krawinkler, H. New trends in seismic design methodology (1994). Proceedings of 10th European Conference on Earthquake Engineering, 2:821-830, Balkema, Rotterdam, Netherlands
- Krawinkler, H., Miranda, E. (2004). Performance-Based Earthquake Engineering. In: Bozorgnia Y. and Bertero V.V. (Editors); Earthquake Engineering: From engineering seismology to performance-based engineering, CRC Press, chapter 9
- Krawinkler, H., Seneviratna, G.D.P.K. (1998). Pros and cons of a pushover analysis of seismic performance evaluation. Engineering structures 20(4-6):452-464
- Krawinkler, H. (1995). New trends in seismic design methodology. Proceedings of the 10th European Conference on Earthquake Engineering, Vienna, 1994. Balkema, Rotterdam, 2:821-830
- Kurose, Y., Guimaraes, G.N., Zuhua, L., Kreger, M.E., Jirsa, J.O. (1991). Evaluation of slab-beam-column connections subjected to bidirectional loading. ACI special publication(123)
- LaFave, J.M., Wight, J.K. (1997). Behavior of reinforced exterior wide beam-column-slab connections subjected to lateral earthquake loading. Report n° UMCEE 97-01. Department of Civil and Environmental Engineering, University of Michigan, Ann Arbor, Michigan, USA
- LaFave, J.M., Wight, J.K. (1999). Reinforced concrete exterior wide beam-column-slab connections subjected to lateral earthquake loading. ACI Structural Journal 96(4):577-586
- LaFave, J.M., Wight, J.K. (2001). Reinforced concrete wide-beam construction vs. conventional construction: resistance to lateral earthquake loads. Earthquake Spectra 17(3):479-505
- Lagomarsino, S., Giovinazzi, S. (2006). Macro seismic and mechanical models for the vulnerability and damage assessment of current buildings. Bulletin of Earthquake Engineering 4:415-443
- Lai, S.P., Biggs, J.M. (1980). Inelastic response spectra for aseismic building design. Journal of the Structural Division (ASCE) 106(ST6):1295-1310

- Lam, N., Wilson, J., Adrian Chandler, A., Hutchinson, G. (2000). Response spectrum modelling for rock sites in low and moderate seismicity regions combining velocity, displacement and acceleration predictions *Earthquake engineering and structural dynamics* 29,1491-1525.
- Lam, N., Wilson, J., Chandler, A., Hutchinson, G. (2000). Response spectrum modelling for rock sites in low and moderate seismicity regions combining velocity, displacement and acceleration predictions. *Earthquake Engineering and Structural Dynamics* 29:1491-1525
- Li, B., Kulkarni, S.A. (2010). Seismic behavior of reinforced concrete exterior wide beam-column joints. *Journal of Structural Engineering (ASCE)* 136(1):26-36
- López Menjívar, M.A. (2004). A review of existing pushover methods for 2-D reinforced concrete buildings. PhD Thesis partial fulfilment study. Rose School, Pavia, Italy.
- López-Almansa, F., Domínguez, D., Benavent-Climent, A. (2013). Vulnerability analysis of RC buildings with wide beams located in moderate seismicity regions. *Engineering Structures* 46:687-702
- Luco, N., Bazzurro, P., Cornell, A. (2004). Dynamic versus static computation of the residual capacity of a mainshock-damaged building to withstand an aftershock. *Proceedings of the 13th World Conference on Earthquake Engineering*, August 1-6, Vancouver, B.C., Canada. Paper n° 2405
- Luo, Y.H., Durrani, A.J., Conte, J.P. (1994). Equivalent frame analysis of flat plate buildings for seismic loading. *Journal of Structural Engineering* 120(7):2137-2155
- MacPherson, C. (2005). Seismic performance and forensic analysis of a precast concrete hollow-core floor super-assembly. Master of Engineering Thesis, University of Canterbury, Christchurch, New Zealand
- Mainstone R.J., (1971). On the stiffnesses and strengths of infilled frames, *Proceedings of the Institution of Civil Engineering*, Supplement IV, 57-90.
- Malhotra, P.K. (2006). Smooth spectra of horizontal and vertical ground motions. *Bulletin of the Seismological Society of America* 96(2):506-518
- Mander, J.B., Priestley, M.J.N., Park, R. (1988). Theoretical stress-strain model for confined concrete. *Journal of Structural Engineering* 114(8):1804-1826

- Manfredi G., Ricci P., Verderame G.M. (2012b), Influence of Infill Panels and Their Distribution on Seismic Behavior of Existing Reinforced Concrete Buildings, *The Open Construction and Building Technology Journal*, 2012, 6, (Suppl 1-M1).
- Manfredi G., Verderame G.M., Prota A., Ricci P., De Luca F., (2012a), 2012 Emilia earthquake, Italy: Reinforced Concrete buildings response, *Bulletin of Earthquake Engineering* (under review).
- Manfredi, G. (2001). Evaluation of seismic energy demand. *Earthquake Engineering and Structural Dynamics* 30,485-499.
- Manfredi, G., Prota, A., Verderame, G.M., De Luca, F., Ricci, P. (2013). 2012 Emilia earthquake, Italy: reinforced concrete buildings response. *Bulletin of Earthquake Engineering* 12(5):2275-2298
- Manfredi, G., Ricci, P., Verderame, G.M. (2012b). Influence of Infill Panels and Their Distribution on Seismic Behavior of Existing Reinforced Concrete Buildings. *The Open Construction and Building Technology Journal*, 2012, 6, (Suppl 1-M1)
- Marefat, M.S., Farzanian, M.Sh. (2008). Evaluation of moment redistribution demand in continuous constructions under gravity and seismic loads. 14th World Conference on Earthquake Engineering, October 12-17, Beijing, China
- Masi, A. (2003). Seismic vulnerability assessment of Gravity Load Designed R/C frames. *Bulletin of Earthquake Engineering* 1(3):371-395
- Masi, A., Santarsiero, G., Mossucca, A., Nigro, D. (2013b). Seismic behaviour of RC beam-column subassemblages with flat beam. *Proceedings of XV Convegno della Associazione Nazionale Italiana di Ingegneria Sismica, ANIDIS. Padova, Italy*
- Masi, A., Santarsiero, G., Nigro, D. (2013a). Cyclic tests on external RC beam-column joints: role of seismic design level and axial load value on the ultimate capacity. *Journal of Earthquake Engineering* 17(1):110-136
- Masi, A., Vona, M. (2008). Estimation of the period of vibration of existing RC building types based on experimental data and numerical results. In: *Increasing seismic safety by combining engineering technologies and seismological data, WB/NATO, Springer, Dubrovnik, Croatia:207-226*

- Mehrabi, A.B., Shing, P.B., Schuller, M.P., Noland, J.L. (1996). Experimental evaluation of masonry-infilled RC frames. *ASCE Journal of Structural Engineering* 122(3):228-237
- MEPP (2000a). Greek Earthquake Resistant Design Code, EAK 2000. Ministry of Environment, Planning and Public Works, Athens, Greece (in Greek)
- MEPP (2000b). Greek Code for the Design and Construction of Concrete Works, EKOS 2000. Ministry of Environment, Planning and Public Works, Athens, Greece (in Greek)
- Mezcua, J., Rueda, J., García, R.M. (2011). A new probabilistic seismic hazard study of Spain. *Natural Hazards* 59,1087-1108
- MH. Norma de acciones en la edificación MV-101. BOE 1963 N° 35, Madrid. 1962, Ministry of Housing, Madrid, Spain (in Spanish)
- Miranda, E. (1993). Site-dependent strength reduction factors. *Journal of Structural Engineering (ASCE)*, 119(12):3503-3519
- Miranda, E., Bertero, V. (1989). Response modification factors for earthquake resistant design of short period buildings. *Earthquake Spectra* 5(1):121-143
- Miranda, E., Bertero, V. (1994). Evaluation of strength reduction factors for earthquake-resistant design. *Earthquake Spectra* 10(2):357-379
- Mohtashami, E., Shooshtari, A. (2013). A multimode adaptive pushover procedure for seismic assessment of integral bridges. *Advances in Civil Engineering* 2013:1-13
- Mostofinejad, D., Farahbod, F. (2007). Parametric study on moment redistribution in continuous RC beams using ductility demand and ductility capacity concept. *Iranian Journal of Science & Technology, Transaction B., Engineering*, 31(B5):459-471
- Mouroux, P., Le Brun, B. (2006). Presentation of RISK-UE project. *Bulletin of Earthquake Engineering* 4(4):323-339
- MPW (2006). Documento Básico SE, Seguridad Estructural. Código Técnico de la Edificación, CTE. Ministry of Public Works, RD 1371/2007, Madrid, Spain (in Spanish)
- Mwafy, A.M., Elnashai, A.S. (2002). Calibration of force reduction factors of RC buildings. *Journal of Earthquake Engineering* 6(2):239-273

- Nassar, A.A., Krawinkler, H. (1991). Seismic demands for SDOF and MDOF systems. Report n° 95, The John A. Blume Earthquake Engineering Center, Stanford University, Stanford, California, USA
- Navarro M., Garcia-Jerez A., Alcalá F.J., Vidal F., Aranda C., Enomoto T. (2012). Analysis of site effects, building response and damage distribution observed due to the 2011 Lorca, Spain, earthquake. Proceedings of the 15th World Conference on Earthquake Engineering, Lisbon, Portugal.
- Navarro, M., García Jerez, A., Alcalá, F.J., Vidal, F., Enomoto, T. (2012). Local site effect microzonation of Lorca town (southern Spain). Bulletin of Earthquake Engineering. DOI 10.1007/s10518-013-9491-y
- Navarro, M., Oliveira, C.S. (2004). Evaluation of dynamic characteristics of reinforced concrete buildings in the City of Lisbon. 4th Assembly of the Portuguese-Spanish of Geodesy and Geophysics, Figueira da foz, Portugal
- Navarro, M., Sánchez, F.J., Feriche, M., Vidal, F., Enomoto, T., Iwatate, T., Matsuda, I., Maeda, T. (2002). Statistical estimation for dynamic characteristics of existing buildings in Granada, Spain, using microtremors. Structural Dynamics, Eurodyn2002, 1:807-812, Balkema
- Newmark, N.M., Hall, W.J. (1973). Seismic design criteria for nuclear reactor facilities. Report n° 46, Building Practices for Disaster Mitigation, National Bureau of Standards, US Department of Commerce:209-236
- NIBS, National Institute of Building Science (1997, 1999 and 2002). Earthquake loss estimation methodology. HAZUS. Technical manuals. Federal Emergency Management Agency (FEMA), Washington, Vol. 1, 2, 3. (<http://www.fema.gov/hazus/>).
- Nudo, R., Sarà, G., Viti, S. (2004). Influence of floor structures on seismic performance of RC frames. 13th World Conference on Earthquake Engineering, Vancouver, B.C., Canada, paper n° 424
- NZS (1976). Code of Practice for General Structural Design and Design Loadings for Buildings, NZS 4203:1976. Standards Association of New Zealand, Wellington, New Zealand
- NZS (2004). Structural Design Actions. Part 5: Earthquake actions, NZS 1170.5. New Zealand Standards, Wellington, New Zealand

- NZS (2006). Concrete Structures Standard: Part 1 – The Design of Concrete Structures, NZS 3101 part 1. New Zealand Standards, Wellington, New Zealand
- Oliveira CS, Navarro M., (2010) Fundamental periods of vibration of RC buildings in Portugal from in-situ experimental and numerical techniques. *Bulletin of Earthquake Engineering*, 8(3), 609–42.
- Oliveira, C.S. (2004). Atualização das bases-de-dados sobre frequências próprias de estruturas de edifícios, pontes, viadutos e passagens de peões a partir de medições in-situ. 3th Portuguese Conference on Earthquake Engineering, University of Minho, Guimarães (in Portuguese)
- Orda, M., Miranda, E., Reinoso, E., Pérez-Rocha, L.E. (2000). Seismic Loss estimation model for Mexico City. *Proceedings of the 12th World conference on Earthquake Engineering*, Auckland, New Zealand, January 30-February 4. Paper nº 1902
- Orsini, G. (1999). A model for buildings' vulnerability assessment using the Parameterless Scale of Seismic Intensity (PSI). *Earthquake Spectra* 15(3):463-483
- Osteraas, J., Krawinkler, H. (1990). Strength and ductility considerations on seismic design. Report #90, The John A. Blume Earthquake Engineering Center, Stanford University, Stanford, California, USA
- Ozdemir, P., Boduroglu, M.H., Ilki, A. (2005). Seismic safety screening method. *Proceedings of the International Workshop on Seismic Performance Assessment and Rehabilitation of Existing Buildings (SPEAR)*, Ispra, Italy, April 4-5. Paper nº 23
- Pan, A., Moehle, J.P. (1989). Lateral displacement ductility of reinforced concrete flat plates. *ACI Structural Journal* 86(3):250-258
- Panagiotakos, T.B., Fardis, M.N. (1996). Seismic response of infilled RC frames structures. 11th World Conference on Earthquake Engineering, Acapulco, México, June 23-28, paper nº 225
- Panagiotakos, T.B., Fardis, M.N. (1998). Effect of column capacity design on earthquake response of reinforced concrete buildings. *Journal of Earthquake Engineering* 2(1):113-145
- Panagiotakos, T.B., Fardis, M.N. (2001). Deformations of reinforced concrete members at yielding and ultimate. *ACI Structural Journal* 98(2):135-148 and Appendix 1 (69 pp.)

- Park, R., Paulay, T. (1975). Reinforced concrete structures. John Wiley & Sons. New York, 769 p.
- Park, Y.J., Ang, A.H.S. (1985). Mechanistic seismic damage model for reinforced concrete. ASCE Journal of Structural Engineering 111(4):722-739
- Paulay, T. (1976). Moment redistribution in continuous beams of earthquake resistant multi-storey reinforced concrete frames. Bulletin of the New Zealand National Society for Earthquake Engineering 9(4):205-212
- Paulay, T. (1988): Seismic design in reinforced concrete: the state of the art in New Zealand. Bulletin of the New Zealand National Society for Earthquake Engineering 21(3):208-232
- Paulay, T., Priestley, M.J.N. (1992). Seismic Design of Reinforced Concrete and Masonry Buildings. John Wiley & Sons, Inc. New York, USA
- PCSC (1968). Reinforced concrete code, EH-68. Permanent Committee of the Structural Concrete, Madrid, Spain (in Spanish)
- PCSC (1973). Reinforced concrete code, EH-73. Permanent Committee of the Structural Concrete, Madrid, Spain (in Spanish)
- PCSC (1980). Reinforced concrete code, EH-80. Permanent Committee of the Structural Concrete, Madrid, Spain (in Spanish)
- PCSC (1988). Reinforced concrete code, EH-88. Permanent Committee of the Structural Concrete, Madrid, Spain (in Spanish)
- PCSC (1991). Reinforced concrete code, EH-91. Permanent Committee of the Structural Concrete, Madrid, Spain (in Spanish)
- PCSC (1999). Reinforced concrete code, EHE. Permanent Committee of the Structural Concrete, Madrid, Spain (in Spanish)
- PCSC (2008). Reinforced concrete code, EHE-08. Permanent Committee of the Structural Concrete, Madrid, Spain (in Spanish)

- Pecce, M., Polese, M., Verderame, G.M. (2004). Seismic vulnerability aspects of RC buildings in Benevento. Proceedings of the Workshop on Multidisciplinary Approach to Seismic Risk Problems. Sant'Angelo dei Lombardi, Italy, September 22. In: Pecce, M., Manfredi, G., Zollo, A. (2004). The many facets of seismic risk: 134-141. CRdC AMRA
- Pinho, R., Bomber, J.J., Glaister, S. (2002). A simplified approach to displacement-based earthquake loss estimation analysis. Proceedings of the 12th European Conference on Earthquake Engineering, London, UK, September 9-13. Paper n° 738.
- Polese, M., Di Ludovico, M., Prota, A., Manfredi, G. (2013). Damage-dependent vulnerability curves for existing buildings. *Earthquake Engineering and Structural Dynamics* 42:853-870
- Porter, K., Kennedy, R., Bachman, R. (2006). Creating fragility functions for Performance-Based Earthquake Engineering. *Earthquake Spectra* 23(2):471-489
- Priestley, M.J.N. (1997). Displacement-based seismic assessment of reinforced concrete buildings. *Journal of Earthquake Engineering* 1(1):157-192
- Priestley, M.J.N. (2000). Performance based seismic design. *Bulletin of the New Zealand Society for Earthquake Engineering*, 33(3):325-346
- Priestley, M.J.N., Calvi, G.M., Kowalsky, M.J. (2007). Direct displacement-based seismic design of structures. Proceedings of the 5th NZSEE Conference, Palmerston North, New Zealand
- Quintero-Febres, C.G., Wight, J.K. (1997). Investigation on the seismic behavior of RC interior wide beam-column connections. Report n° UMCEE 97-15. Department of Civil and Environmental Engineering, University of Michigan, Ann Arbor, Michigan, USA
- Quintero-Febres, C.G., Wight, J.K. (2001). Experimental study of Reinforced concrete interior wide beam-column connections subjected to lateral loading. *ACI Structural Journal* 98(4):572-582
- Regalado, F., Lloret, V. (2011). Análisis y reflexiones sobre los terremotos del 11 de mayo del 2011 acontecidos en Lorca (sugerencias para el futuro). Alicante, Spain (in Spanish)


- Ricci, P. (2010). Seismic vulnerability of existing RC buildings. PhD Thesis. University of Naples Federico II, Naples, Italy
- Ricci, P., De Luca, F., Verderame, G.M. (2011a). 6th April 2009 L'Aquila earthquake, Italy – Reinforced concrete building performance. *Bulletin of Earthquake Engineering* 9(1),285-305.
- Ricci, P., De Risi, M.T., Verderame, G.M., Manfredi, G. (2013). Influence of infill distribution and design typology on seismic performance of low- and mid-rise RC buildings. *Bulletin of Earthquake Engineering* 11:1585-1616
- Ricci, P., Verderame G. M., Manfredi G. (2011c). Analytical investigation of elastic period of infilled RC MRF buildings. *Engineering Structures* 33(2):308-319.
- Ricci, P., Verderame, G.M., Manfredi, G., Pollino, M., Borfecchia, F., De Cecco, L., Martini, S., Pascale, C., Ristore, E., James, V. (2011b). Seismic vulnerability assessment using field survey and Remote Sensing techniques. In: B. Murgante, O. Gervasi, A. Iglesias, D. Taniar, B.O. Apduhan (editors). *Computational Science and its Applications – ICCSA 2011*. Springer-Verlag Berlin Heidelberg, 2011.
- Riddell, R., Hidalgo, P., Cruz, E. (1989). Response modification factors for earthquake resistant design of short period structures. *Earthquake Spectra* 5(3):571-590
- Riddell, R., Newmark, N.M. (1979). Statistical analysis of the response of nonlinear systems subjected to earthquakes. *Structural Research Series n° 468*, Department of Civil Engineering, University of Illinois, Urbana, Illinois, USA
- Romão, X., Costa, A.A., Paupérico, E., Rodrigues, H., Vicente, R., Varum, H., Costa, A. (2013). Field observations and interpretation of the structural performance of constructions after the 11 May 2011 Lorca earthquake. *Engineering Failure Analysis* 34:670-692
- Rossetto, T., Elnashai, A. (2003). Derivation of vulnerability functions for European-type RC structures based on observational data. *Engineering Structures* 25:1241-1263
- Rossetto, T., Peiris, N. (2009). Observations of damage due to the Kashmir earthquake of October 8, 2005 and study of current seismic provisions for buildings in Pakistan. *Bulletin of Earthquake Engineering* 7(3):681-699

- Rota, M., Penna, A., Strobbia, C., Magenes, G. (2008). Direct derivation of fragility curves from Italian post-earthquake survey data. Proceedings of the 14th World Conference on Earthquake Engineering, Beijing, China, October 12-17. Paper 09-01-0148
- Rueda, J., Mezcuca, J., García-Blanco, R.M. (2011). Directivity effects of the May 11, 2011 Lorca (Spain) Mw=5.1 earthquake. Proceedings of AGU Fall Meeting, 5-9 december, San Francisco, California, USA
- Sabetta, F., Goretti, A., Lucantoni, A. (1998). Empirical fragility curves from damage surveys and estimated strong ground motion. Proceedings of the 11th European Conference on Earthquake Engineering, Paris, France, September 6-11
- Sabetta, F., Pugliese, A. (1987). Attenuation of peak horizontal acceleration and velocity from Italian strong-motion records. Bulletin of the Seismological Society of America 77(5):1491-1513
- Sabetta, F., Pugliese, A. (1996). Estimation of response spectra and simulation of nonstationary earthquake ground motions. Bulletin of the Seismological Society of America 86(2):337-352
- Sánchez, F.J., Navarro, M., García, J.M., Enomoto, T., Vidal, F. (2002). Evaluation of seismic effects on buildings structures using microtremor measurements and simulation response. Structural Dynamics, Eurodyn2002, 2:1003-1008, Balkema
- SEAOC (1988). Recommended lateral force requirements. Structural Engineers Association of California, San Francisco, California, USA
- Serna-Ros, P., Fernández-Prada, M.A., Miguel-Sosa, P., Debb, O.A.R. (2001). Influence of stirrup distribution and support width on the shear strength of reinforced concrete wide beams. Magazine of Concrete Research 54(00):1-11
- Sezen, H., Moehle, J.P. (2004). Shear strength model for lightly reinforced concrete columns. ASCE Journal of Structural Engineering 130(11), 1692-1703.
- Shing, P.B., Mehrabi, A.B. (2002). Behaviour and analysis of masonry-infilled frames. Progress in Structural Engineering and Materials 4(3):320-331
- Shuraim, A.B. (2012). Transverse stirrup configurations in RC wide shallow beams supported on narrow columns. Journal of Structural Engineering 138(3):416-424

- Siah, W.L., Stehle, J.S., Mendis, P., Goldsworthy, H. (2003). Interior wide beam connections subjected to lateral earthquake loading. *Engineering Structures* 25:281-291
- Singhal, A., Kiremidjian, A.S. (1996). Method for probabilistic evaluation of seismic structural damage. *ASCE Journal of Structural Engineering* 122(12):1459-1467
- Singhal, A., Kiremidjian, A.S. (1998). Bayesian updating of fragilities with application to RC frames. *ASCE Journal of Structural Engineering* 124(8):922-929
- Spence, R.J.S., Coburn, A.W., Sakai, S., Pomonis, A. (1991). A parameterless scale of seismic intensity for use in the seismic risk analysis and vulnerability assessment. *International Conference on Earthquake, Blast and Impact, Manchester, UK, September 19-20:19-30*
- Trifunac, M.D. (1999). Comments on “Period formulas for concrete shear wall buildings” by R.K. Goel and A.K. Chopra. *Journal of Structural Engineering (ASCE)* 125(7):797-798
- Trifunac, M.D., Ivanović, S.S., Todorovska, M.I. (2001a). Apparent periods of a building. I: Fourier analysis. *Journal of structural engineering* 127:517-526
- Trifunac, M.D., Ivanović, S.S., Todorovska, M.I. (2001b). Apparent periods of a building. II: Time-frequency analysis. *Journal of structural engineering* 127:527-537
- TSI (2007). Specifications for buildings to be built in seismic areas. Turkish Standards Institution, Ministry of Public Works and Settlement, Ankara, Turkey (in Turkish)
- Tso, W.K. (1990). Static eccentricity concept for torsional moment estimations. *Journal of Structural Engineering* 116(5):1199-1212
- Uang C., Bertero V.V. (1990). Evaluation of seismic Energy in structures. *Earthquake Engineering and Structural Dynamics*, 19, 77-90
- Uang, C., Maarouf, A. (1993). Safety and economy considerations of UBC seismic force reduction factors. *Proceedings of the National Earthquake Conference, Central United States Earthquake Consortium, Memphis, Tennessee: 121-130*
- Vamvatsikos, D., Cornell, C.A. (2002). Incremental dynamic analysis. *Earthquake Engineering and Structural Dynamics* 31:491-514

- Verderame G.M., Ricci P., De Luca F., Del Gaudio C., De Risi M.T., (2012). Seismic response of RC buildings during the 2012 Emilia (Italy) sequence. *Soil Dynamics and Earthquake Engineering* (under review).
- Verderame, G.M., De Luca, F., Ricci, P., Manfredi, G. (2011). Preliminary analysis of a soft-storey mechanism after the 2009 L'Aquila earthquake. *Earthquake Engineering and Structural Dynamics* 40(8):925-944
- Verderame, G.M., Iervolino, I., Manfredi, G. (2010b). Elastic period of sub-standard reinforced concrete moment resisting frame buildings. *Bulletin of Earthquake Engineering* 8:955-972
- Verderame, G.M., Polese, M., Mariniello, C., Manfredi, G. (2010a). A simulated design procedure for the assessment of seismic capacity of existing reinforced concrete buildings. *Advances in Engineering Software* 41(2):323-335
- Verderame, G.M., Ricci, P., De Luca, F., Del Gaudio, C., De Risi, M.T. (2013). Damage scenarios for RC buildings during the 2012 Emilia (Italy) earthquake. *Soil Dynamics and Earthquake Engineering* 66:385-400
- Vidal, F., Alguacil, G., Feriche, M., Aranda, C., Morales, J., Stich, D., Pérez Muelas, J., Benito, J., López, J.M. (2011). El terremoto de Lorca: Mayo 2011. Causas del impacto y primeras medidas. Análisis preliminar. Informe IAGPDS, Universidad de Granada. http://www.ugr.es/~iag/lorca/Impacto_Lorca.pdf
- Vidal, F., Navarro, M., Aranda, C., Enomoto, T. (2013). Changes in dynamic characteristics of Lorca RC buildings from pre- and post-earthquake ambient vibration data. *Bulletin of Earthquake Engineering* 12:2095-2110
- Vidic, T., Fajfar, P., Fischinger, M. (1994). Consistent inelastic design spectra: strength and displacement. *Earthquake engineering and structural dynamics* 23,502-521.
- Vielma, J.C., Barbat, A.H., Oller, S. (2006). Factores de reducción de respuesta. Estado del arte y estudio comparativo entre códigos. *Revista internacional de Ingeniería de Estructuras* 11(1):77-106
- Vielma, J.C., Barbat, A.H., Oller, S. (2010). Seismic safety of low ductility structures used in Spain. *Bulletin of Earthquake Engineering* 8:135-155

- VV.AA. (2006): Riesgo Sísmico de la Comunidad Autónoma de la Región de Murcia (RISMUR). 6 Vols. Instituto Geográfico Nacional y Dirección General de Protección Civil CARM. Murcia, Spain (in Spanish)
- Whitman, R.V., Anagnos, T., Kircher, C.A., Lagorio, H.J., Lawson, R.S., Schneider, P. (1997). Development of a national earthquake loss estimation methodology. *Earthquake Spectra* 13(4):643-661
- Whitman, R.V., Reed, J.W., Hong, S.T. (1973). Earthquake Damage Probability Matrices. Proceedings of the 5th World Conference on Earthquake Engineering, Rome, Italy, June 25-29 (2):2531-2540
- Yakut, A. (2004). Preliminary seismic performance assessment procedure for existing RC buildings. *Engineering Structures* 26(10):1447-1461
- Zhu, L., Elwood, K.J., Haukaas, T. (2007). Classification and seismic safety evaluation of existing reinforced concrete columns. *Journal of structural engineering* 133(9):1316-1330
- Zhu, T., Tso, W. and Heidebrecht, A. (1992). Seismic performance of reinforced concrete ductile moment-resisting frame buildings located in different seismic regions. *Canadian Journal of Civil Engineering* 19(4):668-710

The background of the page is a photograph of a brick wall. A semi-transparent grid pattern is overlaid on the image, creating a technical or architectural feel. The grid lines are light blue and intersect to form a series of squares across the entire page.

A simplified analytical spectral-based method (FAST) for the estimation of large-scale vulnerability of RC infilled frames is proposed and tested by using the real damage scenario after the 2011 Lorca earthquake as a benchmark. FAST allows predicting the average non-structural damage state expected for each class of building (defined by number of storeys, age of construction, infills ratio in plan and location), accounting for any reduction of infills ratio on the ground floor. It is based on the approximate definition of capacity curves and on the assumption of “a priori” deformed shapes.

Information regarding the 2011 Lorca earthquake (ground motion, damage scenario and building design practice) is collected. A critical review of Spanish seismic codes in comparison with current performance-based codes such as Eurocode 8 is carried out, especially regarding the prescription of lower behaviour factor for wide-beam frames with respect to deep-beam frames, which may be obsolete.

FAST is applied to the Lorca earthquake: predicted damage scenarios are obtained for different assumptions, showing proper agreement when compared to real damages. FAST proves that infills provided additional strength to RC frames, which is actually the main cause of the few structural collapses registered, even though the registered PGA was three times higher than the typical acceleration of design for the site.